

Legacy & emerging contaminants in the aquatic environment

Edited by

Abdul Qadeer, Mengyang Liu and Sanjeeb Mohapatra

Coordinated by

Racliffe Weng Seng Lai

Published in

Frontiers in Environmental Science

Frontiers in Toxicology



FRONTIERS EBOOK COPYRIGHT STATEMENT

The copyright in the text of individual articles in this ebook is the property of their respective authors or their respective institutions or funders. The copyright in graphics and images within each article may be subject to copyright of other parties. In both cases this is subject to a license granted to Frontiers.

The compilation of articles constituting this ebook is the property of Frontiers.

Each article within this ebook, and the ebook itself, are published under the most recent version of the Creative Commons CC-BY licence. The version current at the date of publication of this ebook is CC-BY 4.0. If the CC-BY licence is updated, the licence granted by Frontiers is automatically updated to the new version.

When exercising any right under the CC-BY licence, Frontiers must be attributed as the original publisher of the article or ebook, as applicable.

Authors have the responsibility of ensuring that any graphics or other materials which are the property of others may be included in the CC-BY licence, but this should be checked before relying on the CC-BY licence to reproduce those materials. Any copyright notices relating to those materials must be complied with.

Copyright and source acknowledgement notices may not be removed and must be displayed in any copy, derivative work or partial copy which includes the elements in question.

All copyright, and all rights therein, are protected by national and international copyright laws. The above represents a summary only. For further information please read Frontiers' Conditions for Website Use and Copyright Statement, and the applicable CC-BY licence.

ISSN 1664-8714
ISBN 978-2-8325-6414-1
DOI 10.3389/978-2-8325-6414-1

About Frontiers

Frontiers is more than just an open access publisher of scholarly articles: it is a pioneering approach to the world of academia, radically improving the way scholarly research is managed. The grand vision of Frontiers is a world where all people have an equal opportunity to seek, share and generate knowledge. Frontiers provides immediate and permanent online open access to all its publications, but this alone is not enough to realize our grand goals.

Frontiers journal series

The Frontiers journal series is a multi-tier and interdisciplinary set of open-access, online journals, promising a paradigm shift from the current review, selection and dissemination processes in academic publishing. All Frontiers journals are driven by researchers for researchers; therefore, they constitute a service to the scholarly community. At the same time, the *Frontiers journal series* operates on a revolutionary invention, the tiered publishing system, initially addressing specific communities of scholars, and gradually climbing up to broader public understanding, thus serving the interests of the lay society, too.

Dedication to quality

Each Frontiers article is a landmark of the highest quality, thanks to genuinely collaborative interactions between authors and review editors, who include some of the world's best academicians. Research must be certified by peers before entering a stream of knowledge that may eventually reach the public - and shape society; therefore, Frontiers only applies the most rigorous and unbiased reviews. Frontiers revolutionizes research publishing by freely delivering the most outstanding research, evaluated with no bias from both the academic and social point of view. By applying the most advanced information technologies, Frontiers is catapulting scholarly publishing into a new generation.

What are Frontiers Research Topics?

Frontiers Research Topics are very popular trademarks of the *Frontiers journals series*: they are collections of at least ten articles, all centered on a particular subject. With their unique mix of varied contributions from Original Research to Review Articles, Frontiers Research Topics unify the most influential researchers, the latest key findings and historical advances in a hot research area.

Find out more on how to host your own Frontiers Research Topic or contribute to one as an author by contacting the Frontiers editorial office: frontiersin.org/about/contact

Legacy & emerging contaminants in the aquatic environment

Topic editors

Abdul Qadeer — Chinese Research Academy of Environmental Sciences, China

Mengyang Liu — City University of Hong Kong, Hong Kong, SAR China

Sanjeeb Mohapatra — Delft University of Technology, Netherlands

Topic coordinator

Racliffe Weng Seng Lai — City University of Hong Kong, Hong Kong, SAR China

Citation

Qadeer, A., Liu, M., Mohapatra, S., Lai, R. W. S., eds. (2025). *Legacy & emerging contaminants in the aquatic environment*. Lausanne: Frontiers Media SA.

doi: 10.3389/978-2-8325-6414-1

Table of contents

- 05 **Editorial: Legacy & emerging contaminants in the aquatic environment—bridging knowledge, policy, and future**
Abdul Qadeer, Mengyang Liu, Sanjeeb Mohapatra and Racliffe Weng Seng Lai
- 09 **Aquatic organisms modulate the bioreactivity of engineered nanoparticles: focus on biomolecular corona**
Wei Liu, Isabelle A. M. Worms, Željko Jakšić and Vera I. Slaveykova
- 22 **First report on atrazine monitoring in drinking water from Ijebu-North, South-West Nigeria: Human health risk evaluation and reproductive toxicity studies**
Folarin Owagboriaye, Rasheed Oladunjoye, Oladunni Adekunle, Mistura Adeleke, Titilola Salisu, Adedamola Adenekan, Abibat Sulaimon, Gabriel Dedeké and Olusegun Lawal
- 38 **A screening study of the spatial distribution and cumulative toxicity of agricultural pesticides in the European Union's waters**
A. Pistocchi, C. Dorati, F. Galimberti, A. Udias, S. Bopp, R. D'Andrimont, R. Catarino and R. B. Schaefer
- 49 **The distribution and metabolism of hexabromocyclododecane isomers varies in the tissues of *Nibea albiflora***
Suping Song, Xiumei Sun, Xin Cheng, Xijian Peng, Qing Hao, Hongmei Hu, Jian Zhu, Tiejun Li and Yuanming Guo
- 59 **Occurrence and path pollution of emerging organic contaminants in mineral water of Hranice hypogenic Karst**
Petra Opletová, Vítězslav Vlček, Milan Geršl, Pavel Chaloupský, Ondřej Ulrich, Jozef Sedláček, Hana Vavrouchová, Kristýna Kohoutková, Radim Klepárník and Jana Šimečková
- 76 **Dechloranes and chlorinated paraffins in sediments and biota of two subarctic lakes**
Aline Arriola, Insam Al Saify, Nicholas A. Warner, Dorte Herzke, Mikael Harju, Per-Arne Amundsen, Anita Evenset, Claudia Möckel and Ingjerd S. Krogseth
- 98 **Regulation of salinity to inhibit 2-methylisoborneol and geosmin: Insights from spatial-scale research in coastal areas of China**
Xi Chen, Zhonghua Li, Huimin Xu, Liping Qiu, Limin Fan, Shunlong Meng, Zexia Gao and Chao Song
- 108 **Effect of cellulose-lignin ratio on the adsorption of U(VI) by hydrothermal charcoals prepared from *Dendrocalamus farinosus***
FanQin Yang, Hanhan Li, Boya Wang, Wei Fan, Xiaoyan Gu, Ying Cao and Shanglian Hu

- 119 **Spatial distribution of available phosphorus in surface road and trackway surface materials on a sheep farm in Ireland**
Owen Fenton, Karen Daly, Pat Tuohy, John Cardiff, Simon Leach, Lungile Senteni Sifundza and John Murnane
- 129 **Cocktail effects of clothianidin and imidacloprid in zebrafish embryonic development, with high and low concentrations of mixtures**
Seonggeun Zee, Moonjung Hyun, Hee-Jung Sim, Kanghee Kim, Ju-Chan Kang and Chang-Beom Park
- 139 **Heterogenous bioluminescence patterns, cell viability, and biofilm formation of *Photobacterium leiognathi* strains exposed to ground microplastics**
Rener De Jesus, Sameera Iqbal, Sunil Mundra and Ruwaya AlKendi



OPEN ACCESS

EDITED AND REVIEWED BY
Sara Cristina Antunes,
University of Porto, Portugal

*CORRESPONDENCE

Abdul Qadeer,
✉ Dr.AQ.Geographer@gmail.com
✉ aqadeer@iu.edu

RECEIVED 14 April 2025

ACCEPTED 18 April 2025

PUBLISHED 15 May 2025

CITATION

Qadeer A, Liu M, Mohapatra S and Lai RWS
(2025) Editorial: Legacy & emerging
contaminants in the aquatic
environment—bridging knowledge, policy,
and future.
Front. Toxicol. 7:1611852.
doi: 10.3389/ftox.2025.1611852

COPYRIGHT

© 2025 Qadeer, Liu, Mohapatra and Lai. This is
an open-access article distributed under the
terms of the [Creative Commons Attribution
License \(CC BY\)](#). The use, distribution or
reproduction in other forums is permitted,
provided the original author(s) and the
copyright owner(s) are credited and that the
original publication in this journal is cited, in
accordance with accepted academic practice.
No use, distribution or reproduction is
permitted which does not comply with these
terms.

Editorial: Legacy & emerging contaminants in the aquatic environment—bridging knowledge, policy, and future

Abdul Qadeer^{1,2,3*}, Mengyang Liu⁴, Sanjeeb Mohapatra⁵ and
Racliffe Weng Seng Lai⁶

¹State Key Laboratory of Environmental Criteria and Risk Assessment, National Engineering Laboratory of Lake Pollution Control and Ecological Restoration, State Environmental Protection Key Laboratory for Lake Pollution Control, Chinese Research Academy of Environmental Sciences, Beijing, China, ²O'Neill School of Public and Environmental Affairs, Indiana University, Bloomington, IN, United States, ³Institute of Soil and Environmental Science, University of Agriculture, Faisalabad, Pakistan, ⁴State Key Laboratory of Marine Pollution, City University of Hong Kong, Kowloon, Hong Kong SAR, China, ⁵Department of Water Management, Delft University of Technology, Delft, Netherlands, ⁶Centre for Regional Oceans and Department of Ocean Science and Technology, Faculty of Science and Technology, University of Macau, Macau, China

KEYWORDS

emerging pollutants (EPs), legacy contaminants, environment, lakes, aquatic bodies

Editorial on the Research Topic

[Legacy & emerging contaminants in the aquatic environment-bridging knowledge, policy, and future](#)

1 Introduction

Aquatic ecosystems are increasingly under threat from a complex mixture of contaminants, including legacy and emerging. Historically, great focus has been given to legacy pollutants such as polychlorinated biphenyls (PCBs), dichlorodiphenyltrichloroethane (DDT), mercury, and heavy metals—substances known for their environmental persistence, bioaccumulative potential, and long-term ecological and human health impacts (Qadeer et al., 2020; Qadeer et al., 2019; Yang et al., 2019; Wang et al., 2018; Hoskins, 2003). Despite regulatory bans or restrictions in many regions (Gao, 2024; Zimmerman and Anastas, 2015; Qadeer et al., 2022a), these chemicals persist in sediments, biota, and water bodies due to their resistance to degradation, thereby causing lasting ecological disruption (Qadeer et al., 2019; Suedel et al., 1994; Streets et al., 2006; Huang et al., 2022; Coelho et al., 2016).

Concurrently, the scientific community is now contending with a new generation of pollutants, broadly referred to as emerging contaminants. These cover a vast number of chemicals, including but not limited to pharmaceuticals (Katsikaros and Chrysikopoulos, 2021), personal care products (Kachhawaha et al., 2021), microplastics (Beginagwa et al., 2016; Qadeer et al., 2021), plasticizers (Qadeer et al., 2022a; Qadeer et al., 2022b; Zhong et al., 2018), nanomaterials (Noguera-Oviedo and Aga, 2016; Li et al., 2021) and industrial additives such as per- and polyfluoroalkyl substances (PFAS) (Liu et al., 2023; Shen et al.,

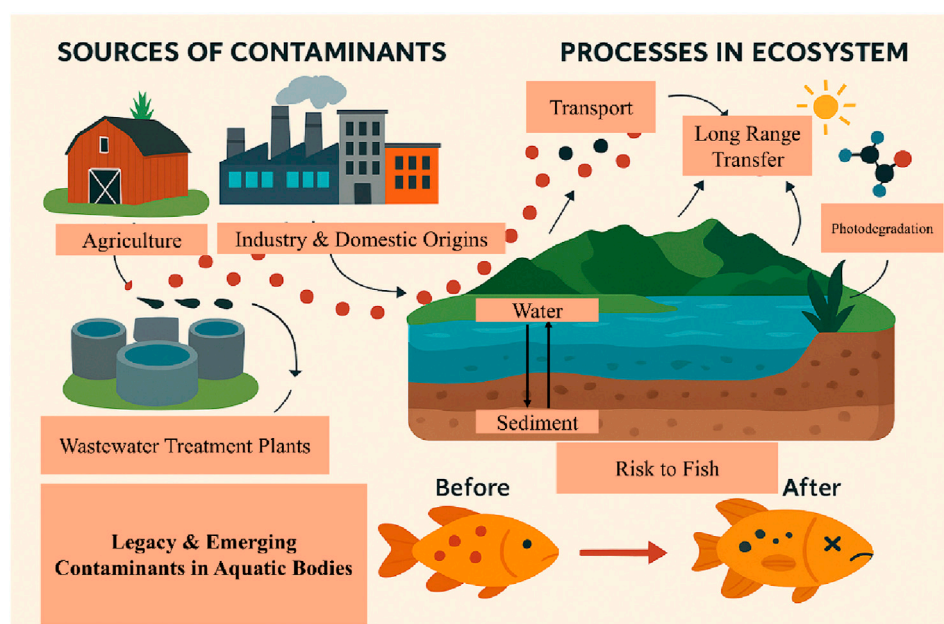


FIGURE 1

This is a general conceptual illustration of the sources, environmental processes, and ecological risks of legacy and emerging contaminants in aquatic ecosystems.

2018) and flame retardants (Noguera-Oviedo and Aga, 2016). Although these chemicals enter the environment through similar processes as legacy pollutants, they are, in general, more poorly monitored and largely unregulated. Our understanding of their long-term impacts remains limited, but growing evidence suggests they can induce sublethal toxicity, disrupt endocrine systems, impair reproduction, and interact synergistically with other stressors to amplify ecological harm (Qadeer et al., 2021; Zota et al., 2018; Folkerson et al., 2023; Ateia and Scheringer, 2024; Roepke and Sadlier, 2021). A general diagram of their sources, transport and risks of legacy and emerging contaminants is provided in Figure 1.

Together, legacy and emerging contaminants present a dual environmental threat to aquatic systems. Their co-occurrence and chemical mixture interactions necessitate urgent, coordinated efforts to reconsider and reshape traditional monitoring frameworks, risk assessment models, and management strategies. Addressing these interconnected challenges requires not only scientific advancement but also effective integration into environmental policy and on-the-ground practice.

2 Overview of the special issue

This Research Topic, “Legacy & Emerging Contaminants in the Aquatic Environment,” features 11 original research articles, offering critical insights into the occurrence, fate, toxicity, and mitigation strategies of both legacy and emerging contaminants across diverse aquatic environments. This collective intellectual property represents efforts from a broad geographic and thematic scope, addressing both long-established and novel pollutants that are gaining increasing scientific and public attention.

Highlights include studies evaluating the impacts of microplastics on marine microbial communities, the toxicological effects of pesticide mixtures on zebrafish embryos, and spatial analyses of phosphorus distribution—linking land use to nutrient runoff. Innovative remediation approaches are also presented, such as the use of hydrothermal charcoals for uranium adsorption and salinity regulation techniques for controlling algal off-flavor compounds in aquaculture systems.

Other contributions examine the presence and distribution of chlorinated paraffins and dechloranes in subarctic lake sediments and biota, the vulnerability of karst aquifers to emerging organic pollutants, and the bioaccumulation of flame retardants in marine fish. A comprehensive assessment of agricultural pesticide residues in European surface waters further emphasizes the complexity of spatial variability and cumulative ecological risks. Collectively, these studies showcase the depth and breadth of current research and underscore the importance of bridging scientific findings with policy development and practical intervention.

3 Bridging science with policy and the future

Effectively addressing legacy and emerging contaminants requires not only scientific knowledge, progress, and breakthroughs but also their timely translation into actionable policy and environmental management strategies. Beyond significant advancements in detection techniques, monitoring, and risk assessment models, scientific findings should be more effectively integrated into regulatory frameworks. Bridging this gap calls for interdisciplinary collaboration among scientists, policymakers, industry professionals, and public health

authorities. By fostering evidence-based policymaking, encouraging stakeholder engagement, and integrating research into local and international regulations, we can enhance the real-world impact of environmental science and promote sustainable stewardship of aquatic ecosystems.

Although progress has been made, critical knowledge gaps still hinder comprehensive contaminant management. In particular, the effects of contaminant mixtures—often more complex and potent than individual compounds remain poorly understood, especially under realistic environmental conditions. There is also a shortage of long-term monitoring data for many emerging contaminants, limiting our ability to assess chronic exposure risks across trophic levels. Furthermore, the fate, transport, and transformation of emerging pollutants in aquatic systems are still largely uncharted.

To address these gaps, future research must prioritize developing integrated monitoring systems, advanced modeling tools, and high-resolution analytical techniques. Studies should also focus on the interactive and cumulative effects of chemical mixtures to reflect real-world exposure scenarios. Strengthening global research collaboration, harmonizing environmental standards, and promoting open-access data sharing will be essential for accelerating this progress. Additionally, engaging local communities, industry partners, and civil society will enhance the implementation of practical, context-specific solutions to aquatic pollution.

Author contributions

AQ: Conceptualization, Formal Analysis, Investigation, Software, Writing – original draft, Writing – review and editing. ML: Investigation, Validation, Writing – original draft, Writing – review and editing. SM: Investigation, Validation, Writing – review and editing. RL: Investigation, Validation, Writing – original draft, Writing – review and editing.

Funding

The author(s) declare that no financial support was received for the research and/or publication of this article.

References

- Ateia, M., and Scheringer, M. (2024). From “forever chemicals” to fluorine-free alternatives. *Science* 385 (6706), 256–258. doi:10.1126/SCIENCE.ADO5019
- Biginagwa, F. J., Mayoma, B. S., Shashoua, Y., Syberg, K., and Khan, F. R. (2016). First evidence of microplastics in the african great lakes: recovery from lake victoria Nile perch and Nile Tilapia. *J. Great Lakes Res.* 42 (1), 146–149. doi:10.1016/j.jglr.2015.10.012
- Coelho, S. D., Sousa, A. C. A., Isobe, T., Kim, J. W., Kunisue, T., Nogueira, A. J. A., et al. (2016). Brominated, chlorinated and phosphate organic contaminants in house dust from Portugal. *Sci. Total Environ.* 569–570, 442–449. doi:10.1016/j.scitotenv.2016.06.137
- Folkerson, A. P., Schneider, S. R., Abbatt, J. P. D., and Mabury, S. A. (2023). Avoiding regrettable replacements: can the introduction of novel functional groups move PFAS from recalcitrant to reactive? *Environ. Sci. Technol.* 57 (44), 17032–17041. doi:10.1021/acs.est.3c06232
- Gao, P. (2024). Chasing “emerging” contaminants: an endless journey toward environmental health. *Environ. Sci. Technol.* 58 (4), 1790–1792. doi:10.1021/acs.est.3c10630
- Hoskins, J. A. (2003). Health effects due to indoor air pollution. *Indoor Built Environ.* 12, 427–433. doi:10.1177/1420326x03037109
- Huang, Z., Qadeer, A., Zheng, S., Ge, F., Zhang, K., Yin, D., et al. (2022). Fatty acid profile as an efficient bioindicator of PCB bioaccumulation in a freshwater lake food web: a stable isotope guided investigation. *J. Hazard. Mater.* 423, 127121. doi:10.1016/J.JHAZMAT.2021.127121
- Kachhawaha, A. S., Nagarnaik, P. M., Labhasetwar, P. K., and Banerjee, K. (2021). Pharmaceuticals and personal care products in aqueous urban environment of western India. *Water Environ. J.* 35 (4), 1302–1312. doi:10.1111/WEJ.12720
- Katsikaros, A. G., and Chrysikopoulos, C. V. (2021). Occurrence and distribution of pharmaceuticals and personal care products (PPCPs) detected in lakes around the world - a review. *Environ. Adv.* 6, 100131. doi:10.1016/J.ENVADV.2021.100131
- Li, F., Meng, X., Wang, X., Ji, C., and Wu, H. (2021). Graphene-triphenyl phosphate (TPP) Co-exposure in the marine environment: interference with metabolism and immune regulation in mussel *Mytilus galloprovincialis*. *Ecotoxicol. Environ. Saf.* 227, 112904. doi:10.1016/j.ecoenv.2021.112904

Acknowledgments

We extend our appreciation to all contributing authors for their innovative research and to the reviewers for their insightful evaluations, which upheld the scientific integrity of this Research Topic. We are also grateful to the editorial team at Frontiers for their continuous support throughout the publication process. This Research Topic represents the collective efforts of a vibrant and globally connected research community committed to safeguarding aquatic environments. We hope this Research Topic serves as a valuable scientific resource and inspires ongoing collaboration, policy innovation, and community engagement in the global fight against aquatic contamination. We are thankful to the Chinese Research Academy of Environmental Science, Beijing, and Indiana University, United States of America, for providing resources and a workplace.

Conflict of interest

The authors declare that the research was conducted in the absence of any commercial or financial relationships that could be construed as a potential conflict of interest.

Generative AI statement

The authors declare that Generative AI was used in the creation of this manuscript. The English language was refined using Grammarly and ChatGPT, and Figure 1 was generated with the assistance of ChatGPT, but manually modified with PowerPiont. The authors take full responsibility for the content, which was carefully reviewed to ensure its accuracy and credibility.

Publisher's note

All claims expressed in this article are solely those of the authors and do not necessarily represent those of their affiliated organizations, or those of the publisher, the editors and the reviewers. Any product that may be evaluated in this article, or claim that may be made by its manufacturer, is not guaranteed or endorsed by the publisher.

- Liu, M., Qadeer, A., Anis, M., Ajmal, Z., Bekele, T. G., Wang, S., et al. (2023). "Occurrence of per- and polyfluoroalkyl substances (PFAS): a special reference to their monitoring, distribution, and environmental fate," in *Emerging aquatic contaminants one health framework for risk assessment and remediation in the post COVID-19 anthropocene*, 173–202. doi:10.1016/B978-0-323-96002-1.00001-8
- Noguera-Oviedo, K., and Aga, D. S. (2016). Lessons learned from more than two decades of research on emerging contaminants in the environment. *J. Hazard. Mater.* 316, 242–251. doi:10.1016/j.jhazmat.2016.04.058
- Qadeer, A., Ajmal, Z., Usman, M., Zhao, X., and Chang, S. (2021). Agricultural plastic mulching as a potential key source of microplastic pollution in the terrestrial ecosystem and consequences. *Resour. Conserv. Recycl.* 175 (July), 105855. doi:10.1016/j.resconrec.2021.105855
- Qadeer, A., Kirsten, K., Ajmal, Z., and Xingru, Z. (2022b). Rebuttal to comment on "alternative plasticizers as emerging global environmental and health threat: another regrettable substitution?" Focus on DINCH as an example. *Environ. Sci. Technol.* 56, 5294–5297. doi:10.1021/acs.est.2c01849
- Qadeer, A., Kirsten, K. L., Ajmal, Z., Jiang, X., and Zhao, X. (2022a). Alternative plasticizers as emerging global environmental and health threat: another regrettable substitution? *Environ. Sci. Technol.* 56 (3), 1482–1488. doi:10.1021/acs.est.1c08365
- Qadeer, A., Sai, L., Min, L., Liu, X., Ajmal, Z., Huang, Y., et al. (2019). Historically linked residues profile of OCPs and PCBs in surface sediments of typical urban river networks, Shanghai: ecotoxicological state and sources. *J. Clean. Prod.* 231, 1070–1078. doi:10.1016/j.jclepro.2019.05.203
- Qadeer, A., Saqib, Z. A., Ajmal, Z., Xing, C., Khan Khalil, S., Usman, M., et al. (2020). Concentrations, pollution indices and health risk assessment of heavy metals in road dust from two urbanized cities of Pakistan: comparing two sampling methods for heavy metals concentration. *Sustain. Cities Soc.* 53, 101959. doi:10.1016/j.scs.2019.101959
- Roepke, T. A., and Sadlier, N. C. (2021). Reproductive toxicology: impact of endocrine disruptors on neurons expressing GnRH or kisspeptin and pituitary gonadotropins. *Reproduction* 162 (5), F131–F145. doi:10.1530/REP-20-0612
- Shen, A., Lee, S., Ra, K., Suk, D., and Moon, H. B. (2018). Historical trends of perfluoroalkyl substances (PFASs) in dated sediments from semi-enclosed bays of Korea. *Mar. Pollut. Bull.* 128 (January), 287–294. doi:10.1016/j.marpolbul.2018.01.039
- Streets, S. S., Henderson, S. A., Stoner, A. D., Carlson, D. L., Simcik, M. F., and Swackhamer, D. L. (2006). Partitioning and bioaccumulation of PBDEs and PCBs in lake Michigan. *Environ. Sci. Technol.* 40 (23), 7263–7269. doi:10.1021/es061337p
- Suedel, B. C., Boraczek, J. A., Peddicord, R. K., Clifford, P. A., and Dillon, T. M. (1994). Trophic transfer and biomagnification potential of contaminants in aquatic ecosystems. *Rev. Environ. Contam. Toxicol.* 136, 21–89. doi:10.1007/978-1-4612-2656-7_2
- Wang, D., Wang, Y., Singh, V. P., Zhu, J., Jiang, L., Zeng, D., et al. (2018). Ecological and health risk assessment of PAHs, OCPs, and PCBs in taihu lake basin. *Ecol. Indic.* 92, 171–180. doi:10.1016/j.ecolind.2017.06.038
- Yang, J., Qadeer, A., Liu, M., Zhu, J., Huang, Y., Du, W., et al. (2019). Occurrence, source, and partition of PAHs, PCBs, and OCPs in the multiphase system of an urban lake, Shanghai. *Appl. Geochem.* 106, 17–25. doi:10.1016/j.apgeochem.2019.04.023
- Zhong, M., Wu, H., Mi, W., Li, F., Ji, C., Ebinghaus, R., et al. (2018). Occurrences and distribution characteristics of organophosphate ester flame retardants and plasticizers in the sediments of the bohai and yellow seas, China. *Sci. Total Environ.* 615, 1305–1311. doi:10.1016/j.scitotenv.2017.09.272
- Zimmerman, J. B., and Anastas, P. T. (2015). Chemistry. Toward substitution with no regrets. *Science* 347 (6227), 1198–1199. doi:10.1126/science.aaa0812
- Zota, A. R., Gellera, R. J., Romano, L. E., Coleman-Phox, K., Adler, N. E., Parry, E., et al. (2018). Association between persistent endocrine-disrupting chemicals (PBDEs, OH-PBDEs, PCBs, and PFASs) and biomarkers of inflammation and cellular aging during pregnancy and postpartum. *Environ. Int.* 115, 9–20. doi:10.1016/j.envint.2018.02.044



OPEN ACCESS

EDITED BY
Monika Mortimer,
China Jiliang University, China

REVIEWED BY
Amitava Mukherjee,
VIT University, India
Hossein Mohammad-Beigi,
Technical University of Denmark,
Denmark

*CORRESPONDENCE
Vera I. Slaveykova,
vera.slaveykova@unige.ch

SPECIALTY SECTION
This article was submitted to
Nanotoxicology,
a section of the journal
Frontiers in Toxicology

RECEIVED 30 April 2022
ACCEPTED 11 July 2022
PUBLISHED 19 August 2022

CITATION
Liu W, Worms IAM, Jakšić Ž and
Slaveykova VI (2022), Aquatic organisms
modulate the bioreactivity of
engineered nanoparticles: focus on
biomolecular corona.
Front. Toxicol 4:933186.
doi: 10.3389/ftox.2022.933186

COPYRIGHT
© 2022 Liu, Worms, Jakšić and
Slaveykova. This is an open-access
article distributed under the terms of the
[Creative Commons Attribution License](#)
(CC BY). The use, distribution or
reproduction in other forums is
permitted, provided the original
author(s) and the copyright owner(s) are
credited and that the original
publication in this journal is cited, in
accordance with accepted academic
practice. No use, distribution or
reproduction is permitted which does
not comply with these terms.

Aquatic organisms modulate the bioreactivity of engineered nanoparticles: focus on biomolecular corona

Wei Liu ¹, Isabelle A. M. Worms ¹, Željko Jakšić ² and Vera I. Slaveykova ^{1*}

¹Department F.-A. Forel for Environmental and Aquatic Sciences, Environmental Biogeochemistry and Ecotoxicology, Faculty of Sciences, Earth and Environment Sciences, University of Geneva, Uni Carl Vogt, Geneva, Switzerland, ²Center for Marine Research Rovinj, Institute Ruder Bošković, Rovinj, Croatia

The increased use of nanoparticle (NP)-enabled materials in everyday-life products have raised concerns about their environmental implications and safety. This motivated the extensive research in nanoecotoxicology showing the possibility that NPs could cause harm to the aquatic organisms if present at high concentrations. By contrast, studies dealing with influence that organisms could exert on the fate and thus effects of NPs are still very rare. Drawing on the existing up-to-date knowledge we critically discuss the formation of biomolecular corona as one of the mechanisms by which organisms exerted control on the NPs fate in the aquatic and biotic environments. We focused the formation of corona by exogenous and endogenous biomolecules and illustrated the discussion with the specific example of phytoplankton and aquatic invertebrate species. We highlighted the necessity to incorporate the concept of biomolecular corona within more general framework considering the feedback of aquatic organisms and the control they exert in shaping the fate and impact of NPs in the aquatic and biological environment. In our view such broader perspective will contribute to get novel insights into the drivers of environmental transformations of NPs and their mechanisms, which are important in environmental risk assessment.

KEYWORDS

Nanotoxicology, nanoparticles, bio-corona, eco-corona, phytoplankton, invertebrates

Introduction

The increased use of nanoparticle (NP)-enabled materials in multiple products have raised concerns about their environmental consequences and safety. Indeed, the increasing evidences demonstrate that if the NPs are released into the environment, during their production, use or disposal, there is a possibility that they could cause harm to the living organisms if present at high concentrations (Nowack and Bucheli, 2007; Navarro et al., 2008; Auffan et al., 2009; Wiesner et al., 2009; Fabrega et al., 2011; Levard

et al., 2012; Bondarenko et al., 2013; Holden et al., 2016; Lead et al., 2018; Grieger et al., 2019; Joonas et al., 2019; Mortimer and Holden, 2019; Kögel et al., 2020; Nguyen et al., 2020; Spurgeon et al., 2020; Sørensen et al., 2020).

The key questions of how the engineered NPs could affect the aquatic organisms and what are the modifying factors guided the research towards development of sound environmental risk assessment and sustainable nanotechnology over past two decades (Nowack et al., 2012; Batley et al., 2013; Collin et al., 2014; Lead et al., 2018; Chen et al., 2019). Indeed, the wealth of information on various NPs and multiple biological models (cells, tissues, organs, and whole organisms) revealed that the reactivity of the NPs towards living organisms is governed by the complex interplay of 1) NP dissolution, 2) organism-dependent cellular uptake, and 3) induction of oxidative stress and consequent cellular damages (Ivask et al., 2014; von Moos and Slaveykova, 2014; Chevallet et al., 2016; Slaveykova et al., 2020). By contrast, studies exploring of how do organisms alter NPs fate in the aquatic environment are still very scarce.

The current state-of-the-art knowledge revealed that phytoplankton could influence the NPs occurrence and fate in the aquatic environment and thus their ultimate impact (Slaveykova, 2022). Various processes were shown to be involved including: 1) uptake of NPs and (intra-) cellular transformation *via* different processes; 2) production of NPs inside the cells and/or on cell surfaces from dissolved metal species; 3) release of various low and high molecular weight biomolecules, which could interact with NPs (e.g., forming a biomolecular corona) (Slaveykova, 2022). No similar conceptual approach has been yet proposed for other aquatic organisms, such as invertebrates. Nevertheless, it is recognized that the interactions of NPs with different biomolecules present in the ambient water and biological environment play a critical role in modulation of the NPs fate, biouptake and toxicity to aquatic organisms in both freshwater and marine environments (Canesi et al., 2016a; Baalousha et al., 2018; Shakiba et al., 2018; Fadare et al., 2019; Fadare et al., 2020; Sikder et al., 2020; Barbero et al., 2021; Liu et al., 2021; Sikder et al., 2021; Wheeler et al., 2021; Baalousha et al., 2022). For example, biomolecules in the aquatic environment can increase or reduce colloidal stability of NPs depending on their quantity and nature, pH and ionic strength: at low ionic strength (e.g., in freshwater) biomolecules can stabilize negatively charged NPs through electrostatic and/or steric interactions, however at high ionic strength (e.g., in marine water) they can reduce NPs stability and favour the aggregation through the formation of cation-biomolecule bridges (Bundschuh et al., 2018). Biomolecular coronas in invertebrate species together with the consequences for the environmental impact of NPs were thoroughly discussed (Canesi et al., 2017). The key role of exogenous biomolecular corona played in mitigating the NPs toxicity towards living organisms has also been comprehensively reviewed (Natarajan

et al., 2021), as well as the environmental dimensions of protein corona (Wheeler et al., 2021).

Drawing on the existing literature on the formation of biomolecular corona, here we discuss the necessity of broader and integrated approach considering the formation of biomolecular corona as one of the mechanisms by which organisms exerted control on the NPs fate in the aquatic and biotic environments. The discussion of how the aquatic organisms could influence the fate and impact of NPs in aquatic environment will be illustrated with selected examples about the key role of exogenous and endogenous corona formation in the case of freshwater and marine phytoplankton and invertebrates (Figure 1A).

Basic principles of biomolecular corona formation

The biomolecular corona is formed by spontaneous adsorption of biomolecules to the highly reactive surface of NPs when they enter in contact with the components of biological or environmental system (Nel et al., 2009; Docter et al., 2015; Moore et al., 2015; Pulido-Reyes et al., 2017; Xu et al., 2020; Wheeler et al., 2021). The scientific understanding on the biomolecular corona formation significantly evolved since the introduction of the term “protein corona” in nano (eco) toxicological research in 2007 through the “eco-corona” and lately “biomolecular corona” encompassing a variety of biomolecules (Wheeler et al., 2021).

The basic principles of formation of biomolecular corona (Lynch and Dawson, 2008; Nel et al., 2009; Tenzer et al., 2011; Monopoli et al., 2012; Walkey and Chan, 2012; Tenzer et al., 2013; Walkey et al., 2014; Docter et al., 2015; Pulido-Reyes et al., 2017; Wheeler et al., 2021) can be summarized briefly as follows:

- The creation of corona is a dynamic adsorption/desorption process where different biomolecules compete for the highly reactive NPs surface; It is accepted that the most abundant biomolecules are adsorbed first, then gradually displaced by the highest affinity biomolecules (Wang et al., 2016). The competition and displacement steps for NPs surface are exhaustively studied for proteins (Hadjidemetriou and Kostarelos, 2017; Wheeler et al., 2021), and also reported for natural organic matter (NOM) (Xu et al., 2020).
- The formation of biomolecular corona on NPs is shown to involve a combination of hydrodynamic, electrodynamic, electrostatic, steric, and bridging interactions. Depending on the characteristics intrinsic for NPs, ambient and biological environments some of the above interactions could prevail (Nel et al., 2009; Pulido-Reyes et al., 2017; Chakraborty et al., 2022).
- Hard and soft coronas are distinguished in the case of proteins. Hard protein corona is characterized by strong binding affinity, long residence time, slow exchange often associated to

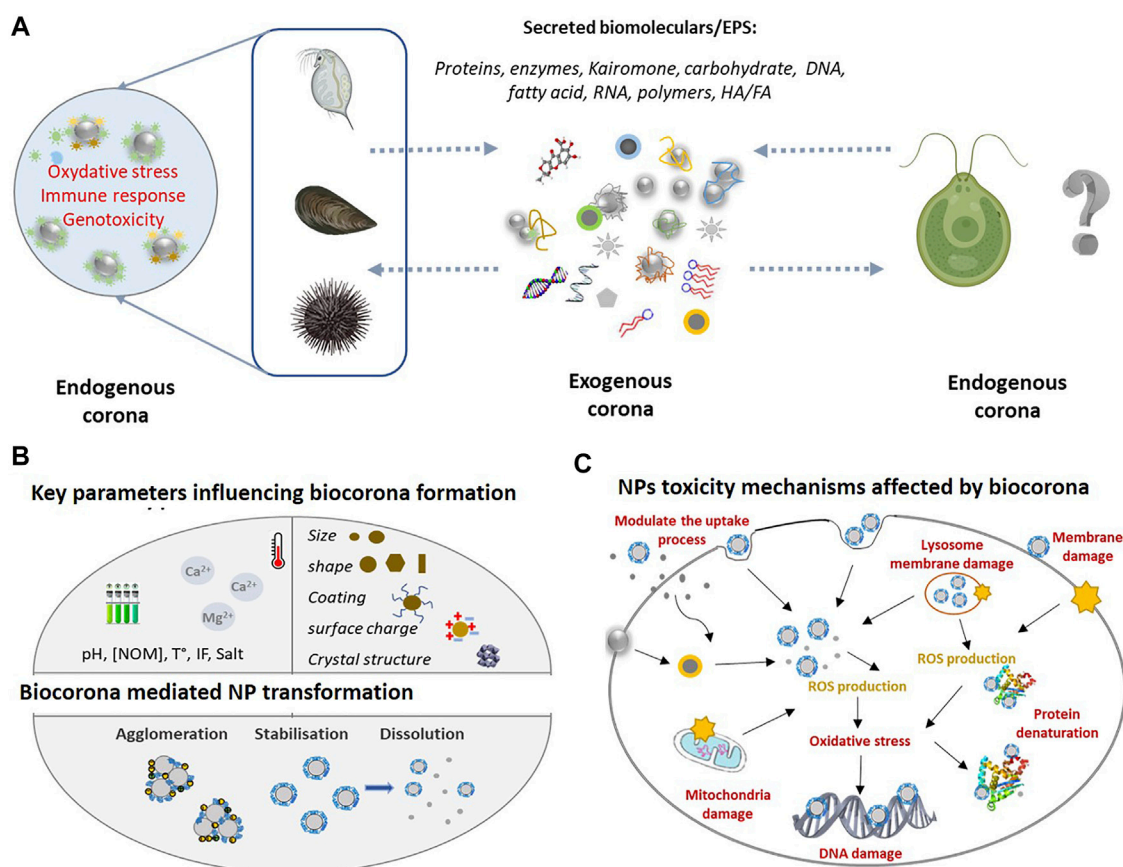


FIGURE 1

(A) Overview of the exogenous and endogenous corona formation in the case of aquatic phytoplankton and invertebrates in the ambient environment the NPs interact with EPS released by aquatic organisms forming exogenous corona. Once inside the organisms in contact with biological fluids, the NPs corona of exogenous biomolecules will be replaced by endogenous biomolecules which will determine the biological identity and toxicity outcome. Given the high diversity of exogenous biomolecules, the exogenous corona is considered to possess more complex composition as compared with endogenous corona. (B) Key environmental variable [e.g., pH, NOM, and temperature (T°)] and NPs intrinsic properties (e.g., size, shape, and coating) influencing corona formation. As a result, the dissolution, stability, and aggregation behaviour of NPs will be affected and thus their bioavailability. (C) NPs toxicological mechanisms and their modulation by corona formation. The formation of exogenous corona can affect the adhesion of NPs to the cell surface, alter the interaction between NPs and cell membrane, modulating the uptake process and resulting the membrane damage. Once inside the cell, exogenous corona may mediate the interaction between NPs and cellular components (e.g., mitochondria and nucleus) and biomolecules (e.g., protein and DNA). Exogenous and endogenous corona may affect the extra- and intra-cellular dissolution of NPs, which can induce the reactive oxygen species (ROS) generation and oxidative stress.

high conformation changes; while the soft-corona or even protein cloud is formed by loosely bound and rapidly exchangeable biomolecules (Docter et al., 2015). Both of hard and soft corona give the novel bio-identity of the NPs. The most of the available knowledge on the role of the biocorona in NP-cell interactions has been acquired from hard-corona forming proteins, analytically accessible “fraction” (Tenzer et al., 2011; Monopoli et al., 2012; Tenzer et al., 2013; Docter et al., 2015). The role of the soft corona, which presumably determine the new surface charge of the protein-coated NPs and steric interactions of the proteins (García-Álvarez and Vallet-Regí, 2021), and thus the association of NPs with cells, are to further explore. It was also mentioned that the distinction between soft and hard corona

seems to mostly “create more confusion than helping to resolve scientific questions” (Docter et al., 2015).

- Biomolecular corona can be formed inside (bio-corona) and outside (eco-corona) of an organism (Pulido-Reyes et al., 2017; Wheeler et al., 2021). It can involve biomolecules released by the organisms or other abiotic material in the aquatic environment (exogenous corona) and biomolecules found in the biofluids, cytosol etc., (endogenous corona). When NPs are taken up by aquatic organisms, the initial corona of NPs evolves as the exogenous biomolecules are replaced by endogenous molecules (Xu et al., 2020; Wheeler et al., 2021). The exogenous and endogenous corona are expected to be tightly linked and require more general conceptual consideration.

- Factors affecting the corona formation and corona composition include (Figure 1B): 1) intrinsic NPs properties (such as size, surface coating and functionalization, shape etc.); 2) ambient medium properties (e.g., ionic strength, pH, presence and characteristics of biomolecules, temperature, light, redox species etc.); and 3) aquatic organisms [for example, feeding pattern, composition and properties of biological fluids, biomolecules or cell structures (cytoplasm, cell and organelle wall/membrane etc.)] (Canesi et al., 2017; Fadare et al., 2020; Xu et al., 2020; Wheeler et al., 2021).

The emergence of the above-mentioned principles was based on wealth of the studies mainly with isolated proteins, *in vitro* assays with blood plasma and cell culture media containing serum (Monopoli et al., 2012; Tenzer et al., 2013; Bertoli et al., 2016), *ex vivo* and *in vivo* investigations on tissues and cells (Monopoli et al., 2012; Docter et al., 2015; Durán et al., 2015; Hadjidemetriou and Kostarelos, 2017). Multiplex *ex situ* (involving isolation of the NPs-protein complexes) and *in situ* (no pre-isolation from the ambient medium) approaches used in combination (Monopoli et al., 2012; Docter et al., 2015; Durán et al., 2015) were employed to address the formation and evolution of the coronas, as well as the consequences for NP stability and biological outcome (Docker et al., 2015; Westmeier et al., 2016). Among different NPs, the formation of protein–NP complex was most studied for silver nanoparticles (nAg). The corona formed by the isolated proteins such as bovine or human serum albumin, ubiquitin, yeast extracted proteins etc., (Durán et al., 2015) affected the dissolution, agglomeration and surface charge of the nAg. Further examples include cytochrome (Cyt) C (Kim et al., 2015), some serum proteins (Wimuktiwan et al., 2015) (Burcz et al., 2015) or intracellular metallothionein (Liu et al., 2017). Conversely, the nAg influenced the protein conformation and activity. Interaction of nAg and metallothionein and blood ceruloplasmin resulted in the replacement of native metals of these proteins by Ag⁺ and conformation changes (Liu et al., 2017). Two key antioxidant enzymes: catalase (CAT) and superoxide dismutase (SOD) formed surface complexes with citrate-coated nAg. Consequently, nAg dissolution was promoted together with conformation changes in the CAT, and an impairment of its enzymatic activity. No effect of the nAg–SOD complex on the protein conformation and its enzymatic activity were observed (Liu et al., 2020b). However, firefly luciferase corona on nAg inhibited the enzymatic activity without affecting the protein conformation (Kakinen et al., 2013).

The relationships between nAg synthetic identity (determined by size, surface functionalization, morphology) and the corona formation was demonstrated in simple model systems (Docker et al., 2015; Durán et al., 2015). For example, more pronounced adsorption of bovine serum albumin (BSA) on citrate stabilized 20 nm nAg as compared with 40 and 70 nm nAg was found and resulted in a destruction of part of the helical

secondary structure of the BSA (Treuel et al., 2010). For the same size of nAg (20 nm), the affinity of BSA was higher to citrate than to polyvinylpyrrolidone (PVP)-stabilized nAg, an observation explained by prevention of the interactions between nAg surface and S-groups of the proteins by existing PVP corona (Treuel et al., 2012). The nAg morphology (cube, sphere, wire, and triangle) of nAg also influenced the concentration and composition of the proteins in the foetal calf serum and thus their antibacterial activity (Ashkarran et al., 2012). The surface charge of NPs also influenced the protein species to be bound to the surface as a higher charge is expected to induce a more significant binding of proteins to the NPs in comparison with low charged surfaces or no-charge surfaces (Deng et al., 2012). Further recent examples illustrating the formation of corona by model biomolecules, mainly proteins can be found in several comprehensive reviews (Chetwynd and Lynch, 2020; Fadare et al., 2020; Nasser et al., 2020; Barbero et al., 2021; Liu et al., 2021; Natarajan et al., 2021; Wheeler et al., 2021).

Despite such significant advancements in the knowledge concerning the interactions between NPs and biomacromolecules, various issues mainly related with the mechanism of corona formation, its time evolution in complex media, long-term effects and the relevance of corona in the organs where NPs are deposited are still to be resolved (Nel et al., 2009; Monopoli et al., 2012; Tenzer et al., 2013; Miclăuş et al., 2016; Bertrand et al., 2017; Hadjidemetriou and Kostarelos, 2017).

Biomolecular corona and phytoplankton

Exogenous corona by biomolecules released by phytoplankton

Phytoplankton release different biomolecules including, extracellular polymeric substances (EPS), which are thought to play a key role in the phycosphere (Seymour et al., 2017; Liu F et al., 2020). EPS are widespread in the aquatic environments (Shou et al., 2018). They are predominant fraction of marine NOM (Corsi et al., 2020) and can represent up to 25% of NOM in freshwaters, particularly during algal blooms (Wilkinson et al., 1997). EPS contain polysaccharides, proteins, lipids, RNA, and DNA, however their composition varied with the species and environmental conditions as reviewed (Naveed et al., 2019).

The EPS produced by marine and freshwater phytoplankton were shown to form biomolecular on different NPs which results in altering NPs colloidal stability and aggregation, dissolution, complexing the released metals, influencing the NPs transformations and favoring formation of the metallic NPs and metal oxide NPs from dissolved metals (Zhou et al., 2016; Zheng et al., 2019; Zhang et al., 2020; Junaid and Wang, 2021; Slaveykova, 2022). Recent reviews have comprehensively

TABLE 1 Selected examples to illustrate the interaction between released biomolecules from phytoplankton and NPs.

Organisms	Biomolecules	Nanoparticles	Main findings (NPs colloidal stability, changes of EPS production)	References
<i>D. tertiolecta</i>	EPS released in culture medium	Aeroxide® P25 nTiO ₂	Stabilization, 20–80 kDa exoproteins involved, No changes in carbohydrate/protein proportion and quantities over 24 h exposure	Morelli et al. (2018)
<i>C. pyrenoidosa</i>	Extracted EPS	5, 10, and 40 nm (anatase) and 25 nm (rutile) nTiO ₂	Increase adsorption with specific surface area of NPs	Gao et al. (2019)
Cyanobacterial bloom	Extracted EPS	nZnO	Increase colloidal stability by electrostatic interaction and surface complexation, Increase dissolution	Xu and Jiang (2015)
<i>Chlorella</i> sp.	EPS released in culture medium	nZnO	Decrease dissolution	Chen et al. (2012)
<i>C. reinhardtii</i>	EPS released in culture medium	Sulfide/silica-modified zerovalent iron (nFeSSi)	Decrease in dissolution, ROS production and increase of algal hetero-aggregation, decreasing the toxic effects related to increase production of EPS within time of growth	Adeleye et al. (2016)
<i>Synechocystis</i> sp	EPS released in culture medium	20 or 50 nm nAg (PVP; citrate; lipoic acid)	Importance of initial NP coating	Jiménez-Lamana and Slaveykova (2016)
<i>Amphora</i> sp., <i>D. tertiolecta</i> , <i>Phaeocystis globosa</i> , <i>T. pseudonana</i>	EPS released in culture medium	Coated (carboxyl- and amine-) or uncoated QDs	Increase colloidal stability for citrate- and lipoic acid-nAg/no effect for PVP-nAg, Decrease colloidal stability, Increase dissolution with increase protein/carbohydrate	Zhang et al. (2012)
<i>I. galbana</i>	EPS released in culture medium	nCu and nCuO	Increase of dissolution	Adeleye et al. (2014)
Cyanobacterial bloom	Extracted EPS, MW fraction	nTiO ₂ , primary particle size of 20 ± 10 nm	Differential adsorption capacities according to MW, Predominance of protein adsorption	Xu et al. (2020a)
<i>Microcystis aeruginosa</i>	EPS released in culture medium	nCeO ₂ , nCuO and nZnO	Alteration of the produced protein vs. polysaccharide composition	Hou et al. (2017)
<i>C. pyrenoidosa</i>	EPS released in culture medium	nTiO ₂	Increase the quantity of released biomolecules	Gao et al. (2020)
<i>Odontella mobiliensis</i> , <i>Skeletonema grethae</i> , <i>Phaeodactylum tricornutum</i> , <i>T. pseudonana</i>	EPS released in culture medium	nTiO ₂	Decrease of the quantities of released biomolecules	Chiu et al. (2017)

PVP, Polyvinylpyrrolidone; MW, Molecular weight; ROS, Reactive oxygen species.

summarized the latest advances concerning the role of EPS on NPs fate and effects (Xu et al., 2020; Ly et al., 2021; Slaveykova, 2022).

Below we will give some selected examples in which the formation of corona by EPS was explicitly considered and the possible mechanisms discussed (Table 1). For example, EPS released from green alga *Dunaliella tertiolecta* and in particularly exoproteins with molecular weight range from 20 to 80 kDa, bound to nTiO₂ stabilizing them in marine waters (Morelli et al., 2018; Corsi et al., 2020). The EPS from green alga *Chlorella pyrenoidosa* adsorbed onto four types of different nTiO₂ materials with primary size of 5, 10, and 40 nm (anatase) and 25 nm (rutile), the adsorption increased with the specific surface area of the NPs and exhibited a selective adsorption of aromatic EPS components (Gao et al., 2019). EPS from bloom-forming cyanobacteria adsorbed to nZnO via electrostatic attraction and surface complexation, thus increasing their stability (Xu and Jiang, 2015). A steric stabilization of sulfide/silica-modified zerovalent iron nanoparticles (nZVI) by organic matter released from green alga *Chlamydomonas*

reinhardtii at different growth stages, demonstrated that the algae may play important role in the environmental fate of NPs (Adeleye et al., 2016). EPS produced by cyanobacterium *Synechocystis* sp. efficiently stabilized 20 and 50 nm citrate-coated and lipoic acid-coated nAg, but had only minor effect on the PVP-coated nAg of similar size (Jiménez-Lamana and Slaveykova, 2016), showing the importance of the primary surface coating of NPs. EPS isolated from four marine diatoms *Amphora* sp., *D. tertiolecta*, *Phaeocystis globosa*, and *Thalassiosira pseudonana* decreased the stability of both non-functionalized and functionalized (carboxyl- and amine-) quantum dots (QDs) in artificial seawater with a degradation rate of QDs positively correlated to the protein content of EPS (Zhang et al., 2012). The EPS excreted by green alga *Chlorella* sp. reduced significantly nZnO dissolution (Chen et al., 2012). By contrast, the EPS released by diatom *Isochrysis galbana* increased the dissolution of nCuO and nCu (Adeleye et al., 2014). Similarly, the EPS extracted from cyanobacterial blooms increased the released of Zn ions from nZnO (Xu and Jiang, 2015).

The EPS are highly diverse in chemical composition and molecular weight, which makes difficult to characterize in depth their molecular specificity when adsorbing onto NPs (Seviour et al., 2019). High molecular weight (HMW, 1 kDa–0.45 μ m) and low MW (LMW, <1 kDa) fractions of cyanobacterial EPS adsorbed on nTiO₂ in molecular weight-dependent manner, with adsorption capacity decreasing in the order HMW-EPS > Bulk-EPS > LMW-EPS (Xu et al., 2020). Given the large variety of microorganisms, and thus the high diversity of released biomolecules, it is likely that each species would modify its external surrounding in a specific way (Ly et al., 2021).

The exposure of phytoplankton species to NPs can modulate the release of EPS, their concentration and composition, thus increasing the complexity of the exogenous biomolecules composition and potentially formed corona. For example, exposure to nCeO₂, nCuO, and nZnO affected the quantity and composition (ratio protein vs. polysaccharide) of the EPS produced by cyanobacterium *M. aeruginosa* (Hou et al., 2017). A significant increase in the release of biomolecules by green alga *C. pyrenoidosa* in response to nTiO₂ was observed (Gao et al., 2020). A decrease of the EPS released by four diatom species *O. mobiliensis*, *S. grethae*, *P. tricornutum*, and *T. pseudonana* upon exposure to nTiO₂ was reported (Chiu et al., 2017). In addition to the intrinsic chemical identity of the NPs, other NPs properties such as size, surface changes have been shown to affect the release of EPS (Hou et al., 2017; Gao et al., 2020; Junaid and Wang, 2021). The above examples clearly illustrated the existing feedbacks between the NPs exposure and the capacity of phytoplankton species to produce EPS.

In addition, the formation of exogenous corona in NPs was shown to decrease their bioavailability and toxicity to phytoplankton species (Figure 1C) by three major mechanisms as reviewed (Natarajan et al., 2021): 1) complexation of the metals ions released soluble NPs and decrease of their bioavailability; 2) decreasing the excessive ROS formation, oxidative stress and damage, and 3) altering the attachments of the NPs to the algal cells by modifying the steric and electrostatic interactions between the NPs and cells. It was suggested that the EPS secretion in algae exposed to NPs can be considered as a possible detoxification mechanism (Zhang et al., 2012).

Endogenous biomolecular corona formation in phytoplankton

In the case of phytoplankton species, no yet studies verified the formation of endogenous corona in the cells. Nevertheless, for the species exhibiting endocytosis, NPs accumulated and transformed into the cell vacuoles as shown for nAg in golden-brown alga *Ochromonas danica*, nAg or nSe in *Poteroiochromonas malhamensis* and ferrihydrite NPs in *Euglena intermedia* (Miao et al., 2010; Wang et al., 2013; Liu et al., 2020a; Chen et al., 2022). However, almost nothing is known regarding the biocorona formed during this process. The

accumulation of nAg, nAu, nCuO, nTiO₂, and QDs in the food vacuoles of *Tetrahymena thermophila* by phagocytosis, endocytosis and other unknown mechanism was evidenced (Mortimer et al., 2014a; Mortimer et al., 2014b). After 24 h exposure the micrometre-size heteroaggregates containing nAg or QDs and biomolecules were ejected from the vacuoles, revealing the importance of the interaction of NPs with the endogenous biomolecules inside the cells (Mortimer et al., 2014b). However, no similar studies yet exist for endocytic phytoplankton species.

Biomolecular corona and invertebrates

Exogenous corona formation by biomolecules released by invertebrates

Invertebrates, such as crustacean *Daphnia magna*, bivalve *M. galloprovincialis* and sea urchin *Paracentrotus lividus*, are known to release different biomolecules as reviewed (Canesi et al., 2017; Xu et al., 2020; Wheeler et al., 2021). For example, *D. magna* is known to release biomolecules into their surroundings including kairomones, enzymes and proteins from expelled gut, chitin-based carbohydrate from moulting, digestive enzymes and undigested or partially digested matter (Nasser et al., 2020), which are likely to form corona and thus to affect the bioreactivity of NPs.

Neonates of *D. magna* were shown to release of proteins, such as Type VI secretion system (74.8 kDa) and Sensor protein QseC (50.4 kDa) (Nasser and Lynch, 2016). These proteins formed exogenous corona on carboxyl- and amine polystyrene NPs (nPS-COOH or nPS-NH₂) resulting in an enhancement of their uptake and less efficient removal from the gut of *D. magna* (Nasser and Lynch, 2016). By contrast, corona on nAu by proteins secreted from daphnids reduced the nAu aggregation and decreased the toxicity by preventing their surface interaction (Mattsson et al., 2018). An exoprotein corona was formed on nPS-NH₂ in *D. magna* culture medium and contained proteins responsible for immune defense, cell maintenance, and antipredator response. The size, surface functionalization and aging of NPs were shown as major factors affecting a formation of exogenous corona (Junaid and Wang, 2021).

The existing literature revealed that the exogenous corona formed in the medium surrounding invertebrates is dominated by proteins and confirm its importance as a modulator of NP uptake and toxicity to invertebrates (Nasser et al., 2020). Corona formed by alginate and chitosan on nCeO₂ did not affect the biouptake, but alginate coated nCeO₂ induced lipidic peroxidation in marine bivalve *Mytilus galloprovincialis* (Nigro et al., 2021) and altered energetic metabolism and osmoregulation in freshwater bivalve *Dreissena polymorpha*.

TABLE 2 Selected examples of biological effects and toxicological consequences of nanoparticles coated with different biomolecules and nature of formed biocorona in marine and freshwater invertebrates.

Organism	Biomolecule	Nanoparticles	NPs main findings (aggregation, effect, MoA, toxicity, and consequence)	References
<i>M. galloprovincialis</i>	hemolymph serum	50.0 nm nPS-HN ₂	180 nm agglomerates formation, interaction with MgC1q6 protein, lysosomal and plasma membrane damage, ROS production, p38 MAPK signalling dysregulation	Canesi et al. (2016a); Canesi et al. (2016b); Canesi et al. (2017)
		9.0 ± 4.0 nm nCeO ₂	interactions with extracellular Cu,Zn-SOD, increased ROS production, activation of O ₂ ⁻ scavenging activity	Auguste et al. (2021b)
		P25 nTiO ₂	interactions with extracellular Cu,Zn-SOD, no immune response observed	
		50.0 nm nPS-HN ₂ s	Z-average size of about 178.0 ± 2.0 nm, smaller and ticker hemocyte, rich of filopodia and formed lace-like pattern, decrease of lysosomal membrane stability and increased lysozyme activity, decrease of phagocytosis	
		60.0 nm nPS-COOH	Z-average size of about 189.1 ± 48.6 nm, short and long filopodia formation, increased lysozyme release by hemocytes	
		18.3 nm nZnO s	NPs surface energy and its uptake efficiency modulation, NPs lipid peroxidation and immune-related generation of ROS (•O ₂ ⁻ , NO)	Efthimiou et al. (2021)
	alginate	5.0 nm nCeO ₂	electron transport system activity modulation, lipid peroxidation, GST activity increase and GR activity decrease	Nigro et al. (2021)
<i>P. lividus</i>	chitosan	5.0 nm nCeO ₂	electron transport system activity modulation, enhanced antioxidant SOD, GPx, and GST activity, GR activity decrease	Nigro et al. (2021)
	coelomic fluid	47.7 ± 1.2 nm nPS-NH ₂ s	Z-average size of about 150 nm, concentration- and time-dependent lysosomal membrane damage and apoptotic-like nuclear alterations in phagocytes	Marques-Santos et al. (2018)
		25.0 ± 3.0 nm PVP-nAu s	concentration-dependent mediation of coelomocytes phagocytosis, inflammation, immunological responses involving TLR4 signalling pathway	Alijagic et al. (2021a)
<i>D. magna</i>		25.0 ± 3.0 nm PVP-nAu	expression of CD45 and CD14 antigens on surface of the particular subset of coelomocytes	Alijagic et al. (2021b)
		100 nm nPS-HN ₂ , nPS-COOH	exogenous corona formation; enhancement of their uptake and less efficient removal from the gut of <i>D. magna</i>	Nasser and Lynch (2016)
		25 nm nAu	Exocorona reduced the nAu aggregation and decreased the toxicity by preventing their surface interaction	Mattsson et al. (2018)
<i>D. polymorpha</i>	alginate	nCeO ₂	energetic metabolism and osmoregulation modulation	Della Torre et al. (2021)
		20.40.100 nm PVP-nAg	accumulation in the soft tissue, the alteration of different morphological and functional characteristics of mussel hemocytes and gill cells, experiencing oxidative stress and the genotoxicity due released Ag	Katsumiti et al. (2015)

GPx, Glutathione peroxidase; GR, Glutathione reductase; GST, Glutathione S-transferase; MAPK, Mitogen-activated protein kinase; MgC1q6 protein, *Mytilus galloprovincialis* putative Complement Component C1q domain; MoA, Mode of action; PS, Polystyrene; PVP, Polyvinylpyrrolidone; ROS, Reactive oxygen species; SOD, Superoxide dismutase.

(Della Torre et al., 2021). Interestingly, long-term exposure at low concentrations to nCeO₂ coated with alginate and chitosan showed significant modulation of electron transport system activity, suggesting a different strategy of defense in response short-term high concentration nCeO₂ exposure (Nigro et al., 2021). Proteins present in gill mucus of blue mussel *Mytilus edulis* formed a corona on nSiO₂ and five different types of nTiO₂ (size and crystal structure); some few proteins in the corona showed a specific recruitment pattern according to the NPs type or crystal structure (Bourgeault et al., 2017). The interactions of NPs with natural bio-molecules, e.g., polysaccharides which and largely present in the marine environment, and impart negative charge to the NPs in particular, could affect NPs toxicity by

altering the interactions towards organisms and enhancing NPs biological effects (Nigro et al., 2021).

Endogenous biomolecular corona formation in invertebrates

Much more extensive is the existing literature considering the formation of the endogenous corona. Endogenous corona determined biological identity of the NPs significantly modulates the cellular uptake, biodistribution of NPs (Treuel et al., 2013) and toxicity outcome in invertebrates (Lynch and Dawson, 2008; Nel et al., 2009; Docter et al., 2015;

Durán et al., 2015; Zimmermann et al., 2017; Rastgar et al., 2022). For example the implication of NPs biomolecular corona in the immune response is also emerged in invertebrate models such as *D. magna*, *M. galloprovincialis*, and *P. lividus* (Wheeler et al., 2021). However, the research of biological effects and toxicological consequences of NPs coated with different biomolecules and formed biocorona in marine invertebrates is very limited. In recent years several researches have been provided for Mediterranean mussel *M. galloprovincialis* hemocytes and sea urchin *P. lividus* coelomocytes (Table 2).

The interaction of NPs with the mussel biofluids, in particular the haemolymph, allowed to identify biomolecular corona formed with haemolymph serum proteins, and to assess the interaction of biomolecular corona-modified NPs with haemocyte. Protein corona formed in haemolymph serum of *M. galloprovincialis* was dependent on the NPs type and size (Canesi et al., 2016b; Canesi et al., 2017). The positively charged nPS-NH₂ were covered rapidly with the corona containing *M. galloprovincialis* putative C1q domain containing protein MgC1q6 (Canesi et al., 2016b). However, nPS-NH₂ of primary size 50 nm, 100 nm, and 1 μm aggregated in haemolymph serum in a size dependent manner, which could explain the discrepancy in their bioaccumulation and translocation into *M. galloprovincialis* hemocytes (Sendra et al., 2020). More recently, study of the specific molecular interactions 100 nm nPS-NH₂ with components in hemolymph serum of *M. galloprovincialis* revealed a formation of corona containing a *M. galloprovincialis* putative putative C1q domain protein MgC1q44 (F0V481) of 23.6 kDa (Auguste et al., 2021a).

nPS-NH₂ in contact with hemolymph serum induced significant changes in *M. galloprovincialis* hemocytes morphology, formation of filopodia network, decrease of phagocytosis activity and lysosomal membrane stability and increase of lysozyme activity. nPS-COOH induced short and long filopodia formation, as well as increased lysozyme release by hemocytes. By contrast, the exposure of *M. galloprovincialis* hemocytes to custom made polyvinylpyrrolidone coated gold nanoparticles (PVP-nAu) in artificial sea water doesn't induce any changes in morphology, phagocytosis activity, lysosomal membrane stability and extracellular ROS production (Auguste et al., 2021b). Cu, Zn—containing superoxide dismutase (Cu,Zn-SOD) prevailed in nCeO₂ and nTiO₂ corona (Canesi et al., 2017).

The formation of different type of biomolecular corona resulted in an increase or decrease in the immunotoxicity of either type of NPs for haemocytes. For example, the formation of MgC1q6 corona on the nPS-NH₂ resulted in an increase of ROS generation, lysosomal and plasma membrane damage and dysregulation of p38 mitogen-activated protein kinase (P38MARK) signalling in *M. galloprovincialis* in comparison with the same NPs in artificial sea water (Canesi et al.,

2016b). However, the formation of a Cu,Zn-SOD corona on nCeO₂ activated O₂^{•−} scavenging activity in mussel haemocytes and thus contributed to a mitigation of ROS production. Under the same conditions Cu,Zn-SOD corona did not affected the response of haemocytes on nTiO₂ (Canesi et al., 2017).

The biomolecular corona formation can be also influenced by the NPs form and shape. The nCeO₂ with negative charge and the rounded shape formed Cu,Zn-SOD biomolecular corona in hemolymph serum which triggered higher changes in the immunological parameters such as ROS and phagocytosis capacity. Thereby, it was observed that difference in surface ζ potential play an important role in NPs association with particular extracellular proteins: *M. galloprovincialis* putative C1q domain containing protein (MgC1q6) with nPS-NH₂ s, and Cu,Zn-SOD protein with the nTiO₂ and nCeO₂ with negative ζ potential (Canesi et al., 2017). However, faceted shape nCeO₂ with neutral surface charge did not show either biocorona formation in hemolymph serum or significant immunological parameters responses (Sendra et al., 2018). In the freshwater mussel *D. polymorpha*, the only known study demonstrated a rapid accumulation of PVP-coated nAg in the soft tissue and the alteration of different morphological and functional characteristics of mussel hemocytes and gill cells, experiencing oxidative stress and the genotoxicity due released Ag (Katsumiti et al., 2015).

Furthermore, the intralysosomal accumulation of nAg in mussel digestive gland was recently evidenced, with accumulation rate depending on the NPs surface coating and size (Jimeno-Romero et al., 2017). The induction of inflammation effect in the gills of mussels exposed to nAg related directly to nanoparticle size and exposure time (Bouallegui et al., 2017). More recently custom made, nZnO promote lipid peroxidation and immune-related generation of ROS, like superoxide anion (O₂^{•−}) and nitric oxide (NO) in hemocytes of *M. galloprovincialis* presumably as a result of protein biomolecular corona modulating the NPs surface energy and uptake efficiency (Efthimiou et al., 2021).

Formation of endogenous corona on the 150 nm nPS-NH₂ dominated by 180 kDa Toposome precursor was shown in the coelomic fluid of purple sea urchin *P. lividus* (Marques-Santos et al., 2018). Under these conditions a concentration- and time-dependent lysosomal membrane damage and apoptotic-like nuclear alterations in *P. lividus* phagocytic coelomocytes were observed. This finding agrees with previous studies on mammalian cell lines and *M. galloprovincialis* hemocytes and further support the idea of ubiquitous “proton-sponge” effect (leading to lysosomal damage and the induction of cytotoxicity by cationic nanoparticles (Nel et al., 2009).

The complexity of the corona composition was further demonstrated in *P. lividus* coelomic fluid exposed to 50 nm

nPS-NH₂ and nPS-COOH by identifying 13 unique proteins on the hard coronas of both nPS: nectin variant 2 precursor, fitolitin-1, actine related protein 1, and guanine nucleotide binding protein β subunit were distinctive for nPS-NH₂ corona, the fascin, actin cytoskeletal 2A, actin cytoskeletal 3B, and muscle actin isoform X1 were features of the nPS-COOH corona, whereas toposome, nectin precursor, actine cytoskeletal 2B and actin 15B were identified in both modified NPs hard biocorona (Grassi et al., 2019). Furthermore, nTiO₂ exposed to cell-free and cell-conditioned media develop distinctive corona of predominantly negatively charged proteins involved in cellular adhesion (toposome, galectin, nectin), and cytoskeletal organization (actin, tubulin). nTiO₂ bound on the outer surface of the cells and within well-organized vesicles, no harmful effects (e.g., oxidative stress and caspase activation) were observed (Alijagic et al., 2019). However, the PVP-nAu in contact with *P. lividus* coelomic fluid acquire biocorona based on three major proteins of about 40, 100, and 170 kDa. A selective biological affinity towards particular proteins (100 kDa proteins in nTiO₂ versus 40 kDa proteins in PVP-nAu biocorona) in contact with sea urchin coelomic fluid modulated recognition of the NPs by the immune cells and their interactions (Alijagic et al., 2021a; Alijagic et al., 2021b). In addition, it is emphasized that PVP-Au NPs may stimulate a subset of *P. lividus* celomocytes to express on their surface CD45 and CD14 antigens, known to be involved in immune cell maturation and macrophage activation in humans (Alijagic et al., 2021a).

Discussion and research gaps

The existing state-of-the-art knowledge revealed that the aquatic phytoplankton and invertebrates could exert an important influence on the behavior and thus toxicological effects of the NPs, in particularly *via* formation of the biomolecular corona with the different endogenous and exogenous biomolecules. Exogenous biomolecules released from phytoplankton were shown to form a corona on NPs and alter their dissolution and stability. The exoprotein fraction of the EPS was suggested to be main components of the exogenous corona (Wheeler et al., 2021). Much less studies explore the formation of exogenous corona with biomolecules released by marine and freshwater invertebrates and could be a topic of future research.

The review of extensive literature on the endogenous corona formation in invertebrates demonstrated that the majority of NPs biomolecular corona studies were performed following *in vitro* exposure in the haemolymph serum of marine bivalve, in a high

NPs concentration range, highlighting the crucial role of biomolecular corona formation in their bioavailability and resulting biological response. Different proteins were shown to be involved in the formation of stable corona according to NPs intrinsic properties and biofluid characteristic. The results obtained so far underline the need to understand how NPs transform in complex environmental matrices *in vivo*, and how NPs interacts with biomolecules present in both environmental media and biological fluids. Moreover, given the large diversity of phyla and species, the data on formation of NPs-protein biomolecular corona in aquatic invertebrates remains scarce, in particular in freshwater invertebrates. The formation of endogenous corona in phytoplankton cells need to be further explored and demonstrated, as biocorona could be expected to be an important modulator of the intracellular handling and effects of NPs.

Regardless of the existing differences in the nature, composition, and molecular weights of the biomolecules produced by various aquatic organisms, the dissimilarity in the NPs uptake patterns, the processes controlling the formation of biomolecular corona and modifying factors are similar. Nevertheless, further mechanistic studies by exhaustive identification and quantitative measurements of various LMW and HMW biomolecules which interact with and form exo- and endogenous corona on NPs are highly sought. Gaps in knowledge concerning the mechanism of formation, stability and evolution of biomolecular corona, exchange between exogenous and endogenous corona components, as well as toxicity outcome in aquatic organisms exposed to NPs, remain to be fully elucidated. Furthermore, a consideration should be given not only on polysaccharides and proteins as main constituents of exogenous and endogenous biomolecular corona, but on different metabolites which are involved in signaling cascades and/or molecular responses to NPs exposure. Indeed, the concept of exometabolite corona has emerged (Chetwynd and Lynch, 2020), and the interplay between exometabolites, important constituents of the phycosphere (Seymour et al., 2017; Liu F et al., 2020), and EPS and the consequences for biocorona formation are still to decipher. With this respect studies combining proteomics and metabolomics approaches could open a novel avenue towards improved understanding of the complexity of biomolecular corona dynamics.

Overall, the present contribution put the concept of biomolecular corona formation in a new perspective and propose its incorporation within more general framework considering the role of aquatic organisms in shaping the fate and effects of NPs in the aquatic and biological environment.

Author contributions

VS conceived the concept, wrote the introduction and overviewed all the work. All authors contributed to the writing biomolecular corona concept section. VS and IW wrote the biocorona and phytoplankton section. WL and ZJ wrote the biocorona and invertebrate section. ZJ and VS wrote the discussion and research gaps section; WL made conceptual figure. All the authors critically commented and revised the manuscript. All the authors have approved the paper submission.

Funding

Authors acknowledge the financial support of Swiss National Science Foundation Projects Nos. 204174 and 197322.

References

- Adeleye, A. S., Conway, J. R., Perez, T., Rutten, P., and Keller, A. A. (2014). Influence of extracellular polymeric substances on the long-term fate, dissolution, and speciation of copper-based nanoparticles. *Environ. Sci. Technol.* 48 (21), 12561–12568. doi:10.1021/es5033426
- Adeleye, A. S., Stevenson, L. M., Su, Y. M., Nisbet, R. M., Zhang, Y. L., Keller, A. A., et al. (2016). Influence of phytoplankton on fate and effects of modified zerovalent iron nanoparticles. *Environ. Sci. Technol.* 50 (11), 5597–5605. doi:10.1021/acs.est.5b06251
- Alijagic, A., Barbero, F., Gaglio, D., Napodano, E., Benada, O., Kofroňová, O., et al. (2021a). Gold nanoparticles coated with polyvinylpyrrolidone and sea urchin extracellular molecules induce transient immune activation. *J. Hazard. Mat.* 402, 123793. doi:10.1016/j.jhazmat.2020.123793
- Alijagic, A., Benada, O., Kofroňová, O., Cigna, D., and Pinsino, A. (2019). sea urchin extracellular proteins design a complex protein corona on titanium dioxide nanoparticle surface influencing immune cell behavior. *Front. Immunol.* 10, 2261. doi:10.3389/fimmu.2019.02261
- Alijagic, A., Bonura, A., Barbero, F., Puentes, V. F., Gervasi, F., Pinsino, A., et al. (2021b). Immunomodulatory function of polyvinylpyrrolidone (PVP)-functionalized gold nanoparticles in vibrio-stimulated sea urchin immune cells. *Nanomater. (Basel, Switz.)* 11 (10), 2646. doi:10.3390/nano11102646
- Ashkarran, A. A., Ghavami, M., Aghaverdi, H., Stroeve, P., and Mahmoudi, M. (2012). Bacterial effects and protein corona evaluations: crucial ignored factors in the prediction of bio-efficacy of various forms of silver nanoparticles. *Chem. Res. Toxicol.* 25 (6), 1231–1242. doi:10.1021/tx300083s
- Auffan, M., Rose, J., Bottero, J.-Y., Lowry, G. V., Jolivet, J.-P., Wiesner, M. R., et al. (2009). Towards a definition of inorganic nanoparticles from an environmental, health and safety perspective. *Nat. Nanotechnol.* 4 (10), 634–641. doi:10.1038/nnano.2009.242
- Auguste, M., Balbi, T., Miglioli, A., Alberti, S., Prandi, S., Narizzano, R., et al. (2021a). Comparison of different commercial nanopolystyrenes: behavior in exposure media, effects on immune function and early larval development in the model bivalve *Mytilus galloprovincialis*. *Nanomaterials* 11 (12), 3291. doi:10.3390/nano11123291
- Auguste, M., Mayall, C., Barbero, F., Hočevár, M., Alberti, S., Grassi, G., et al. (2021b). Functional and morphological changes induced in *Mytilus* hemocytes by selected nanoparticles. *Nanomaterials* 11 (2), 470. doi:10.3390/nano11020470
- Baalousha, M., Afshinnia, K., and Guo, L. D. (2018). Natural organic matter composition determines the molecular nature of silver nanomaterial-NOM corona. *Environ. Sci. Nano* 5 (4), 868–881. doi:10.1039/c8en00018b
- Baalousha, M., Sikder, M., Poulin, B. A., Tfaily, M. M., and Hess, N. J. (2022). Natural organic matter composition and nanomaterial surface coating determine the nature of platinum nanomaterial-natural organic matter corona. *Sci. Total Environ.* 806, 150477. doi:10.1016/j.scitotenv.2021.150477
- Barbero, F., Mayall, C., Drobne, D., Saiz-Poseu, J., Bastus, N. G., Puentes, V., et al. (2021). Formation and evolution of the nanoparticle environmental corona: the

Conflict of interest

The authors declare that the research was conducted in the absence of any commercial or financial relationships that could be construed as a potential conflict of interest.

Publisher's note

All claims expressed in this article are solely those of the authors and do not necessarily represent those of their affiliated organizations, or those of the publisher, the editors and the reviewers. Any product that may be evaluated in this article, or claim that may be made by its manufacturer, is not guaranteed or endorsed by the publisher.

case of Au and humic acid. *Sci. Total Environ.* 768, 144792. doi:10.1016/j.scitotenv.2020.144792

Batley, G. E., Kirby, J. K., and McLaughlin, M. J. (2013). Fate and risks of nanomaterials in aquatic and terrestrial environments. *Acc. Chem. Res.* 46 (3), 854–862. doi:10.1021/ar2003368

Bertoli, F., Garry, D., Monopoli, M. P., Salvati, A., and Dawson, K. A. (2016). The intracellular destiny of the protein corona: a study on its cellular internalization and evolution. *ACS Nano* 10 (11), 10471–10479. doi:10.1021/acsnano.6b06411

Bertrand, N., Grenier, P., Mahmoudi, M., Lima, E. M., Appel, E. A., Dormont, F., et al. (2017). Mechanistic understanding of *in vivo* protein corona formation on polymeric nanoparticles and impact on pharmacokinetics. *Nat. Commun.* 8 (1), 777. doi:10.1038/s41467-017-00600-w

Bondarenko, O., Juganson, K., Ivask, A., Kasemets, K., Mortimer, M., Kahru, A., et al. (2013). Toxicity of Ag, CuO and ZnO nanoparticles to selected environmentally relevant test organisms and mammalian cells *in vitro*: a critical review. *Arch. Toxicol.* 87 (7), 1181–1200. doi:10.1007/s00204-013-1079-4

Bouallegui, Y., Ben Younes, R., Bellamine, H., and Oueslati, R. (2017). Histopathology and analyses of inflammation intensity in the gills of mussels exposed to silver nanoparticles: role of nanoparticle size, exposure time, and uptake pathways. *Toxicol. Mech. Methods* 27 (8), 582–591. doi:10.1080/15376516.2017.1337258

Bourgeault, A., Legros, V., Gonnet, F., Daniel, R., Paquirissamy, A., Bénatar, C., et al. (2017). Interaction of TiO₂ nanoparticles with proteins from aquatic organisms: the case of gill mucus from blue mussel. *Environ. Sci. Pollut. Res. Int.* 24 (15), 13474–13483. doi:10.1007/s11356-017-8801-3

Bundschuh, M., Filser, J., Lüderwald, S., McKee, M. S., Metreveli, G., Schaumann, G. E., et al. (2018). Nanoparticles in the environment: where do we come from, where do we go to? *Environ. Sci. Eur.* 30 (1), 6. doi:10.1186/s12302-018-0132-6

Burcza, A., Graf, V., Walz, E., and Greiner, R. (2015). Impact of surface coating and food-mimicking media on nanosilver-protein interaction. *J. Nanopart. Res.* 17 (11), 428. doi:10.1007/s11051-015-3235-7

Canesi, L., Balbi, T., Fabbri, R., Salis, A., Damonte, G., Volland, M., et al. (2017). Biomolecular coronas in invertebrate species: implications in the environmental impact of nanoparticles. *NanoImpact* 8, 89–98. doi:10.1016/j.impact.2017.08.001

Canesi, L., Ciacci, C., and Balbi, T. (2016a). Invertebrate models for investigating the impact of nanomaterials on innate immunity: the example of the marine mussel *Mytilus* spp. *Curr. Bionanotechnol.* 2 (2), 77–83. doi:10.2174/2213529402666160601102529

Canesi, L., Ciacci, C., Fabbri, R., Balbi, T., Salis, A., Damonte, G., et al. (2016b). Interactions of cationic polystyrene nanoparticles with marine bivalve hemocytes in a physiological environment: role of soluble hemolymph proteins. *Environ. Res.* 150, 73–81. doi:10.1016/j.envres.2016.05.045

Chakraborty, D., Giri, S., Natarajan, L., Chandrasekaran, N., and Mukherjee, A. (2022). Recent advances in understanding the facets of eco-corona on engineered nanomaterials. *J. Indian Inst. Sci.* 102, 621–637. doi:10.1007/s41745-021-00266-w

- Chen, F., Xiao, Z., Yue, L., Wang, J., Feng, Y., Zhu, X., et al. (2019). Algae response to engineered nanoparticles: current understanding, mechanisms and implications. *Environ. Sci. Nano* 6 (4), 1026–1042. doi:10.1039/C8EN01368C
- Chen, P., Powell, B. A., Mortimer, M., and Ke, P. C. (2012). Adaptive interactions between zinc oxide nanoparticles and *Chlorella* sp. *Environ. Sci. Technol.* 46 (21), 12178–12185. doi:10.1021/es303303g
- Chen, Y. Y., Liu, W., Leng, X. J., and Stoll, S. (2022). Toxicity of selenium nanoparticles on *Poteroiochromonas malhamensis* algae in Waris-H culture medium and Lake Geneva water: effect of nanoparticle coating, dissolution, and aggregation. *Sci. Total Environ.* 808, 152010. doi:10.1016/j.scitotenv.2021.152010
- Chetwynd, A. J., and Lynch, I. (2020). The rise of the nanomaterial metabolite corona, and emergence of the complete corona. *Environ. Sci. Nano* 7 (4), 1041–1060. doi:10.1039/C9EN00938H
- Chevallet, M., Gallet, B., Fuchs, A., Jouneau, P. H., Um, K., Mintz, E., et al. (2016). Metal homeostasis disruption and mitochondrial dysfunction in hepatocytes exposed to sub-toxic doses of zinc oxide nanoparticles. *Nanoscale* 8 (43), 18495–18506. doi:10.1039/c6nr05306h
- Chiu, M.-H., Khan, Z. A., Garcia, S. G., Le, A. D., Kagiri, A., Ramos, J., et al. (2017). Effect of engineered nanoparticles on exopolymeric substances release from marine phytoplankton. *Nanoscale Res. Lett.* 12 (1), 620. doi:10.1186/s11671-017-2397-x
- Collin, B., Auffan, M., Johnson, A. C., Kaur, I., Keller, A. A., Lazareva, A., et al. (2014). Environmental release, fate and ecotoxicological effects of manufactured ceria nanomaterials. *Environ. Sci. Nano* 1 (6), 533–548. doi:10.1039/C4EN00149D
- Corsi, I., Bergami, E., and Grassi, G. (2020). Behavior and bio-interactions of anthropogenic particles in marine environment for a more realistic ecological risk assessment. *Front. Environ. Sci.* 8, 21. doi:10.3389/fenvs.2020.00060
- Della Torre, C., Maggioni, D., Nigro, L., Farè, F., Hamza, H., Protano, G., et al. (2021). Alginate coating modifies the biological effects of cerium oxide nanoparticles to the freshwater bivalve *Dreissena polymorpha*. *Sci. Total Environ.* 773, 145612. doi:10.1016/j.scitotenv.2021.145612
- Deng, Z. J., Liang, M., Toth, I., Monteiro, M., and Minchin, R. F. (2012). Plasma protein binding of positively and negatively charged polymer-coated gold nanoparticles elicits different biological responses. *Nanotoxicology* 7 (3), 314–322. doi:10.3109/17435390.2012.655342
- Docter, D., Westmeier, D., Markiewicz, M., Stolte, S., Knauer, S. K., Stauber, R. H., et al. (2015). The nanoparticle biomolecule corona: lessons learned - challenge accepted? *Chem. Soc. Rev.* 44 (17), 6094–6121. doi:10.1039/c5cs00217f
- Durán, N., Silveira, C. P., Durán, M., and Martínez, D. S. T. (2015). Silver nanoparticle protein corona and toxicity: a mini-review. *J. Nanobiotechnology* 13 (1), 55. doi:10.1186/s12951-015-0114-4
- Efthimiou, I., Kalamaras, G., Papavasileiou, K., Anastasi-Papathanasi, N., Georgiou, Y., Dailianis, S., et al. (2021). ZnO, Ag and ZnO-Ag nanoparticles exhibit differential modes of toxic and oxidative action in hemocytes of mussel *Mytilus galloprovincialis*. *Sci. Total Environ.* 767, 144699. doi:10.1016/j.scitotenv.2020.144699
- Fabrega, J., Luoma, S. N., Tyler, C. R., Galloway, T. S., and Lead, J. R. (2011). Silver nanoparticles: behaviour and effects in the aquatic environment. *Environ. Int.* 37 (2), 517–531. doi:10.1016/j.envint.2010.10.012
- Fadare, O. O., Wan, B., Guo, L. H., Xin, Y., Qin, W. P., Yang, Y., et al. (2019). Humic acid alleviates the toxicity of polystyrene nanoplastic particles to *Daphnia magna*. *Environ. Sci. Nano* 6 (5), 1466–1477. doi:10.1039/c8en01457d
- Fadare, O. O., Wan, B., Liu, K., Yang, Y., Zhao, L., Guo, L.-H., et al. (2020). Eco-corona vs protein corona: effects of humic substances on corona formation and nanoplastic particle toxicity in *Daphnia magna*. *Environ. Sci. Technol.* 54 (13), 8001–8009. doi:10.1021/acs.est.0c00615
- Gao, X., Deng, R., and Lin, D. H. (2020). Insights into the regulation mechanisms of algal extracellular polymeric substances secretion upon the exposures to anatase and rutile TiO₂ nanoparticles. *Environ. Pollut.* 263, 114608. doi:10.1016/j.envpol.2020.114608
- Gao, X., Middepogu, A., Deng, R., Liu, J. F., Hao, Z. N., Lin, D. H., et al. (2019). Adsorption of extracellular polymeric substances from two microbes by TiO₂ nanoparticles. *Sci. Total Environ.* 694, 133778. doi:10.1016/j.scitotenv.2019.133778
- García-Álvarez, R., and Vallet-Regí, M. (2021). Hard and soft protein corona of nanomaterials: analysis and relevance. *Nanomaterials* 11 (4), 888. doi:10.3390/nano11040888
- Grassi, G., Landi, C., Della Torre, C., Bergami, E., Bini, L., Corsi, I., et al. (2019). Proteomic profile of the hard corona of charged polystyrene nanoparticles exposed to sea urchin *Paracentrotus lividus* coelomic fluid highlights potential drivers of toxicity. *Environ. Sci. Nano* 6 (10), 2937–2947. doi:10.1039/C9EN00824A
- Grieger, K., Jones, J. L., Hansen, S. F., Hendren, C. O., Jensen, K. A., Kuzma, J., et al. (2019). Best practices from nano-risk analysis relevant for other emerging technologies. *Nat. Nanotechnol.* 14 (11), 998–1001. doi:10.1038/s41565-019-0572-1
- Hadjidemetriou, M., and Kostarelos, K. (2017). Nanomedicine: evolution of the nanoparticle corona. *Nat. Nanotechnol.* 12 (4), 288–290. doi:10.1038/nnano.2017.61
- Holden, P. A., Gardea-Torresdey, J. L., Klaessig, F., Turco, R. F., Mortimer, M., Hund-Rinke, K., et al. (2016). Considerations of environmentally relevant test conditions for improved evaluation of ecological hazards of engineered nanomaterials. *Environ. Sci. Technol.* 50 (12), 6124–6145. doi:10.1021/acs.est.6b00608
- Hou, J., Yang, Y., Wang, P., Wang, C., Miao, L., Wang, X., et al. (2017). Effects of CeO₂, CuO, and ZnO nanoparticles on physiological features of *Microcystis aeruginosa* and the production and composition of extracellular polymeric substances. *Environ. Sci. Pollut. Res. Int.* 24 (1), 226–235. doi:10.1007/s11356-016-7387-5
- Ivask, A., Juganson, K., Bondarenko, O., Mortimer, M., Aruoja, V., Kasemets, K., et al. (2014). Mechanisms of toxic action of Ag, ZnO and CuO nanoparticles to selected ecotoxicological test organisms and mammalian cells *in vitro*: a comparative review. *Nanotoxicology* 8, 57–71. doi:10.3109/17435390.2013.855831
- Jiménez-Lamana, J., and Slaveykova, V. I. (2016). Silver nanoparticle behaviour in lake water depends on their surface coating. *Sci. Total Environ.* 573, 946–953. doi:10.1016/j.scitotenv.2016.08.181
- Jimeno-Romero, A., Bilbao, E., Izaguirre, U., Cajaraville, M., Marigómez, I., and Soto, M. (2017). Digestive cell lysosomes as main targets for Ag accumulation and toxicity in marine mussels, *Mytilus galloprovincialis*, exposed to maltose-stabilised Ag nanoparticles of different sizes. *Nanotoxicology* 11 (2), 168–183. doi:10.1080/17435390.2017.1279358
- Joonas, E., Aruoja, V., Olli, K., and Kahru, A. (2019). Environmental safety data on CuO and TiO₂ nanoparticles for multiple algal species in natural water: filling the data gaps for risk assessment. *Sci. Total Environ.* 647, 973–980. doi:10.1016/j.scitotenv.2018.07.446
- Junaid, M., and Wang, J. (2021). Interaction of nanoplastics with extracellular polymeric substances (EPS) in the aquatic environment: a special reference to eco-corona formation and associated impacts. *Water Res.* 201, 117319. doi:10.1016/j.watres.2021.117319
- Kakinen, A., Ding, F., Chen, P., Mortimer, M., Kahru, A., Ke, P. C., et al. (2013). Interaction of firefly luciferase and silver nanoparticles and its impact on enzyme activity. *Nanotechnology* 24 (34), 345101. doi:10.1088/0957-4484/24/34/345101
- Katsumiti, A., Gilliland, D., Arostegui, I., and Cajaraville, M. P. (2015). Mechanisms of toxicity of Ag nanoparticles in comparison to Bulk and ionic Ag on mussel hemocytes and gill cells. *PLoS ONE* 10 (6), e0129039. doi:10.1371/journal.pone.0129039
- Kim, S. T., Lee, Y. J., Hwang, Y. S., and Lee, S. (2015). Study on aggregation behavior of Cytochrome C-conjugated silver nanoparticles using asymmetrical flow field-flow fractionation. *Talanta* 132, 939–944. doi:10.1016/j.talanta.2014.05.060
- Kögel, T., Bjørøy, Ø., Toto, B., Bienfait, A. M., and Sanden, M. (2020). Micro- and nanoplastic toxicity on aquatic life: determining factors. *Sci. Total Environ.* 709, 136050. doi:10.1016/j.scitotenv.2019.136050
- Lead, J. R., Batley, G. E., Alvarez, P. J. J., Croteau, M. N., Handy, R. D., McLaughlin, M. J., et al. (2018). Nanomaterials in the environment: behavior, fate, bioavailability, and effects. An updated review. *Environ. Toxicol. Chem.* 37 (8), 2029–2063. doi:10.1002/etc.4147
- Levard, C., Hotze, E. M., Lowry, G. V., and Brown, G. E. (2012). Environmental transformations of silver nanoparticles: impact on stability and toxicity. *Environ. Sci. Technol.* 46 (13), 6900–6914. doi:10.1021/es2037405
- Liu, F., Tan, Q.-G., Weiss, D., Crémazy, A., Fortin, C., Campbell, P. G. C., et al. (2020). Unravelling metal speciation in the microenvironment surrounding phytoplankton cells to improve predictions of metal bioavailability. *Environ. Sci. Technol.* 54 (13), 8177–8185. doi:10.1021/acs.est.9b07773
- Liu, F., Li, S. X., Feng, H., Li, L. Z., Yue, T. T., Yan, B., et al. (2021). Modulation of cell uptake and cytotoxicity by nanoparticles with various physicochemical properties after humic acid adsorption. *Environ. Sci. Nano* 8 (12), 3746–3761. doi:10.1039/d1en00773d
- Liu, W., Majumdar, S., Li, W. W., Keller, A. A., and Slaveykova, V. I. (2020a). Metabolomics for early detection of stress in freshwater alga *Poteroiochromonas malhamensis* exposed to silver nanoparticles. *Sci. Rep.* 10 (1), 20563. doi:10.1038/s41598-020-77521-0
- Liu, W., Worms, I. A. M., Herlin-Boime, N., Truffier-Boutry, D., Michaud-Soret, I., Mintz, E., et al. (2017). Interaction of silver nanoparticles with metallothionein and ceruloplasmin: impact on metal substitution by Ag(I), corona formation and enzymatic activity. *Nanoscale* 9 (19), 6581–6594. doi:10.1039/c7nr01075c

- Liu, W., Worms, I., and Slaveykova, V. I. (2020b). Interaction of silver nanoparticles with antioxidant enzymes. *Environ. Sci. Nano* 7 (5), 1507–1517. doi:10.1039/C9EN01284B
- Ly, Q. V., Maqbool, T., Zhang, Z., Le, Q. V., An, X. C., Hu, Y. X., et al. (2021). Characterization of dissolved organic matter for understanding the adsorption on nanomaterials in aquatic environment: a review. *Chemosphere* 269, 128690. doi:10.1016/j.chemosphere.2020.128690
- Lynch, I., and Dawson, K. A. (2008). Protein-nanoparticle interactions. *Nano Today* 3 (1), 40–47. doi:10.1016/S1748-0132(08)70014-8
- Marques-Santos, L. F., Grassi, G., Bergami, E., Faleri, C., Balbi, T., Salis, A., et al. (2018). Cationic polystyrene nanoparticle and the sea urchin immune system: biocorona formation, cell toxicity, and multixenobiotic resistance phenotype. *Nanotoxicology* 12 (8), 847–867. doi:10.1080/17435390.2018.1482378
- Mattsson, K., Aguilar, R., Torstensson, O., Perry, D., Bernfur, K., Linse, S., et al. (2018). Disaggregation of gold nanoparticles by *Daphnia magna*. *Nanotoxicology* 12 (8), 885–900. doi:10.1080/17435390.2018.1485982
- Miao, A. J., Luo, Z. P., Chen, C. S., Chin, W. C., Santschi, P. H., Quigg, A., et al. (2010). Intracellular uptake: a possible mechanism for silver engineered nanoparticle toxicity to a freshwater alga *Ochromonas danica*. *Plos One* 5 (12), e15196. doi:10.1371/journal.pone.0015196
- Miclăuș, T., Beer, C., Chevallier, J., Scavenius, C., Bochenkov, V. E., Enghild, J. J., et al. (2016). Dynamic protein coronas revealed as a modulator of silver nanoparticle sulphidation *in vitro*. *Nat. Commun.* 7 (1), 11770. doi:10.1038/ncomms11770
- Monopoli, M. P., Åberg, C., Salvati, A., and Dawson, K. A. (2012). Biomolecular coronas provide the biological identity of nanosized materials. *Nat. Nanotechnol.* 7, 779–786. doi:10.1038/nnano.2012.207
- Moore, T. L., Rodriguez-Lorenzo, L., Hirsch, V., Balog, S., Urban, D., Jud, C., et al. (2015). Nanoparticle colloidal stability in cell culture media and impact on cellular interactions. *Chem. Soc. Rev.* 44 (17), 6287–6305. doi:10.1039/c4cs00487f
- Morelli, E., Gabbellieri, E., Bonomini, A., Tognotti, D., Grassi, G., Corsi, I., et al. (2018). TiO₂ nanoparticles in seawater: aggregation and interactions with the green alga *Dunaliella tertiolecta*. *Ecotoxicol. Environ. Saf.* 148, 184–193. doi:10.1016/j.ecoenv.2017.10.024
- Mortimer, M., Gogos, A., Bartolomé, N., Kahru, A., Bucheli, T. D., Slaveykova, V. I., et al. (2014a). Potential of hyperspectral imaging microscopy for semi-quantitative analysis of nanoparticle uptake by Protozoa. *Environ. Sci. Technol.* 48 (15), 8760–8767. doi:10.1021/es500898j
- Mortimer, M., and Holden, P. A. (2019). “Chapter 3 - fate of engineered nanomaterials in natural environments and impacts on ecosystems,” in *Exposure to engineered nanomaterials in the environment*. Editors N. Marmiroli, J. C. White, and J. Song (Amsterdam: Elsevier), 61–103.
- Mortimer, M., Kahru, A., and Slaveykova, V. I. (2014b). Uptake, localization and clearance of quantum dots in ciliated protozoa *Tetrahymena thermophila*. *Environ. Pollut.* 190, 58–64. doi:10.1016/j.envpol.2014.03.021
- Nasser, F., Constantinou, J., and Lynch, I. (2020). Nanomaterials in the environment acquire an “eco-corona” impacting their toxicity to *Daphnia magna*—A call for updating toxicity testing policies. *Proteomics* 20 (9), 1800412. doi:10.1002/pmic.201800412
- Nasser, F., and Lynch, I. (2016). Secreted protein eco-corona mediates uptake and impacts of polystyrene nanoparticles on *Daphnia magna*. *J. Proteomics* 137, 45–51. doi:10.1016/j.jprot.2015.09.005
- Natarajan, L., Jenifer, M. A., and Mukherjee, A. (2021). Eco-corona formation on the nanomaterials in the aquatic systems lessens their toxic impact: a comprehensive review. *Environ. Res.* 194, 110669. doi:10.1016/j.envres.2020.110669
- Navarro, E., Baun, A., Behra, R., Hartmann, N. B., Filser, J., Miao, A. J., et al. (2008). Environmental behavior and ecotoxicity of engineered nanoparticles to algae, plants, and fungi. *Ecotoxicology* 17 (5), 372–386. doi:10.1007/s10646-008-0214-0
- Naveed, S., Li, C. H., Lu, X. D., Chen, S. S., Yin, B., Zhang, C. H., et al. (2019). Microalgal extracellular polymeric substances and their interactions with metal(loid)s: a review. *Crit. Rev. Environ. Sci. Technol.* 49 (19), 1769–1802. doi:10.1080/10643389.2019.1583052
- Nel, A. E., Mädler, L., Velegol, D., Xia, T., Hoek, E. M. V., Somasundaran, P., et al. (2009). Understanding biophysicochemical interactions at the nano–bio interface. *Nat. Mat.* 8, 543–557. doi:10.1038/nmat2442
- Nguyen, M. K., Moon, J. Y., and Lee, Y. C. (2020). Microalgal ecotoxicity of nanoparticles: an updated review. *Ecotoxicol. Environ. Saf.* 201, 110781. doi:10.1016/j.ecoenv.2020.110781
- Nigro, L., Freitas, R., Maggioni, D., Hamza, H., Coppola, F., Protano, G., et al. (2021). Coating with polysaccharides influences the surface charge of cerium oxide nanoparticles and their effects to *Mytilus galloprovincialis*. *NanoImpact* 24, 100362. doi:10.1016/j.impact.2021.100362
- Nowack, B., and Bucheli, T. D. (2007). Occurrence, behavior and effects of nanoparticles in the environment. *Environ. Pollut.* 150 (1), 5–22. doi:10.1016/j.envpol.2007.06.006
- Nowack, B., Ranville, J. F., Diamond, S., Gallego-Urrea, J. A., Metcalfe, C., Rose, J., et al. (2012). Potential scenarios for nanomaterial release and subsequent alteration in the environment. *Environ. Toxicol. Chem.* 31 (1), 50–59. doi:10.1002/etc.726
- Pulido-Reyes, G., Leganes, F., Fernandez-Pinas, F., and Rosal, R. (2017). Bio-nano interface and environment: a critical review. *Environ. Toxicol. Chem.* 36, 3181–3193. doi:10.1002/etc.3924
- Rastgar, S., Alijani Ardeshir, R., Segner, H., Tyler, C. R., Peijnenburg, J. G. M. W., Wang, Y., et al. (2022). Immunotoxic effects of metal-based nanoparticles in fish and bivalves. *Nanotoxicology* 16, 88–113. doi:10.1080/17435390.2022.2041756
- Sendra, M., Saco, A., Yeste, M. P., Romero, A., Novoa, B., and Figueras, A. (2020). Nanoplastics: from tissue accumulation to cell translocation into *Mytilus galloprovincialis* hemocytes. resilience of immune cells exposed to nanoplastics and nanoplastics plus *Vibrio splendidus* combination. *J. Hazard. Mat.* 388, 121788. doi:10.1016/j.jhazmat.2019.121788
- Sendra, M., Volland, M., Balbi, T., Fabbri, R., Yeste, M., Gatica, J., et al. (2018). Cytotoxicity of CeO₂ nanoparticles using *in vitro* assay with *Mytilus galloprovincialis* hemocytes: relevance of zeta potential, shape and biocorona formation. *Aquat. Toxicol.* 200, 13–20. doi:10.1016/j.aquatox.2018.04.011
- Seviour, T., Derlon, N., Dueholm, M. S., Flemming, H. C., Girbal-Neuhaus, E., Horn, H., et al. (2019). Extracellular polymeric substances of biofilms: suffering from an identity crisis. *Water Res.* 151, 1–7. doi:10.1016/j.watres.2018.11.020
- Seymour, J. R., Amin, S. A., Raina, J.-B., and Stocker, R. (2017). Zooming in on the phycosphere: the ecological interface for phytoplankton–bacteria relationships. *Nat. Microbiol.* 2 (7), 17065. doi:10.1038/nmicrobiol.2017.65
- Shakiba, S., Hakimian, A., Barco, L. R., and Louie, S. M. (2018). Dynamic intermolecular interactions control adsorption from mixtures of natural organic matter and protein onto titanium dioxide nanoparticles. *Environ. Sci. Technol.* 52 (24), 14158–14168. doi:10.1021/acs.est.8b04014
- Shou, W., Kang, F., and Lu, J. (2018). Nature and value of freely dissolved EPS ecosystem services: insight into molecular coupling mechanisms for regulating metal toxicity. *Environ. Sci. Technol.* 52 (2), 457–466. doi:10.1021/acs.est.7b04834
- Sikder, M., Croteau, M. N., Poulin, B. A., and Baalousha, M. (2021). Effect of nanoparticle size and natural organic matter composition on the bioavailability of polyvinylpyrrolidone-coated platinum nanoparticles to a model freshwater invertebrate. *Environ. Sci. Technol.* 55 (4), 2452–2461. doi:10.1021/acs.est.0c05985
- Sikder, M., Wang, J. J., Poulin, B. A., Tfaily, M. M., and Baalousha, M. (2020). Nanoparticle size and natural organic matter composition determine aggregation behavior of polyvinylpyrrolidone coated platinum nanoparticles. *Environ. Sci. Nano* 7 (11), 3318–3332. doi:10.1039/d0en00659a
- Slaveykova, V. I., Li, M., Worms, I. A., and Liu, W. (2020). When environmental chemistry meets ecotoxicology: bioavailability of inorganic nanoparticles to phytoplankton. *Chim. (Aarau)* 74 (3), 115–121. doi:10.2533/chimia.2020.115
- Slaveykova, V. (2022). “Phytoplankton controls on the transformations of metal-containing nanoparticles in aquatic environments,” in *Environmental nanoparticles: sources, occurrence, analysis and fate*. Editors J. Jimenez and L. J. Szpunar (Cambridge: Royal Society of Chemistry).
- Sørensen, S. N., Wigger, H., Zabeo, A., Semenzin, E., Hristozov, D., Nowack, B., et al. (2020). Comparison of species sensitivity distribution modeling approaches for environmental risk assessment of nanomaterials – a case study for silver and titanium dioxide representative materials. *Aquat. Toxicol.* 225, 105543. doi:10.1016/j.aquatox.2020.105543
- Spurgeon, D. J., Lahive, E., and Schultz, C. L. (2020). Nanomaterial transformations in the environment: effects of changing exposure forms on bioaccumulation and toxicity. *Small* 16, e2000618. doi:10.1002/smll.202000618
- Tenzer, S., Docter, D., Kuharev, J., Musyanovych, A., Fetz, V., Hecht, R., et al. (2013). Rapid formation of plasma protein corona critically affects nanoparticle pathophysiology. *Nat. Nanotechnol.* 8 (10), 772–781. doi:10.1038/nnano.2013.181
- Tenzer, S., Docter, D., Rosfa, S., Wlodarski, A., Kuharev, J., Reik, A., et al. (2011). Nanoparticle size is a critical physicochemical determinant of the human blood plasma corona: a comprehensive quantitative proteomic analysis. *ACS Nano* 5 (9), 7155–7167. doi:10.1021/nn201950e
- Treuel, L., Jiang, X., and Nienhaus, G. U. (2013). New views on cellular uptake and trafficking of manufactured nanoparticles. *J. R. Soc. Interface* 10 (82), 20120939. doi:10.1098/rsif.2012.0939
- Treuel, L., Malissek, M., Gebauer, J. S., and Zellner, R. (2010). The influence of surface composition of nanoparticles on their interactions with serum albumin. *ChemPhysChem* 11 (14), 3093–3099. doi:10.1002/cphc.201000174

- Treuel, L., Malissek, M., Grass, S., Diendorf, J., Mahl, D., Meyer-Zaika, W., et al. (2012). Quantifying the influence of polymer coatings on the serum albumin corona formation around silver and gold nanoparticles. *J. Nanopart. Res.* 14 (9), 1102. doi:10.1007/s11051-012-1102-3
- von Moos, N., and Slaveykova, V. I. (2014). Oxidative stress induced by inorganic nanoparticles in bacteria and aquatic microalgae - state of the art and knowledge gaps. *Nanotoxicology* 8 (6), 605–630. doi:10.3109/17435390.2013.809810
- Walkey, C. D., and Chan, W. C. W. (2012). Understanding and controlling the interaction of nanomaterials with proteins in a physiological environment. *Chem. Soc. Rev.* 41 (7), 2780–2799. doi:10.1039/C1CS15233E
- Walkey, C. D., Olsen, J. B., Song, F. Y., Liu, R., Guo, H. B., Olsen, D. W. H., et al. (2014). Protein corona fingerprinting predicts the cellular interaction of gold and silver nanoparticles. *ACS Nano* 8 (3), 2439–2455. doi:10.1021/nn406018q
- Wang, H. X., Shang, L., Maffre, P., hmann, S., Kirschhöfer, F., Fenner-Weiß, G., et al. (2016). The Nature of a Hard Protein Corona Forming on Quantum Dots Exposed to Human Blood Serum 42 (12), 5836–5844. doi:10.1002/smll.201602283
- Wang, Y., Miao, A. J., Luo, J., Wei, Z. B., Zhu, J. J., Yang, L. Y., et al. (2013). Bioaccumulation of CdTe quantum dots in a freshwater alga *Ochromonas danica*: a kinetics study. *Environ. Sci. Technol.* 47 (18), 10601–10610. doi:10.1021/es4017188
- Westmeier, D., Stauber, R. H., and Docter, D. (2016). The concept of bio-corona in modulating the toxicity of engineered nanomaterials (ENM). *Toxicol. Appl. Pharmacol.* 299, 53–57. doi:10.1016/j.taap.2015.11.008
- Wheeler, K. E., Chetwynd, A. J., Fahy, K. M., Hong, B. S., Tochihiuti, J. A., Foster, L. A., et al. (2021). Environmental dimensions of the protein corona. *Nat. Nanotechnol.* 16 (6), 617–629. doi:10.1038/s41565-021-00924-1
- Wiesner, M. R., Lowry, G. V., Jones, K. L., Hochella, M. F., Di Giulio, R. T., Casman, E., et al. (2009). Decreasing uncertainties in assessing environmental exposure, risk, and ecological implications of nanomaterials. *Environ. Sci. Technol.* 43 (17), 6458–6462. doi:10.1021/es803621k
- Wilkinson, K. J., Joz-Roland, A., and Buffle, J. (1997). Different roles of pedogenic fulvic acids and aquagenic biopolymers on colloid aggregation and stability in freshwaters. *Limnol. Oceanogr.* 42 (8), 1714–1724. doi:10.4319/lo.1997.42.8.1714
- Wimuktiwan, P., Shiowatana, J., and Siripinyanond, A. (2015). Investigation of silver nanoparticles and plasma protein association using flow field-flow fractionation coupled with inductively coupled plasma mass spectrometry (FIFFF-ICP-MS). *J. Anal. At. Spectrom.* 30 (1), 245–253. doi:10.1039/c4ja00225c
- Xu, H. C., and Jiang, H. L. (2015). Effects of cyanobacterial extracellular polymeric substances on the stability of ZnO nanoparticles in eutrophic shallow lakes. *Environ. Pollut.* 197, 231–239. doi:10.1016/j.envpol.2014.10.031
- Xu, H. C., Li, F. F., Kong, M., Lv, X. Z., Du, H. Y., Jiang, H. L., et al. (2020). Adsorption of cyanobacterial extracellular polymeric substance on colloidal particle: influence of molecular weight. *Sci. Total Environ.* 715, 136959. doi:10.1016/j.scitotenv.2020.136959
- Xu, L., Xu, M., Wang, R., Yin, Y., Lynch, I., Liu, S., et al. (2020). The crucial role of environmental coronas in determining the biological effects of engineered nanomaterials. *Small* 16 (36), 2003691. doi:10.1002/smll.202003691
- Zhang, S. J., Jiang, Y. L., Chen, C. S., Spurgin, J., Schwehr, K. A., Quigg, A., et al. (2012). Aggregation, dissolution, and stability of quantum dots in marine environments: importance of extracellular polymeric substances. *Environ. Sci. Technol.* 46 (16), 8764–8772. doi:10.1021/es301000m
- Zhang, Z., Si, R., Lv, J., Ji, Y., Chen, W., Guan, W., et al. (2020). Effects of extracellular polymeric substances on The formation and methylation of mercury sulfide nanoparticles. *Environ. Sci. Technol.* 54 (13), 8061–8071. doi:10.1021/acs.est.0c01456
- Zheng, S. M., Zhou, Q. X., Chen, C. H., Yang, F. X., Cai, Z., Li, D., et al. (2019). Role of extracellular polymeric substances on the behavior and toxicity of silver nanoparticles and ions to green algae *Chlorella vulgaris*. *Sci. Total Environ.* 660, 1182–1190. doi:10.1016/j.scitotenv.2019.01.067
- Zhou, K. J., Hu, Y., Zhang, L. Q., Yang, K., and Lin, D. H. (2016). The role of exopolymeric substances in the bioaccumulation and toxicity of Ag nanoparticles to algae. *Sci. Rep.* 6, 32998. doi:10.1038/srep32998
- Zimmermann, S., Ruchter, N., Loza, K., Eppe, M., and Sures, B. (2017). Nanoparticulate versus ionic silver: behavior in the tank water, bioaccumulation, elimination and subcellular distribution in the freshwater mussel *Dreissena polymorpha*. *Environ. Pollut.* 222, 251–260. doi:10.1016/j.envpol.2016.12.048



OPEN ACCESS

EDITED BY

Rosaria Meccariello,
University of Naples Parthenope, Italy

REVIEWED BY

Massimo Venditti,
Second University of Naples, Italy
Chibuisi Gideon Alimba,
University of Ibadan, Nigeria

*CORRESPONDENCE

Folarin Owagboriaye,
owagboriaye.folarin@
ouagoiwoye.edu.ng

SPECIALTY SECTION

This article was submitted to
Developmental and Reproductive
Toxicology,
a section of the journal
Frontiers in Toxicology

RECEIVED 23 June 2022

ACCEPTED 26 August 2022

PUBLISHED 26 September 2022

CITATION

Owagboriaye F, Oladunjoye R,
Adekunle O, Adeleke M, Salisu T,
Adenekan A, Sulaimon A, Dedeke G and
Lawal O (2022), First report on atrazine
monitoring in drinking water from Ijebu-
North, South-West Nigeria: Human
health risk evaluation and reproductive
toxicity studies.
Front. Toxicol. 4:975636.
doi: 10.3389/ftox.2022.975636

COPYRIGHT

© 2022 Owagboriaye, Oladunjoye,
Adekunle, Adeleke, Salisu, Adenekan,
Sulaimon, Dedeke and Lawal. This is an
open-access article distributed under
the terms of the [Creative Commons
Attribution License \(CC BY\)](#). The use,
distribution or reproduction in other
forums is permitted, provided the
original author(s) and the copyright
owner(s) are credited and that the
original publication in this journal is
cited, in accordance with accepted
academic practice. No use, distribution
or reproduction is permitted which does
not comply with these terms.

First report on atrazine monitoring in drinking water from Ijebu-North, South-West Nigeria: Human health risk evaluation and reproductive toxicity studies

Folarin Owagboriaye^{1*}, Rasheed Oladunjoye¹,
Oladunni Adekunle¹, Mistura Adeleke¹, Titilola Salisu¹,
Adedamola Adenekan², Abibat Sulaimon¹, Gabriel Dedeke³ and
Olusegun Lawal¹

¹Department of Zoology and Environmental Biology, Faculty of Science, Olabisi Onabanjo University Ago-Iwoye, Ago Iwoye, Ogun State, Nigeria, ²Department of Environmental Management and Toxicology, College of Environmental Management, Federal University of Agriculture, Abeokuta, Ogun State, Nigeria, ³Department of Pure and Applied Zoology, College of Bioscience, Federal University of Agriculture, Abeokuta, Ogun State, Nigeria

There are no available data on the level of atrazine in drinking water from rural agricultural areas in Nigeria and its potential health implications. Here, we measured atrazine residue in 69 hand-dug wells (HDW), 40 boreholes (BH), and four major streams from the six communities (Ago-Iwoye, Ijebu-Igbo, Oru, Awa, Ilaporu, and Mamu) in Ijebu North Local Government Area, Southwest Nigeria. Values of atrazine obtained were further used for the evaluation of non-carcinogenic risk associated with ingestion and dermal contact in adults and children as well as reproductive toxicity evaluation. A total of 41 HDW, 22 BH, and the four streams showed varying concentrations of atrazine, which was higher in HDW than BH and stream. Ago-Iwoye recorded the highest concentration of 0.08 mg/L in its HDW while the lowest concentration of 0.01 mg/L was recorded in HDW from Oru. Although the Hazard Index (HI) values associated with ingestion and dermal contact for children were higher than in adults, the values were below the acceptable limit for all the communities. Significant ($p < 0.05$) alterations in the oxidative stress parameters, reproductive hormones, sperm parameters, and mild testicular lesions were only observed in rats exposed to atrazine at 0.08 mg/L compared to control. But atrazine at 0.01, 0.03, and 0.04 mg/L triggered a defence mechanism capable of protecting the structural integrity of the testes and preventing reproductive dysfunction.

KEYWORDS

environmental pollution, herbicide, health risk, atrazine monitoring, reproductive dysfunction

Introduction

Atrazine (2-chloro-4-ethylamino-6-isopropylamino-1,3,5-triazine) is one of the major herbicides used to control pre- and post-emergence broadleaf weeds on maize farms in Nigeria (Farmsquare, 2020). Since Nigeria is one of the largest producers of maize in Africa (Adeite, 2021), farmers solely depend on atrazine to maintain or improve the rate at which maize is produced. The increasing overdependence and use of atrazine on maize farms in Nigeria is now a major public health concern of national interest.

Since contaminated drinking water is the main route of exposure to atrazine in adults and children (US EPA, 2007), the Food Quality Protection Act of 1996 (FQPA) mandated the USEPA and other bodies to monitor dietary risk associated with exposure to atrazine from community water systems (CWS). This prompted the regulatory body to establish a contamination limit of 3 µg/L for atrazine in water bodies under the safe drinking water act (US EPA, 2003).

A rural hand-dug well surveyed in Minnesota by the Minnesota Department of Agriculture (MDA) for atrazine recorded the highest atrazine concentration of 3.4 µg/L (MDH. Human Health, 2009). In addition, a national survey of herbicides in domestic well water carried out by the USEPA revealed atrazine as the common herbicide contaminating the well water (Ritter, 1990; Quackenboss et al., 2000; Focazio et al., 2006). Meanwhile, up to 40% of surface water in 31 states and 10% of groundwater in 13 states had earlier tested positive for atrazine (US EPA, 1989). On the other hand, out of 351 hand-dug wells monitored for atrazine on Ontario farms by the Ontario Ministry of Environment in Canada, 17% of the hand-dug wells recorded atrazine concentrations that were above 1 µg/L (Ontario Ministry of the Environment, 1987). This later prompted Canada to establish a safe limit of 5 µg/L for atrazine in drinking water (Health Canada, 1993). Up till now, no study has been conducted in some rural agricultural areas in Nigeria to monitor atrazine in drinking water from hand-dug well and surface waters as well as its potential health implications.

Although the toxicological profiles of atrazine in experimental animals and human studies have been widely documented (US EPA, 2007; WHO, 2011). Of major interest is its potential to induce reproductive dysfunction in animals. Atrazine has been reported to negatively alter some reproductive hormones in animals (Stoker et al., 2000; Zirkin et al., 2001; Hayes, 2004; Swan, 2006; WHO, 2011) and decrease fertility in rats at 120 mg/kg/day of exposure (Simic et al., 1994; McElroy et al., 2000). Disruptions of plasma and gonadal sex steroids in fish exposed to atrazine were observed (Spano et al., 2004). Furthermore, atrazine induced gonadal-histo-functional alteration in crocodilian reptiles (Rey et al., 2009) and spermatogenesis disruption in birds (Hussain et al., 2011). Abarikwu et al. (2010) studied changes in sperm characteristics and oxidative stress parameters in the testis and epididymis of rats exposed to atrazine at 0, 100, and 200 mg/kg body weight for 7 and 16 days. The herbicide was observed to impair reproductive

function and elicits a depletion of the antioxidant defence system in the testis and epididymis, indicating the induction of oxidative stress (Abarikwu et al., 2010). Although studies have documented the reproductive toxicity of atrazine in animals, there is a need to ascertain this toxicity by considering environmentally relevant concentrations found in drinking water from rural agricultural communities to which the inhabitants may be directly exposed.

Moreover, ensuring sustainable access to clean and safe water is one of the major targets of the 2030 Agenda for Sustainable Development Goals (SDGs) (WHO, UNICEF, 2017), and achieving this target will involve significant improvements in rural areas of Sub-Saharan Africa, which have been denied access to safe and clean drinking water (Sogbanmu et al., 2020). More than one-third of the Nigerian population has been denied access to quality drinking water sources due to uncontrolled anthropogenic activities (WHO, UNICEF, 2017; Sogbanmu et al., 2020). Therefore, the majority of Nigerians in rural communities (where there are higher agricultural activities) still depend on streams, rivers, and hand-dug wells for their drinking water. In the year 2007, the governing council of the Standard Organization of Nigeria established a maximum permissible level of 0.02 mg/L for 2, 4, 6—trichlorophenol in drinking water (Standards Organization of Nigeria, 2007) but provided no limits for the widely used atrazine herbicide.

We designed this study to 1) determine the residue of atrazine in water from the rural communities of Ijebu-North LG, Southwest Nigeria. 2) Evaluate the potential human health risk associated with exposure to atrazine 3) carry out reproductive toxicity of atrazine concentrations found in the water from the study area.

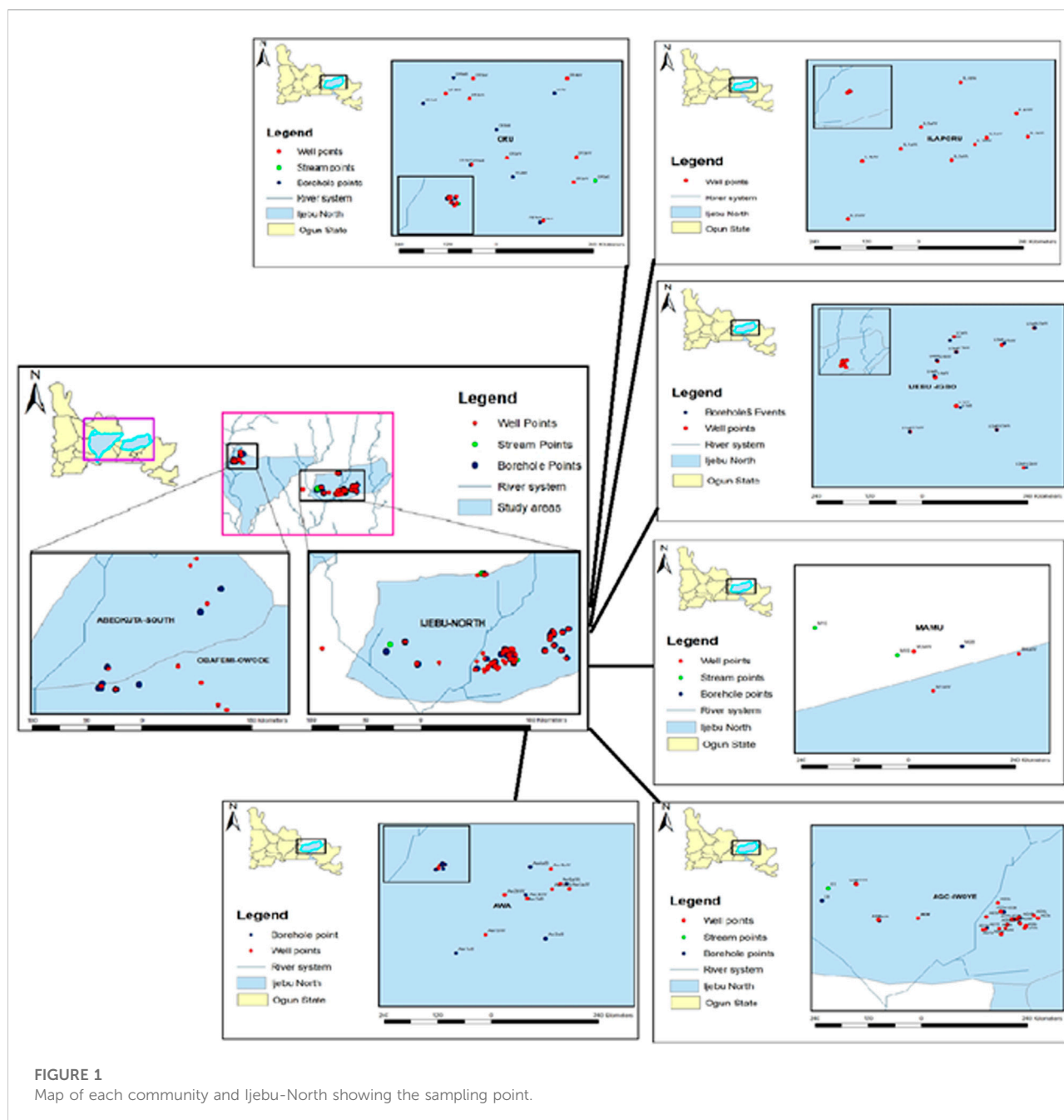
Materials and methods

Study area

This study was carried out in Ijebu-North LGA of Ogun State Nigeria because agriculture is the economic mainstay of the LGA. The local government comprises six communities including Ago-Iwoye, Ijebu-Igbo, Oru, Ilaporu, Awa, and Mamu with a major farm village in each community. The LGA has a 2016 population projection of 390, 200 (National Population Commission, 2016) and a total land area of 967 km². Ijebu North LGA is bounded by Oluyole LGA of Oyo State in the North, Ijebu East L.G in the west, Odogbolu and Ijebu Ode L.G. in the south, and Ikenne L.G. in the east.

Water sample collection

Hand-dug well (HDW), borehole (BH), and stream waters from each of the communities in Ijebu-North (Figure 1) were



collected in 20 ml amber glass bottles according to the procedures of the United States Geological Survey (Koterba et al., 1995). We also collected waters from HDW and BH from the state capital, Abeokuta urban area and this serves as the control location. The number of HDW, BH, and streams sampled from the community is shown in [Supplementary Table S1](#). In total, 69 HDW, 40 BH, and four streams were sampled. The water sample was collected from the farm settlement and collection was maintained within at least a 400-m distance from each sampling point throughout the community. The depths of all the HDW and the coordinates of

each sampling point are shown in [Supplementary Tables S2A-G](#). The depth of all the HDWs sampled was less than 12 m. However, the depths of the boreholes could not be measured. All the water samples were filtered at the point of collection and transported on ice to the laboratory for atrazine concentration analysis. Values obtained were used for the evaluation of human health risks posed by the herbicide. The highest concentration of atrazine observed in a water sample from each of the communities was administered to experimental rats in a sub-chronic hepatotoxicity study.

Determination of atrazine residue

The residue of atrazine was determined in the water sample by using the approved protocols for drinking water monitoring of contaminants (Huang et al., 2003; US EPA, 2009) with few modifications. A stock standard of atrazine was prepared by weighing 10 mg of analytical standard (Sigma-Aldrich, St. Louis, MO, United States) into a 100 ml flask, diluted to the mark with methanol, and stored at -18°C in the dark. Solid-Phase Extraction (SPE) technique was employed with a C18 SPE cartridge, which was conditioned under gravity with 10 ml each of methanol and deionized water. Another 2 ml of deionized water was added to avoid dryness and the valve was closed to the vacuum manifold. The configuration was completed by attaching a 75-ml solvent reservoir to the top of the C18 cartridge that was connected to the manifold. The water sample (200 ml, pH adjusted to 6) was transferred to the reservoir and pumped through the cartridge at a flow rate of 10 ml/min. The cartridge was later washed with 20 ml of deionized water. The cartridge was subjected to a vacuum system for 25 min to remove water and then, totally dried with a stream of nitrogen gas. The elution of the compound retained was done with 2 ml of methanol and the organic extract was completely dried with a rotary evaporator at 40°C and a stream of nitrogen gas. The final sample was reconstituted in acetone to a final volume of 1.0 ml that is ready for GC-MS analysis. The analysis was performed on GC (Agilent Technologies, Model; 7890A) with Mass Selective Detector (Model; 5975C) and the analytical procedures follow the USEPA good laboratory practice standards (40 CFR Part 79.60, 1994). The initial oven temperature was programmed at 110°C for 2 min at $10^{\circ}\text{C}/\text{minute}$ to 180°C at $20^{\circ}\text{C}/\text{minute}$ to 250°C for 8 min. The electron ionization (70v) and ion source temperature (230°C) were also programmed. A total of $1\mu\text{L}$ of the sample was injected and Agilent technologies HP5MS column ($30\text{ m} \times 0.25\text{ mm} \times 0.320\mu\text{m}$) was used for separation. Helium gas was used as the carrier gas at 65 psi. Quantification and identification of the peak areas were done by comparison with the standard used to prepare the calibration standard solution.

Human health risk evaluations

We carried out non-carcinogenic human health risks for adults and children through ingestion and dermal routes in this study. The health risk was evaluated following the standard protocol (EPA, 1989; Resources, 2006; Health Canada, 2010; Almasi et al., 2020; Dehghani et al., 2022). The average daily exposure concentration known as average daily intake (ADI) was computed using Eqs 1, 2 as below

$$\text{ADI}_{\text{ingestion}} = \frac{\text{CW} \times \text{IRW} \times \text{EF} \times \text{ED}}{\text{BW} \times \text{AT}} \quad (1)$$

where CW- atrazine level in water (mg/L); IRW- ingestion rate of water (L); EF- exposure frequency (days/year); ED-exposure

duration (years); BW -body weight (kg); AT-average exposure time (days) (EPA, 1989; Resources, 2006; Health Canada, 2010; Almasi et al., 2020; Dehghani et al., 2022).

$$\text{ADI}_{\text{dermal}} = \frac{\text{CW} \times \text{KP} \times \text{EF} \times \text{SA} \times \text{ET} \times \text{ED} \times \text{CF}}{\text{BW} \times \text{AT}} \quad (2)$$

SA-skin area (cm^2), KP- coefficient for dermal permeability (cm/h), ET-exposure time (hrs/day), CF- conversion factor (mg/kg) (EPA, 1989; Resources, 2006; Health Canada, 2010; Almasi et al., 2020; Dehghani et al., 2022).

The hazard quotient (HQ) of atrazine via ingestion and dermal routes was estimated with the standard United States EPA reference dose (RfD) ($0.035\text{ mg}/\text{kg}/\text{day}$) shown in Equation 3 below

$$\text{HQ} = \frac{\text{ADI}}{\text{RfD}} \quad (3)$$

The hazard index (HI) of atrazine exposure for adults and children was estimated through the summation of the HQ obtained for ingestion and dermal contact.

Toxicity study

Experimental animal and study design

A total of thirty (Huang et al., 2003) male albino rats ($140 \pm 10\text{ g}$) were randomized into five groups (four treatments and one control) of six rats/group and orally exposed to atrazine (PESTANAL, Sigma Aldrich St Louis, United States; purity 98.2%) at $0.01\text{ mg}/\text{L}$, $0.03\text{ mg}/\text{L}$, $0.04\text{ mg}/\text{L}$, and $0.08\text{ mg}/\text{L}$ concentrations. Atrazine was diluted in a watery suspension and orally administered, with gavage, to the rats once a day in a volume of $0.25\text{ ml}/100\text{ g}$ of body weight as previously described (Romano et al., 2010; Owagboriaye et al., 2017). Distilled water was administered to the control group and the exposure scenario lasted for 12 weeks. The concentrations were selected because they were the highest values of atrazine recorded in the water from each of the communities. We handled the rats by following the guidelines of the local ethical committee in the Animal Care Unit (ACU) of Olabisi Onabanjo University as well as ethical guidelines (regulation CEE 86/609).

Collection of samples and preparation

Samples were collected and prepared according to the methods described in Owagboriaye et al. (2022). Retro orbital sinus technique with the microhematocrit tube was used to collect blood samples into a plain sample tube and serum was separated within 1 h after collection. The testis was excised and rinsed in saline solution. The excised testis was divided into two portions. A portion was homogenized in 10%, w/v phosphate buffer (pH 7.4), centrifuged and the supernatant was used for the

biochemical assays. The second portion was fixed in 10% neutral-buffered formalin for histopathological investigations. The rat's epididymis was dissected and sperm cells were collected for sperm parameters analysis.

Hormonal assay

Enzyme-Linked immunosorbent Assay (ELISA) kit (Bio check, United States) was used to determine the concentration of Follicle Stimulating Hormone (FSH), testosterone, prolactin, and Luteinizing hormone (LH) and the protocols follow the manufacturer's guide.

Estimation of ROS and oxidative stress parameters in the testis

The level of ROS in the testicular tissue was determined by incubating 100 µL of an aliquot from testicular homogenate with 5 µL 2',7'-dichloro-dihydro fluorescein diacetate (DCFH-DA) at 37°C for 60 min as previously described in Pérez-Severiano et al. (2004) and Owagboriaye et al. (2021), Owagboriaye et al. (2022). The thiobarbituric acid reactive substance (TBARS) assay described in Okhawa et al. (1979), which involves the measurement of malondialdehyde (MDA) was employed for the determination of lipid peroxidation. The activity of superoxide dismutase (SOD) was determined according to Asada et al. (1974). The amount of enzyme needed to yield 50% inhibition of nitroblue tetrazolium (NBT) per minute indicates a unit of SOD. The method of Hassan and Barakat (2008) was followed for the determination of reduced glutathione (GSH) concentration. The activity of catalase was determined by monitoring the disappearance of hydrogen peroxide at 240 nm (Aebi, 1984). A decrease of 1 µmol in a hydrogen peroxide/minute denotes one unit of the enzyme. We adopted the protocol of Necheles et al. (1968) for the determination of GPx activity using hydrogen peroxide and GSH as substrates. A total of 1 µg of GSH consumed/minute indicates a unit of GPx. The standard protocol of Habig et al. (1974) was adopted for the determination of GST activity. The method of Lowry et al. (1951) was used for protein determination and the expressions of all the antioxidant enzyme activities are in units per milligram of protein.

Estimation of the testis membrane-bound ATPase enzyme

The amount of phosphorus liberated from the incubation mixture of the testis homogenate and 5 mM of ATP, 60 mM of NaCl, 2 mM of MgCl₂, 20 mM of KCl, 2 Mm of CaCl₂, and protein enzyme was estimated for the determination of Ca²⁺ATPase, Na⁺/K⁺ATPase and Mg²⁺ATPase activities (Dedeke et al., 2018; Owagboriaye et al., 2022). We also set up

control through the addition of enzyme after trichloroacetic acid at the end of the incubation period. We adopted the established protocol of Lowry et al. (1951) for protein estimation.

Epididymis sperm parameter assessment

Assessments of sperm count and percentage motility were carried out according to the protocol described in Hassan and Barakat (2008). Epididymides contents were dissected into 10 ml of 0.87% normal saline and dropped on clean slides. The movement or percentage motility of the sperm cells was determined using Eq. 4 as below

$$\% \text{ motility} = \frac{\text{number of sperm cells with progressive movements}}{200} \times 100\% \quad (4)$$

The sperm cells were also counted using a Hausser Scientific haemocytometer (Hausser Scientific 3,520, Horsham, PA, United States). Sperm abnormality assessment was done according to the modified method of Bakare et al. (2005). Epididymal sperm cells were suspended in normal saline and 1% eosin Y stain. A smear was prepared on slides, which were allowed to air-dry and coded for subsequent microscopic examination. A total of 1,000 sperm cells were assessed for morphological abnormalities for each rat.

Histopathological examinations

The testis excised was routinely processed for histopathological investigation, sectioned at 4-5 thick, stained with Hematoxylin-Eosin stain, and mounted in a neutral DPX medium as previously described (Owagboriaye et al., 2022). The prepared slides were viewed at ×400 magnifications.

Statistical methods

IBM Statistical Package (SPSS) version 20.0 was used to analyze the data obtained. We compared the mean values with the Analysis of Variance (ANOVA) and the results were presented as Mean ± Standard Error of Mean (SEM). Student-Newman-Keuls (SNK) was used for the post hoc test and a Probability value less than 0.05 was considered to be statistically significant.

Results

Level of atrazine in water from Ijebu-North

Residues of atrazine in hand-dug wells, boreholes, and streams water from the six communities in Ijebu-North and

TABLE 1 Concentration of atrazine (mg/L) in water from the communities in Ijebu-North Local Government of Ogun State, Nigeria.

	Abeokuta		Ijebu-Igbo		Oru			Ilaporu	Awa		Ago-iwoye			Mamu		
Point	Well	BH	Well	BH	Well	BH	Stream	Well	Well	BH	Well	BH	Stream	Well	BH	Stream
SP1	ND	ND	0.03	0.01	0.01	0.005	0.004	0.01	0.04	0.01	0.08	0.01	0.003	0.04	0.003	BDL
SP2	ND	ND	0.03	0.003	0.01	BDL		ND	0.02	BDL	0.03	BDL		0.03		0.003
SP3	BDL	ND	ND	ND	0.007	ND		0.003	0.04	0.01	0.02	0.003		0.01		
SP4	ND	ND	0.01	ND	ND	0.004		BDL	0.03	0.01	0.03	BDL				
SP5	ND	ND	0.02	0.003	ND	ND		ND	0.04	BDL	0.02	BDL				
SP6	BDL	ND	ND	ND	ND	ND		0.01	ND		0.02	0.003				
SP7	ND	ND	ND	BDL	0.01	0.003		0.003	0.03		0.01	BDL				
SP8	BDL	ND	ND	ND	0.004			ND			0.02					
SP9	ND	ND	0.02	0.003	ND			ND			ND					
SP10	ND	ND	ND	ND				ND			0.02					
SP11											ND					
SP12											0.01					
SP13											0.01					
SP14											ND					
SP15											0.01					
SP16											0.004					
SP17											ND					
SP18											0.003					
SP19											ND					
SP20											ND					

SP-sampling point; ND-not, detected; BH- borehole; BDL-below detection limit.

Abeokuta are shown in Table 1. A total of 41 hand-dug wells, 22 boreholes, and all four streams showed varying concentrations of atrazine. Ago-Iwoye recorded the highest concentration of 0.08 mg/L in its hand-dug well water. This is followed by well water from Awa and Mamu (0.04 mg/L). Ijebu-Igbo and Oru recorded the highest atrazine concentration of 0.03 and 0.01 mg/L respectively. Atrazine was not detected in borehole water from Abeokuta.

Human health risk evaluation

The estimated HQ for children and adults according to the atrazine concentrations detected in each community are shown in Supplementary Tables S3,4,5,6,7. Ago-Iwoye recorded the highest HQ values of 0.146 and 0.063 for ingestion in children and adults, and HQ values of 0.082 and 0.045 for dermal contact in children and adults respectively. This was followed by the Awa community where the HQ values of 0.074 and 0.016 for ingestion in children and adults, and HQ values of 0.040 and 0.023 for dermal contact in children and adults respectively were observed. The estimated HI for children and adults according to the atrazine concentrations detected in Ijebu-

Igbo and Ago-Iwoye, Oru, Awa, Mamu and Ilaporu are shown in Figures 2, 3, respectively. However, the estimated HI for children and adults according to the atrazine concentrations detected in Oru, Awa, Mamu and Ilaporu are shown in Supplementary Figures S1,S2,S3,S4. The HI value in children ranges from 0.020 to 0.228 while the value ranges from 0.004 to 0.108 for adults. However, the values were less than one, which is the standard acceptable value.

Levels of serum testosterone and prolactin hormones in the experimental rats

Levels of serum testosterone and prolactin hormones of male albino rat exposed to atrazine concentrations in drinking water from Ijebu-North, Southwest Nigeria is presented in Figure 4. Results showed a reduction in the serum level of testosterone hormone with an increase in the concentration of atrazine exposure. However, the reduction was only significant ($p < 0.05$) in rats exposed to 0.08 mg/L concentration of atrazine compared to control and those exposed to 0.01, 0.03, and 0.04 mg/L concentrations of atrazine. On the other hand, the level of serum prolactin

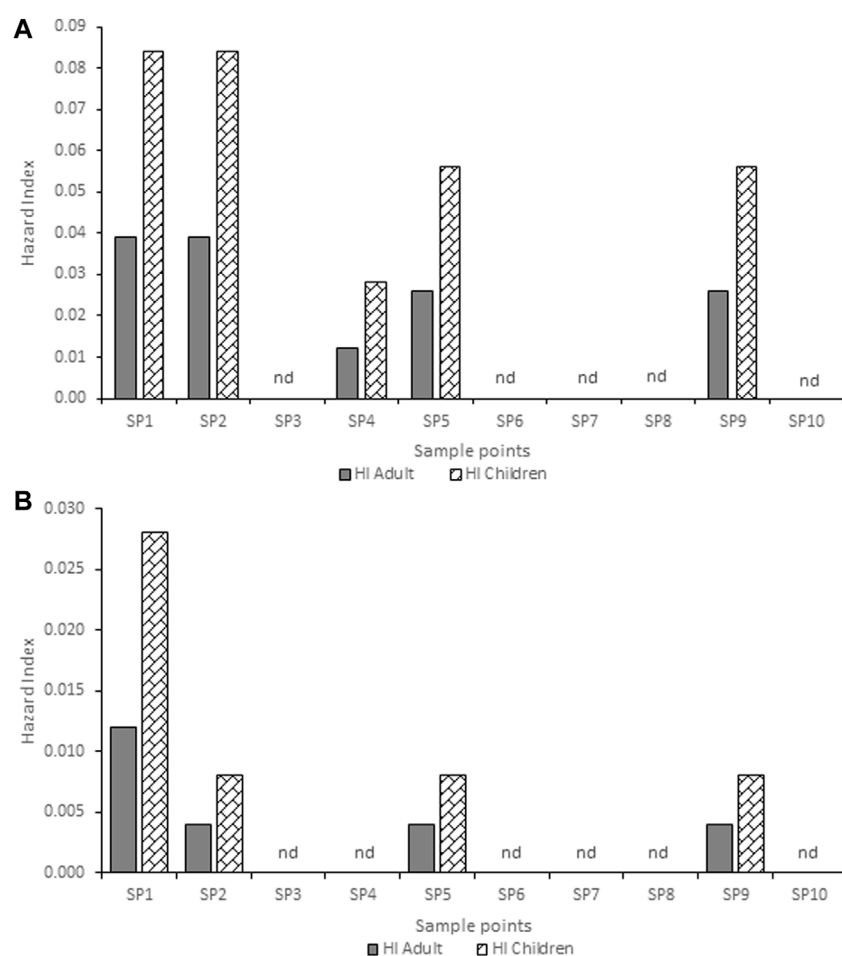


FIGURE 2

Hazard index for adults and children associated with exposure to atrazine concentration in (A) hand-dug well (B) borehole water from Ijebu-Igbo community. SP-Sampling point; nd-non-detected.

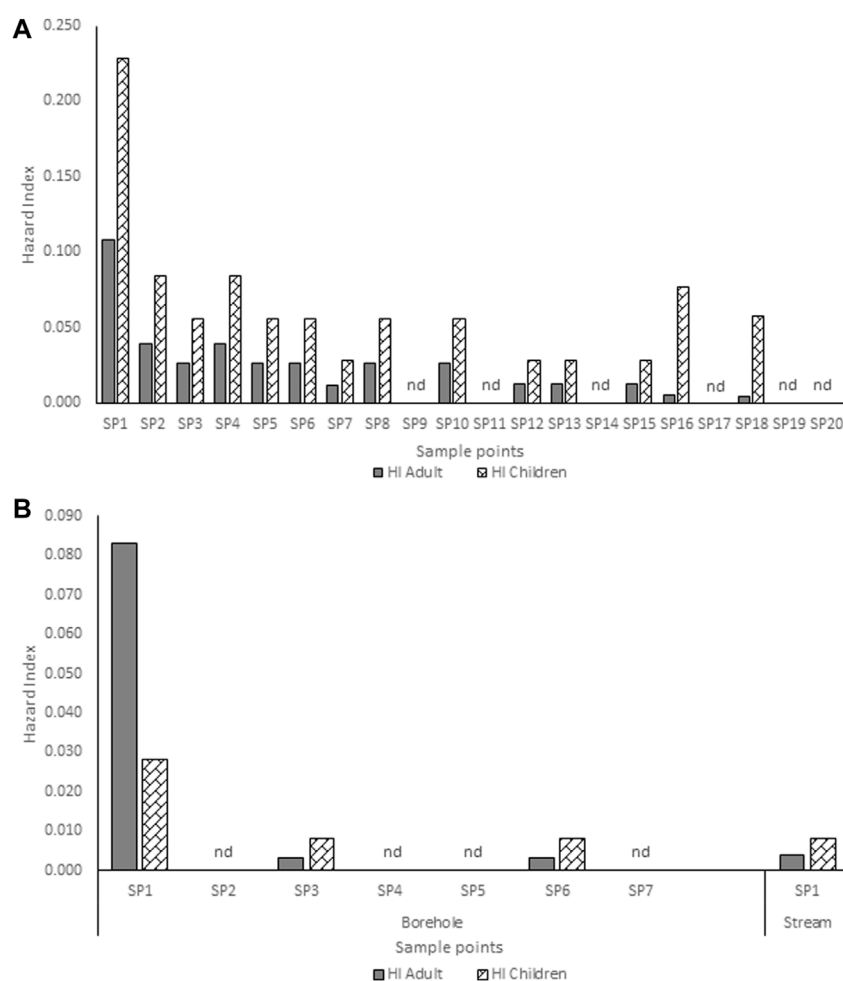
was observed to significantly ($p < 0.05$) increase in the experimental animals exposed to atrazine at 0.04 and 0.08 mg/L concentrations. However, there was no significant ($p > 0.05$) difference in the level of serum prolactin hormone in the control rats and those exposed to 0.01 mg/L and 0.03 mg/L concentrations of atrazine.

Levels of follicle-stimulating and luteinizing hormones in the experimental rats

The serum levels of FSH and LH of male albino rat exposed to atrazine concentrations in drinking water from Ijebu-North, Southwest Nigeria is shown in Figure 5. Although the level of the gonadotropic hormone was higher in all the rats exposed to the varying concentrations of atrazine, not significant ($p > 0.05$) compared to control.

Antioxidant enzymes activities in the testicular tissue of the experimental rats

Antioxidant enzyme activities and concentration of GSH in the testicular tissue of male albino rats exposed to atrazine concentrations in drinking water from Ijebu-North, Southwest Nigeria are shown in Table 2. A significant ($p < 0.05$) increase in SOD activity was observed in the testicular tissue of rats exposed to 0.03 mg/L and 0.04 mg/L concentrations of atrazine compared to other groups. On the other hand, the concentration of GSH was observed to significantly ($p < 0.05$) reduce in the experimental rats with an increase in the concentration of atrazine exposure. In a similar trend, CAT activity was significantly ($p < 0.05$) reduced only in rats exposed to a 0.08 mg/L concentration of atrazine. However, there was no significant difference ($p > 0.05$) in the CAT activity in the control rats and those exposed to 0.01, 0.03, and 0.04 mg/L concentrations of atrazine. Also, the activity of GPx

**FIGURE 3**

Hazard index for adults and children associated with exposure to atrazine concentrations in (A) hand-dug well (B) borehole and stream water from Ago-Iwoye community. SP-Sampling point; nd-non-detected.

observed in the control rats was not significantly different ($p > 0.05$) from that observed in the rats exposed to 0.01 mg/L and 0.03 mg/L concentrations of atrazine. However, GPx activity was significantly reduced ($p < 0.05$) in the rats exposed to a 0.08 mg/L concentration of atrazine.

Levels of reactive oxygen species (ROS) and lipid peroxidation in the testicular tissue

Levels of ROS and MDA in the testicular tissue of male albino rats exposed to atrazine concentrations in drinking water from Ijebu-North, Southwest Nigeria are shown in Figure 6. Although ROS generation and MDA levels were observed to increase with an increase in atrazine concentration, the levels of ROS and MDA recorded in the control rats were not significantly ($p > 0.05$)

different from those recorded in the rats exposed to 0.01 mg/L, 0.03 mg/L and 0.04 mg/L concentrations of atrazine. However, levels of ROS and MDA were significantly ($p < 0.05$) increased in the rats exposed to 0.08 mg/L concentrations of atrazine.

Activities of glutathione-S-transferase in the testicular tissue

The activity of GST in the testicular tissue of male albino rats exposed to atrazine concentrations in drinking water from Ijebu-North, Southwest Nigeria is shown in Figure 7. The enzyme activity was observed to significantly ($p < 0.05$) increase in all the rats exposed to varying concentrations of atrazine compared to control. GST activity was significantly increased in the testicular tissue of rats exposed to 0.03 and 0.04 mg/L concentrations of atrazine. But there was no significant difference ($p > 0.05$) in the

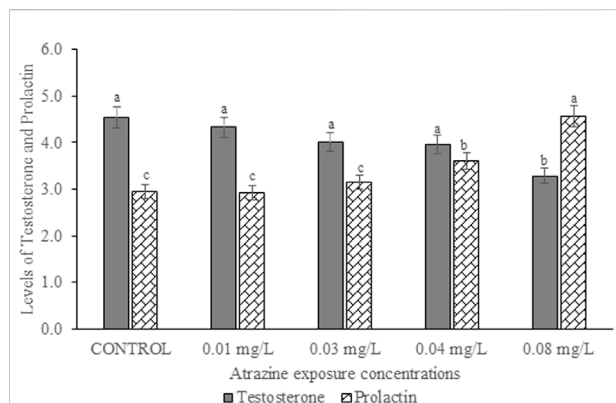


FIGURE 4

Levels of serum testosterone (ng/ml) and prolactin hormones (ng/ml) of male albino rat exposed to atrazine concentrations in drinking water from Ijebu-North, Southwest Nigeria; Error bars represent standard deviation; abc = bars with similar alphabets are not significantly different between the concentration ($p > 0.05$).

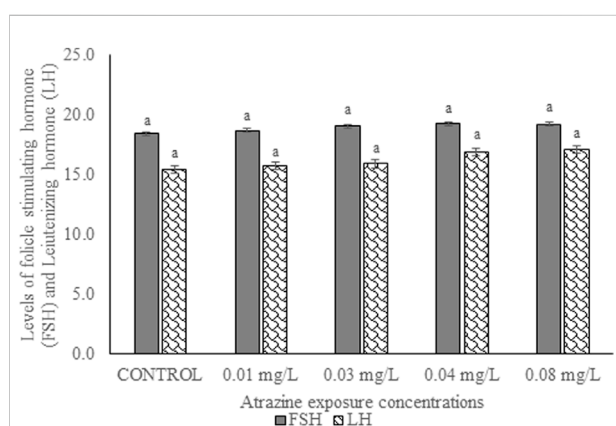


FIGURE 5

Levels of follicle-stimulating (mlu/mL) and luteinizing hormones (mlu/mL) of male albino rat exposed to atrazine concentrations in drinking water from Ijebu-North, Southwest Nigeria; Error bars represent standard deviation; abc = bars with similar alphabets are not significantly different between the concentration ($p > 0.05$).

enzyme activity in the testis of rats exposed to 0.01 and 0.08 mg/L concentrations of atrazine.

Activities of membrane-bound ATPase enzymes in the testis of albino rats

Activities of membrane-bound ATPase enzymes in the testis of albino rats exposed to atrazine concentrations in drinking water from Ijebu-North, Southwest Nigeria are represented in

Figure 8. Although the activity of Ca^{2+} ATPase was highest in the control rats, there were no significant ($p > 0.05$) differences in the activities of Ca^{2+} ATPase, Mg^{2+} ATPase, and $\text{Na}^{+}/\text{K}^{+}$ ATPase in the control rats and those exposed to 0.01, 0.03, 0.04 and 0.08 mg/L concentrations of atrazine.

Sperm motility and sperm count of the experimental rat

Sperm motility and sperm count of experimental rats exposed to atrazine concentrations in drinking water from Ijebu-North, Southwest Nigeria are shown in **Figure 9**. Percentage sperm motility was observed to significantly ($p < 0.05$) reduce in the experimental rats with an increase in the concentration of atrazine exposure. Sperm motility observed in control rats was not significantly ($p > 0.05$) different from that of rats exposed to a 0.01 mg/L concentration of atrazine. Also, the sperm motility observed in rats exposed to 0.04 mg/L and 0.08 mg/L atrazine concentration was not significantly ($p > 0.05$) different. Although sperm count was observed to reduce in the experimental rats with an increase in the concentration of atrazine exposure, the reduction was not significant ($p > 0.05$) compared to control.

Sperm morphology of male albino rat

The results of sperm abnormality assessment in rats exposed to atrazine concentrations in drinking water from Ijebu-North, Southwest Nigeria are displayed in **Table 3** and **Figure 10**. Total sperm abnormality and percentage abnormality were significantly ($p < 0.05$) increased in rats exposed to atrazine at 0.08 mg/L concentration. Also, sperm abnormalities were observed to significantly ($p < 0.05$) increase in the experimental rats with an increase in the concentration of atrazine exposure. However, the number of sperms with abnormal tails was observed to significantly contribute to the total abnormal sperm of the experimental rats. On the other hand, there were no significant ($p > 0.05$) differences in the number of sperms without hook, sperms with damaged head, and banana-shaped sperms recorded in the control rats and those exposed to 0.01, 0.03, 0.04, and 0.08 mg/L concentrations of atrazine.

Testicular cytoarchitectural examination

Figure 11 displays the photomicrographs of the testes of rats exposed to atrazine concentrations in drinking water from Ijebu-North, Southwest Nigeria. Normal testicular structure, characterized by darkly stained oval and round spermatogonia on the basement membrane with myofibroblast, was observed in control rats and those exposed to atrazine at 0.01, 0.03, and 0.04 mg/L concentrations. In addition, the spermatocytes and

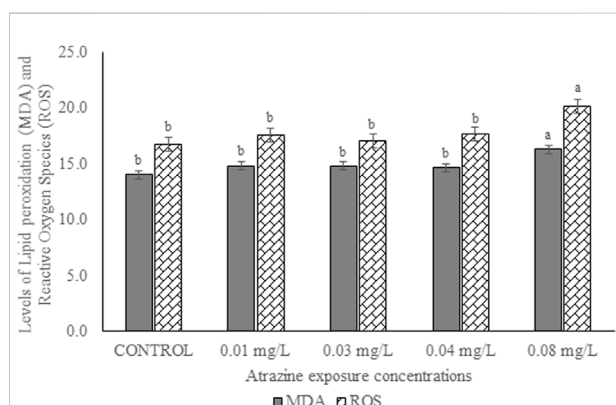
TABLE 2 Antioxidant enzymes activities in the testicular tissue of male albino rat exposed to atrazine concentrations in drinking water from Ijebu-North, Southwestern Nigeria.

Treatments	SOD (U/mg protein)	GSH (U/g tissue)	CAT (U/mg protein)	GPx (U/mg protein)
Control	6.96 ± 1.49 ^c	11.56 ± 2.22 ^a	13.33 ± 0.75 ^a	19.74 ± 1.12 ^a
0.01 mg/L	8.98 ± 1.26 ^b	10.17 ± 0.69 ^b	12.19 ± 1.49 ^a	19.37 ± 0.82 ^a
0.03 mg/L	10.24 ± 0.81 ^a	8.85 ± 0.47 ^c	13.04 ± 7.32 ^a	18.15 ± 0.72 ^a
0.04 mg/L	10.50 ± 0.99 ^a	8.69 ± 0.51 ^c	13.16 ± 1.57 ^a	16.27 ± 1.27 ^b
0.08 mg/L	8.35 ± 0.42 ^b	7.76 ± 0.48 ^c	11.29 ± 1.26 ^b	10.32 ± 1.88 ^c

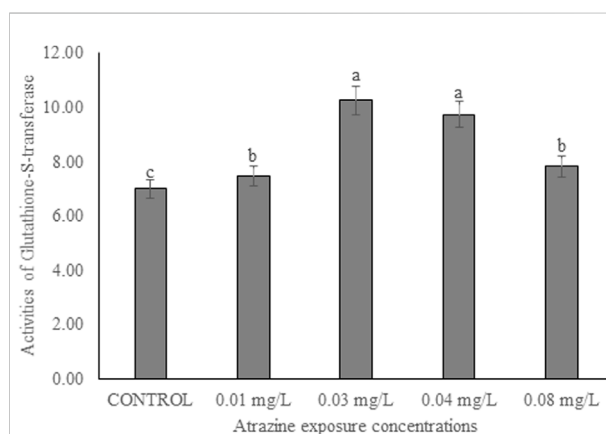
^aMean values (±Standard deviation) in the same column having similar superscripts are not significantly different ($p > 0.05$); SOD, Superoxide dismutase; GPx, Glutathione peroxidase; GSH, Reduced glutathione

^bMean values (±Standard deviation) in the same column having similar superscripts are not significantly different ($p > 0.05$); SOD, Superoxide dismutase; GPx, Glutathione peroxidase; GSH, Reduced glutathione

^cMean values (±Standard deviation) in the same column having similar superscripts are not significantly different ($p > 0.05$); SOD, Superoxide dismutase; GPx, Glutathione peroxidase; GSH, Reduced glutathione

**FIGURE 6**

Levels of ROS (nmol/DCF/g tissue/min) and MDA (nmol/g tissue) in the testes of male albino rat exposed to atrazine concentrations in drinking water from Ijebu-North, Southwest Nigeria; Error bars represent standard deviation; abc = bars with similar alphabets are not significantly different between the concentration ($p > 0.05$).

**FIGURE 7**

Activities of glutathione-S-transferase (U/mg protein) in the testicular tissue of male albino rat exposed to atrazine concentrations in drinking water from Ijebu-North, Southwestern Nigeria.

spermatids are well seen with a large number of spermatozoa found in the lumen of the seminiferous tubule. The Leydig cells appear normal within the interstitium. Meanwhile, mild disoriented seminiferous tubule, as well as displacement and depletion of spermatogonia, spermatocytes, and spermatids with uneven resting of spermatogonia along the membranes, were observed in the testes structure of rats exposed to atrazine at 0.08 mg/L concentration.

Discussion

The concentrations of atrazine detected in water from Oru and Ilaporu communities were all below the MAC of 0.005 mg/L

established by Canada and 0.003 mg/L established by the United States EPA. Hand-dug well from Ijebu-Igbo contained atrazine concentration up to the MAC of United States EPA. Meanwhile, well waters from Awa and Mamu communities both recorded atrazine concentration that is above the United States EPA limit, but lower than the limit set by Canada. However, the concentration of atrazine above the United States EPA and Canada limits was detected in sampling point 1 of the hand-dug well from the Ago-Iwoye community. This is an indication that hand-dug well water from Awa, Mamu, and Ago-Iwoye communities is polluted with atrazine herbicide. The higher level of atrazine observed in the hand-dug well water from Awa, Mamu, and Ago-Iwoye could be attributed to the possible higher use of atrazine in these farming communities since a high level of atrazine detected in some sites was attributed to the

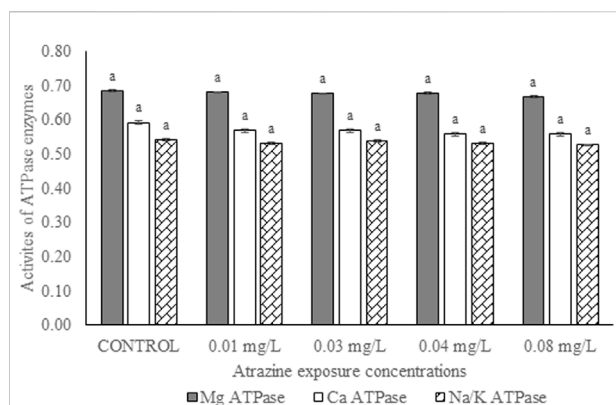


FIGURE 8

Activities of ATPase enzymes ($\mu\text{g pi liberated/min/mg protein}$) in the testis of male albino rats exposed to atrazine concentrations in drinking water from Ijebu-North, Southwest Nigeria; Error bars represent standard deviation; abc = bars with similar alphabets are not significantly different between the concentration ($p > 0.05$).

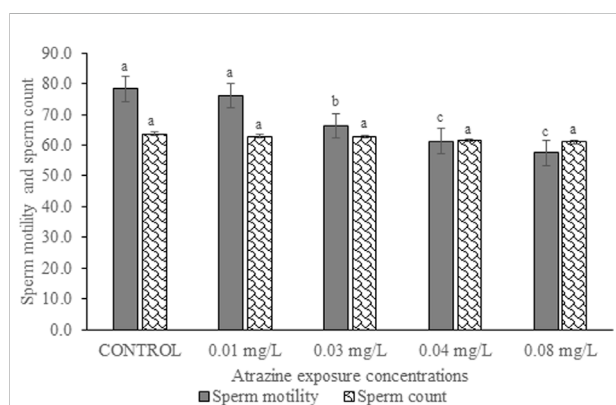


FIGURE 9

Sperm motility (%) and sperm count ($\times 10^6$ cells/ml) of rats exposed to atrazine concentrations in drinking water from Ijebu-North, Southwest Nigeria; Error bars represent standard deviation; abc = bars with similar alphabets are not significantly different between the concentration ($p > 0.05$).

higher use of the herbicide (Sun et al., 2017). Meanwhile, variations and reductions in atrazine concentration detected in water were observed as we moved away from the farm villages of each community. This may be due to the geographical structure, depth of the hand-dug well as well as agricultural activities of the sampled area, which have been reported to influence the spatial distribution of atrazine (Sun et al., 2017; Almasi et al., 2020). The influence of depth on the concentration of atrazine detected in hand-dug well is a possibility. Since the concentration of atrazine in the boreholes was lower than that recorded in the well, it is expected that the depth of boreholes will be greater than that of hand-dug wells.

The HQ values for non-carcinogenic effect through ingestion and dermal routes of exposure for adults and children were less than 1 in all of the community. This indicates that the water from each of the communities may be safe for domestic use. However, the HQ values through the exposure routes for children were higher than that of adults. Our findings confirm Almasi et al. (2020) and Dehghani et al. (2022) who documented higher HQ values for the two exposure routes in adults and children. HQ values for children through dermal contact ranges from 0.001 to 0.030 in Ijebu-Igbo; 0.001 to 0.082 in Ago-Iwoye; 0.001 to 0.010 in Oru; 0.000102 to 0.040 in Awa and 0.001 to 0.041 in Mamu. While for adults, it ranged from 0.002 to 0.016 in Ijebu-Igbo; 0.001 to 0.045 in Ago-Iwoye; 0.001 to 0.006 in Oru; 0.00056 to 0.023 in Awa and 0.0006 to 0.023 in Mamu. This shows that dermal contact poses a higher risk for children than adults. In addition, Ago-Iwoye and Awa communities are more contaminated and pose the highest risk of water use. But here in this study, we did not evaluate the health risk arising from ingestion of atrazine through food such as corn, as this can also increase the health risk (Sánchez et al., 2019). Thus, our findings in this study should be applied with caution.

The present study shows a significant reduction in the serum level of testosterone hormone only in rats exposed to atrazine at 0.08 mg/L, but no significant difference in the hormone level was observed between control and those exposed to atrazine at 0.01, 0.03, and 0.04 mg/L. Our finding is, in part, supported by Stoker et al. (2000), Stoker et al. (2002) and Abarikwu et al. (2015) who observed no effect on plasma testosterone levels in rats following exposure to atrazine at 12.5 mg/kg. However, Victor-Costa et al. (2010) reported decreased testosterone levels in rats at higher doses of atrazine. A high level of prolactin or hyperprolactinemia observed in rats exposed to atrazine at 0.04 and 0.08 mg/L may possibly explain their reduced testosterone level. Although hyperprolactinemia impairs the proper function of the male gonad by either decreasing the pulse generating activity of gonadotropin-releasing hormone (GnRH) or directly inhibiting the secretion of testosterone at the Leydig cells (Horseman et al., 2006), the insignificant increase in FSH and LH of the exposed rats suggests a dysfunction in the testis of the exposed rats. On the contrary, exposure to atrazine at 200 mg/kg in rats was observed to inhibit GnRH, consequently affecting the synthesis of LH and FSH (Foradori et al., 2013; Wirbisky and Freeman, 2015). Furthermore, a decreased serum LH and FSH in rats exposed to atrazine at 200 and 400 mg/kg has been witnessed (Trentacoste et al., 2001; Mokhtari et al., 2011).

Oxidative stress biomarkers (MDA), the concentration of GSH, and antioxidant enzymes were studied in the testis of rats exposed to atrazine. Exposure to atrazine at concentrations found in water from Ijebu-North induced an increase in MDA level with an increase in atrazine concentration mostly at 0.08 mg/L. This might suggest oxidative stress at this concentration. SOD, an endogenous scavenger that dismutates superoxide radical, was observed to increase at 0.03 and 0.04 mg/L of atrazine exposure

TABLE 3 Sperm morphology of male albino rat exposed to atrazine concentrations in drinking water from Ijebu-North, Southwestern Nigeria.

Parameters	Control	0.01 mg/L	0.03 mg/L	0.04 mg/L	0.08 mg/L
Abnormal Tail	10.40 ± 1.52 ^d	10.80 ± 1.48 ^d	31.20 ± 2.59 ^c	40.20 ± 1.92 ^b	45.20 ± 4.49 ^a
Without head	0.20 ± 0.45 ^c	0.80 ± 0.84 ^b	1.20 ± 1.30 ^b	1.60 ± 1.14 ^b	2.60 ± 1.14 ^a
Damaged Head	0.80 ± 0.84 ^a	1.00 ± 0.71 ^a	1.40 ± 0.89 ^a	1.40 ± 0.89 ^a	1.60 ± 0.55 ^a
Without hook	0.80 ± 0.84 ^a	1.00 ± 0.71 ^a	1.20 ± 0.84 ^a	1.60 ± 0.55 ^a	1.60 ± 0.55 ^a
Banana shaped	1.40 ± 1. ^a	2.20 ± 0.45 ^a	2.80 ± 1.48 ^a	3.20 ± 1.30 ^a	3.60 ± 1.52 ^a
Without Tail	1.00 ± 1.22 ^d	1.00 ± 0.71 ^d	9.80 ± 3.70 ^c	21.00 ± 3.16 ^b	25.00 ± 2.24 ^a
Total Abnormal	14.60 ± 2.30 ^d	16.80 ± 2.59 ^d	47.60 ± 1.95 ^c	70.00 ± 4.85 ^b	77.60 ± 6.07 ^a
% Abnormality	1.46 ± 0.23 ^d	1.68 ± 0.26 ^d	4.76 ± 0.19 ^c	7.00 ± 0.48 ^b	7.76 ± 0.61 ^a

^aMean values (±Standard deviation) in the same column having similar superscripts are not significantly different ($p > 0.05$).

^bMean values (±Standard deviation) in the same column having similar superscripts are not significantly different ($p > 0.05$).

^cMean values (±Standard deviation) in the same column having similar superscripts are not significantly different ($p > 0.05$).

^dMean values (±Standard deviation) in the same column having similar superscripts are not significantly different ($p > 0.05$).

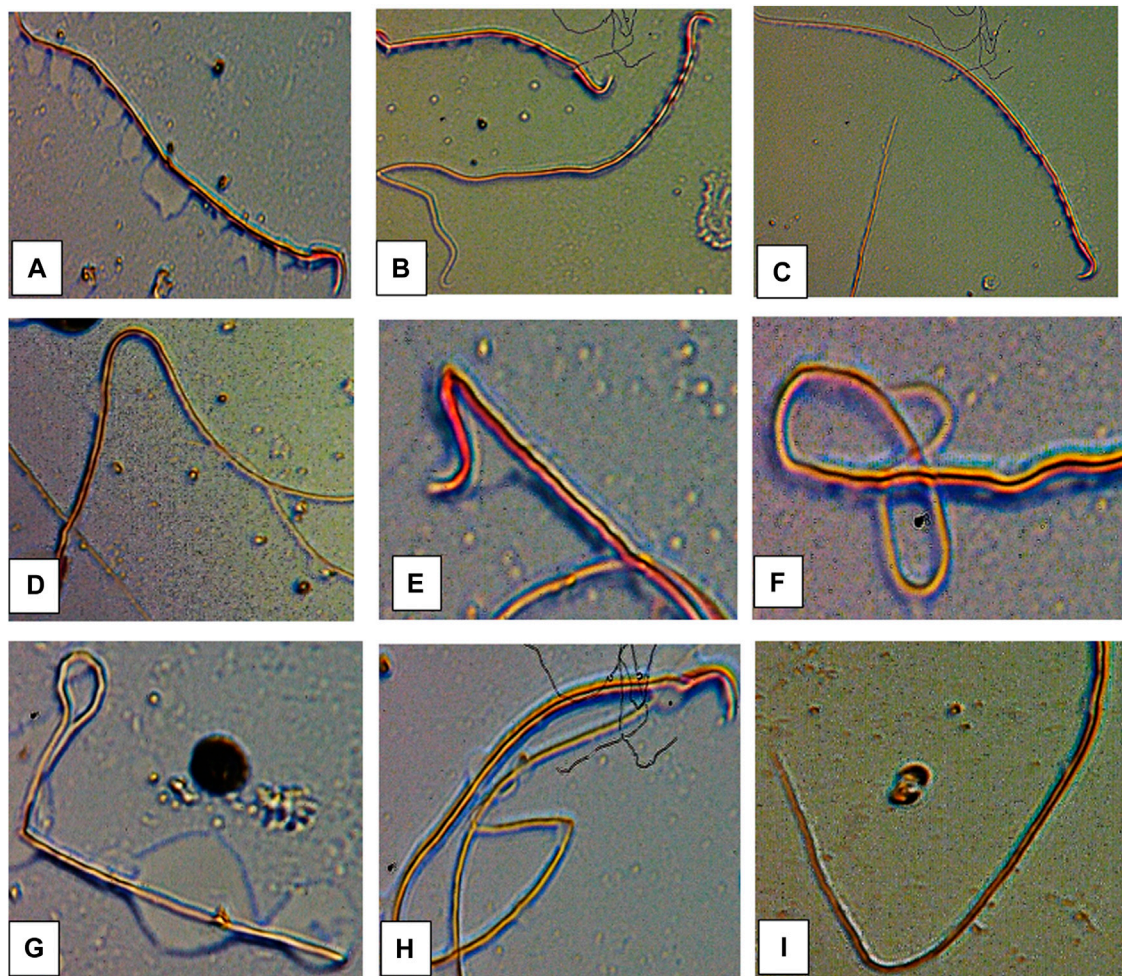


FIGURE 10

Abnormal sperm cells induced in rats exposed to atrazine (A) normal sperm cell (B) sperm with abnormal tail (C) normal sperm cell (D) sperm with bent body (E) sperm with damaged head (F) sperm with bent tail (G) bent tail with damaged head (H) banana shape (I) bent tail.

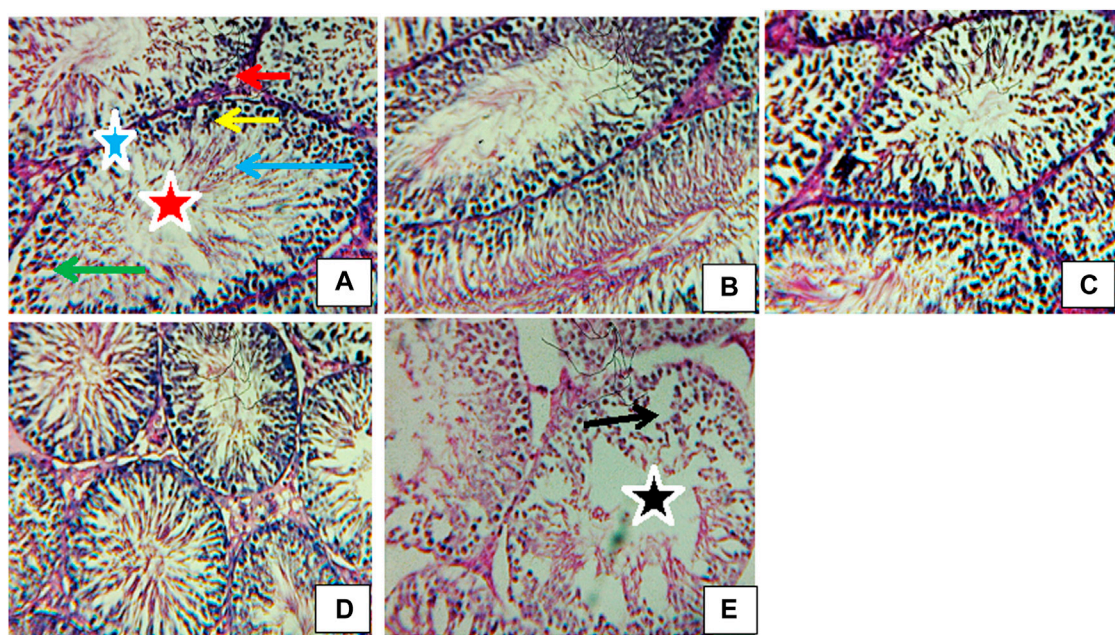


FIGURE 11

Transverse section of testes (H&E stain; x 400) of (A) control revealing normal structure spermatogonia (yellow arrow), spermatids (green arrow), spermatozoa (blue arrow), Leydig cells (red arrow), myofibroblasts (blue star), lumen (red star). (B) Rat exposed to atrazine at 0.01 mg/L revealing a normal structure similar to control. (C) Rat exposed to atrazine at 0.03 mg/L revealing normal structure similar to control (D) rat exposed to atrazine at 0.04 mg/L revealing normal structure similar to control (E) rat exposed to atrazine at 0.08 mg/L revealing mild disoriented seminiferous tubule (black star) as well as displacement and depletion of spermatogonia, spermatocytes and spermatids (black arrow) with uneven resting of spermatogonia along the membranes.

but decrease at 0.08 mg/L concentration. The decrease in SOD activity may be due to the inactivation of SOD by interaction with oxygen radicals (Kaushik and Kaur, 2003). Catalase is known to scavenge hydrogen peroxide at higher concentrations (Alptekin et al., 1996) and at lower concentrations by GPx (Cohen and Hochstein, 1963). In this study, the relative contributions of CAT and GPx in the decomposition of hydrogen peroxide are concentration-specific with CAT being more potent at 0.01, 0.03, and 0.04 mg/L of atrazine concentration but at 0.08 mg/L, while GPx is being impotent at the increasing concentration of atrazine. An increased CAT activity observed in the testes of atrazine-exposed rats signifies that the enzyme is more responsive to the increased hydrogen peroxide concentration in the testes tissue, therefore, emphasizing its role in the control of cellular lipid peroxide concentration (Spasic' et al., 1993). This is very important and significant, especially in the maintenance of cellular proliferation and differentiation in the testes. The decreased activity of GPx in the testes of the atrazine-exposed rats indicates its inability or reduced capacity to scavenge hydrogen peroxide generated in the tissue in response to atrazine exposure. Our finding is, in part, supported by Singh et al. (2010) and Qian et al. (2008) who found increased activities of CAT and SOD as a compensatory or adaptive mechanism in response to oxidative stress induced by atrazine. This claim is

reflected in the insignificant alteration seen in the testicular MDA level of the atrazine-exposed rats at 0.01, 0.03, and 0.04 mg/L, which enables us to suggest that the antioxidant defence system in the testes protects the organ from ROS induced by the herbicide. Meanwhile, our finding partially contradicts Abarikwu et al. (2014) who reported a decreased SOD activity, unchanged GSH concentration and increased MDA level in the testes of rats exposed to atrazine at 120 mg/kg, but CAT activity was unaffected (Abarikwu et al., 2010).

GST is one of the primary detoxification enzymes and a rise in the activity of this enzyme may therefore indicate its ability to rapidly detoxify environmental xenobiotics. In addition, a rise in the GST activity observed in the testis of rats in response to atrazine exposure is accompanied by a significant reduction in its GSH concentration suggesting a rise in conjugation reactions. While Kaushik and Kaur (2003) suggested that a decreased GSH concentration may directly result from a reduction in its synthesis or an increase in its breakdown during stress, Simmons et al. (1990) and Alptekin et al. (1996) attributed a decreased GSH concentration to increased lipid peroxidation. But here in this study, increased consumption of GSH in conjugation reactions due to increased GST seems to explain the GSH concentration reductions in the testis of atrazine-exposed rats. This is understandable since the detoxification of

pesticides is mainly through a reaction catalyzed by GST, which utilizes GSH. On the contrary, a decreased GST activity and unchanged GSH concentration in the testes of rats exposed to 120 and 200 mg/kg atrazine after 16 days has been reported (Abarikwu et al., 2010).

As reported by Kempaiah and Srinivasan (Kempaiah and Srinivasan, 2006), membrane-bound ATPase enzymes are good markers of membrane dysfunctions under oxidative stress. The enzymes supply energy via hydrolytic reaction to control membrane permeability and transportation of ions such as Ca^{2+} , K^{+} , and Na^{+} across the membrane (Langeswaran et al., 2012). We showed for the first time in the present study that exposure to atrazine at 0.01, 0.03, 0.04, and 0.08 mg/L has no significant effect on the activities of membrane-bound ATPases in the testes of exposed rats. This suggests that atrazine at those concentrations may not disturb the ion homeostasis of the testes or alter cellular metabolism. Atrazine at those concentrations may not also change cell membrane integrity and permeability or induce a rise in membrane fluidity and disturbances in vital functions (Chodon et al., 2008).

A significant reduction in percentage sperm motility was observed in the experimental rats with an increase in the concentration of atrazine exposure. However, sperm count was relatively unaffected in the experimental rats. Our finding is, in part, supported by Kniewald et al. (2000) and Abarikwu et al. (2014) who observed a decrease in sperm count and motility in rats exposed to atrazine. Atrazine seems to target the sperm tail of the experimental rats since the number of sperms with the abnormal tail was observed to significantly contribute to the total abnormal sperm of the experimental rats. This may possibly explain the low motility observed in the sperm. Although the mechanism underlying the tail abnormality by atrazine is unknown in the present study, a further mechanism-based approach study focusing on this area is hereby recommended. However, atrazine did not induce significant sperm head abnormalities in this present study. Our findings on sperm morphology agree with Abarikwu et al. (2014) who reported insignificant head abnormalities of sperms, but higher sperm tail and midpiece abnormalities in rats exposed to atrazine at 120 mg/kg.

The observed mild changes in the testicular cytoarchitectural structure of rats exposed to atrazine at 0.08 mg/L may indicate mild toxicity to the male reproductive system of the rats, which may consequently interfere with the spermatogenesis process (Thakur et al., 2014). Although a concentration-dependent increase in sperm motility and morphology was observed in rats exposed to atrazine at 0.01, 0.03, and 0.04 mg/L concentrations, unlike atrazine at 0.08 mg/L, the testicular antioxidant defence was strong enough to protect the structural integrity of the testes of rats exposed to these concentrations.

Conclusion

Our findings show the presence of atrazine residue in HDW, boreholes, and stream waters from the communities in Ijebu-North LGA, southwest Nigeria. The HI values for non-carcinogenic effect via ingestion and dermal routes for children and adults were below the acceptable limit for all the communities. But children from the LGA seem to be more at risk than adults. In addition, Ago-Iwoye and Awa communities were more contaminated and may pose the highest risk of water use. Atrazine at environmentally relevant concentrations of 0.01, 0.03, and 0.04 mg/L was observed to induce testicular antioxidant defence capable of protecting the tissue against oxidative damage, degenerative lesions, and reproductive dysfunction. However, atrazine at 0.08 mg/L may induce mild reproductive toxicity in the exposed animal. As part of the requirements of FQPA on water quality assessment, this is the first study to monitor the level of atrazine in water from HDW, boreholes, and streams of rural areas in Nigeria and could contribute to the establishment of MCL of atrazine in drinking water in Nigeria. This study could also contribute to the ongoing USDA Pesticide Data Program monitoring for pesticide residues in food and water. We recommend prompt intervention by the regulatory agencies and policymakers on the use of atrazine herbicide in rural agricultural areas of Ijebu-North southwest, Nigeria. In addition, there is a need to further analyse the testis of the exposed animal for any evidence of atrazine accumulation. Since the exposure to atrazine concentrations for 12 weeks (sub-chronic toxicity study) in the present study was observed to induce little or no effect on the testis, there is a need for chronic exposure to the same atrazine concentrations in the future study.

Data availability statement

The raw data supporting the conclusion of this article will be made available by the authors, without undue reservation.

Ethics statement

The animal study was reviewed and approved by the local ethics committee in the Animal Care Unit (ACU) of Olabisi Onabanjo University (OOU/SCIENG/EC/0003/140621).

Author contributions

Conceptualization (FO; GD; and OL); methodology, (FO; GD; and OL); Formal analysis and investigation (FO; RO; OA; MA; TS; AA; AS); Writing Original draft preparation, (FO);

Writing review and editing (All the authors); Resources, (RO; OA; MA; TS); Supervision, (GD and OL).

Acknowledgments

The management of Olabisi Onabanjo University and the Department of Zoology and Environmental Biology granted us permission to use its facilities for this study.

Conflict of interest

The authors declare that the research was conducted in the absence of any commercial or financial relationships that could be construed as a potential conflict of interest.

References

- Abarikwu, S. O., Adesiyun, A. C., Oyeloja, T. O., Oyeyemi, M. O., and Farombi, E. O. (2010). Changes in sperm characteristics and induction of oxidative stress in the testis and epididymis of experimental rats by a herbicide, atrazine. *Arch. Environ. Contam. Toxicol.* 58, 874–882. doi:10.1007/s00244-009-9371-2
- Abarikwu, S. O., Akiri, O. F., Durojaiye, M. A., and Adenike, A. (2014). Combined effects of repeated administration of Bretmont Wipeout (glyphosate) and Ultrazin (atrazine) on testosterone, oxidative stress and sperm quality of Wistar rats. *Toxicol. Mech. Methods* 25, 70–80. doi:10.3109/15376516.2014.989349
- Abarikwu, S. O., Akiri, O. F., Durojaiye, M. A., and Adenike, A. (2015). Combined effects of repeated administration of Bretmont Wipeout (glyphosate) and Ultrazin (atrazine) on testosterone, oxidative stress and sperm quality of Wistar rats. *Toxicol. Mech. Methods* 25, 70–80. doi:10.3109/15376516.2014.989349
- Adeite, A. (2021). Maize farming in Nigeria: Exciting facts you should know. Available at: <https://babbangona.com/maize-farming-in-nigeria-exciting-facts-you-should-know/> (Assessed January 10, 2022).
- Aebi, H. (1984). Catalase *in vitro* Methods. *Enzym.* 105, 121–126. doi:10.1016/s0076-6879(84)05016-3
- Almasi, H., Takdastanb, A., Jaafarzadeh, N., Babaeib, A. A., Birganib, Y. T., Cheraghianc, B., et al. (2020). Spatial distribution, ecological and health risk assessment and source identification of atrazine in Shadegan international wetland, Iran. *Mar. Pollut. Bull.* 160, 111569. doi:10.1016/j.marpolbul.2020.111569
- Alptekin, N., Seckin, S., Yelkenci, F., Toker, N. K., Toker, G., Uysal, M., et al. (1996). Lipid peroxides, glutathione, gamma-glutamylcysteine synthetase and gamma-glutamyltranspeptidase activities in several tissues of rats following water-immersion stress. *Pharmacol. Res.* 34, 167–169. doi:10.1006/phrs.1996.0084
- Asada, K., Takahashi, M., and Nagate, M. (1974). Assay and inhibitors of spinach superoxide dismutase. *Agric. Biol. Chem.* 38, 471–473. doi:10.1080/00021369.1974.10861178
- Bakare, A. A., Mosuro, A. A., and Osibanjo, O. (2005). An *in vivo* evaluation of induction of abnormal sperm morphology in mice by land fill leachates. *Mutat. Res.* 582, 28–34. doi:10.1016/j.mrgentox.2004.12.007
- Chodon, D., Arumugam, A., Rajasekaran, D., and Dhanapal, S. (2008). Effect of genistein on modulating lipid peroxidation and membrane-bound enzymes in N-Nitrosodiethylamine-induced and Phenobarbital-promoted rat liver carcinogenesis. *J. Health Sci.* 54 (2), 137–142. doi:10.1248/jhs.54.137
- Cohen, G., and Hochstein, P. (1963). Glutathione peroxidase: The primary agent for the elimination of H₂O₂ in erythrocytes. *Biochemistry* 2, 1420–1428. doi:10.1021/bi00906a038
- Dedeke, G. A., Owagboriaye, F. O., Ademolu, K. O., Olujimi, O. O., and Aladesida, A. A. (2018). Comparative assessment on mechanism underlying renal toxicity of commercial formulation of roundup herbicide and glyphosate alone in male albino rat. *Int. J. Toxicol.* 37 (4), 285–295. doi:10.1177/109158181779553
- Dehghani, M., Gharehchahi, E., Jafari, S., Moeini, Z., Derakhshan, Z., Ferrante, M., et al. (2022). Health risk assessment of exposure to atrazine in the soil of Shiraz farmlands, Iran. *Environ. Res.* 204, 112090. doi:10.1016/j.envres.2021.112090
- EPA (1989). *Risk assessment guidance for superfund. Volume I: Human health evaluation manual (part A)*. Washington, DC: Office of Emergency and Remedial Response, U.S. Environmental Protection Agency. EPA/540/1-89/002
- Farmsquare (2020). ATRAFORCE (Selective Herbicide). Available at: <https://farmsquare.ng/shop/atrafence-selective-herbicide/> (Retrieved September 17, 2020).
- Focazio, M. J., Tipton, D., Dunkle Shapiro, S., and Geiger, L. H. (2006). The chemical quality of self-supplied domestic well water in the United States. *Ground Water Monit. Remediat.* 26 (3), 92–104. doi:10.1111/j.1745-6592.2006.00089.x
- Foradori, C. D., Zimmerman, A. D., Hinds, L. R., Zuloaga, K. L., Breckenridge, C. B., and Handa, R. J. (2013). Atrazine inhibits pulsatile gonadotropin-releasing hormone (GnRH) release without altering GnRH messenger RNA or protein levels in the female Rat1. *Biol. Reprod.* 88, 1–7. doi:10.1095/biolreprod.112.102277
- Habig, W. H., Pabst, M. J., and Jakoby, W. B. (1974). Glutathione S-transferases. *J. Biol. Chem.* 249 (22), 7130–7139. doi:10.1016/s0021-9258(19)42083-8
- Hassan, A. M., and Barakat, A. H. (2008). Assessment of oxidative stress induced by nickel chloride and antioxidant effects of basil (*ocimum basilicum* L) and thyme (*thymus vulgaris* L). *J. Genet. Eng Biotech* 6 (2), 29–38.
- Hayes, T. B. (2004). There is no denying this: Defusing the confusion about atrazine. *Bioscience* 54, 1138–1149. doi:10.1641/0006-3568(2004)054[1138:tindtd]2.0.co;2
- Health Canada (1993). Guidelines for Canadian drinking water quality guideline technical document atrazine.
- Health Canada (2010). *Federal contaminated site risk assessment in Canada, Part V: Guidance on human health detailed quantitative risk assessment for chemicals (DQRACChem.)*. ON, Canada: Health Canada Ottawa.
- Horseman, N. D., and Gregerson, K. A. (2006). “Prolactin,” in *Endocrinology*. Editors L. J. DeGroot and J. L. Jameson (Philadelphia: Elsevier Saunders), 309–321.
- Huang, S. B., Tanton, J. S., Lin, Y., and Yokley, R. A. (2003). Analytical method for the determination of atrazine and its dealkylated chlorotriazine metabolites in water using SPE sample preparation and GC-MSD analysis. *J. Agric. Food Chem.* 51, 7252–7258. doi:10.1021/jf0349578
- Hussain, R., Mahmood, F., Khan, M. Z., Khan, A., and Muhammad, F. (2011). Pathological and genotoxic effects of atrazine in male Japanese quail (*Coturnix japonica*). *Ecotoxicology* 20, 1–8. doi:10.1007/s10646-010-0515-y
- Kaushik, S., and Kaur, J. (2003). Chronic cold exposure affects the antioxidant defense system in various rat tissues. *Clin. Chim. Acta.* 333, 69–77. doi:10.1016/s0009-8981(03)00171-2
- Kempaiiah, R. K., and Srinivasan, K. (2006). Beneficial influence of dietary curcumin, capsaicin and garlic on erythrocyte integrity in high-fat fed rats. *J. Nutr. Biochem.* 17, 471–478. doi:10.1016/j.jnutbio.2005.09.005
- Kniwald, J., Jakominic, M., Tomljenovic, A., Simic, B., Romac, P., Vranesic, D., et al. (2000). Disorders of male rat reproductive tract under the influence of atrazine. *J. Appl. Toxicol.* 20, 61–68. doi:10.1002/(sici)1099-1263(200001/02)20:1<61::aid-jat628>3.0.co;2-3

Publisher's note

All claims expressed in this article are solely those of the authors and do not necessarily represent those of their affiliated organizations, or those of the publisher, the editors and the reviewers. Any product that may be evaluated in this article, or claim that may be made by its manufacturer, is not guaranteed or endorsed by the publisher.

Supplementary material

The Supplementary Material for this article can be found online at: <https://www.frontiersin.org/articles/10.3389/ftox.2022.975636/full#supplementary-material>

- Koterba, M. T., Wilde, F. D., and Lapham, W. W. (1995). Ground-water data-collection protocols and procedures for the national water-quality assessment Program: Collection and documentation of water-quality samples and related data. *U.S. Geol. Surv.* 95, 399 doi:10.3133/ofr95399
- Langeswaran, K., Jagadeesan, A. J., and Balasubramanian, M. P. (2012). Modulation of membrane bound ATPases and metabolizing enzymes against N-Nitrosodiethylamine (DEN) induced primary liver cancer in Wistar albino rats. *Int. J. Pharma Bio Sci.* 3 (2), 156–165.
- Lowry, O. H., Rosebroug, N. J., Farr, A. L., and Randall, R. J. (1951). Protein measurement with the Folin phenol reagent. *J. Biol. Chem.* 193, 265–275. doi:10.1016/s0021-9258(19)52451-6
- McElroy, W. K., Goldman, J. M., Tyrey, L., Stoker, T. E., and Cooper, R. L. (2000). Atrazine disrupts the hypothalamic control of pituitary-ovarian function. *Toxicol. Sci.* 53, 297–307. doi:10.1093/toxsci/53.2.297
- MDH. Human Health (2009). *Assessment: Atrazine report for the Minnesota*. St. Paul, MN: Department of Health.
- Mokhtari, M., Sharifi, E., and Soltani, A. (2011). Effects of atrazine toxin on levels of LH, FSH and testosterone hormones in adult male rat. *Nat. Environ. Pollut. Technol.* 10 (2), 201–206.
- National Population Commission (2016). Nigeria: Administrative division States and local government area. Available at: <https://www.citypopulation.de/php/nigeria-admin.php> (Accessed February 17, 2020).
- Necheles, T. F., Boles, T. A., and Allen, D. M. (1968). Erythrocyte glutathione-peroxidase deficiency and hemolytic disease of the newborn infant. *J. Pediatr.* 72, 319–324. doi:10.1016/s0022-3476(68)80202-1
- Okhawa, H., Ohishi, N., and Yagi, K. (1979). Assay for lipid peroxides in animal tissues by thiobarbituric acid reaction. *Anal. Biochem.* 95, 351–358. doi:10.1016/0003-2697(79)90738-3
- Ontario Ministry of the Environment (1987). *Pesticides in Ontario drinking water — 1985*. Toronto: Ontario Ministry of the Environment, Water Resources Branch, Drinking Water Section.
- Owagboriaye, F. O., Aina, S. A., Oladunjoye, R. Y., Salisu, T., and Adenekan, A. (2021). Insights into the potential mechanism underlying liver dysfunction in male albino rat exposed to gasoline fumes. *Egypt. J. Basic Appl. Sci.* 8 (1), 302–316. doi:10.1080/2314808X.2021.1992118
- Owagboriaye, F. O., Aina, S. A., Salisu, T., Oladunjoye, R. Y., Adenekan, A., Aladesida, A. A., et al. (2022). Insights into the mechanism underlying reproductive toxicity of gasoline fumes in male albino rat. *Comp. Clin. Path.* 31, 439–452. doi:10.1007/s00580-022-03343-3
- Owagboriaye, F. O., Dedeke, G. A., Ademolu, K. O., Olujimi, O. O., Ashidi, J. S., and Aladesida, A. A. (2017). Reproductive toxicity of Roundup herbicide exposure in male albino rat. *Exp. Toxicol. Pathol.* 69, 461–468. doi:10.1016/j.etp.2017.04.007
- Pérez-Severiano, F., Santamaría, A., Pedraza-Chaverri, J., Medina-Campos, O. N., Ríos, C., and Segovia, J. (2004). Increased formation of reactive oxygen species, but no changes in glutathione peroxidase activity, in striata of mice transgenic for the Huntington's disease mutation. *Neurochem. Res.* 29, 729–733. doi:10.1023/b:ncere.0000018843.83770.4b
- Qian, H. F., Sheng, G. D., Liu, W. P., Lu, Y. C., Liu, Z. H., and Fu, Z. W. (2008). Inhibitory effects of atrazine on *Chlorella vulgaris* as assessed by real-time polymerase chain reaction. *Environ. Toxicol.* 27, 182–187. doi:10.1897/07-163.1
- Quackenboss, J. J., Pellizzari, E. D., Shubat, P., Whitmore, R. W., Adgate, J. L., Thomas, K. W., et al. (2000). Design strategy for assessing multi-pathway exposure for children: The Minnesota children's pesticide exposure study (MNCPPES). *J. Expo. Anal. Environ. Epidemiol.* 10 (2), 145–158. doi:10.1038/sj.jea.7500080
- Resources, M. D. N. (2006). *Departmental Missouri risk-based corrective action (MRBCA) technical guidance (appendices), table B-1, lowest default target levels, all soil types and all pathways*. Washington, DC: Missouri Department of Natural Resources.
- Rey, F., Gonzalez, M., Zayas, M. A., Stoker, C., Durando, M., Luque, E. H., et al. (2009). Prenatal exposure to pesticides disrupts testicular histoarchitecture and alters testosterone levels in male *Caiman latirostris*. *Gen. Comp. Endocrinol.* 162, 286–292. doi:10.1016/j.ygcen.2009.03.032
- Ritter, W. F. (1990). Pesticide contamination of ground water in the United States—a review. *J. Environ. Sci. Health.* B 25 (1), 1–29. doi:10.1080/03601239009372674
- Romano, R. M., Romano, M. A., Bernardi, M. M., Furtado, P. V., and Oliveira, C. A. (2010). Prepubertal exposure to commercial formulation of the herbicide glyphosate alters testosterone levels and testicular morphology. *Arch. Toxicol.* 84, 309–317. doi:10.1007/s00204-009-0494-z
- Sánchez, V., Lopez-Bellido, J., Rodrigo, M. A., and Rodriguez, L. (2019). Enhancing the removal of atrazine from soils by electrokinetic-assisted phytoremediation using ryegrass (*Lolium perenne* L.). *Chemosphere* 232, 204–212. doi:10.1016/j.chemosphere.2019.05.216
- Simic, B., Kniewald, J., and Kniewald, Z. (1994). Effects of atrazine on reproductive performance in the rat. *J. Appl. Toxicol.* 14, 401–404. doi:10.1002/jat.2550140603
- Simmons, H. F., James, R. C., Harbison, R. D., and Roberts, S. M. (1990). Depression of glutathione by cold-restraint in mice. *Toxicology* 61, 59–71. doi:10.1016/0300-483x(90)90007-4
- Singh, M., Sandhir, R., and Kiran, R. (2010). Effects on antioxidant status of liver following atrazine exposure and its attenuation by vitamin E. *Exp. Toxicol. Pathol.* 63, 269–276. doi:10.1016/j.etp.2010.01.005
- Sogbanmu, T. O., Aitsegeme, S. O., Otubanjo, O. A., and Odiyo, J. O. (2020). Drinking water quality and human health risk evaluations in rural and urban areas of Ibeju-Lekki and Epe local government areas, Lagos, Nigeria. *Hum. Ecol. Risk Assess. Int. J.* 26 (4), 1062–1075. doi:10.1080/10807039.2018.1554428
- Spano, L., Tyler, C. R., van Aerle, R., Devos, P., Mandiki, S. N., Silvestre, F., et al. (2004). Effects of atrazine on sex steroid dynamics, plasma vitellogenin concentration and gonad development in adult goldfish (*Carassius auratus*). *Aquat. Toxicol.* 66, 369–379. doi:10.1016/j.aquatox.2003.10.009
- Spasic, M. B., Saicic, Z. S., Buzadzic, B., Korac, B., Blagojevic, D., and Petrovic, V. M. (1993). Effect of long-term exposure to cold on the antioxidant defense system in the rat. *Free Radic. Biol. Med.* 15, 291–299. doi:10.1016/0891-5849(93)90076-7
- Standards Organization of Nigeria (2007). Unicef.org. Available at: http://www.unicef.org/nigeria/ng_publications_Nigerian_Standard_for_Drinking_Water_Quality.pdf (Retrieved August 20, 2020).
- Stoker, T. E., Guidici, D. L., Laws, S. C., and Cooper, R. L. (2002). The effects of atrazine metabolites on puberty and thyroid function in the male Wistar rat. *Toxicol. Sci.* 67, 198–206. doi:10.1093/toxsci/67.2.198
- Stoker, T. E., Laws, S. C., Guidici, D. L., and Cooper, R. L. (2000). The effect of atrazine on puberty in male wistar rats: An evaluation in the protocol for the assessment of pubertal development and thyroid function. *Toxicol. Sci.* 58, 50–59. doi:10.1093/toxsci/58.1.50
- Sun, J., Pan, L. L., Zhan, Y., Tsang, D. C. W., Zhu, L. Z., and Li, X. D. (2017). Atrazine contamination in agricultural soils from the Yangtze River Delta of China and associated health risks. *Environ. Geochem. Health* 39, 369–378. doi:10.1007/s10653-016-9853-x
- Swan, S. H. (2006). Semen quality in fertile US men in relation to geographical area and pesticide exposure. *Int. J. Androl.* 29, 62–68. doi:10.1111/j.1365-2605.2005.00620.x
- Thakur, M., Gupta, H., Singh, D., Mohanty, I. R., Maheswari, U., Vanage, G., et al. (2014). Histopathological and ultra-structural effects of nanoparticles on rat testis following 90 days (Chronic study) of repeated oral administration. *J. Nanobiotechnology* 12, 42. doi:10.1186/s12951-014-0042-8
- Trentacoste, S. V., Friedmann, A. S., Youker, R. T., Breckenridge, C. B., and Zirkin, B. R. (2001). Atrazine effects on testosterone levels and androgen-dependent reproductive organs in peripubertal male rats. *J. Androl.* 22, 142–148. doi:10.1002/j.1939-4640.2001.tb02164.x
- US EPA (2009). *Analytical methods approved for drinking water compliance monitoring of organic contaminants*. Washington, DC: United States Environmental Protection Agency, National Primary Drinking Water Regulations, 23. Revised December 2009.
- US EPA (2007). Archie document on atrazine chemical summary for toxicity and exposure assessment for children's health.
- US EPA (2003). Interim reregistration eligibility decision (IRED) for atrazine. Cast: No. 0362 2003.
- US EPA (1989). "Office of drinking water Atrazine," in *Drinking water health advisory: Pesticides* (Chelsea, MI: Lewis Publishers), 43.
- Victor-Costa, A. B., Bandeira, S. M. C., Oliveira, A. G., and Mahecha, G. A. B. (2010). Changes in testicular morphology and steroidogenesis in adult rats exposed to atrazine. *Reprod. Toxicol.* 29, 323–331. doi:10.1016/j.reprotox.2009.12.006
- WHO, UNICEF (2017). *Progress on drinking water, sanitation and hygiene. 2017 update and SDG baselines*. Geneva: WHIO. Available at: https://en.m.wikipedia.org/wiki/Sustainable_Development_Goals16/02/2018,9C48AM (Accessed February 26, 2020).
- WHO (2011). *Atrazine and its Metabolites in drinking-water background document for development of WHO guidelines for drinking-water quality*. 20 Avenue Appia, 1211 Geneva 27, Switzerland: WHO Press, World Health Organization.
- Wirbisky, S. E., and Freeman, J. L. (2015). Atrazine exposure and reproductive dysfunction through the hypothalamus-pituitary-gonadal (HPG) Axis. *Toxics* 3, 414–450. doi:10.3390/toxics3040414
- Zirkin, R. B., Stephanie, V. T., Andrew, S. F., Robert, T. Y., and Charles, B. B. (2001). Atrazine effects on testosterone levels and androgen-dependent reproductive organs in peripubertal male rats. *J. Androl.* 22, 142–148.



OPEN ACCESS

EDITED BY

Sanjeeb Mohapatra,
National University of Singapore,
Singapore

REVIEWED BY

Pooja Sharma,
Environmental Research Institute,
National University of Singapore,
Singapore
Khalid Muzamil Gani,
National Institute of Technology,
Srinagar, India
Bhanu Vellanki,
Indian Institute of Technology Roorkee,
India
Monika Dubey,
Indian Institute of Technology Roorkee,
Roorkee, India in collaboration with
reviewer BV

*CORRESPONDENCE

A. Pistocchi,
✉ alberto.pistocchi@ec.europa.eu

SPECIALTY SECTION

This article was submitted to Toxicology,
Pollution and the Environment,
a section of the journal
Frontiers in Environmental Science

RECEIVED 17 November 2022

ACCEPTED 30 March 2023

PUBLISHED 25 April 2023

CITATION

Pistocchi A, Dorati C, Galimberti F,
Udias A, Bopp S, D'Andrimont R,
Catarino R and Schaefer RB (2023), A
screening study of the spatial distribution
and cumulative toxicity of agricultural
pesticides in the European
Union's waters.
Front. Environ. Sci. 11:1101316.
doi: 10.3389/fenvs.2023.1101316

COPYRIGHT

© 2023 Pistocchi, Dorati, Galimberti,
Udias, Bopp, D'Andrimont, Catarino and
Schaefer. This is an open-access article
distributed under the terms of the
Creative Commons Attribution License
(CC BY). The use, distribution or
reproduction in other forums is
permitted, provided the original author(s)
and the copyright owner(s) are credited
and that the original publication in this
journal is cited, in accordance with
accepted academic practice. No use,
distribution or reproduction is permitted
which does not comply with these terms.

A screening study of the spatial distribution and cumulative toxicity of agricultural pesticides in the European Union's waters

A. Pistocchi^{1*}, C. Dorati¹, F. Galimberti¹, A. Udias², S. Bopp¹,
R. D'Andrimont¹, R. Catarino¹ and R. B. Schaefer³

¹European Commission, Joint Research Centre (JRC), Ispra, Italy, ²Escuela Técnica Superior de Ingeniería Informática, Rey Juan Carlos University, Móstoles, Spain, ³Institute for Environmental Sciences, University of Koblenz and Landau, Landau, Germany

Pesticides can be an important stressor to aquatic ecosystems, and their use is strictly regulated in the European Union (EU). However, data on the use of pesticides are rather limited and poorly available, and monitoring is often insufficient to characterize their actual exposure and impact. The aim of the work presented here is to harness the limited data available and assess, for the first time, the distribution of concentrations and toxicity of 148 pesticide active substances (AS) for the whole EU. Starting from available estimates of pesticide use in agriculture and a simple screening-level model of their fate and transport, we quantify pesticide concentrations in soil and water. A comparison with monitoring data shows that predicted water concentrations are in plausible orders of magnitude, hence the model can be regarded as a first-approximation representation of the distribution of pesticides in the environment. The toxicity of individual pesticide active substances (AS) is characterized by their concentrations divided by the respective no observed effect concentrations (NOEC) for aquatic organisms, which represents the "toxic units" (TU) of each AS. The cumulative toxicity of pesticides in soils and streams of the EU is obtained by summing the TU of individual AS. We estimate that the toxicity of individual AS is generally well below 0.1 TU, indicating relatively safe environmental exposure. However, the cumulative toxicity of a mixture of AS can exceed 0.1 toxic units (TU) for more than 27% of the length of the EU's stream network, and 1 TU for more than 4%. The cumulative toxicity at a given location is driven by only a handful of AS, but these differ from site to site reflecting the variability of pesticide use. Still, we estimate that only about 20 AS out of 148 appear among the top contributors to cumulative toxicity in most cases. While our assessment suggests a relatively widespread risk due to pesticide pollution, it also points to the important limitations concerning knowledge of pesticide use and monitoring of pesticide occurrence in the environment. These limitations need to be addressed in order to evaluate more accurately the effectiveness of EU pesticide policies. The assessment represents a proof-of-concept of a method that can be applied in support of the monitoring of pesticide

Abbreviations: AS, (pesticide) active substance; CA, concentration addition; EU, European Union; GIS, geographic information system; MoA, mode of action; NOEC, no observed effect concentration; PPDP, Pesticide Properties Database; SI, supporting information; SSD, species sensitivity distribution; TU, toxic unit(s); LOQ, limit of quantification.

policies implementation in the EU and elsewhere, once pesticide use can be estimated.

KEYWORDS

pesticides, freshwater, cumulative toxicity, spatial model, soil

Introduction

Pesticide fate in the environment has long been an issue of concern for the civil society around the world. Early ecologist literature, including famous Rachel Carson's *Silent spring* (Carson, 1962), has flagged the presence of these chemicals even in areas remote from their application as a strong evidence of the capability of mankind to poison the global environment. Besides the decline in the abundance and diversity of terrestrial organisms, such as Lepidoptera (butterflies), Hymenoptera (honeybees, bumblebees) and beetles (ladybirds, carabids) mainly found in agricultural areas, also freshwater organisms show a high proportion of threatened species as a consequence of exposure to a number of stressors including pesticides (Sala et al., 2000; Vörösmarty et al., 2010). The concern has fostered the ongoing development of stringent legislation on the management of pesticides (EU, 2009b; EU, 2005; European Commission, 2006a; European Commission, 2002; EU, 2009a; European Commission, 2022). The use of pesticides, and related risks, are also considered a criterion to assess the environmental performance of agriculture in the EU (European Commission, 2006b), and is addressed as one of the key aspects of concern in the recent European Farm to Fork (European Commission, 2020b) and Biodiversity strategies (European Commission, 2015; European Commission, 2020a). Moreover, a number of pesticides are included in the list of priority substances targeted by the European Water Framework Directive and related directives (EU, 2000; EU, 2006), which aim at an overall reduction of chemical risk in aquatic ecosystems. Pesticides are widely applied in modern agriculture, typically in sequence during the vegetation period, where pesticide products may contain multiple active substances (Auber et al., 2011; Chiaia-Hernandez et al., 2017). Consequently, in agricultural regions pesticides occur as mixtures in soils (Chiaia-Hernandez et al., 2017), ground waters (Gilliom, 2007; Munira et al., 2018) and surface water bodies (Schäfer et al., 2013; Schreiner et al., 2016). The distribution of pesticides in the environment and their cumulative risks must be quantified when assessing the implementation of EU policies in the field.

Assessments of pesticide risk at European scale have been performed in the past several years based on a variety of approaches (e.g., by Schriever et al. (2007), using an empirical indicator of runoff potential; by Tiktak et al. (2004), using a physical modeling approach; by Delbaere and Nieto Serradilla (2004), using a pesticide fate indicator, among others). Risk assessment usually rests on exposure/toxicity ratios, i.e., environmental concentrations divided by threshold values indicating toxic risks with reference to specified receptors (ecosystems, non-target species, humans) (e.g., Gutsche and Rossberg, 1997; Reus and Leendertse, 2000; FOCUS, 2001; Chen et al., 2002; Reus et al., 2002; Padovani et al., 2004; de Zwart, 2005; HAIR project, undated). Concentrations may derive from direct measurements, but these are affected by limitations (e.g., Wolfram

et al., 2021). Therefore estimates based on models, ideally using monitored concentration for comparison and validation, in practice are often the only possibility of quantification, especially when addressing a large area.

When concentrations represent the actual conditions in the environment, we can consider the indicators to represent a “true” risk. Conversely, if they reflect a conventional “reasonable worst case” scenario assuming a given pesticide use, they represent a conditional risk. This is typically the subject of assessments for the authorization of pesticide active substances on the market (FOCUS, 2001).

Currently ca. 300 chemical substances are reported in use in the EU as agricultural pesticides (Galimberti et al., 2020). However, little is known about their actual use patterns and emission rates, hence their expected concentrations in the environment.

These knowledge limitations have so far undermined any attempt at assessing the cumulative environmental risk of pesticides at EU level, although there is expanding evidence that the latter may represent an important pressure on aquatic ecosystems (Oliver et al., 2022). In this contribution, we draw a first EU scale cumulative environmental risk assessment of 148 pesticide active substances (AS) in soil and water across Europe, based on recent estimates of pesticide use derived from available data (Udias et al., 2022). In the following sections, we clarify the method used to compute environmental concentrations of pesticide AS, compare our calculations with available monitoring data, present and discuss the cumulative toxicity resulting from computed concentrations. In the final section, we draw conclusions for pesticide assessment and management in the EU including a set of policy recommendations focusing on identified agricultural regions with high cumulative water toxicity, in support of the implementation of EU Strategies and Targets.

Materials and methods

Throughout this paper, we refer to the amounts of pesticides released in the environment as “emissions”. We make use of the estimates of emissions by Udias et al. (2022) for 148 pesticide active substances (AS) in Europe, listed in the [Supplementary Material S1](#), Annex 1, together with their physicochemical properties used for modelling. These represent total amounts of each AS applied in agriculture around the reference year 2015, within EU regions (in kg per year). The regional total application was apportioned to land surfaces within each region on the basis of land cover information, as explained in details in the [Supplementary Material S1](#), Annex 2. This resulted in 148 maps of pesticide AS emission, expressed in kg per hectare and year. Consistent with the resolution of environmental data used for subsequent model calculations, we produced these emission maps with a resolution of 1 km² (see [Supplementary Material S1](#), Annex 2).

The mass of pesticides in soil and the loads to the stream network were predicted using a simple steady state box model (Pistocchi, 2010; Pistocchi, 2013). The model describes the soil as a linear continuous stirred tank reactor; we assume an emission of pesticides that is constant in time, although it is well known that pesticides are applied intermittently and often only during a few days in a year. The implications of this assumption will be discussed later. The model accounts for pesticide removal from the soil due to degradation, runoff and leaching, erosion, and volatilization. From steady state mass balance in soils, we compute the loads of pesticide to the stream network through runoff and leaching as well as erosion. Moreover, we consider that a fixed proportion of emissions reaches the stream network after bypassing the soil, to account for direct losses of pesticides (e.g., through wind drift, dripping from distribution equipment and rinsing of chemical tanks). Direct losses of pesticides are intrinsically difficult to model due to their dependence on local management variables. Here we tentatively set direct losses to 1% of emissions. The implications of this assumption are further discussed below.

The loads of pesticide AS coming from agricultural soils through runoff, leaching and erosion, and the assumed fixed proportion of emissions that bypasses the soil ending up directly in water, are then considered as an input to the stream network. For the stream network, we use a steady state plug-flow model accounting for first-order dissipation. In this way it is possible to estimate the concentration of each pesticide AS at each section of the stream network, taking into account all loads coming from its contributing area subject to dissipation along the respective trajectories. [Supplementary Material S1](#), Annex 2 provides a more detailed description of the calculations used for the mass balance in soils and the stream network. The soil model equations are solved in spatially distributed form using map algebra within a geographic information system (GIS) (Pistocchi, 2014). The stream network model equations are solved in a vector format on a network of sub-basins with a spatial resolution varying from a few to a few tens of squared km (Vogt, 2007), similar to the modelling exercise shown in (Pistocchi et al., 2019). Soil properties and water flow in the stream network are described using European-scale datasets further described in the [Supplementary Material S1](#), Annex 2.

The model is deliberately kept very simple. An alternative could have been to use a complex model incorporating an accurate description of chemical fate and transport processes. When applied to predict environmental concentrations from detailed input data including on pesticide use and observations for calibration and verification, complex models promise to yield the most accurate assessment. Application of these models at European scale has been limited so far to assessing conditional risks (e.g., Tiktak et al., 2002; Holman et al., 2004; Centofanti et al., 2008; Hendley et al., 2009; Urionabarrenetxea et al., 2022) capitalizing on the increasing availability of datasets supporting the definition of model scenarios (e.g. Schneider et al., 2007; Blenkinsop et al., 2008; FOOTPRINT, 2008). Assessing “true” risk at EU scale using complex models, though, is not proportionate to the knowledge available in practice. In the absence of detailed data, models entail assumptions (hence uncertainties) that may jeopardize the advantages of an accurate description of processes. Moreover, when model parameters cannot be calibrated on the basis of observations, models of very different structure and complexity

are expected to give results of comparable prediction quality, and use of complex models is only advisable after testing simpler screening-level models (Pistocchi, 2013).

The estimates of emissions by Udias et al. (2022), used as input for our calculation, are an extrapolation of reported emissions in selected countries. For a comparison of model results with monitoring data, observed concentrations of pesticides in water were extracted from the IPCHEM platform (see Galimberti et al., 2020 for details). No suitable data could be found on pesticide concentrations in soils to compare with model results.

Once concentrations are estimated for all 148 individual AS, we can refer to two fundamental models to predict the toxicity of chemical mixtures: the model of concentration addition (CA) for chemicals with a similar Mode of Action (MoA) (Loewe and Muischnek, 1926) and the model of independent action (IA) (Bliss, 1939), also called effect addition or response addition, for chemicals with a dissimilar MoA. The CA model posits that the concentrations of the chemicals in a mixture are exchangeable if scaled by an appropriate effect concentration (Belden and Brain, 2018). On the contrary, IA accounts for the probability that multiple chemicals contribute to an effect. Several studies have analysed the performance of CA and IA when used to predict the joint toxicity of pesticides, indicating overall similar performances, although in different cases one approach has shown a better match with observations compared to the other (Backhaus et al., 2004a; Backhaus et al., 2004b; Belden et al., 2007; Cedergreen et al., 2008; Norgaard and Cedergreen, 2010; Schäfer et al., 2013; Cedergreen, 2014). In the light of this evidence, the literature tends to suggest CA as the first step in ecological risk assessment irrespective of the MoA, as it provides a precautionary but not overprotective estimation for pesticide mixtures (Junghans et al., 2006; Backhaus and Faust, 2012; Schell et al., 2018) while more complex approaches may not be applicable widely due to data limitations (e.g. Kim et al., 2018). Another recent review confirmed that synergisms with high deviations from CA based predictions are rare and the use of CA as default approach is recommended, still keeping in mind some exceptions for specific classes of chemicals (Martin et al., 2021). Therefore, CA has become in practice the standard tool for a first tier pesticide risk assessment in China (Chen et al., 2020), the European Union (Frische et al., 2014), and the USA (Belden and Brain, 2018). In this work, we refer only to the CA model and compute a toxicity indicator as the sum of individual AS concentrations divided by their respective effect concentration. For the latter, we use the median of chronic no observed effect concentration (NOEC) species sensitivity distributions (SSD) provided by Posthuma et al., 2019. For chemicals not covered by these SSD, we refer to the 21-days NOEC for aquatic invertebrates reported in the Pesticide Properties Database (PPDB) developed by the University of Hertfordshire (<http://sitem.herts.ac.uk/aeru/ppdb/en/index.htm>). The assumed effect concentrations are provided in the [Supplementary Material S1](#), Annex 1, for the 148 AS considered here.

Results

Figure 1 shows the ranges of concentrations of all active substances predicted in the stream network (rivers water), together with the assumed effect concentration. All substances appear to be below the effect concentration. Concentrations in soils show a similar pattern, as shown in the [Supplementary](#)

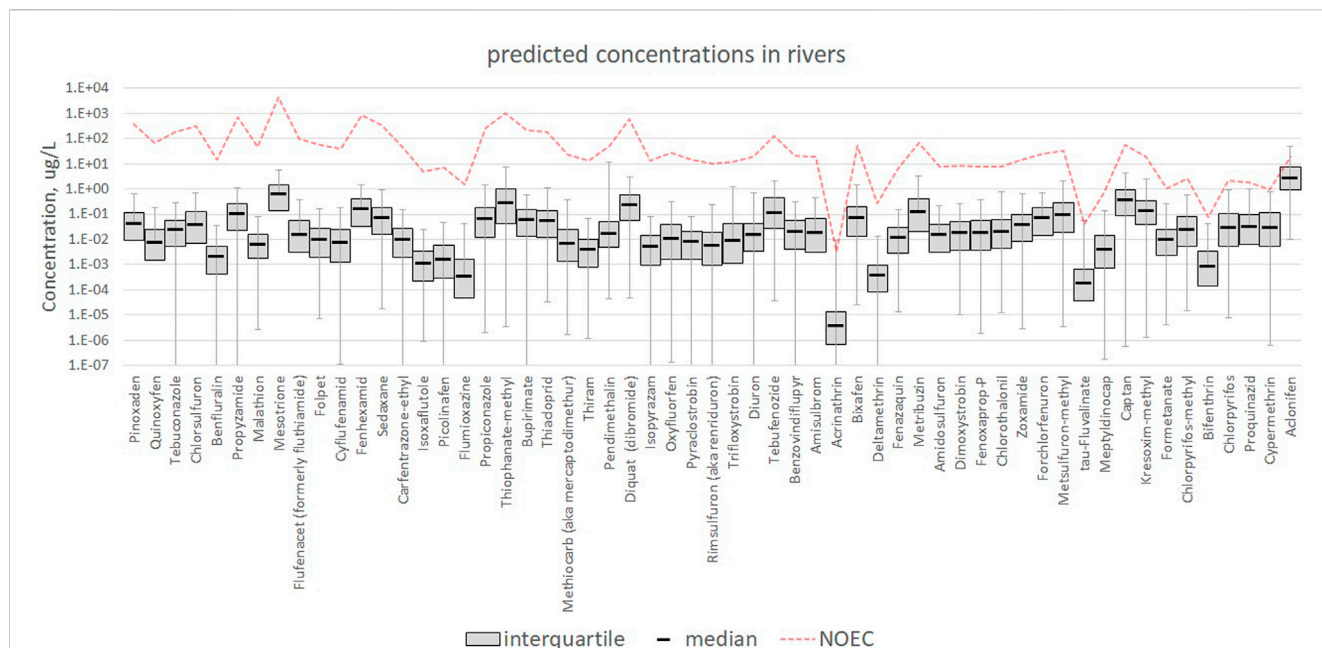


FIGURE 1

Concentrations in freshwater. The whiskers represent the 1st and 99th percentiles of computed concentrations. For the sake of readability, we show only the individual AS for which the NOEC is 4 orders of magnitude larger or less with respect to the median concentration. For all other AS, the computed concentrations are much smaller than the NOEC. A more detailed picture is provided in the [Supplementary Material S1](#), annex 2.

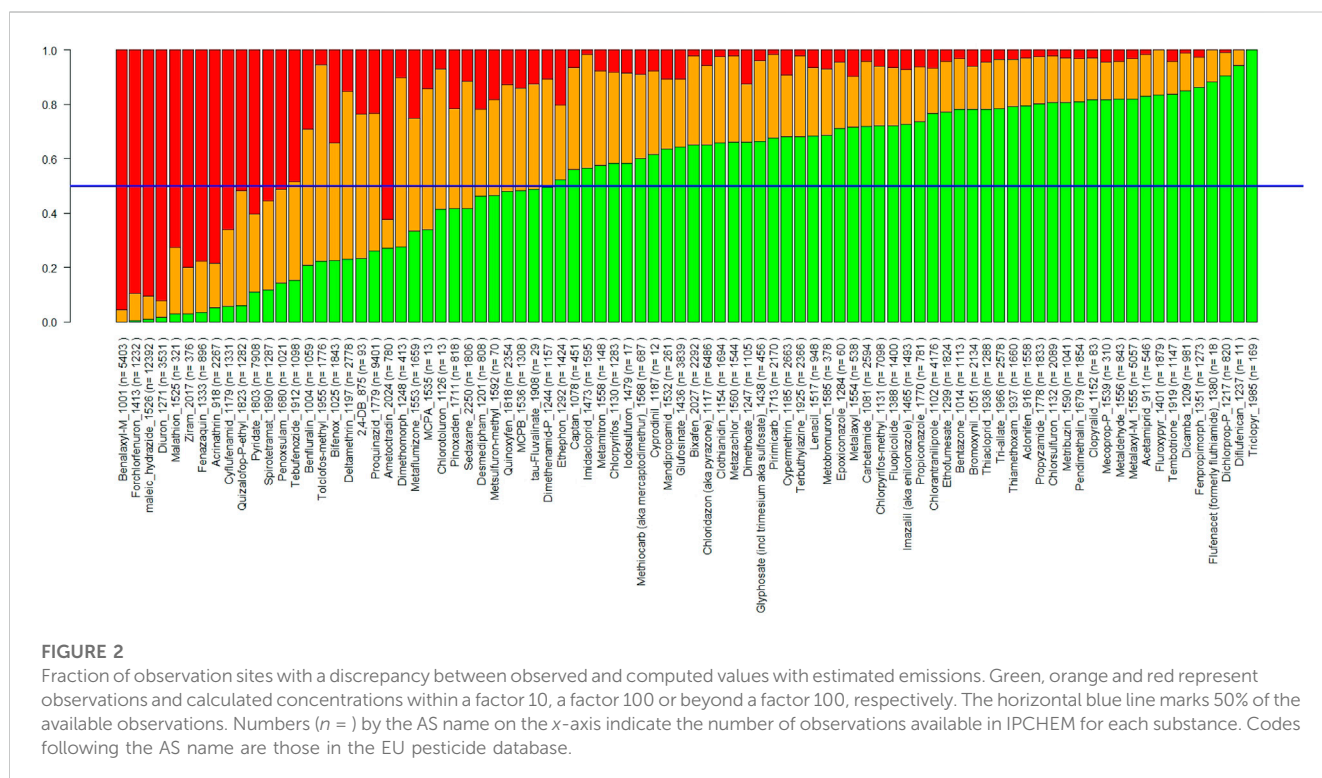


FIGURE 2

Fraction of observation sites with a discrepancy between observed and computed values with estimated emissions. Green, orange and red represent observations and calculated concentrations within a factor 10, a factor 100 or beyond a factor 100, respectively. The horizontal blue line marks 50% of the available observations. Numbers ($n =$) by the AS name on the x-axis indicate the number of observations available in IPCHEM for each substance. Codes following the AS name are those in the EU pesticide database.

Material S1, Annex 2. Liquid phase concentrations in soil tend to be lower than in rivers water because river concentrations reflect also the direct loss of 1% of emissions that we assumed to fall directly on

water due to spray drift, dripping and other causes, hence not contributing to soil concentrations. Direct losses may be an important, and in some cases a dominant contribution.

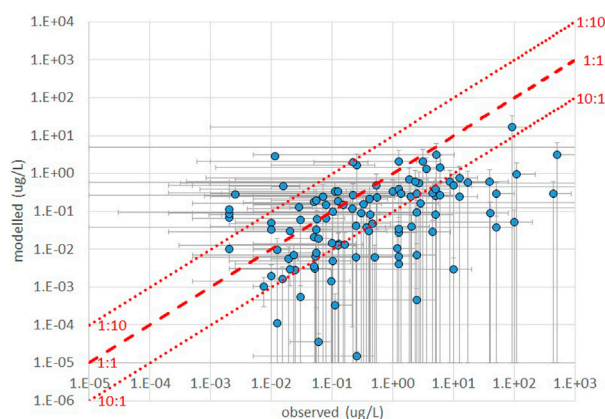


FIGURE 3

comparison of ranges of concentrations from observations and model calculations based on estimated emissions.

To underline the potential importance of direct losses compared to losses through leaching and soil erosion, we also compute the ratio of combined losses through runoff and leaching to emissions, and the one of losses through erosion to emissions, for all 148 AS (Supplementary Material S1, Annex 2), indicating runoff and leaching losses are mostly below 10%, and rather often below 1% of emissions, while losses with erosion rarely exceed 0.1%.

Figure 2 shows the frequency of occurrence of discrepancies (computed as the ratios between observed and computed concentrations) if within a factor 10, between a factor 10 and a factor 100, or above a factor 100, for each of the AS for which monitoring data were available, across all monitoring sites. We can observe that, using estimated emissions, for a majority of substances (53 out of 86) observed and computed concentrations are within a factor 10 at least in 50% of the cases, while 63 out of 86 AS exceed a factor 100 discrepancy in 20% of the cases or less. However, for 10 substances discrepancies are above a factor 100 in more than 50% of the cases. The scatter plot of the central value of the observed and computed concentration ranges (Figure 3) indicates a tendency of the model to underestimate observations, and generally mirrors the pattern of Figure 2.

Many of the cases where discrepancies are larger can be explained with the quantification limits of the observations. For a large proportion of the monitoring data for some AS, true concentrations are likely lower than reported, since measurements below the limit of quantification (LOQ) have been substituted by the value of the LOQ or LOQ/2 in the underlying datasets. For example, the chemical with the worst performance (Benalaxyl-M) has more than 5,000 observations, but all except 4 in the database indicate a constant value of 0.035 ug/L, whereas the calculated values span a range of much lower values. Ametoctradin, a chemical showing mostly discrepancies beyond a factor 100, has 780 observations, all but one at the value of 0.1 ug/L vis-à-vis calculated values ranging over several orders of magnitude, but well below 0.1 ug/L. Observations for all AS suffer from similar limitations, but when concentrations are higher above or around quantification limits the match with calculated values tends to improve. Scatter plots of observations and modelled concentrations for individual substances across measurement

sites are provided in the Supplementary Material S1, Annex 3, for the worst-matching AS.

As a benchmark for the model's skill at matching observed concentrations, we repeated the model calculations with original reported emissions, in the reference countries (Germany, France, Spain, Italy, Ireland, Denmark, Belgium and the Netherlands) for which these were available. A comparison of the calculation results with observations (Supplementary Material S1, Annex 3) does not show clear improvements over the model based on estimated emissions: than the model with reported emissions: for the latter, 46 out of 82 substances are within a factor 10 in 50% of the cases or more, and 53 out of 82 beyond a factor 100 in 20% of the cases or more, while the scatter plot of central values is slightly worse than with estimated emissions.

Figure 4 shows a map of cumulative toxicity in the stream network, computed under a CA model assumption as the sum of concentrations divided by the respective NOEC for all 148 pesticide AS, with estimated emissions as input. The sum of concentrations divided by NOEC represents the amount of "toxic units" (TU) of the mixture. The Supplementary Material S1, Annex 2 also shows a map of the sum of the corresponding losses from soils due to erosion, leaching and runoff and direct losses (1% of emissions) for all 148 pesticide AS, also in this case divided by the respective NOEC. The sum of NOEC-normalized losses can be read as the losses in mass equivalents of a hypothetical substance with unit toxicity. The two maps, shown in Figure 4; Supplementary Material S1 Annex 2 respectively, visualize the estimated distribution of toxicity in rivers and "toxic load" coming from the catchment, hence the parts of the stream network at highest risk and the parts of the catchments contributing the most to pollution. The two maps are rather consistent with each other and highlight a pattern of higher risk in Southern and eastern countries, but with presence of hot spots in various countries. Figure 5 summarizes the distribution of toxicity in the stream network by country, indicating that a cumulative toxicity between 0.1 TU and 1 TU is widespread across the EU, and a cumulative toxicity of 1 TU is also relatively often exceeded. In aggregated terms, 27.4% of the length of the EU's stream network is above 0.1 TU and 4.3% above 1 TU due to the 148 pesticide AS considered in the model.

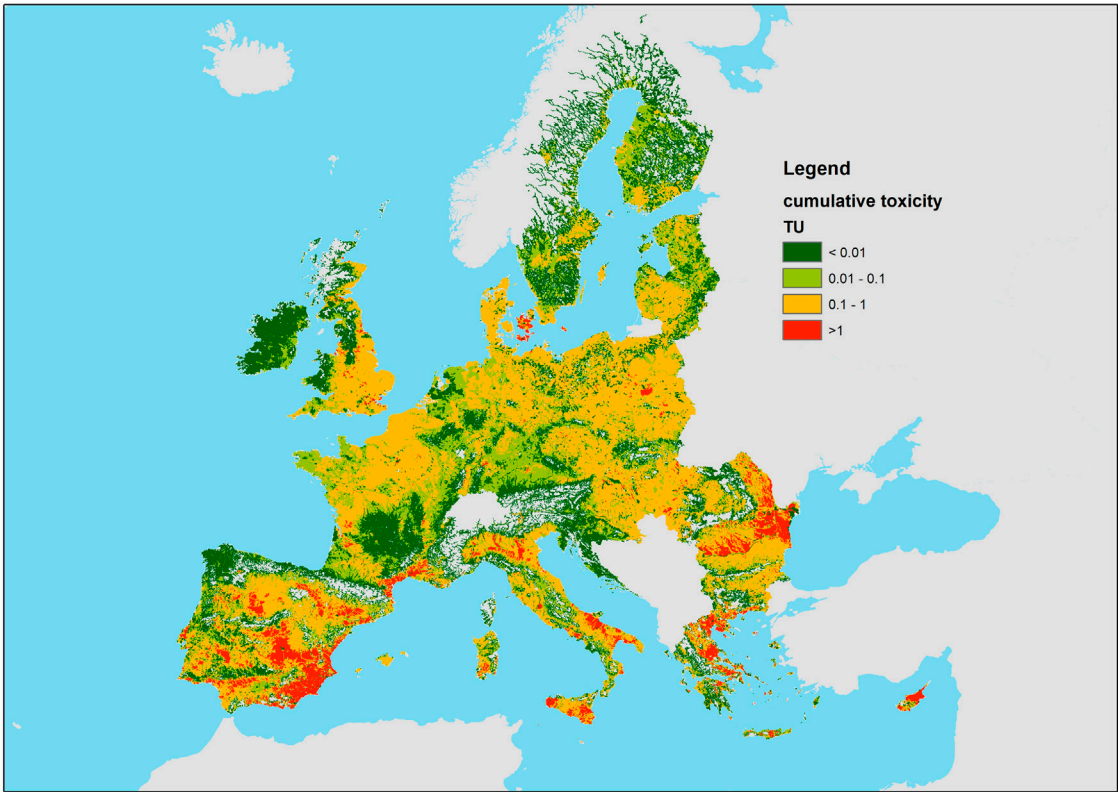
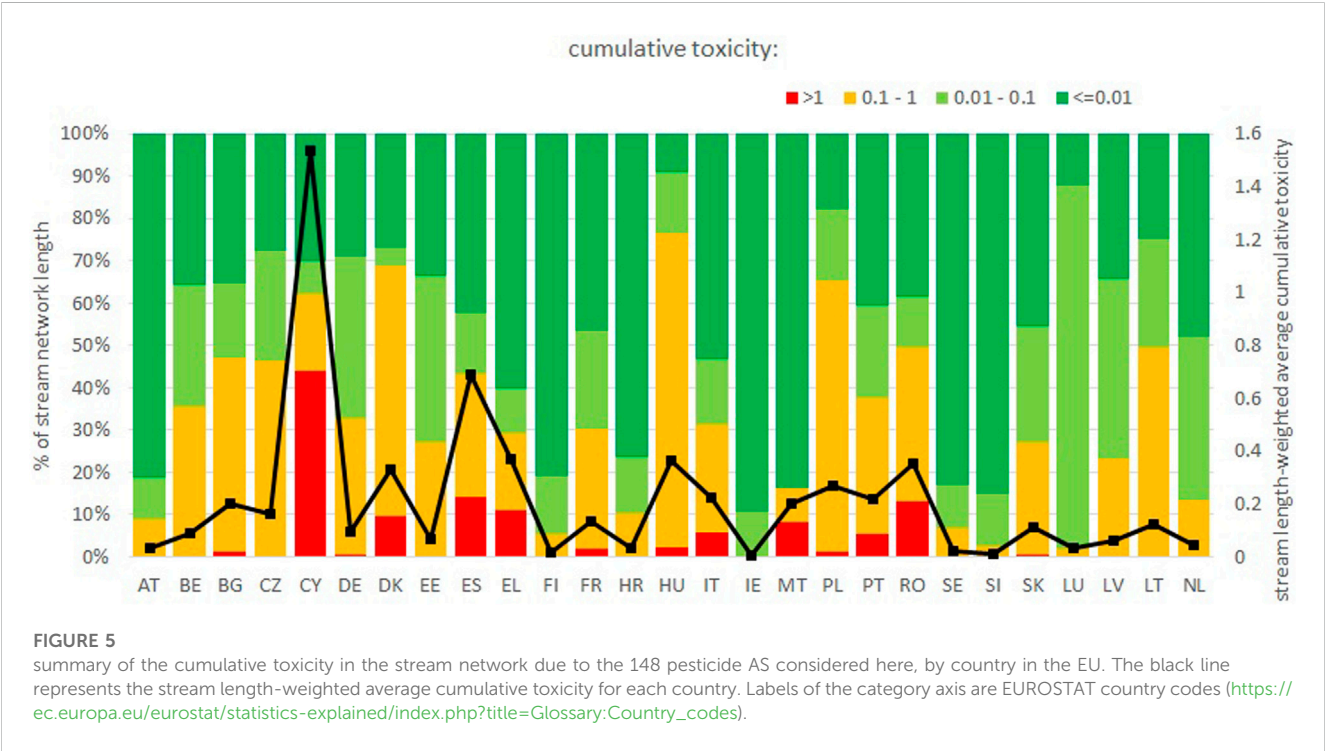
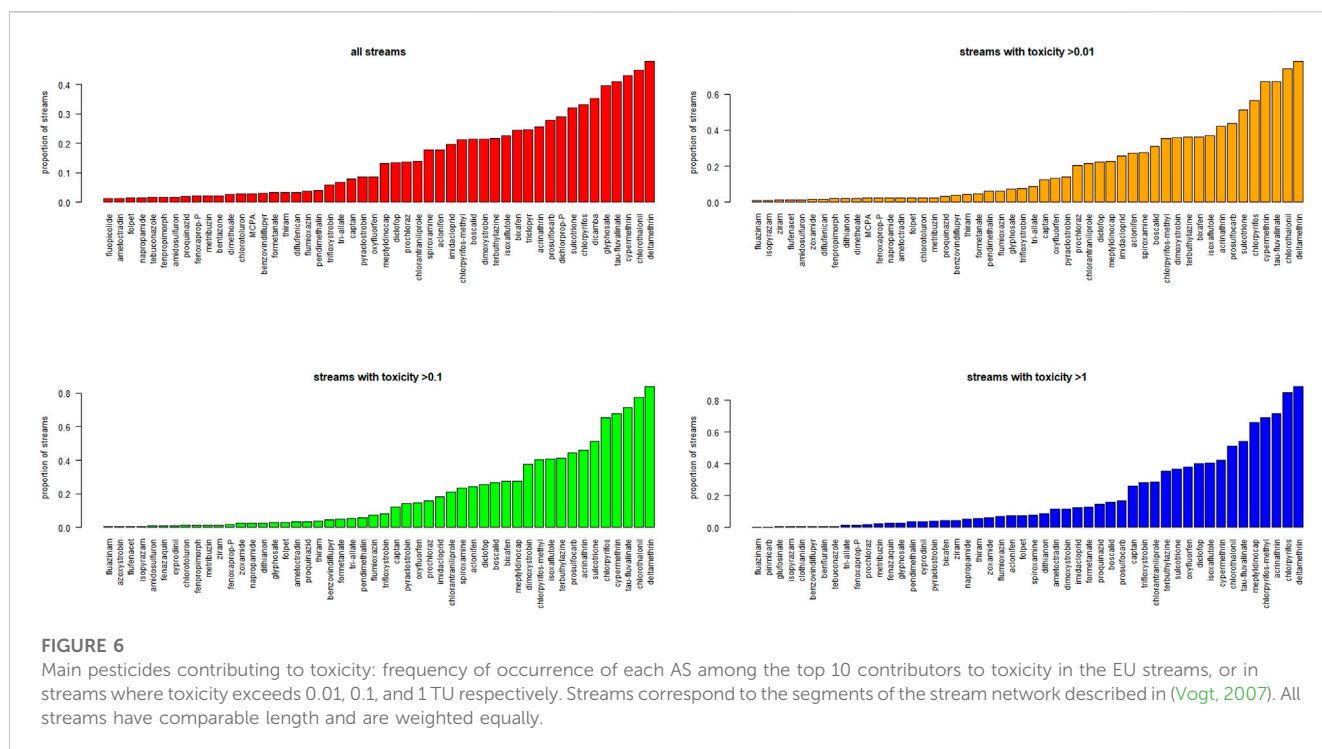


FIGURE 4
Map of the cumulative water toxicity due to the pesticides considered in this study.





The individual maps of concentration normalized by NOEC for the 148 pesticide AS enable also an analysis of which substances contribute the most to overall toxicity. In Figure 6 we plot the frequency of appearance, across the stream network, of each AS among the top 10 contributors to cumulative toxicity. For instance, a frequency of 0.1 would indicate that an AS is among the top 10 contributors in 10% of the stream network. If we consider the whole EU stream network, including also stretches where the cumulative toxicity is low, we tend to identify the most widespread AS. Conversely, if we focus on those parts of the stream network with toxicity above 0.1 TU or 1 TU, we can identify the substances contributing the most to toxicity. For instance, herbicide Glyphosate appears as the 5th most frequent top contributor with reference to the whole stream network, but only as the 37th when looking at the network with toxicity >10 (and similarly above 0.1 and above 1). However, some substances consistently appear among the top contributors irrespective of the toxicity threshold considered. These include deltamethrin, acrinathrin, cypermethrin, chlorpyrifos, tau-fluvalinate, chlorotalonil, which are mostly insecticides.

Discussion

Using a simple model, we have presented an analysis of the cumulative risk of toxicity for aquatic organisms due to 148 pesticide AS in the EU. We have shown how more than 27% of the EU's stream network is affected by a pesticide mixture with concentrations resulting in a cumulative toxicity of 0.1 TU or more, and more than 4% above 1 TU. This indicates that pesticide pollution is widespread, and could be a relevant pressure on aquatic ecosystems in Europe. As a first extensive model-based assessment of pesticides at the EU scale, our quantification is laden with uncertainties further addressed

below. The uncertainty affecting model estimates of concentrations of each pesticide active substance is at least one order of magnitude, as shown by the comparison with observations presented above. The uncertainty owes to all parameters used in the calculation. Pesticide properties (degradation half-life, soil-water partition coefficient) are usually characterized in controlled experiments, not necessarily accounting for the variability of environmental conditions. However, in many cases concentrations depend critically on the assumed direct losses of pesticides. An additional uncertainty in the assessment of risks is related to the assumed NOEC, which may also be regarded as uncertain within at least one order of magnitude. The two aspects together cause a potentially very large uncertainty on each of the 148 AS considered in this work. The sum of toxicities could suffer from lower uncertainty, if errors were completely random, as underestimations of toxicity for some AS would be canceled out by overestimations for others. A formal uncertainty analysis of the model, anyway beyond the scope of this work, would add limited benefit for the following overarching reasons.

First of all, we focus on 148 pesticide AS out of a total of about 300 chemical AS in current use. Under a concentration addition model, neglecting substances implies underestimating cumulative toxicity.

Furthermore, our assessment of toxicity is based on concentrations in water calculated by the model. These are quite consistent with reported observations in terms of orders of magnitude and ranges, in the majority of the cases. The model tends to underestimate concentrations in comparison with observations (see Figure 2; Figure 3). The correlation between observed and calculated concentrations, though, is rather weak (Figure 3 and Annex 3). This can be explained by uncertainties and bias related to both observed and calculated concentrations.

Pesticide concentrations vary significantly in space and time, and the current sampling schemes with regular grab sampling tend to underestimate true concentrations as relevant exposure periods can be missed (Stehle et al., 2013; Oliver et al., 2022). Indeed, the monitoring data used in this exercise contained frequent records below levels of quantification while calculated concentrations were still significant for cumulative toxicity.

Discrepancies between observations and calculations may owe in part to the simplicity of the model: our steady-state calculation apparently does not account for the highly dynamical nature of certain pesticide applications. A systematic bias of our steady state calculation, in particular, is the approximation of emissions as stationary, while a more realistic model should take into account at least the fact that pesticides are released impulsively, once or a few times in a year. In the [Supplementary Material S1](#), Annex 4, we present and discuss a correction factor to account for the effect of an impulsive release of pesticides when using steady state models initially proposed in (Pistocchi, 2010; Pistocchi, 2013; Pistocchi, 2014). In general, however, the simulation of an impulsive release yields lower annual average concentrations than a steady state calculation, which would further exacerbate our underestimation of observations. Therefore, we should assume higher emissions in order to match the available observations. More complex models, describing processes at a finer spatial and temporal resolution, are not expected to show better predictive capacity, because the key fate and transport parameters (degradation rates and, to some extent, partitioning properties) cannot be calibrated under field conditions (see, e.g., Knäbel et al., 2012). Based on the above considerations, we regard our modelled concentrations as a provisionally acceptable generalization of observed concentrations.

Another aspect to consider is the effect concentration used to compute the TU of the mixture. We rest on existing estimates of the NOEC affecting 50% of the species in aquatic ecosystems, according to the species sensitivity distributions (SSD) modelled by Posthuma et al. (Posthuma et al., 2019), and our assessment is therefore conditional to the validity of this threshold. For example, (EFSA, 2013), recommends applying an assessment factor of 3 for toxicity data based on chronic NOEC based SSDs considering the 5th percentile of the distribution, while here the 50th percentile of the distribution was used and no assessment factor was applied, likely leading to an underestimation of risks. Moreover, for substances with missing SSD-based values (Posthuma et al., 2019), we used the 21-day NOEC for aquatic invertebrates. These NOEC values may not be consistent with the other SSD-based values for those AS which are most toxic towards organisms other than invertebrates.

We flag a relatively high risk from chronic exposure when the mixture toxicity calculated from the NOEC exceeds 1 TU, and a lower but somehow significant risk when it is between 0.1 and 1 TU. However, we could not verify any relationship between our calculated mixture toxicity, hence risk, and impacts on aquatic ecosystems. The NOEC may be about one order of magnitude lower than concentrations at which an acute exposure has observable effects on aquatic organisms [e.g., 67], but the relationship between exceedance of NOEC and the risk of ecological effects is still problematic (Smetanová et al., 2014).

Nutrients and hydromorphological degradation often co-occur with toxicants above ecological risk levels in freshwater ecosystems

(Schäfer and Piggott, 2018). Although our knowledge of the combined impacts is limited, stressors can interact in different ways (Schäfer and Piggott, 2018): by exerting a combined pressure on ecosystems (Holmstrup et al., 2010; Stampfli et al., 2013; Link et al., 2017), by influencing the sensitivity of organisms towards other stressors (Holmstrup et al., 2010), and by differentially affecting age stages, populations or species within an ecosystem, triggering disruptions in the population dynamics (Bracewell et al., 2019; Van den Brink et al., 2019). Pesticides frequently co-occur (Matthaei et al., 2010; Moschet et al., 2014; Lemm and Feld, 2017; Szöcs et al., 2017) and interact with other stressors (Holmstrup et al., 2010), (Lange et al., 2011; Magbanua et al., 2013; Piggott et al., 2015; Elbrecht et al., 2016; Jackson et al., 2016; Liess et al., 2016; Magbanua et al., 2016; Chará-Serna and Richardson, 2018; Davis et al., 2018; European Environment Agency, 2018; Bray et al., 2019; Chará-Serna et al., 2019; Juvigny-Khenafou et al., 2020), often in a synergistic way (Holmstrup et al., 2010; Jackson et al., 2016; Liess et al., 2016). Maps of pesticide concentrations as discussed here may support the assessment of combinations of stressors on aquatic ecosystems, which so far have struggled to disentangle the effect of chemical pollutants (Vigiak et al., 2021).

Conclusion

This paper presents what, to our knowledge, is the first EU-scale model-based assessment of the cumulative toxicity of pesticide active substances presently authorized on the market, based on a spatially explicit estimation of pesticide use. We have used a simple, spatially explicit model to quantify the cumulative toxicity of 148 pesticide AS in the stream network of the EU. We find a relatively high frequency of exceedance of safe chronic exposure to pesticides, mainly driven by less than 20 of those substances. While our model is theoretically prone to overestimation, available measurements rather suggest an underestimation of concentrations, hence we do not expect to exaggerate the extent and severity of pesticide environmental contamination. Reference to NOEC and the CA model make the assessment precautionary for the goals we have pursued. In this modelling exercise, we have used an improved estimation of emissions compared to a previous exercise that we regard as an “ancestor” (provided for reference in the [Supplementary Material S1](#), Annex 5). However, this has led only to limited improvements in the overall prediction, consistent with the persisting knowledge gaps on actual pesticide use in Europe. In particular, the data currently available at the EU scale do not allow predicting pesticide AS concentrations more accurately than within one order of magnitude. In the future, an accurate characterization of spatial patterns of pesticide emissions remains key to improve model predictions and the overall assessment of pesticides in the framework of current European pesticide legislation. A recently proposed regulation of statistics on agricultural input and output (European Commission, 2021) requires better harmonization and quality of data from 2025 on, possibly enabling more sophisticated modelling in the future. However, pending an improved representation of emissions, the simple approach presented here may still prove sufficient for a first assessment. For the time being, what we present here is a proof of concept for spatially explicit pesticide risk indicators, which could also be presented in aggregated form (see [Supplementary Material S1](#), Annex 6), in support to the

monitoring of policy implementation and EU scale pesticide management, compatible with the available knowledge.

Data availability statement

The raw data supporting the conclusion of this article will be made available by the authors, without undue reservation.

Author contributions

AP conceived, led and executed the research, wrote the manuscript and managed resources and funding. CD curated the data and executed processing and calculations under the supervision of AP. RS, AU, and FG provided data, advice, scientific discussion, and contributed to writing and reviewed the manuscript. SB, RC, and RD reviewed the manuscript and contributed to clarification and improvement of the presentation and discussion.

Acknowledgments

This work was partly developed in the context of the project “Nature-based solutions for climate and water pollution mitigation in agricultural regions” under an administrative arrangement

between the JRC and the Directorate General for Environment of the European Commission.

Conflict of interest

The authors declare that the research was conducted in the absence of any commercial or financial relationships that could be construed as a potential conflict of interest.

Publisher's note

All claims expressed in this article are solely those of the authors and do not necessarily represent those of their affiliated organizations, or those of the publisher, the editors and the reviewers. Any product that may be evaluated in this article, or claim that may be made by its manufacturer, is not guaranteed or endorsed by the publisher.

Supplementary material

The Supplementary Material for this article can be found online at: <https://www.frontiersin.org/articles/10.3389/fenvs.2023.1101316/full#supplementary-material>

References

- Auber, A., Roucaute, M., Togola, A., and Caquet, T. (2011). Structural and functional effects of conventional and low pesticide input crop-protection programs on benthic macroinvertebrate communities in outdoor pond mesocosms. *Ecotoxicology* 20, 2042–2055. doi:10.1007/s10646-011-0747-5
- Backhaus, T., Arrhenius, A., and Blanck, H. (2004a). Toxicity of a mixture of dissimilarly acting substances to natural algal communities: Predictive power and limitations of independent action and concentration addition. *Environ. Sci. Technol.* 38, 6363–6370. doi:10.1021/es0497678
- Backhaus, T., and Faust, M. (2012). Predictive environmental risk assessment of chemical mixtures: A conceptual framework. *Environ. Sci. Technol.* 46, 2564–2573. doi:10.1021/es2034125
- Backhaus, T., Faust, M., Scholze, M., Gramatica, P., Vighi, M., and Grimme, L. H. (2004b). Joint algal toxicity of phenylurea herbicides is equally predictable by concentration addition and independent action. *Environ. Toxicol. Chem.* 23, 258–264. doi:10.1897/02-497
- Belden, J. B., and Brain, R. A. (2018). Incorporating the joint toxicity of co-applied pesticides into the ecological risk assessment process. *Integr. Environ. Assess. Manag.* 14, 79–91. doi:10.1002/ieam.1957
- Belden, J. B., Gilliom, R. J., and Lydy, M. J. (2007). How well can we predict the toxicity of pesticide mixtures to aquatic life? *Integr. Environ. Assess. Manag.* 3, e1–e5. doi:10.1002/ieam.5630030326
- Blenkinsop, S., Fowler, H. J., Dubus, I. G., Nolan, B. T., and Hollis, J. M. (2008). Developing climatic scenarios for pesticide fate modelling in Europe. *Environ. Pollut.* 154, 219–231. doi:10.1016/j.envpol.2007.10.021
- Bliss, C. I. (1939). The toxicity of poisons applied jointly. *Ann. Appl. Biol.* 26, 585–615. doi:10.1111/j.1744-7348.1939.tb06990.x
- Bracewell, S., Verdonchot, R. C. M., Schäfer, R. B., Bush, A., Lapen, D. R., and Van den Brink, P. J. (2019). Qualifying the effects of single and multiple stressors on the food web structure of Dutch drainage ditches using a literature review and conceptual models. *Sci. Total Environ.* 684, 727–740. doi:10.1016/j.scitotenv.2019.03.497
- Bray, J. P., Nichols, S. J., Keely-Smith, A., Thompson, R., Bhattacharyya, S., Gupta, S., et al. (2019). Stressor dominance and sensitivity-dependent antagonism: Disentangling the freshwater effects of an insecticide among co-occurring agricultural stressors. *J. Appl. Ecol.* 56, 2020–2033. doi:10.1111/1365-2664.13430
- Carson, R. (1962). *Silent spring*. Boston: Houghton Mifflin Co.
- Cedergreen, N., Christensen, A. M., Kamper, A., Kudsk, P., Mathiassen, S. K., Streibig, J. C., et al. (2008). A review of independent action compared to concentration addition as reference models for mixtures of compounds with different molecular target sites. *Environ. Toxicol. Chem.* 27, 1621–1632. doi:10.1897/07-474.1
- Cedergreen, N. (2014). Quantifying synergy: A systematic review of mixture toxicity studies within environmental toxicology. *PLoS ONE* 9, 965800–e96612. doi:10.1371/journal.pone.0096580
- Centofanti, T., Hollis, J. M., Blenkinsop, S., Fowler, H. J., Truckell, I., Dubus, I. G., et al. (2008). Development of agro-environmental scenarios to support pesticide risk assessment in Europe. *Sci. Total Environ.* 407, 574–588. doi:10.1016/j.scitotenv.2008.08.017
- Chará-Serna, A. M., Epele, L. B., Morrissey, C. A., and Richardson, J. S. (2019). Nutrients and sediment modify the impacts of a neonicotinoid insecticide on freshwater community structure and ecosystem functioning. *Sci. Total Environ.* 692, 1291–1303. doi:10.1016/j.scitotenv.2019.06.301
- Chará-Serna, A. M., and Richardson, J. S. (2018). Chlorpyrifos interacts with other agricultural stressors to alter stream communities in laboratory microcosms. *Ecol. Appl.* 28, 162–176. doi:10.1002/eap.1637
- Chen, L., Li, S., Zhou, Y., Zhou, X., Jiang, H., Liu, X., et al. (2020). Risk assessment for pesticide mixtures on aquatic ecosystems in China: A proposed framework. *Pest Manag. Sci.* 76, 444–453. doi:10.1002/ps.5529
- Chen, P., Hertl, P., Chen, S., and Tierney, D. (2002). A pesticide surface water mobility index and its relationship with concentrations in agricultural drainage watersheds. *Environ. Toxicol. Chem.* 21 (2), 298–308. doi:10.1002/etc.5620210211
- Chiaia-Hernandez, A. C., Keller, A., Wächter, D., Steinlin, C., Camenzuli, L., Hollender, J., et al. (2017). Long-term persistence of pesticides and TPs in archived agricultural soil samples and comparison with pesticide application. *Environ. Sci. Technol.* 51, 10642–10651. doi:10.1021/acs.est.7b02529
- Davis, S. J., Ó hUallacháin, D., Mellander, P.-E., Kelly, A.-M., Matthaei, C. D., Piggott, J. J., et al. (2018). Multiple-stressor effects of sediment, phosphorus and nitrogen on stream macroinvertebrate communities. *Sci. Total Environ.* 637–638, 577–587. doi:10.1016/j.scitotenv.2018.05.052
- de Zwart, D. (2005). Ecological effects of pesticide use in The Netherlands: Modeled and observed effects in the field ditch. *Integr. Environ. Assess. Manag.* 1 (2), 123–134. doi:10.1897/ieam_2004-015.1
- EU (2000). Directive 2000/60/EC of the European Parliament and of the Council of 23 October 2000 establishing a framework for Community action in the field of water policy. *Off. J. Eur. Commun. L* 327, 22.

- EU (2005). No 396/2005 of the European Parliament and of the Council of 23 February 2005 on maximum residue levels of pesticides in or on food and feed of plant and animal origin and amending Council Directive 91/414/EEC with EEA relevance. *Off. J. Eur. Commun. L* 70, 16–23.
- EU (2006). Directive 2006/118/EC of the European parliament and of the council of 12 december 2006 on the protection of groundwater against pollution and deterioration. *Off. J. Eur. Commun. L* 327, 27.
- EU (2009a). Directive 2009/128/EC of the European Parliament and of the council of 21 October 2009 establishing a framework for Community action to achieve the sustainable use of pesticides.
- EU (2009b). No 1107/2009 of the European Parliament and of the Council of 21 October 2009 concerning the placing of plant protection products on the market and repealing Council Directives 79/117/EEC and 91/414/EEC. Available at: <https://eur-lex.europa.eu/legal-content/EN/TXT/HTML/?uri=CELEX:32009R1107&from=EN>.
- EFSA (2013). EFSA Panel on Plant Protection Products and their Residues, Guidance on tiered risk assessment for plant protection products for aquatic organisms in edge-of-field surface waters. *EFSA J.* 11(7, 3290, doi:10.2903/j.efsa.2013.3290
- Elbrecht, V., Beermann, A. J., Goessler, G., Neumann, J., Tollrian, R., Wagner, R., et al. (2016). Multiple-stressor effects on stream invertebrates: A mesocosm experiment manipulating nutrients, fine sediment and flow velocity. *Freshw. Biol.* 61, 362–375. doi:10.1111/fwb.12713
- European Commission (2020a). Communication From The Commission To The European Parliament, The Council, The European Economic And Social Committee And The Committee Of The Regions. EU Biodiversity Strategy for 2030 Bringing nature back into our lives. Available at: https://eur-lex.europa.eu/resource.html?uri=cellar:a3c806a6-9ab3-11ea-9d2d-01aa75ed71a1.0001.02/DOC_1&format=PDF.
- European Commission (2020b). Communication From The Commission To The European Parliament, The Council, The European Economic And Social Committee And The Committee Of The Regions. A Farm to Fork Strategy for a fair, healthy and environmentally-friendly food system. Available at: https://eur-lex.europa.eu/resource.html?uri=cellar:ea0f9f73-9ab2-11ea-9d2d-01aa75ed71a1.0001.02/DOC_1&format=PDF.
- European Commission (2006a). A thematic strategy on the sustainable use of pesticides. Available at: <http://ec.europa.eu/environment/ppps/home.htm>.
- European Commission (2006b). Communication from the Commission to the Council and the European Parliament. Development of Agri-environmental indicators for monitoring the integration of environmental concerns into the common agricultural policy/COM.
- European Commission (2022). COM(2022) 305 final 2022/0196 (COD) proposal for a regulation of the European parliament and of the council on the sustainable use of plant protection products and amending regulation. Available at: https://ec.europa.eu/info/law/better-regulation/have-your-say/initiatives/12413-Pesticides-sustainable-use-updated-EU-rules_en.
- European Commission (2002). Communication from the commission to the council, the European parliament and the economic and social committee towards A thematic strategy on the sustainable use of pesticides/com.
- European Commission (2021). Proposal for a Regulation of the European Parliament and of the Council on statistics on agricultural input and output and repealing Regulations (EC) No 1165/2008. Available at: <https://eur-lex.europa.eu/legal-content/EN/TXT/?uri=CELEX:52021PC0037>.
- European Commission (2015). Report from the Commission to the European Parliament and the Council the mid-term review of the EU biodiversity strategy to 2020. Brussels, Belgium: European Commission.
- European Environment Agency (2018). European waters Assessment of status and pressures 2018. Luxembourg: Publications Office of the European Union.
- FOCUS (2001). FOCUS surface water scenarios in the EU evaluation process under 91/414/EEC. Report of the FOCUS working group on surface water scenarios, EC document reference SANCO/4802/2001-rev.2. Available at: <https://esdac.jrc.ec.europa.eu/projects/focus-dg-sante>.
- Footprint (2008). FOOTPRINT SUGAR, the SURface water/GroundwAter contribution index. Prod. as part EU-funded Footpr. Proj. SSPI-CT-2005-022704. Available at: <http://www.herts.ac.uk/aeru/footprint/tools/sugar.htm>.
- Frische, T., Matezki, S., and Wogram, J. (2014). Environmental risk assessment of pesticide mixtures under regulation 1107/2009/EC: A regulatory review by the German federal environment agency (UBA). *J. für Verbraucherschutz und Lebensmittelsicherheit* 9, 377–389. doi:10.1007/s00003-014-0916-6
- Galimberti, F., Dorati, C., Udias Moineiro, A., and Pistocchi, A. (2020). Estimating pesticide use across the EU. Luxembourg: Publications Office of the European Union.
- Gilliom, R. J. (2007). Pesticides in U.S. Streams and groundwater. *Environ. Sci. Technol.* 41, 3408–3414. doi:10.1021/es072531u
- Gutscheand Rossberg, D. (1997). SYNOPSIS 1.1 — A model to assess and to compare the environmental risk potential of active ingredients in plant protection products. *Agric. Ecosyst. Environ.* 64, 181–188. doi:10.1016/s0167-8809(97)00037-6
- HAIR project HAIR project reports on Terrestrial, Aquatic, Consumer indicators. Available at: http://www.rivm.nl/rvs/risbeoor/Modellen/Results_of_HAIR_project.jsp.
- Hendley, P., Harbourn, C., Prenger, J., and Miller, P. (2009). Use of SSURGO, NHDPlus and other spatial data to assess potential watershed vulnerability to herbicide runoff and to extend monitoring study findings. *Poster Present. UP119, 30th SETAC N. Am. Annu. Meet.*
- Holman, I. P., Dubus, I., Hollis, J. M., and Brown, C. D. (2004). Using a linked soil model emulator and unsaturated zone leaching model to account for preferential flow when assessing the spatially distributed risk of pesticide leaching to groundwater in England and Wales. *Sci. total Environ.* 318, 73–88. doi:10.1016/S0048-9697(03)00375-9
- Holmstrup, M., Bindesbol, A. M., Oostingh, G. J., Duschl, A., Scheil, V., Köhler, H. R., et al. (2010). Interactions between effects of environmental chemicals and natural stressors: A review. *Sci. Total Environ.* 408, 3746–3762. doi:10.1016/j.scitotenv.2009.10.067
- Jackson, M. C., Loewen, C. J. G., Vinebrooke, R. D., and Chimimba, C. T. (2016). Net effects of multiple stressors in freshwater ecosystems: A meta-analysis. *Glob. Change Biol.* 22, 180–189. doi:10.1111/gcb.13028
- Junghans, M., Backhaus, T., Faust, M., Scholze, M., and Grimme, L. H. (2006). Application and validation of approaches for the predictive hazard assessment of realistic pesticide mixtures. *Aquat. Toxicol.* 76, 93–110. doi:10.1016/j.aquatox.2005.10.001
- Juigney-Khenafou, N. P. D., Zhang, Y., Piggott, J. J., Atkinson, D., Matthaei, C. D., Van Bael, S. A., et al. (2020). Anthropogenic stressors affect fungal more than bacterial communities in decaying leaf litter: A stream mesocosm experiment. *Sci. Total Environ.* 716, 135053. doi:10.1016/j.scitotenv.2019.135053
- Kim, J., Fischer, M., and Helms, V. (2018). Prediction of synergistic toxicity of binary mixtures to *Vibrio fischeri* based on biomolecular interaction networks. *Chem. Res. Toxicol.* 31, 1138–1150. doi:10.1021/acs.chemrestox.8b00164
- Knäbel, A., Stehle, S., Schäfer, R. B., and Schulz, R. (2012). Regulatory FOCUS surface water models fail to predict insecticide concentrations in the field. *Environ. Sci. Technol.* 46 (15), 8397–8404.
- Lange, K., Liess, A., Piggott, J. J., Townsend, C. R., and Matthaei, C. D. (2011). Light, nutrients and grazing interact to determine stream diatom community composition and functional group structure. *Freshw. Biol.* 56, 264–278. doi:10.1111/j.1365-2427.2010.02492.x
- Lemm, J. U., and Feld, C. K. (2017). Identification and interaction of multiple stressors in central European lowland rivers. *Sci. Total Environ.* 603–604, 148–154. doi:10.1016/j.scitotenv.2017.06.092
- Liess, M., Foit, K., Knillmann, S., Schäfer, R. B., and Liess, H.-D. (2016). Predicting the synergy of multiple stress effects. *Sci. Rep.* 6, 32965. doi:10.1038/srep32965
- Link, M., Ohevon der, P. C., Voß, K., and Schäfer, R. B. (2017). Comparison of dilution factors for German wastewater treatment plant effluents in receiving streams to the fixed dilution factor from chemical risk assessment. *Sci. Total Environ.* 598, 805–813. doi:10.1016/j.scitotenv.2017.04.180
- Loewe, S., and Muischnek, H. (1926). Über kombinationswirkungen. *Schmiedeb. Arch. für Exp. Pathol. Pharmacol.* 114, 313–326. doi:10.1007/BF01952257
- Magbanua, F. S., Townsend, C. R., Hageman, K. J., and Matthaei, C. D. (2013). Individual and combined effects of fine sediment and the herbicide glyphosate on benthic macroinvertebrates and stream ecosystem function. *Freshw. Biol.* 58, 1729–1744. doi:10.1111/fwb.12163
- Magbanua, F. S., Townsend, C. R., Hageman, K. J., Piggott, J. J., and Matthaei, C. D. (2016). Individual and combined effects of fine sediment and glyphosate herbicide on invertebrate drift and insect emergence: A stream mesocosm experiment. *Freshw. Sci.* 35, 139–151. doi:10.1086/684363
- Martin, O., Martin, S., Ermler, S., McPhie, J., Stephanie, K., Kienzler, A., et al. (2021). Ten years of research on synergisms and antagonisms in chemical mixtures: A systematic review and quantitative reappraisal of mixture studies. *Environ. Int.* 146, 106206. doi:10.1016/j.envint.2020.106206
- Matthaei, C. D., Piggott, J. J., and Townsend, C. R. (2010). Multiple stressors in agricultural streams: Interactions among sediment addition, nutrient enrichment and water abstraction. *J. Appl. Ecol.* 47, 639–649. doi:10.1111/j.1365-2664.2010.01809.x
- Moschet, C., Wittmer, I., Simovic, J., Junghans, M., Piazzoli, A., Singer, H., et al. (2014). How a complete pesticide screening changes the assessment of surface water quality. *Environ. Sci. Technol.* 48, 5423–5432. doi:10.1021/es500371t
- Munira, S., Farenhorst, A., Sapkota, K., Nilsson, D., and Sheedy, C. (2018). Auxin herbicides and pesticide mixtures in groundwater of a canadian prairie province. *J. Environ. Qual.* 47, 1462–1467. doi:10.2134/jeq2018.05.0202
- Delbaere, B., and Nieto Serradilla, A. (2004). Environmental risks from agriculture in Europe: Locating environmental risk zones in Europe using agri-environmental indicators – tilburg. (ECNC).
- Norgaard, K. B., and Cedergreen, N. (2010). Pesticide cocktails can interact synergistically on aquatic crustaceans. *Environ. Sci. Pollut. Res.* 17, 957–967. doi:10.1007/s11356-009-0284-4
- Oliver, W., Arle, J., Liebmann, L., Link, M., Schäfer, R. B., Anke Schneeweiss, et al. (2022). Three reasons why the Water Framework Directive (WFD) fails to identify pesticide risks. *Water Res.* 208, 117848. doi:10.1016/j.watres.2021.117848

- Padovani, L., Trevisan, M., and Capri, E. (2004). A calculation procedure to assess potential environmental risk of pesticides at the farm level. *Ecol. Indic.* 4, 111. doi:10.1016/j.ecolind.2004.01.002
- Piggott, J. J., Salis, R. K., Lear, G., Townsend, C. R., and Matthaei, C. D. (2015). Climate warming and agricultural stressors interact to determine stream periphyton community composition. *Glob. Change Biol.* 21, 206–222. doi:10.1111/gcb.12661
- Pistocchi, A. (2013). Some considerations on the use of simple box models of contaminant fate in soils. *Environ. Monit. Assess.* 185 (3), 2855–2867. doi:10.1007/s10661-012-2755-1
- Pistocchi, A. (2014). *GIS based chemical fate modeling: Principles and applications*. Hoboken: Wiley, 520. 978-1-.
- Pistocchi, A., Dorati, C., Alberto, A., Ginebreda, A., and Marcé, R. (2019). River pollution by priority chemical substances under the water framework directive: A provisional pan-European assessment. *Sci. Total Environ.* 662, 434–445. doi:10.1016/j.scitotenv.2018.12.354
- Pistocchi, A. (2010). On the temporal resolution of mass balance models for soluble chemicals in soils. *Hydrol. Process* 24, 1172–1186. doi:10.1002/hyp.7581
- Posthuma, L., van Gils, J., Zijp, M. C., van de Meent, D., and de Zwart, D. (2019). Species sensitivity distributions for use in environmental protection, assessment, and management of aquatic ecosystems for 12 386 chemicals. *Environ. Toxicol. Chem.* 38, 905–917. doi:10.1002/etc.4373
- Reus, J., Lenndertse, C., Bockstaller, C., Fomsgaard, I., Gutsche, V., and Lewis, K. (2002). Comparison and evaluation of eight pesticide environmental risk indicators developed in Europe and recommendations for future use. *Agri Ecosyst. Environ.* 90, 177–187. doi:10.1016/S0167-8809(01)00197-9
- Reus, J. A. W., and Leendertse, A. P. C. (2000). The environmental yardstick for pesticides: A practical indicator used in The Netherlands. *Issues* 19 (8–10), 637–641. doi:10.1016/S0261-2194(00)00084-3
- Sala, O. E., Chapin, F. S., Armesto, J. J., Berlow, E., Bloomfield, J., Dirzo, R., et al. (2000). Global biodiversity scenarios for the year 2100. *Science* 287, 1770–1774. doi:10.1126/science.287.5459.1770
- Schäfer, R. B., Gerner, N., Kefford, B. J., Rasmussen, J. J., Beketov, M. A., de Zwart, D., et al. (2013). How to characterize chemical exposure to predict ecologic effects on aquatic communities? *Environ. Sci. Technol.* 47, 7996–8004. doi:10.1021/es4014954
- Schäfer, R. B., and Piggott, J. J. (2018). Advancing understanding and prediction in multiple stressor research through a mechanistic basis for null models. *Glob. Change Biol.* 24, 1817–1826. doi:10.1111/gcb.14073
- Schell, T., Goedkoop, W., Zubrod, J. P., Feckler, A., Lüderwald, S., Schulz, R., et al. (2018). Assessing the effects of field-relevant pesticide mixtures for their compliance with the concentration addition model – an experimental approach with *Daphnia magna*. *Sci. Total Environ.* 644, 342–349. doi:10.1016/j.scitotenv.2018.06.334
- Schneider, M. K., Brunner, F., Hollis, J. M., and Stamm, C. (2007). Towards a hydrological classification of European soils: Preliminary test of its predictive power for the base flow index using river discharge data. *Hydrol. Earth Syst. Sci.* 11, 1501–1513. doi:10.5194/hess-11-1501-2007
- Schreiner, V. C., Szöcs, E., Bhowmik, A. K., Vijver, M. G., and Schäfer, R. B. (2016). Pesticide mixtures in streams of several European countries and the USA. *Sci. Total Environ.* 573, 680–689. doi:10.1016/j.scitotenv.2016.08.163
- Schriever, C. A., and Liess, M. (2007). Mapping ecological risk of agricultural pesticide runoff. *Sci. Total Environ.* 384, 264–279. doi:10.1016/j.scitotenv.2007.06.019
- Smetanová, S., Bláha, L., Liess, M., Schäfer, R. B., and Beketov, M. A. (2014). Do predictions from Species Sensitivity Distributions match with field data? *Environ. Pollut.* 189 (0), 126–133. doi:10.1016/j.envpol.2014.03.002
- Stampfli, N. C., Knillmann, S., Liess, M., Noskov, Y. A., Schäfer, R. B., and Beketov, M. A. (2013). Two stressors and a community – effects of hydrological disturbance and a toxicant on freshwater zooplankton. *Aquat. Toxicol.* 127, 9–20. doi:10.1016/j.aquatox.2012.09.003
- Stehle, S., Knabel, A., and Schulz, R. (2013). Probabilistic risk assessment of insecticide concentrations in agricultural surface waters: A critical appraisal. *Environ. Monit. Assess.* 185 (8), 6295–6310. doi:10.1007/s10661-012-3026-x
- Szöcs, E., Brinke, M., Karaoglan, B., and Schäfer, R. B. (2017). Large scale risks from agricultural pesticides in small streams. *Environ. Sci. Technol.* 51, 7378–7385. doi:10.1021/acs.est.7b00933
- Tiktak, A., de Nie, D. S., Pineros Garcet, J. D., Jones, A., and Vanclooster, M. (2004). Assessment of the pesticide leaching risk at the Pan-European level. The EuroPEARL approach. *J. Hydrology* 289, 222–238. doi:10.1016/j.jhydrol.2003.11.030
- Tiktak, A., de Nie, D. S., van der Linden, A. M. A., and Kruijne, R. (2002). Modelling the leaching and drainage of pesticides in The Netherlands: The GeoPEARL model. *Agronomie* 22, 373–387. doi:10.1051/agro:2002022
- Udias, A., Galimberti, F., Dorati, C., and Pistocchi, A. (2022). *Emissions of pesticide active substances in the European Union, extrapolated from country reports*. Submitted.
- Uriónabarrenetxea, E., Casás, C., García-Velasco, N., Santos, M., Tarazona, J. V., and Soto, M. (2022). Predicting environmental concentrations and the potential risk of Plant Protection Products (PPP) on non-target soil organisms accounting for regional and landscape ecological variability in European soils. *Chemosphere* 303, 135045. doi:10.1016/j.chemosphere.2022.135045
- Van den Brink, P. J., Bracewell, S. A., Bush, A., Chariton, A., Choung, C. B., Compson, Z. G., et al. (2019). Towards a general framework for the assessment of interactive effects of multiple stressors on aquatic ecosystems: Results from the Making Aquatic Ecosystems Great Again (MAEGA) workshop. *Sci. Total Environ.* 684, 722–726. doi:10.1016/j.scitotenv.2019.02.455
- Vigiak, O., Udias, A., Pistocchi, A., Zanni, M., Alberto, A., and Grizzetti, B. (2021). Probability maps of anthropogenic impacts affecting ecological status in European rivers. *Ecol. Indic.* 126, 107684. doi:10.1016/j.ecolind.2021.107684
- Vogt, J. V. (2007). A pan-European river and catchment database. *EC-JRC Rep. Eur. 22920 En. Luxemb.*, 120. Available at: https://ccm.jrc.ec.europa.eu/documents/CCM2-Report_EUR-22920-EN_2007_STD.pdf.
- Vörösmarty, C. J., McIntyre, P. B., Gessner, M. O., Dudgeon, D., Prusevich, A., Green, P., et al. (2010). Global threats to human water security and river biodiversity. *Nature* 467, 555–561. doi:10.1038/nature09440
- Wolfram, J., Stehle, S., Bub, S., Petschick, L. L., and Schulz, R. (2021). Water quality and ecological risks in European surface waters – monitoring improves while water quality decreases. *Environ. Int.* 152, 106479. doi:10.1016/j.envint.2021.106479



OPEN ACCESS

EDITED BY

Abdul Qadeer,
Chinese Research Academy of
Environmental Sciences, China

REVIEWED BY

Jingqian Xie,
Shanghai Ocean University, China
Shangwei Zhang,
Beijing Normal University, China
Xixi Li,
Chinese Research Academy of
Environmental Sciences, China

*CORRESPONDENCE

Xiumei Sun,
✉ xiumeisun250438667@163.com

RECEIVED 09 August 2023

ACCEPTED 07 November 2023

PUBLISHED 20 November 2023

CITATION

Song S, Sun X, Cheng X, Peng X, Hao Q,
Hu H, Zhu J, Li T and Guo Y (2023), The
distribution and metabolism of
hexabromocyclododecane isomers
varies in the tissues of *Nibea albiflora*.
Front. Environ. Sci. 11:1274997.
doi: 10.3389/fenvs.2023.1274997

COPYRIGHT

© 2023 Song, Sun, Cheng, Peng, Hao, Hu,
Zhu, Li and Guo. This is an open-access
article distributed under the terms of the
[Creative Commons Attribution License](#)
(CC BY). The use, distribution or
reproduction in other forums is
permitted, provided the original author(s)
and the copyright owner(s) are credited
and that the original publication in this
journal is cited, in accordance with
accepted academic practice. No use,
distribution or reproduction is permitted
which does not comply with these terms.

The distribution and metabolism of hexabromocyclododecane isomers varies in the tissues of *Nibea albiflora*

Suping Song^{1,2}, Xiumei Sun^{1,2*}, Xin Cheng^{1,2}, Xijian Peng³,
Qing Hao^{1,2}, Hongmei Hu^{1,2}, Jian Zhu^{1,2}, Tiejun Li^{1,2} and
Yuanming Guo^{1,2}

¹Marine and Fisheries Research Institute of Zhejiang Ocean University, Zhoushan, China, ²Key Laboratory of Sustainable Utilization of Technology Research for Fisheries Resources of Zhejiang Province, Zhejiang Marine Fisheries Research Institute, Zhoushan, China, ³Zhejiang Huanneng Environmental Technology Co., Ltd., Hangzhou, China

Hexabromocyclododecanes (HBCDs), as brominated flame retardants, have increasingly drawn concern due to their detection in various marine organisms in recent years. The present test investigated the selective accumulation, depuration, and bioisomerization of HBCDs in different tissues and organs of *Nibea albiflora*, as well as the genetic metabolic behavior of HBCDs between parents and offspring. In a semi-static water environment, *N. albiflora* were exposed to individual HBCD diastereoisomers (α -HBCD, β -HBCD, or γ -HBCD) at a concentration of 0.4 $\mu\text{g/L}$ for bioaccumulation, followed by clean food for depuration. During the exposure period, the highest concentrations of these HBCDs were observed in the intestine and gill of *N. albiflora*. α -HBCD was detected in all exposure groups, suggesting that both β -HBCD and γ -HBCD could be bioisomerized to α -HBCD in *N. albiflora*. In addition, there was no bioisomerization of α -HBCD to either β -HBCD or γ -HBCD, and there was no bioisomerization between β -HBCD and γ -HBCD. The half-lives ($t_{1/2}$) were variable among different diastereoisomers, following an order of α -HBCD > γ -HBCD > β -HBCD. The most rapid depuration rate of HBCDs was discovered in the liver while muscle showed the least. Additionally, prior to spawning, the parent fish were exposed to contaminated feed (silkworms sprayed with 200 μL of a 30 $\mu\text{g/mL}$ HBCD solution) for 6 days. By comparing the HBCDs concentrations in the maternal gonad, fertilized eggs, hatching eggs, larvae, and juveniles, it was determined that the maternal transfer coefficients for HBCDs were approximately 1, indicating dynamic equilibrium of HBCDs throughout the process from maternal tissue to progeny development. Differences in HBCDs pattern between organs observed in the experiment support a proposal of an organ-specific diastereomer accumulation.

KEYWORDS

hexabromocyclododecanes, isomers, bioisomerization, selective-accumulation, distribution, depuration

1 Introduction

Hexabromocyclododecanes (HBCDs), as non-bonded additive brominated flame retardants (BFRs), have been extensively utilized in construction, textiles, and electronic products due to their effective flame-retardant properties and minimal impact on material properties (Lopes and Elisa, 2023). During the lifecycle phases (i.e., production, application,

transportation, or disposal) of these products, HBCDs can be easily released into the environment. In recent years, HBCDs have been widely detected in environmental (e.g., soil, water, and offshore sediments) (Goto et al., 2020; Pan et al., 2022; Wu et al., 2023), as well as in organisms (e.g., birds, aquatic animals, plants, and humans) (Fournier et al., 2012; Lu et al., 2019; Feiteiro et al., 2021; Tavoloni et al., 2021). HBCDs have even been detected in remote regions such as the South Pole and Arctic (Koch et al., 2015; Kim et al., 2018). Due to their long-distance transport, persistence, bioaccumulation and toxicity, HBCDs were included as persistent organic pollutants on the Stockholm Convention Persistent Organic Pollutants (POPs) list in May 2013. The widespread distribution of HBCDs in marine organisms has attracted great concerns, due to their adverse impacts on marine organisms and human health (Zhang et al., 2022; Ghzela et al., 2023).

The lipophilic and hydrophobic properties of HBCDs facilitates their bioaccumulation within organisms. Furthermore, HBCDs accumulated mainly in adipose tissues, with annual increments observed (Ruan et al., 2018). A wide detection spectrum of HBCDs in fish along China's coastline revealed concentrations spanning from non-detectable levels to 2,970 ng/g lw (Zhang et al., 2022). Concentrations in *Neophocaena phocaenoides* and *Sousa chinensis* in China's South Sea were significantly elevated compared to their environment. The accumulation of HBCDs in fish tissues followed the order: fat > liver > gill > muscle, exhibiting a positive correlation with tissue lipid content (Tang et al., 2015). Such observations underscore HBCDs' proclivity for organismal fat layers. These compounds pose degradation challenges for organisms and can inflict extensive effects on various biota, including humans. HBCDs have been associated with toxic effects affecting various physiological systems, including the liver, nerves, and thyroid, as well as the immune, endocrine, and reproductive systems (Darnierud, 2003; Lilienthal et al., 2009; Koch et al., 2015). While previous research primarily examined the exposure to a mix of HBCDs, it is actually divided into many isomers, each with distinct properties. HBCDs exhibit isomer-selective bioaccumulation, metabolic and toxic effects. Therefore, a more nuanced analysis of individual HBCD isomers is warranted for a thorough and precise ecological risk assessment in environmental contexts.

Among the 16 possible stereoisomers, the HBCDs products contain predominantly three isomers: γ -(75–89%), α -(10–13%) and β -HBCD (1–12%) (Tavoloni et al., 2020). In addition, industrial HBCDs also contain slight amounts of δ -HBCD and ϵ -HBCD (Zoeller, 2012). The polarity, dipole moment, and water solubility of the three main isomers differ, resulting in variable environmental stability and biological uptake rates (Oh et al., 2014). The octanol-water partition coefficients ($\log K_{ow}$) of α -, β -, and γ -HBCD at 25°C were 5.59, 5.44, and 5.53, respectively (Gerecke et al., 2006; Goss et al., 2008; Oh et al., 2014), indicating a strong predisposition for these compounds to accumulate in organisms. In particular, α -HBCD has been identified as a preferred enantiomer in various species (Ruan et al., 2018; Ruan et al., 2018; Zhang et al., 2018), with its enantioselectivity varying among organisms (Zhang et al., 2014; Huang et al., 2017). It has been reported that γ - and β -HBCD may not bioaccumulate (Zhang et al., 2018). Brandon et al. (2020) notably observed that shrimp fed with whiteflies containing HBCDs exhibited neither enrichment nor accumulation but maintained a metabolic equilibrium. However, in-depth studies on the causes of selective enrichment are lacking.

Given the distinct behaviors of HBCDs in biota accumulation, disposition, and effects, understanding the mechanisms behind these processes is crucial for both regulatory and toxicological considerations. The selective enrichment of HBCD stereoisomers in environmental and biological samples, results from multiple factors. These include differences in exposure sources, water solubility of isomers, bioavailability, selective absorption, organs excreting the compound, biological metabolic rates, and selective conversion of stereoisomers within organisms. These factors must be comprehensively considered in the ecological hazard assessments of HBCDs, along with accurate qualitative and quantitative analyses of their stereoisomers. To understand the selective enrichment, transformation, and distribution mechanism of HBCDs in different tissues and organs of *N. albiflora*, as well as its genetic metabolic behavior between parents and offsprings, controlled laboratory accumulation studies are necessary. In the present study, *N. albiflora* were exposed to individual compounds in water and purification experiments were conducted. Additionally, parental exposure experiments using HBCD-containing feed were also conducted. The diastereomer-specific bioaccumulation, distribution, metabolic behavior, and mechanisms of each HBCD isomer in various organs or tissues of *N. albiflora* (including blood, gonad, liver, intestine, gallbladder, spleen, kidney, gill, brain, and muscle) were assessed, as well as the maternal transfer capability of HBCDs.

2 Materials and methods

2.1 Chemicals and reagents

α -HBCD (CAS 134237-50-6), β -HBCD (CAS 134237-51-7) and γ -HBCD (CAS 134237-52-8), as 100.8 $\mu\text{g/mL}$ in toluene (1 mL), were purchased from AccuStandard, Inc. (USA). HBCD (unequal mix of 3 isomers of $^{13}\text{C}_{12}$, 99%, 50 $\mu\text{g/mL}$ in toluene, 1.2 mL, CAS 25637-99-4) was purchased from Cambridge Isotope Laboratories, Inc. (United States). *n*-Hexane (CAS 110-54-3), acetone (CAS 67-64-1), acetonitrile (CAS 75-05-8), and anhydrous sodium sulfate (CAS 7757-82-6) were purchased from ANPEL Laboratory Technologies Inc. (Shanghai, China). Dichloromethane (CAS 75-09-2) was purchased from J. T. Baker (United States). Methanol (CAS 67-56-1) was purchased from Merck. (Germany). Concentrated sulfuric acid (95.0%–98.0%, CAS 7664-93-9) was purchased from Sinopharm Chemical Reagent Co., Ltd. (Shanghai, China).

2.2 Biological experiments

2.2.1 Exposure and purification experiment of *Nibea albiflora* in semi-static water

HBCDs were pre-equilibrated at designated concentrations to eliminate any potential adsorption to the walls of fiberglass tanks. In a preliminary trial, *N. albiflora* were exposed to pollutants at concentrations of 0, 0.2, and 0.4 $\mu\text{g/L}$. A discernible accumulation in the organisms was observed at the 0.4 $\mu\text{g/L}$ concentration within a brief duration. Notably, previous research reported an ambient HBCD concentration of $0.35 \pm 0.06 \text{ ng/L}$ in seawater from

aquaculture areas (Pan et al., 2023). The exposure level of 0.4 µg/L was selected based on the concentration of HBCDs in natural environment, aiming to facilitate discernible accumulation of HBCD isomers within a short time. *N. albiflora* without obvious diseases and deformities were randomly selected for the investigation. After being acclimated for over 2 weeks, sixty adult *N. albiflora* were randomly divided into four groups, including three experimental groups and one control group. *N. albiflora* were exposed to 0.4 µg/L of α -HBCD, β -HBCD, or γ -HBCD using the semi-static water exposure method. Specifically, 50% of the water containing a single compound was renewed every day to maintain each isomer concentration. Acetone was used as the control. Fish were fed an amount equivalent to 1% of their body weight daily at a fixed time. The exposure period lasted 6 d. The exposure test lasted for 6 d followed by 9 d of depuration test. The depuration test was conducted in seawater without HBCDs. During the experiment, the tanks remained under the same conditions as acclimation process. Sufficient oxygen was provided, with a constant temperature at $24^{\circ}\text{C} \pm 1^{\circ}\text{C}$ throughout the experiment. The health and behavior of the experimental fish were monitored daily.

Samples from various tissues and organs were collected at 1, 3, and 6 d post-exposure, and days 4 and 9 post-depuration. At each sampling time, 2 *N. albiflora* specimens were randomly selected from each tank to make up pooled samples, ensuring a representative analysis. After washing and removing surface moisture, the specimens were dissected to collect samples from different tissues and organs, including blood, liver, intestine, spleen, kidney, gallbladder, gill, brain, muscle, and gonad. These samples were sealed in glass containers and frozen at -20°C until HBCD chemical analysis.

2.2.2 Exposure of broodstock and hatching of fertilized eggs

2.2.2.1 Exposed breeding of parent fish

Initially, the *N. albiflora* were cultivated in earthen ponds where they were fed a mixture of small fish, after which, they were transferred indoors for overwintering and given frozen squid as bait. The ponds floors were cleaned daily to maintain hygiene. During the pre-oviposition period, female and male brood fish were segregated and fed separately. They were fed with uncontaminated silkworms in the morning and with silkworms contaminated (sprayed with the 200 µL of 30 µg/mL HBCDs) in the afternoon. The exposure continued for 6 d. During this period, special attention was given to the brood *N. albiflora*, with emphasis on tracking their gonadal development. After gonadal maturation, males and females were transferred to seawater without HBCDs and allowed to interbreed, concentrating on spawning. Normal eggs were subsequently selected, counted, and hatched in fresh seawater. Both brood fish and fertilized eggs were utilized in subsequent analysis.

2.2.2.2 Incubation of fertilized eggs

Fertilized eggs were incubated in standing water at 26°C , then reared in static water with micro-aeration at 22°C – 25°C . After an embryonic development of 20–36 h, larval were separated from the membranes. From 3 to 4 d post-hatching, they were fed rotifers as opening bait for 8–10 d. Feeding occurred at 4-h intervals, with quantities adjusted according to consumption. Water quality was

monitored daily, and any remaining membrane were removed if necessary. Following the rotifer-feeding period, water was renewed and maintained at a depth of 5 cm. By 14 d post-hatching, larvae grew to approximately 10 mm, with morphology and organs development resembling parent fish, marking their transition into the juvenile phase. Samples were collected and analyzed at 0 d (fertilized eggs), 1 d (hatching eggs), 3 d (larval fish, 2.84 mm), 10d (larval fish, ~5 mm) and 14 d (juvenile fish, ~10 mm).

2.3 Sample preparation and analytical methods

2.3.1 Sample extraction and clean up

After freeze-drying, 2.00 g of the homogenized sample was accurately weighed into a 50 mL centrifuge tube (Polypropylene, Corning Life Sciences (Wujiang) Co., Ltd.) with 2.0 g of anhydrous sodium sulfate to enhance sample dispersion and improve extraction efficiency. Subsequently, 100 µL of internal standard solution (mixed internal standard solution of ^{13}C - α -HBCD, ^{13}C - β -HBCD, and ^{13}C - γ -HBCD with a mass concentration of 100 ng/mL) was added. A total of 30 mL of acetone/*n*-hexane (1:1, v/v) was added to the centrifuge tube, which were completely mixed by shaking for 2 min. After that, the tubes were ultrasonicated for 10 min, followed by centrifugation at 5,000 rpm for 5 min to separate the supernatant. The supernatant was then transferred to a rotary evaporator. The residue was re-extracted with the above-mentioned method. All separated supernatants were combined and reduced to dryness at 40°C using the vacuum-rotary evaporation. The residue was reconstituted with 10 mL of *n*-hexane and transferred to a centrifuge tube for sulfonation with 10 mL of concentrated sulfuric acid (China National Pharmaceutical Group, Beijing, China). The mixture was shaken and separated by centrifugation at 5,000 rpm for 5 min. The supernatant was transferred to a rotary evaporator. The lower layer was re-extracted with 10 mL of *n*-hexane. The whole organic extract was concentrated under reduced pressure in a vacuum concentrator to a volume of 1 mL of hexane for the cleanup step.

Sample cleanup procedure was performed using solid phase extraction (SPE). The SPE cartridges (silica, 1 g/6 mL, ANPEL Laboratory Technologies Inc., Shanghai, China) were previously conditioned with 5 mL of *n*-hexane. After loading the extracts, cartridges were cleaned with 1 mL of *n*-hexane. The HBCDs retained in the cartridges were eluted with 10 mL of a mixture *n*-hexane and dichloromethane (1:3, v/v). The eluent obtained from the cartridge was evaporated to dryness, and then the residue was redissolved in 1 mL of methanol, subsequently filtrated with a 0.22 µm organic phase membrane filter (13 mm × 0.22 µm, ANPEL Laboratory Technologies Inc., Shanghai, China) and transferred to an injection vial prior to ultra performance liquid chromatography-triple quadrupole tandem mass (UPLC-QqQ-MS/MS) analysis.

2.3.2 UPLC-QqQ-MS/MS analysis

The separation and quantification of HBCDs were performed by UPLC-QqQ-MS/MS (Acquity-Quattro Premier XE, Waters, United States) with electrospray ionization. The mobile phase consisted of ultra-pure Milli-Q (with a resistivity of 18.2 MΩ cm)

TABLE 1 Mobile phase elution program.

Time (min)	A (%)	B (%)
0	80	20
1.00	25	75
8.00	15	85
10.00	80	20

and methanol-acetonitrile (4:6, v/v). The composition and ramp of mobile phase were listed in Table 1. The separation of HBCDs in the extracts was performed on a BEH C18 column (100 mm × 2.1 mm × 1.7 μm, Waters, United States) with a mobile phase flow rate of 0.3 mL/min at 40°C. The injection volume was 10 μL. Electrospray ionization was performed in the negative ion mode. The identification and quantitation of HBCDs were performed using multiple reaction monitoring mode (MRM). The parent ions, daughter ions, and collision voltages were listed in Table 2. Specifically, the ion pair m/z 640.4–80.9 was monitored for quantitation, while the ion pair m/z 640.4–78.9 was monitored for qualitative analysis. The labeled HBCD isomers were identified using the ion pair m/z 652.3–78.9.

2.4 Quality assurance/quality control

The HBCDs mixed standard solution was serially diluted with methanol to prepare six concentrations (0, 1.00, 5.00, 10.0, 20.0, and 50.0 ng/mL) of standard solutions. The concentration of the internal standard was set at 10 ng/mL. A standard curve was plotted based on these standard solutions. The correlation coefficients (r^2) of all three isomers exceeded 0.99. The limit of quantitation (LOD) was calculated based on a 10-fold signal-to-noise ratio and was established as 0.20 μg/kg for the UPLC-MS/MS analytical method. Blanks and samples were analyzed concurrently, and no analytes were detected in any blank samples. At three spiked concentration levels of 0.5, 2.5, and 10 μg/kg, the recovery rate for HBCDs was 85.8%–97.3%, and the relative standard deviation was less than 9.10%. This method demonstrated good recovery, high

accuracy, and excellent precision, fulfilling the requirements for subsequent experimental analyses.

2.5 Data processing

A first-order kinetic model was used to fit the purification-stage data (Geng et al., 2019):

$$C_t = C_0 e^{-kt} \quad (1)$$

Purification half-lives (Li et al., 2017):

$$t_{1/2} = \frac{\ln 2}{k} \quad (2)$$

where, C_t is the analyte concentration in *N. albiflora* at time t , C_0 is the analyte concentration in *N. albiflora* at time 0 of purification, and k is the purification rate constant, which also corresponds to the slope of regression curve.

Statistical analyses were performed using SPSS (Statistical Package for the Social Sciences; v 24, IBM). Kruskal–Wallis H tests and one-way analyses of variance were used to determine statistical significance. The criterion for statistical significance was set at $p < 0.05$ throughout the study.

3 Results and discussions

3.1 Distribution characteristics and selective accumulation of HBCDs in *Nibea albiflora*

Figure 1 shows the concentrations of α -, β -, and γ -HBCD in various tissues from *N. albiflora* following exposures of 3 and 6 days. These variations underscore the differential impacts of pollution sources and exposure durations on the accumulation of these compounds, as suggested by Bertucci et al. (2020). The HBCDs accumulated with time in all tissues (except the β - and γ -HBCD-treated group in gallbladder), though the rates were inconsistent. Exposed to α -HBCD for 3 d, the highest concentration were recorded in the intestine (125.20 ng/g dw)

TABLE 2 Selective reaction monitoring of parent ions, daughter ions, and collision voltages.

Compounds	Parent ions (m/z)	Daughter ions (m/z)	Collision voltages (V)
α -HBCD	640.4	80.9	15
		78.9	15
β -HBCD	640.4	80.9	15
		78.9	15
γ -HBCD	640.4	80.9	15
		78.9	15
^{13}C - α -HBCD	652.3	78.9	15
^{13}C - β -HBCD	652.3	78.9	15
^{13}C - γ -HBCD	652.3	78.9	15

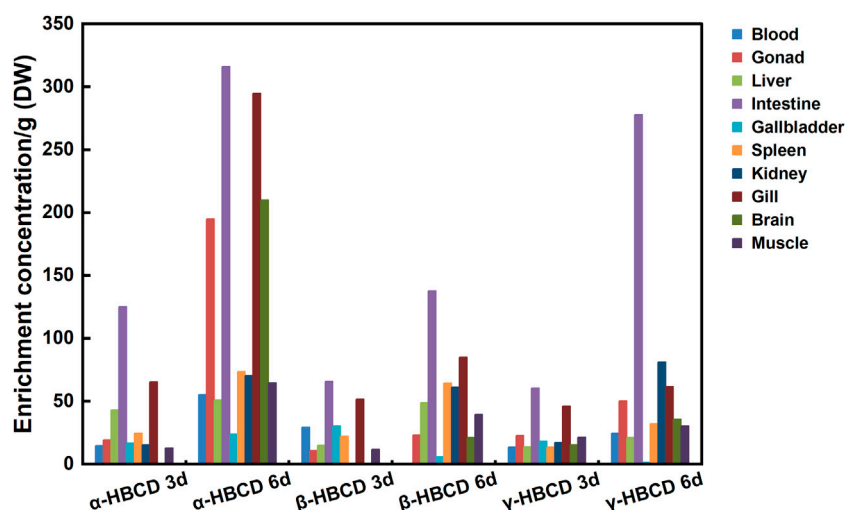


FIGURE 1

Distribution characteristics and selective enrichment of α -HBCD, β -HBCD, and γ -HBCD in the tissues/organs of *N. albiflora*. Note: HBCD, hexabromocyclododecane; DW, dry weight.

and gill (65.43 ng/g dw), whereas the lowest being in the brain. Following 6 d of exposure to α -HBCD, the concentrations of α -HBCD in the intestine, gill, and gonad increased significantly to 316.10, 294.90, and 194.9 ng/g dw, respectively, with the lowest concentration at this juncture was in the gallbladder (24.00 ng/g dw). After β -HBCD exposure for 3 d, the highest concentrations were observed in the intestine (65.93 ng/g dw) and gill (51.57 ng/g dw). In contrast, β -HBCD was undetectable in brain and kidney, whereas α -HBCD was detected, indicating a bioisomerization of β -HBCD to α -HBCD. After 6 d of exposure to β -HBCD, the concentrations in the intestine (137.85 ng/g dw) and gill (85.20 ng/g dw) were notably higher than in other tissues, with the gallbladder (5.71 ng/g dw) showing the lowest. Additionally, α -HBCD was detected in the kidney, intestine, and liver, indicating that β -HBCD was metabolized into α -HBCD in these tissues to varying degrees. Regarding γ -HBCD exposure at 3 d, its concentrations peaked in the intestine (60.65 ng/g dw) and gill (46.16 ng/g dw), while the spleen (13.67 ng/g dw) and kidney (17.22 ng/g dw) recorded the lowest concentrations. Interestingly, α -HBCD was identified in the brain, indicating that γ -HBCD was metabolized into α -HBCD. By the 6th day, the concentrations of γ -HBCD were more pronounced in the intestine (277.80 ng/g dw) and kidney (81.26 ng/g dw) compared to other tissues, with the gallbladder (1.40 ng/g dw) showing the lowest concentration. Furthermore, α -HBCD was detected in the brain, intestine, and gonad, indicating that γ -HBCD was metabolized into α -HBCD to varying degrees in these tissues. It may be attributed to conditions within the organism and the influence of thermal factors (Koeppen et al., 2008; Szabo et al., 2010). In summary, it is notable that α -HBCD was detected in all exposure groups, whereas no other diastereomers were found in the group spiked with β - or γ -HBCD only. Throughout the exposure, a bioisomerization of β - and γ -HBCD to α -HBCD was observed, whereas no isomerization of α -HBCD to β - or γ -HBCD was noted,

aligning with previous studies (Law et al., 2006; Zhang et al., 2016; Sun et al., 2018).

On the 3rd and 6th days post-exposure, the total concentrations of the HBCD isomers were compared across the three exposure groups. α -HBCD emerged as the dominant isomer in *N. albiflora*, with its concentration significantly higher those of β - and γ -HBCD ($p < 0.01$). The results further support the proposal of selective bioaccumulation of HBCD diastereoisomers. Likewise, Du et al. (Du M et al., 2012) observed the highest accumulation of α -HBCD in their experiments with zebrafish. A similar selective enrichment was also reported by Wang et al. (Wang et al., 2021) in their studies on human cells, attributing to the high affinity of efflux protein P-gp. Beyond binding affinity, transcriptomic expression patterns, protein levels, and enzymatic activities are paramount in influencing HBCD metabolism and transport within organisms. Further molecular studies are required to elucidate these underlying mechanisms.

Regarding tissue enrichment patterns, all exposure groups exhibited the highest concentrations in the intestine and gill. The distribution variability across different tissues could be attributed to both dynamic and thermodynamic factors. From a dynamic standpoint, intestine and gill have a heightened exposure to chemicals in water. Chemicals predominantly enter the intestine via ingestion or the gill via respiration, subsequently reaching various tissues and organs via the bloodstream. From a thermodynamic standpoint, the elevated lipid content in gill and intestine might account for the pronounced accumulation of hydrophobic chemicals within these tissues (Zhang et al., 2014). Similarly, Sun et al. (2009) found that the bioaccumulation of arsenate occurred through gill and intestinal uptake. In *Cyprinus carpio*, the sequence for HBCDs accumulation in intake tissues as intestine > gill > skin and distributed them as adipose > liver > brain > muscle (Zhang et al., 2016). Li et al. (2017) consistently observed tissues concentrations in *Eisenia fetida* following the order

TABLE 3 Purification parameters of HBCD diastereomers during the exposure experiment.

Pollutant	Organization	<i>k</i>	<i>t</i> _{1/2} (d)
α -HBCD	gonad	0.03	22.80
	liver	0.06	12.36
	muscle	0.02	29.62
β -HBCD	gonad	0.07	9.90
	liver	0.13	5.27
	muscle	0.06	11.67
γ -HBCD	gonad	0.05	14.97
	liver	0.06	11.46
	muscle	0.04	16.08

of intestine > body fluid > body wall. The gill and intestine emerge as critical interfaces of aquatic contaminant exposure on fish.

Compared to the concentrations observed on the 3rd day post-exposure, the concentration of HBCDs in the intestine increased noticeably by day 6. In addition to lipid partitioning, which is the principal mechanism underlying the bioaccumulation of HBCDs (Shin et al., 2020; Hou et al., 2022), inter-tissue- and organ-specific metabolic variations also modulate pollutant enrichment within an organism (Wang et al., 2020). We hypothesized that HBCDs, similar to other highly lipophilic compounds, are incorporated into lipoproteins during cellular assembly within intestinal cells. They are then absorbed by chylomicrons, which influences their free concentration *in vivo*. Since most of these compounds are chelated, their bioavailability to metabolic enzymes diminishes (Jandacek et al., 2009). In the present study, on the 3rd day of α -HBCD exposure, the detected concentration of α -HBCD in the brain at a mere 0.626 ng/g, surging to 210.10 ng/g by the 6th day. Concentrations of HBCDs in the brain also showed an increasing trend in the β -HBCD- and γ -HBCD-exposure groups. These findings suggest that HBCDs possess the capability to traverse the blood-brain barrier and accumulate within the brain (Zhang et al., 2016), warranting further research.

3.2 Depuration of HBCDs in *Nibea albiflora*

Consistent with the findings of previous research (Susanne et al., 2011), we observed that the purification curve in each tissue or organ largely adhered to first-order kinetics. The *k* and *t*_{1/2} for α -HBCD, β -HBCD, and γ -HBCD, calculated from the fit of the experimental data to Eqs 1, 2, are detailed in Table 3.

The values of *t*_{1/2} for α -HBCD, β -HBCD and γ -HBCD were in the range of 12.36–29.62, 5.27–11.67, and 11.46–16.06 respectively, and the values of *k* were 0.0234–0.0561, 0.0594–0.1316, and 0.0431–0.0605 respectively. Therefore, α -HBCD persisted the longest within *N. albiflora*, while β -HBCD and γ -HBCD metabolized quicker. This aligns with findings in both biota and liver cells, where α -HBCD exhibited the longest half-life (Gerecke et al., 2006; Huang et al., 2016). This finding supports

the notion that α -HBCD is the dominant isomer accumulating within marine fish species. The distinct physicochemical properties of the three HBCD diastereomers may have contributed to the varying depuration capabilities of *N. albiflora*. Previous isomer metabolism experiments have revealed variations in the metabolic pathways of different diastereomers. For instance, α -HBCD mainly undergoes oxidation without evidence of debromination or stereoisomerization. In contrast, β -HBCD and γ -HBCD have exhibited multiple metabolic pathways, including stereoisomerization, oxidation, dehydrogenation, reductive debromination, and ring-opening (Szabo et al., 2010; Taylor et al., 2011; Heldur, 2016). These metabolic differences make α -HBCD the predominant isomer within biological tissues, as it is the most resistant to metabolism and accumulates through the stereoisomerization of the β - and γ -HBCD diastereomers. This observation is further substantiated by marine sample analyses (N et al., 2005; Zhang et al., 2018). Compared to β -HBCD and γ -HBCD, α -HBCD exhibits greater resistance to metabolic degradation and transformation within biological systems (Zhang et al., 2014). The results of single-dose exposure experiments in rodents, specifically involving α -HBCD and γ -HBCD, demonstrated distinct metabolic pathways for these two diastereomers, and the extent of metabolism of γ -HBCD substantially surpassed that of α -HBCD. Research on the biometabolites of HBCDs in rats and mice has shown that HBCDs can activate Phase I and II metabolic enzyme systems, particularly the cytochrome P450 enzyme system (CYP2B and CYP3A). These enzyme systems, which are involved in pollutant degradation, facilitate the debromination or hydroxylation of HBCDs. This leads to cumulative or magnified toxicological effects (Zegers et al., 2005; Germer et al., 2006; Hakk et al., 2012). Additionally, in contrast to the isomer depuration rates found in both zebrafish and human HepG2 cells (α -HBCD < β -HBCD < γ -HBCD) (Du et al., 2012; Wang et al., 2021), we observed the depuration rate for β -HBCD to be greater than that for γ -HBCD in *N. albiflora*. It is noteworthy that Zhang et al. (2016) found no conversion between HBCD diastereomers in incubation experiments with chicken liver microsomes. Therefore, the ability of HBCD diastereomers to be metabolized varies between organisms. These suggest metabolic variability between organisms due to the unique interplay of metabolic enzymes and transport proteins.

In this study, marked differences were observed in the *k* and *t*_{1/2} values across different organs. The order of *k* for α -, β -, and γ -HBCD in different tissues was the same, liver > gonad > muscle. Specifically, the liver showed the highest depuration rate, supporting its role as the primary site of HBCDs metabolism (Topić Popović et al., 2023). Similar observations were made in experiments where *E. fetida* was exposed to soil containing HBCDs. For β -HBCD and γ -HBCD, the elimination rate constant (*k*_e) values were found to be in the sequence of intestine > body fluid > body wall, whereas for α -HBCD, the *k*_e values followed the order of body wall > intestine > body fluid (Li et al., 2017). Furthermore, Zhang et al. (2014) also reported the varying *k*₂ values of HBCDs across tissues of *C. carpio* following aquatic exposure. Therefore, the tissue distribution of chemicals is influenced by multiple factors, encompassing both kinetic aspects and the properties of the tissues. In the context of HBCDs, this distribution becomes even more intricate due to the distinct metabolic and isomerization tendencies of the three diastereomers across various tissues.

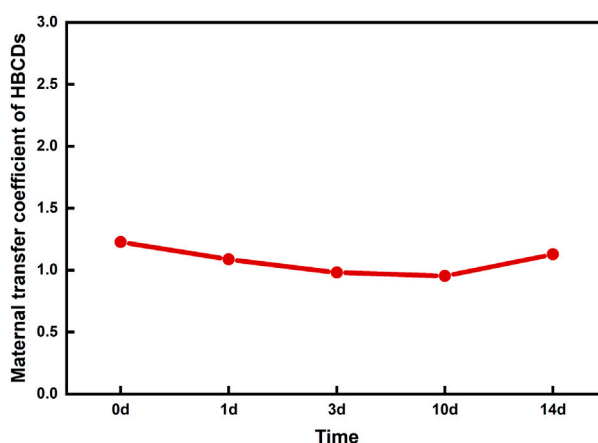


FIGURE 2
Maternal transfer coefficient of HBCDs in *N. albiflora*.

3.3 Selective genetic metabolism of HBCDs in *Nibea albiflora*

Maternal gonads, fertilized eggs and fry were used to evaluate the transmissibility of HBCDs to offspring. By analyzing the contaminant concentration and isomer composition across the three maternal tissues (i.e., gonads, liver, and muscle), fertilized eggs, and fish fry, selecting the most representative tissue to evaluate maternal transfer. We found that the concentrations and isomer characteristics of gonads align more closely with fertilized eggs than with the liver and muscle. Therefore, maternal gonads were selected to represent maternal concentrations during the transfer assessment. In oviparous organisms, should organic pollutants maintain an equilibrium distribution within the body throughout the egg-laying process, the maternal transfer coefficient—defined as the ratio of pollutant concentration in the egg to that in the maternal tissue—would consistently equate to 1 (Ross et al., 2008). Intriguingly, the maternal transfer coefficient for α -, β -, and γ -HBCD did not follow a discernible trend, which might due to isomer transformations during biological processes. Therefore, analyzing the total concentration of compounds, rather than focusing solely on isomerism, provides a more accurate evaluation of the progeny transfer ability. The maternal transfer coefficient for HBCDs was determined by calculating the ratio of the total concentration of HBCDs across various developmental stages in the progeny to that in the gonads. As depicted in Figure 2, the maternal transfer coefficients of the total HBCDs were approximately 1, which indicates that HBCDs were balanced during the transfer process from the maternal tissue to the progeny and the development of the progeny.

The HBCD isomer composition remained consistent in maternal gonads, as well as fertilized and hatching eggs, indicating that the accumulation pattern of HBCDs remain static during the formation and development of fertilized eggs. Similarly, the concentrations and characteristics of the diastereomers were consistent between larvae and juveniles, suggesting a stable HBCD accumulation pattern across these developmental stages. However,

transformations were observed among HBCD diastereomers during the transition from fertilized eggs to larvae and juveniles. The compositional patterns of diastereomers in maternal gonads, fertilized eggs, and various developmental stages are illustrated in Figure 3. Specifically, during the stages spanning maternal gonad to hatching eggs (gonad–1 d), the α -HBCD dominated with a concentration of approximately 45%. This was followed by β -HBCDs (~40%) and γ -HBCD (~15%). However, the composition changed dramatically during the larval to juvenile stage (3–14d). Here, α -HBCD accounted for only ~15% of the total, being the least prevalent, β -HBCDs at around 10%. Notably, γ -HBCD emerged as the dominant isomer, comprising roughly 75% of the overall HBCDs.

By comparing the characteristics of diastereomers in maternal gonads, fertilized eggs, and fry, we found that a transformation occurred from α -HBCD and β -HBCD to γ -HBCD during the developmental transition from embryos to larvae and subsequently to juveniles. This observation challenges the conventional understanding that α -HBCD cannot transform into other diastereomers and β -HBCDs cannot convert into γ -HBCD. Huang et al. (2016) also found trace amounts of γ -HBCD in HepG2 cells 6 d after incubation with α - or β -HBCD. Similarly, in female C57L/6 mice exposed to ^{14}C -labeled α -, β -, and γ -HBCD, β -HBCD could be bioisomerized to γ -HBCD (Sanders et al., 2013). While it is uncertain whether this conversion is attributed to microflora activity in the gut or metabolic activity within the tissues, the ability to convert HBCD diastereomers in *N. albiflora* does vary across their developmental stages. The precise underlying mechanism requires further exploration.

4 Conclusion

In exposure studies where *N. albiflora* was individually exposed to α -HBCD, β -HBCD, or γ -HBCD, α -HBCD was detected in all exposure groups, suggesting that both β -HBCD and γ -HBCD could be bioisomerized to α -HBCD. Diastereomers concentrations

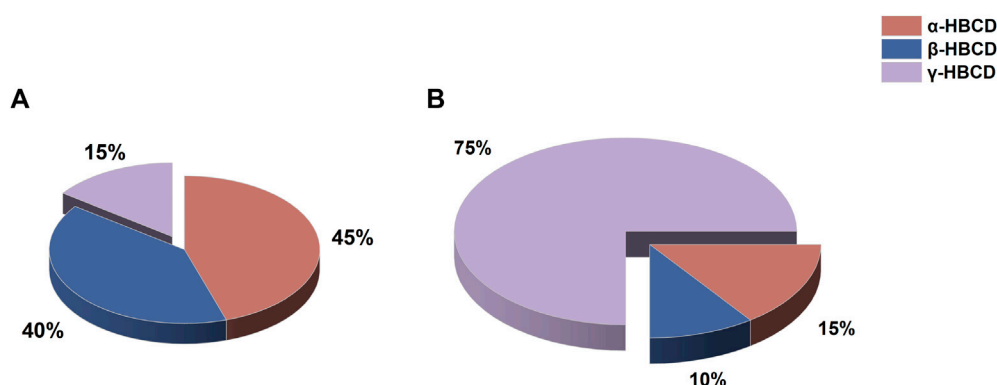


FIGURE 3

Composition of HBCD diastereomers at different developmental stages of the *N. albiflora*. Note: (A), gonad-1d (gonad, fertilized eggs, eggs hatched for 1d); (B), 3-14d (larvae and juveniles).

varied across tissues, with the intestine and gill exhibiting the highest levels. The half-lives sequence for the three diastereomers varied among tissues and organs, but consistently was α -HBCD > γ -HBCD > β -HBCD. Notably, the concentrations of HBCDs remained equilibrated during transmission from the maternal tissue to progeny and throughout progeny development. However, the mechanism of transformation among the three HBCD diastereomers differed at various developmental stages of *N. albiflora*.

Data availability statement

The raw data supporting the conclusion of this article will be made available by the authors, without undue reservation.

Ethics statement

The animal study was approved by the Zhejiang Marine Fisheries Research Institute, Key Laboratory of Sustainable Utilization of Technology Research for Fisheries Resources of Zhejiang Province, Zhoushan. The study was conducted in accordance with the local legislation and institutional requirements.

Author contributions

SS: Data curation, Software, Writing-original draft, Writing-review and editing, Conceptualization, Formal Analysis, Investigation. XS: Methodology, Project administration, Resources, Validation, Visualization, Writing-review and editing. XC: Conceptualization, Data curation, Investigation, Methodology, Writing-original draft.

References

Bertucci, J. I., Malala Irugal Bandaralage, S., and Hecker, M. (2020). Assessing the cytotoxic effect of hexabromocyclododecane (hbcdd) on liver tissue cultures from fathead minnow (*pimephales promelas*). *Aquat. Toxicol.* 225, 105523. doi:10.1016/j.aquatox.2020.105523

XP: Software, Writing-review and editing. QH: Formal Analysis, Writing-review and editing. HH: Methodology, Software, Writing-review and editing. JZ: Data curation, Investigation, Writing-review and editing. TL: Validation, Writing-review and editing. YG: Supervision, Writing-review and editing.

Funding

The author(s) declare financial support was received for the research, authorship, and/or publication of this article. This work was supported by the Zhejiang Basic Public Welfare Plan Project under contract LGF22B070004 and the National Natural Science Foundation of China under contract 21407127.

Conflict of interest

Author XP is employed by Zhejiang Huanneng Environmental Technology Co., Ltd.

The remaining authors declare that the research was conducted in the absence of any commercial or financial relationships that could be construed as a potential conflict of interest.

Publisher's note

All claims expressed in this article are solely those of the authors and do not necessarily represent those of their affiliated organizations, or those of the publisher, the editors and the reviewers. Any product that may be evaluated in this article, or claim that may be made by its manufacturer, is not guaranteed or endorsed by the publisher.

Brandon, A. M., Abbadi, S. H. E., Ibekwe, U. A., Cho, Y. M., Wu, W. M., and Criddle, C. S. (2020). Fate of hexabromocyclododecane (hbcdd), a common flame retardant, in polystyrene-degrading mealworms: elevated hbcdd levels in egested polymer but no bioaccumulation. *Environ. Sci. Technol.* 54, 364-371. doi:10.1021/acs.est.9b06501

- Darnerud, P. O. (2003). Toxic effects of brominated flame retardants in man and in wildlife. *Environ. Int.* 29, 841–853. doi:10.1016/S0160-4120(03)00107-7
- Du, M., Lin, L., Yan, C., and Zhang, X. (2012). Diastereoisomer- and enantiomer-specific accumulation, depuration, and bioisomerization of hexabromocyclododecanes in zebrafish (*Danio rerio*). *Environ. Sci. Technol.* 46, 11040–11046. doi:10.1021/es302166p
- Feiteiro, J., Mariana, M., and Cairrao, E. (2021). Health toxicity effects of brominated flame retardants: from environmental to human exposure. *Environ. Pollut.* 285, 117475. doi:10.1016/j.envpol.2021.117475
- Fournier, A., Feidt, C., Marchand, P., Vénisseau, A. S., Bizet, B. L., Sellier, N., et al. (2012). Kinetic study of γ -hexabromocyclododecane orally given to laying hens (*Gallus domesticus*). *Environ. Sci. Pollut. Res. Int.* 19, 440–447. doi:10.1007/s11356-011-0573-6
- Geng, J., Han, M., Yang, X., Li, Y., Bartlam, M., and Wang, Y. (2019). Different biotransformation of three hexabromocyclododecane diastereoisomers by *Pseudomonas* sp. under aerobic conditions. *Chem. Eng. J.* 374, 870–879. doi:10.1016/j.cej.2019.05.232
- Gerecke, A. C., Giger, W., Hartmann, P. C., Heeb, N. V., Kohler, H. E., Schmid, P., et al. (2006). Anaerobic degradation of brominated flame retardants in sewage sludge. *Chemosphere* 64, 311–317. doi:10.1016/j.chemosphere.2005.12.016
- Gerecke, A. C., Law, R. J., Voorspoels, S., Kohler, M., Heeb, N. V., Leslie, H., et al. (2006). Hexabromocyclododecanes (hbcds) in the environment and humans: a review. *Environ. Sci. Technol.* 40, 3679–3688. doi:10.1021/es0602492
- Germer, S., Piersma, A. H., van der Ven, L., Kamyschnikow, A., Fery, Y., Schmitz, H., et al. (2006). Subacute effects of the brominated flame retardants hexabromocyclododecane and tetrabromobisphenol A on hepatic cytochrome p450 levels in rats. *Toxicology* 218, 229–236. doi:10.1016/j.tox.2005.10.019
- Ghzel, M., Ben, A. W., Philippe, S., Soufiane, T., Ridha, D. M., and Laure, J. (2023). Correction to: first study of bromophenols and hexabromocyclododecanes in seafood from north africa (case of bizerte lagoon, Tunisia): occurrence and human health risk. *Environ. Sci. Pollut. Res. Int.* 30, 67914–67917. doi:10.1007/S11356-023-27268-8
- Goss, K. U., Arp, H. P. H., Bronner, G., and Niederer, C. (2008). Partition behavior of hexachlorocyclohexane isomers. *J. Chem. Eng. Data* 53, 750–754. doi:10.1021/jc700595y
- Goto, A., Tue, N. M., Isobe, T., Takahashi, S., Tanabe, S., and Kunisue, T. (2020). Nontarget and target screening of organohalogen compounds in mussels and sediment from hiroshima bay, Japan: occurrence of novel bioaccumulative substances. *Environ. Sci. Technol.* 54, 5480–5488. doi:10.1021/acs.est.9b06998
- Hakk, H., Szabo, D. T., Huwe, J., Diliberto, J., and Birnbaum, L. S. (2012). Novel and distinct metabolites identified following a single oral dose of α - or γ -hexabromocyclododecane in mice. *Environ. Sci. Technol.* 46, 13494–13503. doi:10.1021/es303209g
- Heldur, H. (2016). Comparative metabolism studies of hexabromocyclododecane (hbcd) diastereoisomers in male rats following a single oral dose. *Environ. Sci. Technol.* 50, 89–96. doi:10.1021/acs.est.5b04510
- Hou, R., Huang, Q., Pan, Y., Lin, L., Liu, S., Li, H., et al. (2022). Novel brominated flame retardants (nbfrs) in a tropical marine food web from the south China sea: the influence of hydrophobicity and biotransformation on structure-related trophodynamics. *Environ. Sci. Technol.* 56, 3147–3158. doi:10.1021/acs.est.1c08104
- Huang, H., Wang, D., Wan, W., and Wen, B. (2017). Hexabromocyclododecanes in soils and plants from a plastic waste treatment area in north China: occurrence, diastereomer- and enantiomer-specific profiles, and metabolism. *Environ. Sci. Pollut. Res. Int.* 24, 21625–21635. doi:10.1007/s11356-017-9792-9
- Huang, X., Chen, C., Shang, Y., Zhong, Y., Ren, G., Yu, Z., et al. (2016). *In vitro* study on the biotransformation and cytotoxicity of three hexabromocyclododecane diastereoisomers in liver cells. *Chemosphere* 161, 251–258. doi:10.1016/j.chemosphere.2016.07.001
- Jandacek, R. J., Rider, T., Yang, Q., Woollett, L. A., and Tso, P. (2009). Lymphatic and portal vein absorption of organochlorine compounds in rats. *American J. Physiology. Gastrointest. Liver Physiology* 296, G226–G234. doi:10.1152/ajpgi.90517.2008
- Kim, J. T., Choi, Y. J., Barghi, M., Yoon, Y. J., Kim, J. H., Kim, J. H., et al. (2018). Occurrence and distribution of old and new halogenated flame retardants in mosses and lichens from the south shetland islands, Antarctica. *Environ. Pollut.* 235, 302–311. doi:10.1016/j.envpol.2017.12.080
- Koch, C., Schmidt-Koetters, T., Rupp, R., and Sures, B. (2015). Review of hexabromocyclododecane (hbcd) with a focus on legislation and recent publications concerning toxicokinetics and -dynamics. *Environ. Pollut.* 199, 26–34. doi:10.1016/j.envpol.2015.01.011
- Koeppe, R., Becker, R., Jung, C., and Nehls, I. (2008). On the thermally induced isomerisation of hexabromocyclododecane stereoisomers. *Chemosphere* 71, 656–662. doi:10.1016/j.chemosphere.2007.11.009
- Law, K., Palace, V. P., Halldorson, T., Danell, R., Wautier, K., Evans, B., et al. (2006). Dietary accumulation of hexabromocyclododecane diastereoisomers in juvenile rainbow trout (*Oncorhynchus mykiss*): bioaccumulation parameters and evidence of bioisomerization. *Environ. Toxicol. Chem.* 25, 1757–1761. doi:10.1897/05-445r.1
- Li, B., Chen, H., Sun, H., and Lan, Z. (2017). Distribution, isomerization and enantiomer selectivity of hexabromocyclododecane (hbcd) diastereoisomers in different tissue and subcellular fractions of earthworms. *Ecotoxicol. Environ. Saf.* 139, 326–334. doi:10.1016/j.ecoenv.2017.01.004
- Lilienthal, H., Ven, L. T. M. V., Piersma, A. H., and Vos, J. G. (2009). Effects of the brominated flame retardant hexabromocyclododecane (hbcd) on dopamine-dependent behavior and brainstem auditory evoked potentials in a one-generation reproduction study in wistar rats. *Toxicol. Lett.* 185, 63–72. doi:10.1016/j.toxlet.2008.12.002
- Lopes, M. M., and Elisa, C. (2023). Occurrence and health effects of hexabromocyclododecane: an updated review. *Toxics* 11, 409. doi:10.3390/toxics11050409
- Lu, H., Ma, X. J., Huang, X. J., Lu, S., Huang, Y. H., Mo, C. H., et al. (2019). Distribution, diastereomer-specific accumulation and associated health risks of hexabromocyclododecanes (hbcds) in soil-vegetable system of the pearl river delta region, south China. *J. Environ. Manage.* 248, 109321. doi:10.1016/j.jenvman.2019.109321
- Oh, J. K., Kotani, K., Managaki, S., and Masunaga, S. (2014). Levels and distribution of hexabromocyclododecane and its lower brominated derivative in Japanese riverine environment. *Chemosphere* 109, 157–163. doi:10.1016/j.chemosphere.2014.01.074
- Pan, Y., Liu, S., Li, H., Lin, L., Hou, R., Cheng, Y., et al. (2023). Expanded polystyrene buoys as an important source of hexabromocyclododecanes for aquatic ecosystem: evidence from field exposure with different substrates. *Environ. Pollut.* 318, 120920. doi:10.1016/j.envpol.2022.120920
- Pan, Y., Liu, S., Lin, L., Cheng, Y., Hou, R., Li, H., et al. (2022). Release behaviors of hexabromocyclododecanes from expanded polystyrene microplastics in seawater and digestive fluids. *Gondwana Res.* 108, 133–143. doi:10.1016/j.gr.2021.10.030
- Ross, M. S., Verreault, J., Letcher, R. J., Gabrielsen, G. W., and Wong, C. S. (2008). Chiral organochlorine contaminants in blood and eggs of glaucous gulls (*Larus hyperboreus*) from the Norwegian arctic. *Environ. Sci. Technol.* 42, 7181–7186. doi:10.1021/es8000147
- Ruan, Y., Lam, J. C. W., Zhang, X., and Lam, P. K. S. (2018). Temporal changes and stereoisomeric compositions of 1,2,5,6,9,10-hexabromocyclododecane and 1,2-dibromo-4-(1,2-dibromoethyl)cyclohexane in marine mammals from the south China sea. *Environ. Sci. Technol.* 52, 2517–2526. doi:10.1021/acs.est.7b05387
- Ruan, Y., Zhang, X., Qiu, J. W., Leung, K. M. Y., Lam, J. C. W., and Lam, P. K. S. (2018). Stereoisomer-specific trophodynamics of the chiral brominated flame retardants hbcd and tbb in a marine food web, with implications for human exposure. *Environ. Sci. Technol.* 52, 8183–8193. doi:10.1021/acs.est.8b02206
- Sanders, J. M., Knudsen, G. A., and Birnbaum, L. S. (2013). The fate of β -hexabromocyclododecane in female c57bl/6 mice. *Toxicol. Sci.* 134, 251–257. doi:10.1093/toxsci/kft121
- Shin, E., Jeong, Y., Barghi, M., Seo, S., Kwon, S. Y., and Chang, Y. (2020). Internal distribution and fate of persistent organic contaminants (pcdd/fs, dl-pcbs, hbcds, tbbpa, and pfass) in a bos taurus. *Environ. Pollut.* 267, 115306. doi:10.1016/j.envpol.2020.115306
- Sun, H., Zhang, X., Zhang, Z., Chen, Y., and Crittenden, J. C. (2009). Influence of titanium dioxide nanoparticles on speciation and bioavailability of arsenite. *Environ. Pollut.* 157, 1165–1170. doi:10.1016/j.envpol.2008.08.022
- Sun, R., Luo, X., Zheng, X., Cao, K., Peng, P., Li, Q. X., et al. (2018). Hexabromocyclododecanes (hbcds) in fish: evidence of recent hbcd input into the coastal environment. *Mar. Pollut. Bull.* 126, 357–362. doi:10.1016/j.marpolbul.2017.11.040
- Susanne, E., Roland, B., Ronald, M., and Irene, N. (2011). Hexabromocyclododecane enantiomers: microsomal degradation and patterns of hydroxylated metabolites. *Environ. Sci. Technol.* 45, 3938–3944. doi:10.1021/es1039584
- Szabo, D. T., Diliberto, J. J., Hakk, H., Huwe, J. K., and Birnbaum, L. S. (2010). Toxicokinetics of the flame retardant hexabromocyclododecane gamma: effect of dose, timing, route, repeated exposure, and metabolism. *Toxicol. Sci.* 117, 282–293. doi:10.1093/toxsci/kfq183
- Tang, B., Zeng, Y. H., Luo, X. J., Zheng, X. B., and Mai, B. X. (2015). Bioaccumulative characteristics of tetrabromobisphenol A and hexabromocyclododecanes in multi-tissues of prey and predator fish from an e-waste site, south China. *Environ. Sci. Pollut. Res. Int.* 22, 12011–12017. doi:10.1007/s11356-015-4463-1
- Tavoloni, T., Stecconi, T., Galarini, R., Bacchiocchi, S., Dörr, A. J. M., Elia, A. C., et al. (2021). Bfrs (pbdes and hbcds) in freshwater species from lake trasimeno (Italy): the singular case of hbcds in red swamp crayfish. *Sci. Total Environ.* 758, 143585. doi:10.1016/j.scitotenv.2020.143585
- Tavoloni, T., Stecconi, T., Galarini, R., Bacchiocchi, S., Piersanti, A., Elia, A. C., et al. (2020). Bfrs (pbdes and hbcds) in freshwater species from lake trasimeno (Italy): the singular case of hbcds in red swamp crayfish. *Sci. Total Environ.* 758, 143585. doi:10.1016/j.scitotenv.2020.143585
- Taylor, S. D., Diliberto, J. J., Hakk, H., Huwe, J. K., and Birnbaum, L. S. (2011). Toxicokinetics of the flame retardant hexabromocyclododecane alpha: effect of dose, timing, route, repeated exposure, and metabolism. *Toxicol. Sci. Official J. Soc. Toxicol.* 121, 234–244. doi:10.1093/toxsci/kfr059
- Topić Popović, N., Čizmek, L., Babić, S., Strunjak-Perović, I., and Čož-Rakovac, R. (2023). Fish liver damage related to the wastewater treatment plant effluents. *Environ. Sci. Pollut. Res. Int.* 30, 48739–48768. doi:10.1007/s11356-023-26187-y
- Wang, H., Huang, W., Gong, Y., Chen, C., Zhang, T., and Diao, X. (2020). Occurrence and potential health risks assessment of polycyclic aromatic hydrocarbons (pahs) in different tissues of bivalves from hainan island, China. *Food Chem. Toxicol.* 136, 111108. doi:10.1016/j.fct.2019.111108

- Wang, X., Tan, X., Zhang, Y., Hu, X., Shen, C., Huang, Y., et al. (2021). The enantiomer-selective metabolism of hexabromocyclododecanes (hbcds) by human hepg2 cells. *Sci. Total Environ.* 768, 144430. doi:10.1016/j.scitotenv.2020.144430
- Wu, T., Li, X., Zheng, Z., Liu, Z., Yang, M., Zhang, N., et al. (2023). Hexabromocyclododecanes in surface soil-maize system around baiyangdian lake in north China: distribution, enantiomer-specific accumulation, transport, temporal trend and dietary risk. *J. Hazard Mater* 451, 131180. doi:10.1016/j.jhazmat.2023.131180
- Zegers, B. N., Mets, A., Van Bommel, R., Minkenberg, C., Hamers, T., Kamstra, J. H., et al. (2005). Levels of hexabromocyclododecane in harbor porpoises and common dolphins from western european seas, with evidence for stereoisomer-specific biotransformation by cytochrome p450. *Environ. Sci. Technol.* 39, 2095–2100. doi:10.1021/es049209t
- Zhang, Y., Li, S., Zhang, Y., Chen, Y., Wang, X., and Sun, Y. (2022). Bioaccumulation and biomagnification of hexabromocyclododecane in marine biota from China: a review. *Toxics* 10, 620. doi:10.3390/toxics10100620
- Zhang, Y., Lu, Y., Wang, P., and Shi, Y. (2018). Biomagnification of hexabromocyclododecane (hbcd) in a coastal ecosystem near a large producer in China: human exposure implication through food web transfer. *Sci. Total Environ.* 624, 1213–1220. doi:10.1016/j.scitotenv.2017.12.153
- Zhang, Y., Sun, H., and Ruan, Y. (2014). Enantiomer-specific accumulation, depuration, metabolism and isomerization of hexabromocyclododecane (hbcd) diastereomers in mirror carp from water. *J. Hazard Mater* 264, 8–15. doi:10.1016/j.jhazmat.2013.10.062
- Zhang, Y., Wang, L., Sun, H., Yao, T., Zhu, H., Xu, J., et al. (2016). Impacts of loach bioturbation on the selective bioaccumulation of hbcd diastereoisomers and enantiomers by mirror carp in a microcosm. *Chemosphere* 163, 471–479. doi:10.1016/j.chemosphere.2016.08.065
- Zoeller, Å. B. A. J., Heindel, J., Jobling, S., Kidd, K., and Zoeller, R. T. (2012). State-of-the-science of endocrine disrupting chemicals, 2012. *Toxicol. Lett.* 211, S3. doi:10.1016/j.toxlet.2012.03.020



OPEN ACCESS

EDITED BY

Abdul Qadeer,
Chinese Research Academy of Environmental
Sciences, China

REVIEWED BY

Zeljko Jakšić,
Rudjer Boskovic Institute, Croatia
Andrés Perez Parada,
Universidad de la República, Uruguay

*CORRESPONDENCE

Petra Oppeltová,
✉ oppeltova@mendelu.cz

RECEIVED 16 November 2023

ACCEPTED 18 January 2024

PUBLISHED 05 February 2024

CITATION

Oppeltová P, Vlček V, Geršl M, Chaloupský P,
Ulrich O, Sedláček J, Vavrouchová H,
Kohoutková K, Klepárník R and Šimečková J
(2024), Occurrence and path pollution of
emerging organic contaminants in mineral
water of Hranice hypogenic Karst.
Front. Environ. Sci. 12:1339818.
doi: 10.3389/fenvs.2024.1339818

COPYRIGHT

© 2024 Oppeltová, Vlček, Geršl, Chaloupský,
Ulrich, Sedláček, Vavrouchová, Kohoutková,
Klepárník and Šimečková. This is an open-
access article distributed under the terms of the
[Creative Commons Attribution License \(CC BY\)](https://creativecommons.org/licenses/by/4.0/).
The use, distribution or reproduction in other
forums is permitted, provided the original
author(s) and the copyright owner(s) are
credited and that the original publication in this
journal is cited, in accordance with accepted
academic practice. No use, distribution or
reproduction is permitted which does not
comply with these terms.

Occurrence and path pollution of emerging organic contaminants in mineral water of Hranice hypogenic Karst

Petra Oppeltová^{1*}, Vítězslav Vlček², Milan Geršl³,
Pavel Chaloupský⁴, Ondřej Ulrich¹, Jozef Sedláček⁵,
Hana Vavrouchová¹, Kristýna Kohoutková⁵, Radim Klepárník⁵
and Jana Šimečková²

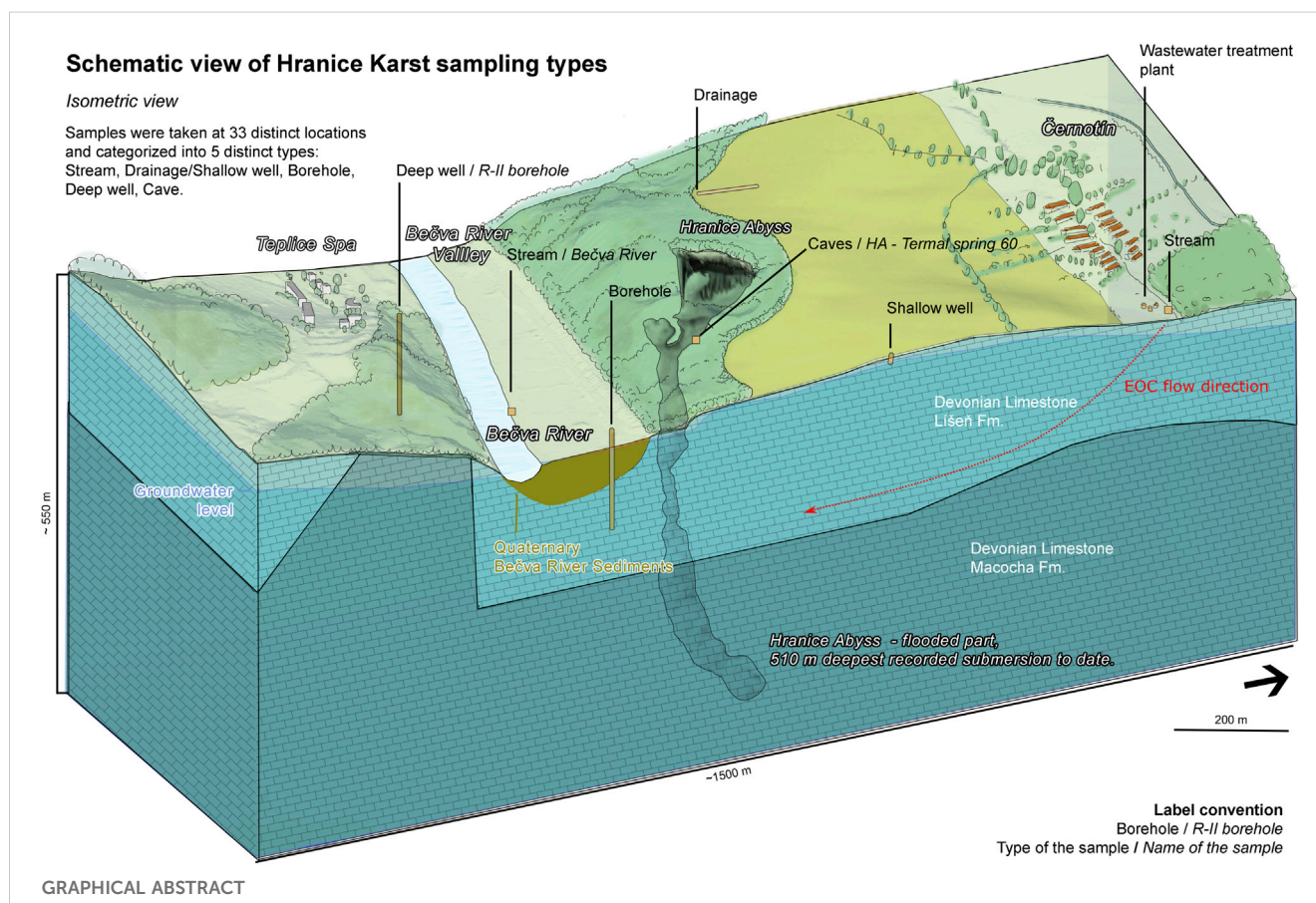
¹Department of Applied and Landscape Ecology, Faculty of AgriScience, Mendel University in Brno, Brno, Czechia, ²Department of Agrochemistry, Soil Science, Microbiology and Plant Nutrition, Faculty of AgriScience, Mendel University in Brno, Brno, Czechia, ³Department of Agricultural, Food and Environmental Engineering, Faculty of AgriScience, Mendel University in Brno, Brno, Czechia, ⁴Department of Chemistry and Biochemistry, Faculty of AgriScience, Mendel University in Brno, Brno, Czechia, ⁵Department of Landscape Planning, Faculty of Horticulture, Mendel University in Brno, Brno, Czechia

The Hranice hypogenic karst region includes urban, spa and agricultural areas and industry complexes that affect water quality in the region. Emerging organic contaminants (EOCs), especially pesticides and pharmaceuticals, are released into the complex aquatic system. These substances and their metabolites can affect aquatic and human life, as well as the regional development of the wider area traditionally associated with the spa. In this study, we conducted preliminary screening for pesticides and pharmaceuticals at 33 sampling sites and across different location types, including surface water, drainage water, a shallow well, groundwater and thermal karst water. Sampling occurred between February 2022 and June 2023. The results generally confirm that current land use is causing pollution in the karst system. The monitored substances were present in all water types, and in most cases the concentrations of pesticides were lower than those of their metabolites. Chloridazon desphenyl (DESPH) is the most widespread pesticide in surface, ground and hypogenic waters. Its concentrations in surface waters were 5.7 ng·L⁻¹–2,230 ng·L⁻¹, in groundwaters were 11.3 ng·L⁻¹–1,490 ng·L⁻¹ and in karst hypogenic waters 5.4 ng·L⁻¹–378 ng·L⁻¹. Diclofenac was the most widespread substance from the pharmaceutical group. Its concentrations ranged from 5.6 ng·L⁻¹–549 ng·L⁻¹ in surface waters, 8.4 ng·L⁻¹–112 ng·L⁻¹ in groundwaters and 5.1 ng·L⁻¹–47.4 ng·L⁻¹ in karst hypogenic waters. Directly in the karst hypogenic waters, the following EOCs were repeatedly detected: atrazine and its metabolites, simazin, metazachlor ethane sulfonic acid (ESA), metolachlor ESA, alachlor ESA, chloridazon DESPH, diclofenac, ibuprofen, azithromycin, bisphenol A and diethyltoluamide (DEET). The initial research hypothesis is that hydrothermal karst waters are of sub-recent

age and deep circulation and, unlike surface and groundwaters, are not contaminated by recent pollutants. A certain component of these waters is therefore a shallow and shorter circulation.

KEYWORDS

pesticide residues, pharmaceuticals, field sampling, contamination control, Karst aquifers, groundwater



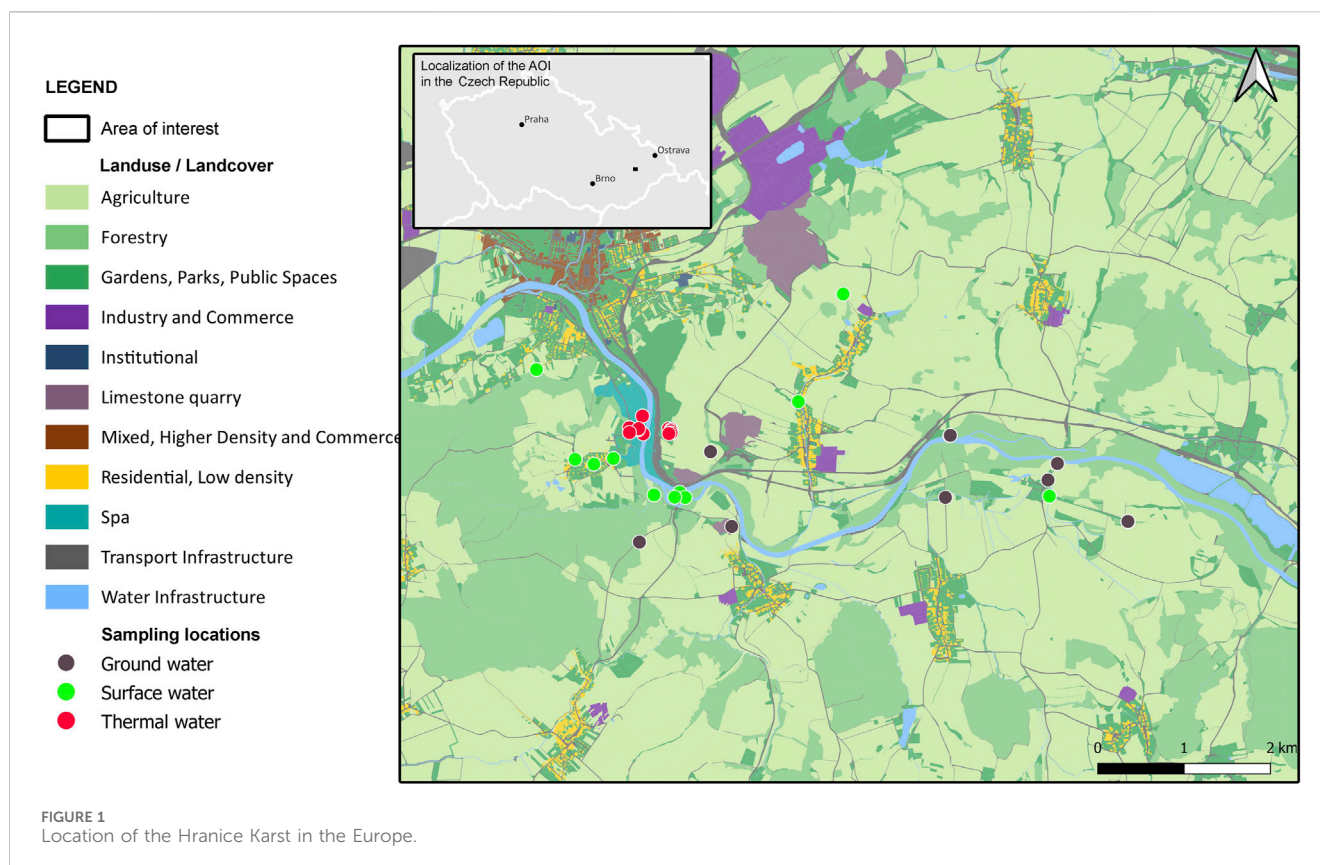
1 Introduction

Karstic aquifers supply 25% of all drinking water in the world, but they are highly vulnerable to contamination, and their preservation is constantly threatened in developing countries (Wilkinson, et al., 2022).

In densely populated and environmentally sensitive areas, the vulnerability of groundwater is in and, more recently, there is concern regarding contamination by pesticides or pharmaceuticals (including their metabolites) and their further spatial distribution question (Wachniew, et al., 2016; Douglas, et al., 2018). The risk of contamination in karst areas can be considered one of the most significant. The results of previous studies explicitly conducted in karst areas have confirmed the considerable flow rate of distribution of substances in the water-soil-geological system (Huang, et al., 2021).

Pesticides and pharmaceuticals belong to a group of chemical compounds called emerging organic contaminants (EOCs) (García,

et al., 2020). EOCs are substances potentially harmful to the environment (Chopra and Kumar 2020; Mali, et al., 2023). Many EOCs can accumulate in aquifers through a process known as leaching, which involves their movement into deeper soil layers and eventually into groundwater sources such as aquifers (Zemann, et al., 2016; Pérez-Lucas, et al., 2019). The accumulation of pesticides in aquifers poses serious environmental and health risks, as these water sources are used for drinking water worldwide. Severe effects on human health resulting from significantly prolonged exposure and accumulation are possible (Zhang, et al., 2006; Bhandari, et al., 2020; Perera-Rios, et al., 2022; Ruomeng, et al., 2023). EOCs are widely used and can accumulate in the environment through various sources. The predominant entry points of EOCs into the environment are via wastewater discharge, agricultural and aquacultural practices, and industry and hospital inputs (Alderton, et al., 2021). The transportation of microorganic pollutants to aquifers is determined by their characteristics and subsurface conditions, such as hydrogeological factors, groundwater



residence time, redox processes, soil type, and chemical properties. In addition, other processes, such as ion exchange, adsorption or desorption onto minerals and organic matter, biodegradation and chemical transformations, may control their migration into aquifer systems (Stoppiello, et al., 2020). Many global studies and research papers have revealed the findings pesticides and their metabolites in surface and groundwaters, including karst waters and drinking water sources (Eurostat, 2018; Ferrando and Matamoros, 2020; Baran, et al., 2021; Syafrudin, et al., 2021; Trolborg, et al., 2022).

Treating water contaminated by new artificial chemical compounds, mainly from pharmaceutical and personal care products, is a significant concern (Metcalf, et al., 2011). Pharmaceutical findings are prevalent in surface waters (Bexfield, et al., 2019; Chopra and Kumar 2020) and also identified in karst aquifers (Morasch, 2013; Dodgen, et al., 2017).

The European Water Framework Directive 2000/60/EC (European Council, 2000) aims to elevate all surface waters to “good” status, involving a range of biological, hydrological and chemical metrics. An Environmental Quality Standard (EQS) is a chemical metric used to assess status. Chemicals selected for EQS derivation are deemed to present a Europe-wide risk, and these EQSs are applied across all European Union countries. The EQSs represent legally binding maximum surface water concentrations, and drive regulatory action to reduce the concentration of chemicals in surface waters (Leverett, et al., 2021).

The occurrence of pesticide residues is repeatedly confirmed in agricultural soils (Karasali, et al., 2016; Hvězdová, et al., 2018; Silva, et al., 2019; Geissen, et al., 2021; Bakanov, et al., 2023; Riedo, et al., 2023), but no limits have yet been set.

This study aims to determine the vulnerability of the hypogene karst study area to pesticide leaching and potential accumulation. We employed advanced analytical methods, supported by geological and topological knowledge, to evaluate the transfer of emerging organic pollutants into hypogene karstic waters.

1.1 Study area

The study of the Hranice karst region (Figure 1) focuses on a distinct type of landscape, namely, hypogene hydrothermal karst. This karstic region is extensively populated and utilised. Its carbonated mineral waters have been used for their healing properties since the 16th century, making the spa in Teplice nad Bečvou one of the oldest in Moravia. The area’s potential is highly diversified and is influenced by various interests—agriculture, surface mining, nature conservation, recreation, spa, industry and housing (Oppeltová, et al., 2022).

The territory is between the Český masif’s geological units and the Outer Western Carpathians. The interaction between the Bohemian Massif and the Western Carpathians has significantly influenced the tectonic structure and present-day form of the Hranice Karst. Carbonate (limestone) rocks of the Devonian and Lower Carboniferous ages emerge in an area of approximately 5×3 km in the eastern part of the Czech Republic (N 49° 31', E 17° 45'). Paleozoic carbonates are partially overlain by younger sediments belonging to the Neogene of the Carpathian foreland, consisting mainly of clays

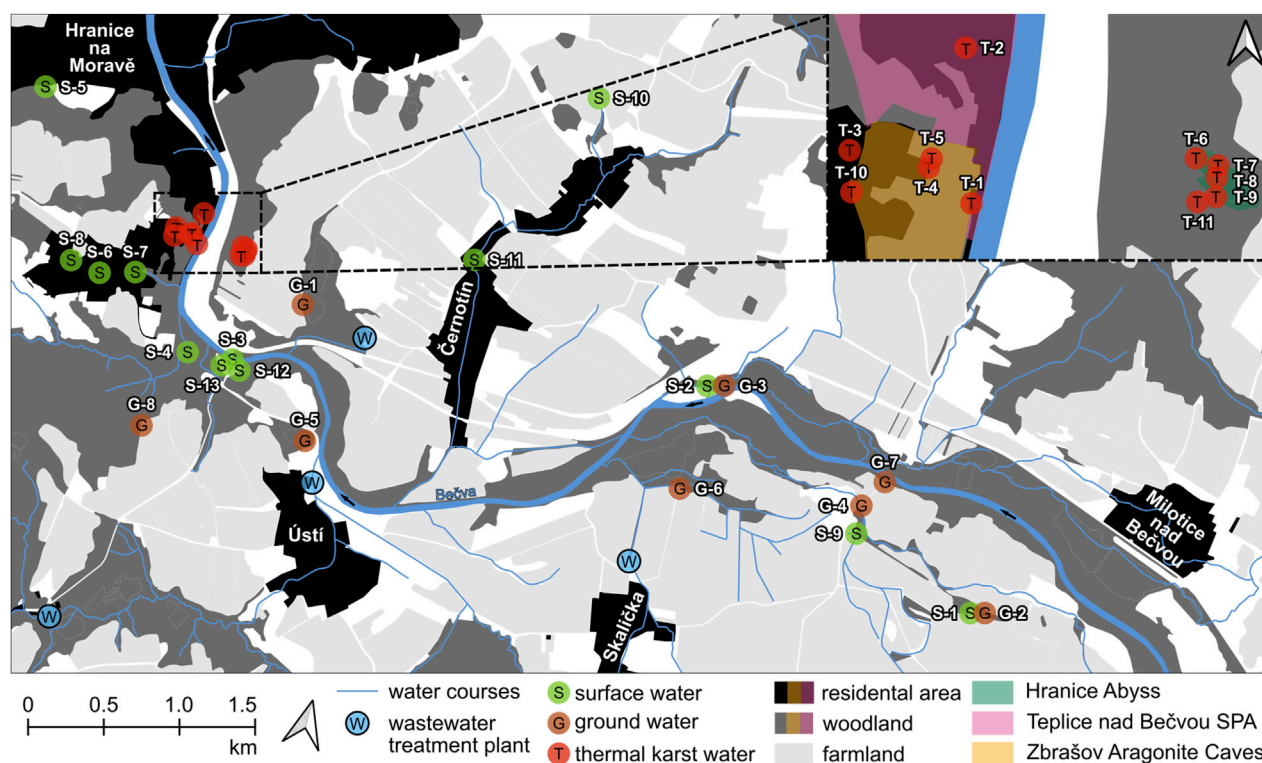


FIGURE 2
Depiction of the sampling sites within the study area.

and sandstones (Šrámek, et al., 2019). The Quaternary cover consists of reference soil groups (RSG) rendzic leptosols, arenosols and regosols on the karst bedrock; on agricultural land, RSG luvisols or retisols and cambisols dominate (IUSS Working Group WRB, 2015).

Regarding limestone, 30 caves are known in the karst area, the largest of which are the Zbrašov aragonite caves (ZAC) with unique their hydrothermal decoration and gas lakes with CO_2 . Hranice Abyss (HA) is also located here and is the deepest freshwater flooded abyss in the world. It is widely accepted that the formation of the abyss and the surrounding mineral springs in the karst area is associated with the influx of juvenile CO_2 from deeper regions of the geosphere (Špaček, et al., 2015). The abyss is filled with mineral water with a high level of CO_2 (Šrámek, et al., 2019), and there are springs of hypogenic mineral water to the depth of 30 m, 40 m, and 60 m.

There are also lakes of warm mineral water covered by a layer of gaseous CO_2 in the Zbrašov aragonite caves. The infiltration areas of the waters from which the mineral waters are created have not yet been identified. However, it appears that the mineral waters result from the mixing of older and younger waters and that some of the waters infiltrate underground at slightly higher elevations (Vysoká, et al., 2019; Šrámek, et al., 2019).

Mean annual air temperature and precipitation within the study area are 8.5°C and 677 mm, respectively (for 1961–2021). The Bečva River and its tributaries drain the whole study site. In the Teplice nad Bečvou municipality, the gauge is managed by the Czech Hydrometeorological Institute (CHMI) with a contributing basin

area of 1275.32 km^2 . According to the CHMI, the average annual flow of the Bečva River in Hranice is $14.8 \text{ m}^3 \cdot \text{s}^{-1}$, and the average water level is 0.89 m.

2 Materials and methods

2.1 Sampling sites

The screening aimed to determine whether and to what extent deep karst mineral waters (i.e., outflows of warm mineral waters) are contaminated with emerging organic contaminants (EOCs). Monitoring focused on EOCs in the area of interest, the Hranice Abyss, has never been conducted.

Samples were collected at locations in the Hranice Abyss where warm mineral waters emerge, presumed to be predominantly of hypogenic origin. Locations of watercourses and shallow subsurface waters, including drainage waters and shallow wells, were sampled. Those were suspected of contamination by agricultural and other anthropogenic EOCs. Deep groundwater was sampled through boreholes, including spa wells, to verify the distribution of EOCs. Collaborating with divers, mineral water samples were obtained from caves and warm outflows in the Hranice Abyss at 30, 40, and 60 m depths. Waters in the Zbrašov Aragonite Caves lakes were also included in this study.

Total 32 locations (Figure 2) were selected for processing in the article, which was divided into three groups: “surface water” (S:

TABLE 1 List of the sampling sites including depth and geographical location (WGS 84) (KMW - karst mineral water).

ID	Type	Depth (m)	La (WGS 84)	Lo (WGS 84)
S-1	Borehole	10	49.52718826	17.82472761
S-2	Borehole	8	49.53441099	17.79503013
S-3	Stream		49.5259388	17.75285
S-4	Stream		49.5254226	17.7487819
S-5	Drainage/Shallow well	3.5	49.5372863	17.7281999
S-6	Shallow well	3.4	49.52803692	17.73874911
S-7	Shallow well	3.2	49.52880707	17.74177451
S-8	Shallow well	2.9	49.52837815	17.73568331
S-9	Shallow well	50	49.529089	17.8117902
S-10	Drainage	3	49.54806	17.7759557
S-11	Shallow well	4	49.53647878	17.77041381
S-12	Borehole	17.1	49.5254621	17.75380825
S-13	Borehole	12	49.52538672	17.75211268
G-1	Borehole	66	49.5304493	17.7571546
G-2	Borehole	40	49.5272186	17.8246736
G-3	Borehole	40	49.53444281	17.79510887
G-4	Borehole	100	49.53074793	17.81133714
G-5	Borehole	100	49.5229036	17.761627
G-6	Borehole	100	49.5279646	17.7952437
G-7	Borehole	20	49.53254796	17.81259474
G-8	Borehole	100	49.5203957	17.7471571
T-1	Deep well. KMW	60	49.5316529	17.7461472
T-2	Deep well. KMW	143	49.5334889	17.7457772
T-3	Deep well. KMW	101	49.5321471	17.7438445
T-4	Caves. KMW	1	49.53202816	17.7453102
T-5	Caves. KMW	1	49.53213892	17.74534988
T-6	Caves. KMW	30	49.5324326	17.7501486
T-7	Caves. KMW	30	49.5323726	17.7505633
T-8	Caves. KMW	40	49.5322292	17.7505631
T-9	Caves. KMW	60	49.531997	17.7505756
T-10	Caves. KMW	3	49.5316544	17.743949
T-11	Caves. KMW	6	49.5319191	17.7502494

13 locations), “groundwater” (G: 8 locations) and “thermal karst water” (TKW: 11 locations) (Table 1).

From February 2022 to June 2023, water monitoring focused on observing selected emerging EOCs—mainly pesticides and their metabolites, pharmaceuticals and their metabolites—was carried out in the Hranice Karst (Figure 2). Sampling was conducted seasonally, depending on hydrometeorological conditions. Due to drying up of some resources, it was not possible to sample regularly. Due to the specific conditions

and dependence on other subjects and circumstances (divers, high CO₂ concentration in caves), water sampling from the abyss and caves was not carried out regularly and took place at different times than the sampling of surface, drainage waters and of boreholes and balneological wells. Seasonal changes in EOCs concentrations were not part of this research. During the monitored period from February 2022 to June 2023, 14 monitor campaigns were carried out. In total 44 surface, 30 groundwater and 45 TKW samples were taken.

TABLE 2 Groundwater Ubiquity Score values.

GUS value	Potential for movement toward groundwater
<0	Extremely Low
0–1.8	Low
>1.8–2.8	Moderate
>2.8	High

2.2 EOCs quantification

The samples were collected in 100 ml glass screw-cap vials. An ultra-high-performance liquid chromatography system (Agilent 1290 Infinity, Agilent Technologies, Inc., California) coupled with a tandem mass spectrometer (Triple Quadrupole 6495C, Agilent Technologies, Inc., California), was used to determine the selected pesticides, pharmaceuticals, and their metabolites in aqueous matrices. An enriched sample was also prepared to verify yield efficiency for each sample. Measurements were carried out in dynamic multiple reaction monitoring (dMRM) mode. The analytes were identified based on their quantification ions, qualifying ions (if applicable), and retention times. Prior to analysis, samples were enriched with internal deuterated standards, if available. Corresponding internal standards in concentration 100 µg·ml⁻¹, diluted in acetone, acetonitrile or methanol, were used. Their list, including their description, is presented in [Supplementary Table S1](#). The analysis was conducted using a direct injection method, where 100 µl of the not-filtered sample was directly introduced into the column. Chromatographic analysis was performed using, 0.002% formic acid and 0.2 mM NH₄F gradient (gradient parameters in [Supplementary Table S2](#)). The column utilized for this study was an Agilent Zorbax Eclipse Plus C18, with dimensions of 2.1 mm × 100 mm and a particle size of 1.8 µm. The quality of analyses was ensured by regular optimization of the working parameters of the mass detector before each measurement—Autotune, Checktune. The quality was additionally monitored, by continuous control of the yield of analytes in enriched samples and in an enriched blank. The method is validated and accredited according to [ČSN, EN, \(2018\)](#).

The ability of chemical compounds to contaminate groundwater and the leaching potential of pesticides was evaluated according to Groundwater Ubiquity Score (GUS). GUS is a technique to predict the ability of chemical compounds to contaminate groundwater and it is also used for assessing leaching potential of pesticides ([Wauchope, et al., 1992](#)) ([Table 2](#)). GUS is an experimentally calculated value by [Gustafson \(1989\)](#) that relates pesticide half-life and sorption potential.

European Union legislation—the Water Framework Directive 2000/60/EC, the related Drinking Water Directive [European Union, \(2020\)](#) and the Groundwater Directive ([European Commission, 2006b](#))—require that the concentration of individual pesticides in groundwater must not exceed 0.1 µg·L⁻¹, and the total concentration of all pesticides must be below 0.5 µg·L⁻¹ “Total” means the sum of all individual pesticides detected and quantified in the monitoring procedure, including their relevant metabolites, degradation and reaction products ([European Commission, 2006a](#)). These values must not be exceeded in drinking water and are

recommended as a groundwater quality standards ([European Commission, 2006a](#)).

3 Results

The data obtained within this study revealed contaminants, such as pesticides, pesticide metabolites, and pharmaceuticals, in the waters of the Hranice Karst. Moreover, bisphenol A (BPA) and DEET were also occasionally found. Pesticides or their metabolites banned in the EU were found in all types of waters ([Tables 3–5](#)). Box plot of all EOCs in the groups surface water (S), groundwater (G), and thermal karst waters (T) in ng·L⁻¹ was created ([Figure 3](#)). Box plot of all EOCs parent compounds and EOCs metabolites in S, G and T groups shows [Figure 4](#). The sum of the contents of the pesticide parent compound and their metabolite shows [Figure 5](#) and the sum of the contents of the pharmaceutical parent compound and their metabolite shows [Figure 6](#). The chart values represent the sums of EOCs substances measured during individual samplings at all monitored locations. Upper whisker: max value of the dataset; lower whisker: min value of the dataset; the box boundaries from top to bottom are as follows: top: 75th percentile; first bar: median; bottom: 25th percentile. The chart shows the cross-arithmetic mean; stars: outliers.

3.1 Surface waters

This category includes 13 sites encompassing surface and shallow subsurface waters, including drainage waters and shallow wells ([Table 1](#)). These are locations where there is a high assumption that EOCs enter the aquatic environment ([Figures 3–6](#)). As for the number of contaminants found, the Bečva River ranks first. The highest concentrations often reached the order of µg·L⁻¹ ([Figures 3–5](#)). As expected for the chloroacetate and pyridazone groups, higher levels of metabolites than parent substances were consistently detected ([Table 3](#)). In none of the cases were the maximum values of primary substances or metabolites associated with a watercourse but with drainages or shallow wells of about 3 m in depth, many of which serve as local drinking water sources.

The highest total of all primary pesticide substances in a single collection (152.6 ng·L⁻¹) was found at the shallow well S-6. The highest pesticide metabolites content (4070.2 ng·L⁻¹) was detected at shallow well S-10 ([Supplementary Table S3, Figure 5](#)).

For triazine pesticides, the maximum value of primary substances was found at S-6 (142 ng·L⁻¹ atrazine) and metabolites at S-7 (105 ng·L⁻¹ desethylatrazine). For chloroacetate pesticides of primary substances, the maximum

TABLE 3 EOCs in surface waters.

		LOD	min		Max		Avg	Med	Sd
		ng·L ⁻¹	ng·L ⁻¹	Location	ng·L ⁻¹	Location	ng·L ⁻¹	ng·L ⁻¹	ng·L ⁻¹
NSAID	Diclofenac	5	5.60	S-3	549.00	S-8	107.32	37.60	160.68
	Ibuprofen	10	11.10	S-3	976.00	S-8	141.46	31.20	296.94
ATB	Azithromycin	25; 200	79.70	S-3	79.70	S-3	79.70	79.70	0.00
	Clarithromycin	25	19.40	S-3	56.60	S-3	41.57	48.70	16.00
	Sulfamethoxacol	5	5.40	S-12	52.20	S-3	29.11	28.50	16.87
	Trimethoprim	5	8.40	S-1	12.20	S-3	10.60	11.20	1.61
ATDe	Venlafaxine	10	5.10	S-3	19.90	S-3	12.50	12.50	7.40
	<i>O-desmethylvenlafaxin</i>	5	13.70	S-3	42.70	S-3	26.42	22.10	10.71
Urea pest	Chlorotoluron	5	10.30	S-3	13.60	S-2	11.65	11.35	1.22
Tria Dia Pest	Atrazin (2005)	10	43.70	S-7	142.00	S-6	88.68	86.70	31.64
	<i>Desethylatrazin</i>	5	6.30	S-10	105.00	S-7	45.50	52.25	34.44
	<i>Atrazine-2-OH</i>	5	6.50	S-8	78.60	S-6	26.88	19.80	20.68
	<i>Atrazin-DES-DI</i>	5	5.30	S-9	86.10	S-7	29.84	24.30	26.25
	Simazin (2004)	5	5.40	S-6	30.80	S-7	13.88	9.65	10.16
	Simetryn (2005)	5	5.20	S-3	5.20	S-3	5.20	5.20	0.00
	Terbutryn (2003)	5	6.50	S-3	66.40	S-11	21.18	8.80	22.82
	Terbutylazin	5	14.10	S-9	14.10	S-9	14.10	14.10	0.00
	<i>Terbutylazin deseth</i>	5	46.00	S-9	46.00	S-9	46.00	46.00	0.00
	<i>Terbutylazin-2-OH</i>	5	5.40	S-4	32.90	S-11	21.42	24.90	9.39
	<i>Terbutylazin-DE2OH</i>	5	5.40	S-9	5.40	S-9	5.40	5.40	0.00
	Propazin (2004)	5	5.20	S-6	6.40	S-6	5.80	5.80	0.60
Chloracet Pest	<i>Metazachlor OA</i>	5	5.90	S-3	282.00	S-11	81.98	43.50	87.07
	<i>Metazachlor ESA</i>	10	10.80	S-8	1,400.00	S-11	231.96	60.10	326.71
	<i>Metolachlor ESA</i>	10	10.40	S-7	155.00	S-8	38.92	29.85	32.86
	<i>Alachlor ESA (2008)</i>	10	12.10	S-8	12.70	S-8	12.40	12.40	0.30
	<i>Acetochlor ESA (2013)</i>	10	28.40	S-9	66.00	S-1	46.35	45.50	16.55
	<i>Acetochlor OA (2013)</i>	5	5.00	S-9	5.00	S-9	5.00	5.00	0.00
	Dimethenamid	5	25.50	S-9	25.50	S-9	25.50	25.50	0.00
	<i>Dimethenamid ESA</i>	5	7.40	S-2	49.30	S-9	27.00	25.65	18.97
	<i>Dimethenamid OA</i>	5	12.90	S-9	18.50	S-9	15.70	15.70	2.80
Pyridazone	Chloridazon (2020)	5	5.10	S-1	14.30	S-10	8.22	7.60	3.14
	<i>Chloridazon DESPH</i>	5	5.70	S-3	2,230.00	S-10	441.75	159.00	635.38
	<i>Chloridazon DESPH ME</i>	5	5.10	S-7	943.00	S-10	160.52	44.70	235.13
	Bisphenol A	5	54.1	S-3	144	S-2	99.05	99.05	44.95
	DEET	100	141	S-13	141	S-13	141	141	0

Primary compounds in bold and their metabolites in italics. The year in parentheses indicates the ban on the application of these substances in the EU from the indicated date.

TABLE 4 EOCs in ground waters.

		LOD	min		Max		Avg	Med	Sd
		ng.L ⁻¹	ng.L ⁻¹	location	ng.L ⁻¹	Location	ng.L ⁻¹	ng.L ⁻¹	ng.L ⁻¹
NSAID	Diclofenac	5	8.40	G-4	112.00	G-4	41.38	34.45	33.66
	Ibuprofen	10	27.60	G-6	150.00	G-4	75.07	37.60	49.20
ATB	Azithromycin	25; 200	115.00	G-6	115.00	G-6	115.00	115.00	0.00
	Sulfamethoxacol	5	25.60	G-7	25.60	G-7	25.60	25.60	0.00
Urea pest	Chlorotoluron	5	43.40	G-8	43.40	G-8	43.40	43.40	0.00
Tria Dia pest	<i>Desethylatrazin</i>	5	25.30	G-8	25.30	G-8	25.30	25.30	0.00
	<i>Atrazine-2-OH</i>	5	5.40	G-3	241.00	G-8	38.18	15.80	62.03
	<i>Atrazin-DES-DI</i>	5	5.20	G-6	6.50	G-6	5.85	5.85	0.65
	Simetryn (2005)	5	6.20	G-6	7.70	G-6	6.95	6.95	0.75
	Terbutryn (2003)	5	7.40	G-6	12.40	G-8	9.90	9.90	2.50
	Prometryn (2004)	5	6.40	G-6	28.50	G-8	17.45	17.45	11.05
	<i>Terbuthylazin-2-OH</i>	5	9.90	G-6	532.00	G-8	72.92	23.60	153.30
	<i>Terbuthylazin-DE2OH</i>	5	7.00	G-6	8.10	G-6	7.55	7.55	0.55
	Prometon (2005)	5	6.00	G-6	6.00	G-6	6.00	6.00	0.00
	Suchumeton	5	6.50	G-6	6.50	G-6	6.50	6.50	0.00
Chloracet Pest	<i>Metazachlor OA</i>	5	6.50	G-5	534.00	G-1	107.46	57.50	129.56
	<i>Metazachlor ESA</i>	10	10.60	G-5	1,050.0	G-1	414.56	348.00	323.65
	<i>Metolachlor OA</i>	15	22.20	G-4	53.80	G-4	38.00	38.00	15.80
	<i>Metolachlor ESA</i>	10	13.00	G-7	97.40	G-4	44.01	41.40	20.42
	<i>Acetochlor ESA (2013)</i>	10	10.00	G-4	35.90	G-8	23.71	22.30	8.80
	<i>Acetochlor OA (2013)</i>	5	12.70	G-6	12.70	G-6	12.70	12.70	0.00
	<i>Dimethenamid ESA</i>	5	6.50	G-2	79.90	G-4	37.91	34.50	23.57
	<i>Dimethenamid OA</i>	5	6.90	G-4	47.00	G-6	22.40	21.75	13.14
	<i>Dimethachlor ESA</i>	5	5.70	G-1	6.30	G-1	6.00	6.00	0.24
Pyridazone	Chloridazon (2020)	5	5.40	G-1	33.50	G-6	10.96	7.80	9.28
	<i>Chloridazon DESPH</i>	5	11.30	G-5	1,490.0	G-4	351.18	265.50	366.47
	<i>Chloridazon DESPH ME</i>	5	5.80	G-3	436.0	G-6	182.98	146.00	151.37
Strobilur	Azoxystrobin	5	5.60	G-6	16.30	G-6	10.95	10.95	5.35
	Bisphenol A	5	268.00	G-6	655.00	G-4	437.75	414.00	149.69
	DEET	100	114.00	G-6	114.00	G-6	114.00	114.00	0

Primary compounds in bold and their metabolites in italics. The year in parentheses indicates the ban on the application of these substances in the EU from the indicated date.

was at S-9 (25.5 ng·L⁻¹ dimethenamid) and metabolites at S-11 (1,400 ng·L⁻¹ metazachlor ESA). Primary substances of pyridazol pesticides and their metabolites had their maximum in drainage S-10 (14.3 ng·L⁻¹ chloridazon and 2,230 ng·L⁻¹ chloridazon-DESPH) (Table 3).

For pharmaceuticals, the maximum values of non-steroidal anti-inflammatory drugs (NSAIDs) were in well S-8 (976 ng·L⁻¹); antibiotics (ATB) and antidepressants (ATDe) were in the Bečva River and S-3 (79.7 and 62.6 ng·L⁻¹) (Table 3).

In S-3 and S-2, Bisphenol A (BPA) was also analysed (54.1 ng·L⁻¹; 144 ng·L⁻¹), and in well S-13, DEET was found (141 ng·L⁻¹) (Table 3).

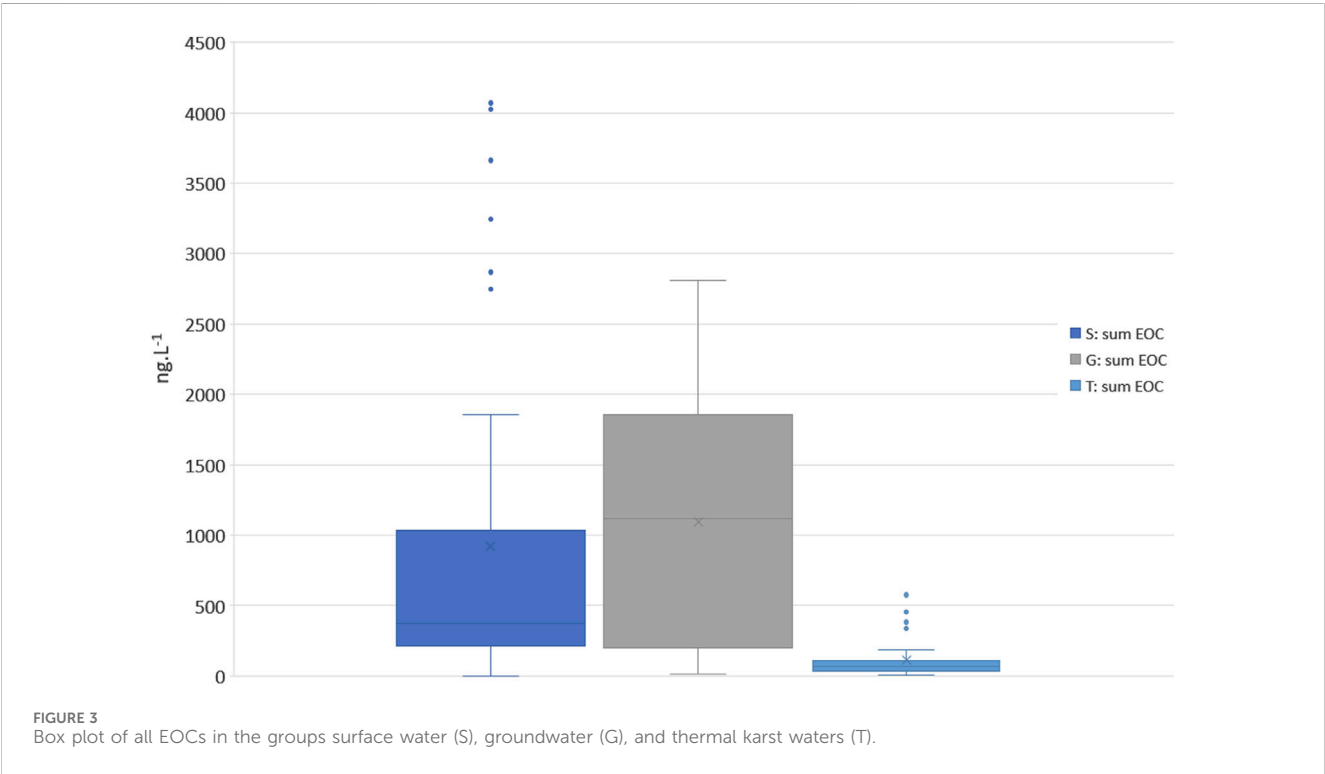
3.2 Groundwater

In this category, eight sites comprising only boreholes (Table 1) with varying depths from 20 m (G-7) to 100 m (G-4, G-5, G-6, and

TABLE 5 EOCs in thermal karst waters.

		LOD	min		Max		Avg	Med	Sd
		ng.L ⁻¹	ng.L ⁻¹	location	ng.L ⁻¹	location	ng.L ⁻¹	ng.L ⁻¹	ng.L ⁻¹
NSAID	Diclofenac	5	5.10	T-5	47.40	T-3	18.41	6.20	17.71
	Ibuprofen	10	13.00	T-4	30.50	T-2	21.75	21.75	8.75
ATB	Azithromycin	25; 200	73.80	T-7	73.80	T-7	73.80	73.80	0.00
Tria Dia Pest	Atrazin (2005)	10	12.50	T-10	16.20	T-10	14.53	14.90	1.53
	<i>Desethylatrazin</i>	5	6.10	T-11	18.50	T-10	10.86	8.95	4.11
	<i>Atrazin-DES-DI</i>	5	5.30	T-11	14.30	T-10	9.56	10.60	3.34
	Simazin (2004)	5	5.70	T-10	5.70	T-10	5.70	5.70	0.00
Chloracet Pest	<i>Metazachlor OA</i>	5	5.30	T-11	5.30	T-11	5.30	5.30	0.00
	<i>Metazachlor ESA</i>	10	10.20	T-7	63.00	T-1	26.01	20.30	14.29
	<i>Metolachlor ESA</i>	10	10.70	T-6	123.0	T-1	20.11	12.00	27.58
	<i>Alachlor ESA (2008)</i>	10	10.10	T-9	23.80	T-10	14.95	14.60	3.72
Pyridazone	<i>Chloridazon DESPH</i>	5	5.10	T-1	378.0	T-11	51.50	28.30	83.49
	<i>Chloridazon DESPH ME</i>	5	5.10	T-9	96.10	T-11	17.72	7.20	22.75
	Bisphenol A	5	125.00	T-1	242.0	T-9	183.5	183.5	58.50
	DEET	100	132.00	T-6	132.0	T-6	132.0	132.0	0.00

Primary compounds in bold and their metabolites in italics. Substances banned in the EU, their metabolites and the year of ban marked in red.



G-8) were included. These are, therefore, sites where further transport of EOC substances from the “S” locations into the hydrogeological system can be assumed. In all monitored

groundwater locations, findings of pesticide metabolites exceeded the parent substances, both in the number of substances found as well as the concentrations (Table 4).

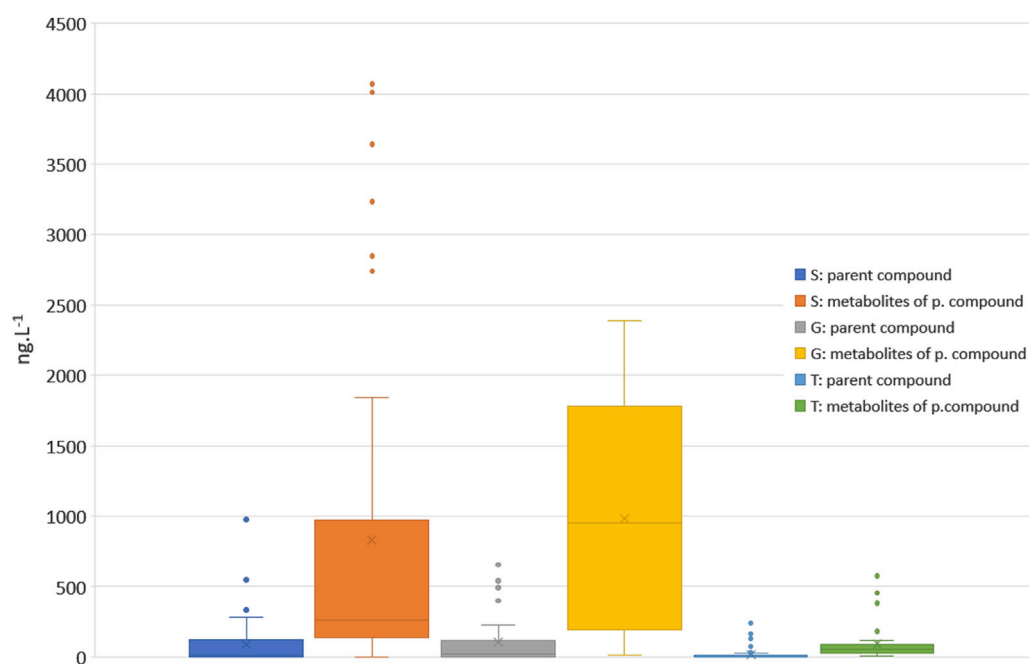


FIGURE 4
Box plot of all EOCs parent compounds and EOCs metabolites in S, G, and T groups.

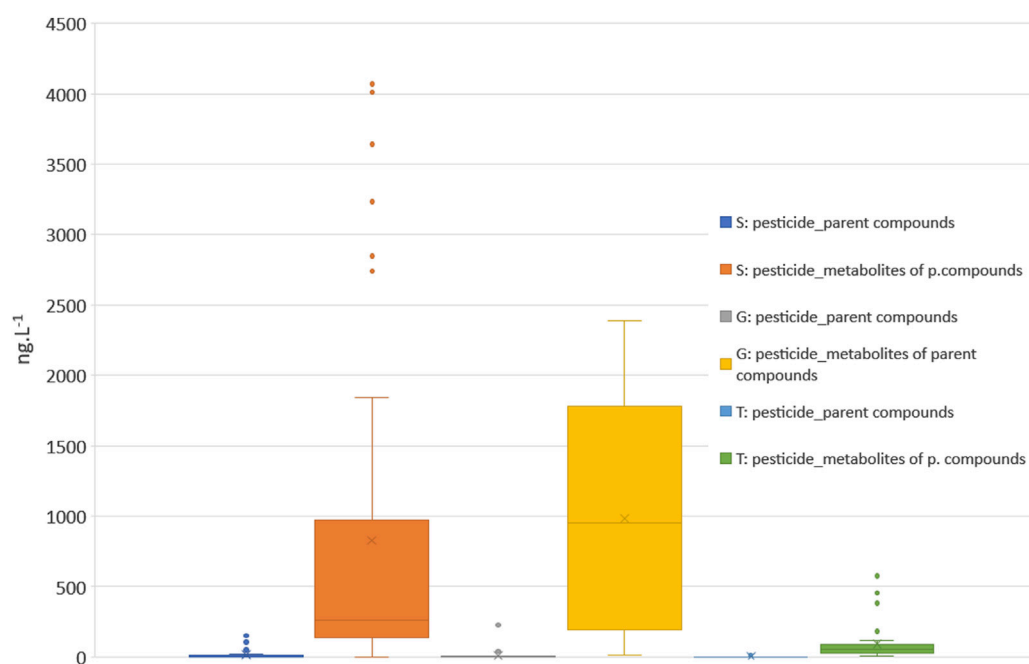


FIGURE 5
Sum of the contents of the pesticide parent compound and their metabolite in S, G, and T groups.

The highest total of all primary pesticide substances in a single collection (226.3 ng.L⁻¹) was detected at G-8. The highest total pesticide metabolites in a single collection (2,390.7 ng.L⁻¹) was at G-1 (Figure 5).

From the urea pesticides, Chlortoluron was detected in G-8 (43.3 ng.L⁻¹) (Table 4).

Most substances belonging to triazine pesticides were found in boreholes G-6 and G-8. In these two boreholes, metabolites and parent substances of triazine pesticides were found to be the only ones in the category of groundwater. For triazine pesticides, the maximum value of primary substances was found in G-8 (28.5 ng.L⁻¹ prometryn). In terms

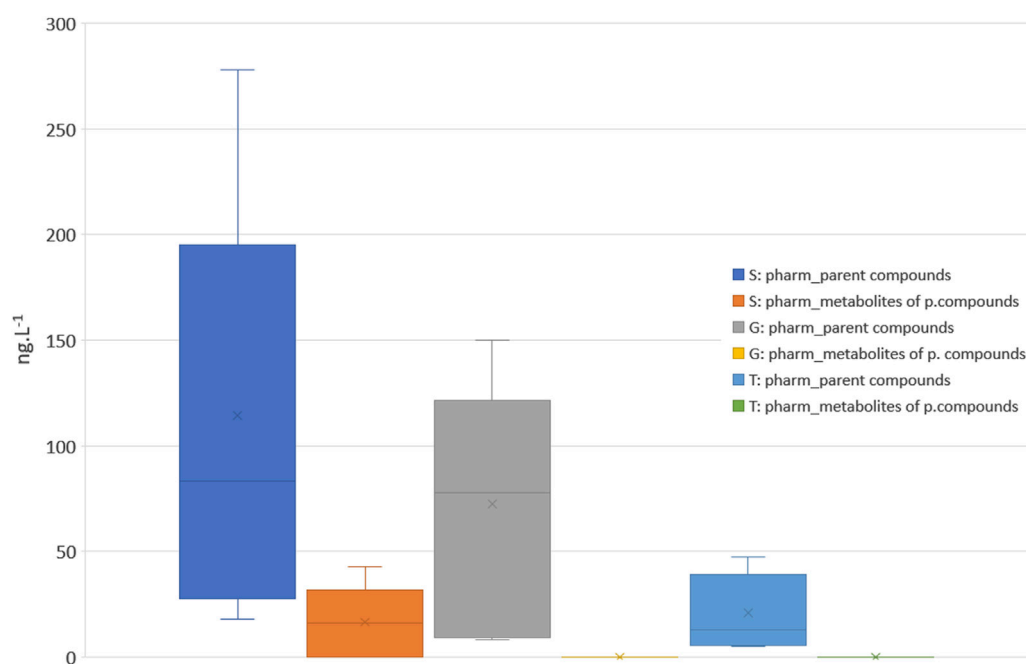


FIGURE 6 Sum of the contents of the pharmaceutical parent compound and their metabolite shows in S, G, and T groups.

of individual metabolite findings, the maximum values were again in borehole G-8, atrazine-2-OH ($241 \text{ ng}\cdot\text{L}^{-1}$) and terbuthylazine-2-OH ($532 \text{ ng}\cdot\text{L}^{-1}$) (Table 4). Triazine pesticide metabolites were also detected by repeated findings in borehole G-1 ($9.8\text{--}39 \text{ ng}\cdot\text{L}^{-1}$). In borehole G-8, triazole pesticide—tetraconazole was detected ($142 \text{ ng}\cdot\text{L}^{-1}$) (Supplementary Table S3).

Chloroacetamide pesticides are represented here only by metabolites; the parent substances were not found in ground waters. The highest concentration of metabolite was found at borehole G-1 ($1,050 \text{ ng}\cdot\text{L}^{-1}$ metazachlor ESA) (Table 4).

In the pyridazone group, both parent substances and metabolites were found. The highest value of the parent substances was found at borehole G-6 ($33.5 \text{ ng}\cdot\text{L}^{-1}$ chloridazon); the highest value of metabolites was found at borehole G-4 ($1,490 \text{ ng}\cdot\text{L}^{-1}$) (Table 4).

No substances from the strobilurin group were found here.

For pharmaceuticals, the maximum values of NSAIDs were in borehole G-4 ($150 \text{ ng}\cdot\text{L}^{-1}$ ibuprofen); antibiotics were found only in borehole G-6 ($115 \text{ ng}\cdot\text{L}^{-1}$ azithromycin) and in borehole G-7 ($25.6 \text{ ng}\cdot\text{L}^{-1}$ sulfamethoxazole). No ATDe were detected at any groundwater sites (Table 4).

BPA was repeatedly found in boreholes G-6 and G-4 at concentrations up to $268 \text{ ng}\cdot\text{L}^{-1}$ and $655 \text{ ng}\cdot\text{L}^{-1}$. DEET was detected in borehole G-6 ($114 \text{ ng}\cdot\text{L}^{-1}$) (Table 4).

3.3 Thermal karst waters

This category included 11 sites encompassing thermal springs of mineral waters, cave lakes and outputs in abysses (Table 5). Therefore, these are locations where the accumulation of EOC substances from areas “S” and “G” was assumed, or they should be areas minimally influenced anthropogenically.

The highest sum of all primary pesticide substances within a single collection ($20.6 \text{ ng}\cdot\text{L}^{-1}$) was found at T-10. The highest sum of all pesticide metabolites within one collection ($576.1 \text{ ng}\cdot\text{L}^{-1}$) was at T-11 (Figure 5).

In TKW, trace amounts of parent substances and metabolites of diazine and triazine pesticides were occasionally found. Specifically, these were atrazine and its metabolites, as well as simazine. The maximum value of parent substances of diazine and triazine pesticides was in T-10 ($16.2 \text{ ng}\cdot\text{L}^{-1}$ atrazine), and the maximum concentration of metabolites was also in T-10 ($18.5 \text{ ng}\cdot\text{L}^{-1}$ desethylatrazine) (Table 5).

As for chloroacetate pesticides in TKW, only metabolite findings were present, with no parent substances of this group found. The highest amount of metabolites was detected in the balneological well T-1, specifically metazachlor ESA ($63 \text{ ng}\cdot\text{L}^{-1}$) and metolachlor ESA ($123 \text{ ng}\cdot\text{L}^{-1}$) (Table 5).

The pyridazone group is also represented only by metabolites. The maximum metabolite value was in T-11 ($378 \text{ ng}\cdot\text{L}^{-1}$ chloridazon-DESPH) (Table 5).

Trace amounts of pharmaceuticals were found at most TKW sites during the monitoring period (Supplementary Table S3). In most cases, these were NSAIDs, with the highest value at the balneological well T-3 ($47.4 \text{ ng}\cdot\text{L}^{-1}$ Diclofenac). The only finding of ATB was T-7 ($73.8 \text{ ng}\cdot\text{L}^{-1}$). Pharmaceuticals in the ATDe group were not detected at any TKW sites (Table 5).

BPA was found at TKW sites only in T-9 ($242 \text{ ng}\cdot\text{L}^{-1}$). DEET was detected in HA at T-6 ($132 \text{ ng}\cdot\text{L}^{-1}$) (Table 5).

4 Discussion

From the above results, variable inputs of primary substances and metabolites into the system are evident. The results indicate that the highest concentrations of pesticides, their metabolites, and

pharmaceuticals (reaching up to $\mu\text{g}\cdot\text{L}^{-1}$) were identified in surface waters group. These sites encompass surface and shallow subsurface waters, including drainage waters and shallow wells. Group surface waters represents areas where pollution from both non-point and point sources enters the hydrological system. These sites are typically situated in intensively cultivated agricultural landscapes, where pesticides and industrial fertilisers are substantially used. In addition, the influence of human habitation in these areas might contribute to potential contamination through wastewater discharge. Contaminants enter the hydrological system mainly via surface runoff infiltration, leaching through soil layers and from wastewater since none of the sewage treatment plants in the area of interest have technology for removal. The degree of pesticide contamination in water is affected by the properties of the pesticide (e.g., solubility), characteristics of the soil (e.g., organic matter content within the soil, soil pH or content of clay and coarse particles) (Park, et al., 2020), site conditions and the application and management of pesticides (Syafudin, et al., 2021). Shallow groundwater is easily contaminated with pesticides, and their distribution is linked to land use and crop growth (Andrade and Stigter, 2009). Land management practices, such as irrigation and application, together with intensive rainfall events, can increase a pesticide's mobility (Menchen, et al., 2017).

Elevated concentrations of EOCs, also in the $\mu\text{g}\cdot\text{L}^{-1}$ range, have been detected in groundwater (Figure 4), specifically in wells ranging from 10 s to 100 m deep. These deep wells contained pesticide metabolites, indicative of contamination originating from agricultural activities, and pharmaceuticals and BPA, both likely derived from wastewater contamination. Given the permeable substrate in these areas, characterised by locally permeable sandy soils and underlying limestone, the EOCs can disperse from these deep groundwater sources. The sandy soils and limestone substrate facilitate the migration and dispersion of these contaminants in the groundwater and allow deep karst mineral waters contamination.

The occurrence of organic micropollutants in the groundwater, such as pesticides, has attracted global attention because of the potential negative effects on human health (Luo, et al., 2014). The threshold value of $0.1 \mu\text{g}\cdot\text{L}^{-1}$ (European Commission, 2006b) was repeatedly exceeded in all monitored groundwater samples, with some contaminants surpassing this limit up to tenfold. The sole exception is well G-7, which did not exceed this threshold throughout the observation period. The geological profile of the borehole G-7 is composed of fluvial gravels and sandy loam sediments with high permeability down to a depth of 6.8 m; below that, to a depth of 20.0 m, it consists of clays and claystones with low permeability. In addition, the limit of $0.5 \mu\text{g}\cdot\text{L}^{-1}$ was surpassed in wells G-1, G-3, G-4, G-6, and G-8 (Supplementary Table S3).

The geological profile of well G-1 at depths of 0–18 m consists of alternating highly permeable and impermeable rocks, specifically Neogene sands and sandstones, or possibly clays. It comprises tectonically fractured and karstified Palaeozoic limestones at 18–66 m depth. Both rock types generally exhibit high permeability, so the studied substances may be transported from greater distances or villages opposite the water flow. The flow here is considered to be conformal with the direction of the river's current. The geological profile of well G-3 up to a depth of 6.8 m consists of fluvial gravels and sandy loam sediments of high permeability and

up to 40 m by weathered and karstified limestones. Well G-4 is formed up to a depth of 4.8 m by sandy and clayey fluvial gravels in the profile. From a depth of 4.8 m onwards, it consists of limestones that show intense weathering, karstification and the presence of cave spaces. The geological profile of well G-6 up to a depth of 8.6 m is made of fluvial gravels and sandy loam sediments of high permeability. At depths of 8.6–28.5 m, there are clays and claystones of minimal permeability. Beneath these clays, karstified Paleozoic limestones have been confirmed down to a depth of 100 m. The geological profile of well G-8 is led by Paleozoic limestones, which exhibit high permeability. The interaction between land use and water quality is essential worldwide, as agriculture has been proven to exert considerable pressure on the quality of groundwater and surface waters due to leaching and erosion processes (Kronvang, et al., 2020).

In wells G-6 and G-4, BPA was repeatedly detected, with concentrations reaching up to $655 \text{ ng}\cdot\text{L}^{-1}$ in G-4 and $268 \text{ ng}\cdot\text{L}^{-1}$ in G-6 (Table 4).

Ibuprofen tends to be detected in various environmental samples: wastewater, sludge, soil, surface water and groundwater. In Europe, groundwater concentrations of ibuprofen occur between $3 \text{ ng}\cdot\text{L}^{-1}$ and $395 \text{ ng}\cdot\text{L}^{-1}$ (Chopra and Kumar 2020). As part of the groundwater quality monitoring, wells located within the built-up areas of the villages Černotín and Teplice nad Bečvou (S-6, S-7, S-8, and S-11) were also included; contamination by pharmaceuticals (diclofenac, ibuprofen) as well as metabolites of pesticides in concentrations reaching up to $1 \mu\text{g}\cdot\text{L}^{-1}$, was detected. The source of this contamination is likely wastewater leaks from sewer systems (or sewage treatment plants with infiltration, but these should not be present) in family homes built above the sampled sites. Once in the groundwater, these pollutants attenuate very slowly and can persist for long periods because of unfavourable redox and degradation conditions (e.g., anaerobic conditions and limited microbial activity) (Sorensen, et al., 2015; Sorensen et al., 2015; Dueñas-Moreno, et al., 2022). Dueñas-Moreno, et al. (2022) pointed out the high-risk BPA represents for human health once introduced into the groundwater.

Negligible to trace concentrations of EOCs (sum of all found substances), on the order of tens to hundreds of $\text{ng}\cdot\text{L}^{-1}$, were detected at the TKW sites (Figure 3), which were presumed to be predominantly of hypogenic origin and hence were not expected to contain EOC-type substances. The threshold values of $0.1 \mu\text{g}\cdot\text{L}^{-1}$ and $0.5 \mu\text{g}\cdot\text{L}^{-1}$ were exceeded at TKW sites only in the case of T-11, located precisely at the Hranice Abyss and in T-6. From the TKW group, significant findings of EOCs were observed in the balneological wells T-1 and T-3 (Table 3, Supplementary Table S3). These findings included trace amounts of diclofenac, ibuprofen, metazachlor ESA, metolachlor ESA, and chloridazon-DESPH. These monitoring results refute the initial hypothesis that deep hydrothermal karst waters are ancient and uncontaminated.

Among all the monitored pesticides and their metabolites within the scope of the Hranice Karst monitoring (refer to our table), metazachlor ESA and metolachlor ESA were among the substances with the highest GUS indices (Table 2), with values of 6.18 and 7.22, respectively. GUS is a technique to predict the ability of chemical compounds to contaminate groundwater and is also used for assessing the leaching potential of pesticides. GUS is an experimentally calculated value that relates pesticide half-life and

sorption potential (from laboratory data). The monitoring results demonstrated that, within the karst system, EOCs with elevated GUS indices can contaminate wells at depths of 60 m and 101 m. When utilising pesticides, particularly within karst terrains and on permeable soils, there should be thorough monitoring of the propensity of chemical compounds to contaminate groundwater. Subsequently, application strategies should be adjusted based on these observations to mitigate contamination risks.

The GUS may be used to rank pesticides for their potential to move toward groundwater (Gustafson, 1989). Pesticides with a short half-life, low water solubility and high sorption potential may have less potential to move through soil. Pesticides with a long half-life, high water solubility and low sorption potential possess a more significant potential to move through soil (Wauchope, et al., 1992).

Chloridazone is an herbicide widely used in agriculture to control beets and corn. The primary chloridazon metabolites are desphenyl-chloridazon (DPC) and methyl-desphenyl-chloridazon (Me-DPC), which can be a threat to surface and groundwater resources (Vidal, et al., 2022). Chloridazon inhibits the photosynthesis process in annual broad-leaf weeds and has been widely used in the past several decades because it was considered relatively harmless (Cioni and Maines, 2010; Jakiene, et al., 2015). Due to the polarity and solubility of metabolites, they are regarded as mobile compounds which cause surface water and groundwater pollution.

Chloridazon-DESPH also possesses a notably high GUS index of 5.64, indicating a significant potential for movement toward groundwater. Furthermore, it exhibits a high Screening Concentration In Ground Water (SCI-GROW) index of $9.25 \mu\text{g}\cdot\text{L}^{-1}$, signifying a pronounced likelihood of appearing in groundwater due to its propensity for leaching and mobility in the soil–water environment. These indices collectively suggest a need for careful management and monitoring of chloridazon-DESPH to prevent groundwater contamination.

SCI-GROW is a screening model which the Office of Pesticide Programs in the US Environmental Protection Agency frequently uses to estimate pesticide concentrations in vulnerable groundwater. The model provides an exposure value to determine the potential risk to the environment and human health from drinking water contaminated with the pesticide. The SCI-GROW estimate is based on the environmental fate properties of the pesticide (aerobic soil degradation half-life and linear adsorption coefficient normalised for soil organic carbon content), the maximum application rate, and existing data from small-scale prospective groundwater monitoring studies at sites with sandy soils and shallow groundwater (USEPA, 2016).

In the lakes within the Zbrašov Aragonite Caves (T-10, T-11), trace amounts of atrazine and its metabolites have been confirmed (Table 5). In the slopes above the caves, intensively farmed fields are located to the south and west. The land use of this area has not changed significantly over the long term. Atrazine is a triazine herbicide extensively used against various dicotyledonous weeds, but it has been banned in the European Union since 2005 due to its environmental and health implications. Despite the ban, the persistence and mobility of atrazine in the environment can result in its continued detection in various water bodies, reflecting its historical use and long-term environmental

persistence. These findings highlight the necessity for ongoing monitoring and assessment of water quality within the cave environment to understand the environmental distribution and fate of banned or restricted substances. Although atrazine use was banned in France in 2003, both atrazine and its metabolite desethylatrazine were detected in French groundwater years after its removal from the market (Baran, et al., 2008). The GUS leaching potential index of atrazine is 2.57 (moderate potential for movement toward groundwater), and the GUS of desethylatrazine is 3.24 (high potential for movement toward groundwater). Atrazine has a high potential to contaminate groundwater, especially in environments with porous soil profiles (de Albuquerque, et al., 2020), as confirmed by the research results in the Hranice Karst. Many studies are published yearly on atrazine's presence in the environment, especially for its metabolites (Kolpin, et al., 1998; Fava, et al., 2007; Iker, et al., 2010; Jablonowski, et al., 2011) modelled atrazine concentrations in shallow groundwater (concentrations ranged from <0.004 to $4.7 \mu\text{g}\cdot\text{L}^{-1}$) and found that atrazine concentrations are controlled mainly by the history of atrazine use in relation to the groundwater age.

Despite banned application, triazines and acetochlor are still detected (Baran, et al., 2021). Furthermore, in the lakes within the Zbrašov Aragonite Caves, trace amounts of chloridazon-DESPH, chloridazon-DESPH-ME, alachlor ESA, and the pharmaceutical diclofenac have been detected (Supplementary Table S3). Although intensively farmed fields are located on the slopes above the caves, pharmaceuticals must be attributed to historical infiltration of wastewater or leaks from sewage systems in the past. Recently, a modern sewage system was built in the village. The detection of these compounds, even in trace amounts, indicates the presence of anthropogenic contaminants within the karstic aquifer, necessitating continued vigilance and monitoring to assess the environmental health and potential risks associated with these residues.

EOCs were also detected in the deep waters of the Hranice Abyss (T-6, T-7, T-8, T-9, and T-11). Noteworthy are the findings of BPA ($242 \text{ ng}\cdot\text{L}^{-1}$ in T-9), DEET ($132 \text{ ng}\cdot\text{L}^{-1}$ in T-6), chloroacetanilide pesticides and their metabolites (including alachlor ESA, metolachlor oxanilic acid (OA), metolachlor ESA, metazachlor OA, and metazachlor ESA), as well as compounds from the pyridazone group (chloridazon-DESPH, chloridazon-DESPH-ME) (Table 5).

The highest concentrations of the pollutants were identified in well T-11 (Table 5). Given the lower water conductivity values' decreased concentrations of bicarbonates (HCO_3), calcium (Ca), and magnesium (Mg) compared to the other inputs (T-9 and T-6), it can be inferred that the water in T-11 is not purely mineral water. Instead, a mixing process appears to have occurred, involving surface waters (which are likely contaminated) blending with the deeper, mineral-rich waters in this location. This mixing introduced pollutants into the deeper water strata, which warrants careful and continuous monitoring to understand the extent and implications of such contamination for the water quality in the area adjacent to Hranice Abyss.

The detection of BPA indicates contamination from wastewater sources. Dueñas-Moreno, et al. (2022) reported that BPA has been globally detected in groundwater reservoirs and landfills. Sewage sludge and wastewater are the primary BPA sources of groundwater

pollution. BPA pollution is caused by anthropogenic activities, including manufacturing processes, the distribution, use, consumption, treatment and disposal of devices and products containing phthalates and BPA, resulting in long-term transport from the environment to groundwater reservoirs. Their physicochemical properties condition the transport and fate of phthalates and BPA, the type of pollution sources, the type of matrix (air, water, and soil) and the environmental conditions (pH, temperature, and pressure) (Tran, et al., 2022).

The continued detection of alachlor ESA in both caves and the abyss (Supplementary Table S3), despite its ban since 2007, raises significant considerations. Despite their prohibited use, many pesticides and their metabolites are still found in water and other areas (Jablonowski, et al., 2011; Baran, et al., 2021; Kruč-Fijałkowska, et al., 2022). The water in the specified areas may exhibit slow movement or circulation dynamics, allowing contaminants introduced before the ban to remain *in situ* for extended periods. Slow-moving or stagnant water bodies can act as reservoirs for these compounds, releasing them gradually (Zhu, et al., 2017). The unique environmental conditions in these areas might hinder the degradation process of alachlor and its metabolites. The environmental persistence of certain compounds can be extended under conditions that are not conducive to their breakdown, resulting in prolonged detectability (Mouvet, et al., 1997). Although alachlor has been banned, illegal or unregulated use might still be occurring, or sources of contamination might not have been identified or mitigated. This continued input can maintain the presence of alachlor and its metabolites in the environment. The persistence of alachlor ESA and its metabolites in the water demands further investigation to understand the dynamics of water movement, the degradation pathways of these compounds under local environmental conditions and potential unidentified sources of contamination.

Trace amounts of the NSAID diclofenac and the antibiotic azithromycin were detected in the waters of the Hranice Abyss. Notably, diclofenac was found at its highest concentration of $47.4 \text{ ng}\cdot\text{L}^{-1}$ in T-3. Azithromycin was detected in T-7 ($73.8 \text{ ng}\cdot\text{L}^{-1}$) (Table 5).

The presence of pharmaceuticals like diclofenac and azithromycin in aquatic environments is often attributed to the incomplete metabolism of these drugs in humans and animals and the insufficient removal of these compounds during wastewater treatment processes (Jones, et al., 2022). Once released into the environment, these pharmaceuticals can persist and be transported through water bodies, leading to their detection in remote and deep-water locations like the Hranice Abyss.

Active pharmaceutical ingredients are emitted into the natural environment during manufacture, use and disposal. There is evidence that environmental exposure to pharmaceuticals has deleterious effects on the health of ecosystems and humans (e.g., by selecting antibiotic-resistant bacteria, feminising fish and increasing the susceptibility of fish to predation) (Kidd, et al., 2007; Brodin, et al., 2013; Wellington, et al., 2013; Horký, et al., 2021).

Diclofenac has thus been detected in trace concentrations in the balneological wells within the ZAC and in the Hranice Abyss (Supplementary Table S3). The limit recommended by European Commission in surface water is $5.4 \text{ ng}\cdot\text{L}^{-1}$ resp. $230 \text{ ng}\cdot\text{L}^{-1}$ to

protect birds from diclofenac secondary poisoning through the food chain (Peters, et al., 2022). The limit of $230 \text{ ng}\cdot\text{L}^{-1}$ was exceeded at two of our monitored sites. In S-8 and S-9, the maximum concentration of diclofenac was $549 \text{ ng}\cdot\text{L}^{-1}$ and $231 \text{ ng}\cdot\text{L}^{-1}$ (Table 3, Supplementary Table S3). The less strict limit of $5.4 \text{ ng}\cdot\text{L}^{-1}$ was exceeded in group S (S-3, S-6, S-9, and S-10), group G (G-1, G-2, G-4, G-5, and G-6) and group T (T-1, T-3, T-4, T-9, and T-10) (Supplementary Table S3).

The correlation between land use and concentrations of EOCs (specifically pharmaceuticals) was also confirmed by other studies (Schäfer, et al., 2016; Chen, et al., 2023). In particular, there is a pattern of positive correlation between contaminant concentrations and land use characterised by cropland and impermeable surfaces (when considering horizontal distribution) and a negative correlation between concentrations and areas covered with vegetation.

5 Conclusion

The monitoring of the Hranice Hypogenic Karst showed the presence of EOCs in all types of waters, including trace concentrations in deep TKW and balneological wells. The detected EOCs were represented by pesticides, pharmaceuticals and their metabolites; BPA and DEET were occasionally found. Thus, the results refute the original hypothesis that deep hydrothermal karst waters are ancient and uncontaminated. The excessive permeability of the karst system leads to an enhanced vulnerability for retention and spread of contaminants. The results generally confirm that current land use is associated with pollution in the karst system.

In groundwater and the Zbrašov Aragonite Caves lakes, trace findings of atrazine and its metabolites were confirmed. In the warm HA springs and Zbrašov Aragonite Caves lakes, trace concentrations of alachlor metabolites were found. In both cases, these are substances whose application has been banned in the European Union for more than 10 years. The unique environmental conditions in these areas might hinder the degradation processes of these substances, and slow-moving or stagnant water bodies can thus act as reservoirs for these compounds.

When using pesticides, especially in karst locations and on permeable soils, one should monitor the ability of chemical compounds to contaminate groundwater. In agricultural practice, this means monitoring the values of the GUS index of the substances used and adapting one's application to these values. This karst area is a highly vulnerable system to anthropogenic activities and it is recommended to be monitored beyond legal requirements. In the future, more extensive sampling of source and ground waters through concerted campaigns or deployed samplers and higher resolution weather and land use measures would bring more certainty to understanding contamination of karst aquifers and their environmental, drinking water and mineral water risks.

Data availability statement

The original contributions presented in the study are included in the article/Supplementary Material, further inquiries can be directed to the corresponding author.

Author contributions

PO: Data curation, Investigation, Methodology, Supervision, Writing—original draft, Writing—review and editing, Conceptualization, Resources. VV: Conceptualization, Data curation, Formal Analysis, Methodology, Writing—review and editing. MG: Conceptualization, Data curation, Funding acquisition, Methodology, Supervision, Validation, Writing—original draft, Writing—review and editing, Investigation. PC: Data curation, Writing—review and editing. OU: Data curation, Visualization, Writing—review and editing, Resources. JS: Funding acquisition, Project administration, Visualization, Writing—review and editing. HV: Writing—review and editing. KK: Writing—review and editing. RK: Visualization, Writing—review and editing. JŠ: Writing—review and editing, Project administration.

Funding

The author(s) declare financial support was received for the research, authorship, and/or publication of this article. This research was funded by the Gregor Johann Mendel Grant Agency of the Mendel University in Brno (Czechia), within the project Landscape in Whole and Landscape in Detail - an Interdisciplinary Research of the Hranice Karst.

Acknowledgments

The authors greatly appreciate Michal Guba, Martin Strnad, Miroslav Lukáš, Petr Hřebejk, Jan Musil, Martin Prachař and

other cave divers, members of the Czech Speleological Society 7–02 Hranický Karst, Czech Republic, for underwater sampling, as well as the staff of the Cave Authority of the Czechia, Zbrašov Aragonite Caves headquarters. We thank Veronika Matušková for help with field sampling and laboratory measurements. We thank Povodí Morava s. p. for allowing access to the sampling sites.

Conflict of interest

The authors declare that the research was conducted in the absence of any commercial or financial relationships that could be construed as a potential conflict of interest.

Publisher's note

All claims expressed in this article are solely those of the authors and do not necessarily represent those of their affiliated organizations, or those of the publisher, the editors and the reviewers. Any product that may be evaluated in this article, or claim that may be made by its manufacturer, is not guaranteed or endorsed by the publisher.

Supplementary material

The Supplementary Material for this article can be found online at: <https://www.frontiersin.org/articles/10.3389/fenvs.2024.1339818/full#supplementary-material>

References

- Alderton, I., Palmer, B. R., Heinemann, J. A., Pattis, I., Weaver, L., Gutiérrez-Ginés, M. J., et al. (2021). The role of emerging organic contaminants in the development of antimicrobial resistance. *Emerg. Contam.* 7, 160–171. doi:10.1016/j.emcon.2021.07.001
- Andrade, A., and Stigter, T. (2009). Multi-method assessment of nitrate and pesticide contamination in shallow alluvial groundwater as a function of hydrogeological setting and land use. *Agric. Water Manag.* 96, 1751–1765. doi:10.1016/j.agwat.2009.07.014
- Bakanov, N., Honert, C., Eichler, L., Lehmann, G. U., Schulz, R., and Brühl, C. A. (2023). A new sample preparation approach for the analysis of 98 current-use pesticides in soil and herbaceous vegetation using hplc-ms/ms in combination with an acetonitrile-based extraction. *Chemosphere* 331, 138840. doi:10.1016/j.chemosphere.2023.138840
- Baran, N., Lepiller, M., and Mouvet, C. (2008). Agricultural diffuse pollution in a chalk aquifer (trois fontaines, France): influence of pesticide properties and hydrodynamic constraints. *J. Hydrology* 358, 56–69. doi:10.1016/j.jhydrol.2008.05.031
- Baran, N., Surdyk, N., and Auterives, C. (2021). Pesticides in groundwater at a national scale (France): impact of regulations, molecular properties, uses, hydrogeology and climatic conditions. *Sci. Total Environ.* 791, 148137. doi:10.1016/j.scitotenv.2021.148137
- Bexfield, L. M., Toccalino, P. L., Belitz, K., Foreman, W. T., and Furlong, E. T. (2019). Hormones and pharmaceuticals in groundwater used as a source of drinking water across the United States. *Environ. Sci. Technol.* 53, 2950–2960. doi:10.1021/acs.est.8b05592
- Bhandari, G., Atreya, K., Scheepers, P. T., and Geissen, V. (2020). Concentration and distribution of pesticide residues in soil: non-dietary human health risk assessment. *Non-dietary Hum. health risk Assess. Chemosphere* 253, 126594. doi:10.1016/j.chemosphere.2020.126594
- Brodin, T., Fick, J., Jonsson, M., and Klaminder, J. (2013). Dilute concentrations of a psychiatric drug alter behavior of fish from natural populations. *Science* 339, 814–815. doi:10.1126/science.1226850
- Chen, M., Hong, Y., Jin, X., Guo, C., Zhao, X., Liu, N., et al. (2023). Ranking the risks of eighty pharmaceuticals in surface water of a megacity: a multilevel optimization strategy. *Sci. Total Environ.* 878, 163184. doi:10.1016/j.scitotenv.2023.163184
- Chopra, S., and Kumar, D. (2020). Ibuprofen as an emerging organic contaminant in environment, distribution and remediation. *Heliyon* 6, e04087. doi:10.1016/j.heliyon.2020.e04087
- Cioni, F., and Maines, G. (2010). Weed control in sugarbeet. *Sugar Tech.* 12, 243–255. doi:10.1007/s12355-010-0036-2
- ČSN, EN (2018). *ISO/IEC 17025: posuzování shody—Všeobecné požadavky na způsobilost zkušebních a kalibračních laboratoří*. Praha: ČNI.
- de Albuquerque, F. P., de Oliveira, J. L., Moschini-Carlos, V., and Fraceto, L. F. (2020). An overview of the potential impacts of atrazine in aquatic environments: perspectives for tailored solutions based on nanotechnology. *Sci. Total Environ.* 700, 134868. doi:10.1016/j.scitotenv.2019.134868
- Dodgen, L., Kelly, W., Panno, S., Taylor, S., Armstrong, D., Wiles, K., et al. (2017). Characterizing pharmaceutical, personal care product, and hormone contamination in a karst aquifer of southwestern Illinois, USA, using water quality and stream flow parameters. *Sci. total Environ.* 578, 281–289. doi:10.1016/j.scitotenv.2016.10.103
- Douglas, S. H., Dixon, B., and Griffin, D. (2018). Assessing the abilities of intrinsic and specific vulnerability models to indicate groundwater vulnerability to groups of similar pesticides. *A Comp. study Phys. Geogr.* 39, 487–505. doi:10.1080/02723646.2017.1406300
- Dueñas-Moreno, J., Mora, A., Cervantes-Avilés, P., and Mählknecht, J. (2022). Groundwater contamination pathways of phthalates and bisphenol a: origin, characteristics, transport, and fate—a review. *Environ. Int.* 170, 107550. doi:10.1016/j.envint.2022.107550
- European Commission (2006a). Directive 2006/118/EC of the European Parliament and of the Council. <https://eur-lex.europa.eu/LexUriServ/LexUriServ.do?uri=OJ:L:2006:372:0019:0031-EN:PDF>.

- European Commission (2006b). Directive 2006/118/ec on the protection of groundwater against pollution and deterioration. Available at: <https://eur-lex.europa.eu/LexUriServ/LexUriServ.do?uri=OJ:L:2006:372:0019:0031:EN:PDF>.
- European Council (2000). Directive 2000/60/ec of the european parliament and of the council of 23 october 2000 establishing a framework for community action in the field of water policy. Available at: <https://eur-lex.europa.eu/eli/dir/2000/60/oj>.
- European Union (2020). Directive 2020/2184 of the European Parliament and of the Council of 16 December 2020 on the quality of water intended for human consumption. Available at: <https://eur-lex.europa.eu/legal-content/EN/TXT/?uri=CELEX:32020L2184>.
- Eurostat (2018). Archive:Agri-environmental indicator - pesticide pollution of water. Available at: https://ec.europa.eu/eurostat/statistics-explained/index.php?title=Archive:Agri-environmental_indicator_-_pesticide_pollution_of_water.
- Fava, L., Orrù, M. A., Scardala, S., and Funari, E. (2007). Leaching potential of carbamates and their metabolites and comparison with triazines. *Microchem. J.* 86, 204–208. doi:10.1016/j.microc.2007.03.003
- Ferrando, L., and Matamoros, V. (2020). Attenuation of nitrates, antibiotics and pesticides from groundwater using immobilised microalgae-based systems. *Sci. Total Environ.* 703, 134740. doi:10.1016/j.scitotenv.2019.134740
- García, J., García-Galán, M. J., Day, J. W., Boopathy, R., White, J. R., Wallace, S., et al. (2020). A review of emerging organic contaminants (eocs), antibiotic resistant bacteria (arb), and antibiotic resistance genes (args) in the environment: increasing removal with wetlands and reducing environmental impacts. *Bioresour. Technol.* 307, 123228. doi:10.1016/j.biortech.2020.123228
- Geissen, V., Silva, V., Lwanga, E. H., Beriot, N., Oostindie, K., Bin, Z., et al. (2021). Cocktails of pesticide residues in conventional and organic farming systems in europe—legacy of the past and turning point for the future. *Environ. Pollut.* 278, 116827. doi:10.1016/j.envpol.2021.116827
- Gustafson, D. I. (1989). Groundwater ubiquity score: a simple method for assessing pesticide leachability. *Environ. Toxicol. Chem.* 8, 339–357. doi:10.1002/etc.5620080411
- Horký, P., Grabic, R., Grabicová, K., Brooks, B. W., Douda, K., Slavík, O., et al. (2021). Methamphetamine pollution elicits addiction in wild fish. *fish J. Exp. Biol.* 224, jeb242145. doi:10.1242/jeb.242145
- Huang, H., Liu, H., Xiong, S., Zeng, F., Bu, J., Zhang, B., et al. (2021). Rapid transport of organochlorine pesticides (ocps) in multimedia environment from karst area. *Sci. Total Environ.* 775, 145698. doi:10.1016/j.scitotenv.2021.145698
- Hvězďová, M., Kosubová, P., Košíková, M., Scherr, K. E., Šimek, Z., Brodský, L., et al. (2018). Currently and recently used pesticides in central european arable soils. *Sci. Total Environ.* 613, 361–370. doi:10.1016/j.scitotenv.2017.09.049
- Iker, B. C., Kambesis, P., Oehrlé, S. A., Groves, C., and Barton, H. A. (2010). Microbial atrazine breakdown in a karst groundwater system and its effect on ecosystem energetics. *J. Environ. Qual.* 39, 509–518. doi:10.2134/jeq2009.0048
- IUSS Working Group WRB (2015). *World Reference Base for Soil Resources 2014, update 2015. International soil classification system for naming soils and creating legends for soil maps*. World Soil Resources Reports No. 106. Rome: FAO.
- Jablonowski, N. D., Schäffer, A., and Buraue, P. (2011). Still present after all these years: persistence plus potential toxicity raise questions about the use of atrazine. *Environ. Sci. Pollut. Res.* 18, 328–331. doi:10.1007/s11356-010-0431-y
- Jakiene, E., Spruogis, V., Dautarte, A., Romaneckas, K., and Avizienyte, D. (2015). The bio-organic nano fertilizer improves sugar beet photosynthesis process and productivity. *Zemdirbyste* 102, 141–146. doi:10.13080/z-a.2015.102.018
- Jones, E. R., Bierkens, M. F., Wanders, N., Sutanudjaja, E. H., van Beek, L. P., and van Vliet, M. T. (2022). Current wastewater treatment targets are insufficient to protect surface water quality. *Earth Environ.* 3, 221. doi:10.1038/s43247-022-00554-y
- Karasali, H., Marousopoulou, A., and Machera, K. (2016). Pesticide residue concentration in soil following conventional and low-input crop management in a mediterranean agro-ecosystem, in central Greece. *Sci. Total Environ.* 541, 130–142. doi:10.1016/j.scitotenv.2015.09.016
- Kidd, K. A., Blanchfield, P. J., Mills, K. H., Palace, V. P., Evans, R. E., Lazorchak, J. M., et al. (2007). Collapse of a fish population after exposure to a synthetic estrogen. *Proc. Natl. Acad. Sci.* 104, 8897–8901. doi:10.1073/pnas.0609568104
- Kolpin, D. W., Barbash, J. E., and Gilliom, R. J. (1998). Occurrence of pesticides in shallow groundwater of the United States: initial results from the national water-quality assessment program. *Environ. Sci. Technol.* 32, 558–566. doi:10.1021/es970412g
- Kronvang, B., Wendland, F., Kovar, K., and Fraters, D. (2020). Land use and water quality. *Encycl. hydrological Sci.* 2020. doi:10.3390/w12092412
- Kruć-Fijałkowska, R., Dragon, K., Drożdżyński, D., and Górski, J. (2022). Seasonal variation of pesticides in surface water and drinking water wells in the annual cycle in western Poland, and potential health risk assessment. *Sci. Rep.* 12, 3317. doi:10.1038/s41598-022-07385-z
- Leverett, D., Merrington, G., Crane, M., Ryan, J., and Wilson, I. (2021). Environmental quality standards for diclofenac derived under the European Water Framework Directive: 1. Aquatic organisms. *Aquat. Org. Environ. Sci. Eur.* 33, 133. doi:10.1186/s12302-021-00574-z
- Luo, Y., Guo, W., Ngo, H. H., Nghiem, L. D., Hai, F. I., Zhang, J., et al. (2014). A review on the occurrence of micropollutants in the aquatic environment and their fate and removal during wastewater treatment. *Sci. total Environ.* 473, 619–641. doi:10.1016/j.scitotenv.2013.12.065
- Mali, H., Shah, C., Raghunandan, B., Prajapati, A. S., Patel, D. H., Trivedi, U., et al. (2023). Organophosphate pesticides an emerging environmental contaminant: pollution, toxicity, bioremediation progress, and remaining challenges. *J. Environ. Sci.* 127, 234–250. doi:10.1016/j.jes.2022.04.023
- Menchen, A., Heras, J. D., and Alday, J. J. G. (2017). Pesticide contamination in groundwater bodies in the júcar river European Union pilot basin (se Spain). *Environ. Monit. Assess.* 189, 146–218. doi:10.1007/s10661-017-5827-4
- Metcalfe, C. D., Beddows, P. A., Bouchot, G. G., Metcalfe, T. L., Li, H., and Van Lavieren, H. (2011). Contaminants in the coastal karst aquifer system along the Caribbean coast of the Yucatan Peninsula, Mexico. *Mex. Environ. Pollut.* 159, 991–997. doi:10.1016/j.envpol.2010.11.031
- Morasch, B. (2013). Occurrence and dynamics of micropollutants in a karst aquifer. *Environ. Pollut.* 173, 133–137. doi:10.1016/j.envpol.2012.10.014
- Mouvet, C., Jeannot, R., Riolland, H., and Maciag, C. (1997). Stability of isoproturon, bentazone, terbuthylazine and alachlor in natural groundwater, surface water and soil water samples stored under laboratory conditions. *Chemosphere* 35, 1083–1097. doi:10.1016/s0045-6535(97)00174-4
- Oppeltová, P., Vavrouchová, H., Sedláček, J., Geršl, M., Ulrich, O., Vlček, V., et al. (2022). *Spatial conflicts management in hranice karst with emphasis on nature protection and tourist management*. Křtiny, Czech Republic: Mendel University Press.
- Pérez-Lucas, G., Vela, N., El Aatik, A., and Navarro, S. (2019). Environmental risk of groundwater pollution by pesticide leaching through the soil profile. *Pesticides-use misuse their impact Environ.* 2019, 1–28. doi:10.5772/intechopen.82418
- Park, W.-P., Chang, K.-M., Hyun, H.-N., Boo, K.-H., and Koo, B.-J. (2020). Sorption and leaching characteristics of pesticides in volcanic ash soils of jeju island. *korea Appl. Biol. Chem.* 63, 1–13. doi:10.1186/s13765-020-00555-5
- Perera-Rios, J., Ruiz-Suarez, E., Bastidas-Bastidas, P. J., May-Euán, F., Uicab-Pool, G., Leyva-Morales, J. B., et al. (2022). Agricultural pesticide residues in water from a karstic aquifer in yucatan, Mexico, pose a risk to children's health. *Int. J. Environ. Health Res.* 32, 2218–2232. doi:10.1080/09603123.2021.1950652
- Peters, A., Crane, M., Merrington, G., and Ryan, J. (2022). Environmental quality standards for diclofenac derived under the european water framework directive: 2. *Avian Second. poisoning Environ. Sci. Eur.* 34, 1–16. doi:10.1186/s12302-022-00601-7
- Riedo, J., Wächter, D., Gubler, A., Wettstein, F. E., Meuli, R. G., and Bucheli, T. D. (2023). Pesticide residues in agricultural soils in light of their on-farm application history. *Environ. Pollut.* 331, 121892. doi:10.1016/j.envpol.2023.121892
- Ruomeng, B., Meihao, O., Siru, Z., Shichen, G., Yixian, Z., Junhong, C., et al. (2023). Degradation strategies of pesticide residue: from chemicals to synthetic biology. *Synthetic Syst. Biotechnol.* 8, 302–313. doi:10.1016/j.synbio.2023.03.005
- Schäfer, R. B., Kühn, B., Malaj, E., König, A., and Gergs, R. (2016). Contribution of organic toxicants to multiple stress in river ecosystems. *Freshw. Biol.* 61, 2116–2128. doi:10.1111/fwb.12811
- Silva, V., Mol, H. G., Zomer, P., Tienstra, M., Ritsema, C. J., and Geissen, V. (2019). Pesticide residues in european agricultural soils—a hidden reality unfolded. *Sci. Total Environ.* 653, 1532–1545. doi:10.1016/j.scitotenv.2018.10.441
- Sorensen, J., Lapworth, D., Nkhuwa, D., Stuart, M., Gooddy, D., Bell, R., et al. (2015). Emerging contaminants in urban groundwater sources in africa. *Water Res.* 72, 51–63. doi:10.1016/j.watres.2014.08.002
- Špaček, P., Bábek, O., Štěpančíková, P., Švancara, J., Pazdírková, J., and Sedláček, J. (2015). The nysa-morava zone: an active tectonic domain with late cenozoic sedimentary grabens in the western carpathians' foreland (ne bohemian massif). *Int. J. Earth Sci.* 104, 963–990. doi:10.1007/s00531-014-1121-7
- Šrámek, O., Geršl, M., Faimon, J., and Bábek, O. (2019). The geochemistry and origin of fluids in the carbonate structure of the Hranice Karst with the world's deepest flooded cave of the Hranicka Abyss, Czech Republic. *czech Repub. Appl. Geochem.* 100, 203–212. doi:10.1016/j.apgeochem.2018.11.013
- Stoppio, M. G., Lofrano, G., Carotenuto, M., Viccione, G., Guarnaccia, C., and Cascini, L. (2020). A comparative assessment of analytical fate and transport models of organic contaminants in unsaturated soils. *Sustainability* 12, 2949. doi:10.3390/su12072949
- Syafrudin, M., Kristanti, R. A., Yuniarto, A., Hadibarata, T., Rhee, J., Al-Onazi, W. A., et al. (2021). Pesticides in drinking water—a review. *Int. J. Environ. Res. public health* 18, 468. doi:10.3390/ijerph18020468
- Tran, H. T., Lin, C., Bui, X.-T., Nguyen, M. K., Cao, N. D. T., Mukhtar, H., et al. (2022). Phthalates in the environment: characteristics, fate and transport, and advanced wastewater treatment technologies. *Bioresour. Technol.* 344, 126249. doi:10.1016/j.biortech.2021.126249
- Troldborg, M., Gagkas, Z., Vinten, A., Lilly, A., and Glendell, M. (2022). Probabilistic modelling of the inherent field-level pesticide pollution risk in a small drinking water catchment using spatial bayesian belief networks. *Hydrology Earth Syst. Sci.* 26, 1261–1293. doi:10.5194/hess-26-1261-2022
- USEPA (2016). *Sci-grow description*. Washington, DC: United States Environmental Protection Agency. Available at: <https://archive.epa.gov/epa/pesticide-science-and-assessing-pesticide-risks/sci-grow-description.html>.

- Vidal, J., Báez, M. E., Calzadilla, W., Aranda, M., and Salazar, R. (2022). Removal of chloridazon and its metabolites from soil and soil washing water by electrochemical processes. *Electrochimica Acta* 425, 140682. doi:10.1016/j.electacta.2022.140682
- Vysoká, H., Bruthans, J., Falteisek, L., Žák, K., Rukavičková, L., Holeček, J., et al. (2019). Hydrogeology of the deepest underwater cave in the world: Hranice Abyss, Czechia. *Journal* 27, 2325–2345. doi:10.1007/s10040-019-01999-w
- Wachniew, P., Zurek, A. J., Stumpp, C., Gemitzi, A., Gargini, A., Filippini, M., et al. (2016). Toward operational methods for the assessment of intrinsic groundwater vulnerability: a review. *A Rev. Crit. Rev. Environ. Sci. Technol.* 46, 827–884. doi:10.1080/10643389.2016.1160816
- Wauchope, R. D., Buttler, T., Hornsby, A., Augustijn-Beckers, P., and Burt, J. (1992). The scs/ars/ces pesticide properties database for environmental decision-making. *Rev. Environ. Contam. Toxicol.* 123, 1–155. doi:10.1007/978-1-4612-2862-2_1
- Wellington, E. M., Boxall, A. B., Cross, P., Feil, E. J., Gaze, W. H., Hawkey, P. M., et al. (2013). The role of the natural environment in the emergence of antibiotic resistance in gram-negative bacteria. *Lancet Infect. Dis.* 13, 155–165. doi:10.1016/s1473-3099(12)70317-1
- Wilkinson, J. L., Boxall, A. B., Kolpin, D. W., Leung, K. M., Lai, R. W., Galbán-Malagón, C., et al. (2022). Pharmaceutical pollution of the world's rivers. *Proc. Natl. Acad. Sci.* 119, e2113947119. doi:10.1073/pnas.2113947119
- Zemann, M., Majewsky, M., and Wolf, L. (2016). Accumulation of pharmaceuticals in groundwater under arid climate conditions—results from unsaturated column experiments. *Chemosphere* 154, 463–471. doi:10.1016/j.chemosphere.2016.03.136
- Zhang, H., Luo, Y., Zhao, Q., Wong, M. H., and Zhang, G. (2006). Residues of organochlorine pesticides in Hong Kong soils. *Chemosphere* 63, 633–641. doi:10.1016/j.chemosphere.2005.08.006
- Zhu, L., Li, X., Zhang, C., and Duan, Z. (2017). Pollutants' release, redistribution and remediation of black smelly river sediment based on re-suspension and deep aeration of sediment. *Int. J. Environ. Res. Public Health* 14, 374. doi:10.3390/ijerph14040374



OPEN ACCESS

EDITED BY

Abdul Qadeer,
Chinese Research Academy of Environmental
Sciences, China

REVIEWED BY

Sisi Liu,
South China Normal University, China
Zeljko Jakšić,
Rudjer Boskovic Institute, Croatia

*CORRESPONDENCE

Aline Arriola,
✉ aar@akvaplan.niva.no

RECEIVED 21 September 2023

ACCEPTED 18 April 2024

PUBLISHED 16 May 2024

CITATION

Arriola A, Al Saify I, Warner NA, Herzke D,
Harju M, Amundsen P-A, Evenset A, Möckel C
and Krogseth IS (2024), Dechloranes and
chlorinated paraffins in sediments and biota of
two subarctic lakes.

Front. Toxicol. 6:1298231.
doi: 10.3389/ftox.2024.1298231

COPYRIGHT

© 2024 Arriola, Al Saify, Warner, Herzke, Harju,
Amundsen, Evenset, Möckel and Krogseth. This
is an open-access article distributed under
the terms of the [Creative Commons
Attribution License \(CC BY\)](https://creativecommons.org/licenses/by/4.0/). The use,
distribution or reproduction in other forums
is permitted, provided the original author(s)
and the copyright owner(s) are credited and
that the original publication in this journal is
cited, in accordance with accepted academic
practice. No use, distribution or reproduction
is permitted which does not comply with
these terms.

Dechloranes and chlorinated paraffins in sediments and biota of two subarctic lakes

Aline Arriola^{1*}, Insam Al Saify², Nicholas A. Warner^{3,4},
Dorte Herzke⁴, Mikael Harju⁴, Per-Arne Amundsen⁵,
Anita Evenset¹, Claudia Möckel⁶ and Ingjerd S. Krogseth^{4,5}

¹Akvaplan-niva, Fram Centre, Tromsø, Norway, ²Waternet Institute for the Urban Water Cycle, Department of Technology, Research and Engineering, Amsterdam, Netherlands, ³Thermo Fisher Scientific, Bremen, Germany, ⁴NILU (Norsk Institutt for Luftforskning), Fram Centre, Tromsø, Norway, ⁵Department of Arctic and Marine Biology, UiT the Arctic University of Norway, Tromsø, Norway, ⁶Department of Materials and Environmental Chemistry, Stockholm University, Stockholm, Sweden

Our understanding of the environmental behavior, bioaccumulation and concentrations of chlorinated paraffins (CPs) and Dechloranes (Dec) in the Arctic environment is still limited, particularly in freshwater ecosystems. In this descriptive study, short chain (SCCPs) and medium chain (MCCPs) CPs, Dechlorane Plus (DP) and analogues, and polychlorinated biphenyls (PCBs) were measured in sediments, benthic organisms, three-spined stickleback (*Gasterosteus aculeatus*), Arctic char (*Salvelinus alpinus*) and brown trout (*Salmo trutta*) in two Sub-Arctic lakes in Northern Norway. Takvannet (TA) is a remote lake, with no known local sources for organic contaminants, while Storvannet (ST) is situated in a populated area. SCCPs and MCCPs were detected in all sediment samples from ST with concentration of 42.26–115.29 ng/g dw and 66.18–136.69 ng/g dw for SCCPs and MCCPs, respectively. Only SCCPs were detected in TA sediments (0.4–5.28 ng/g dw). In biota samples, sticklebacks and benthic organisms showed the highest concentrations of CPs, while concentrations were low or below detection limits in both char and trout. The congener group patterns observed in both lakes showed SCCP profiles dominated by higher chlorinated congener groups while the MCCPs showed consistency in their profiles, with C₁₄ being the most prevalent carbon chain length. Anti- and syn-DP isomers were detected in all sediment, benthic and stickleback samples with higher concentrations in ST than in TA. However, they were only present in a few char and trout samples from ST. Dec 601 and 604 were below detection limits in all samples in both lakes. Dec 603 was detected only in ST sediments, sticklebacks and 2 trout samples, while Dec 602 was the only DP analogue found in all samples from both lakes. While there were clear differences in sediment concentrations of DP and Dec 602 between ST and TA, differences between lakes decreased with increasing $\delta^{15}\text{N}$. This pattern was similar to the PCB behavior, suggesting the lake characteristics in ST are playing an important role in the lack of biomagnification of pollutants in this lake. Our results suggest that ST receives pollutants from local sources in addition to atmospheric transport.

KEYWORDS

emerging contaminants, chlorinated paraffins, dechloranes, Lakes, sub-arctic

1 Introduction

Persistent organic pollutants (POPs) are man-made compounds that have been used extensively in agriculture, industrial and manufacturing processes (Markowitz, 2018; Ontiveros-Cuadras et al., 2019). Due to their physicochemical properties, POPs can undergo long-range atmospheric transport (LRAT), which results in a global distribution and lead to POPs being present in regions far from where they are used and released, such as the Arctic (Hageman et al., 2015; Kallenborn et al., 2015). POPs also have long half-lives and are highly resistant to degradation. This makes them highly persistent in ecosystems and increases the risk for biomagnification in food webs, potentially causing adverse effects in top predators, including humans. While many POPs have been recognized as harmful and have been regulated by the Stockholm Convention since 2004 (Fiedler et al., 2019), new chemicals are continuously introduced in industrial applications, in many cases as replacements for regulated compounds. Around 150,000 chemicals are currently in use by the industry, with many more entering the market every year (AMAP, 2016). Many are organic contaminants with similar properties to legacy POPs (persistent, bioaccumulative, toxic and/or with LRAT potential) but their potential role as environmental contaminants remains poorly understood.

Short and medium chain chlorinated paraffins (SCCPs and MCCPs) and Dechlorane plus (DP) and related compounds (Dec 601, 602, 603, and 604) are examples of contaminants that have 1) recently been regulated (SCCPs, DP), 2) are currently under review for regulation (MCCPs) or, 3) are not regulated (Dec 601–604). Chlorinated paraffins (CPs) are polychlorinated n-alkanes, which can be categorized according to their number of carbons: short chain (SCCPs, C_{10–13}), medium chain (MCCPs, C_{14–17}) and long chain (LCCPs, C ≥ 18). Differences in carbon chain length and degree of chlorination (30%–70% by weight) give these compounds a wide variety of physico-chemical properties (Glüge et al., 2013). CPs were first introduced on an industrial scale in the 1930s and are now among the most widely produced chemicals in the world (Glüge et al., 2018) with China being the largest producer and consumer (Chen et al., 2021). CPs are stable across a wide range of temperatures and physical conditions, which make them useful in many applications such as in metalworking fluids, in paints and lubricants, as flame retardants, as plasticizers, or as extreme pressure additives (Glüge et al., 2016; Glüge et al., 2018; van Mourik et al., 2016). Despite having been in use for many decades, CPs have only relatively recently been detected in the Arctic environment (Tomy et al., 1999; Tomy et al., 2000; Muir et al., 2000; Reth et al., 2006), mostly due to the development of more sensitive analytical methods and to their inclusion in monitoring programs (Bohlin-Nizzetto and Aas, 2014).

SCCPs have been included in several regulatory bodies in the last years. In Norway, production, sales, import or export of products with more than 0.1% by weight of SCCPs was prohibited in 2002 (ECHA, 2008). SCCPs were included in the Stockholm convention of POPs (Annex A—elimination) in 2017 (UNEP, 2017). While MCCPs have not been regulated, they have been proposed for listing under the Stockholm Convention on persistent organic pollutants (UNEP, 2021). As a result of the regulation of SCCPs, there has been an increase in production and use of MCCPs (Glüge et al., 2018).

This is already reflected in the environment, with MCCP mass fractions in biota surpassing those of SCCPs (Vorkamp et al., 2019a).

Dechlorane plus has been in use since the 1960s, first as an insecticide to replace Mirex, and later as a flame retardant additive mainly in wire and electronic appliances (Hoh et al., 2006; Guo et al., 2017; Hansen et al., 2020). It is considered a chemical of high production volume in the US and of low production volume in the EU (Tomy et al., 2007; Wang et al., 2016). DP has two stereoisomers, *syn*-DP and *anti*-DP that are found in an approximate ratio of 1:3 in commercial products (Wang et al., 2016). The isomer ratio has been used to assess the fate and distribution of DP in the environment and it is normally represented as f_{anti} ($f_{anti} = antiDP/(antiDP + synDP)$). In comparison to DP, information on production and use of the related compounds Dec 602, 603, and 604 is very limited (Shen et al., 2011a; Feo et al., 2012).

CPs, DP and Dec 602, Dec 603 have been found in air, water, sediments, and biota in remote areas such as the Arctic and Antarctic (Möller et al., 2010; Möller et al., 2012; Xiao et al., 2012; Vorkamp and Riget, 2014; Vorkamp et al., 2015; Vorkamp et al., 2019a; Vorkamp et al., 2019b; AMAP, 2017; Gao et al., 2018). These chemicals have been measured in top predators, such as whales and seals, indicating biomagnification in the environment (Simond et al., 2017; Vorkamp et al., 2019a). However, the number of studies in freshwater ecosystems is limited to only a few studies in Canada, Sweden and Norway (Schlabach et al., 2017). A review by Vorkamp et al. (2019a) highlights that only 3 studies include MCCPs in fish from Norwegian and Canadian Arctic lakes. Studies including DP in the Arctic/Sub-Arctic focus mainly on marine and terrestrial environments. Given the small number of studies in freshwater ecosystems and the importance of data from the Arctic documenting the LRAT, bioaccumulation, and persistence of contaminants of emerging concern, the 2017 AMAP assessment on contaminants of emerging concern strongly emphasized the need for more information on levels and better understanding of the sources and distribution of these contaminants. Accordingly, this study aims to provide data for CPs, DP and related compounds in freshwater ecosystems in the Norwegian Sub-Arctic. We specifically address the potential biomagnification by sampling different organisms of the food web, and also evaluate the importance of local sources for these compounds by contrasting a pristine lake assumed only to receive contamination through LRAT, against a lake in an urban area with known local sources of contaminants like PCBs, DDTs, PAHs (polycyclic aromatic hydrocarbons) and cVMS (cyclic volatile methyl siloxanes) (Christensen, 2009; Krogseth et al., 2017a).

2 Materials and methods

2.1 Study area

Two lakes in Northern Norway were selected for this study: Storvannet (70°39' N 23° E) and Takvannet (69°07' N 19°05' E) (Figure 1). Both lakes are oligotrophic, have similar food webs, same top predators and have been well described and studied (Rikardsen and Elliott, 2000; Rikardsen et al., 2000; Amundsen et al., 2007; Amundsen et al., 2009; Amundsen et al., 2019; Eloranta et al., 2013; Eloranta et al., 2015; Krogseth et al., 2017a; Krogseth et al., 2017b).

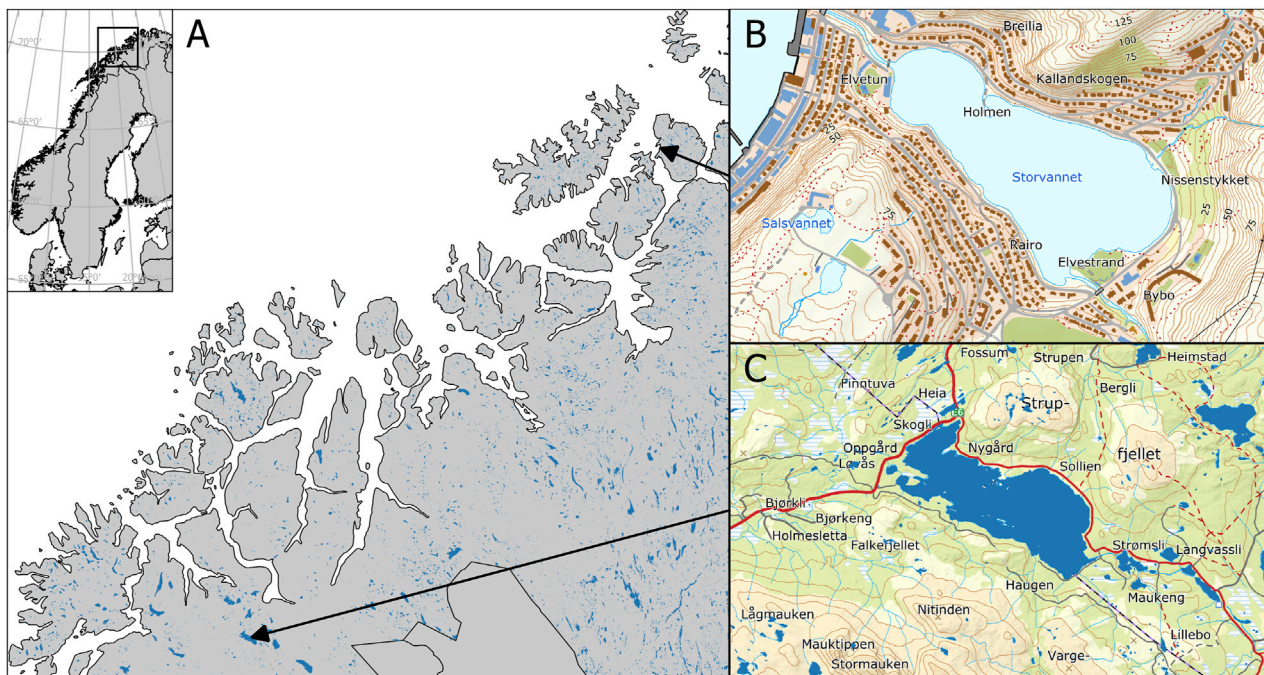


FIGURE 1
Map of Northern Norway (A) showing the location of Storvannet (B) and Takvannet (C). (B) is based on data from the Norwegian Lake Database, available from The Norwegian Water Resources and Energy Directorate (NVE). Map data in (A, C) are from the Kartdata3 WMS service.

However, they are assumed to have different sources of contamination. Storvannet is in a residential area of Hammerfest city (population approx. 8000) and has a long history of contamination with legacy POPs from local sources (Christensen et al., 2009; Krogseth et al., 2017a; Krogseth et al., 2017b). The lake has an area of 0.23 km², with an average depth of 9 m, maximum depth of 18 m, and a water renewal time of ca. 9 days in summer and 38 days in winter (Rikardsen et al., 1997). The lake is covered with ice from November until late May/early June (Krogseth et al., 2017b). Water temperatures through the whole water column are close to zero during winter (0°–1°C) and increase rapidly in June to a maximum of ca. 12°C in July (Rikardsen et al., 2000). Takvannet is located at 214 m above sea level with no known local sources of pollution. It has an area of 15 km² with a maximum depth of 80 m. The lake is usually ice covered from late November to early June. During wintertime, the littoral temperature is close to zero while the profundal waters reach 2°C and during summer a maximum temperature of 12°–14°C can be reached (Klemetsen et al., 1989; Amundsen et al., 2009; Prati et al., 2020; Prati et al., 2021).

2.2 Sample collection

Samples were collected in Storvannet and Takvannet during September and October 2018, respectively. In both lakes, brown trout (*Salmo trutta*), Arctic char (*Salvelinus alpinus*), three-spined sticklebacks (*Gasterosteus aculeatus*), benthic invertebrates and sediments were sampled. Trout and char were caught with multineets (40 m long and 1.5 m high with a mesh size 10, 12.5, 15, 18.5, 22, 26, 35, 45 mm (knot to knot) (Supplementary Table

SI.1). Sticklebacks were sampled either by deploying traps baited with shrimp wrapped in fine mesh (so the fish could not eat it) or by electrofishing in the shallow areas of the lakes. Fish were identified and their fork length and body weight measured. Otoliths were removed for age determination in both char and trout. Samples were individually wrapped in double aluminum foil and stored in zip-lock bags. Benthic organisms were collected from sieving sediment obtained with an Ekman grab (area 225 cm²). Organisms were sorted to taxa and stored in glass jars. Sediments were taken with an Ekman grab (area 225 cm²) at 5 different locations in TA and 4 at ST, at water depths between 12 and 16 m in Storvannet and between 18 and 25 m in Takvannet. The top 2 cm of each sediment sample was transferred to glass jars. All samples were stored at –20°C until further sample preparation in the lab.

2.3 Quality control procedures

All dissection and laboratory procedures were performed in an ISO class 6 clean room with both gas and particle filtration to limit the risk of contamination of samples. Detailed quality control procedures are described in SI. Samples were extracted by batches corresponding to a given lake and type of sample (trout, char, sticklebacks, benthic organisms or sediments) to avoid cross-contamination. Three laboratory blanks consisting of sodium sulphate were analyzed for each batch of samples, and one SRM (sample reference material) was analyzed for each sample type. Samples were spiked with isotopic labeled internal standards prior to extraction, and a recovery standard was added just before instrumental analysis (Detail information can be found in the SI).

2.4 Sample preparation

2.4.1 Fish and benthic organisms

Extraction and clean-up of tissue samples was performed as described by [Herzke et al. \(2009\)](#) and [Bouwman et al. \(2008\)](#). For trout and char, 2 g of muscle were homogenized by finely chopping the tissue with a scalpel in a petri dish. For sticklebacks, 3 g of whole fish (pooled from 3 to 4 fish of similar size) were homogenized, while for benthos 3–5 g of whole organisms of each taxa were homogenized. Homogenized tissues were then mixed with 1:10 parts of sodium sulfate until they formed a fine powder and left in a freezer (−20°C) overnight. Internal recovery standards (see SI for more details) were added to each sample, before they were extracted for 15 min three times using cyclohexane/acetone (3:1) in an ultrasonic bath. Extracts were transferred to 100 mL glass vials and evaporated to 0.5 mL using a RapidVap (Labconco™ RapidVap™ Vacuum Evaporation System) and then left for evaporation to dryness under loose foil in the cleanroom. Lipid content was determined gravimetrically ([Herzke et al., 2009](#)). Samples were reconstituted with 1 mL of n-hexane and transferred to a glass centrifuge tube. Acid clean-up was performed by adding approximately 4–5 mL of concentrated H₂SO₄ to the sample followed by vortexing. Samples were left overnight in darkness. The following day, samples were centrifuged for 20 min at 2000 rpm. The hexane layer was then transferred to a new glass centrifuge tube, new acid was added, and samples were left for 1 h in darkness. This procedure was repeated 3 times. Further clean-up was performed using a 250 mm Pasteur pipette packed with sodium sulphate and preconditioned with 4 mL of n-hexane. The sample was eluted with 4 mL of n-hexane. The eluate was reduced to 0.5 mL using RapidVap and the solvent changed to isooctane. Samples were then evaporated to a final volume of 0.2 mL and transferred to GC-vials, to which recovery standards were added.

2.4.2 Sediments

Sediment samples were thawed and spread out in aluminum trays and left to dry in the clean room for 48 h. Extraction of sediments was performed on an ASE Dionex Accelerated Solvent Extraction system (Thermo Fisher Scientific) equipped with 34 mm stainless steel extraction cells and 80 mL collection bottles. The extraction was performed with acetone:hexane (1:1 v/v) solvent at 150°C and 1500Psi. The packing of the cell was as follows: first a cellulose filter was placed into the cell outlet, followed by 5.0 g of silica, another filter, and a mixture of 5 g of dried sediments mixed with diatomaceous earth. All samples were spiked with internal standards before extraction. Extracts were transferred to 100 mL glass vials and evaporated with RapidVap to 1 mL and acid clean-up was performed as described above for fish and benthic organisms. Once the extract was clean, activated copper (−40 + 100 mesh, 99.5%) was added to remove all traces of sulfur. A second clean-up procedure was performed with Silica columns, previously rinsed with 10% dichloromethane in hexane. Samples were eluted with 40 mL of the same solvent and collected in a 100 mL glass vial. Samples were then evaporated to approximately 10 mL before transferring them to 15 mL vials and further reduced to 0.5 mL and then solvent changed to isooctane. Samples were then evaporated to a final 0.2 mL and transferred to GC vials.

2.4.3 Total organic carbon and stable isotopes

Total organic carbon (TOC) was measured in sediment samples following the method DIN19539:2016-12. Biota and sediments from both lakes were analyzed for stable isotopes of carbon and nitrogen, and isotopic ratios were calculated ($\delta^{13}\text{C}$ and $\delta^{15}\text{N}$). Detailed description for both methodologies can be found in the SI. The isotopic ratio of nitrogen ($\delta^{15}\text{N}$) was used to investigate the bioaccumulation of the chemicals in the two lakes, by regressing chemical concentrations against $\delta^{15}\text{N}$.

2.5 Instrumental analyses and quantification

2.5.1 PCBs

PCBs were analyzed on an Agilent Technology 7890 GC and detection on an Agilent Technology 5975 MSD. For more detailed information, please refer to ([Herzke et al., 2009](#)).

2.5.2 Dechloranes and chlorinated paraffins

Dechlorane analysis was performed on a Thermo Scientific Q Exactive Orbitrap GC/HRAM mass spectrometer (Thermo Fisher Scientific, Waltham, MA United States) with 1 μL injections into a PTV (program temperature vaporizer) with a deactivated baffled glass liner at 70°C and after 0.1 min ramped to 320°C at 12°C/sec and held for 6 min. Helium was used as carrier gas at 1.4 mL/min in constant flow mode. A Thermo Scientific TG-5SilMS capillary column (15 m x 0.25 mmID, 0.25 μm df) was used. The GC oven was programmed from 60°C (2 min) and ramped at 50°C/min to 320°C and held for 6 min with a total runtime of 13.2 min. Transfer line of MS was held at 300°C while ion source was set at 180°C in NCI mode with methane at 1.4 mL/min at 70 eV with a mass resolution of 60,000 @ m/z 200, scanning at 250–700 m/z. The dechlorane standard was injected as a single point calibration. Results were processed in Tracefinder 4.1.

2.5.3 Quantification of chlorinated paraffins

The CP calibration standards were prepared in isooctane from the stock solutions and ranged from 0.5 ng/ μL to 5 ng/ μL with observed linear relationships of $R^2 = 0.99$ (ZS/MCCPs). The pattern deconvolution approach was used to quantify the CPs ([Bogdal et al., 2015](#)). A detailed description of the statistical analysis was reported by [Al Saify et al. \(2021\)](#), using the same commercially available technical formulations with two additional single-chain length standards (C₁₁ 60% and C₁₂ 70% Cl) to reconstruct the CP sample patterns.

2.6 Data analyses

Data are presented on both lipid normalized (lw) and wet weight (ww) basis for biota and normalized for total organic carbon (oc) and dry weight (dw) for sediments. However, statistical analyses were performed on lw and dw. Due to the overall small sample sizes and associated likely deviation from normal distributions, data were summarized using median and range. The median is much less affected by extreme observations in either the upper or lower tails of the distribution ([Huston and Juarez-Colunga, 2009](#)) and is therefore

often chosen as a more “robust” and better measure of center than the more commonly used mean.

We used the Wilcoxon rank sum test to test differences between lakes for all the morphometrics, lipid percent, isotopes and TOC.

To test for differences in contaminant mass fraction between lakes and compartments, we performed an Aligned Rank Transform two-way factorial ANOVA (Wobbrock et al., 2011), using the ARTool package for R (Elkin et al., 2021). This is a non-parametric equivalent of a normal two-way factorial ANOVA, appropriate for data that cannot be assumed to conform to the requirements for traditional parametric methods. We performed a contrast analysis on the estimated marginal means (a.k.a. The least squares means) from the ART analysis, across the reference grid of predictor variables, using functions available in the emmeans package for R (Russell, 2020). For PCBs the analysis was performed on the $\Sigma 7$ PCBs (28, 52, 101, 118, 138, 153, 180) which is often used for comparison of mass fractions over time or between different locations unless specified otherwise. It is important to highlight that caution should be made in interpreting results due to low sampling numbers, especially for benthic species. For Statistical analyses, values below limit of detection (LOD) were substituted with a value of LOD/2 (Giskeødegård and Lydersen, 2022).

Biota sediment accumulation factor (BSAF) can be used as an approach to estimate the bioaccumulation potential of organic contaminants. BSAFs were calculated as the lipid normalized concentration in biota divided by the mean of the OC-normalized concentration in sediments in the lake (Burkhard et al., 2004) for samples that had values above LOD.

All statistical analyses were performed in R (R Core Team, 2020).

3 Results and discussion

3.1 Morphometrics and stable isotopes

Summary statistics for organism morphometrics (length, weight and age for char and trout), total organic carbon (TOC) in sediments, stable isotopes, and lipid content for samples from both lakes are shown in [Supplementary Tables SI.1, SI.2](#). There were no significant differences in length, weight, age and lipid content between the two lakes for either trout (Wilcoxon rank sum test length: $W_x = 58.5$, $p = 0.83$, weight: $W = 59$, $p = 0.81$, age: $W = 70$, $p = 0.3$, lipid: $W = 53$, $p = 0.92$) or char (length: $W = 63$, $p = 0.15$, weight: $W = 60$, $p = 0.24$, age: $W = 59$, $p = 0.26$, lipid: $W = 42$, $p = 0.84$). Surface sediment samples from Storvannet had significantly higher proportions of TOC compared to Takvannet (4.3%–6.5% vs 2.0%–2.3%, $W = 20$, $p = 0.015$).

[Supplementary Figure SI.1](#) presents the stable isotope ratios in both lakes. $\delta^{15}\text{N}$ ratios were significantly higher in Storvannet than in Takvannet for both char ($W = 82$, $p < 0.001$) and trout ($W = 101$, $p < 0.001$), while no significant differences were observed between lakes for sediments, benthic organisms, or sticklebacks. Within lakes there were no significant differences between char and trout. However, a few trout individuals had higher $\delta^{15}\text{N}$ ratios than char in both lakes ([Supplementary Figure SI.1](#)). Trout is

TABLE 1 Mass fractions of $\Sigma 7$ -PCB and of PCB-153 in sediments (ng/g dw) and biota (ng/g lw) in Storvannet and Takvannet.

Lake	n	Σ PCB 7		PCB 153	
		Median	Range	Median	Range
Storvannet					
Sediment	4	44	21–66	11	6–18
Benthos	2	839	708–971	262	215–309
Stickleback	5	1121	1030–1357	371	342–455
Trout	11	633	55–3866	145	17–909
Char	10	1121	57–2401	262	15–638
Takvannet					
Sediment	5	0.21	0.1–0.5	0.04	0.03–0.1
Benthos	5	28	9–36	7	3–10
Stickleback	3	67	58–80	22	19–25
Trout	10	40	17–532	10	4–106
Char	9	145	83–1078	36	21–269

considered to be competitively superior to char and it has been observed that the main prey of trout over 300 mm in length is three-spined sticklebacks but they can also become cannibalistic (Prati et al., 2021). Char and trout are omnivorous and feed on different prey depending on their ontogenetic development (Klemetsen et al., 2003) but may also be influenced by the environmental conditions of the lakes and interspecific competition which can vary between lakes (Guildford et al., 2008; Cabrerizo et al., 2018; Prati et al., 2021). Although there were no statistically differences in length within or between lakes, the fish over 300 mm had higher $\delta^{15}\text{N}$ values and were more abundant in the samples from Storvannet. The differences between the fish from the two lakes may indicate that fish in Storvannet rely to a greater extent on fish prey compared to fish in Takvannet. In addition, these differences may be explained by potentially higher microbial activity in Storvannet. The microbial loop has been shown to play an important role in the uptake of terrestrial material into the food-web (Poste et al., 2019) and can also add additional trophic levels (Karlsson et al., 2012; Mc Govern et al., 2019).

Values of $\delta^{13}\text{C}$ were not significantly different between lakes for char, trout, stickleback, and benthos, but were significantly enriched in sediments from Takvannet compared to Storvannet. This may indicate a higher terrestrial input into Takvannet, which has a larger catchment area (59.2 km²) than Storvannet (42.4 km²) (Norwegian Water Resources and Energy Directorate (NVE), 2020). This is coupled with the shorter water turnover time in Storvannet due to its large drainage basin and small size.

3.2 PCBs

Overviews of $\Sigma 7$ -PCB and PCB-153 mass fractions in sediments and biota from both lakes are provided in [Table 1](#), [Supplementary Table SI.3](#), and [Supplementary Figures SI.2A, B](#). Mass fractions in

sediment were assessed according to the guidelines given by the Norwegian Environment Agency (Miljødirektoratet, 2016) to obtain information on the environmental condition of the lakes. Sediment mass fraction of $\Sigma 7$ -PCB in Storvannet ranged from 21.4 to 65.9 ng/g dw, with a median of 43.9 ng/g dw. This is comparable to those measured in 2006 (range of 54.9–58.4 ng/g dw, Evenset et al., 2006), and corresponds to condition class III (moderately polluted) (Miljødirektoratet, 2016). Storvannet is more polluted than other lakes both on mainland Norway (average $\Sigma 7$ -PCB 1.9 ng/g dw, $n = 49$) and on Svalbard (average $\Sigma 7$ -PCB 10.1 ng/g dw, $n = 5$) (Gabrielsen et al., 2011). This, together with its classification as “moderately polluted” corroborates that it receives PCBs from local sources (Christensen, 2009; Krogseth et al., 2017a; Krogseth et al., 2017b). Mass fractions of $\Sigma 7$ -PCB in Takvannet sediments were significantly lower than those in Storvannet ($W = 20$, $p = 0.01$), ranging from 0.14 to 0.49 ng/g dw. Mass fractions in Takvannet were also significantly lower than those from Storvannet when normalized to TOC content, despite lower TOC content in Takvannet sediments. The $\Sigma 7$ -PCB in Takvannet correspond to background conditions (Miljødirektoratet, 2016). This suggests that Takvannet mainly receives PCBs through LRAT.

Consistent with this, $\Sigma 7$ -PCB mass fractions in biota were higher in Storvannet than in Takvannet for all organisms, except char. This was especially evident at lower trophic levels, where mass fractions could differ by as much as 100-fold, while differences become gradually smaller for species higher up the food chain. As a result, in Takvannet, mass fractions increase considerably with increasing $\delta^{15}\text{N}$, while in Storvannet mass fractions do not increase as sharply (Supplementary Figures SI.2A, B, SI.5). The correlation between PCB-153 and $\delta^{15}\text{N}$ differs between lakes. In Takvannet we observed a significant positive relationship (linear model of $\log_{10}(\text{conc}_{\text{PCB-153}}) \sim \delta^{15}\text{N}$; slope = 1.39, 95% CI: 1.191–1.561), while in Storvannet the correlation was slightly negative but not significant (slope = 0.96, 95% CI: 0.826–1.104) (Supplementary Figures SI.3, SI.5). The opposing relationship of PCB-153 and ΣPCB7 observed in Storvannet resembles the observed and modelled behavior of cyclic volatile methyl siloxanes (cVMS) in Storvannet (Krogseth et al., 2017b). This was explained by the particular characteristics of both the physical environment and food web of Storvannet. This lake has a rapid water turnover time, resulting in a disequilibrium situation between water and sediments (with higher fugacity in sediment than in water). This results in lower mass fractions in the benthic-feeding fish due to more efficient elimination of contaminants through ventilation to water (Krogseth et al., 2017a; Krogseth et al., 2017b). Hence, the lack of biomagnification of PCB-153 in Storvannet is likely a result of these processes. See the Supplementary Material for a more detailed discussion of the bioaccumulation behavior and BSAFs of PCBs in these two lakes. Supplementary Figure SI.5 shows the results of a principal component analysis (PCA) highlighting differences between compartments and lakes. The first two principal components (PC) explained 66.8% of the variance in the data (PC 1: 41.9%, PC 2: 24.9%). The first PC mainly accounts for differences between lakes while the second PC is related to differences between compartments.

3.3 Dechloranes

3.3.1 Dechlorane Plus

Mass fractions of *syn*- and *anti*-DP in sediments and biota of Storvannet and Takvannet are provided in Table 2 and Supplementary Table SI.4. Both DP isomers were detected in all sediment samples. Mass fractions (in ng/g dw and ng/g OC) were higher in Storvannet (*syn*-DP median: 9.56 ng/g OC range: 3.50–38.0 ng/g OC, $n = 4$; *anti*-DP median: 43.6 ng/g OC; range: 9.16–153 ng/g OC, $n = 4$), than in Takvannet (*syn*-DP median: 0.26 ng/g OC, range: 0.08–0.41 ng/g OC, $n = 5$; *anti*-DP median: 0.86 ng/g OC; range: 0.44–3.72 ng/g OC, $n = 5$), with consistently higher *anti*-DP than *syn*-DP mass fractions in both lakes. Higher mass fractions of ΣDP in Storvannet than in Takvannet indicate that Storvannet also receives DP from local sources around the lake, as it does for other organic contaminants including PCBs and cVMS (Krogseth et al., 2017a; b; Christensen et al., 2009; Christensen, 2009). Mass fraction ranges of the sum of *anti*-DP and *syn*-DP (ΣDP) in sediment samples from Storvannet were comparable to those found in Lake Erie (0.061–8.62 ng/g dw) (Sverko et al., 2008), but higher than in Lake Huron and Lake Michigan (ΣDP 0.87 ng/g dw and 0.55 ng/g dw, respectively) (Shen et al., 2011b). However, in Storvannet, mass fractions were lower than in Lake Ontario (*syn*-DP median: 30 and 35 ng/g dw; *anti*-DP median: 115 and 176 ng/g dw, respectively) (Qiu et al., 2007; Tomy et al., 2007), which has elevated ΣDP mass fractions because of its location downstream of a DP manufacturing plant (Shen et al., 2011a). Ranges of ΣDP in sediment samples from Takvannet were comparable to those found in Lake Winnipeg of $\Sigma \text{DP} = 0.03$ ng/g; *syn*-DP: 0.011 ng/g dw, *anti*-DP: 0.018 ng/g dw. Takvannet is considered a remote lake, and the low mass fractions suggest that it only receives DP through LRAT as it was seen in Lake Winnipeg (Qiu et al., 2007; Tomy et al., 2007).

In biota from Storvannet, *syn*- and *anti*-DP were above detection limits in all samples of benthos and sticklebacks. In biota from Takvannet, *syn*- and *anti*-DP were above detection limits in most samples of benthos and sticklebacks, but not in any of the char or trout. Like for sediments, mass fractions of both isomers in biota were significantly higher in Storvannet than in Takvannet (Figure 2), and *anti*-DP were consistently higher than *syn*-DP mass fractions (Table 2 and Supplementary Table SI.4). *Syn*-DP and *anti*-DP in benthos ranged from 0.67 to 1.16 ng/g lw ($n = 2$) and 2.49–3.26 ng/g lw ($n = 2$), respectively, in Storvannet. In Takvannet, amphipods were the only benthic sample with mass fractions of *syn*-DP below LOD. The rest of the benthic samples had *syn*-DP that ranged from 0.17–0.77 ng/g lw ($n = 4$) and mass fractions of *anti*-DP that ranged from 0.07–1.90 ng/g lw ($n = 5$) with the lowest mass fraction found in amphipods.

In Storvannet, mass fractions of *syn*-DP and *anti*-DP in sticklebacks ranged from 0.08–0.15 ng/g lw ($n = 5$) and 0.13–0.28 ng/g lw ($n = 5$), respectively. In Takvannet, only one stickleback out of three had mass fractions above LOD (0.05 ng/g lw) of *syn*-DP. In contrast, mass fractions for *anti*-DP were measured in all three-spined stickleback with ranges of 0.03–0.09 ng/g lw ($n = 3$). In both lakes there was a decrease in mass fractions from benthic organisms to sticklebacks for both isomers.

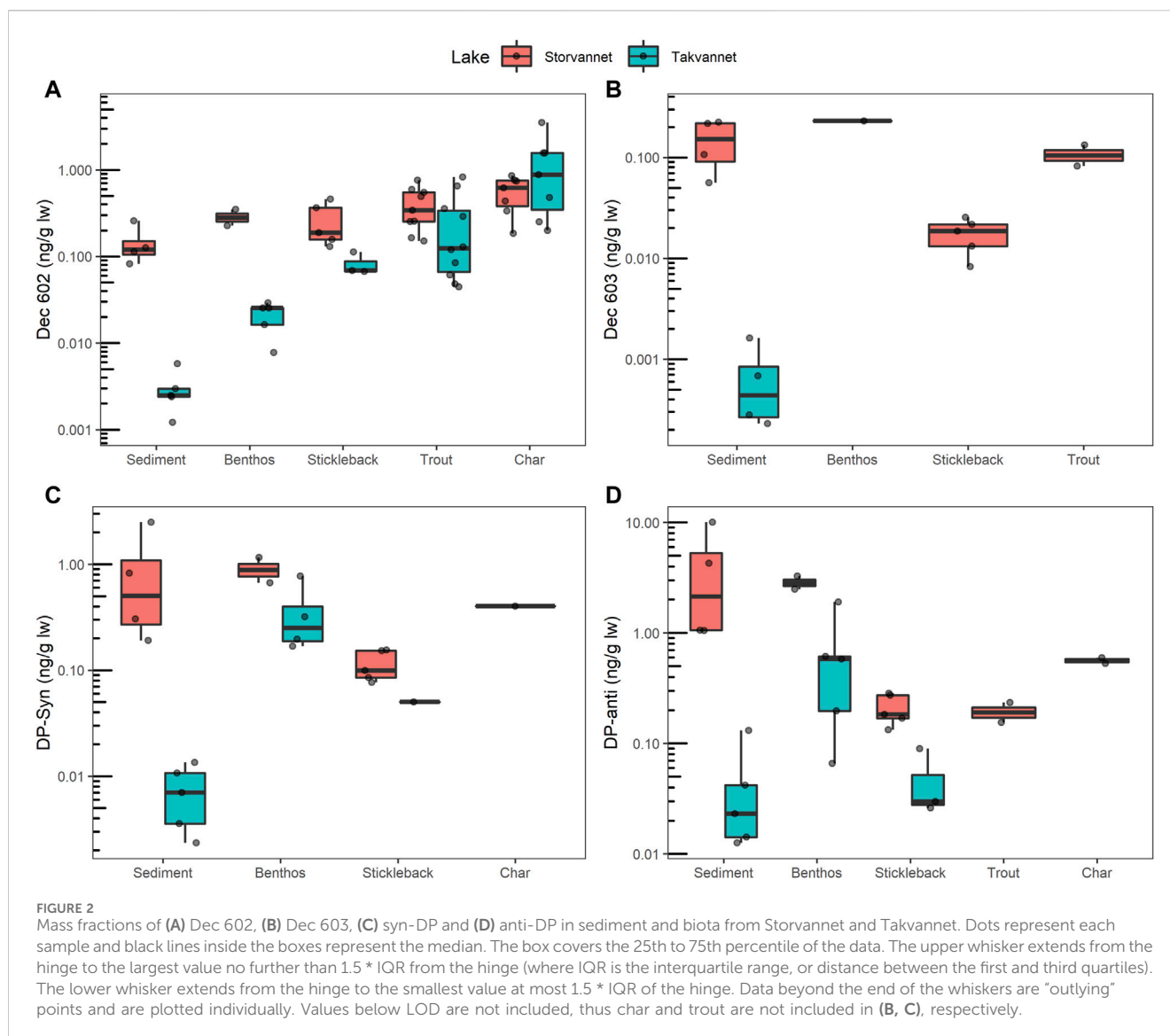
In Storvannet, *syn*-DP was detected in one char (0.40 ng/g lw) and *anti*-DP was found in two char samples (0.53–0.60 ng/g lw) and

TABLE 2 Mass fractions of *syn*-DP, *anti*-DP, and DP total (*syn*-DP + *anti*-DP) measured in sediment (ng/g OC) and biota (ng/g lw) in Storvannet and Takvannet, as well as the calculated f_{anti} fraction. The numbers in parenthesis indicate the number of samples > LOD. Mass fractions < LOD are not included in medians and ranges. "na" indicates that the *fanti* fraction and DP total concentration was not calculated because none of the DP isomers were detected > LOD.

Lake	n	<i>syn</i> -DP		n	<i>anti</i> -DP		n	<i>Fanti</i>		n	DP total	
		Median	Range		Median	Range		Median	Range		Median	Range
Storvannet												
Sediment	4 (4)	9.56	3.50–38.0	4 (4)	43.6	9.16–153	4 (4)	0.82	0.78–0.85	4 (4)	3.23	1.24–12.5
Mollusc	1 (1)	0.67	-	1 (1)	2.49	-	1 (1)	0.79	-	1 (1)	3.15	-
Chironomid	1 (1)	1.16	-	1 (1)	3.26	-	1 (1)	0.74	-	1 (1)	4.42	-
Stickleback	5 (5)	0.10	0.08–0.15	5 (5)	0.18	0.13–0.28	5 (5)	0.65	0.63–0.66	5 (5)	0.28	-
Arctic char	10 (1)	0.40	-	10 (2)	0.56	0.53–0.60	10 (1)	0.6	-	10 (2)	0.77	0.53–1.00
Brown trout	10 (0)	< LOD	-	10 (2)	0.19	0.15–0.23	10 (0)	na	-	10 (2)	0.19	0.15–0.23
Takvannet												
Sediment	5 (5)	0.26	0.08–0.41	5 (5)	0.86	0.44–3.72	5 (5)	0.80	0.77–0.91	5 (5)	0.03	0.01–0.14
Amphipods	1 (0)	< LOD	-	1 (1)	0.07	-	1 (0)	na	-	1 (1)	0.07	-
Valvatidae	1 (1)	0.20	-	1 (1)	0.61	-	1 (1)	0.76	-	1 (1)	0.80	-
Lymnae	1 (1)	0.30	-	1 (1)	1.90	-	1 (1)	0.86	-	1 (1)	2.22	-
Mollusc	1 (1)	0.77	-	1 (1)	0.58	-	1 (1)	0.43	-	1 (1)	1.35	-
Chironomid	1 (1)	0.17	-	1 (1)	0.20	-	1 (1)	0.54	-	1 (1)	0.37	-
Stickleback	3 (1)	0.05	-	3 (3)	0.03	0.03–0.09	3 (1)	0.64	-	3 (3)	0.03	0.03–0.14
Arctic char	9 (0)	< LOD	-	9 (0)	< LOD	-	9 (0)	na	-	9 (0)	na	-
Brown trout	10 (0)	< LOD	-	10 (0)	< LOD	-	10 (0)	na	-	10 (0)	na	-

two trout samples (0.15–0.23 ng/g lw). The detected mass fractions were comparable to, or higher than, the mass fractions measured in sticklebacks from the same lake. Our results are similar to other studies, where DPs were detected in low mass fractions in fish despite elevated mass fractions in sediments (Guo et al., 2017). In Southern Norway, 95% of DP mass fractions in fish samples were below the limit of quantification in the urban lake Mjøsa and in the pristine lake Femunden with detected Σ DP values ranging between 0.05–0.10 ng/g ww. (Jartun et al., 2020). The few detected *syn*-DP and *anti*-DP mass fractions in Storvannet char were slightly higher than in Trout or Walleye from all of the Great Lakes, except for *anti*-DP in Lake Huron which were higher than in Storvannet (Guo et al., 2017). Moreover, they were also comparable to those in Arctic char from Greenland (Vorkamp et al., 2019b), where *syn*-DP was not detected, and *anti*-DP was detected in low mass fractions in 3 out of 6 samples (0.047–0.188 ng/g lw). The trout samples from Storvannet had *anti*-DP mass fractions that were only slightly higher than those from Lakes Michigan and Superior (Guo et al., 2017). Other studies of trout from the Great Lakes have found higher Σ DP mass fractions with a mean of 0.35 ng/g lw (Kurt-Karakus et al., 2019) and also in a range from 2.3–7.2 ng/g lw (Lake Ontario only) with the highest mass fractions from 1988 (Ismail et al., 2009). In Takvannet neither of the DP isomers were found in char or trout. Supplementary Figure SI.7 shows the PCA biplot for DPs and DP related compounds. The plot highlights a clear separation between compartments and to a lower degree between lakes. The low

detection frequency of *syn*-DP and *anti*-DP in char and trout species in both Storvannet and Takvannet compared with levels in samples from benthic organisms or stickleback samples in the same lake, indicate a lack of magnification for DP isomers in both lakes. BSAF for both *anti* and *syn* DP (Supplementary Figure SI.8) suggest low bioaccumulation potential. In Takvannet, BSAF could only be estimated for benthic organisms (average 1.11 and 0.46 for *syn* and *anti* DP) and sticklebacks (average of 0.03 for *syn* DP and 0.06 for *anti* DP). In Storvannet, BSAF values were lower than 1 in all organisms, including benthos (0.04 and 0.06 for *anti* and *syn* DP), sticklebacks (0.003 and 0.01 for *anti* and *syn* DP) and char (0.002 and 0.003 for *anti* and *syn* DP). The low BSAF values of both DPs in both lakes indicate a lack of biomagnification. However, these BSAFs should be interpreted with care due to the small sample size. Similar results were observed but with trophic magnification factors (TMFs) in Lake Ontario by Tomy et al. (2007), where low TMF values for *syn*- and *anti*-DP indicated a lack of biomagnification. Results from Lake Winnipeg were more ambiguous, with an estimated TMF of 2.5 for *anti*-DP, but a lack of biomagnification for *syn*-DP (Tomy et al., 2007). In contrast, Wu et al. (2010) found TMFs of 6.5 and 11.3 for *anti*-DP and *syn*-DP, respectively. It has been suggested that the lack of increasing DP with increasing trophic level may be explained by DPs low water solubility and high octanol water partition coefficient ($\log K_{ow} = 11.3$, Shen et al., 2011b). DPs high hydrophobicity means that it binds to organic carbon both in sediments and in the water column



and hence is less bioavailable. The high log K_{OW} limits the transfer efficiency across the gastrointestinal tract, hence decreasing the organism's uptake of DP from the diet (Hoh et al., 2006; Guo et al., 2017). It is also possible that DPs become biotransformed by fish, as has been described by Hoh et al. (2006). Previous studies have concluded that DP bioaccumulation patterns are species-specific rather than simply correlated with general trophic level, and that differences in biomagnification also can be related to differences in ecosystem structure (Tomy et al., 2007; Vorkamp et al., 2015; Schlabach et al., 2017; Vorkamp et al., 2019b). Biomagnification of DP isomers has been detected in freshwater food webs (Tomy et al., 2007; Wu et al., 2010) but also in marine food webs (Peng et al., 2014; Na et al., 2017; Zhang and Kelly, 2018). The reasons why they display biomagnification in certain species/food-webs, but not in others, is not clearly known yet.

3.3.2 DP stereoisomer profiles

The commercial DP products consist of around 65% *anti*-DP and 35% *syn*-DP, giving an f_{anti} value of 0.65. However, this can

range between 0.59 and 0.80 due to differences in production batches and manufacturers (Hoh et al., 2006). Isomer (f_{anti}) ratios found in the environment that deviate from this may show the extent of environmental degradation and/or biotransformation of the different isomers as the two stereoisomers may degrade at different rates (Xian et al., 2011). The median f_{anti} values in sediments from Storvannet and Takvannet were 0.82 (range 0.78–0.85) and 0.80 (range 0.77–0.91), respectively (Table 2). These are at the high end of those reported for technical mixtures (Hoh et al., 2006; Wang et al., 2010), suggesting a depletion of the *syn*-DP isomer. This agrees with observations in sediments from Lake Ontario ($f_{anti} = 0.86$) (Tomy et al., 2007). It also agrees with higher f_{anti} in sediment samples closer to source regions (Hoh et al., 2006).

The f_{anti} values in benthos were higher in Storvannet than in Takvannet for both mollusks (ST: $f_{anti} = 0.79$, TA: $f_{anti} = 0.43$) and chironomids (ST: $f_{anti} = 0.74$, TA: $f_{anti} = 0.54$). This indicates a depletion of *anti*-DP in benthos from Takvannet compared to in Storvannet. It also indicates a depletion of *anti*-DP in benthos

TABLE 3 Mass fractions of Dec 602 and 603 measured in sediment (pg/g OC) and biota (pg/g ww) in Storvannet and Takvannet. The numbers in parentheses indicate the number of samples > LOD. Mass fractions < LOD are not included in medians and range.

Lake	n	Dec 602		n	Dec 603	
		Median	Range		Median	Range
Storvannet						
Sediment	4 (4)	2.10	1.67–3.95	4 (4)	2.45	1.28–3.95
Mollusc	1 (1)	0.23	-	1 (0)	<LOD	-
Chironomid	1 (1)	0.35	-	1 (1)	0.23	-
Stickleback	5 (5)	0.19	0.13–0.46	5 (5)	0.02	0.01–0.03
Arctic char	10 (7)	0.62	0.18–0.86	10 (0)	<LOD	-
Brown trout	11 (8)	0.34	0.15–0.76	11 (2)	0.11	0.08–0.13
Takvannet						
Sediment	5 (5)	0.11	0.04–0.16	5 (5)	0.014	0.01–0.05
Amphipods	1 (1)	0.01	-	1 (0)	<LOD	-
Valvatidae	1 (1)	0.03	-	1 (0)	<LOD	-
Lymnae	1 (1)	0.03	-	1 (0)	<LOD	-
Mollusc	1 (1)	0.03	-	1 (0)	<LOD	-
Chironomid	1 (1)	0.02	-	1 (0)	<LOD	-
Stickleback	3 (3)	0.07	0.07–0.11	3 (0)	<LOD	-
Arctic char	9 (7)	0.88	0.20–3.51	9 (0)	<LOD	-
Brown trout	10 (10)	0.12	0.04–0.82	10 (0)	<LOD	-

compared to sediments in Takvannet. However, when all benthic samples in Takvannet were considered, the range in f_{anti} was large (0.43–0.86), and it is hard to draw conclusions due to a low number of samples. The median f_{anti} values in sticklebacks were not different between the two lakes (ST: 0.65, TA: 0.64) and were within the range observed for commercial DP products.

Due to low detection frequencies of DP in trout and char, f_{anti} could only be estimated for one char sample from Storvannet (0.60). This value is in the same range as f_{anti} in fish from Lake Ontario (0.65 ± 0.06) (Tomy et al., 2007), Lake Superior (0.63 ± 0.07) and Lake Erie (0.60 ± 0.07) (Guo et al., 2017). As in other studies (Tomy et al., 2007; Shen et al., 2011a), we observed lower f_{anti} values for benthic organisms and fish than in sediments. In the food web from Lake Ontario, the values declined from 0.65 in plankton to 0.51 in trout (Tomy et al., 2007). This might be explained by a stereoselective accumulation of *syn*-DP, since *anti*-DP is more reactive and susceptible to photodegradation and biodegradation (Möller et al., 2010; Wang et al., 2015). Experiments have shown that the *syn* isomer had higher assimilation and lower depuration in rainbow trout than the *anti*-isomer (Tomy et al., 2008). It is not known if this happens in other organisms to the same extent (Wang et al., 2016).

3.3.3 Other dechloranes

Dec 601 and 604 were below LOD in all samples in both Storvannet and Takvannet. This is in agreement with findings from the limited number of studies describing the presence of

DP related compounds in freshwater ecosystems (Shen et al., 2010; Shen et al., 2011a; 2011b; Jartun et al., 2020). Neither Dec 601 nor 604 were detected in sediments or fish from Lake Mjøsa or Lake Femunden (Jartun et al., 2020), and were also not detected in sediments, fish or birds from the Oslofjord (Ruus et al., 2019). While Dec 604 has been described in sediments and fish samples from the Great Lakes (Sverko et al., 2011) it was only present in the sediment samples from Michigan, Huron, Erie and Ontario lakes and only in four samples from Lake Superior (Shen et al., 2010; Shen et al., 2011a), while in fish samples it was only present in trout from Lake Ontario (Shen et al., 2010). This suggests that the manufacturing plants along the Niagara River were the main sources of the detected Dec 604. Thus, it is not surprising that we did not detect Dec 604 in Storvannet and Takvannet. Moreover, this also agrees with a spatial study of Dechlorane Plus and related compounds in European background air, including Norwegian sites, where Dec 601 and 604 were not detected in air samples (Skogeng et al., 2023).

Dec 603 (Table 3; Supplementary Table SI.5; Figure 2) was detected in all sediment samples from both lakes (ST: 2.54 pg/g OC, range: 1.28–3.95 pg/g OC; TA: 0.014 pg/g OC, range: 0.01–0.05 pg/g OC), and in the chironomid sample (0.23 ng/g lw, $n = 1$), all sticklebacks (0.02 ng/g lw, range: 0.01–0.03 ng/g lw, $n = 5$) and two trout samples (0.08–0.13 ng/g lw) in Storvannet. Dec 603 was not detected in biota from Takvannet. Similarly low Dec 603 mass fractions were found in sediment in the Oslofjord (average 0.069 ng/g dw (Ruus et al., 2019)) and in two studies in the Great Lakes (0.001–0.6 ng/g dw (Shen et al., 2010) and < LOD–1.1 ng/g dw

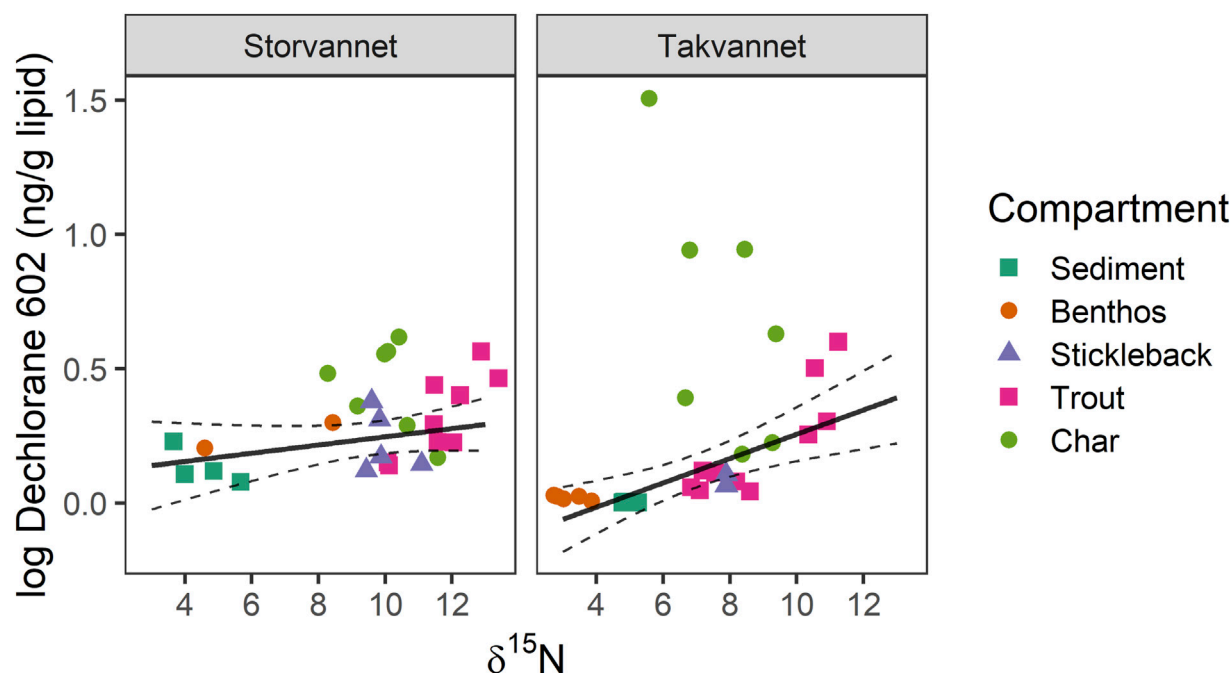


FIGURE 3
Relationship between $\delta^{15}\text{N}$ and the logarithmic Dec 602 mass fractions for all samples in Takvannet and Storvannet. Solid black line represents the fit of the robust linear model and the dash lines represent the 95% confidence interval of the fit.

(Shen et al., 2011b)). The Dec 603 mass fractions measured in Storvannet are in the low range in comparison to measurements in trout from Lake Superior, Huron and Ontario and in whitefish from Lake Erie, with mass fractions ranging from 0.014–0.500 ng/g lw (Shen et al., 2010). There is no clear current point source of Dec 603, thus this compound might enter the lakes mainly through atmospheric transport (Shen et al., 2010). However, Dec 603 was not measured above detection limits in air samples from background regions in Europe (Skogeng et al., 2023).

Dec 602 was found in all sediment samples from both lakes, with mass fractions ranging between 1.67–3.95 pg/g OC in Storvannet (median 2.10 pg/g OC), and 0.04–0.16 pg/g OC (median 0.11 pg/g OC) in Takvannet (Figure 2; Table 3; Supplementary Table S1.5). Dec 602 was detected more frequently than Dec 603 in the biota samples. Dec 602 was detected in all benthos and stickleback samples, and in over 70% of trout and char samples, from both lakes. Dec 602 was higher in the single chironomid sample (0.35 ng/g lw) than in the single mollusk sample (0.23 ng/g lw) from Storvannet. Mass fractions in benthic organisms from Takvannet were lower than in Storvannet and ranged between 0.008–0.029 ng/g lw ($n = 5$). Similarly, Dec 602 in sticklebacks were higher in Storvannet (0.19 ng/g lw (range: 0.13–0.46, $n = 5$)) than in Takvannet (0.07 ng/g lw (range: 0.07–0.11, $n = 3$)) (Figure 2). Mass fractions in trout from Storvannet had a median of 0.34 ng/g lw (range: 0.15–0.76 ng/g lw, $n = 9$) while in Takvannet the median value was 0.12 ng/g lw (range: 0.04–0.82, $n = 10$). In contrast, char from Takvannet (0.88 ng/g lw, range 0.20–3.51, $n = 7$) had higher mass fractions than Storvannet char (0.62 ng/g lw, range: 0.18–0.86, $n = 7$). However, these differences between lakes for char and trout were not significant.

Takvannet had lower Dec 602 mass fractions in sediment than those reported for any of the Great Lakes (Shen et al., 2010), while Dec 602 in Storvannet sediment was higher in all of the Great Lakes except Lake Ontario h (0.160–11 ng/g dw) (Shen et al., 2010). Dec 602 median mass fractions in trout from Takvannet and Storvannet were 61 and 21 times lower, respectively, than those in trout from Lake Ontario (7.38 ng/g lw). Dec 602 mass fractions in char from Storvannet and Takvannet were lower than in char from all the Great Lakes, except Lake Superior.

While there were clear differences in sediment Dec 602 mass fractions between Storvannet and Takvannet, differences between lakes decreased with increasing $\delta^{15}\text{N}$ (Figure 2 and Supplementary Figure S1.9). This pattern was similar to the PCB behavior, suggesting that the lake characteristics in Storvannet play an important role in the biomagnification (or lack thereof) of pollutants in this lake (Krogseth et al., 2017a; Krogseth et al., 2017b). The linear model between Dec 602 and $\delta^{15}\text{N}$ showed a slightly positive correlation (slope: 1.01, 95% CI: 0.99–1.04) for Storvannet and (slope: 1.04, 95% CI: 1.02–1.05) for Takvannet (Figure 3). Increasing Dec 602 mass fractions with increasing $\delta^{15}\text{N}$ was significant in Takvannet which agrees with previous studies (Shen et al., 2011a; Feo et al., 2012; Barón et al., 2014a). It has been suggested that this chemical is more bioaccumulative and may have a higher bioavailability compared to Dec 602 due to a $\log K_{ow}$ lower than 8.1 (Wang et al., 2016). BSAF values for Dec 602 (Supplementary Figure S1.8) show a clear bioaccumulation potential, particularly in Takvannet, while the values observed in Storvannet are low, which is in accordance with what we have previously described, and we attribute this to differences in lake characteristics. In Takvannet BSAF values increased from benthos (0.20) < sticklebacks (0.78) < trout (2.45) < char (11.3). In

TABLE 4 Mass fractions of SCCP homologue groups (denoted by the carbon chain length) in sediments (ng/g dw) and biota (ng/g lw) in Storvannet and Takvannet, as well as the Σ SCCPs. N = number of samples analyzed, number between parentheses represents the number of samples that were above LOD. Mass fractions < LOD were not included in the median and ranges.

Lake	n	Σ C10		n	Σ C11		n	Σ C12		n	Σ C13		Σ SCCP	
		Median	Range		Median	Range		Median	Range		Median	Range	Median	Range
Storvannet														
Sediment	4 (4)	6.37	3.580–11.61	(4)	29.16	21.99–55.99	(4)	21.89	17.59–39.02	(4)	5.965	2.980–9.580	63.32	46.26–115.2
Mollusc	1 (1)	27.6	-	(1)	118	-	(1)	52.8	-	(1)	108	-	307	-
Chironomid	1 (0)	-	-	(0)	-	-	(0)	-	-	(0)	-	-	-	-
Stickleback	4 (4)	14.2	10.5–101	(4)	47.4	27.2–187	(4)	52.8	25.3–177	(4)	76.2	36.4–230	190	99.4–695
Arctic char	10 (3)	2.55	0.15–31.4	(4)	3.03	1.87–147	(4)	7.07	0.34–130	(4)	4.09	0.14–99.9	27.9	10.9–817
Brown trout	11 (2)	3.94	0.45–7.42	(3)	4.34	1.09–28.3	(3)	3.13	3.06–50.9	(3)	2.09	2.03–32.2	19.9	12.5–238
Takvannet														
Sediment	5 (3)	0.072	0.041–0.101	(3)	0.325	0.225–1.885	(3)	0.251	0.129–3.296	(3)	0.008	0.003–0.013	0.661	0.399–5.281
Amphipods	1 (1)	11.5	-	(1)	9.54	-	(1)	2.41	-	(1)	2.853	-	26.3	-
Valvatidae	1 (1)	3.87	-	(1)	10.3	-	(1)	4.91	-	(1)	10.54	-	29.6	-
Lymnae	1 (1)	16.5	-	(1)	49.9	-	(1)	26.6	-	(1)	32.05	-	125	-
Mollusc	1 (1)	5.40	-	(1)	1.79	-	(1)	0.56	-	(1)	2.125	-	9.86	-
Chironomid	1 (0)	-	-	(0)	-	-	(0)	-	-	(0)	-	-	-	-
Stickleback	3 (3)	3.64	0.19–6.32	(3)	5.79	0.83–6.61	(3)	1.36	0.24–11.7	(3)	0.83	0.05–46.6	11.6	1.31–71.2
Arctic char	9 (2)	2.24	1.04–3.45	(2)	26.1	9.80–42.4	(2)	5.16	1.09–9.23	(1)	0.24	-	67.2	23.8–110
Brown trout	10 (3)	0.23	0.03–0.63	(4)	3.00	1.13–7.00	(4)	1.43	0.23–9.68	(1)	5.67	-	5.99	1.36–20.2

TABLE 5 Mass fractions of MCCP homologue groups (denoted by the carbon chain length) in sediments (ng/g dw) and biota (ng/g lw) in Storvannet and Takvannet, as well as the Σ MCCPs. N = number of samples analyzed, number between parentheses represents the number of samples that were above LOD. Mass fractions < LOD were not included in the median and ranges.

Lake	n	ΣC14		n	ΣC15		n	ΣC16		n	ΣC17		ΣMCCP	
		Median	Range		Median	Range		Median	Range		Median	Range		
Storvannet														
Sediment	4 (4)	41.86	37.09–68.88	(4)	24.65	19.27–45.40	(4)	9.419	7.410–19.99	(4)	1.921	1.280–4.410	77.30	66.18–136.7
Mollusc	1 (1)	14047	-	(1)	9365	-	(1)	6302	-	(1)	2041	-	31757	-
Chironomid	1 (0)	-	-	(0)	-	-	(0)	-	-	(0)	-	-	-	-
Stickleback	4 (4)	459	107–1588	(4)	154	35.5–498	(4)	45.0	9.77–147	(4)	6.61	1.38–28.7	1330	307–4527
Arctic char	10 (2)	857	202–1510	(2)	118	17.8–218	(2)	3.26	0.42–6.10	(0)	-	-	977	220–1735
Brown trout	11 (4)	213	51.9–2228	(4)	42.5	3.63–1493	(3)	3.19	0.38–1004	(1)	111.8	-	258	55.6–4837
Takvannet														
Sediment	5 (0)	<LOD	-	(0)	<LOD	-	(0)	<LOD	-	(0)	<LOD	-	<LOD	-
Amphipods	1 (1)	225	-	(1)	116	-	(1)	52.8	-	(1)	14.8	-	409	-
Valvatidae	1 (1)	572	-	(1)	277	-	(1)	105	-	(1)	8.76	-	963	-
Lymnae	1 (1)	4081	-	(1)	2735	-	(1)	1888	-	(1)	634	-	9340	-
Mollusc	1 (1)	202	-	(1)	92	-	(1)	24.1	-	(1)	2.28	-	320	-
Chironomid	1 (1)			(1)			(1)			(1)				
Stickleback	3 (3)	196	29.2–3004	(3)	142	5.70–2291	(3)	62.5	0.12–1013	(2)	103	3.70–203	404	35.0–6512
Arctic char	9 (3)	182	85.9–660	(2)	25.9	12.2–499	(2)	8.46	3.90–254	(2)	11.7	-	1149	39.9–15255
Brown trout	10 (4)	380	18.1–4837	(3)	315	10.8–4412	(3)	361	11.0–4404	(1)	892	-	212	106–1425

Storvannet values for benthos (0.12) were very similar to sticklebacks (0.11) followed by trout (0.14) and highest value of 0.23 for char.

The higher mass fractions of DP, Dec 602 and Dec 603 in Storvannet sediments compared to those in Takvannet suggest that Storvannet may receive not only LRAT input but also contribution from local emissions of these compounds. This is not unexpected, since DP and related compounds have been widely used as flame retardants in industrial applications and household products such as in electrical and electronic equipment (Wang et al., 2016). Production, use, recycling, waste handling, as well as leachate and run-off from landfills, wastewater treatment plants and more, can lead to their release (Wang et al., 2016; Schlabach et al., 2017; Wang and Kelly, 2017). High levels of DPs have been measured in sewage sludge and wastewater treatment plants from urban areas (de la Torre et al., 2012; Barón et al., 2014b; Schlabach et al., 2017), and they have also been found in dust and electronic appliances from residential areas (Newton et al., 2015; Schlabach et al., 2017; Wong et al., 2018; Sørensen and Larsen, 2019). Storvannet has received both intentional and unintentional emissions of untreated wastewater (Krogseth et al., 2017a; Krogseth et al., 2017b), which could potentially be a source of DP and related compounds to Storvannet.

3.4 Chlorinated paraffins

3.4.1 SCCPs and MCCPs

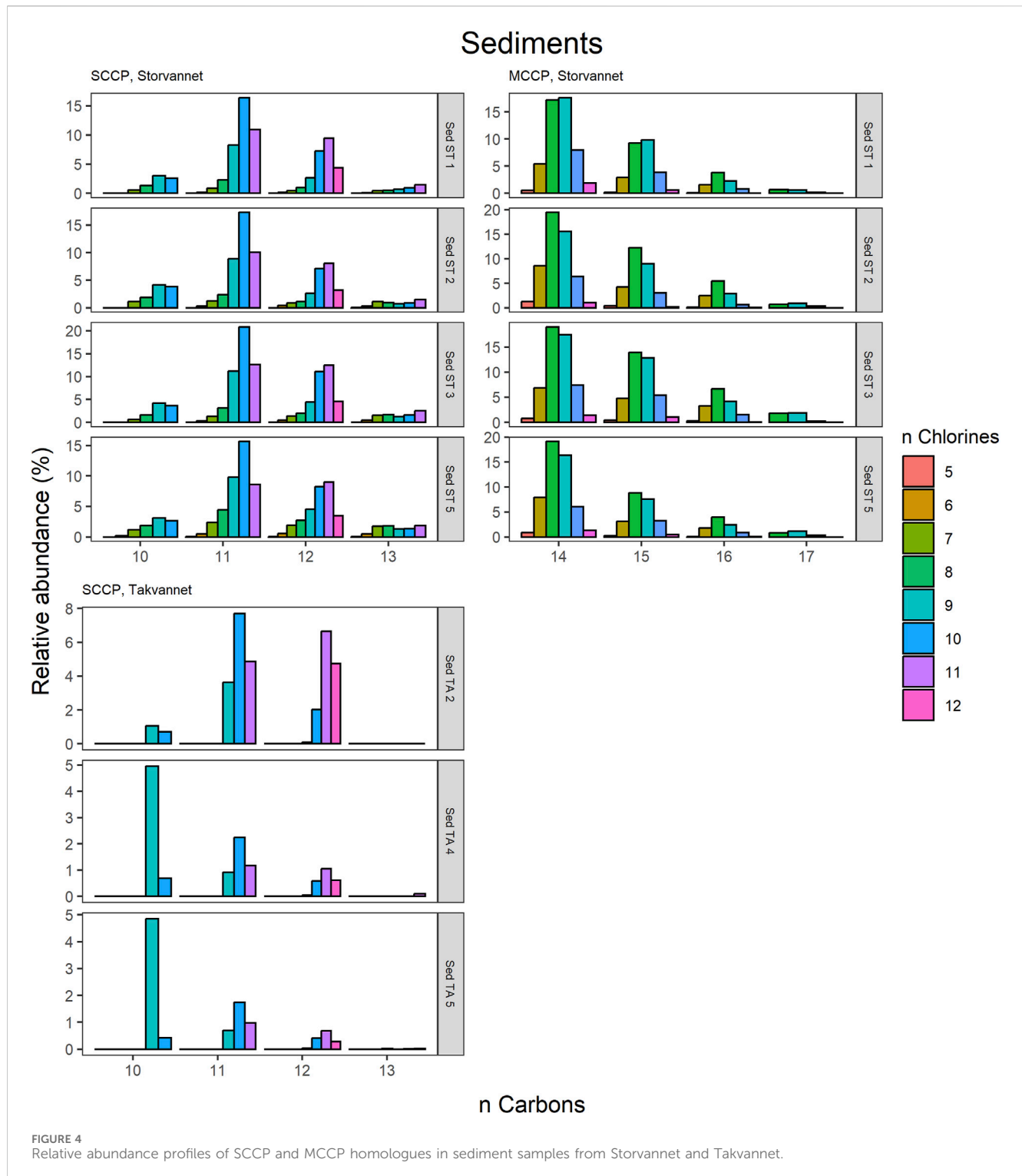
SCCPs and MCCPs are presented in Table 4, Table 5 and Supplementary Table SI.6, 7. Supplementary Figure SI.9 shows a PCA biplot which highlights the difference between MCCPs and SCCPs between compartments and lakes. Although only 57.1% of variation was explained by the first two principal components, the PCA biplot is still useful to identify clusters. Storvannet sediments and sticklebacks and benthic samples from both lakes are more influenced by MCCPs than SCCPs. While trout and char from both Storvannet and Takvannet are more influenced by SCCPs. Both SCCPs and MCCPs were detected in all sediment samples from Storvannet with median mass fractions of 63 ng/g dw (range: 46–115 ng/g dw) and 77 ng/g dw (range of 66–137 ng/g dw) for Σ SCCPs and Σ MCCPs, respectively. Higher mass fractions of MCCPs relative to SCCPs agree with current emission profiles for CPs, where MCCP usage and emissions have increased in recent years due to regulatory scrutiny and regulation of SCCPs. The MCCP:SCCP ratio was relatively consistent, and in most cases >1 (0.9, 1.2, 1.5, and 1.6 in the four samples respectively). Overall, total SCCP tended to be at least one order of magnitude higher in Storvannet than in Takvannet (median: 0.661 ng/g dw, range: 0.399–5.281 ng/g dw), but due to the small sample size, this difference was not statistically significant (Wilcoxon rank sum test, $W = 12$, $p = 0.057$). While MCCPs were detected in samples from Storvannet, they were not detected in samples from Takvannet. This may be due to the higher molecular mass and therefore low degree of LRAT of MCCPs (Wu et al., 2019). The presence of MCCPs in Storvannet may therefore be a result of local use of products containing CPs (Li et al., 2021).

In Storvannet, CPs were only detected in a mollusk sample with a Σ SCCP 2.41 ng/g ww (307 ng/g lw) and 124 ng/g ww (31757 ng/lw) of Σ MCCPs. In Takvannet SCCPs and MCCPs were measured in 4 benthic organisms, with Lymnae having the highest mass

fractions for both CPs (Σ SCCPs: 1.38 ng/g ww (125 ng/g lw), Σ MCCPs: 102 ng/g ww (9340 ng/g lw)) > Amphipods (SCCPs: 0.34 ng/g ww (26.3 ng/g lw), MCCPs: 5.27 ng/g ww (409 ng/g lw) > Valvatidae (SCCPs: 0.16 ng/g ww (29.6 ng/g lw), MCCPs: 5.31 ng/g ww (963 ng/g lw)) > Mollusc (SCCPs: 0.05 ng/g ww (9.86 ng/g lw), MCCPs: 1.65 ng/g ww (320 ng/g lw)) (Table 4; Table 5; Supplementary Table SI.6, 7).

Σ SCCPs were observed in sticklebacks from both lakes, Storvannet (median: 10.2 ng/g ww, 191 ng/g lw) and Takvannet (median: 0.6 ng/g ww, 11.6 ng/g lw). Interestingly, in Storvannet, mass fractions detected in trout and char were lower than those found in Sticklebacks, while comparable mass fractions were found among all fish in Takvannet. Median mass fractions of Σ MCCPs in sticklebacks were 1331 ng/g lw (range: 308–4528 ng/g lw) in Storvannet and 404 ng/g lw (range: 35.0–6513 ng/g lw) in Takvannet, however they were not significantly different (Wilcoxon, $W = 7$, $p = 0.86$). For top predatory fish, the detection frequency for MCCPs was low for both trout (40%) and char (<30%) in both lakes. In Storvannet, Σ MCCPs mass fractions in trout with values above LOD ranged from 56 to 4838 ng/g lw (median: 258 ng/g lw) and in Takvannet they ranged from 106–1425 ng/g lw (median: 212 ng/g lw). These mass fractions were not significantly different between lakes (Wilcoxon, $W = 7$, $p = 0.89$). For char, Σ MCCPs in Storvannet ranged from 220 to 1735 ng/g lw (median: 978 ng/g lw), and in Takvannet from 39 to 15255 ng/g lw (median: 1149 ng/g lw). However, this maximum value is from one individual with an extremely low lipid content. Again, mass fractions were not significantly different between lakes (Wilcoxon, $W = 5$, $p = 0.4$). Within lakes there were no significant differences between char and trout (Storvannet: $W = 3$, $p = 0.8$; Takvannet: $W = 8$, $p = 0.629$). Although nonparametric tests were performed, results should be interpreted with caution due to the very small number of samples with values above LOD. Nevertheless, among the small number of fish with mass fractions above LOD, the medians were very similar in the two lakes. This was unexpected due to the proximity of Storvannet to an urban area. Similar to SCCPs, MCCPs did not show an increase in mass fractions with increasing $\delta^{15}\text{N}$. The Σ SCCPs observed in trout in this study are only similar to those found in trout from Lake Erie (12 ± 7 ng/g lw) but are low in comparison to those found in trout from other Canadian lakes that ranged from 22 to 288 ng/g lw (Basconillo et al., 2015). In comparison to char from Lake Ellasjøen on Bear Island (Σ SCCPs 7–27 ng/g ww) (Katsoyiannis, 2013), both lakes from this study had also lower mass fractions. Comparison to other studies should be done with caution as different analytical and quantification methodologies may not be comparable (Pellizzato et al., 2009; van Mourik et al., 2020). Dick et al. (2010) observed similar results in Canada, where mass fractions in sticklebacks were higher than those in Arctic char. This is probably a reflection of sticklebacks feeding on benthic organisms.

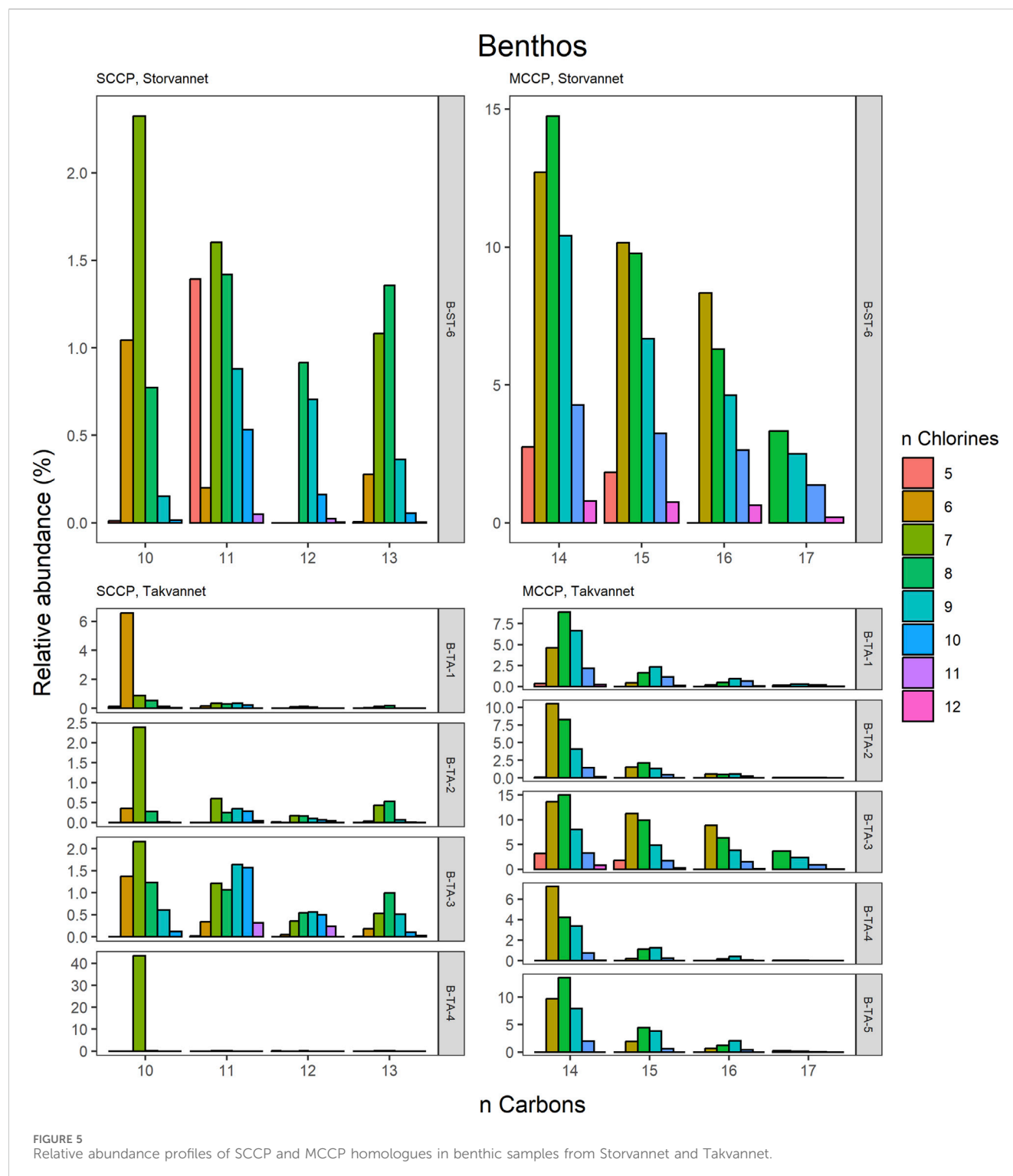
BSAF values for SCCPs and MCCPs are shown in Supplementary Figures SI.10–12. BSAF values greater than 1 were found for several homologues in Storvannet benthos (C_{10}Cl_6 , C_{10}Cl_7 , C_{11}Cl_6 , C_{11}Cl_7 , C_{12}Cl_5 , C_{12}Cl_6 , C_{12}Cl_7 , C_{13}Cl_6 , C_{13}Cl_7 , C_{13}Cl_8) and sticklebacks (C_{10}Cl_6 , C_{10}Cl_7 , C_{11}Cl_6 , C_{12}Cl_8 , C_{13}Cl_7 , C_{13}Cl_8 , C_{13}Cl_9), and for only a few homologues in Takvannet benthos (C_{10}Cl_9 , C_{11}Cl_9 , C_{12}Cl_9 , $\text{C}_{13}\text{Cl}_{10}$), sticklebacks (C_{12}Cl_9 , $\text{C}_{13}\text{Cl}_{10}$) and char (C_{10}Cl_9 , C_{11}Cl_9 , $\text{C}_{11}\text{Cl}_{10}$). BSAF for MCCPs could only be estimated for organisms in Storvannet, and the only benthic organism was not included due to its very



low lipid content. BSAF values were above 1 also for several MCCP homologues in sticklebacks ($C_{14}Cl_8$, $C_{14}Cl_9$, $C_{14}Cl_{10}$, $C_{15}Cl_{10}$, $C_{16}Cl_{10}$), trout ($C_{14}Cl_5$, $C_{14}Cl_6$, $C_{15}Cl_5$, $C_{15}Cl_6$, $C_{15}Cl_7$, $C_{16}Cl_5$, $C_{16}Cl_6$, $C_{17}Cl_7$) and char ($C_{14}Cl_8$, $C_{14}Cl_9$, $C_{14}Cl_{10}$). Previous studies have shown a negative correlation between BSAFs and $\log K_{ow}$ (Sun et al., 2017; Huang et al., 2019), suggesting that bioaccumulation of SCCPs decreases with increasing $\log K_{ow}$ (Sun et al., 2017). While there was no evidence for such a

relationship in our study (see Fig SI 10–12), this may be a result of the small sample size.

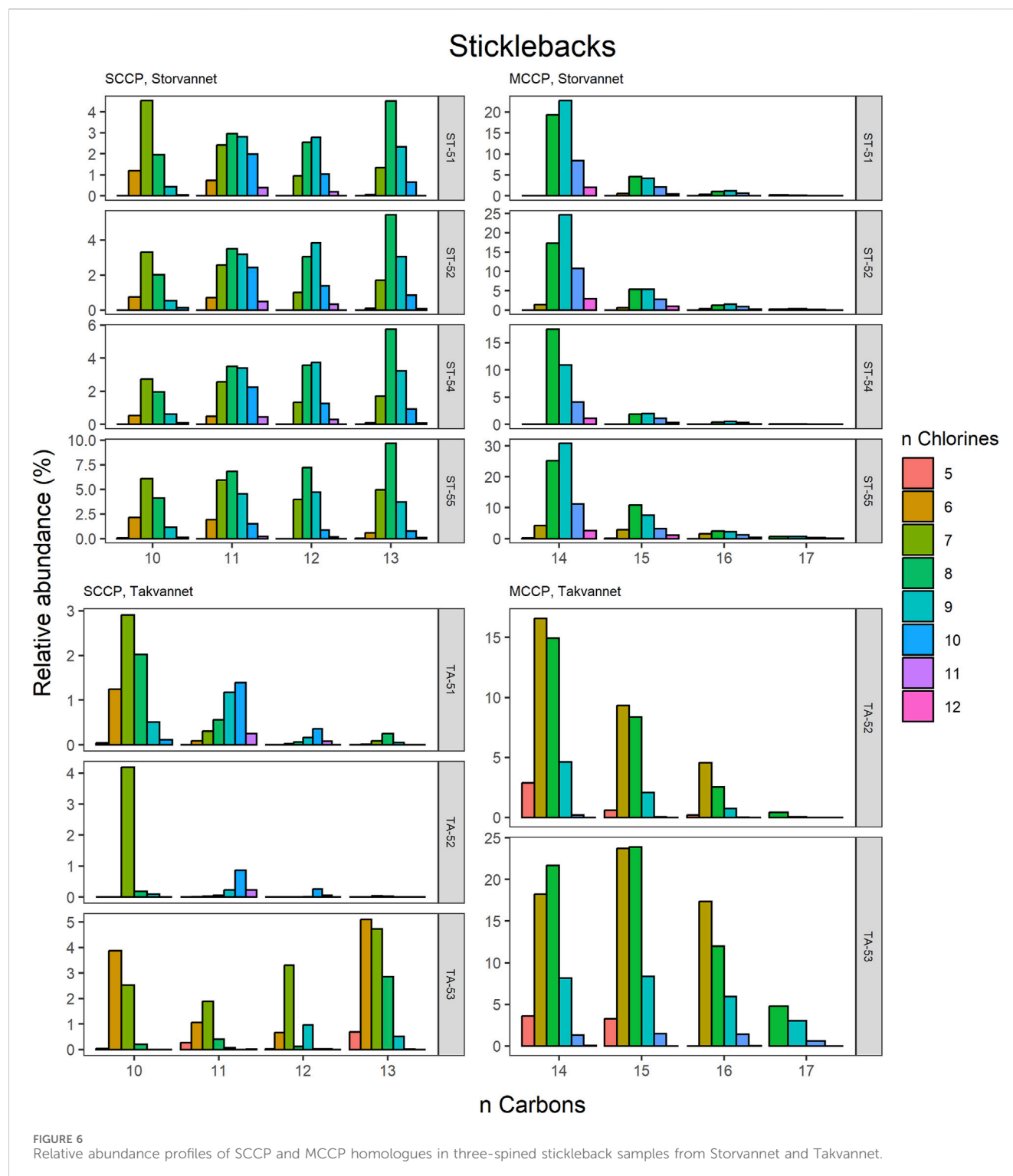
Although mass fractions of both SCCPs and MCCPs were low in this study, their presence in sub-Arctic lakes reflects that CPs can undergo LRAT (Wu et al., 2019; Jiang et al., 2021). Our results are in agreement with previous studies where higher mass fractions of CPs have been observed close to urban areas with industrial and anthropogenic activity (Li et al., 2021).



3.4.2 CP homologue and congener group patterns

The congener group patterns for both SCCPs and MCCPs are provided in Figures 4–8. The patterns observed in both lakes showed SCCP profiles dominated by higher chlorinated congener groups while the MCCPs showed consistency in their profiles with C_{14} being the prevalent carbon chain length. Within the sediment samples, the C_{11} and C_{12} homologues contributed highest to the sum of SCCPs in both Storvannet ($47\% \pm 1.5\%$ and $35\% \pm 2.5\%$,

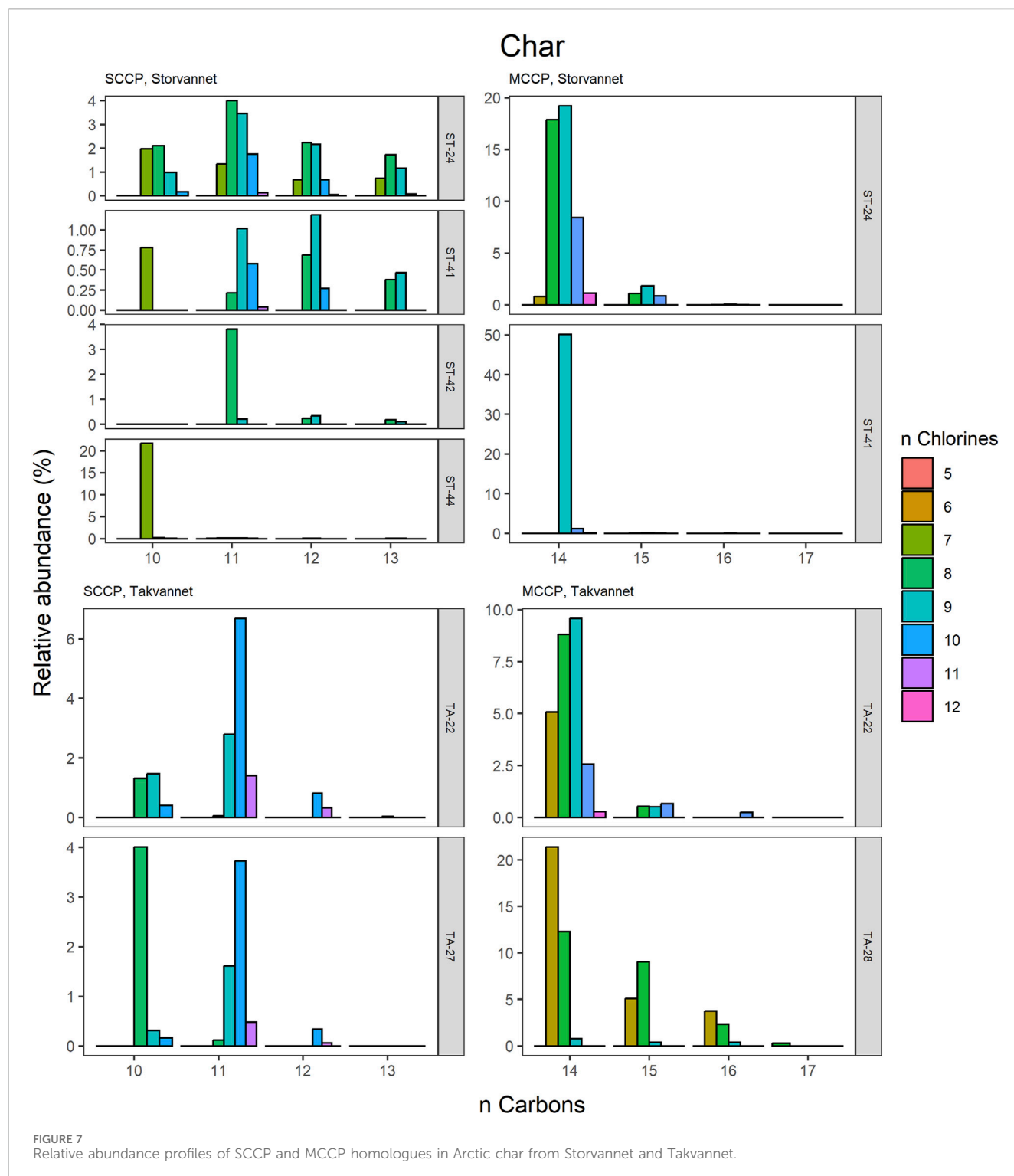
respectively) and Takvannet ($47\% \pm 10\%$ and $44\% \pm 16\%$, respectively). The most abundant SCCP congener groups in sediment were C_{11}, Cl_{9-11} and C_{12}, Cl_{10-12} (Figure 4). This is in good agreement with sediment core samples from a rural lake in Switzerland showing a C_{11-12} contribution of 66–87% (mean: 79%) (Iozza et al., 2008). The SCCP profiles we observed are very different compared to those observed in the technical mixtures where congeners with Cl_{5-8} dominate in the SCCP 51% and 55% Cl and



Cl₇₋₁₀ in the SCCP 63% Cl. Similar findings, i.e., high chlorination (Cl₈₋₁₁) SCCP profiles, were observed in rubber granulates (Brandsma et al., 2019). This profile is most likely caused by use of different technical CP mixtures available worldwide for use in product manufacturing, in addition to recycling of materials to produce new products containing various technical mixes (Krätschmer and Schächtele, 2019). With adoption of recent regulations on the use of SCCPs under the Stockholm

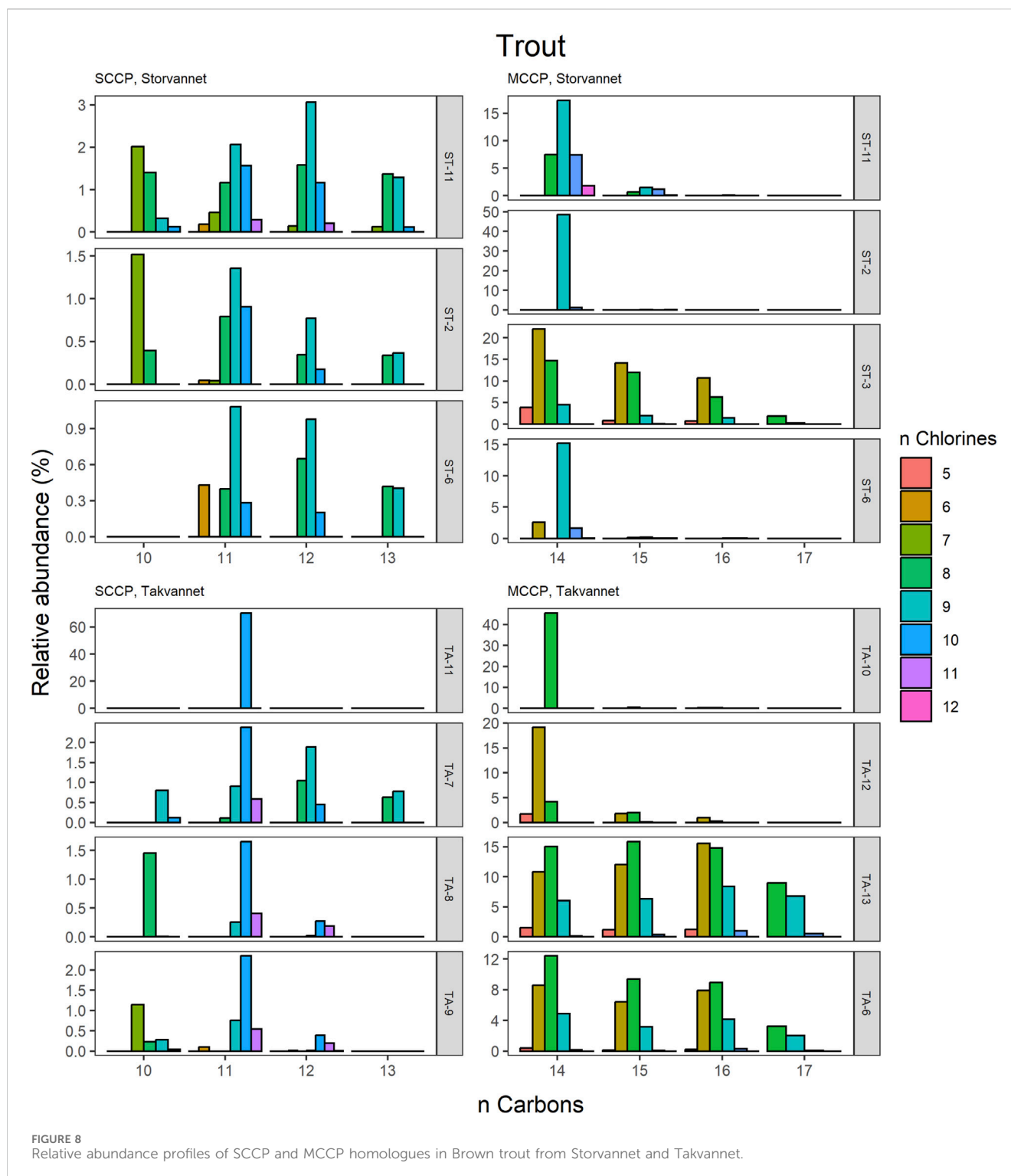
convention, SCCPs present in the environment will represent a very different profile to those observed prior to regulations. This is either as a result of degradation or use/recycling of different technical mixtures for production of products which warrants further investigation.

The MCCPs were only detected in sediments from Storvannet (Section 4.2.1) with C₁₄ as the major contributor (54% ± 2.4%), followed by C₁₅, C₁₆ and C₁₇ (32% ± 1.8%, 12% ± 1.0% and 2.6% ±



0.6%, respectively). The MCCP profiles are in good agreement with sediment samples from the North and Baltic Sea (Hüttig and Oehme, 2006) with contributions of 45%–50% and 31%–40% for the C_{14} and C_{15} homologues and from Lake Thun in Switzerland (C_{14} : 41%–64%, mean: 48%). The MCCP profiles observed in sediment are almost identical to those in benthic organisms from both Storvannet and Takvannet ($52\% \pm 9.9\%$, $30\% \pm 1.4\%$, $15\% \pm 6.3\%$ and $3.3\% \pm 2.8\%$ for C_{14-17} , respectively) (Figure 5),

highlighting the importance of organism-sediment coupling in driving food chain exposure to MCCPs. The SCCPs, however, showed differences in profiles between the sediment and benthic organisms. Comparable to the sediment samples, the C_{11} homologue was found to be the most dominant in almost all organisms (ranging from 18% to 40%) but was followed by the contribution of the C_{13} homologue (11%–36%) instead of the C_{12} homologue (9%–21%). The Chironomidae in both lakes showed SCCP profiles deviating



from the other organisms with the C_{13} chain length as major contributor (Storvannet: 95% and Takvannet: 70%).

The high contributions of C_{13} were also observed in stickleback in Storvannet with profiles very similar between the individuals (Figure 6). The relative proportion increased with increasing carbon length, with C_{13} being the most dominant group of the SCCPs ($18\% \pm 1.3\%$). One stickleback sample in Takvannet showed a profile similar to those in Storvannet, while the other two showed profiles

comparable to the sediment samples with dominance of the C_{11} homologue followed by the C_{12} . This could be attributed to the fact that shorter and less chlorinated CPs will have a greater volatility and be more easily transported via LRAT. The MCCP profiles of the sticklebacks in Storvannet showed consistency among all samples with the C_{14-15} as most abundant homologues ($70\% \pm 0.7\%$ and $23\% \pm 0.6\%$, respectively). The composition of the MCCPs in sediment and biota were found to be a combination of the

MCCPs with 52% and 57% CI, implying that their occurrence within the environment is a result from production and use of materials containing these mixtures. There was no significant difference found between the SCCP profiles detected in the top predatory fish in Takvannet (Figure 7; Figure 8). The C_{11} and C_{12} homologues were found to be most abundant in the trout and char samples ($68\% \pm 23\%$ and $24\% \pm 14\%$, respectively), different from the profiles observed in the biota samples from Storvannet where C_{13} was observed as greatest contributor. The C_{10} homologues dominated in both fish, but with a much higher contribution in char ($71\% \pm 20\%$) than in trout ($40\% \pm 16\%$). The opposite was observed with C_{13} homologue, which had higher contribution in trout ($6.6\% \pm 5.7\%$) than in char ($0.3\% \pm 0.5\%$). No clear explanation could be found for this occurrence and therefore more research is needed to understand the CP homologue behavior.

In conclusion, we have shown the presence of emerging and legacy pollutants in two lakes in the Norwegian sub-Arctic. Our results confirm higher mass fractions in a lake close to an urbanized area (Storvannet). This suggests that Storvannet may receive not only long-range transport input but in addition has local sources of pollution. This is not unexpected, since these chemicals have been widely used as flame retardants in industrial applications and household products such as in electrical and electronic equipment. The fact that these pollutants were also detected (albeit in low mass fractions) in the pristine Takvannet lake, suggests that this lake receives contaminants via atmospheric transport. Increase in mass fractions with increasing $\delta^{15}\text{N}$ was only observed for PCBs and Dec 602 in Takvannet. The lack of trophic magnification in Storvannet resembles the previously observed and modelled concentrations of cyclic volatile methyl siloxanes (cVMS) in this lake. This could be explained by the characteristics of both the physical environment and food web structure. Storvannet has a rapid water turnover, causing a non-equilibrium situation between water and sediments, resulting in the highest mass fractions being present in benthic invertebrates. Mass fractions of CPs and DPBs were observed in sediments, benthic organisms and sticklebacks but were detected in only few samples in trout and char. Higher mass fractions of MCCPs over SCCPs agrees with current emission profiles for CPs, where MCCP use, and emissions have increased in recent years due to regulatory scrutiny and regulation on SCCPs. These results contribute to our understanding of mass fractions of legacy and emerging contaminants in lake ecosystems and provide evidence of both long-range and locally sourced contamination in the subarctic.

Data availability statement

The raw data supporting the conclusion of this article will be made available by the authors, without undue reservation.

Ethics statement

Ethical approval was not required as the study was based on dead fish obtained from UiT in Takvannet and with a fishing permit in Storvannet. Fish were sampled in lakes that are open to public fishing.

Author contributions

AA: Conceptualization, Data curation, Formal Analysis, Investigation, Methodology, Software, Validation, Visualization, Writing—original draft, Writing—review and editing. IA: Data curation, Formal Analysis, Investigation, Methodology, Software, Writing—original draft, Writing—review and editing. NW: Data curation, Investigation, Methodology, Software, Writing—review and editing. DH: Data curation, Investigation, Methodology, Writing—review and editing. MH: Data curation, Investigation, Methodology, Writing—review and editing. P-AA: Resources, Writing—review and editing. AE: Writing—review and editing, Conceptualization, Funding acquisition, Project administration. CM: Writing—review and editing, Investigation. IK: Conceptualization, Funding acquisition, Investigation, Methodology, Supervision, Visualization, Writing—review and editing.

Funding

The author(s) declare that financial support was received for the research, authorship, and/or publication of this article. This study was funded by the Research Council of Norway (RCN) (#244298, #267574, and #287114) and the FRAM Centre Flagship for Hazardous Substances—effects on ecosystems and human health (#132018).

Acknowledgments

We thank Guttorm Christensen for field assistance and logistics support and Merete Miøen for advice and assistance in the laboratory.

Conflict of interest

The authors declare that the research was conducted in the absence of any commercial or financial relationships that could be construed as a potential conflict of interest.

Publisher's note

All claims expressed in this article are solely those of the authors and do not necessarily represent those of their affiliated organizations, or those of the publisher, the editors and the reviewers. Any product that may be evaluated in this article, or claim that may be made by its manufacturer, is not guaranteed or endorsed by the publisher.

Supplementary material

The Supplementary Material for this article can be found online at: <https://www.frontiersin.org/articles/10.3389/ftox.2024.1298231/full#supplementary-material>

References

- Al Saify, I., Cioni, L., Van Mourik, L. M., Brandsma, S. H., and Warner, N. A. (2021). Optimization of a low flow sampler for improved assessment of gas and particle bound exposure to chlorinated paraffins. *Chemosphere* 275, 130066. doi:10.1016/j.chemosphere.2021.130066
- AMAP (2016). in *AMAP assessment 2016: chemicals of emerging arctic concern*. AMAP), A. M. A. A. P. Oslo, Norway.
- AMAP (2017). "Chemical of emerging arctic concern. Summary for policy-makers," in *Arctic monitoring and assessment programme (AMAP)*. Oslo, Norway.
- Amundsen, P. A., Knudsen, R., and Klemetsen, A. (2007). Intraspecific competition and density dependence of food consumption and growth in Arctic charr. *J. Anim. Ecol.* 76, 149–158. doi:10.1111/j.1365-2656.2006.01179.x
- Amundsen, P. A., Lafferty, K. D., Knudsen, R., Primicerio, R., Klemetsen, A., and Kuris, A. M. (2009). Food web topology and parasites in the pelagic zone of a subarctic lake. *J. Anim. Ecol.* 78, 563–572. doi:10.1111/j.1365-2656.2008.01518.x
- Amundsen, P.-A., Primicerio, R., Smalås, A., Henriksen, E. H., Knudsen, R., Kristoffersen, R., et al. (2019). Long-term ecological studies in northern lakes—challenges, experiences, and accomplishments. *Limnol. Oceanogr.* 64, S11–S21. doi:10.1002/lno.10951
- Barón, E., Manez, M., Andreu, A. C., Sergio, F., Hiraldo, F., Eljarrat, E., et al. (2014a). Bioaccumulation and biomagnification of emerging and classical flame retardants in bird eggs of 14 species from Donana Natural Space and surrounding areas (South-western Spain). *Environ. Int.* 68, 118–126. doi:10.1016/j.envint.2014.03.013
- Barón, E., Santín, G., Eljarrat, E., and Barceló, D. (2014b). Occurrence of classic and emerging halogenated flame retardants in sediment and sludge from Ebro and Llobregat river basins (Spain). *J. Hazard Mater.* 265, 288–295. doi:10.1016/j.jhazmat.2013.10.069
- Basconcillo, L. S., Backus, S. M., McGoldrick, D. J., Zaruk, D., Sverko, E., and Muir, D. C. (2015). Current status of short- and medium chain polychlorinated n-alkanes in top predatory fish across Canada. *Chemosphere* 127, 93–100. doi:10.1016/j.chemosphere.2015.01.016
- Bogdal, C., Alsberg, T., Diefenbacher, P. S., Macleod, M., and Berger, U. (2015). Fast quantification of chlorinated paraffins in environmental samples by direct injection high-resolution mass spectrometry with pattern deconvolution. *Anal. Chem.* 87, 2852–2860. doi:10.1021/acs.504444d
- Bohlén-Nizzetto, P., and Aas, W. (2014). *Monitoring of environmental contaminants in air and precipitation, annual report 2013*. Oslo, Norway: Norwegian Institute for Air Research (NILU. I.S., K).
- Bouwman, H., Polder, A., Venter, B., and Skaare, J. U. (2008). Organochlorine contaminants in cormorant, darter, egret, and ibis eggs from South Africa. *Chemosphere* 71, 227–241. doi:10.1016/j.chemosphere.2007.09.057
- Brandsma, S. H., Brits, M., Groenewoud, Q. R., Van Velzen, M. J. M., Leonards, P. E. G., and De Boer, J. (2019). Chlorinated paraffins in car tires recycled to rubber granulates and playground tiles. *Environ. Sci. Technol.* 53, 7595–7603. doi:10.1021/acs.est.9b01835
- Burkhard, L. P., Cook, P. M., and Lukasewycz, M. T. (2004). Biota–sediment accumulation factors for polychlorinated biphenyls, dibenzo-p-dioxins, and dibenzofurans in southern Lake Michigan lake trout (*Salvelinus namaycush*). *Environ. Sci. Technol.* 38, 5297–5305. doi:10.1021/es035215y
- Cabrerizo, A., Muir, D. C. G., Köck, G., Iqaluk, D., and Wang, X. (2018). Climatic influence on temporal trends of polychlorinated biphenyls and organochlorine pesticides in landlocked char from lakes in the Canadian high arctic. *Environ. Sci. Technol.* 52, 10380–10390. doi:10.1021/acs.est.8b01860
- Chen, C., Chen, A., Li, L., Peng, W., Weber, R., and Liu, J. (2021). Distribution and emission estimation of short- and medium-chain chlorinated paraffins in Chinese products through detection-based mass balancing. *Environ. Sci. Technol.* 55, 7335–7343. doi:10.1021/acs.est.0c07058
- Christensen, G. N. (2009). *Storvatn, Hammerfest, Undersøkelse av miljøgifter i utløpsvannet*. Tromsø, Norway: Akvaplan-niva.
- Christensen, G. N., Evensen, A., Dahl-Hansen, G., and GoTsch, A. (2009). *Storvatn i Hammerfest kommune. Undersøkelse av miljøgifter i vann, sediment og fisk, 2008*. Tromsø, Norway: Akvaplan-niva AS.
- De La Torre, A., Alonso, M. B., Martinez, M. A., Sanz, P., Shen, L., Reiner, E. J., et al. (2012). Dechlorane-related compounds in franciscana dolphin (*Pontoporia blainvillei*) from southeastern and southern coast of Brazil. *Environ. Sci. Technol.* 46, 12364–12372. doi:10.1021/es302934p
- Dick, T. A., Gallagher, C. P., and Tomy, G. T. (2010). Short- and medium-chain chlorinated paraffins in fish, water and soils from the iqualuit, nunavut (Canada), area. *World Rev. Sci. Technol. Sustain. Dev.* 7, 387–401. doi:10.1504/wrstd.2010.032747
- ECHA (2008). in *Data on manufacture, import, export, uses and releases of alkanes, C10-13, chloro, SCCPs as well as information on potential alternatives to its use*. AGENCY, E. C.
- Elkin, L., Kay, M., Higgins, J., and Wobbrock, J. (2021). *An aligned rank Transform procedure for multifactor contrast test*.
- Eloranta, A. P., Kahilainen, K. K., Amundsen, P.-A., Knudsen, R., Harrod, C., and Jones, R. I. (2015). Lake size and fish diversity determine resource use and trophic position of a top predator in high-latitude lakes. *Ecol. Evol.* 5, 1664–1675. doi:10.1002/ecs3.1464
- Eloranta, P., Knudsen, R., and Amundsen, P. A. (2013). Niche segregation of coexisting Arctic charr (*Salvelinus alpinus*) and brown trout (*Salmo trutta*) constrains food web coupling in subarctic lakes. *Freshw. Biol.* 58, 207–221. doi:10.1111/fwb.12052
- Evenset, A., Götsch, A., and Dahl-Hansen, G. (2006). *Miljøundersøkelser i Hammerfest havn og Storvatn*. Tromsø, Norway: Akvaplan-niva.
- Feo, M. L., Baron, E., Eljarrat, E., and Barcelo, D. (2012). Dechlorane Plus and related compounds in aquatic and terrestrial biota: a review. *Anal. Bioanal. Chem.* 404, 2625–2637. doi:10.1007/s00216-012-6161-x
- Fiedler, H., Kallenborn, R., Boer, J. D., and Sydes, L. K. (2019). The Stockholm Convention: a tool for the global regulation of persistent organic pollutants. *Chem. Int.* 41, 4–11. doi:10.1515/ci-2019-0202
- Gabrielsen, G. W., Evensen, A., Frantzen, S., Gwynn, J., Hallanger, I. G., Kallenborn, R., et al. (2011). *MOSJ statusrapport 2011 Miljøgifter*. Tromsø, Norway: Norsk Polarinstitutt.
- Gao, H., Na, G., Yao, Y., Li, R., Gao, Y., Zhang, Z., et al. (2018). Distribution characteristics and source of dechloranes in soil and lichen of the fildes peninsula (Antarctica). *Int. J. Environ. Res. Public Health* 15, 2312. doi:10.3390/ijerph15102312
- Giskeødegård, G. F., and Lydersen, S. (2022). Measurements below the detection limit. *Tidsskr Nor Laegeforen*. Sep 19;142(13). English, Norwegian. doi:10.4045/tidsskr.22.0439
- Glüge, J., Bogdal, C., Scheringer, M., Buser, A., and Hungerbühler, K. (2013). Calculation of physicochemical properties for short- and medium-chain chlorinated paraffins. *J. Phys. Chem. Reference Data* 42. doi:10.1063/1.4802693
- Glüge, J., Schinkel, L., Hungerbühler, K., Cariou, R., and Bogdal, C. (2018). Environmental risks of medium chain chlorinated paraffins (MCCPs): a review. *Environ. Sci. Technol.* 52, 6743–6760. doi:10.1021/acs.est.7b06459
- Glüge, J., Wang, Z., Bogdal, C., Scheringer, M., and Hungerbühler, K. (2016). Global production, use, and emission volumes of short-chain chlorinated paraffins - a minimum scenario. *Sci. Total Environ.* 573, 1132–1146. doi:10.1016/j.scitotenv.2016.08.105
- Guldford, S. J., Muir, D. C., Houde, M., Evans, M. S., Kidd, K. A., Whittle, D. M., et al. (2008). PCB concentrations in lake trout (*Salvelinus namaycush*) are correlated to habitat use and lake characteristics. *Environ. Sci. Technol.* 42, 8239–8244. doi:10.1021/es801218m
- Guo, J., Venier, M., Salamova, A., and Hites, R. A. (2017). Bioaccumulation of Dechloranes, organophosphate esters, and other flame retardants in Great Lakes fish. *Sci. Total Environ.* 583, 1–9. doi:10.1016/j.scitotenv.2016.11.063
- Hageman, K., Bogdal, C., and Scheringer, M. (2015). "Long-range and regional atmospheric transport of POPs and implications for global cycling," in *Persistent organic pollutants (POPs): analytical techniques, environmental fate and biological effects*. Editor E. ZENG (Amsterdam, Netherlands: Elsevier).
- Hansen, K. M., Fauser, P., Vorkamp, K., and Christensen, J. H. (2020). Global emissions of dechlorane plus. *Sci. Total Environ.* 742, 140677. doi:10.1016/j.scitotenv.2020.140677
- Herzke, D., Nygård, T., Berger, U., Huber, S., and Rø, N. (2009). Perfluorinated and other persistent halogenated organic compounds in European shag (*Phalacrocorax aristotelis*) and common eider (*Somateria mollissima*) from Norway: a suburban to remote pollutant gradient. *Sci. Total Environ.* 408, 340–348. doi:10.1016/j.scitotenv.2009.08.048
- Hoh, E., Zhu, and Hites, R. A. (2006). Dechlorane plus, a chlorinated flame retardant, in the Great lakes. *Environ. Sci. Technol.* 40, 1184–1189. doi:10.1021/es051911h
- Huang, Y., Chen, L., Jiang, G., He, Q., Ren, L., Gao, B., et al. (2019). Bioaccumulation and biomagnification of short-chain chlorinated paraffins in marine organisms from the Pearl River Estuary, South China. *Sci. Total Environ.* 671, 262–269. doi:10.1016/j.scitotenv.2019.03.346
- Huston, C., and Juarez-Colunga, E. (2009). *Guidelines for computing summary statistics for datasets containing non-detects*, 178. British Columbia, Canada: Bulkley Valley Research Center.
- Hüttig, J., and Oehme, M. (2006). Congener group patterns of chloroparaffins in marine sediments obtained by chloride attachment chemical ionization and electron capture negative ionization. *Chemosphere* 64, 1573–1581. doi:10.1016/j.chemosphere.2005.11.042
- Iozza, S., Müller, C. E., Schmid, P., Bogdal, C., and Oehme, M. (2008). Historical profiles of chlorinated paraffins and polychlorinated biphenyls in a dated sediment core from Lake Thun (Switzerland). *Environ. Sci. Technol.* 42, 1045–1050. doi:10.1021/es702383t
- Ismail, N., Gewurtz, S. B., Pleskach, K., Whittle, D. M., Helm, P. A., Marvin, C. H., et al. (2009). Brominated and chlorinated flame retardants in Lake Ontario, Canada, lake trout (*Salvelinus namaycush*) between 1979 and 2004 and possible

influences of food-web changes. *Environ. Toxicol. Chem.* 28, 910–920. doi:10.1897/08-162.1

Jartun, M., Økelsrud, T. R., Kine, B., Enge, E. K., Halse, A. K., Götsch, A., et al. (2020). Monitoring of environmental contaminants in freshwater ecosystems 2019 – occurrence and biomagnification. *Miljødirektoratet M-1805|2020* ISSN 1894-7948.

Jiang, L., Gao, W., Ma, X., Wang, Y., Wang, C., Li, Y., et al. (2021). Long-term investigation of the temporal trends and gas/particle partitioning of short- and medium-chain chlorinated paraffins in ambient air of king george Island, Antarctica. *Environ. Sci. Technol.* 55, 230–239. doi:10.1021/acs.est.0c05964

Kallenborn, R., Hung, H., and Brorstrom-Lunden, E. (2015). “Atmospheric long range transport of persistent organic pollutants (POPs) into polar regions,” in *Persistent organic pollutants (POPs): analytical techniques, environmental fate and biological effect*. Editor E. ZENG (Amsterdam, Netherlands: Elsevier).

Karlsson, J., Berggren, M., Ask, J., Byström, P., Jonsson, A., Laudon, H., et al. (2012). Terrestrial organic matter support of lake food webs: evidence from lake metabolism and stable hydrogen isotopes of consumers. *Limnol. Oceanogr.* 57, 1042–1048. doi:10.4319/lo.2012.57.4.1042

Katsoyiannis, A. (2013). *Perfluorinated alkylated substances, brominated flame retardants and chlorinated paraffins in the Norwegian Environment - screening 2013*. Oslo, Norway: Norwegian Environment Agency.

Klemetsen, A., Amundsen, P.-A., Dempson, J. B., Jonsson, B., Jonsson, N., O’connell, M. F., et al. (2003). Atlantic salmon *Salmo salar* L., brown trout *Salmo trutta* L. and Arctic charr *Salvelinus alpinus* (L.): a review of aspects of their life histories. *Ecol. Freshw. Fish* 12, 1–59. doi:10.1034/j.1600-0633.2003.00010.x

Klemetsen, A., Amundsen, P. A., Muladal, H., Rubach, S., and Solbakken, J. I. (1989). Habitat shifts in a dense, resident arctic charr *Salvelinus Alpinus* population. *Physiol. Ecol. Jpn.* 1, 187–200.

Krätschmer, K., and Schächtele, A. (2019). Interlaboratory studies on chlorinated paraffins: evaluation of different methods for food matrices. *Chemosphere* 234, 252–259. doi:10.1016/j.chemosphere.2019.06.022

Krogseth, I. S., Undeman, E., Evenset, A., Christensen, G. N., Whelan, M. J., Breivik, K., et al. (2017a). Elucidating the behavior of cyclic volatile methylsiloxanes in a subarctic freshwater food web: a modeled and measured approach. *Environ. Sci. Technol.* 51, 12489–12497. doi:10.1021/acs.est.7b03083

Krogseth, I. S., Whelan, M. J., Christensen, G. N., Breivik, K., Evenset, A., and Warner, N. A. (2017b). Understanding of cyclic volatile methyl siloxane fate in a high latitude lake is constrained by uncertainty in organic carbon–water partitioning. *Environ. Sci. Technol.* 51, 401–409. doi:10.1021/acs.est.6b04828

Kurt-Karakus, P. B., Muir, D. C. G., De Jourdan, B., Teixeira, C., Epp Martindale, J., Embers, H., et al. (2019). Bioaccumulation of selected halogenated organic flame retardants in Lake Ontario. *Environ. Toxicol. Chem.* 38, 1198–1210. doi:10.1002/etc.4413

Li, F., Shi, R., Wang, Y., He, A., Han, Z., Zheng, X., et al. (2021). The effect of anthropogenic activities on the environmental fate of chlorinated paraffins in surface soil in an urbanized zone of northern China. *Environ. Pollut.* 288, 117766. doi:10.1016/j.envpol.2021.117766

Markowitz, G. (2018). From industrial toxins to worldwide pollutants: a brief history of polychlorinated biphenyls. *Public Health Rep.* 133, 721–725. doi:10.1177/0033549118801578

Mc Govern, M., Evenset, A., Borgå, K., De Wit, H. A., Braaten, H. F. V., Hessen, D. O., et al. (2019). Implications of coastal darkening for contaminant transport, bioavailability, and trophic transfer in northern coastal waters. *Environ. Sci. Technol.* 53, 7180–7182. doi:10.1021/acs.est.9b03093

Miljødirektoratet 2016. Grenseverdier for klassifisering av vann, sediment og biota – revidert 30.10.2020.

Möller, A., Xie, Z., Cai, M., Sturm, R., and Ebinghaus, R. (2012). Brominated flame retardants and dechlorane plus in the marine atmosphere from Southeast Asia toward Antarctica. *Environ. Sci. Technol.* 46, 3141–3148. doi:10.1021/es300138q

Möller, A., Xie, Z., Sturm, R., and Ebinghaus, R. (2010). Large-scale distribution of dechlorane plus in air and seawater from the Arctic to Antarctica. *Environ. Sci. Technol.* 44, 8977–8982. doi:10.1021/es103047n

Muir, D., Bennie, D., Teixeira, C., Fisk, A., Tomy, T., Stern, G., et al. (2000). *Short chain chlorinated paraffins: are they persistent and bioaccumulative?*

Na, G., Yao, Y., Gao, H., Li, R., Ge, L., Titley, I. A., et al. (2017). Trophic magnification of dechlorane plus in the marine food webs of fildes peninsula in Antarctica. *Mar. Pollut. Bull.* 117, 456–461. doi:10.1016/j.marpolbul.2017.01.049

Newton, S., Sellstrom, U., and De Wit, C. A. (2015). Emerging flame retardants, PBDEs, and HBCDDs in indoor and outdoor media in Stockholm, Sweden. *Environ. Sci. Technol.* 49, 2912–2920. doi:10.1021/es505946e

Norwegian Water Resources and Energy Directorate (Nve) (2020). *Innsjødatabase*. Available at: <https://www.nve.no/kart/kartdata/vassdragsdata/innsjodatabase/>.

Ontiveros-Cuadras, J. F., Ruiz-Fernández, A. C., Sanchez-Cabeza, J. A., Sericano, J., Pérez-Bernal, L. H., Páez-Osuna, F., et al. (2019). Recent history of persistent organic

pollutants (PAHs, PCBs, PBDEs) in sediments from a large tropical lake. *J. Hazard Mater* 368, 264–273. doi:10.1016/j.jhazmat.2018.11.010

Pellizzato, F., Ricci, M., Held, A., Emons, H., Böhmer, W., Geiss, S., et al. (2009). Laboratory intercomparison study on the analysis of short-chain chlorinated paraffins in an extract of industrial soil. *TrAC Trends Anal. Chem.* 28, 1029–1035. doi:10.1016/j.trac.2009.05.002

Peng, H., Wan, Y., Zhang, K., Sun, J., and Hu, J. (2014). Trophic transfer of dechloranes in the marine food web of liaodong bay, North China. *Environ. Sci. Technol.* 48, 5458–5466. doi:10.1021/es500229y

Poste, A. E., Hoel, C. S., Andersen, T., Arts, M. T., Færøvig, P.-J., and Borgå, K. (2019). Terrestrial organic matter increases zooplankton methylmercury accumulation in a brown-water boreal lake. *Sci. Total Environ.* 674, 9–18. doi:10.1016/j.scitotenv.2019.03.446

Prati, S., Henriksen, E. H., Knudsen, R., and Amundsen, P.-A. (2020). Seasonal dietary shifts enhance parasite transmission to lake salmonids during ice cover. *Ecol. Evol.* 10, 4031–4043. doi:10.1002/ece3.6173

Prati, S., Henriksen, E. H., Smalås, A., Knudsen, R., Klemetsen, A., Sánchez-Hernández, J., et al. (2021). The effect of inter- and intraspecific competition on individual and population niche widths: a four-decade study on two interacting salmonids. *Oikos* 130, 1679–1691. doi:10.1111/oik.08375

Qiu, X., Marvin, C. H., and Hites, R. A. (2007). Dechlorane plus and other flame retardants in a sediment core from Lake Ontario. *Environ. Sci. Technol.* 41, 6014–6019. doi:10.1021/es070810b

Reth, M., Ciric, A., Christensen, G. N., Heimstad, E. S., and Oehme, M. (2006). Short- and medium-chain chlorinated paraffins in biota from the European Arctic -- differences in homologue group patterns. *Sci. Total Environ.* 367, 252–260. doi:10.1016/j.scitotenv.2005.12.014

Rikardsen, A. H., Amundsen, P.-A., Bjørn, P. A., and Johansen, M. (2000). Comparison of growth, diet and food consumption of sea-run and lake-dwelling Arctic charr. *J. Fish Biol.* 57, 1172–1188. doi:10.1006/jfbi.2000.1380

Rikardsen, A. H., and Elliott, J. M. (2000). Variations in juvenile growth, energy allocation and life-history strategies of two populations of Arctic charr in North Norway. *J. Fish Biol.* 56, 328–346. doi:10.1111/j.1095-8649.2000.tb02110.x

Rikardsen, A. H., Svenning, M.-A., and Klemetsen, A. (1997). The relationships between anadromy, sex ratio and parr growth of Arctic charr in a lake in North Norway. *J. Fish Biol.* 51, 447–461. doi:10.1111/j.1095-8649.1997.tb01503.x

Russell, L. (2020). *Emmeans: estimated marginal means, aka least-squares means*.

Ruus, A., Bæk, K., Petersen, K., Allan, I., Beylich, B., Schlabach, M., et al. (2019). *Environmental contaminants in an urban fjord, 2017*. Oslo, Norway: The Norwegian Environment Agency: The Norwegian Environment Agency.

Schlabach, M., Van Bavel, B., Lomba, J. A., Borgen, A., Fjeld, E., Halse, A. K., et al. (2017). *Screening programme 2016 - selected compounds with relevance for EU regulation*. Oslo, Norway: Norwegian Environment Agency.

Shen, L., Reiner, E. J., Helm, P. A., Marvin, C. H., Hill, B., Zhang, X., et al. (2011a). Historic trends of dechloranes 602, 603, 604, dechlorane plus and other norbornene derivatives and their bioaccumulation potential in Lake Ontario. *Environ. Sci. Technol.* 45, 3333–3340. doi:10.1021/es104328r

Shen, L., Reiner, E. J., Macpherson, K. A., Kolic, T. M., Helm, P. A., Richman, L. A., et al. (2011b). Dechloranes 602, 603, 604, dechlorane plus, and chlordene plus, a newly detected analogue, in tributary sediments of the Laurentian Great lakes. *Environ. Sci. Technol.* 45, 693–699. doi:10.1021/es1027844

Shen, L., Reiner, E. J., Macpherson, K. A., Kolic, T. M., Sverko, E., Helm, P. A., et al. (2010). Identification and screening analysis of halogenated norbornene flame retardants in the Laurentian Great lakes: dechloranes 602, 603, and 604. *Environ. Sci. Technol.* 44, 760–766. doi:10.1021/es902482b

Simond, A. E., Houde, M., Lesage, V., and Verreault, J. (2017). Temporal trends of PBDEs and emerging flame retardants in belugas from the St. Lawrence Estuary (Canada) and comparisons with minke whales and Canadian Arctic belugas. *Environ. Res.* 156, 494–504. doi:10.1016/j.envres.2017.03.058

Skogeng, L. P., Lunder Halvorsen, H., Breivik, K., Eckhardt, S., Herzke, D., Moeckel, C., et al. (2023). Spatial distribution of Dechlorane Plus and dechlorane related compounds in European background air. *Front. Environ. Sci.* 10. doi:10.3389/fenvs.2022.1083011

Sørensen, P., and Larsen, A. K. (2019). *Screening survey of hazardous substances in articles*. Oslo, Norway: Norwegian Environment Agency.

Sun, R., Luo, X., Tang, B., Chen, L., Liu, Y., and Mai, B. (2017). Bioaccumulation of short chain chlorinated paraffins in a typical freshwater food web contaminated by e-waste in south China: bioaccumulation factors, tissue distribution, and trophic transfer. *Environ. Pollut.* 222, 165–174. doi:10.1016/j.envpol.2016.12.060

Sverko, E., Tomy, G. T., Marvin, C. H., Zaruk, D., Reiner, E., Helm, P. A., et al. (2008). Dechlorane plus levels in sediment of the lower Great lakes. *Environ. Sci. Technol.* 42, 361–366. doi:10.1021/es0710104

Sverko, E., Tomy, G. T., Reiner, E. J., Li, Y.-F., Mccarry, B. E., Arnot, J. A., et al. (2011). Dechlorane plus and related compounds in the environment: a review. *Environ. Sci. Technol.* 45, 5088–5098. doi:10.1021/es2003028

- Tomy, G. T., Muir, D. C. G., Stern, G. A., and Westmore, J. B. (2000). Levels of C10–C13 polychloro-n-alkanes in marine mammals from the arctic and the st. Lawrence river estuary. *Environ. Sci. Technol.* 34, 1615–1619. doi:10.1021/es990976f
- Tomy, G. T., Pleskach, K., Ismail, N., Whittle, D. M., Helm, P. A., Sverko, E., et al. (2007). Isomers of dechlorane plus in Lake Winnipeg and Lake Ontario food webs. *Environ. Sci. Technol.* 41, 2249–2254. doi:10.1021/es062781v
- Tomy, G. T., Stern, G. A., Lockhart, W. L., and Muir, D. (1999). Occurrence of C10–C13 polychlorinated n-alkanes in Canadian midlatitude and Arctic lake sediments. *Environ. Sci. Technol.* 33, 2858–2863. doi:10.1021/es990107q
- Tomy, G. T., Thomas, C. R., Zidane, T. M., Murison, K. E., Pleskach, K., Hare, J., et al. (2008). Examination of isomer specific bioaccumulation parameters and potential *in vivo* hepatic metabolites of syn- and anti-dechlorane plus isomers in juvenile rainbow trout (*Oncorhynchus mykiss*). *Environ. Sci. Technol.* 42, 5562–5567. doi:10.1021/es800220y
- UNEP (2017). *Report of the conference of the parties of the Stockholm convention on persistent organic pollutants on the work of its eighth meeting*. Geneva, Switzerland: United Nations.
- UNEP (2021). Proposal to list chlorinated paraffins with carbon chain lengths in the range C14–17 and chlorination levels at or exceeding 45 per cent chlorine by weight in Annexes A, B and/or C to the Stockholm Convention on Persistent Organic Pollutants. *Persistent Org. Pollut. Rev. Comm.*
- Van Mourik, L. M., Gaus, C., Leonards, P. E. G., and De Boer, J. (2016). Chlorinated paraffins in the environment: a review on their production, fate, levels and trends between 2010 and 2015. *Chemosphere* 155, 415–428. doi:10.1016/j.chemosphere.2016.04.037
- Van Mourik, L. M., Lava, R., O'Brien, J., Leonards, P. E. G., De Boer, J., and Ricci, M. (2020). The underlying challenges that arise when analysing short-chain chlorinated paraffins in environmental matrices. *J. Chromatogr. A* 1610, 460550. doi:10.1016/j.chroma.2019.460550
- Vorkamp, K., Balmer, J., Hung, H., Letcher, R. J., and Rigét, F. F. (2019a). A review of chlorinated paraffin contamination in Arctic ecosystems. *Emerg. Contam.* 5, 219–231. doi:10.1016/j.emcon.2019.06.001
- Vorkamp, K., Bossi, R., Rigét, F. F., Skov, H., Sonne, C., and Dietz, R. (2015). Novel brominated flame retardants and dechlorane plus in Greenland air and biota. *Environ. Pollut.* 196, 284–291. doi:10.1016/j.envpol.2014.10.007
- Vorkamp, K., Rigét, F., Sanderson, H., Bossi, R., Hansen, K. M., and Skov, H. (2019b). *POP/PBT characterisation of dechlorane plus and novel brominated flame retardants based on data from Greenland*. Scientific Report from DCE – Danish Centre for Environment and Energy No. 339. Denmark; Aarhus: Aarhus University, DCE – Danish Centre for Environment and Energy ©: Aarhus University, Department of Environmental Science.
- Vorkamp, K., and Rigét, F. F. (2014). A review of new and current-use contaminants in the Arctic environment: evidence of long-range transport and indications of bioaccumulation. *Chemosphere* 111, 379–395. doi:10.1016/j.chemosphere.2014.04.019
- Wang, D., Guo, M.-X., Pei, W., Byer, J. D., and Wang, Z. (2015). Trophic magnification of chlorinated flame retardants and their dechlorinated analogs in a fresh water food web. *Chemosphere* 118, 293–300. doi:10.1016/j.chemosphere.2014.09.057
- Wang, P., Zhang, Q., Zhang, H., Wang, T., Sun, H., Zheng, S., et al. (2016). Sources and environmental behaviors of Dechlorane Plus and related compounds - a review. *Environ. Int.* 88, 206–220. doi:10.1016/j.envint.2015.12.026
- Wang, Q., and Kelly, B. (2017). Occurrence and distribution of halogenated flame retardants in an urban watershed: comparison to polychlorinated biphenyls and organochlorine pesticides. *Environ. Pollut. (Barking, Essex 1987)* 231, 252–261. doi:10.1016/j.envpol.2017.07.092
- Wobbrock, J. O., Findlater, L., Gergle, D., and Higgins, J. J. (2011). “The aligned rank transform for nonparametric factorial analyses using only anova. procedures,” in *Proceedings of the SIGCHI Conference on Human Factors in Computing Systems*, Vancouver, BC, Canada (Association for Computing Machinery).
- Wong, F., De Wit, C. A., and Newton, S. R. (2018). Concentrations and variability of organophosphate esters, halogenated flame retardants, and polybrominated diphenyl ethers in indoor and outdoor air in Stockholm, Sweden. *Environ. Pollut.* 240, 514–522. doi:10.1016/j.envpol.2018.04.086
- Wu, J., Cao, D., Gao, W., Lv, K., Liang, Y., Fu, J., et al. (2019). The atmospheric transport and pattern of Medium chain chlorinated paraffins at Shergyla Mountain on the Tibetan Plateau of China. *Environ. Pollut.* 245, 46–52. doi:10.1016/j.envpol.2018.10.112
- Wu, J.-P., Zhang, Y., Luo, X.-J., Wang, J., Chen, S.-J., Guan, Y.-T., et al. (2010). Isomer-specific bioaccumulation and trophic transfer of dechlorane plus in the freshwater food web from a highly contaminated site, south China. *Environ. Sci. Technol.* 44, 606–611. doi:10.1021/es902744b
- Xian, Q., Siddique, S., Li, T., Feng, Y.-L., Takser, L., and Zhu, J. (2011). Sources and environmental behavior of dechlorane plus — a review. *Environ. Int.* 37, 1273–1284. doi:10.1016/j.envint.2011.04.016
- Xiao, H., Shen, L., Su, Y., Barresi, E., Dejong, M., Hung, H., et al. (2012). Atmospheric concentrations of halogenated flame retardants at two remote locations: the Canadian High Arctic and the Tibetan Plateau. *Environ. Pollut.* 161, 154–161. doi:10.1016/j.envpol.2011.09.041
- Zhang, H., and Kelly, B. C. (2018). Sorption and bioaccumulation behavior of multi-class hydrophobic organic contaminants in a tropical marine food web. *Chemosphere* 199, 44–53. doi:10.1016/j.chemosphere.2018.01.173



OPEN ACCESS

EDITED BY

Abdul Qadeer,
Chinese Research Academy of Environmental
Sciences, China

REVIEWED BY

Qinghui Huang,
Tongji University, China
Shiyang Zhang,
Wuhan University of Technology, China

*CORRESPONDENCE

Zexia Gao,
✉ 3817258494@qq.com
Chao Song,
✉ songc@ffrc.cn

[†]These authors have contributed equally to
this work

RECEIVED 16 May 2024

ACCEPTED 19 August 2024

PUBLISHED 29 August 2024

CITATION

Chen X, Li Z, Xu H, Qiu L, Fan L, Meng S, Gao Z
and Song C (2024) Regulation of salinity to
inhibit 2-methylisoborneol and geosmin:
Insights from spatial-scale research in coastal
areas of China.
Front. Environ. Sci. 12:1433586.
doi: 10.3389/fenvs.2024.1433586

COPYRIGHT

© 2024 Chen, Li, Xu, Qiu, Fan, Meng, Gao and
Song. This is an open-access article distributed
under the terms of the [Creative Commons
Attribution License \(CC BY\)](#). The use,
distribution or reproduction in other forums is
permitted, provided the original author(s) and
the copyright owner(s) are credited and that the
original publication in this journal is cited, in
accordance with accepted academic practice.
No use, distribution or reproduction is
permitted which does not comply with these
terms.

Regulation of salinity to inhibit 2-methylisoborneol and geosmin: Insights from spatial-scale research in coastal areas of China

Xi Chen^{1,2,3†}, Zhonghua Li^{2†}, Huimin Xu^{3,4}, Liping Qiu^{3,4},
Limin Fan^{2,3,4,5,6}, Shunlong Meng^{2,3,4,5,6}, Zexia Gao^{1*} and
Chao Song^{2,3,4,5,6*}

¹College of Fisheries, Huazhong Agricultural University, Wuhan, China, ²Wuxi Fisheries College, Nanjing Agricultural University, Wuxi, China, ³Freshwater Fisheries Research Center, Chinese Academy of Fishery Sciences, Wuxi, China, ⁴Laboratory of Quality and Safety Risk Assessment for Aquatic Products on Environmental Factors (Wuxi), Ministry of Agriculture and Rural Affairs, Wuxi, China, ⁵Key Laboratory of Control of Quality and Safety for Aquatic Products, Ministry of Agriculture and Rural Affairs, Beijing, China, ⁶Key Laboratory of Freshwater Fisheries and Germplasm Resources Utilization, Ministry of Agriculture and Rural Affairs, Freshwater Fisheries Research Center, Chinese Academy of Fishery Sciences, Wuxi, China

Drinking water quality and the commercial value of aquatic items are both significantly impacted by odor molecules like 2-methylisoborneol (2-MIB) and geosmin (GSM). Many investigations have been conducted to identify the microorganisms involved in the synthesis of 2-MIB and GSM. However, few studies have attempted to identify potential degradation factors in the natural environment. Here, pathway analysis of the relationship between water quality parameters and the distribution of odor compounds in water bodies led to a more significant connection ($p < 0.05$) between total nitrogen, total phosphorus, chemical oxygen demand, and salinity in water bodies for the distribution of their odor compounds. Salinity among them exhibited the strongest connection and had a direct impact. The establishment of a larger spatial scale statistical research method, mainly using the water environment with different salinities formed in different geographical areas, and the distribution of odor compounds in this water body as a research vehicle helped to find the most concise relationship between the two variables. The results show that the concentration of odor compounds is lower in waters with higher salinity, which proves the negative correlation between the two. The results of this study provide a theoretical basis for solving the problem of odorous pollutants in water bodies, with the aim of improving the utilization of water resources more effectively and, secondly, leading to a new guiding direction for the conservation and exploitation of impact plains and mudflats.

KEYWORDS

2-methylisoborneol, geosmin, water quality parameters, pathway analysis, coastal mudflat, natural inhibitor

1 Introduction

A healthy, odor-free water environment is what people expect, but with rapid socio-economic development, increased human activity, and the discharge of pollutants, the problem of water pollution often arises (Ajibade et al., 2021). The presence of odorous substances in water bodies is still a major concern. The production of odorous substances in water bodies is often accompanied by eutrophication of the water body and is generally produced by the metabolism of algae and bacteria, mainly 2-methylisoborneol (2-MIB) and geosmin (GSM). As they are trace amounts of volatile organic pollutants, they have a very low olfactory threshold concentration of 10 ng/L and can be detected by human olfaction (Young et al., 1996), posing a threat to water quality and public health (Zhang et al., 2009; Fu et al., 2021). Odor substances in water not only have an impact on the health of drinking water, but also on the survival, development, and reproduction of aquatic organisms, for example, 2-MIB has an impact on the development of embryos and offspring of fish such as *Danio rerio* (Zhou et al., 2021).

Currently, many studies have focused on the identification of microorganisms involved in the generation of odor compounds, as well as on the techniques for the removal of odor compounds already present in water, and it is more generally accepted that algae and bacteria in the water column are the direct and main cause of odor compound production (Son et al., 2015). Secondly, some studies have also conducted correlation analysis on water quality factors on the distribution of odor compounds in water bodies, but the effects of these water quality factors on the distribution of odor compounds in different study water bodies are uncertain, which show both positive and negative effects (Shu-Chu et al., 2008; Tung et al., 2008; Ding et al., 2014; Zhen et al., 2014; Hu et al., 2017), which arises from the complexity and uncertainty in the production and volatilization of odor compounds in water bodies. There are also a significant number of findings showing a negative correlation between salinity and the concentration of odor compounds in this water body (Tosi and Sola, 1993; Nam-Koong et al., 2016), which is an interesting phenomenon, but the mechanistic principles involved are not clear. The production of odor compounds in water bodies mainly originates from algae and bacteria, and the concentration distribution in the aqueous environment is subject to a combination of pathways including production and disappearance. The production is mainly through the metabolic production of algae and bacteria, while the disappearance is mainly through dissipation and volatilization, etc. Current research has shown that water quality factors have a certain correlation between algae and bacteria (Naughton et al., 2020), which will undoubtedly indirectly affect the distribution of odor compounds in the water column. However, it is not reported whether water quality factors have a facilitative or mitigating effect on the storage of odor compounds in water bodies, i.e., whether there is a direct relationship between them is unclear.

China is a vast country with huge differences in climate, topography, population density, and economic development levels, and its watershed environment may show different states in different regions. For example, in the coastal areas of southeast China, the waters are densely distributed; however, in northwest China, there are mostly arid and semi-arid areas. Water resources

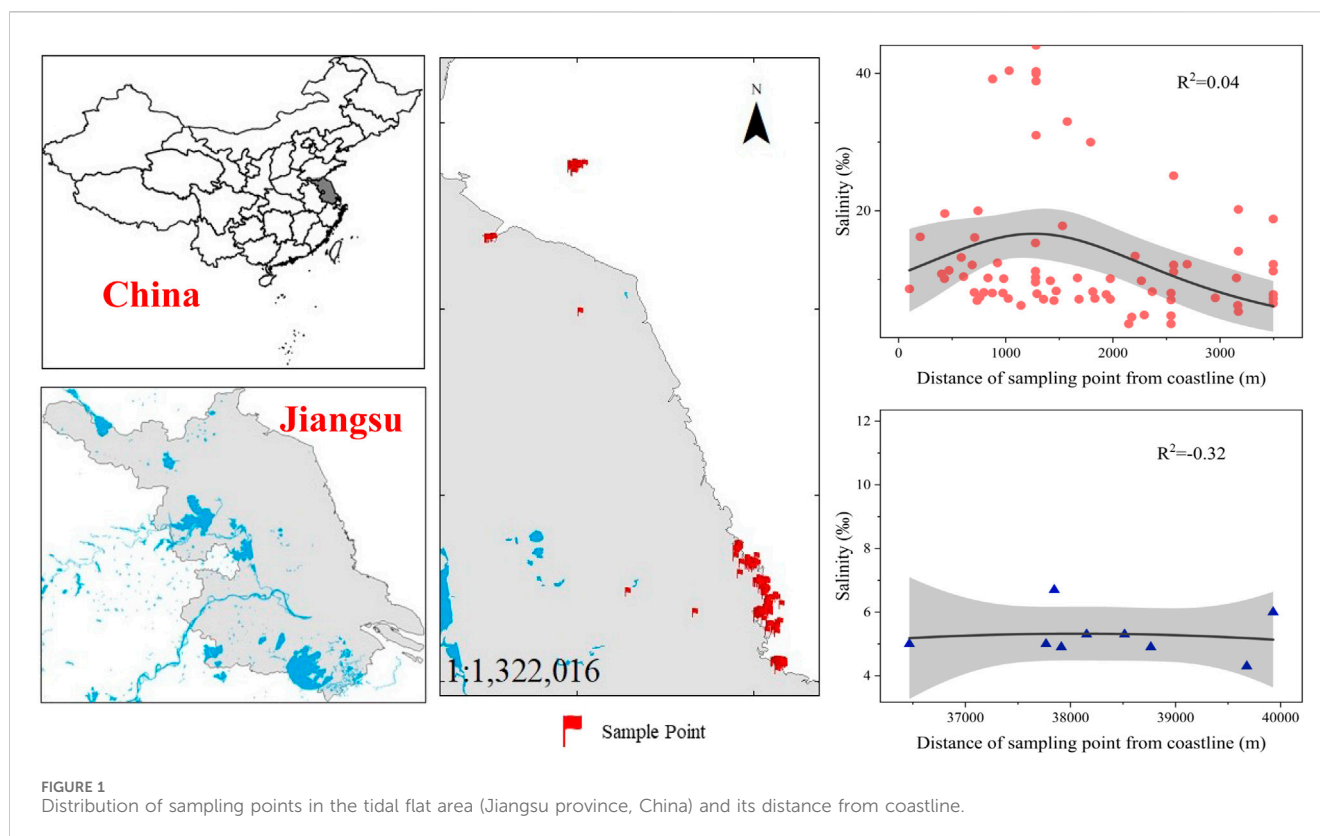
are also more abundant in southern China than in northern China. Different water environments and geographical differences also cause differences in water quality factors, which also include salinity. The variation of salinity distribution is an important factor that influences and restricts the distribution and variation of other hydrological factors (Bai et al., 2012). For example, the salinity at the mouth of the Yangtze River Delta and Pearl River Delta is significantly higher than that of other waters and shows a pattern of higher salinity the closer to the coastline (Chen et al., 2008; Xie et al., 2021). Precipitation is also an important factor affecting the salinity of regional waters. Northern China is dominated by a temperate continental climate and temperate monsoon climate, with low precipitation throughout the year, while southern regions have abundant precipitation (Zhou and Yu, 2005). This geographical difference in water quality may affect the distribution of odor-producing algae and bacteria in water, but it is unknown whether odor compounds in their water bodies are directly affected and the mechanism of the effect.

Coastal mudflats, located in the transition zone between terrestrial and marine ecosystems, are one of the important environmental resources, while the abundant vegetation on tidal flats accumulates a large amount of organic carbon, which is important for global climate change, sea level rise, and fall, and material cycling (e.g., water, sand and nutrient transport, carbon, nitrogen, and phosphorus cycling and fate, etc.). Especially with a series of high-intensity developments such as rapid urbanization in China's coastal areas, there will also be some impacts on their water environment (Selkoe et al., 2008). The coastal mudflat area of Jiangsu is one of the few typical pristine coasts in China and the world, which has largely maintained its natural ecological structure and function (Chi et al., 2011; Xu et al., 2011; Wang et al., 2020). In addition, as the largest silty tidal flats in China, the tidal flats are well developed and have obvious zonation due to the large tidal difference and strong tidal action along its coast (Zone et al., 2005). We investigated the correlation between water quality factors and the presence and distribution of odor compounds in the mudflats of Jiangsu coastal mudflats, and combined the results of the survey data to further investigate the possible effects of mudflat formation processes and geospatial differences on the odor compounds in the water bodies. In this paper, the innovative research objective is to identify the potential degradation factors of odor compounds in the natural environment, which provides a research basis for solving the problem of odor pollutants in water bodies, to improve the utilization of water resources more effectively, and secondly, to lead a new guiding direction for the conservation and development of impact plains and mudflats.

2 Materials and methods

2.1 Sampling deployment and water sample collection

A strategy was developed to select sampling points in the tidal flat area of Jiangsu province, China, based on distance from the coastline (represented in Figure 1). 252 samples were collected from 84 sites, with water samples collected from three uniform points at each site. The samples were extracted from a depth of 0.5 m, mixed



into one sample for analysis, and stored in amber glass bottles and refrigerated to 4°C. Most samples were tested within 72 h.

2.2 Determination of 2-MIB and GSM concentrations

The headspace solid phase microextraction (HSPME) method with gas chromatography-mass spectrometry (GC-MS) was used for the detection of odorants in the water samples.

We used HSPME to extract 2-MIB and GSM from water samples by sorption. We measured 10.0 mL of water sample (natural water should be filtered by 0.45 μ m membrane) in a 20 mL headspace vial, added 10 μ L of internal standard spiking solution (IBMP, mass concentration of 10 μ g/L), i.e., the mass concentration of IBMP in water was 10 ng/L, then added 2 g of NaCl, immediately capped the vial and gently shaken well, and put it in a 70 °C water bath after the NaCl was completely dissolved. The extracted fibers were heated and pressed down to the top space for sorptive extraction. After the extraction for 30 min, the extracted fiber was removed, the sorbent needle was dried, and the extracted fiber was inserted into the gas chromatography injection port and desorbed at the injection port temperature of 250 °C for 5 min and chromatographed by mass spectrometry.

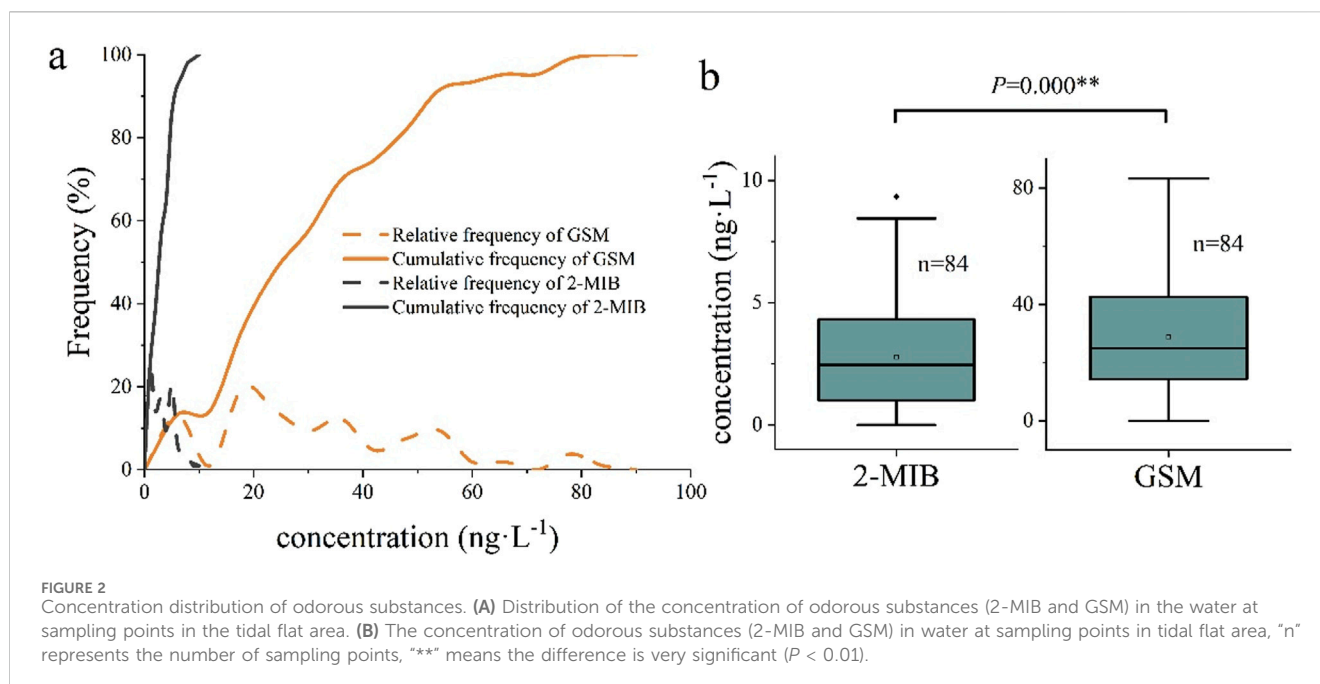
Gas chromatography-mass spectrometry (GC-MS) was used for the detection of 2-MIB and GSM concentrations in water samples. A DB-5 column (30 m \times 0.25 mm \times 0.25 μ m) was selected as the separation part of the chromatography, and the starting temperature of the column chamber was set to 50 °C and held for 1 minute, ramped up to 120 °C at a rate of 10 °C per minute and held for 1 min,

and ramped up to 220 °C at a rate of 20 °C per minute and held for 1 min. In the specific chromatographic conditions, we set the injection mode as non-split, the inlet temperature as 250 °C, the inlet pressure as 7.66 psi, the total flow rate as 44 mL/min, and the carrier gas as helium high-purity (purity >99.999%) with a flow rate of 1.0 mL/min to achieve better chromatographic results. In the mass spectrometry, an electron ionization source (EI) was selected as the ion source with ionization energy of 70 eV, ion source temperature of 230 °C; MS quadrupole temperature of 150 °C; transmission line temperature of 250 °C; solvent delay of 5 min; and scan mode of ion detection (SIM) ([Supplementary Table S1](#)).

The detection limit of both odorants was 0.5 ng/L, with recoveries ranging from 91.2% to 112.5% for 2-MIB and 88.4%–109.7% for GSM, based on a signal-to-noise ratio of 10.

2.3 Seven basic water quality factors and salinity determination methods

The study measured water quality indicators such as salinity (SA), pH, dissolved oxygen (DO), temperature (T), chemical oxygen demand (COD), total nitrogen (TN), total phosphorus (TP), and total suspended solids (TSS). These were measured using handheld refractometers, pH meter, dissolved oxygen meter, and national standards of the People's Republic of China. The results for TN, TP, COD, ammonia nitrogen, and suspended matter were determined using neutral reagent photometric and gravimetric methods, while the national standards for potassium persulfate oxidation and ammonium molybdate spectrophotometry were also used (GB11894-89).



2.4 Path analysis

Path analysis is a technical approach to distinguish between causal models and is used to establish hypothetical pathways that explain the relative importance of environmental water quality factors on changes in odor compound concentrations (Luo et al., 2020; Shao et al., 2022). Before modeling, a K-S (Kolmogorov-Smirnov) test was performed on odor compound concentrations and water quality factors to determine whether the data conformed to a normal distribution. This study included six main water quality impact factors, namely, salinity, pH, dissolved oxygen, temperature, chemical oxygen demand, total nitrogen, total phosphorus, and suspended solids. These factors interact with each other and determine the changes in the concentration of odor compounds to varying degrees through direct or indirect effects. For example, TN and TP play an important role in the production of odor compounds by influencing the distribution of odor-producing algae and bacteria in the water column, especially during the hot summer season. In this study, it was first assumed that all environmental factors have a direct effect on the levels of 2-MIB and GSM in the water column, which can be explained by the standardized path coefficient (β). β represents the relative contribution of each environmental factor, and the positive and negative values of the coefficients represent positive and negative effects, respectively, and the higher the absolute value of the coefficient, the more important it is for the distribution of odor compounds. Secondly, it is assumed that water quality factors also exist to indirectly influence the content of odor compounds in water. Based on the above assumptions, a path analysis model was established, and the model was debugged through regression analysis by gradually adding or removing paths. During the debugging process, the significance of each path test parameter needed to be determined, and when $p < 0.05$, the model was accepted and the optimal results of the model were determined, and the relative importance of different water quality factors on controlling

the changes in the distribution of 2-MIB and GSM and the complex interactions between these factors were obtained.

3 Results and discussion

3.1 Distribution and influencing factors of odorous substances in water in coastal tidal flats area

Currently, 2-MIB and GSM are the two most dominant odor-producing compounds in water (Ma et al., 2018; Rongfang et al., 2018; Yuan et al., 2018). In this study, we collected water samples and examined 2-MIB and GSM in water bodies from coastal mudflat areas in Jiangsu province. The results are shown in Figure 2. The concentrations of 2-MIB and GSM in 84 water samples from this region were 2.60 ± 2.30 ng/L and 27.83 ± 20.07 ng/L, respectively, with GSM concentrations significantly higher than 2-MIB concentrations ($p < 0.001$). The formation of this difference in distribution may be related to the type and amount of algae and bacteria in the water column, and the proof of the main producers of these two odor compounds has been given successively by researchers, with 2-MIB mainly originating from actinomycetes and cyanobacteria in the substrate, and GSM mainly originating from *Streptomyces*, which is also one of its producers (Sugiura et al., 1998; Sugiura and Nakano, 2000). And, likely, the producers of odor compounds in the water bodies of the region are mainly bacteria.

3.2 Analysis of concentration relationship between main water quality factors and 2-MIB and GSM

Water bodies are a complex environment, but the conventional test indicators in water have been able to reflect the quality of a water

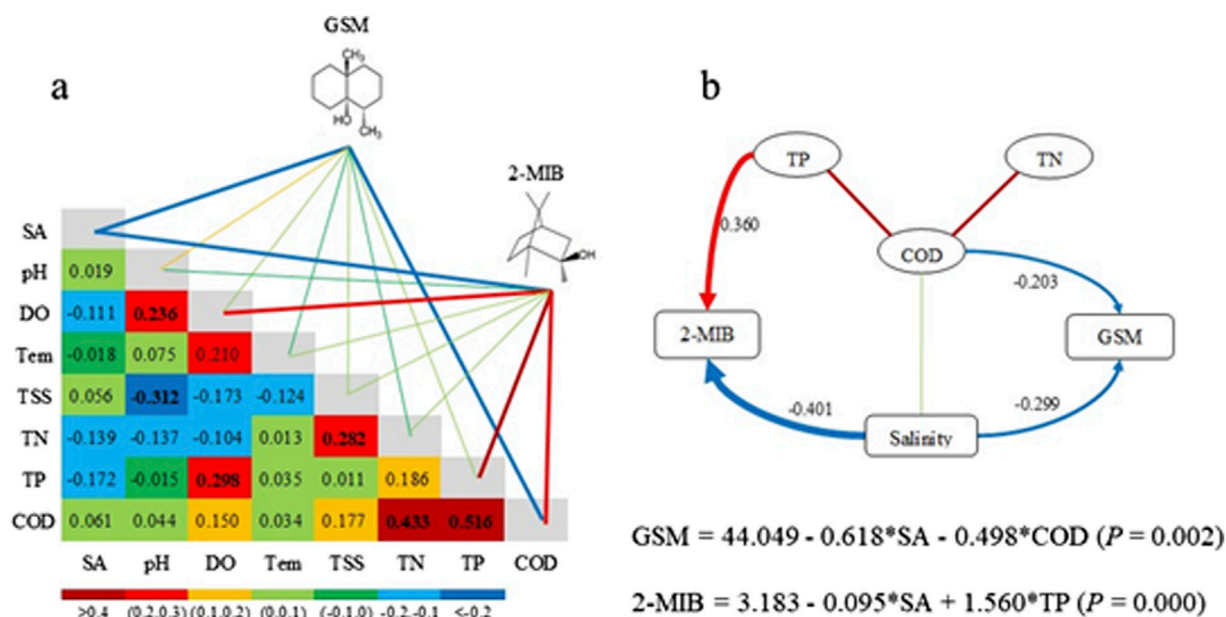


FIGURE 3 Relationship between environmental factors of water quality and two kinds of odor substances. (A) The relationship between the two odor substances (2-MIB and GSM) in the water samples in the beach area and the basic water quality factors. The larger correlation coefficient is shown as the darker color, and the red and blue respectively represent the positive and negative effects. (B) Size analysis describes two odor material and the main environmental factors, the relationship between the larger path coefficient is shown as broad arrow, positive and negative influences in red and blue, respectively. The formulas are multiple linear equations.

body relatively well, such as total nitrogen (TN), total phosphorus (TP), dissolved oxygen (DO), pH, temperature (T), chemical oxygen demand (COD), total suspended solids (TSS), and salinity (SA), and there are also interactions between the various water quality factors in a water body (Muhid et al., 2013; Vandergucht et al., 2013). In this study (Figure 3), there is a strong positive correlation between TN, TP, and COD with correlation coefficients of 0.433 and 0.516, respectively, since COD is a comprehensive indicator of water quality in response to water bodies. Few studies have focused on the effects of water quality factors on the concentration and distribution of odor compounds and their mechanistic mechanisms. Since it is not possible to identify the direct or indirect influence of water quality factors on the distribution of odor compounds, the choice of using statistical methods of through-way analysis is a reasonable approach (Park et al., 2021). We quantified the degree of influence of multiple influencing factors on the distribution of odor compounds in water bodies using path analysis, which decomposes the correlation coefficients of each independent variable with the dependent variable into the direct effect of the respective variable on the dependent variable and the indirect effect on that dependent variable through other independent variables, and therefore, the via analysis was used to examine the complex relationship between water quality factors and odor compounds (Fei-Yun et al., 2014). Herein, the screening results by path analysis showed (Supplementary Table S2; Supplementary Table S3) that 2-MIB concentrations were positively correlated with TP concentrations, while GSM concentrations were more influenced

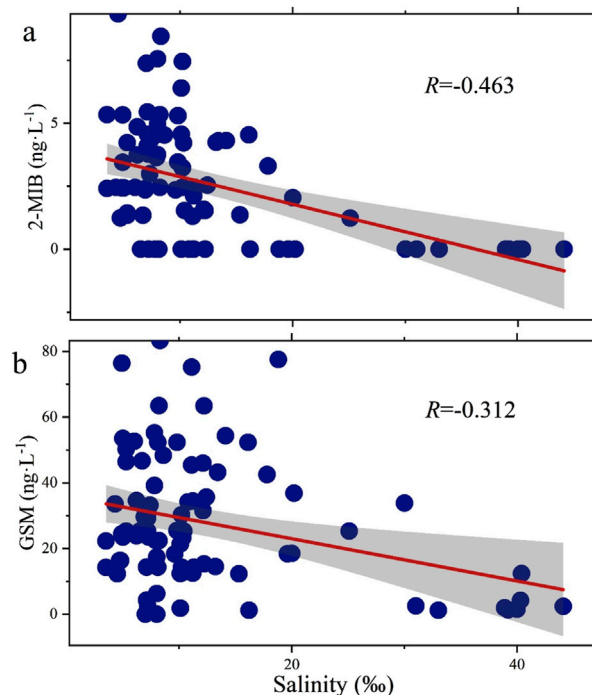


FIGURE 4 Relationship between 2-MIB (A) and GSM (B) and salinity in water samples, "R" is the Pearson correlation coefficient between them.

by COD, which in turn was correlated with TN and TP concentrations. Therefore, among the basic water quality indicators, TN, TP, and COD are strongly associated with the concentrations of two odor compounds, and these three water quality indicators also interact with each other (Figures 3B). TP also acts as a limiting factor for water eutrophication in many cases (Parinet et al., 2004), and the nitrogen and phosphorus content in the water column also directly determines the value-added of phytoplankton. The nitrogen and phosphorus content in the water column also directly determines the rate of phytoplankton appreciation, which in turn affects the eutrophication process in the water column (Muhid et al., 2013; Sims et al., 2013; Vandergucht et al., 2013). In conclusion, TN, TP, and COD in water bodies can reveal the distribution of odor compounds in water bodies to some extent, but it is not certain that other water quality factors do not affect odor compounds due to the complexity of water quality changes, such as elevated temperature and dissolved oxygen, which can also affect other water quality factors.

Salinity also had a significant effect on the levels of odor compounds in the water column (Figures 3B; Figure 4), with correlation coefficients of -0.463 and -0.312 for 2-MIB and GSM concentrations, respectively, both showing relatively significant direct negative correlations and slightly greater than the path model coefficients between them (i.e., -0.401 and -0.299). The producers of 2-MIB and GSM in the water column, although slightly different, are mainly algae and bacteria (Wu and Duirk, 2013; Sauvé and Desrosiers, 2014). It has been shown that low salinity may promote the growth of algae, while high salinity shows some inhibition of algal growth, including many freshwater cyanobacteria, suggesting an indirect relationship between salinity and odorant substance concentration in the water column (Goncalves et al., 2006). However, this is not sufficient as a theoretical basis for a strong correlation between salinity and odor compounds, for example, the indirect correlation between factors such as TN and TP, which is more strongly correlated with algal bacteria, and odor compounds are abrupt. Since salinity is not all through indirect effects on algae and bacteria and thus inhibits the production of odor compounds in water, the direct significant difference between salinity and odor substances derived in the path model analysis ($p < 0.05$) may be that salinity directly destroys the persistence of odor compounds in water. Salinity mainly affects the ionic strength in the water column, while some related studies have shown that the higher the ionic strength in the water column, the more volatile the volatile substances in the water column, which likely include volatile odor compounds such as 2-MIB and GSM (Sauvé and Desrosiers, 2014; Baker et al., 2016; Watson et al., 2016). Moreover, the results of the separation analysis of odor compounds reveal that 2-MIB is more present in the dissolved fraction, while GSM is mainly present in the cells (Clerc et al., 2021), which explains well the greater effect of high salinity on the concentration of 2-MIB in water.

3.3 Tidal flat formation and regional salinity differences in relation to the distribution of odorants

Salinity differences in the water column not only indirectly affect the production of odor compounds, but also may be directly involved in the elimination or volatilization of odor compounds. It is difficult to verify the direct or indirect relationship through

simulation experiments since the carrying capacity of odor compounds such as 2-MIB and GSM in the water column cannot be controlled. A large spatial scale study can eliminate the effects caused by chance errors between the independent and dependent variables. In addition to the distribution of odor compounds in water quality due to human activities, do natural geographic differences also affect the distribution of odor compounds in water bodies, e.g., does the formation of mudflats lead to different salinities in different waters, and what is the extent of the effect on the distribution of the corresponding odor compounds? We try to investigate the formation of mudflats and the distribution patterns of odor compounds in water bodies in different regions and their causes, by establishing a statistical study method at a large spatial scale.

Salt and freshwater mixing is a common natural hydrological phenomenon in estuarine waters. Freshwater runoff from rivers and seawater with high salinity are mixed with each other under the action of tidal currents in estuarine waters, and saltwater intrusion is formed upstream along the estuary at high tide. The formation of mudflats is the result of shoreline migration, and due to the difference in formation time and shoreline extension (Figures 5B), the salinity of mudflats varies from location to location. In this study, by collecting water samples from the coastal mudflats in Jiangsu province (Figure 5), the distance between the sampling point and the shoreline was measured using the sampling point as input elements and the adjacent actual shoreline as adjacent elements (Figures 5C). The results of the study showed that the salinity in the water body exhibited a distribution pattern of lower salinity in the water body at different locations of the mudflats, the further away from the present shoreline (Figures 5D).

In addition, the establishment of a larger spatial scale statistical study method (Figure 6), which focuses on a water environment with different salinities formed in different geographical areas, and the distribution of odor compounds in that water body as a study vehicle, helps to find the most concise relationship between the two variables. Wu (2021) in his studies of Fengman Reservoir (FMR), Miyun Reservoir (MYR), Tianmu Lake (TMH), Tangpu Reservoir (TPR), Qiandao Lake (QDH), Tingxi Reservoir (TXR), and Xinfengjiang Reservoir (XFJ), which the results are shown in Figure 6A–G and Figures 6A. It was found that the distribution of odor compounds in these seven large reservoirs had obvious differences. In TMH and TPR near the outlet of the Yangtze River, the concentrations of odor compounds were high, basically exceeding the olfactory threshold concentration of 10 ng/L . However, the species differed, with 2-MIB dominating in TMH and GSM almost undetected, while in TPR it was GSM dominating and 2-MIB at a lower concentration. The overall performance can be tentatively analyzed that the concentration of odor compounds in water bodies is higher the closer to the coast, which is also tentatively consistent with our predicted results. Moreover, the concentration of odor compounds in water bodies in the southern region is higher than that in the northern region. Since the coastal areas of China span three climate zones, warm temperate, subtropical, and tropical, and are gradually arid from south to north, the salinity of soil and water bodies increases from small to large accordingly. The salt content of the surface layer of coastal soils in southern China generally does not exceed 2%, while the salt content of the surface layer of salt soils in northern and northeastern China reaches 2%–3%, and even up to 5%–8% individually (Xu et al., 2013; Yu et al.,

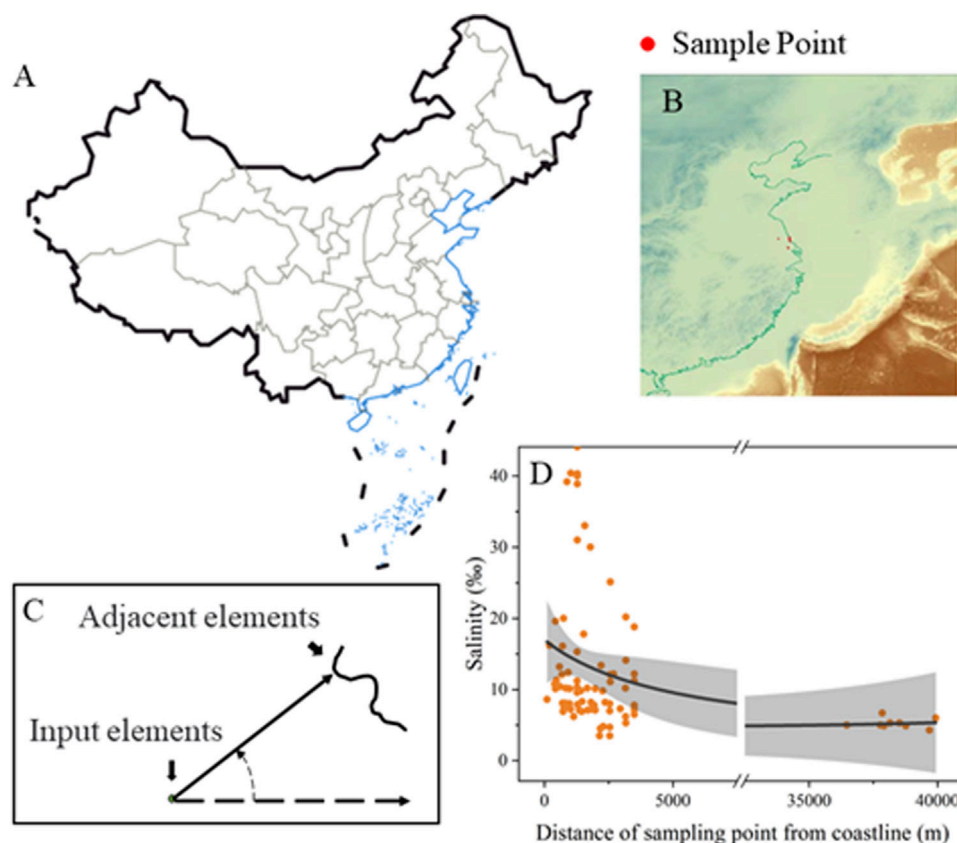


FIGURE 5

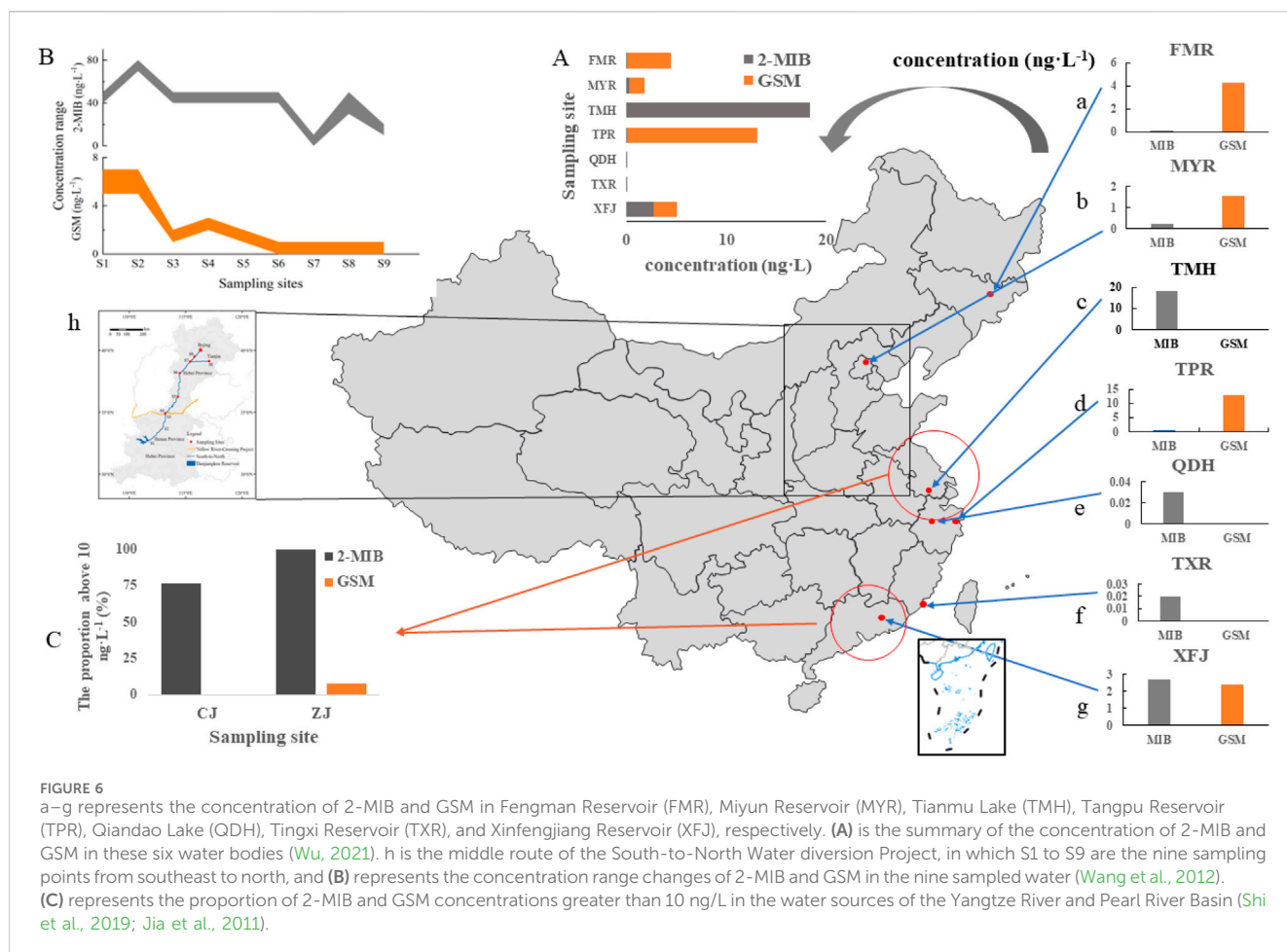
(A) is the map of China's coastline, (B) is the satellite map of China's coastline and the sampling site of water samples, (C) is the calculation model of the distance between the sampling site and the coastline, with the sampling site as input elements and the adjacent actual coastline as adjacent elements to measure the distance between the sampling site and the coastline. (D) represents the relationship between water salinity and distance from the coastline.

2014; Wang et al., 2018). This unique southern-northern difference is likely to be one of the dominant factors in the difference in the concentration of odor compounds in the southern and northern water bodies, and also mirrors our conclusion that salinity in water bodies is negatively correlated with the concentration of odor compounds.

We collected data from water bodies in the middle section of the South-North Water Transfer Line for statistical analysis (XIA et al., 2012). Since the water potential is flowing from south to north of the Yellow River (from S1 to S9 in Figures 6H), the odor compounds in its water bodies also show a trend of getting smaller from south to north during the water transportation (Figures 6B). In addition, the Yangtze River Delta and the Pearl River Delta regions, as the most economically developed regions in China, were studied by researchers on the spatial and temporal characteristics of salinity in the Yangtze River Delta inlet and the Pearl River Delta inlet, respectively, and it was found that the salinity in the water in the Yangtze River inlet (mostly higher than 31 during the flood season) was greater than that in the Pearl River inlet (9.95 during the flood season, with a concentration range of 0.03–31.72). Later, another researcher measured odor compounds in most water bodies (including reservoirs, lakes, etc.) in both regions (Figures 6C), and by comparison, it can be found that there are 14 water sources in the Yangtze River Delta where 2-MIB can be detected,

and 76.9% of them have 2-MIB concentrations greater than 10 ng/L. There are 7 water sources where GSM can be detected, and all of their (Shi et al., 2019); 22 water sources in the Pearl River Delta region were able to detect 2-MIB, with all of them having 2-MIB concentrations greater than 10 ng/L, and 7 water sources were able to detect GSM, with 7.69% of them having GSM concentrations greater than 10 ng/L (Jia et al., 2011). In this larger spatial statistical study, the results were as we expected, i.e., waters with high salinity had lower concentrations of odor compounds in the water, although the differences may not be statistically significant. In the next studies, further validation is needed, as well as a more in-depth investigation of the direct and indirect effects of geographical differences and salinity differences on the distribution of odor compounds in water bodies, and their mechanistic mechanisms.

Odor contamination of water bodies has been taken seriously and how to go about identifying, measuring, and removing odor compounds such as 2-MIB and GSM from water is necessary to satisfy the end consumer. The taste and odor of water are now a global phenomenon, especially in the drinking water and aquaculture industries, which may cause concerns about the safety of drinking and food safety of aquatic products (Kakimoto et al., 2014; Zamyadi et al., 2015; Mustapha et al., 2021). More importantly, studies have demonstrated that odor compounds in water, such as 2-MIB, can be developmentally toxic to fish (Zhou et al., 2021). The removal of odor



compounds in water, especially 2-MIB and GSM, is now a research focus, and different removal techniques using ultrafine powdered activated carbon (SPAC), coagulation, sedimentation, membrane filtration, flocculation, ozonation, powdered activated carbon (PAC), electrodialysis, sedimentation, co-precipitation, and multiphase photocatalysis have been applied to remove color, taste, or odor from water (Zamyadi et al., 2015; Fotiou et al., 2016; Guo et al., 2016; Garrido-Cardenas et al., 2019). However, all these methods have their inherent drawbacks. For example, the photochemical treatment with UV-assisted has a good removal effect for two pollutants, but it is not suitable for a large-scale replication due to the high cost (Huang et al., 2022). In recent years, with the increasing area of coastal mudflats, the management of mudflats has been paid more and more attention, as well as the high-speed development of coastal cities such as impact plains, the water quality requirements of this water body, have become more and more strict, and the rational use of its pollutant generation mechanism and potential degradation factors in the natural environment can be more efficient and targeted. Then, in addition to artificial removal, different waters can be managed in a targeted manner according to the geographical area, which can effectively solve the problem of odor pollution in water. For example, in coastal mudflat areas near the shore water sources and farming water, due to its salinity

and other environmental factors inhibiting the residual odor compounds in the water, more attention can be paid to the control and removal of other pollutants as appropriate. In the management of waters in the north and south of China, the differences in water use characteristics and water environment should be treated differently. In the process of water management, we can pay more attention to the ecological safety of reclaimed water. For the management of southern waters, it is more urgent to prevent cyanobacteria outbreaks and eutrophication of water bodies. Secondly, in the development and use of coastal cities and mudflats, we should not only prevent the salinization of fresh water but also pay more attention to the odor pollution of water bodies.

4 Conclusion

In this paper, we take 2-MIB and GSM as the representative of odor compounds in water, and then explain the relationship between the basic water quality factors in water bodies and the distribution of odor compounds in water as an expansion, extending an interesting phenomenon that salinity in water samples, compared to other water quality factors, shows a particularly negative correlation with the concentration of odor compounds in water, showing a clear direct relationship. This is somewhat different from many studies that have

concluded that water quality factors indirectly affect the distribution of odor compounds by influencing the producers of odor compounds in water, such as cyanobacteria and actinomycetes. Salinity in water may reduce the concentration of odor compounds by inhibiting their retention in water. This conclusion was confirmed by a statistical study on a large spatial scale to investigate the differences in the distribution of odor compounds in coastal areas of China and in northern and southern waters and to compare them with salinity. The salinity of water plays a key role in the variation of odor compounds concentration. In the process of future water management, the management of different geographical locations and different water environments should be targeted to enhance management efficiency, improve water quality, and solve the problem of odor pollution in water more efficiently and conveniently. It will point out a new guiding direction in the more effective development and utilization of impact plains and coastal mudflats.

Data availability statement

The original contributions presented in the study are included in the article/[Supplementary Material](#), further inquiries can be directed to the corresponding authors.

Author contributions

XC: Investigation, Methodology, Writing—original draft. ZL: Investigation, Methodology, Writing—original draft. HX: Validation, Writing—review and editing. LQ: Supervision, Writing—review and editing. LF: Supervision, Writing—review and editing. SM: Supervision, Writing—review and editing. ZG: Writing—review and editing. CS: Funding acquisition, Project administration, Writing—review and editing.

References

- Ajibade, F. O., Adelodun, B., Lasisi, K. H., Fadare, O. O., Ajibade, T. F., Nwogwu, N. A., et al. (2021). Environmental pollution and their socioeconomic impacts. *Microbe Mediat. Remediat. Environ. Contam.*, 321–354. doi:10.1016/b978-0-12-821199-1.00025-0
- Bai, J., Xiao, R., Zhang, K., and Gao, H. (2012). Arsenic and heavy metal pollution in wetland soils from tidal freshwater and salt marshes before and after the flow-sediment regulation regime in the Yellow River Delta, China. *J. Hydrology* 450, 244–253. doi:10.1016/j.jhydrol.2012.05.006
- Baker, P., Watson, S., Monson, B., and Giglio, S. (2016). Biochemistry and genetics of taste- and odor-producing cyanobacteria. *Harmful Algae* 54, 112–127. doi:10.1016/j.hal.2015.11.008
- Chen, C.-T. A., Wang, S.-L., Lu, X.-X., Zhang, S.-R., Lui, H.-K., Tseng, H.-C., et al. (2008). Hydrogeochemistry and greenhouse gases of the Pearl River, its estuary and beyond. *Quat. Int.* 186 (1), 79–90. doi:10.1016/j.quaint.2007.08.024
- Chi, Xu, Sheng, S., Wen, Z., Cui, L., and Liu, M. (2011). Characterizing wetland change at landscape scale in Jiangsu Province, China. *Environ. Monit. and Assess.* 179, 279–292. doi:10.1007/s10661-010-1735-6
- Clerc, N. A., Druschel, G. K., and Gray, M. (2021). Occurrences of 2-methylisoborneol and geosmin-degrading bacteria in a eutrophic reservoir and the role of cell-bound versus dissolved fractions. *J. Environ. Manag.* 297 (4), 113304. doi:10.1016/j.jenvman.2021.113304
- Ding, Z., Peng, S., Jin, Y., Xuan, Z., Chen, X., and Yin, L. (2014). Geographical and seasonal patterns of geosmin and 2-methylisoborneol in environmental water in Jiangsu province of China. *J. Anal. Methods Chem.* 2014, 1–6. doi:10.1155/2014/743924
- Fei-Yun, Z., Lan-Hai, L., Sajjad, A., and Xue-Mei, L. (2014). Using path analysis to identify the influence of climatic factors on spring peak flow dominated by snowmelt in an alpine watershed. *J. Mt. Sci.* 11 (04), 990–1000. doi:10.1007/s11629-013-2789-z
- Fotouhi, T., Triantis, T. M., Kaloudis, T., O'Shea, K. E., Dionysiou, D. D., and Hiskia, A. (2016). Assessment of the roles of reactive oxygen species in the UV and visible light photocatalytic degradation of cyanotoxins and water taste and odor compounds using C-TiO₂. *Water Res.* 90, 52–61. doi:10.1016/j.watres.2015.12.006
- Fu, S., Zhao, X., Zhou, Z., Li, M., and Zhu, L. (2021). Effective removal of odor substances using intimately coupled photocatalysis and biodegradation system prepared with the silane coupling agent (SCA)-enhanced TiO₂ coating method. *Water Res.* 188, 116569. doi:10.1016/j.watres.2020.116569
- Garrido-Cardenas, J. A., Esteban-Garcia, B., Agüera, A., Sánchez-Pérez, J. A., and Manzano-Agugliaro, F. (2019). Wastewater treatment by advanced oxidation process and their worldwide research trends. *Int. J. Environ. Res. Public Health* 17 (1), 170. doi:10.3390/ijerph17010170
- Goncalves, A., Figueiredo, D., and Pereira, M. J. (2006). The effects of different salinity concentrations on growth of three freshwater green algae. *Fresenius Environ. Bull.* 15 (11), 1382–1386.
- Guo, Q., Yang, K., Yu, J., Wang, C., Wen, X., Zhang, L., et al. (2016). Simultaneous removal of multiple odorants from source water suffering from septic and musty odors: verification in a full-scale water treatment plant with ozonation. *Water Res.* 100, 1–6. doi:10.1016/j.watres.2016.05.017
- Hu, Y., Yu, D., Guo, L., and Xie, P. (2017). Relationships of water taste and odor compounds and their related environmental factors in Lake Donghu, Wuhan. *J. Lake Sci.* 29 (1), 87–94. doi:10.18307/2017.0110
- Huang, X., Wang, S., Wang, G., Zhu, S., and Ye, Z. (2022). Kinetic and mechanistic investigation of geosmin and 2-methylisoborneol degradation using UV-assisted

Funding

The author(s) declare that financial support was received for the research, authorship, and/or publication of this article. This work was supported by the Center Public Interest Scientific Institution Basal Research Fund, the Freshwater Fisheries Research Center, CAFS (No. 2023JBFM03), China Agricultural Research System (CARS-46), Central Public-Interest Scientific Institution Basal Research Fund, CAFS (NO. 2023TD18), and Jiangsu Graduate Practice Innovation Project (SJCX23_0218).

Conflict of interest

The authors declare that the research was conducted in the absence of any commercial or financial relationships that could be construed as a potential conflict of interest.

Publisher's note

All claims expressed in this article are solely those of the authors and do not necessarily represent those of their affiliated organizations, or those of the publisher, the editors and the reviewers. Any product that may be evaluated in this article, or claim that may be made by its manufacturer, is not guaranteed or endorsed by the publisher.

Supplementary material

The Supplementary Material for this article can be found online at: <https://www.frontiersin.org/articles/10.3389/fenvs.2024.1433586/full#supplementary-material>

- photoelectrochemical. *Chemosphere* 290, 133325. doi:10.1016/j.chemosphere.2021.133325
- Jia, H., Xie, J., Wu, S., and He, G. (2011). Temporal and spatial variations of salinity in Pearl River Estuary in recent years. *Trans. Oceanol. Limnol.* 2, 142–146.
- Kakimoto, M., Ishikawa, T., Miyagi, A., Saito, K., Miyazaki, M., Asaeda, T., et al. (2014). Culture temperature affects gene expression and metabolic pathways in the 2-methylisoborneol-producing cyanobacterium *Pseudanabaena galeata*. *J. Plant Physiology* 171 (3–4), 292–300. doi:10.1016/j.jplph.2013.09.005
- Luo, H., Guan, Q., Lin, J., Wang, Q., Wang, N., Tan, Z., et al. (2020). Air pollution characteristics and human health risks in key cities of northwest China. *J. Environ. Manag.* 269, 110791. doi:10.1016/j.jenvman.2020.110791
- Ma, L., Wang, C., Li, H., Peng, F., and Yang, Z. (2018). Degradation of geosmin and 2-methylisoborneol in water with UV/chlorine: influencing factors, reactive species, and possible pathways. *Chemosphere* 211 (NOV), 1166–1175. doi:10.1016/j.chemosphere.2018.08.029
- Muhid, P., Davis, T. W., Bunn, S. E., and Burford, M. A. (2013). Effects of inorganic nutrients in recycled water on freshwater phytoplankton biomass and composition. *Water Res.* 47 (1), 384–394. doi:10.1016/j.watres.2012.10.015
- Mustapha, S., Tijani, J. O., Ndamitso, M. M., Abdulkareem, A. S., and Mohammed, A. K. (2021). A critical review on geosmin and 2-methylisoborneol in water: sources, effects, detection, and removal techniques. *Environ. Monit. Assess.* 193 (4), 204. doi:10.1007/s10661-021-08980-9
- Nam-Koong, H., Schroeder, J., Petrick, G., and Schulz, C. (2016). Removal of the off-flavor compounds geosmin and 2-methylisoborneol from recirculating aquaculture system water by ultrasonically induced cavitation. *Aquac. Eng.* 70, 73–80. doi:10.1016/j.aquaeng.2015.10.005
- Naughton, S., Kavanagh, S., Lynch, M., and Rowan, N. J. (2020). Synchronizing use of sophisticated wet-laboratory and in-field handheld technologies for real-time monitoring of key microalgae, bacteria and physicochemical parameters influencing efficacy of water quality in a freshwater aquaculture recirculation system: a case study from the Republic of Ireland. *Aquaculture* 526, 735377. doi:10.1016/j.aquaculture.2020.735377
- Parinet, B., Lhote, A., and Legube, B. (2004). Principal component analysis: an appropriate tool for water quality evaluation and management-application to a tropical lake system. *Ecol. Model.* 178, 295–311. doi:10.1016/j.ecolmodel.2004.03.007
- Park, E. S., Fitzpatrick, K., Das, S., and Avelar, R. (2021). Exploration of the relationship among roadway characteristics, operating speed, and crashes for city streets using path analysis. *Accid. Analysis Prev.* 150 (2), 105896. doi:10.1016/j.aap.2020.105896
- Rongfang, Y., Shaona, W., Dan, L., Shao, X., and Zhou, B. (2018). Effect of the wavelength on the pathways of 2-MIB and geosmin photocatalytic oxidation in the presence of Fe-N co-doped TiO₂. *Chem. Eng. J.* 353, 319–328. doi:10.1016/j.cej.2018.07.123
- Sauvé, S., and Desrosiers, M. (2014). A review of what is an emerging contaminant. *Chem. Central J.* 8 (1), 15–17. doi:10.1186/1752-153x-8-15
- Selkoe, K. A., Kappel, C. V., Halpern, B. S., Micheli, F., and Lenihan, H. S. (2008). Response to comment on 'A global map of human impact on marine ecosystems'. *Science* 321 (5895), 948–952.
- Shao, W. Y., Wang, Q. Z., Guan, Q. Y., Luo, H. P., Ma, Y. R., and Zhang, J. (2022). Distribution of soil available nutrients and their response to environmental factors based on path analysis model in arid and semi-arid area of northwest China. *Sci. Total Environ.* 827, 154254. doi:10.1016/j.scitotenv.2022.154254
- Shi, P., Zhu, G., Yang, W., Xu, H., Zhu, M., Zou, W., et al. (2019). Occurrence and influencing factors of odorous compounds in reservoirs used as drinking water resources in Jiangsu province. *Environmental Science (in Chinese)* 40, 4000–4008. doi:10.13227/j.hjkt.201812024
- Shu-Chu, T., Tsair, F., Feng, C., and Yang Chia, L. (2008). Seasonal change and correlation with environmental parameters for 2-MIB in Feng-Shen Reservoir, Taiwan. *Environ. Monit. and Assess.* 145, 407–416. doi:10.1007/s10661-007-0049-9
- Sims, A., Zhang, Y., Gajraj, S., Brown, P. B., and Hu, Z. (2013). Toward the development of microbial indicators for wetland assessment. *Water Res.* 47 (5), 1711–1725. doi:10.1016/j.watres.2013.01.023
- Son, M., Cho, D.-g., Lim, J. H., Park, J., Hong, S., Ko, H. J., et al. (2015). Real-time monitoring of geosmin and 2-methylisoborneol, representative odor compounds in water pollution using bioelectronic nose with human-like performance. *Biosens. Bioelectron.* 74, 199–206. doi:10.1016/j.bios.2015.06.053
- Sugiura, N., Iwami, N., Inamori, Y., Nishimura, O., and Sudo, R. (1998). Significance of attached cyanobacteria relevant to the occurrence of musty odor in Lake Kasumigaura. *Wat Res.* 32 (12), 3549–3554. doi:10.1016/s0043-1354(98)00153-5
- Sugiura, N., and Nakano, K. (2000). Causative microorganisms for musty odor occurrence in the eutrophic Lake Kasumigaura. *Hydrobiologia* 434 (1), 145–150. doi:10.1023/a:1004000511610
- Tosi, L., and Sola, C. (1993). Role of geosmin, a typical inland water odour, in guiding glass eel *Anguilla anguilla* (L.) migration. *Ethology* 95 (3), 177–185. doi:10.1111/j.1439-0310.1993.tb00468.x
- Tung, S.-C., Lin, T.-F., Yang, F.-C., and Liu, C.-L. (2008). Seasonal change and correlation with environmental parameters for 2-MIB in Feng-Shen Reservoir, Taiwan. *Environ. Monit. Assess.* 145 (1), 407–416. doi:10.1007/s10661-007-0049-9
- Vandergucht, D. M., Sereda, J. M., Davies, J. M., and Hudson, J. J. (2013). A comparison of phosphorus deficiency indicators with steady state phosphate in lakes. *Water Res.* 47 (5), 1816–1826. doi:10.1016/j.watres.2013.01.004
- Wang, C., Wang, G., Guo, Z., Dai, L., Cheng, H., Li, Y., et al. (2020). Effects of land-use change on the distribution of the wintering red-crowned crane (*Grus japonensis*) in the coastal area of northern Jiangsu Province, China. *Land Use Policy* 90, 104269. doi:10.1016/j.landusepol.2019.104269
- Wang, Y., Deng, C., Liu, Y., Niu, Z., and Li, Y. (2018). Identifying change in spatial accumulation of soil salinity in an inland river watershed, China. *Sci. Total Environ.* 621, 177–185. doi:10.1016/j.scitotenv.2017.11.222
- Wang, Y., Zhang, C., Bi, Y., Zhu, Y., Song, G., Wang, S., et al. (2022). Spatio-temporal pattern of odorous compounds and its influencing factors in the canal of the middle-route of south-to-north water diversion project. *Acta Hydrobiologica Sinica (in Chinese)* 46 (2), 149–159. doi:10.7541/2022.2020.206
- Watson, S. B., Monis, P., Baker, P., and Giglio, S. (2016). Biochemistry and genetics of taste- and odor-producing cyanobacteria. *Harmful Algae* 54, 112–127. doi:10.1016/j.hal.2015.11.008
- Wu, D., and Duirk, S. E. (2013). Quantitative analysis of earthy and musty odors in drinking water sources impacted by wastewater and algal derived contaminants. *Chemosphere* 91 (11), 1495–1501. doi:10.1016/j.chemosphere.2012.12.024
- Wu, T. (2021). The production mechanism and influencing factors of odor compounds in drinking water reservoirs. *University of Chinese Academy of Sciences*.
- Xia, J., Zeng, S., Zhang, L., and DU, H. (2012). Hydrological responses to climate change in the water receiving area of the middle route project for South-to-North Water Transfer. *Bull. Chin. Acad. Sci.* 26 (1), 17–31.
- Xie, W., Yang, J., Yao, R., and Wang, X. (2021). Spatial and temporal variability of soil salinity in the Yangtze River estuary using electromagnetic induction. *Remote Sens.* 13 (10), 1875. doi:10.3390/rs13101875
- Xu, C., Sheng, S., Zhou, W., Cui, L., and Liu, M. (2011). Characterizing wetland change at landscape scale in Jiangsu Province, China. *Environ. Monit. Assess.* 179 (1), 279–292. doi:10.1007/s10661-010-1735-6
- Xu, Y., Pu, L., Zhu, M., Li, J., Zhang, M., Li, P., et al. (2013). Spatial variation of soil salinity in the coastal reclamation area, eastern China. *J. Coast. Res.* 30 (2), 411–417. doi:10.2112/jcoastres-d-13-00078.1
- Young, W. F., Horth, H., Crane, R., Ogden, T., and Arnott, M. (1996). Taste and odour threshold concentrations of potential potable water contaminants. *Water Res.* 30 (2), 331–340. doi:10.1016/0043-1354(95)00173-5
- Yu, J., Li, Y., Han, G., Zhou, D., Fu, Y., Guan, B., et al. (2014). The spatial distribution characteristics of soil salinity in coastal zone of the Yellow River Delta. *Environ. Earth Sci.* 72, 589–599. doi:10.1007/s12665-013-2980-0
- Yuan, R., Wang, S., Liu, D., Shao, X., and Zhou, B. (2018). Effect of the wavelength on the pathways of 2-MIB and geosmin photocatalytic oxidation in the presence of Fe-N co-doped TiO₂. *Chem. Eng. J.* 353, 319–328. doi:10.1016/j.cej.2018.07.123
- Zamyadi, H., Stuetz, H., Hofmann, R., Ho, L., and Newcombe, G. (2015). Fate of geosmin and 2-methylisoborneol in full-scale water treatment plants. *WATER Res.* 83, 171–183. doi:10.1016/j.watres.2015.06.038
- Zhang, T., Lin, L., Song, L., and Chen, W. (2009). Effects of temperature and light on the growth and geosmin production of *Lyngbya kuetzingii* (Cyanophyta). *J. Appl. Phycol.* 21 (3), 279–285. doi:10.1007/s10811-008-9363-z
- Zhen, D., Shifu, P., Yuqin, J., Xuan, Z., Chen, X., and Yin, L. (2014). Geographical and seasonal patterns of geosmin and 2-methylisoborneol in environmental water in Jiangsu province of China. *J. Anal. Methods Chem.* 2014, 1–6. doi:10.1155/2014/743924
- Zhou, T. J., and Yu, R. C. (2005). Atmospheric water vapor transport associated with typical anomalous summer rainfall patterns in China. *J. Geophys. Res. Atmos.* 110 (D8). doi:10.1029/2004jd005413
- Zhou, W., Li, X., Wang, Y., Wang, J., Li, D., Wei, H., et al. (2021). Physiological and transcriptomic changes of zebrafish (*Danio rerio*) embryos-larvae in response to 2-MIB exposure. *J. Hazard. Mater.* 416, 126142. doi:10.1016/j.jhazmat.2021.126142
- Zone, L., Kremer, H., Tissier, M., Burbridge, P., Talaue-Mcmanus, L., Rabalais, N., et al. (2005). Land-ocean interactions in the coastal zone: science plan and implementation strategy. *Environ. Policy Collect.* 20 (11), 1262–1268.



OPEN ACCESS

EDITED BY

Abdul Qadeer,
Chinese Research Academy of Environmental
Sciences, China

REVIEWED BY

Meifang Li,
Central South University Forestry and
Technology, China
Qinhe Pan,
Hainan University, China
Shiyu Fu,
South China University of Technology, China

*CORRESPONDENCE

Ying Cao,
✉ yingcao@swust.edu.cn
Shanglian Hu,
✉ hushanglian@swust.edu.cn

RECEIVED 19 June 2024

ACCEPTED 19 August 2024

PUBLISHED 05 September 2024

CITATION

Yang F, Li H, Wang B, Fan W, Gu X, Cao Y and
Hu S (2024) Effect of cellulose-lignin ratio on
the adsorption of U(VI) by hydrothermal
charcoals prepared from
Dendrocalamus farinosus.
Front. Environ. Sci. 12:1451496.
doi: 10.3389/fenvs.2024.1451496

COPYRIGHT

© 2024 Yang, Li, Wang, Fan, Gu, Cao and Hu.
This is an open-access article distributed under
the terms of the [Creative Commons Attribution
License \(CC BY\)](#). The use, distribution or
reproduction in other forums is permitted,
provided the original author(s) and the
copyright owner(s) are credited and that the
original publication in this journal is cited, in
accordance with accepted academic practice.
No use, distribution or reproduction is
permitted which does not comply with these
terms.

Effect of cellulose-lignin ratio on the adsorption of U(VI) by hydrothermal charcoals prepared from *Dendrocalamus farinosus*

FanQin Yang, Hanhan Li, Boya Wang, Wei Fan, Xiaoyan Gu,
Ying Cao* and Shanglian Hu*

College of Life Sciences and Engineering, Southwest University of Science and Technology, Mianyang, China

Herein, the impact of varying proportions of cellulose/lignin in bamboo on the production of hydrothermal biochar was investigated. Different characterization techniques were applied to explore the structure of hydrothermal biochar derived from three different genotypes (215, 30-A, 52-B) of *Dendrocalamus farinosus*, and the adsorption behavior of uranium by these hydrothermal biochars was evaluated. It was found that a decrease in cellulose/lignin ratio (3.08, 2.68, and 2.58) positively influenced the specific surface area and pore volume of hydrothermal biochar. Consequently, the prepared hydrothermal biochars exhibited adsorption capacities for U(VI) ions at levels of 14.78 mg/g, 24.68 mg/g, and 26.02 mg/g respectively under these three ratios. The adsorption process by 52-B-220 well complied with the Freundlich isotherm, which indicated that the multi-layer adsorption occurred on the solid liquid interface, but single-layer adsorption was evident in those prepared from genotypes 30-A and 215. This study demonstrated that adjusting biomass feedstock composition as an effective strategy for enhance the quality of biochar.

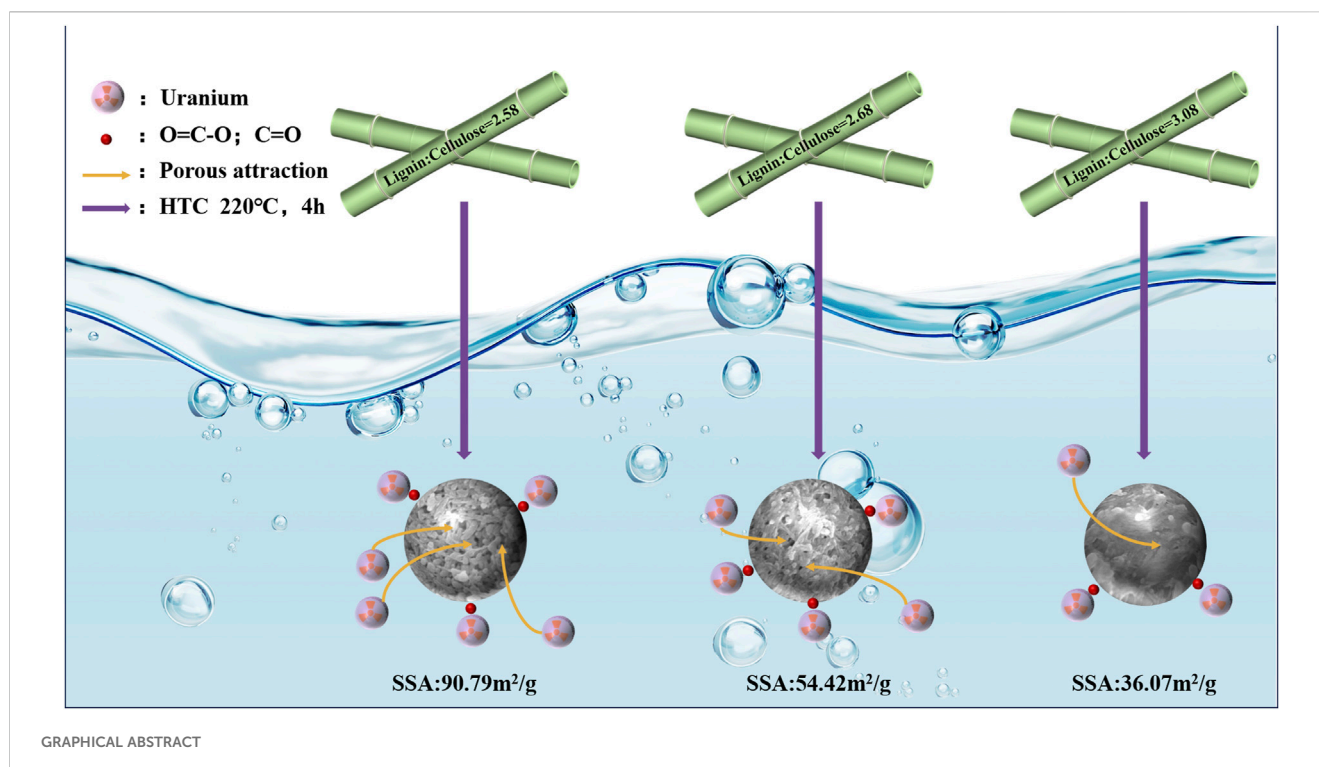
KEYWORDS

cellulose-lignin ratio, *Dendrocalamus farinosus*, hydrothermal biochar, adsorption, uranium

1 Introduction

As the global nuclear industry expands, an increasing number of radionuclides are being released into aquatic environments, posing significant health risks to both wildlife and humans (Hinck et al., 2021; Li et al., 2019; Liu et al., 2023). U(VI), one of the most prevalent radionuclides, has garnered extensive attention owing to its significant radioactivity and toxicity (Domingo, 2001; Liang et al., 2022). Biochar, used as an adsorbent, is widely employed in wastewater treatment processes to remove heavy metal pollutants from water due to its low environmental impact, cost-effectiveness, and superior pore structure (Ahmad et al., 2014). Biochar is produced using various biomass as raw materials, with lignocellulosic biomass being the primary source (Cuong et al., 2021). Variations in lignocellulosic biomass result in distinct physical and chemical properties of biochar (Elnour et al., 2019), thereby influencing its adsorption capacity for U(VI). Consequently, it is imperative to investigate how raw materials influence biochar and subsequently affect its adsorption capacity.

Recent research has extensively explored the formation of biochar. Yu, Titirici, Falco, and colleagues have examined the effects of individual components on biochar formation,



thereby establishing a theoretical framework for the role of raw materials (Falco et al., 2011; Titirici et al., 2008; Yu et al., 2012). In their pursuit to minimize costs and maximize efficiency, Lawal et al. assessed the influence of cellulose content on the physicochemical properties and adsorption capacity of biochar, utilizing materials such as cellulose, oil palm frond, and palm kernel shell. They concluded that a higher cellulose content significantly enhances the adsorption capacity of biochar (Lawal et al., 2021). However, these investigations primarily concentrated on the impacts of individual components. Biomass materials, principally consisting of cellulose, hemicellulose, and lignin, form the essential structural foundation for post-carbonized biochar. During the preparation of biochar, each polymer is subjected to pyrolysis at varying temperature ranges (Wu et al., 2018; Zhu and Zhong, 2020). Consequently, enhancing the microporous and mesoporous structure of biochar for improved pollutant adsorption necessitates a detailed analysis of the biomass's chemical composition and thermal decomposition properties, particularly the cellulose-lignin ratio.

Bamboo, as a lignocellulosic biomass, is an ideal material for biochar production due to its abundance and renewable nature. In our recent study, we reported the development of novel germplasm resources for *D. farinosus* (Hu, 2022), emphasizing the cultivation of diverse genotypes in our initial experiments. Several mutagenized strains of *D. farinosus* exhibited significant intraspecific variation in chemical composition, allowing us to negate the impact of variability among different lignocellulosic biomasses. Ideal experimental materials derived from these mutagenized strains were used to investigate the influence of chemical components in raw materials on the physicochemical properties and adsorption capacities of biochar.

Consequently, this study aimed to produce biochar from *D. farinosus* with varied cellulose-lignin ratios and to assess the effects of these variations on the physicochemical properties and

adsorption capacities of the biochar. An in-depth characterization of various genotypes of *D. farinosus* and their respective biochars was conducted to elucidate the relationship between cellulose-lignin ratios and both the physicochemical properties and the adsorption capacities of the biochar. Based on these insights, it becomes feasible to tailor the physicochemical properties and adsorption capacities of biochar through precise adjustments of the cellulose-lignin ratio.

2 Materials and methods

2.1 Materials

Three genotypes of *D. farinosus* (i.e., 52-B, 30-A, and 215) were provided by the Bamboo Institute of Southwest University of Science and Technology (Sichuan, China). Uranyl nitrate hexahydrate ($\text{UO}_2(\text{NO}_3)_2 \cdot 6\text{H}_2\text{O}$), and arsenazo III ($\text{C}_{22}\text{H}_{18}\text{As}_2\text{N}_4\text{O}_{14}\text{S}_2$) were obtained from Rhawn Reagents (Shanghai, China). Other reagents, such as anhydrous ethanol and hydrochloric acid was purchased from Chengdu Jinshan Chemical Reagent Co., Ltd., (Chengdu, China) and Chengdu United Chemical Reagent Research Institute (Chengdu, China), respectively.

2.2 Preparation of hydrothermal charcoals

Bamboo stems were harvested at breast height from the different genotypes of two-year-old *D. farinosus*. All samples were rinsed by deionized water three times and then oven dried at 65°C to ensure consistent weight. The dried bamboo stems were milled by a commercial grinding machine with the powder passing through a 200-mesh sieve. Approximately 4.0 g of each bamboo powder was

transferred to a sealed reactor with 200 mL deionized water, and kept at 220°C for 4 h and then cooled naturally. The processed material was centrifuged at 7500 rpm for 10 min, the liquid was discarded, and the precipitate was repeatedly centrifuged in aliquots of anhydrous ethanol until the supernatant was clear and transparent. Then filtered, neutralized by washing with deionized water and oven-dried at 65°C overnight. The resulting solids from different bamboo samples were marked as 52-B-220, 30-A-220, and 215-220, respectively. where the samples were identified by the genotype of the biomass and the heating temperature. The yield of the hydrothermal charcoal (Y, %) was calculated from Equation 1:

$$Y = \frac{M_1}{M_0} \times 100\% \quad (1)$$

M_0 (g): the mass of the dry matter;

M_1 (g): the mass of the hydrothermal charcoal.

2.3 Characterization of the adsorbents

The surface morphology was observed by Scanning Electron Microscope (SEM, SU8020 instrument, Hitachi, Japan). FTIR spectra were obtained by the KBr pellet method, within the range of 4,000–1,000 cm^{-1} a (Nicolet iS10, Thermo Scientific, United States). Specific surface areas and pore volumes were measured with ASAP® 2,460 Surface Area and Porosimetry System Analyzer (Micromeritics Instrument Corporation, Norcross, GA, United States). Elemental composition was obtained by Vario EL cube elemental analyzer (Elementar, Germany). Zeta equipotential was obtained by Zetasizer Nano ZS90 (Malvern, Britain). The electrochemical reduction of uranium was measured on an electrochemical station (CHI 660E).

2.4 Batch adsorption experiments

To investigated the influence of (a) adsorbent mass (0.02–0.4 g); (b) pH (2–6); (c) contact time (0–24 h); (d) temperature (15°C–55°C); and (e) initial concentration of U(VI) (5–45 mg/L) on U(VI) adsorption performance. First, several solutions of uranyl nitrate were obtained with different concentrations and adjusted to the required pH using NaOH (0.1 M) and HNO_3 . Then, the prepared solutions (50 mL) were placed into conical flasks, the adsorbent was then added (as required), and the resulting mixture was reacted in an oscillating (150 rpm) air-bath shaker for predetermined periods of time at the required temperatures. Finally, determination of U(VI) with arsenazoIII as complexing agent, its concentration being determined by absorbance at 520 nm on a T6 New Century UV spectrophotometer (Beijing Puxi General Instrument Co., Ltd., Beijing, China). Overall, repeated three times at each condition, the average concentrations of U(VI) were used for data analysis. The adsorption capacity and removal rate of U(VI) by biochar were used to characterize the adsorption performance of the charcoals; their values were calculated from Equations 2, 3 (Zhao et al., 2017):

$$q_e = \frac{(C_0 - C_e)V}{m} \quad (2)$$

$$\text{RE} = \frac{C_0 - C_e}{C_0} \times 100\% \quad (3)$$

q_e (mg/g): the adsorption capacity;

RE (%):the removal rate at adsorption equilibrium;

C_0 (mg/L): the initial concentration of uranyl ion before adsorption;

C_e (mg/L): the concentration of U(VI) at equilibrium, mg/L; V (L): the volume of the adsorption solution;

m (g): the mass of adsorbent.

2.5 Elution/regeneration study

We conducted an elution/regeneration study using an improved version of the method of Li et al. (2019), to investigate the reusability of 52-B-220 through five adsorption-desorption cycles.

2.6 Statistical analyses

Statistical product and service solutions (SPSS) software (SPSS statistics 22, IBM Corporation) was used to perform the significance analysis between chemical composition. Letters indicate differences in chemical composition of the three genotypes of *D. farinosus* according to Tukey b's honestly significant difference ($p < 0.05$).

3 Results and discussion

3.1 Characterization of the biomass

3.1.1 Composition

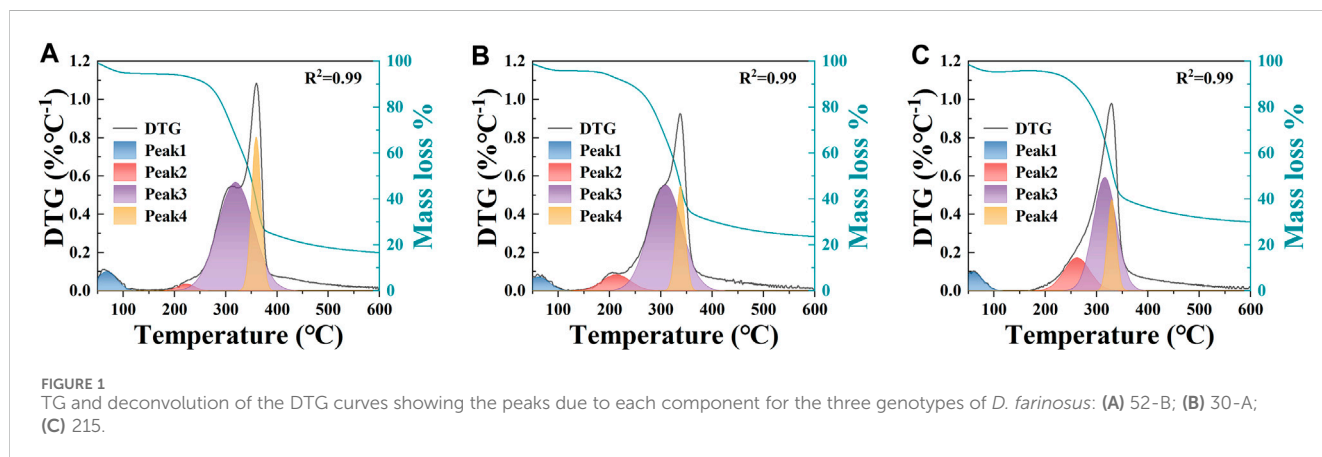
The chemical compositions of the three *D. farinosus* genotypes are detailed in Table 1. Among the various raw materials, the largest difference in cellulose content (12%) was observed between genotypes 215 and 52-B. No significant differences in lignin content were observed. Consequently, the cellulose-to-lignin ratio varied significantly across the genotypes. Additionally, the carbon content among the three *D. farinosus* genotypes remained consistent at 44.6%–46.2%, whereas substantial variations in oxygen content were observed, ranging from 30.7% to 40.1% (Table 1). Therefore, the *D. farinosus* genotypes exhibited significant differences both individually and in their relative compositions.

3.1.2 Thermogravimetric analysis

TG (thermogravimetry) and DTG (derivative thermogravimetry) analyses were conducted to evaluate the properties of raw biomass following thermal decomposition (Figure 1). The devolatilization zone (150°C–400°C) for each genotype showed variations in mass loss, ranging from 70.46% (52-B) to 59.08% (215), attributed to the differing compositions of the biomasses. Finally, mass loss within the continuous devolatilization zone (400°C–600°C) ranged from 7.47% (52-B) to 6.45% (30-A).

TABLE 1 Cellulose content, lignin content, cellulose-lignin ratio, and elemental abundance of the three genotypes of *D. farinosus*.

Sample	Cellulose %	Lignin %	Cellulose-lignin	Element abundance %			
				C	H	O	N
52-B	42.4 ± 0.26c	16.4 ± 0.07b	2.58 ± 0.01c	45.3	6.09	40.1	0.38
30-A	43.8 ± 0.38b	16.4 ± 0.20b	2.68 ± 0.03b	44.6	6.10	30.7	0.54
215	53.5 ± 0.06a	17.4 ± 0.36a	3.08 ± 0.06a	46.2	5.87	33.2	0.41



To determine the optimal hydrothermal temperature for preserving lignin as the structural framework of hydrothermal charcoal and for forming cellulose-associated carbon microspheres, the DTG curve was deconvoluted to isolate the pyrolysis peaks of each component (Wu et al., 2018). The DTG curve revealed four distinct peaks at approximately 60°C (peak 1), 200°C (peak 2), 300°C (peak 3), and 350°C (peak 4), corresponding to moisture, hemicellulose, cellulose, and lignin, respectively (Figure 1). A thorough examination of these component peaks revealed that their pyrolysis onset temperatures varied significantly. Specifically, the pyrolysis onset temperatures were 180°C for hemicellulose, 200°C for cellulose, and 300°C for lignin, consistent with findings from previous studies (Liang et al., 2018; Tong Thi et al., 2014; Yang et al., 2017). Furthermore, during the hydrothermal reaction, the subcritical state of the liquid phase (i.e., water) can accelerate the reaction rate and induce sample corrosion (Zanon Costa et al., 2020). To ensure the complete reaction of hemicellulose and cellulose into carbon microspheres and retention of the lignin-based hydrothermal charcoal framework, a final hydrothermal temperature of 220°C was selected.

3.2 Characteristics of hydrothermal charcoals

3.2.1 Surface morphology and pore structure

SEM images of the hydrothermal charcoals were captured to elucidate the surface morphologies of the three *D. farinosus* genotypes (Figures 2A–C). The agglomeration of carbon microspheres intensified with increasing cellulose/lignin ratios, ultimately resulting in the complete envelopment of the surface. At this final stage, the filamentous structure became

indistinguishable, and the pore structure significantly diminished (215–220).

A lignin skeleton with attached carbon microspheres was observed in 52-B-220 (Figure 2A), signifying its superior efficacy in biochar production. This observation is consistent with previous studies that demonstrate the effective cross-linking of hemicellulose, cellulose, and lignin within a three-dimensional matrix (Deanin et al., 1978; Kang et al., 2019). Consequently, the lower cellulose-to-lignin ratio in 52-B likely enhanced the exposure of the polymer network to the processing conditions at 220°C.

The FTIR spectra of the three hydrothermal charcoals are shown in Figure 2D. No significant differences were observed in the peaks associated with functional groups among the three hydrothermal charcoals. The characteristic bands and their corresponding assignments are as follows: 3348 cm⁻¹ (broad, O-H stretching vibration); 1700 cm⁻¹ [C=O stretching vibrations of aldehyde, ketone, ester, and carboxyl (Fang et al., 2014)]; 1,608 cm⁻¹ (C=O stretching vibrations of the benzene ring) and 1,316 cm⁻¹ [C-O stretching vibration of the carboxylate anion (Chen et al., 2018)]; 1,265 cm⁻¹ (C-O-C and phenolic -OH stretching vibration of aromatic hydrocarbons); 1,160 cm⁻¹, 1,110 cm⁻¹, and 1,058 cm⁻¹ (C-O vibrations of ethers, alcohols, phenols). The presence of these characteristic bands indicates that the surface composition of hydrothermal charcoal is predominantly composed of hydroxyl and carboxyl groups. However, the peaks at 1,510 cm⁻¹, 1,425 cm⁻¹, and 1,265 cm⁻¹ are attributed to lignin (Aleeva et al., 2020; Liu et al., 2017), indicating that its structure was preserved during the preparation process, a finding consistent with SEM observations.

The yields of hydrothermal charcoals from the three *D. farinosus* genotypes are shown in Figure 2E. No significant differences ($p > 0.05$) were observed in the yields among the three *D. farinosus*

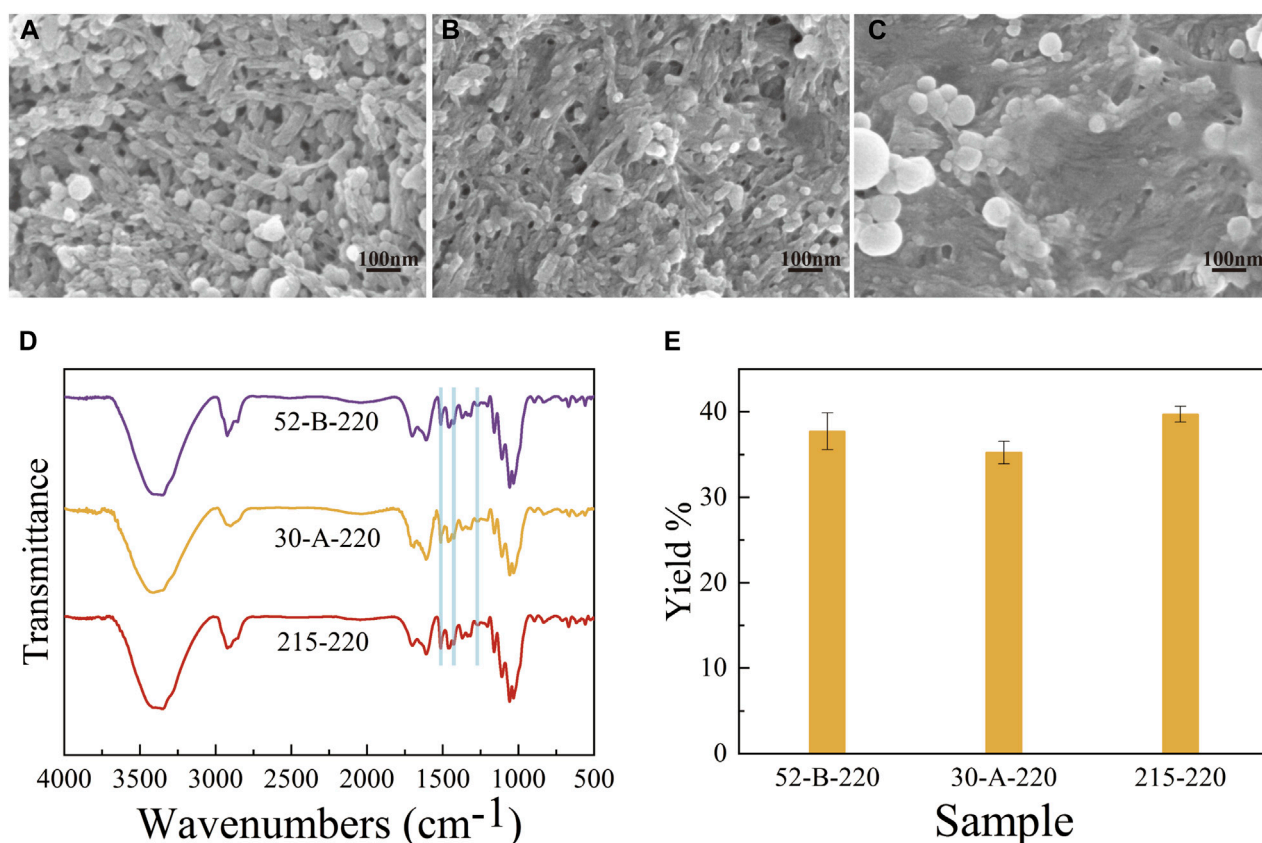


FIGURE 2
The SEM images of hydrothermal charcoals (A) for 52-B-220, (B) for 30-A-220, (C) for 215-220. (D) FTIR spectra of hydrothermal charcoals. (E) Yields of hydrothermal charcoals.

genotypes, indicating that utilizing *D. farinosus* with low cellulose/lignin ratios for hydrothermal charcoal production is unlikely to raise production costs.

Given that pore structure is a critical factor influencing sorbent adsorption performance, the pore diameters, specific surface areas, and pore volumes of each hydrothermal charcoal are shown in Table 2. No significant differences were observed in the pore diameters among the three-genotype charcoals, while specific surface areas and pore volumes decreased with increasing cellulose/lignin ratios. This phenomenon can be attributed to the increase in carbon microsphere formation, as cellulose is the primary precursor for these structures (Sevilla and Fuertes, 2009; Titirici et al., 2008). The subsequent agglomeration of excess carbon microspheres blocks the formation of new pores or constricts existing ones, leading to a reduction in specific surface area and pore volume (Yu et al., 2012).

3.3 Adsorption performance

3.3.1 The effect of experimental parameters on adsorption

pH is a crucial factor in adsorption processes as it significantly influences charge transfer at the solid–liquid interface (Fang et al., 2020). Consequently, it is imperative to systematically investigate

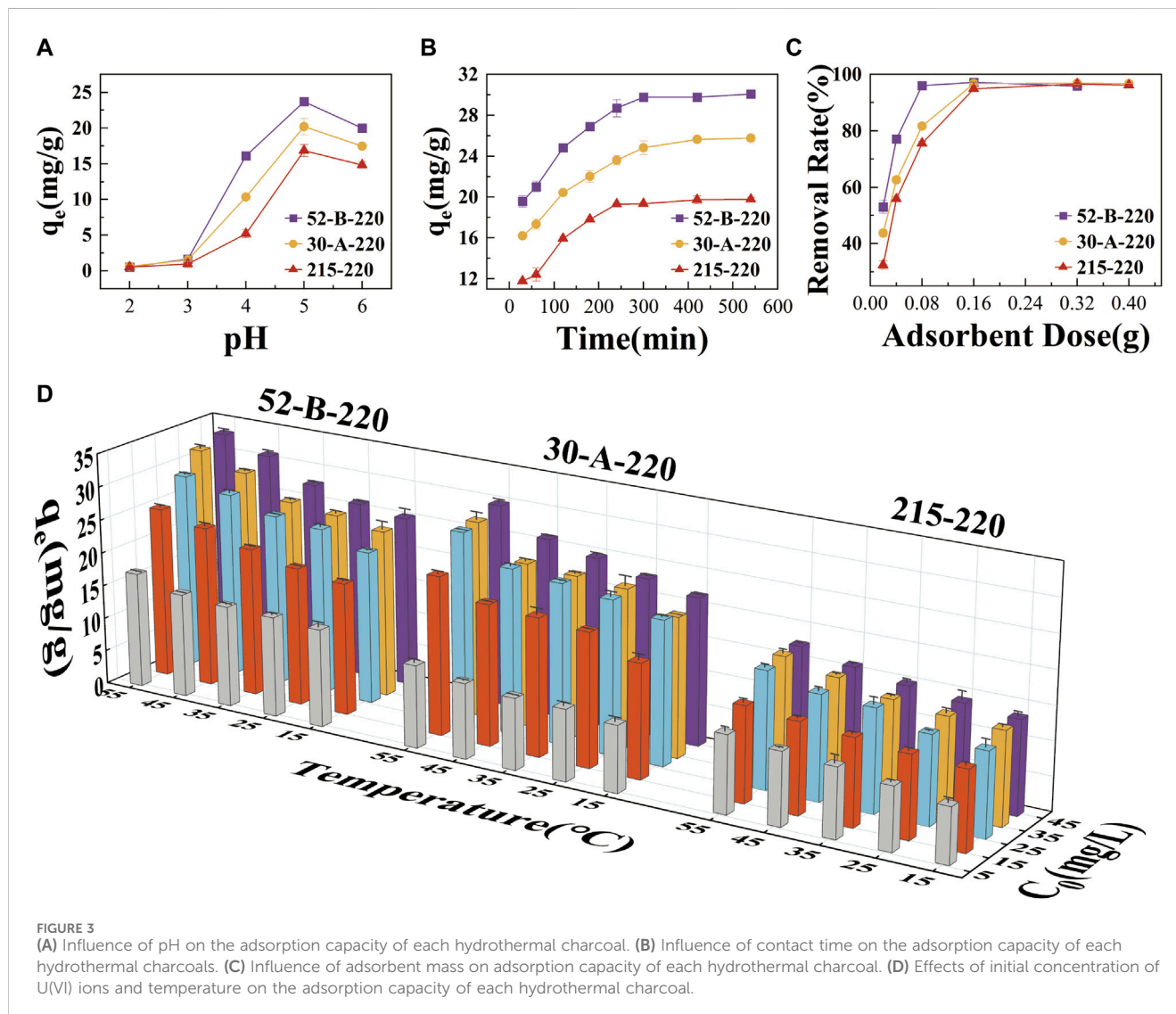
the effect of pH on U(VI) adsorption (Hui et al., 2019). The surface charge of the adsorbent was evaluated across a pH range of 2.0–8.0, while the adsorption performance of hydrothermal charcoals was assessed at pH 2.0–6.0. The surface charge of the adsorbent continues to decline until pH 6.0 (Supplementary Figure S1), indicating that the adsorbent surface is severely protonated at low pH. That leads to adsorption competition between UO_2^{2+} and H^+ , as well as electrostatic repulsion occurred between the adsorbent and UO_2^{2+} . As pH increases, protonation weakens, and the adsorption capacity of the adsorbent gradually increases (Zhao et al., 2017). Additionally, when the pH exceeds 5.0, the species of U in the solution change and begin to form precipitates rather than adsorb, leading to a decrease in adsorption capacity (Liao et al., 2022). This observation is consistent with the results shown in Figure 3A and those reported in previous studies (Abdi et al., 2017; Humelnicu et al., 2014). Therefore, pH 5.0 is considered more suitable for U(VI) adsorption.

Furthermore, Figure 3B illustrates the influence of contact time, ranging from 0 to 300 min, on the adsorption capacity of the hydrothermal charcoals. The adsorption of U(VI) increased rapidly during the first 120 min, then gradually slowed as it approached equilibrium at 300 min. This trend is consistent with the decrease in available adsorption sites, which are progressively occupied by U(VI) ions.

Notably, the adsorption capacity of each hydrothermal charcoal exhibited an inverse relationship with the mass of

TABLE 2 Pore diameter, specific surface area, and pore volume measurements were obtained from the analysis of each hydrothermal charcoal.

Sample	Surface area (m ² /g)	Pore volume (cm ³ /g)	Average pore diameter (nm)
52-B-220	90.7914	0.198,307	7.5515
30-A-220	54.4164	0.113,982	7.4554
215-220	36.0689	0.077575	7.3017



the adsorbent, while their removal rates increased with higher adsorbent masses (>95%) (Figure 3C). The optimal adsorbent masses for 52-B-220, 30-A-220, and 215-220 were determined to be 0.08 g, 0.16 g, and 0.16 g, respectively. The observed increase in removal rate can be attributed to the greater availability of adsorption sites for U(VI) ions due to the increased mass of the adsorbent. Given that a larger specific surface area enhances the adsorption capacity per unit mass, an equivalent removal rate can be achieved with a smaller adsorbent mass. Consequently, 52-B-220 exhibited optimal adsorption performance at the lowest adsorbent mass.

As illustrated in Figure 3D, the effects of a broad temperature range (15°C–55°C) and varying initial concentrations of U(VI) ions (5–45 mg/L) on the adsorption performance of each hydrothermal charcoal were examined. Consistent with published data, the adsorption capacities of each hydrothermal charcoal increased with rising temperature, likely due to the enhanced mass transfer of ions in solution at elevated temperatures. This effect accelerates the mass transfer rate of the adsorbate from the outer layer of the adsorbent to the inner pores (Inyang et al., 2016; Mishra et al., 2006). The adsorption capacity also exhibited a direct correlation with the initial concentration of U(VI) ions, reaching saturation at 35 mg/L.

Previous studies have demonstrated that increasing the initial concentration enhances adsorption capacity by amplifying both the driving force for mass transfer and the contact rate of U(VI) ions with adsorption sites (Wegener et al., 2009). Adsorption saturation was achieved when the concentration of uranyl ions in the solution became sufficient to fully occupy the adsorption sites on the hydrothermal charcoal.

3.3.2 Adsorption kinetics

The adsorption mechanism of U(VI) ions in the solid-liquid system was examined using Lagergren's pseudo-first-order and McKay's pseudo-second-order kinetic models. The relevant fitting parameters are summarized in [Supplementary Figure S1](#); [Supplementary Table S1](#). The kinetic data for each hydrothermal charcoal showed a better fit with the pseudo-second-order kinetic model ($R^2 = 0.999, 0.998$, and 0.998) than with the pseudo-first-order kinetic model ($R^2 > 0.96$ for 30-A-220; $R^2 < 0.96$ for 52-B-220 and 215-220). This suggests that chemisorption is the primary adsorption mechanism (Li et al., 2019; Rodríguez-Reinoso, 1998).

3.3.3 Adsorption isotherms

To validate the adsorption behavior and assess the adsorption capacity of hydrothermal charcoal, the U(VI) adsorption isotherm was thoroughly examined. The isotherm data were analyzed using the Langmuir and Freundlich adsorption models ([Supplementary Figure S2](#); [Supplementary Table S2](#)). The adsorption data for U(VI) on 52-B-220 exhibited a superior fit to the Freundlich adsorption model ($R^2 = 0.998$) compared to the Langmuir model ($R^2 = 0.980$), indicating that adsorption occurred as a multilayer process on a heterogeneous surface (Xu et al., 2019). Given that the value of n ranged between 1 and 10, increasing temperature and concentration were favorable for enhancing adsorption performance. For 30-A-220 and 215-220, [Supplementary Table S2](#) shows that the Langmuir model's fitting coefficients (R^2) were all greater than 0.99, slightly outperforming those of the Freundlich model. This indicates that the primary driving force for U(VI) adsorption was point-to-point monolayer adsorption on a homogeneous surface (Im and Choi, 2018).

Additionally, [Supplementary Table S3](#) provides a comparative analysis of the q_m values of hydrothermal charcoals from this study and those reported in other studies.

In its unmodified form, 52-B-220 biochar exhibits superior adsorption capacity. This enhanced capacity is attributed to methodological adjustments made in this study, which fully exploit the natural template provided by the raw material's three-dimensional lignin network structure, thereby increasing the specific surface area and pore volume of 52-B-220. Although the adsorption capacity of functionalized biochar exceeds that of 52-B-220, the improvements in physical adsorption in 52-B-220 do not hinder subsequent functionalization processes. Future studies can employ adaptable functionalization processes tailored to specific adsorbates, positioning 52-B-220 as an ideal precursor for further enhancements. The cellulose/lignin adjustment strategy has proven successful, establishing 52-B-220 as a cost-effective, readily available adsorbent, particularly well-suited for large-scale pollution control applications. Moreover, 52-B-220 serves as an outstanding precursor for developing highly efficient adsorbents.

3.3.4 Thermodynamics of adsorption

The results for each hydrothermal charcoal are illustrated in [Supplementary Figure S3](#) and outlined in [Supplementary Table S4](#). The thermodynamic curves and parameters for U(VI) ion adsorption by each hydrothermal charcoal suggest that the process is both spontaneous and endothermic. According to the equation $\Delta G = \Delta H - T\Delta S$, where $\Delta H^\circ > 0$ (endothermic) and $\Delta S^\circ > 0$, the ΔG° values for U(VI) adsorption by each charcoal between 288.15 K and 328.15 K were negative.

3.3.5 Elution/regeneration study

The regeneration study of hydrothermal charcoal is of substantial importance for its practical applications. Following adsorption, biochar can be regenerated by washing with hydrochloric acid, which restores adsorption sites and renders the biochar reusable (Chen et al., 2016). The experiment was performed under optimal adsorption conditions ($T = 25^\circ\text{C}$, $t = 6$ h, $\text{pH} = 5$, $C_0 = 20$ ppm, Dose = 0.02 g) ([Figure 4](#)). After five cycles, the adsorption capacity of 52-B-220 decreased from 22.58 mg/g to 19.94 mg/g, retaining 86.13% of its original adsorption capacity. The slight reduction in adsorption capacity is attributed to the incomplete desorption of U(VI) ions from the biochar surface. The regeneration results indicate that 52-B-220 is a promising candidate for U(VI) adsorption.

3.3.6 Effect of the coexisting ions

Given the diverse array of coexisting ions in natural wastewater, it is crucial to investigate the selective adsorption of U. [Figures 4B, C](#) illustrate that the adsorption capacity and distribution factor of 52-B-220 for U(VI) are 23.35 mg/g and 2.24 L/g, respectively. These values are significantly higher than those for other coexisting ions, indicating that 52-B-220 exhibits strong adsorption affinity and capacity for U(VI), making it a suitable adsorbent for separating U(VI) from multicomponent systems.

3.4 Adsorption mechanism

In order to further clarify the possible adsorption mechanism of U(VI) by the hydrothermal charcoals, the chemical composition, and surficial chemical states of 52-B-220 before and after adsorption are characterized by FTIR, XPS and LSV. As depicted in [Supplementary Figure S4](#), comparison of the FTIR spectra of 52-B-220 ([Supplementary Figure S4](#)) revealed a new absorption band at 915 cm^{-1} post-adsorption. This peak technically corresponds to the asymmetric stretching vibration of U(VI) (Quilès and Burneau, 2000; Su et al., 2022). Indicating that uranyl ions were successfully adsorbed onto the surface of 52-B-220. Meanwhile, the FTIR spectra of the adsorbent-before and after adsorption-shows that the peak at $1,696\text{ cm}^{-1}$ slightly shifted to 1703 cm^{-1} after adsorption, what indicates the involvement of -C=O group in the adsorption of U(VI) (Jin et al., 2018); the intensity of peak at $1,205\text{ cm}^{-1}$ decreases after adsorption, suggesting the participation of -OH (phenol) in the adsorption of U(VI) (Liu et al., 2013); and peaks at $1,058\text{ cm}^{-1}$, $1,110\text{ cm}^{-1}$, and $1,160\text{ cm}^{-1}$ also decrease after adsorption, indicating the involvement of -OH (alcohol) in the adsorption of U(VI) (Mishra et al., 2017).

Prior to the adsorption of U(VI) ions, the XPS survey spectra of 52-B-220 peaked at 286 eV and 533 eV corresponding to C1s and

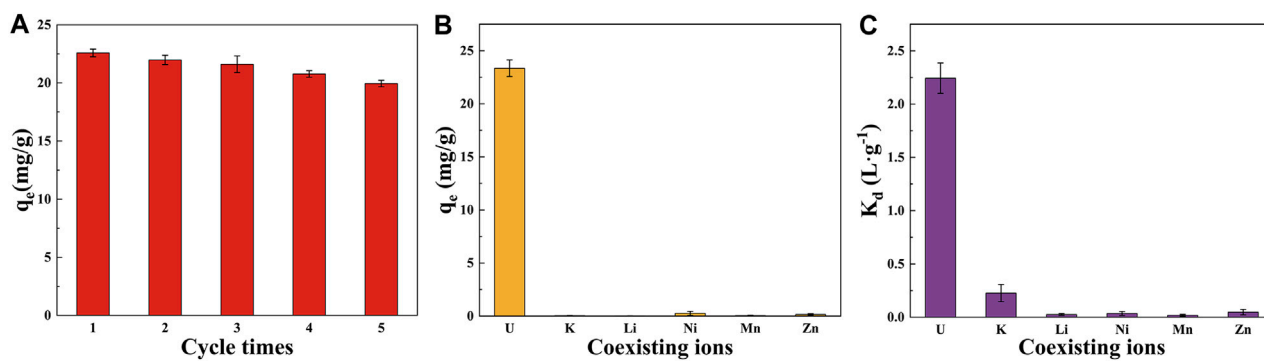


FIGURE 4
(A) Regeneration of U(VI) adsorption on 52-B-220. (B) Adsorption capacity and (C) distribution factor of 52-B-220 for co-existing ions.

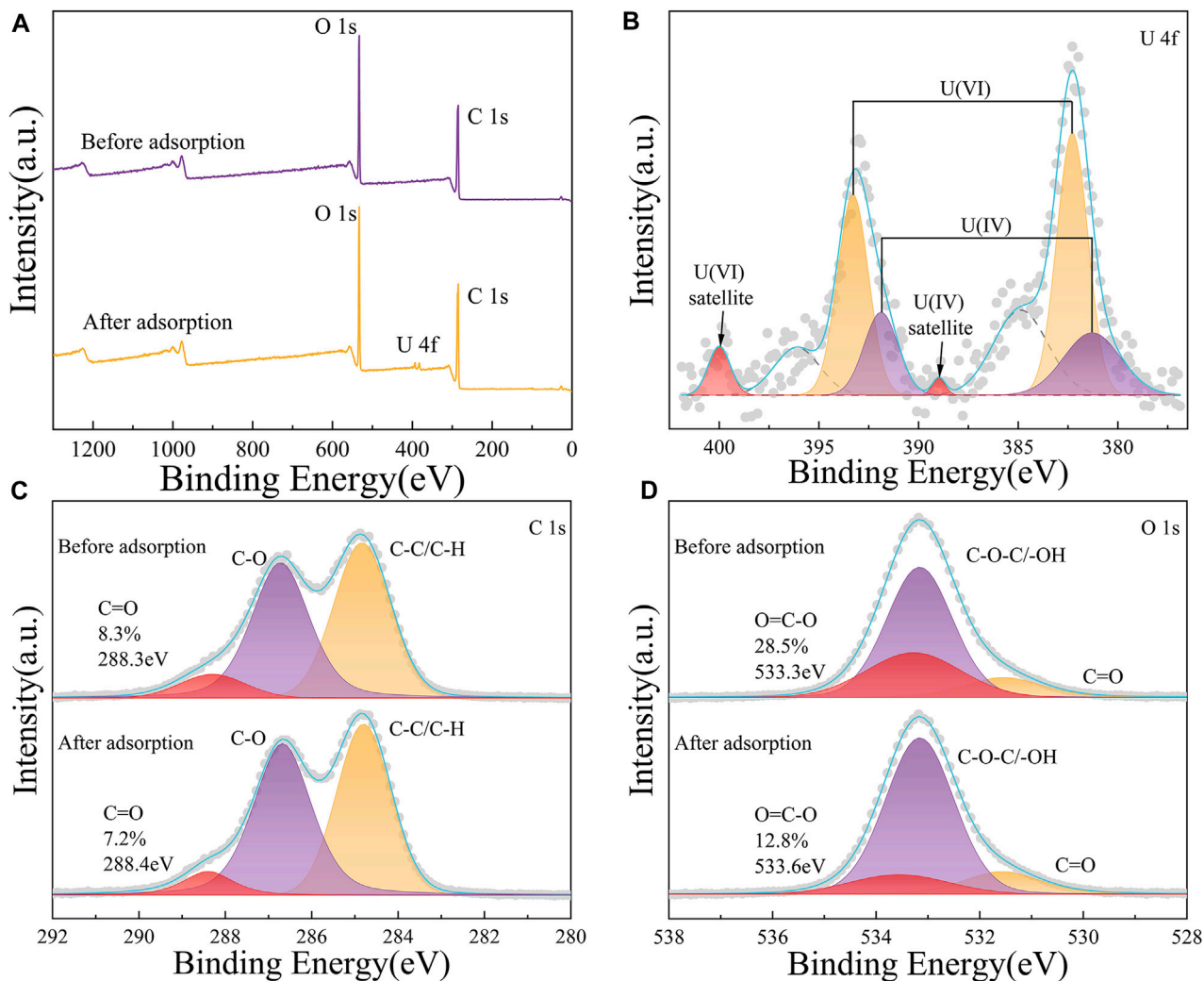


FIGURE 5
XPS spectra of 52-B-220 before and after the adsorption of U(VI) ions: (A) XPS survey spectra; (B–D) high-resolution XPS spectra of U4f, C1s, and O1s, respectively, obtained post adsorption.

O1s, respectively (Figure 5A). The new peak binding energy at 390 eV is attributed to U(VI), implying that U(VI) was successfully adsorbed onto the surface of 52-B-220. Two peaks with binding energies of 382.3 and 393.2 eV are detected in the U 4f spectrum, which are related to U 4f_{7/2} and U 4f_{5/2} peaks, respectively (Figure 5B). Notably, each of these were deconvoluted to peak at 381.3 eV and 391.9 eV, and 382.3 eV and 393.3 eV, which agreed with U(IV) and U(VI). The satellite peaks of U(VI) 4f_{5/2} (400.0 eV), and U(IV) 4f_{7/2} (389.0 eV) verified the existence of both U species, implying that some U(VI) was reduced to U(IV) during the processing of the biomass (Ilton and Bagus, 2011; Xiang et al., 2018).

The high-resolution C1s signals were deconvoluted to peak at 284.8 eV (C-C/C-H), 286.7 eV (C-O of hydroxyl and ether), and 288.3 eV (C=O of carboxyl and ester) (Figure 5C) (Biesinger, 2022; Chen et al., 2022; Moeini et al., 2022; Yang et al., 2022). After adsorption, due to the involvement of C=O, the peak at 288.3 eV shifted slightly to 288.4 eV, and its relative intensity decreased. Additionally, the high-resolution O1s signal was deconvoluted to give three peaks located at 531.5 eV (C=O), 533.2 eV (C-O-C/-OH), and 533.3 eV (O=C-O) (Figure 5D). After adsorption, the peaks at 533.3 eV and 531.5 eV shifted to 533.56 eV and 531.6 eV, respectively, due to the participation of O=C-O and C=O; and their relative intensities decreased accordingly. The small shifts in binding energy and decrease in signal intensity of O=C-O and C=O were indicative of their interaction with U(VI) (Chen et al., 2022; Yu et al., 2019; Zhang et al., 2020). Meanwhile, we recorded the linear sweep voltammetry (LSV) curves in the presence of 20 ppm U(VI) within a 0.5 M Na⁺ electrolyte solution (Supplementary Figure S6). In the presence of uranium, two distinct peaks were recorded at -0.67 V and -0.89 V vs. Ag/AgCl, corresponding to the reduction of U(VI) to U(V) and U(V) to U(IV), respectively. These results suggest that the observed processes may occur via electron transfer and coordinate bond formation between the carboxyl and ester groups of 52-B-220 and U(VI).

4 Conclusion

The increase in the cellulose/lignin ratio in *D. farinosus* resulted in enhanced aggregation of carbon microspheres within the hydrothermal biochar, leading to a reduction in specific surface area and pore volume, ultimately resulting in decreased adsorption capacity of the hydrothermal biochar. In comparison to biochar with a high cellulose/lignin ratio, 52-B-220 exhibited a significantly larger specific surface area (an increase of 151.71%) and higher adsorption capacity (an increase of 76.05%), indicating that adjusting raw materials is a viable approach for achieving higher adsorption capacity. Batch adsorption results revealed that the adsorption process of 52-B-220 primarily involved multi-layer endothermic chemisorption. FT-IR and XPS spectra demonstrated that U(VI) adsorption by 52-B-220 mainly occurred through carboxyl and hydroxyl groups. Reducing the cellulose/lignin ratio serves as a fundamental method for enhancing the performance of hydrothermal biochar while reducing post-treatment costs. Modifying the structure of raw materials offers a feasible solution for cost reduction and efficiency improvement in biochar adsorption.

Data availability statement

The original contributions presented in the study are included in the article/Supplementary Material, further inquiries can be directed to the corresponding authors.

Author contributions

FY: Conceptualization, Data curation, Formal Analysis, Investigation, Methodology, Project administration, Software, Validation, Visualization, Writing—original draft, Writing—review and editing. HL: Conceptualization, Supervision, Visualization, Writing—review and editing. BW: Conceptualization, Formal Analysis, Investigation, Project administration, Supervision, Writing—review and editing. WF: Project administration, Supervision, Writing—review and editing. XG: Supervision, Writing—review and editing. YC: Funding acquisition, Project administration, Supervision, Writing—review and editing. SH: Conceptualization, Funding acquisition, Project administration, Resources, Supervision, Writing—review and editing.

Funding

The author(s) declare that financial support was received for the research, authorship, and/or publication of this article. This study was supported by the Science and Technology Project of Sichuan Province, China (2022NSFSC0093 and 2021YFYZ0006), the National Key R&D Program of China (2021YFD2200504_1 and 2021YFD2200505_2), the Ph.D. Foundation of Southwest University of Science and Technology (No. 18zx7128).

Conflict of interest

The authors declare that the research was conducted in the absence of any commercial or financial relationships that could be construed as a potential conflict of interest.

Publisher's note

All claims expressed in this article are solely those of the authors and do not necessarily represent those of their affiliated organizations, or those of the publisher, the editors and the reviewers. Any product that may be evaluated in this article, or claim that may be made by its manufacturer, is not guaranteed or endorsed by the publisher.

Supplementary material

The Supplementary Material for this article can be found online at: <https://www.frontiersin.org/articles/10.3389/fenvs.2024.1451496/full#supplementary-material>

References

- Abdi, S., Nasiri, M., Mesbahi, A., and Khani, M. H. (2017). Investigation of uranium (VI) adsorption by polypyrrole. *J. Hazard. Mater.* 332, 132–139. doi:10.1016/j.jhazmat.2017.01.013
- Ahmad, M., Rajapaksha, A. U., Lim, J. E., Zhang, M., Bolan, N., Mohan, D., et al. (2014). Biochar as a sorbent for contaminant management in soil and water: a review. *Chemosphere* 99, 19–33. doi:10.1016/j.chemosphere.2013.10.071
- Aleeva, S. V., Lepilova, O. V., and Koksharov, S. A. (2020). Study of reducing destruction of lignin by FT-IR spectroscopy. *J. Appl. Spectrosc.* 87, 779–783. doi:10.1007/s10812-020-01069-0
- Biesinger, M. C. (2022). Accessing the robustness of adventitious carbon for charge referencing (correction) purposes in XPS analysis: insights from a multi-user facility data review. *Appl. Surf. Sci.* 597, 153681. doi:10.1016/j.apsusc.2022.153681
- Chen, L., Zhao, D., Chen, S., Wang, X., and Chen, C. (2016). One-step fabrication of amino functionalized magnetic graphene oxide composite for uranium(VI) removal. *J. Colloid Interface Sci.* 472, 99–107. doi:10.1016/j.jcis.2016.03.044
- Chen, Z., He, X., Li, Q., Yang, H., Liu, Y., Wu, L., et al. (2022). Low-temperature plasma induced phosphate groups onto coffee residue-derived porous carbon for efficient U(VI) extraction. *J. Environ. Sci.* 122, 1–13. doi:10.1016/j.jes.2021.10.003
- Chen, Z., Liu, T., Tang, J., Zheng, Z., Wang, H., Shao, Q., et al. (2018). Characteristics and mechanisms of cadmium adsorption from aqueous solution using lotus seedpod-derived biochar at two pyrolytic temperatures. *Environ. Sci. Pollut. Res. Int.* 25, 11854–11866. doi:10.1007/s11356-018-1460-1
- Cuong, D. V., Matsagar, B. M., Lee, M. S., Hossain, M. S. A., Yamauchi, Y., Vithanage, M., et al. (2021). A critical review on biochar-based engineered hierarchical porous carbon for capacitive charge storage. *Renew. & Sustain. Energy Rev.* 145, 111029. doi:10.1016/j.rser.2021.111029
- Deanin, R. D., Driscoll, S. B., Cook, R. J., Dubreuil, M. P., and Shaker, W. A. (1978). Lignin as a filler in commodity thermoplastics.
- Domingo, J. L. (2001). Reproductive and developmental toxicity of natural and depleted uranium: a review. *Reprod. Toxicol. (Elmsford, N.Y.)* 15, 603–609. doi:10.1016/s0890-6238(01)00181-2
- Elnour, A. Y., Alghayam, A. A., Shaikh, H. M., Poulouse, A. M., Al-Zahrani, S. M., Anis, A., et al. (2019). Effect of pyrolysis temperature on biochar microstructural evolution, physicochemical characteristics, and its influence on biochar/polypropylene composites. *Appl. Sciences-Basel* 9, 1149. doi:10.3390/app9061149
- Falco, C., Baccile, N., and Titirici, M.-M. (2011). Morphological and structural differences between glucose, cellulose and lignocellulosic biomass derived hydrothermal carbons. *Green Chem.* 13, 3273–3281. doi:10.1039/c1gc15742f
- Fang, Q., Chen, B., Lin, Y., and Guan, Y. (2014). Aromatic and hydrophobic surfaces of wood-derived biochar enhance perchlorate adsorption via hydrogen bonding to oxygen-containing organic groups. *Environ. Sci. Technol.* 48 (1), 279–288. doi:10.1021/es403711y
- Fang, R., Lu, C., Zhong, Y., Xiao, Z., Liang, C., Huang, H., et al. (2020). Puffed rice carbon with coupled sulfur and metal iron for high efficiency mercury removal in aqueous solution. *Environ. Sci. Technol.* 54, 2539–2547. doi:10.1021/acs.est.9b07385
- Hinck, J. E., Cleveland, D., and Sample, B. E. (2021). Terrestrial ecological risk analysis via dietary exposure at uranium mine sites in the Grand Canyon watershed (Arizona, USA). *Chemosphere* 265, 129049. doi:10.1016/j.chemosphere.2020.129049
- Hu, S. L. (2022). *Research on the creation and breeding of new germplasm of cluster bamboo for industrial use: the creation and breeding of new germplasm of Dendrocalamus farinosus*. Beijing: Science Press.
- Hui, J. J., Wang, Y. Q., Liu, Y. H., Cao, X. H., Zhang, Z. B., Dai, Y., et al. (2019). Effects of pH, carbonate, calcium ion and humic acid concentrations, temperature, and uranium concentration on the adsorption of uranium on the CTAB-modified montmorillonite. *J. Radioanalytical Nucl. Chem.* 319, 1251–1259. doi:10.1007/s10967-019-06415-x
- Humelnicu, D., Blegescu, C., and Ganju, D. (2014). Removal of uranium(VI) and thorium(IV) ions from aqueous solutions by functionalized silica: kinetic and thermodynamic studies. *J. Radioanalytical Nucl. Chem.* 299, 1183–1190. doi:10.1007/s10967-013-2873-4
- Ilton, E. S., and Bagus, P. S. (2011). XPS determination of uranium oxidation states. *Surf. Interface Analysis* 43, 1549–1560. doi:10.1002/sia.3836
- Im, H.-J., and Choi, K.-S. (2018). Investigation of gaseous wet methyl iodide adsorption on Ag nanoparticles embedded in organic-inorganic hybrid silica gels. *J. Radioanalytical Nucl. Chem.* 316, 1323–1328. doi:10.1007/s10967-018-5866-5
- Inyang, M. I., Gao, B., Yao, Y., Xue, Y., Zimmerman, A., Mosa, A., et al. (2016). A review of biochar as a low-cost adsorbent for aqueous heavy metal removal. *Crit. Rev. Environ. Sci. Technol.* 46, 406–433. doi:10.1080/10643389.2015.1096880
- Jin, J., Li, S., Peng, X., Liu, W., Zhang, C., Yang, Y., et al. (2018). HNO₃ modified biochars for uranium (VI) removal from aqueous solution. *Bioresour. Technol.* 256, 247–253. doi:10.1016/j.biortech.2018.02.022
- Kang, X., Kirui, A., Widanage, M. C. D., Mentink-Vigier, F., Cosgrove, D. J., and Wang, T. (2019). Lignin-polysaccharide interactions in plant secondary cell walls revealed by solid-state NMR. *Nat. Commun.* 10, 347. doi:10.1038/s41467-018-08252-0
- Lawal, A. A., Hassan, M. A., Zakaria, M. R., Yusoff, M. Z. M., Norrrahim, M. N. F., Mokhtar, M. N., et al. (2021). Effect of oil palm biomass cellulosic content on nanopore structure and adsorption capacity of biochar. *Bioresour. Technol.* 332, 125070. doi:10.1016/j.biortech.2021.125070
- Li, M. X., Liu, H. B., Chen, T. H., Dong, C., and Sun, Y. B. (2019). Synthesis of magnetic biochar composites for enhanced uranium (VI) adsorption. *Sci. Total Environ.* 651, 1020–1028. doi:10.1016/j.scitotenv.2018.09.259
- Liang, F., Wang, R., Xiang, H., Yang, X., Zhang, T., Hu, W., et al. (2018). Investigating pyrolysis characteristics of moso bamboo through TG-FTIR and Py-GC/MS. *Bioresour. Technol.* 256, 53–60. doi:10.1016/j.biortech.2018.01.140
- Liang, Y., Xia, M., Yu, Q., Li, Y., Sui, Z., Yuan, Y., et al. (2022). Guanidinium-based ionic covalent organic frameworks for capture of uranyl tricarbonate. *Adv. Compos. Hybrid Mater.* 5, 184–194. doi:10.1007/s42114-021-00311-3
- Liao, J., Xiong, T., Ding, L., Xie, Y., Zhang, Y., and Zhu, W. (2022). Design of a renewable hydroxyapatite-biocarbon composite for the removal of uranium(VI) with high-efficiency adsorption performance. *Biochar* 4, 29. doi:10.1007/s42773-022-00154-1
- Liu, C., Huang, X., and Kong, L. Z. (2017). Efficient low temperature hydrothermal carbonization of Chinese reed for biochar with high energy density. *Energies* 10, 2094. doi:10.3390/en10122094
- Liu, F., Wang, S., Zhao, C., and Hu, B. (2023). Constructing coconut shell biochar/MXenes composites through self-assembly strategy to enhance U(VI) and Cs(I) immobilization capability. *Biochar* 5, 31–16. doi:10.1007/s42773-023-00231-z
- Liu, J., Li, J., Yang, X., Song, Q., Bai, C., Shi, Y., et al. (2013). Facile preparation of polyphenolic hydroxyl functionalized uranium-selective chelating sorbent: simple oxidation of styrene-divinylbenzene copolymer microparticles by Hummers method. *Mater. Lett.* 97, 177–180. doi:10.1016/j.matlet.2013.01.120
- Mishra, S. P., Tiwari, D., Prasad, S. K., Dubey, R. S., and Mishra, M. (2006). Inorganic ion-exchangers in radioactive waste management: Part XVI: uptake of some metal phosphates (stannic and zirconium) for 134Cs. *J. Radioanalytical & Nucl. Chem.* 268, 191–199. doi:10.1556/JRNC.268.2006.2.3
- Mishra, V., Sureshkumar, M. K., Gupta, N., and Kaushik, C. P. (2017). Study on sorption characteristics of uranium onto biochar derived from Eucalyptus wood. *Water Air Soil Pollut.* 228, 309. doi:10.1007/s11270-017-3480-8
- Moeini, B., Linford, M. R., Fairley, N., Barlow, A., Cumpson, P., Morgan, D., et al. (2022). Definition of a new (Doniach-Sunjic-Shirley) peak shape for fitting asymmetric signals applied to reduced graphene oxide/graphene oxide XPS spectra. *Surf. Interface Analysis* 54, 67–77. doi:10.1002/sia.7021
- Quilès, F., and Burneau, A. (2000). Infrared and Raman spectra of uranyl(VI) oxo-hydroxo complexes in acid aqueous solutions: a chemometric study. *Vib. Spectrosc.* 23, 231–241. doi:10.1016/S0924-2031(00)00067-9
- Rodríguez-Reinoso, F. (1998). The role of carbon materials in heterogeneous catalysis. *Carbon* 36, 159–175. doi:10.1016/s0008-6223(97)00173-5
- Sevilla, M., and Fuertes, A. B. (2009). The production of carbon materials by hydrothermal carbonization of cellulose. *Carbon* 47, 2281–2289. doi:10.1016/j.carbon.2009.04.026
- Su, Y., Wenzel, M., Paasch, S., Seifert, M., Doert, T., Brunner, E., et al. (2022). One-pot synthesis of brewer's spent grain-supported superabsorbent polymer for highly efficient uranium adsorption from wastewater. *Environ. Res.* 212, 113333. doi:10.1016/j.envres.2022.113333
- Titirici, M. M., Antonietti, M., and Baccile, N. (2008). Hydrothermal carbon from biomass: a comparison of the local structure from poly- to monosaccharides and pentoses/hexoses. *Green Chem.* 10, 1204–1212. doi:10.1039/b807009a
- Tong Thi, P., Ma, Z., Chen, D., and Zhang, Q. (2014). Pyrolysis characteristics and kinetics study of bamboo holo-cellulose using TG-FTIR. *J. Zhejiang a&f Univ.* 31, 495–501. doi:10.11833/j.jissn.2095-0756.2014.04.001
- Wegener, M., Eppinger, T., Baeumler, K., Kraume, M., Paschedag, A. R., and Baensch, E. (2009). Transient rise velocity and mass transfer of a single drop with interfacial instabilities-Numerical investigations. *Chem. Eng. Sci.* 64, 4835–4845. doi:10.1016/j.ces.2009.07.023
- Wu, X., Ba, Y., Wang, X., Niu, M., and Fang, K. (2018). Evolved gas analysis and slow pyrolysis mechanism of bamboo by thermogravimetric analysis, Fourier transform infrared spectroscopy and gas chromatography-mass spectrometry. *Bioresour. Technol.* 266, 407–412. doi:10.1016/j.biortech.2018.07.005
- Xiang, S., Cheng, W., Nie, X., Ding, C., Yi, F., Asiri, A. M., et al. (2018). Zero-valent iron-aluminum for the fast and effective U(VI) removal. *J. Taiwan Inst. Chem. Eng.* 85, 186–192. doi:10.1016/j.jtice.2018.01.039
- Xu, W., Zhang, W., Kang, J., and Li, B. (2019). Facile synthesis of mesoporous Fe-based MOFs loading bismuth with high speed adsorption of iodide from solution. *J. Solid State Chem.* 269, 558–565. doi:10.1016/j.jssc.2018.10.028

- Yang, H., Huang, L., Liu, S., Hou, M., Sun, K., and Sun, Y. (2017). Study on bamboo pyrolysis process and product characteristics. *Acta Energiæ Solaris Sin.* 38, 1431–1439.
- Yang, W., Peng, D., Kimura, H., Zhang, X., Sun, X., Pashameah, R. A., et al. (2022). Honeycomb-like nitrogen-doped porous carbon decorated with Co₃O₄ nanoparticles for superior electrochemical performance pseudo-capacitive lithium storage and supercapacitors. *Adv. Compos. Hybrid Mater.* 5, 3146–3157. doi:10.1007/s42114-022-00556-6
- Yu, J., Yuan, L., Wang, S., Lan, J., Zheng, L., Xu, C., et al. (2019). Phosphonate-Decorated covalent organic frameworks for actinide extraction: a breakthrough under highly acidic conditions. *J. Chin. Chem. Soc.* 003, 286–295. doi:10.31635/ccschem.019.20190005
- Yu, L. H., Falco, C., Weber, J., White, R. J., Howe, J. Y., and Titirici, M. M. (2012). Carbohydrate-derived hydrothermal carbons: a thorough characterization study. *Langmuir* 28, 12373–12383. doi:10.1021/la3024277
- Zanon Costa, C., Falabella Sousa-Aguiar, E., Peixoto Gimenes Couto, M. A., and Souza de Carvalho Filho, J. F. (2020). Hydrothermal treatment of vegetable oils and fats aiming at yielding hydrocarbons: a review. *Catalysts* 10, 843. doi:10.3390/catal10080843
- Zhang, S., Yuan, D., Zhang, Q., Wang, Y., Liu, Y., Zhao, J., et al. (2020). Highly efficient removal of uranium from highly acidic media achieved using a phosphine oxide and amino functionalized superparamagnetic composite polymer adsorbent. *J. Mater. Chem. A* 8, 10925–10934. doi:10.1039/d0ta01633k
- Zhao, W. H., Lin, X. Y., Cai, H. M., Mu, T., and Luo, X. G. (2017). Preparation of mesoporous carbon from sodium lignosulfonate by hydrothermal and template method and its adsorption of uranium(VI). *Industrial & Eng. Chem. Res.* 56, 12745–12754. doi:10.1021/acs.iecr.7b02854
- Zhu, L., and Zhong, Z. (2020). Effects of cellulose, hemicellulose and lignin on biomass pyrolysis kinetics. *Korean J. Chem. Eng.* 37, 1660–1668. doi:10.1007/s11814-020-0553-y



OPEN ACCESS

EDITED BY

Sanjeeb Mohapatra,
Delft University of Technology, Netherlands

REVIEWED BY

Nitish Venkateswarlu Mogili,
National Institute of Technology, India
Monika Dubey,
Indian Institute of Technology Roorkee, India
Arnab Ghosh,
Dong-A University, Republic of Korea

*CORRESPONDENCE

Owen Fenton,
✉ owen.fenton@teagasc.ie

RECEIVED 01 July 2024

ACCEPTED 03 September 2024

PUBLISHED 17 September 2024

CITATION

Fenton O, Daly K, Tuohy P, Cardiff J, Leach S,
Sifundza LS and Murnane J (2024) Spatial
distribution of available phosphorus in surface
road and trackway surface materials on a sheep
farm in Ireland.
Front. Environ. Sci. 12:1457970.
doi: 10.3389/fenvs.2024.1457970

COPYRIGHT

© 2024 Fenton, Daly, Tuohy, Cardiff, Leach,
Sifundza and Murnane. This is an open-access
article distributed under the terms of the
[Creative Commons Attribution License \(CC BY\)](https://creativecommons.org/licenses/by/4.0/).
The use, distribution or reproduction in other
forums is permitted, provided the original
author(s) and the copyright owner(s) are
credited and that the original publication in this
journal is cited, in accordance with accepted
academic practice. No use, distribution or
reproduction is permitted which does not
comply with these terms.

Spatial distribution of available phosphorus in surface road and trackway surface materials on a sheep farm in Ireland

Owen Fenton^{1*}, Karen Daly¹, Pat Tuohy², John Cardiff¹,
Simon Leach¹, Lungile Senteni Sifundza^{1,3} and John Murnane³

¹Teagasc, Environmental Research Centre, Wexford, Ireland, ²Teagasc, Animal and Grassland Research and Innovation Centre, Moorepark, Ireland, ³School of Engineering, University of Limerick, Limerick, Ireland

Farm roadway runoff is a high-risk source of pollution when connectivity with waters occurs. Nutrients in this runoff are dominated by fresh animal deposits, but recent dairy and beef farm studies showed that available phosphorus (P) accumulates in roadway surface material and can be lost in runoff. A current knowledge gap is to examine available P concentrations in unsealed roadway and trackway (non-maintained) network of a lowland sheep farm. The present study focused on a 45 ha farm stocked with 544 sheep in south-east Ireland. Ten locations were sampled along with the adjacent fields for available P (i.e., Morgan's P) and ancillary parameters (e.g., pH, total P and heavy metals) in December 2022. The first sampling location was on an aggregate roadway and the other nine were on trackways representing an older aggregate roadway network used by the flock but now covered with soil and grass. Results showed a distinct difference in surface material pH between roadway and trackway locations. Trackways had a pH that mimicked adjacent fields around the agronomic optimum for grassland of ~6.2. All sampling locations had elevated available P concentrations, ranging from 26.3 to 111.0 mg L⁻¹ (mean 62.8 mg L⁻¹), similar to the spatial distribution for dairy farms but above those found at beef farms previously studied. The highest available P concentrations were found in roadway and trackway sections adjacent to the farmyard. Other elevated sampling areas were on trackways (87.3 or 97.7 mg P L⁻¹) away from the farmyard where sheep are funnelled to pasture, stop to seek shade, urinate and defecate but do not graze. By contrast the average available P concentration for the surrounding fields was 8.4 mg L⁻¹ with a range of 2.7–15.9 mg L⁻¹. Two sampling areas combine to create a critical source area where a high available P source becomes visibly mobilised as runoff during rainfall, discharges into an open drainage ditch, which is then connected to a local stream. Breaking the pathway before runoff enters the open ditch could be a cheap and effective way of mitigating nutrient losses at these two locations.

KEYWORDS

agriculture, nutrient transfer continuum, critical source area, water quality, soil

1 Introduction

Previous international research on roadway runoff and its impacts on connected waters has largely focused on planning, building, and operating roadway networks in urban and rural environments (Gillis et al., 2022). Other research on characterization and mitigation of forest road and trackways has been well developed (Wemple and Jones, 2003). It is known that farm roadways and tracks contribute sediments and particulates to waterways (Adams et al., 2014). Some recent research has focused on roadway runoff from internal farm roadways (called laneways in New Zealand (Monaghan and Smith, 2012); farm tracks Australia (Adams et al., 2014) or stock lanes in EU (Lucci et al., 2010) trafficked by machinery and livestock (Sifundza et al., 2024). In all cases, contaminants originating from roadway runoff can be deposited to surfaces and may be bioaccumulated directly or partitioned to sediments, or dissolve in surface waters (Gillis et al., 2022). In temperate regions, nutrient loads lost in farm roadway runoff can have significant negative impacts on water quality and this has led to regulation of soiled water runoff. For example, in Ireland soiled roadway runoff is strictly regulated since 2021 and is prohibited from entering waters (e.g., dry ditches and streams). Article 17.20 states “There shall be no direct runoff of soiled water from farm roadways to waters from 1 January 2021. The occupier of such a holding shall comply with the minimum specification for farm roadways.” (Current specification S199 July 2020).

Temporal and spatial concentrations of phosphorus (P) stored in farm roadway surface materials as a source distinct from fresh urine and faeces deposited on the roadways is a new area of research. It has been shown that this source of P can be lost throughout the year (i.e., in open and closed periods when animals are outside and housed, respectively). These materials act as storage reservoirs for P, which can become available in runoff during rainfall events with (i.e., soiled runoff) or without (i.e., non-soiled runoff) the presence of animal wastes (Fenton et al., 2022).

Recent work on dairy and beef farms in the south-east of Ireland, investigated the spatial and temporal distribution of available P in surface roadway material (Fenton et al., 2022; Sifundza et al., 2024). In Fenton et al. (2022), the range of available P in roadway surface materials (to 1 cm depth and excludes fresh excreta) on a dairy farm during a spatial survey conducted at the end of the open period (i.e., period where livestock actively used the roadway) was 10–110 mg L⁻¹. The highest concentrations were found near farmyards, before underpasses and wherever animals slowed down due to roadway design and roadway features. In Sifundza et al. (2024), a temporal survey showed available P concentrations ranged from 15.9–101.4 mg L⁻¹ (includes open and closed periods) which was higher than on two neighbouring beef farms (4.1–24.4 mg L⁻¹). Temporal results showed that mean available P concentrations (5.4, 14.9, 13.4 mg L⁻¹ for dairy, beef farm 1 and beef farm 2, respectively) increased in the open period (from February to September), whereas mean concentrations (40.3, 10.4, 9.8 mg L⁻¹ for dairy, beef farm 1 and beef farm 2, respectively) declined over the closed period (October to January). On all farms examined, approximately 3 roadway locations were considered connected to surface waters forming a critical source area (CSA) (McDowell et al., 2024; Shore et al., 2014)

and therefore needed mitigation intervention. Typically, the installation of low cost diversion bars to divert runoff into a vegetated buffer (>3 m) or swale, changing the slope of the roadway away from waters towards a buffer or swale and minimising the nutrient source through stock management (e.g., increasing the flow of animal traffic minimises deposits) were all noted as possible ways to break the pathway thereby minimising chemical and ecological impacts (Boger et al., 2018; Fenton et al., 2021).

Consideration of available P concentrations of roadways and trackways within different farms accessed by animals is important as fresh faeces and urine patches are deposited from large numbers of animals both spatially and temporally on these pervious unsealed surfaces. To date, research has focused on the loads of nutrients in runoff delivered to waters from roadways, while presenting the P source stemming only from fresh materials, e.g., McDowell et al. (2020). This approach limits losses to the open period and does not consider losses from the storage of P in the roadway itself, which can be lost during the closed period in addition to the open period. It is therefore important to consider the spatial distribution of available P in roadway and trackway materials across the major farming types where animals access roadways on a regular or *ad hoc* basis. An understanding of this available P store will help with the management of this source and mitigation of this source in both open and closed periods in the farming calendar. Such knowledge will also be important for consideration of the contribution of roadway runoff at catchment scale.

In previous studies (Fenton et al., 2022; Sifundza et al., 2024), it was hypothesised for temperate climates that the mean spatial and temporal available P roadway material concentration would be greatest during the open period when animals trafficked the roadway network and highest where animal movement was impeded (e.g., at bends, at entrance or exit to farmyard, before underpasses). In addition roadway condition and width have an influence on cow flow, e.g., farm roadways should be at least 3.5 m wide (for a 50 cow herd) with another 0.5 m allowed for each additional 50 cows (Maher et al., 2023). Also it was hypothesised that the mean available P concentration would be larger on a dairy farm than beef farms due to the amount of time animals traffic roadways due to milking operations (morning and evening). The temperate climate allows for high-quality pasture production over a long growing season and the efficient utilisation of pasture is critical for profitability, and farm roadways are essential for rotational grazing systems (Maher et al., 2023). Results from Sifundza et al. (2024) which compared dairy and beef farms, showed that the mean available P concentration on dairy farms was up to 4 times higher than that of beef farms. Overall, the P concentrations on both dairy and beef farms followed the same trend over the months, whereby the P concentration declined over the winter months, i.e., December and January and increased in the open period. The present study examines for the first time the spatial nature of available P on a lowland sheep farm roadway and trackway network. It is often the case in the south east of Ireland that dairy, beef and sheep farms are in close proximity to each other and could be within the same catchment area. There is a similar number of dairy and sheep farms in Co. Wexford where the present study site is located, e.g., 836 sheep farms *versus* 1048 dairy farms (Central Statistics Office, 2024; Teagasc, 2024). It is hypothesised as the sheep

rarely use the roadway network but use the trackway system more frequently the available P concentration on the trackway system will be higher than that of the roadway. As the animal numbers can greatly exceed those of a dairy or beef system it is hypothesised that the mean and available P range spatially on the sheep farm in the closed period sampling event could be similar to a beef farm for the roadways and similar to a dairy farm for the trackways.

On sheep farms, internal roadways enable animals to access grazing areas but are less common and indeed less commonly used by animals when compared to other farming systems such as beef and dairy farms. After using the roadway network, sheep tend to stick to defined routes within fields to reach grazing areas where they spread out. However, original roadway networks on sheep farms can become covered by soil and grass over time, can slump and become degraded. Such trackways are still obvious linear features on the landscape and can be fenced off from the surrounding paddock or field. Farm roadways or trackways within these systems still can provide runoff connectivity with waters, thus, information pertaining to the pollutant concentrations needs to be collated. To date no study has investigated surface material available P concentrations on sheep farms along internal roadways or trackways. The present farm scale study examines available P concentrations in surface materials on a sheep farm to assess if a temporal survey is warranted. For that purpose, a sheep farm in south-east Ireland was selected, the roadway and trackway network was mapped and ten representative locations were sampled to 1 cm and tested for available P, pH and metals. In addition the adjacent fields were sampled as a comparison. Each sampling point was assessed with respect to its connectivity to surface waters (i.e., open drainage ditch or surface streams in the vicinity).

2 Materials and methods

2.1 Study farm

The 45 ha sheep farm used in the study is located in a lowland area in the south-east of Ireland, with average annual rainfall of 1,100 mm. The land slopes gently from the farm yard in one direction to a river bounding the farm. At the time of roadway sampling (December 2022) the number of sheep was as follows: breeding Ewes over 12 months of age ($n = 370$), breeding Rams over 12 months ($n = 12$), replacement Ewe lambs ($n = 162$). Average stocking density over the last number of years is 1.44 Livestock Units ha^{-1} . Sheep graze outside for most of the year and are only housed briefly during winter months. Movement around the roadway and trackway network is to access different grazing areas. Sheep also use the roadway or trackways for resting, seek shade by bounding trees but tend not to graze these areas due to the high level of urination and defecation.

In Ireland, typically a farm internal roadway is constructed by first removing the topsoil layer (10–15 cm), before placing stone (shale, limestone or sandstone) aggregate (20–30 cm layer) as the main construction material, overlain by a surface dust or blinding layer (25 mm layer of 0–4 mm in size). Each individual layer is rolled with a heavy vibrating roller to keep it in place. The crossfall on the roadway ensures drainage from the surface

and should be either a continuous crossfall of 1:25 or from center to both sides (Teagasc, 2021). Over time as animals and machinery use the roadway, soil from the fields may become incorporated into the dust layer. If not maintained or replaced these roadways become relics of the original network and turn into trackways, which become grassed over. On the farm, only one roadway fits the above description and runs with slope through location 1, 2, 3, 4, and 6 (Figure 1). All other roadways are orientated across slope and can be described as trackways. These trackways, (e.g., location 5, Figure 1) appear sunken from their original positions, are waterlogged and act as overland flow interceptors, which causes sediment to build up on the old roadway surfaces. Some old field boundaries were removed over time to make larger fields. Sample locations are presented in Figure 1 with a detailed description of each sampling location together with a photograph in Table 1.

2.2 Farm roadway, trackway and field sampling and analysis

At each location a duplicate roadway or trackway material sample of 200 g was taken from the top 1 cm, bagged and transported to the laboratory for analysis. Fresh animal deposits were avoided during the sampling process. Each field was sampled using a zig-zag sampling pattern covering the entire area as outlined in Teagasc (2020). All samples (i.e., roadway, trackway and field samples) were oven dried at 40°C, sieved through 2 mm sieve to remove debris and stored at room temperature before analysis. To determine available P, soil samples (3 g) were shaken for 30 min at room temperature with 15 mL Morgan's solution (sodium acetate and acetic acid and buffered at pH 4.8) at a ratio of 1:5 and then filtered (Morgan, 1941). The filtrates were then analysed for P concentration on the Lachat system using the principle of flow injection analysis. Two-gram (2 g) samples were also shaken on a reciprocating shaker for 5 min and the supernatant was filtered (0.45 μm) and tested for aluminium (Al), iron (Fe), calcium (Ca), boron (B), cobalt (Co), copper (Cu), manganese (Mn), and zinc (Zn) using a soil solution ratio of 1: 10 in Mehlich 3 reagent (0.2 M CH_3COOH + 0.25M NH_4NO_3 + 0.015 M NH_4F + 0.13 M HNO_3 + 0.001 M EDTA). Analyses was conducted on an Agilent 5100 ICP-OES.

3 Results

3.1 Spatial patterns of pH and heavy metals

The pH across the roadway and trackway locations is at or near the agronomic target for grassland of 6.2 (Table 2). Only the pH at the first roadway location (Figure 1) beside the farm yard and associated housing shed is elevated (i.e., pH 7.54 ± 0.09). These are similar for farm roadways as found by Sifundza et al. (2024) on a dairy and two beef farms in the south-east of Ireland (7.56 ± 0.30 , 7.89 ± 0.43 and 7.71 ± 0.49 , respectively). The mean pH at locations 2–10 (pH 6.30 ± 0.28) are similar to fields found within the current farm (6.04 ± 0.26).

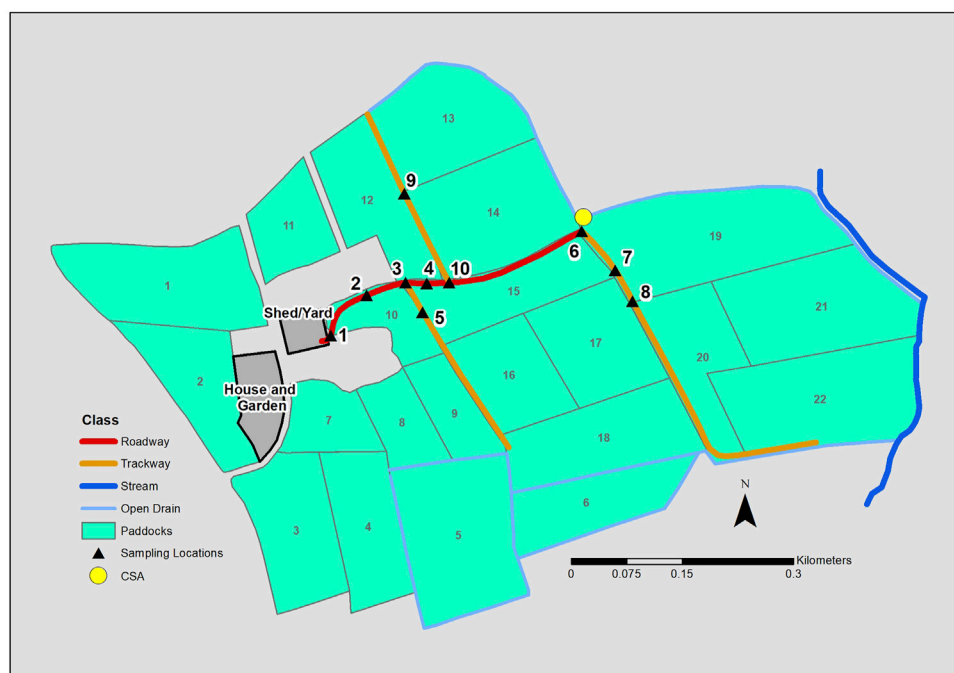


FIGURE 1
Sheep farm internal roadway and trackway system with location of shed/yard, sampling locations (1–10), field numbers, position of open drain and stream with critical source area (CSA) delivery point marked.

3.2 Spatial distribution of available P

Available P (Morgan's P) for roadways and trackways ranged from 26.3 to 111.0 mg L⁻¹ (Table 2; Figure 2 presents available P mean and standard deviation per location). The highest P concentrations were at location 1 (adjacent to the farmyard) and two locations 400 and 500 m away from the farmyard, respectively, i.e., location 7 (connected to open drainage ditch) and 10 (receives run-on from up-gradient areas) (See Table 1 for specific details). Another elevated area is at location 3 where sheep are slowed as they channel through a narrow fence gap. In contrast the average available P concentration for the surrounding fields was 8.4 mg L⁻¹ (Index 4) with a range 2.7–15.9 mg L⁻¹.

4 Discussion



4.1 pH and metal concentrations

The pH values found were similar to fields with mineral soils found on the farms studied by Sifundza et al. (2024) i.e., dairy, beef farm 1 and beef farm 2 with 6.2 ± 0.28 , 6.3 ± 0.35 , and 6.4 ± 0.27 , respectively. These results indicate that over time the older roadway network and trackways have become subsumed (as the landowner suggests) into the field network on the farm. The soil test results for the field samples are similar to locations 2–10. Metal concentrations for roadway and trackway locations are within similar ranges for dairy and beef farms studied in the south-east of Ireland and are indicative of an aggregate and soil mix. However, mean field soil metal concentrations are all lower than adjacent roadway and trackways, except for Fe.

4.2 Spatial distribution of available P





The spatial concentration range of available P was similar to that of a dairy farm roadway network (i.e. 15.9 ± 13.0 to 101.4 ± 61.1) but considerably higher than surface materials on roadways within the two beef farms (e.g., 6.31 ± 1.7 to 23.2 ± 9.6 mg L⁻¹) as reported by Sifundza et al. (2024). The lowest values here represent highest values on the beef farms. Source factors will be determined by the concentration of animals on the roadway as influenced by stocking rate, roadway density and animal type. For example, Marsden et al. (2020) document that sheep urinate 8–11 times a day (mean urine event volume recorded was 289 ± 14 mL) with an estimated daily urine production value of 2.77 ± 0.15 L urine sheep⁻¹ d⁻¹. By way of comparison, Ravera et al. (2015) document that cows (wintering system in New Zealand) urinate 8–12 times a day with 2.37 L per event indicating an estimated daily urine production value of between 18–30 L urine cow⁻¹ d⁻¹. The concentration of P in faeces and urine for cows and sheep is largely a product of the diet. It can vary across studies, e.g., McDowell (2006) tested cattle and sheep dung and found 5.5 and 8.0 g TP kg⁻¹ dry matter, respectively. Scott et al. (1972) examined the P content of faeces and urine in sheep fed with different diets and found 5.6 ± 0.3 g d⁻¹ in faeces and 0.3 ± 0.2 g d⁻¹ in urine (fed with roughage), which can increase if concentrates are introduced. In cows, dung P concentration ranges between 4 and 8 g P kg⁻¹ (McDowell, 2006; McDowell et al., 2020; Vadas et al., 2015) and dairy cows defecate 10.5 times cow⁻¹ d⁻¹, with only a fraction of this likely to be on roadways (Oudshoorn et al., 2008). Vebriyanti et al. (2022) showed that with varied diets the P concentration in cow urine ranged from 130.94 mg L⁻¹ \pm 4.11 – 156.67 mg L⁻¹ \pm 2.49 . Using the numbers

TABLE 1 General descriptions of the farm roadway sampling locations on the Sheep Farm with representative images.

Location	Description	Image
1	<div>Entrance/Exit of Farm Yard</div> <ul style="list-style-type: none">• After gateway, 5 m from farmyard• Stone aggregate roadway• Slight gradient, wide to narrow, straight, transition from field to yard• Obstruction to animal flow• Evidence of relatively high P loads from excreta, as movement of animals slows down	
2	<div>Roadway bend leaving Farm Yard</div> <ul style="list-style-type: none">• 30 m from farmyard• Slight gradient, bend, narrow, smooth surface• Previous aggregate internal roadway grassed over• Treeline continues with slope all the way down to location 6. Sheep can use this line for shading and resting	
3	<div>First narrow gap on roadway</div> <ul style="list-style-type: none">• After gateway• 100 m from farmyard• Gentle gradient, straight, narrow, rough uneven surface• High levels of excreta evident as sheep slow to move through narrow gap• Previous aggregate internal roadway grassed over	
4	<div>Straight section of roadway</div> <ul style="list-style-type: none">• Further down slope after location 3• 150 m from farmyard• Gentle gradient, wide, straight, smooth surface• Previous aggregate internal roadway grassed over• Facing location 6 in the distance	



(Continued on following page)

TABLE 1 (Continued) General descriptions of the farm roadway sampling locations on the Sheep Farm with representative images.

Location	Description	Image
5	<p>First trackway branching to right</p> <ul style="list-style-type: none"> • Offshoot of location 3 • 200 m from farmyard • Trackway along hedgerow with some shading • Trackway receives run-on from up-gradient fields • Significant camber and gradient towards field, wide, straight, smooth surface • Previous aggregate internal roadway grassed over. Obvious distinction from field 	
6	<p>Second narrow gap on roadway</p> <ul style="list-style-type: none"> • 350 m from farmyard • Obstructions to sheep flow due to narrow unevenly surfaced gap • Gentle gradient, narrow, straight, rough surface • Greater nutrient loads from excreta deposited at location, as movement of sheep slowed down • CSA (Figure 1). Roadway, trackway and field runoff connects with open drainage ditch, which delivers water to a stream • Maintenance of open ditch created bank, but evidence that this bank has been breached by runoff 	
7	<p>Second trackway branching to right</p> <ul style="list-style-type: none"> • 400 m from farmyard • Flat gradient, steep camber, wide, straight, grassed over surface • Gives sheep access to fields on left side • Previous aggregate internal roadway grassed over • Interaction of trackway runoff at this location with location 6 containing high P source. Locations 6 and 7 combine to form a CSA. 	
8	<p>Narrow gap on straight trackway</p> <ul style="list-style-type: none"> • 500 m from farmyard • Flat gradient, narrow, rough waterlogged surface • Along hedgerow with shading • Previous aggregate internal roadway grassed over • Puddle under gateway, prone to ponding as little relief available to drain off naturally • Not always used for stock as it is so wet. 	

(Continued on following page)

TABLE 1 (Continued) General descriptions of the farm roadway sampling locations on the Sheep Farm with representative images.

Location	Description	Image
9	<div>Straight trackway to gate at public road</div> <ul style="list-style-type: none">• 600 m from farmyard• Gentle gradient, wide, smooth grassed over surface• Access to fields on both sides• Previous aggregate internal roadway grassed over	
10	<div>T junction to internal road accessing public road</div> <ul style="list-style-type: none">• 500 m from farmyard• Gentle gradient, narrow, lots of evidence of receiving roadway runoff from up-gradient roadway sections, rough waterlogged surface• Ponding of water interacts with fields but not open drainage ditch• Previous aggregate internal roadway grassed over	

above for sheep urine the concentration of P could be as high as 108 mg L⁻¹ (0.3 g P d⁻¹/2.77 L d⁻¹). The number of sheep (Ewe, Rams and Lambs) on this farm at time of sampling was 544. This number coupled with the concentration of P and volumes in urine and faeces documented above gives an indication of daily loads deposited on the farm.

As the sheep are outside nearly all year (i.e., some housing in Winter months to protect fields from treading damage) and have access to all the roadway and trackway networks when grazing different parts of the farm, the concentrations found during the testing period herein (i.e., December) may be conservative and warrants a temporal study. For example, in the dairy and beef unit farm study of Sifundza et al. (2024) the mean available P concentration for December was 32.4 mg L⁻¹ (min: 6.5 and max: 67.7), and 10.8 mg L⁻¹ (min: 3.1 and max: 37.1), respectively. This month compares to the mean available P concentration for May was 64.5 mg L⁻¹ (min: 14.2 and max: 149.5) and 15.3 (min: 3.1 and max: 71.2), respectively. In reality for the dairy farm all locations except one were higher in available P concentration in May than in December. For the beef farm the vast majority of locations were higher in May with some staying the same. It could be hypothesized that sheep farm locations will also follow seasonal trends as with dairy and beef farms.

It appears that P losses in runoff (both surface and subsurface) from pasture-based livestock (cattle and sheep) farming areas will generally not exceed 2 kg TP ha⁻¹ year⁻¹ (Hooda et al., 2000). The problem here is that such losses do not have a negative economic

consequence to the landowner (equate to < 5% of nutrients applied) but can have large impacts on water quality. To put these numbers into perspective, phosphate impacts on water quality even at very low concentrations. The Environmental Quality Standard (EQS) for good status water bodies is 0.035 mg P L⁻¹ and 0.025 mg P L⁻¹ for high status water bodies. Therefore, as little as 1 kg P when present as phosphate, lost in roadway runoff will pollute approximately 29 million litres of water (NFGWS, 2020). As the wetting and drying cycle impacts the P concentration in sediments and soil and their subsequent release (Smith et al., 2023) a temporal survey of the road and trackway network is advised. This would match the approach of Fenton et al. (2022) whereby a spatial survey established the range of available P concentrations on a dairy roadway network and a follow-up study by Sifundza et al. (2024) established both the spatial and temporal trends of available P on the same roadway network.

Future work should consider other farm and animal types (e.g., pigs) that have access to roadways or trackways and examine the spatial and temporal nature of available P on those networks. In addition the influence of soil type may be important, e.g., mineral soils *versus* high organic soils. This could be a large difference for upland sheep farms where grazing occurs in upland areas on peat soils with little or no capacity to hold onto P. In addition an examination of the sampling and laboratory techniques would be beneficial. For example, the sampling depth of 1 cm may capture the highest concentrations of available P but other stores may be present

below this 1 cm layer. At present an agronomic test is being used to examine available P in a mixed material (aggregate and soil) and there could be other appropriate tests to examine P storage and loss dynamics in these materials. For example, Ezzati et al. (2020) examined source-sink P dynamics of sediment along an agricultural ditch network using equilibrium P concentrations (EPC₀) and developed sorption isotherms to examine the binding strength in these materials.

4.3 Connectivity of available P source with waters and potential management solutions

One area (combines locations 6–7) on the farm was identified as a CSA (Table 2). These CSAs are small areas of the farm and suitable for targeted mitigation (Doody et al., 2012). The delivery point to the open ditch is presented in Figure 1 and identified in the image of location 6 in Table 1 (yellow dot). The first contributing area is at location 7 where a high source in the surface materials could be mobilised during rainfall towards a connected open drainage ditch. Another area that contributes to the CSA is location 6, where connectivity exists with the open ditch and the available P source in the roadway materials is 41 mg L⁻¹.

In terms of environmental management across dairy *versus* beef *versus* sheep farms, as the regulation pertaining to roadway runoff on farms in Ireland covers all farm types, the onus is on the landowner to identify where runoff enters waters and to come up with a mitigation solution to “break the pathway” the soiled roadway runoff delivery point and waters. The number of connectivity points on a dairy farm seems to be consistent with approx. 10% of roadway sections in connectivity with waters (Maher et al., 2023; Rice et al., 2022). A similar number of connectivity points was also found by Sifundza et al. (2024) on both dairy and beef farms studied. So although the source concentration may be different (combination of available P from fresh and roadway materials) within a CSA across dairy, beef and sheep farms, environmental management through mitigation will still be needed.

The CSA concept refers to small areas of fields, farms or catchments. The best application of CSAs to target mitigation actions should be at such small areas but only where they account for most contaminant loss (McDowell et al., 2024). With respect to roadway and trackway runoff the contribution to overall P losses at farm and catchment scales has not been established and this needs further investigation and indeed consideration in future regulation and policy. At present all CSAs within the roadway and trackway network regardless of their contribution to overall catchment losses require environmental management through source minimization and mitigation.

Possible mitigation solutions for the present farm would be to prevent runoff from these areas entering the open ditch (considered water under current regulations in Ireland) by breaking the pathway. A suggestion would be installation of a diversion bar or to change the camber of the trackway towards the field or to bund the open drainage ditch. Options and costs of these mitigation measures are detailed in Fenton et al. (2021). It is important to note that waterlogged soils have the potential to release available P to a greater extent than the surrounding soils. This is the case along flow pathways, e.g., roadway or trackway runoff pathways which are constantly wetting and drying. The work of Smith et al. (2023) indicate that high soil profile saturation, low nitrate (NO₃⁻), and increased temperature induce P release, potentially via reductive dissolution. Without the buffering influence of NO₃⁻ in a soil profile, anaerobic conditions caused by inundation could cause a soil profile to become Fe- and Mn-reducing and release associated P. Therefore, the period of greatest risk is likely to be when saturation (i.e., anaerobia and reduction) overlaps with increasing temperatures. This established winter to spring as risky periods for P loss, due to the combination of: existing moisture; warmer temperatures; minimal rainfall quantities required to saturate the soil profile; and, NO₃⁻ is likely to be depleted via leaching from the soil. This again highlights why it is important to understand where saturation and wetting and drying cycles occurs on a given farm. For instance: in typically poorly-drained soils; in low-lying areas where flow from upslope would accumulate (e.g., locations 5 and 10); or on soils or roadways over poorly-permeable layers.

TABLE 2 Sample mean results for the spatial sampling in December 2022.

Location	pH	Morgan’s P	Total P	Morgan’s K	Al	B	Ca	Co	Cu	Fe	Mn	Zn
		mg L ⁻¹			mg kg ⁻¹							
1	7.54	111.00	256.66	344.00	30.92	0.07	4135.57	0.48	3.57	284.39	120.59	26.25
2	6.26	42.95	212.97	375.50	569.48	0.48	2986.36	0.38	3.56	318.05	80.32	21.52
3	6.86	79.60	274.89	573.50	491.60	1.00	2772.06	0.79	4.33	437.73	110.12	37.24
4	6.36	58.15	253.31	628.00	621.68	0.32	2292.91	0.61	2.81	346.11	107.62	14.67
5	6.30	48.45	272.31	488.50	642.72	0.96	2952.34	0.70	3.39	351.19	121.58	15.34
6	6.23	41.60	231.54	459.50	575.40	0.93	2443.63	0.78	3.91	468.73	121.37	22.82
7	6.10	87.35	415.97	575.00	559.46	1.36	3170.15	0.63	2.52	323.54	101.75	28.27
8	6.23	35.55	261.94	372.00	717.45	0.81	2127.20	0.49	3.48	449.34	88.95	9.21
9	5.87	26.30	140.29	272.50	514.32	0.50	2950.10	0.37	3.22	474.31	85.22	10.77
10	6.53	97.70	341.72	776.50	367.98	1.03	3419.97	0.73	3.33	386.01	119.05	23.50
Mean	6.43	62.87	266.16	486.50	509.10	0.75	2925.03	0.60	3.41	383.94	105.66	20.96

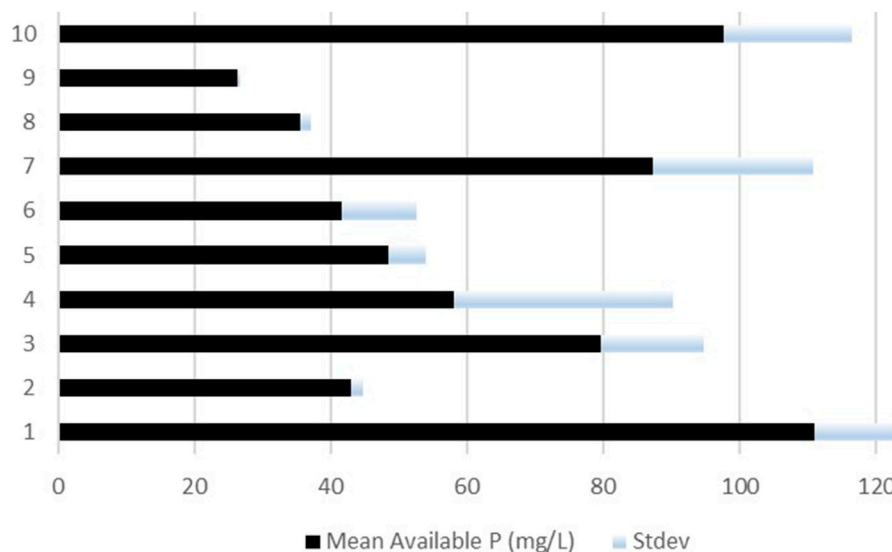


FIGURE 2
Mean available phosphorus (P) concentrations and standard deviation (stdev) for each sampling location.

5 Conclusion

Roadways and trackways used by sheep exhibited high concentrations of available P across the ten locations sampled and exhibited a different signature to that of field soil. Concentrations were above previously studied beef farms but on a par with dairy farms studied. One location was considered critical source areas (combination of locations 6–7), where a source from a soiled roadway runoff entered a dry open ditch connecting directly with a nearby stream. Mobilisation of roadway and trackway runoff to these delivery points occurs during rainfall events. These locations are in need of mitigation, e.g., installation of a diversion bar or establishment of a buffer area to break the pathway and block nutrients and sediment entering waters. As sheep have access to the entire roadway and trackway system throughout the year (apart for a brief winter housing period) the temporal distribution of available P on sheep farm roadways and trackways should be investigated and compared in lowland and upland areas.

Data availability statement

The original contributions presented in the study are included in the article/supplementary material, further inquiries can be directed to the corresponding author.

Author contributions

OF: Visualization, Validation, Supervision, Software, Resources, Project administration, Writing–review and editing, Writing–original draft, Methodology, Investigation, Funding acquisition, Formal Analysis, Data curation, Conceptualization. SL: Writing–review and editing, Visualization, Investigation, Formal Analysis, Data curation. KD: Funding acquisition, Writing–review and editing, Resources, Formal Analysis. PT: Funding acquisition, Writing–review and

editing, Methodology, Formal Analysis. JC: Investigation, Data curation, Writing–review and editing. LS: Writing–review and editing. JM: Writing–review and editing, Visualization, Methodology, Investigation, Formal Analysis.

Funding

The author(s) declare that financial support was received for the research, authorship, and/or publication of this article. The funding for the present project was under the Teagasc core-funded ROAD-READY project.

Acknowledgments

Special thanks goes to farm and laboratory staff members for their time, advice and patience and to those who helped with training and testing of samples.

Conflict of interest

The authors declare that the research was conducted in the absence of any commercial or financial relationships that could be construed as a potential conflict of interest.

Publisher's note

All claims expressed in this article are solely those of the authors and do not necessarily represent those of their affiliated organizations, or those of the publisher, the editors and the reviewers. Any product that may be evaluated in this article, or claim that may be made by its manufacturer, is not guaranteed or endorsed by the publisher.

References

- Adams, R., Arafat, Y., Eate, V., Grace, M. R., Saffarpour, Sh., Weatherley, A. J., et al. (2014). A catchment study of sources and sinks of nutrients and sediments in south-east Australia. *J. Hydrology* 515, 166–179. doi:10.1016/j.jhydrol.2014.04.034
- Boger, A. R., Ahiablame, L., Mosase, E., and Beck, D. (2018). Effectiveness of roadside vegetated filter strips and swales at treating roadway runoff: a tutorial review. *Environ. Sci. Water Res. & Technol.* 4 (4), 478–486. doi:10.1039/c7ew00230k
- Central Statistics Office (2024). Census of agriculture 2020. Available at: <https://www.cso.ie/en/releasesandpublications/ep/p-coa/censusofagriculture2020-preliminaryresults/livestock/>.
- Doody, D. G., Archbold, M., Foy, R. H., and Flynn, R. (2012). Approaches to the implementation of the Water Framework Directive: targeting mitigation measures at critical source areas of diffuse phosphorus in Irish catchments. *J. Environ. Manage* 93 (1), 225–234. doi:10.1016/j.jenvman.2011.09.002
- Ezzati, G., Fenton, O., Healy, M. G., Christianson, L., Feyereisen, G. W., and Thornton, S. (2020). Impact of P inputs on source-sink P dynamics of sediment along an agricultural ditch network. *J. Environmen. Manage.* 257, 109988.
- Fenton, O., Rice, P., Murnane, J., Tuohy, P., and Daly, K. (2022). Dairy farm roadway surface materials as a P-source within the nutrient transfer continuum framework. *Front. Environ. Sci.* 10, 878166. doi:10.3389/fenvs.2022.878166
- Fenton, O., Tuohy, P., Daly, K., Moloney, T., Rice, P., and Murnane, J. G. (2021). A review of on-farm roadway runoff characterisation and potential management options for Ireland. *Water Air Soil Pollut.* 232, 89. doi:10.1007/s11270-021-05027-0
- Gillis, P. L., Parrott, J. L., and Helm, P. (2022). Environmental fate and effects of road run-off. *Arch. Environ. Contam. Toxicol.* 82 (2), 159–161. doi:10.1007/s00244-021-00906-3
- Hooda, P. S., Edwards, A. C., Anderson, H. A., and Miller, A. (2000). A review of water quality concerns in livestock farming areas. *Sci. Total Environ.* 250, 143–167. doi:10.1016/s0048-9697(00)00373-9
- Lucci, G. M., McDowell, R. W., and Condon, L. M. (2010). Potential phosphorus and sediment loads from sources within a dairy farmed catchment. *Soil Use Manag.* 26, 44–52. doi:10.1111/j.1475-2743.2009.00247.x
- Maher, P., Egan, M., Murphy, M. D., and Tuohy, P. (2023). Assessment of the current performance of grazing infrastructure across Irish dairy farms. *J. Dairy Sci.* 106, 4759–4772. doi:10.3168/jds.2022-22799
- Marsden, K. A., Lush, L., Holmberg, J. A., Whelan, M. J., King, A. J., Wilson, R. P., et al. (2020). Sheep urination frequency, volume, N excretion and chemical composition: implications for subsequent agricultural N losses. *Agric. Ecosyst. Environ.* 302 (2020), 107073. doi:10.1016/j.agee.2020.107073
- McDowell, R. W. (2006). Contaminant losses in overland flow from cattle, deer and sheep dung. *Water, Air, Soil Pollut.* 174, 211–222. doi:10.1007/s11270-006-9098-x
- McDowell, R. W., Daly, K., and Fenton, O. (2020). Mitigation of phosphorus, sediment and *Escherichia coli* losses in runoff from a dairy farm roadway. *Ir. J. Agric. Food Res.* 59. doi:10.15212/ijafr-2020-0117
- McDowell, R. W., Kleinman, P. J. A., Haygarth, P., McGrath, J. M., Smith, D., Heathwaite, L., et al. (2024). A review of the development and implementation of the critical source area concept: a reflection of Andrew Sharpley's role in improving water quality. *J. Environ. Qual.* doi:10.1002/jeq2.20551
- Monaghan, R. M., and Smith, L. C. (2012). Contaminant losses in overland flow from dairy farm laneways in southern New Zealand. *Agric. Ecosyst. Environ.* 159, 170–175. doi:10.1016/j.agee.2012.07.022
- Morgan, M. F. (1941). Chemical soil diagnosis by the Universal soil testing system. Connecticut, USA: Connecticut Agricultural Experimental Station. *Bulletin* 450.
- NFGWS (2020). *A handbook for source protection and mitigation actions for farming*. Dublin, Ireland : Published by the National Federation of Group Water Schemes. Available at: www.nfgws.ie.
- Oudshoorn, F. W., Kristensen, T., and Nadimi, E. S. (2008). Dairy cow defecation and urination frequency and spatial distribution in relation to time-limited grazing. *Livest. Sci.* 113, 62–73. doi:10.1016/j.livsci.2007.02.021
- Rice, P., Daly, K., Tuohy, P., Murnane, J. G., Nag, R., and Fenton, O. (2022). Evaluating connectivity risk of farm roadway runoff with waters-Development and sensitivity analysis of a semi quantitative risk model. *Scie. Total Environ.* 851, 158114.
- Ravera, B. L., Bryant, R. H., Cameron, K. C., Di, H. J., Edwards, G. R., and Smith, N. (2015). Use of a urine meter to detect variation in urination behaviour of dairy cows on winter crops. *Proc. N. Z. Soc. Animal Prod.* 75, 84–88.
- Scott, D. (1972). Excretion of phosphorus and acid in the urine of sheep and calves fed either roughage or concentrate diets. *Quarter. J. Experimen. Physiol.* 57,, 379–392.
- Shore, M., Jordan, P., Mellander, P.-E., Kelly-Quinn, M., Wall, D. P., Murphy, P. N. C., et al. (2014). Evaluating the critical source area concept of phosphorus loss from soils to water-bodies in agricultural catchments. *Sci. Total Environ.* 490, 405–415. doi:10.1016/j.scitotenv.2014.04.122
- Sifundza, L. S., Murnane, J., Daly, K., Lopez-Sangil, L., Leach, S., Tuohy, P., et al. (2024). Phosphorus in farm roadway substrates: contrasting spatial and temporal patterns in dairy and beef farms. *Front. Environ. Sci.* 12, 1405378. doi:10.3389/fenvs.2024.1405378
- Smith, G. J., McDowell, R. W., Daly, K., hUallacháin, D. Ó., Condon, L. M., and Owen, F. (2023). Factors controlling shallow subsurface dissolved reactive phosphorus concentration and loss kinetics from poorly drained saturated grassland soils. *J. Environ. Qual.* 52, 355–366. doi:10.1002/jeq2.20442
- Teagasc (2020). in *Major & micro nutrient advice for productive agricultural crops* Editors D. P. Wall and M. Plunkett
- Teagasc (2021). Building a farm roadway. Available at: <https://www.teagasc.ie/news-events/daily/dairy/building-a-farm-roadway.php> (Accessed).
- Teagasc (2024). National farm survey small farms report 2022. Available at: <https://www.teagasc.ie/publications/2024/national-farm-survey-small-farms-report-2022.php> (Accessed May, 2024).
- Vadas, P. A., Busch, D. L., Powell, J. M., and Brink, G. E. (2015). Monitoring runoff from cattle-grazed pastures for a phosphorus loss quantification tool. *Agric. Ecosyst. & Environ.* 199, 124–131. doi:10.1016/j.agee.2014.08.026
- Vebriyanti, E., Arief, I. I., and Dewi, S. P. (2022). Utilization of cow urine waste for the manufacture of urine as a form of environmentally friendly dairy farming business. *IOP Conf. Ser. Earth Environ. Sci.* 950, 012028.
- Wemple, B. C., and Jones, J. A. (2003). Runoff production on forest roads in a steep, mountain catchment. *Water Resour. Res.* 39 (8), 1220. doi:10.1029/2002wr001744



OPEN ACCESS

EDITED BY

Mengyang Liu,
City University of Hong Kong, Hong Kong, SAR
China

REVIEWED BY

Neha Tyagi,
Indian Institute of Technology Delhi, India
Manjari Mishra,
Stanford University, United States

*CORRESPONDENCE

Chang-Beom Park,
✉ changbeom.park@kitox.re.kr

[†]These authors have contributed equally to this work on this work

RECEIVED 13 July 2024

ACCEPTED 06 September 2024

PUBLISHED 18 September 2024

CITATION

Zee S, Hyun M, Sim H-J, Kim K, Kang J-C and Park C-B (2024) Cocktail effects of clothianidin and imidacloprid in zebrafish embryonic development, with high and low concentrations of mixtures.
Front. Toxicol. 6:1464069.
doi: 10.3389/ftox.2024.1464069

COPYRIGHT

© 2024 Zee, Hyun, Sim, Kim, Kang and Park. This is an open-access article distributed under the terms of the [Creative Commons Attribution License \(CC BY\)](https://creativecommons.org/licenses/by/4.0/). The use, distribution or reproduction in other forums is permitted, provided the original author(s) and the copyright owner(s) are credited and that the original publication in this journal is cited, in accordance with accepted academic practice. No use, distribution or reproduction is permitted which does not comply with these terms.

Cocktail effects of clothianidin and imidacloprid in zebrafish embryonic development, with high and low concentrations of mixtures

Seonggeun Zee^{1,2,3†}, Moonjung Hyun^{4†}, Hee-Jung Sim¹, Kanghee Kim¹, Ju-Chan Kang² and Chang-Beom Park^{1*}

¹Environmental Exposure and Toxicology Research Center, Korea Institute of Toxicology (KIT), Jinju, Republic of Korea, ²Department of Aquatic Life Medicine, Pukyong National University Graduate School, Busan, Republic of Korea, ³Food Safety Risk Assessment Division, National Institute of Food and Drug Safety Evaluation, Cheongju, Republic of Korea, ⁴Bioenvironmental Science and Toxicology Division, Gyeongnam Branch Institute, Korea Institute of Toxicology (KIT), Jinju, Republic of Korea

There is growing concern that sprayed neonicotinoid pesticides (*neonics*) persist in mixed forms in the environmental soil and water systems, and these concerns stem from reports of increase in both the detection frequency and concentration of these pollutants. To confirm the toxic effects of *neonics*, we conducted toxicity tests on two *neonics*, clothianidin (CLO) and imidacloprid (IMD), in embryos of zebrafish. Toxicity tests were performed with two different types of mixtures: potential mixture compounds and realistic mixture compounds. Potential mixtures of CLO and IMD exhibited synergistic effects, in a dose-dependent manner, in zebrafish embryonic toxicity. Realistic mixture toxicity tests that are reflecting the toxic effects of mixture in the aquatic environment were conducted with zebrafish embryos. The toxicity of the CLO and IMD mixture at environmentally-relevant concentrations was confirmed by the alteration of the transcriptional levels of target genes, such as cell damage linked to oxidative stress response and thyroid hormone synthesis related to zebrafish embryonic development. Consequently, the findings of this study can be considered a strategy for examining mixture toxicity in the range of detected environmental concentrations. In particular, our results will be useful in explaining the mode of toxic action of chemical mixtures following short-term exposure. Finally, the toxicity information of CLO and IMD mixtures will be applied for the agricultural environment, as a part of chemical regulation guideline for the use and production of pesticides.

KEYWORDS

Clothianidin, Imidacloprid, binary mixtures, developmental toxicity, zebrafish embryos

Abbreviations: ahr2, Aryl hydrocarbon receptor; cyp1a1 and cyp1b1, cytochrome P450 subunits; CLO, clothianidin; IMD, imidacloprid; nAChRs, nicotinic acetylcholine receptors; neonics, neonicotinoid pesticides; nrf1a and nrf2a, nuclear factor erythroid 2-related factor; p53, proto-oncogene; tsh- β , thyroid stimulating hormone beta; thraa and thrb, thyroid hormone receptor alpha and beta.

1 Introduction

Neonicotinoid pesticides (*neonics*) strongly bind to postsynaptic nicotinic acetylcholine receptors (*nAChRs*), which are mainly distributed in the central nervous system of insects, resulting in a variety of neurotoxic symptoms, such as convulsions, paralysis, and ultimately death (Casida and Durkin, 2013; Morrissey et al., 2015; Van der Sluijs et al., 2015). Because of the effectiveness of *neonics* against insect pests, the production and use of *neonics* have continuously increased to the point that they are the most widely used pesticides in the agricultural environment (Douglas and Tooker, 2015; Simon-Delso et al., 2015; Sparks, 2013). However, with increasing application of *neonics* in cultivated land, the environmental threat has also increased, and the concentration of *neonics* in soil has been reported to range from 0.4 to 13.28 ng/g in monitoring samples from North America and Europe (Wood and Goulson, 2017). With an increase in the concentration and toxic effects of *neonics*, which are considered emerging pollutants, the European Union (EU) and the United States have imposed sanctions to curtail agricultural applications of *neonics*, with the aim of reducing the health risks stemming from contamination in soil- and aquatic environments (European Food Safety Authority, 2013; United States Environmental Protection Agency, 2020). However, because there are still no regulations for environmental exposure to *neonics*, their production and use have continued in several East Asian countries (Chen et al., 2019; Christen et al., 2018). Furthermore, the sprayed *neonics* can migrate from the terrestrial to aquatic environments via natural routes, such as rainfall, meltwater, and polluted dust. Indeed, *neonics* have been detected in surface water, at concentration ranging from 0.13 to 0.63 ng/mL (Botías et al., 2015; Hladik and Kolpin, 2016; Limay-Rios et al., 2016; Main et al., 2016). Thus, to clearly understand the eco-health risks of *neonics* used in agricultural, an assessment of the toxic effects of *neonics* in both terrestrial- and aquatic environments is required.

Clothianidin (CLO) and imidacloprid (IMD) are believed to be the most widely used *neonics* worldwide (Miles et al., 2017; Woodward et al., 2022). CLO and IMD can be directly introduced into the terrestrial environment during the application season before the harvest of agricultural products (Struger et al., 2017), and their release at high concentrations into aquatic environments is possible due to their high solubility and slow rate of chemical decomposition (Morrissey et al., 2015). For example, in soil samples from agricultural land in the United States, CLO at concentrations of 0.02–13.6 ng/g and IMD at 0.09–10.7 ng/g were detected at the time of application (Jones et al., 2014). In term of water pollution, concentrations of *neonics* as high as 59–61 ng/L (CLO) and 70–149 ng/L (IMD) have been found in water samples from vicinity of wastewater treatment plants in the United States (Sadaria et al., 2016).

Generally, CLO and IMD residues that accumulated on the plant surface or soils after spraying on agricultural environment can mainly transported into the surface water by precipitation or runoff. Interestingly, CLO and IMD were detected in 100% of the runoff samples from agricultural environment in the Salinas Valley, California, simultaneously. The detected concentrations were varied 32–576 ng/L for CLO and 11–274 ng/L for IMD after seed treatment and their concentrations were elevated from 4,877 ng/L in runoff

samples after drench treatment (Woodward et al., 2022). These reports indicate that CLO and IMD residues are existed the form of chemical mixture in soil and aquatic environment. Indeed, the measured concentrations of CLO and IMD in the mixed form were approximately 1:1 in soil and aquatic environments (Bonmatin et al., 2015; Sánchez-Bayo et al., 2016). These results are not irrelevant the increase of health risks of co-exposure to CLO and IMD in both soil and aquatic environment (Sánchez-Bayo et al., 2016; Simon-Delso et al., 2015). For this reason, the toxic effects of pesticide mixtures, including *neonics* mixtures, have become an important issue in the field of environmental health. In previously studies, acute and chronic exposure to different combinations of CLO and IMD has been shown to have a dose-dependent synergistic toxic effect on bloodworm larvae (Maloney et al., 2017; 2018). However, although aquatic organisms may be directly exposed to a mixture of CLO and IMD at high concentrations during the pesticide spraying period, the information of toxicity caused by the combination of CLO and IMD at environmental concentrations is insufficient.

The objective of this study is to assess the mixture toxicity of CLO and IMD at environmental concentrations reflecting both low and high concentrations (e.g., from ng/mL to µg/mL) during the intensive spraying season in agricultural lands. To confirm the mixture toxicity of CLO and IMD at environmental concentrations, zebrafish embryos were selected as test model organisms. Because developmental defects caused by exposure to mixtures of CLO and IMD in zebrafish embryos indicate non-negligible ecological risks at the individual and the population level (Embry et al., 2010). To ascertain the developmental toxicity of mixtures of CLO and IMD, which are dependent on exposure levels (e.g., mixed concentrations), the toxicity tests using zebrafish embryos were conducted with mixtures of CLO and IMD at different exposure levels through the intrinsic toxicity of a single chemical. In this study, we report differences in toxicity between mixture compounds that is potential mixtures based on the effective concentration of a single chemical and realistic mixtures, which are based on actual measured environmental concentrations. The potential toxic effects in zebrafish embryonic development were quantified in terms of the degree of alterations of target genes expression, namely cell damage and thyroids imbalance.

2 Material and methods

2.1 Target chemicals

Clothianidin (CLO, CAS no. 210880-92-5, >98%) and imidacloprid (IMD, CAS no. 138261-41-3, >98%) were purchased from Sigma-Aldrich (St. Louis, MO, United States). Stock solutions were prepared in dimethyl sulfoxide (DMSO; Sigma-Aldrich, St. Louis, MO, United States). ≤ 1% (v/v) DMSO was used as solvent control for the toxicity tests. Because there was not significant different between the developmental toxicity of zebrafish, including the activation of stress response, when compared to 0.1% DMSO exposed group with the control group through the previous study (Xiong et al., 2017).

TABLE 1 Effective concentrations (ECx) of clothianidan (CLO) and imidacloprid (IMD) in zebrafish at the embryo-larva stage after exposure for 6 days. The 95% confidence limits (95% CI) were calculated using the probit method (CETIS program version 1.8.7.15, Tidepool Scientific Software, United States).

Toxicity test	EC5 (95% CI)	EC15 (95% CI)	EC25 (95% CI)	EC50 (95% CI)
CLO (µg/mL)	65.28 (N.C.–104.61)	255.72 (224.61–289.12)	292.89 (247.77–332.07)	411.11 (345.75–535.54)
IMD (µg/mL)	60.80 (N.C.–108.36)	145.69 (113.89–158.99)	175.04 (146.25–196.54)	267.96 (205.83–294.60)

N.C., no calculation.

2.2 Single toxicity tests for zebrafish embryos

Zebrafish embryos were obtained from adult zebrafish continuously sub-cultured in Korea Institute Toxicology Laboratory, Republic of Korea and were maintained at 26°C ± 1°C in a climate chamber (16 h daylight: 8 h darkness) until use for toxicity tests (Park et al., 2022). To confirm the intrinsic toxicity of CLO and IMD in zebrafish embryos, 20 zebrafish embryos in each exposure group were used for single toxicity tests at nine nominal concentrations [0 (DMSO >0.1%), 7.8, 15.6, 31.3, 62.5, 125, 250, 500, and 1,000 µg/mL] in a sterilized cell culture 6-well plate filled with 15 mL working solution (Effendorf, Hamburg, Germany). At 6 days after exposure, embryonic toxicity (%) was scored as follows: [embryonic toxicity (%) = lethality (dead embryo + dead larva) + abnormality (unhatched eggs + abnormal larva)/initial embryos × 100]. Developmental abnormality of zebrafish was investigated based on apical phenotypic observation, such as coagulated embryos, lack of somite formation, non-detachment of the tail, and lack of heartbeat for 6 days after exposure (OECD, 2013). Embryonic toxicity (%) was used for estimating the effective concentration values (ECx) for each chemical and 95% confidence limits, by concentration-response curves (CETIS program version 1.8.7.15, Tidepool Scientific Software, United States) (Park et al., 2022).

2.3 Mixture toxicity tests for zebrafish embryos

Based on the intrinsic toxicity levels of each chemical in and zebrafish embryos, mixture toxicity tests were conducted with two different mixture compounds: a potential mixture compounds that can occur high concentrations during pesticide spraying period or long-term exposure, and realistic mixture compounds that reflect environmental concentrations.

All toxicity tests were approved by the Institutional Animal Care and Use Committee (IACUC) in Korea Institute of Toxicology, Republic of Korea (IACUC no. 2006-0003).

2.3.1 Potential mixture toxicity tests

Both CLO and IMD, individually, were found to be toxic to zebrafish embryos at high concentrations, namely 500 and 1,000 µg/mL (Supplementary Figure S1). Potential mixture toxicity tests for zebrafish embryos were designed with ECx values estimated from a single toxicity test (Table 1; Supplementary Figure S1), which involved a range from the lowest effective concentration (EC5) to the half effective concentration (EC50) for each target chemical. Potential mixture toxicity tests in the embryonic stages of zebrafish

were performed under the same conditions as the single toxicity tests, and the mixing ratios of CLO and IMD were fixed at 1:1, reflecting the detected mixing ratio in the natural environment (Bonmatin et al., 2015; Sánchez-Bayo et al., 2016).

2.3.2 Realistic mixture toxicity tests

To verify the developmental effects in zebrafish embryos caused by exposure to realistic mixtures, mixture toxicity tests with zebrafish embryos were performed at a range of environmentally relevant concentrations, and three exposure concentrations at a 1:1 mixing ratio (i.e., 1, 10, and 100 ng/mL of each chemical). The exposure concentrations and mixing ratios of CLO and IMD in the mixtures reflected actual measured environmental concentrations (Bonmatin et al., 2015; Sánchez-Bayo et al., 2016). In addition, to examine the toxicity pathway related to embryonic development, zebrafish embryos exposed to mixtures of CLO and IMD were sampled at 6 days after exposure and placed in a sterilized 1.5 mL microtube with 100 µL of RNAlater™ (Thermo Fisher Scientific, Massachusetts, United States) and were stored at –40°C until use in the expression change analysis of target genes. Realistic mixture toxicity tests using zebrafish embryos were performed under the same conditions as the single-toxicity tests.

2.3.3 Residual concentrations of CLO and IMD in the test media

The concentrations of CLO and IMD in the zebrafish test media were analyzed using high performance liquid chromatography–tandem mass spectrometry (HPLC-MS/MS) with an Agilent 6,420 Triple Quadrupole MS instrument connected to an Agilent 1,260 Infinity HPLC system containing a binary pump, autosampler, and degasser (Agilent, Santa Clara, CA, United States). Chromatographic separation was performed using a Poroshell 120 EC-C18 column (2.1 × 100 mm, 2.7 µm particle size; Agilent, Santa Clara, CA, United States) connected to a C18 guard column (Phenomenex, Torrance, CA, United States). Mobile phase A was 0.1% formic acid in water, and mobile phase B was acetonitrile. HPLC was run using a linear gradient as follows: 0–5 min, 20%–40% B; 5–7 min, 40%–70% B. The column was then equilibrated with 20% B for 4.9 min. The flow rate was set at 0.4 mL/min, and the injection volume was set at 10 µL. MS analysis was conducted in the positive ion mode using electrospray ionization. The MS conditions were optimized as follows: capillary voltage, 4000 V; sheath gas temperature, 370°C; sheath gas flow, 12 L/min; gas temperature, 350°C; gas flow, 8 L/min; nebulizer gas pressure, 40 psi; fragmentor voltage, 75 V for CLO and 80 V for IMD. On the selected reaction monitoring mode (SRM), the collision energy (CE) and selected reaction monitoring channels for the analytes were as follows: CLO, CE

10 V and m/z 250.0→169.0; CLO-d3, CE 10 V and m/z 253.0→172.0; IMD, CE 12 V and m/z 256.0→209.0; IMD-d4, CE 10 V and m/z 260.1→213.1. HPLC-MS/MS data were collected and processed using MassHunter Workstation Software Qualitative Analysis (ver. B.06.00, Agilent, Santa Clara, CA, United States). The relative error (RE) values for the residual concentration of each target chemical were calculated as: $RE (\%) = \frac{(\text{mean concentration of media samples} - \text{nominal concentration})}{\text{nominal concentration}} \times 100$.

2.3.4 Transcriptional alteration of target genes

To examine the transcriptional alteration of target genes linked to zebrafish embryonic development, The total RNA from 20 zebrafish embryos was extracted using a RNeasy Mini kit (Qiagen, Hilden, Germany), following the manufacturer's instructions. The total RNA concentration was measured spectrophotometrically at 260/280 nm using a Gen5™ spectrophotometer (BioTek®, Winooski, VT, United States). First-strand cDNA was synthesized with 0.5 µg of total RNA using a Superscript III First-Strand Synthesis System kit (Thermo Fisher Scientific, Vilnius, Lithuania) according to the manufacturer's manual.

The primer sequences for target genes were designed to use for quantitative real-time polymerase chain reaction (qRT-PCR): namely aryl hydrocarbon receptor 2 (*ahr2*), cytochrome P450 monooxygenases (i.e., *cyp1a1* and *cyp1b1*), nuclear factor erythroid 2-related factors (i.e., *nrf1a* and *nrf2a*), tumor suppressor gene (*p53*), thyroid stimulating hormone beta subunit (*tsh-β*), and thyroid hormone receptors (i.e., *thraa* and *thrb*) (Supplementary Table S1) (Fan et al., 2018; Liu et al., 2011; Ren et al., 2020; Williams et al., 2013). The qRT-PCR was performed using a Thermal Cycler Dice® Real Time System III (Takara, Tokyo, Japan) using the Go Taq® qPCR Master Mix (Promega, Madison, WI, United States). The qRT-PCR reactions were conducted as follows: an initial hot-start activation step at 95°C for 2 min, followed by 40 cycles at 95°C for 15 s and 60°C for 60 s. Melting curve analyses were performed to optimize primers for qRT-PCR performance. These transcript abundances for the target genes were normalized to a housekeeping gene (i.e., *β-actin*). The relative quantification of target genes expression was calculated using the $2^{-\Delta\Delta CT}$ method (Park et al., 2022).

2.4 Statistical analysis

All data are represented as mean ± standard error of the mean (SE). Data comparisons between the exposure groups in the toxicity tests were conducted using the *post hoc* least squares distance (LSD) test method of one-way analysis of variance (ANOVA) (SigmaPlot version 12.5; Systat Software, Inc., San Jose, CA, United States). *P*-values less than 0.05 ($P < 0.05$) were considered statistically significant.

To determine the combined effect for binary mixtures of CLO and IMD in zebrafish embryo toxicity tests, we used the combination index (CI) equation, which is given by $CI = (D)_1/(Dx)_1 + (D)_2/(Dx)_2$ for a combination of two substances; where $(Dx)_1$ and $(Dx)_2$ in the

denominator are the dose of each substance “alone” that provides x % effect (EC_x), and $(D)_1$ and $(D)_2$ in the numerator are the dose of each substance in the mixture that provides x % effect (Chou, 2011). The CI value was calculated with regard to CompuSyn software (ComboSyn, Inc., NJ, United States), and the isobologram was plotted using sigmaplot software (version 15.0, Systat Software, Inc., Canada).

3 Results and discussion

In this study, we hypothesized that exposure to a mixture of CLO and IMD could induce developmental toxicity in aquatic organisms through cumulative exposure to low concentrations (non-lethality); i.e., the lowest observed effect concentration. To verify our hypothesis, binary mixture toxicity tests for CLO and IMD were performed with zebrafish embryos under mixture combinations from half effective concentrations for each chemical (potential mixture toxicity) to environmental concentrations (realistic mixture toxicity).

3.1 Potential mixture toxicity of CLO and IMD

In binary mixture toxicity tests, owing to the effective concentrations of CLO and IMD, the combined effects of CLO and IMD on embryonic toxicity development in zebrafish were observed. In potential mixture toxicity tests, the mixtures of CLO and IMD based on EC_x values for each chemical (i.e., 60–400 µg/mL of CLO and IMD) showed higher toxicity than single chemical exposure, and elevated with exposure concentrations (Figure 1A). To confirm the combined effect for binary mixtures of CLO and IMD, the concept of CI equation was introduced based on the median-effect equation of the law of mass action; where $CI = 1$, <1 , and >1 indicate additive effect, synergism, and antagonism, respectively (Chou, 2011). In this study, CI value for binary mixture of CLO and IMD values was <1 , and these results indicated that binary mixtures of CLO and IMD have synergistic effect in zebrafish embryonic toxicity with a dose-dependent manner (Figure 1B) (Maloney et al., 2017; 2018). Our results confirmed that combinations of potential toxicity test of mixtures may amplify the toxic effects of single CLO and IMD those were observed. Therefore, we should consider the toxic effects of both individual pesticides and their mixtures in the risk management of pesticides for protecting the soli and aquatic ecosystems (Wu et al., 2018).

We, also, confirmed that IMD may act as an accelerator of toxic effects in binary mixtures of CLO and IMD, due to that IMD exposure showed a strong toxicity when compared to CLO exposure in this study: EC_{50} values were 411.11 µg/mL for CLO and 267.96 µg/mL for IMD, respectively (Table 1). In a study of CLO and IMD acute toxicity in sheepshead minnow (Gibbons et al., 2015), it was found that IMD triggered mixture toxicity due to higher toxicity of IMD than that of CLO; the 50% lethal concentration (LC_{50}) was 161 µg/mL for CLO and 93.6 µg/mL for IMD. However, it is difficult to determine whether IMD is the main toxic compound in the CLO and IMD mixtures from the toxic

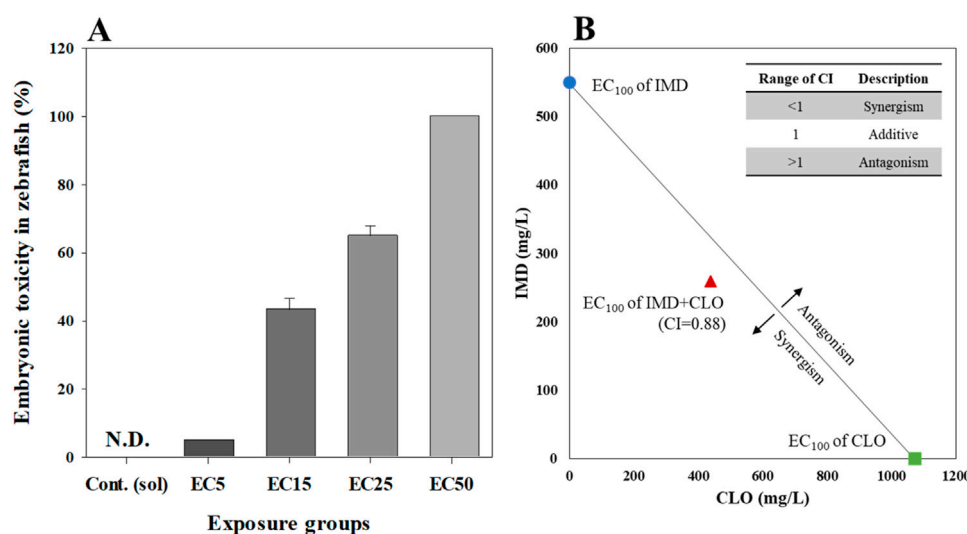


FIGURE 1 Embryonic toxicity (A) and combination index (CI) value (B) for binary mixtures of clothianidin (CLO) and imidacloprid (IMD) in zebrafish at 6 days after exposure. Zebrafish toxicity tests were designed with ECx values estimated from single toxicity: the mixture included from 5% to 50% effective concentrations of each of the two chemicals, and the mixing ratio was 1:1. All data represent the mean value \pm standard error (SEM) of triplicate experiments.

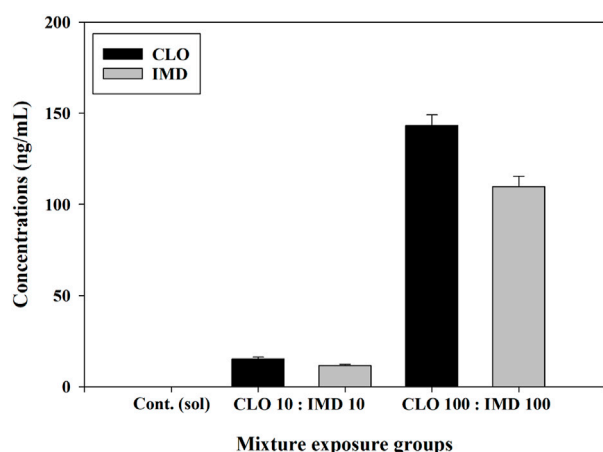


FIGURE 2 Residual concentrations of clothianidin (CLO) and imidacloprid (IMD) in binary mixtures for zebrafish embryos. The media combined with CLO and IMD at high and low concentrations (i.e., 10 and 100 ng/mL) were analyzed using the HPLC-MS/MS method in triplicate experiments. Seven-point calibration curves were generated from 2 to 500 ng/mL with an R^2 value >0.999 , and the recovery test of this method was conducted at three concentrations (5, 75, and 400 ng/L).

units (i.e., ECx) for zebrafish embryos in potential mixture toxicity tests. Mixture toxicity tests under different mixture combinations (e.g., ratios and concentrations) are required to clearly identify the toxic compounds in the mixtures. Consequently, our findings indicate that toxicity tests for zebrafish embryos are appropriate for applying the combined effects of CLO and IMD in natural environments. In this study, realistic mixture toxicity tests were conducted with zebrafish embryos, to confirm the adverse effects of mixtures at environmental concentration of CLO and IMD.

3.2 Realistic mixture toxicity of CLO and IMD

3.2.1 Residual concentrations of CLO and IMD

The stability and persistence of CLO and IMD in binary mixtures were assessed through two different types of mixing combinations, high and low concentrations (i.e., mixtures containing 10 and 100 ng/mL of each chemical, respectively), at 6 days after exposure. CLO and IMD were not detected in the control solution. Residual concentrations (compared to initial concentrations) of CLO and IMD in the mixture solutions ranged from 92.1% to 103.0% in the case of CLO and from 91.6% to 101.7% in the case of IMD, which indicates that both of these *neonics* were stable in the mixtures; that is, no or negligible volatilization or denaturation (Figure 2). Furthermore, the half-life of CLO reaches 56 days in sediment and up to 1,386 days in soil, and the half-life of IMD reaches 129 days in sediment and up to 228 days in soil (Mason et al., 2013). These results indicate that mixtures of CLO and IMD can steadily accumulate and persist in aquatic environments after agriculture or soil applications. These phenomena are not independent of the continuous increase in the detected concentrations of CLO and IMD in surface waters over the past 15 years and may lead to acute toxicity in aquatic organisms, as well as chronic toxicity (Sánchez-Bayo et al., 2016; Simon-Delso et al., 2015). Therefore, to better understand the toxic effects of CLO and IMD mixtures, considering their detected environmental concentrations, further studies on the phenotypic toxicity caused by short-term exposure and the toxic mechanisms for predicting chronic toxicity are required.

3.2.2 Mixture toxicity reflecting the environmental concentrations

Some studies reported that CLO and IMD might be remained in high concentrations in surface waters, through leaching and runoff

TABLE 2 Embryonic toxicity of clothianid (CLO), imidacloprid (IMD), and binary mixtures for 6 days after exposure. Mix. 1, 10, and 100 indicate binary mixtures consisting of 1, 10, and 100 ng/mL of each two chemicals. All data represent the mean value \pm standard errors (n = 20 embryos in each group with triplicate experiments).

Toxicity tests	Exposure groups (ng/mL)					
	Cont. (Sol)	CLO 10	IMD 10	Mix. 1	Mix. 10	Mix. 100
Embryonic toxicity (%)	3.3 \pm 1.7	12.5 \pm 3.4	12.5 \pm 2.8	8.3 \pm 1.7	11.7 \pm 2.5	7.5 \pm 1.7

under worst-case environmental scenarios (e.g., incorrect handling or improper disposal): up to IMD 320 ng/mL in Netherlands (Van Dijk et al., 2013) and CLO up to 170 ng/mL in United States (Miles et al., 2017). Therefore, we hypothesized that single and mixture of ≤ 100 ng/mL CLO and IMD can reflect as the detectable concentrations in the aquatic environment, including worst-case scenarios. In the present study, phenotypic toxicity was not observed in binary mixtures of CLO and IMD that reflected the detectable concentrations in the aquatic environment. There was no significant difference between all exposure groups compared with solvent control group, indicating that embryonic toxicity on zebrafish embryos, i.e., lethality and abnormality, were less than 15% after binary mixture exposure (Table 2). Thus, when exposed to detectable concentrations in the aquatic environment (i.e., ≤ 100 ng/mL), CLO and IMD, whether singly or in mixtures, are little to cause short-term developmental toxicity in zebrafish embryos. However, a strong acute toxicity to zebrafish was shown in the *neonics* mixtures-exposure groups and this phenomenon was exerted by synergistic effects with mixing ratio and concentration of components in the mixtures. These results imply that *neonics* mixture toxicity was associated with co-existing components and concentrations in the mixtures (Shukla et al., 2017; Wang et al., 2017). Therefore, although there was no phenotypic toxicity in zebrafish embryos, developmental defects in zebrafish embryos may appear upon co-exposure at low concentrations by mixing ratio and concentrations of CLO and IMD (Wu et al., 2018).

In this study, because ≤ 10 ng/mL CLO and IMD were simultaneously detected in runoff samples after spraying on agricultural environment (Woodward et al., 2022), the combined effects of CLO and IMD on zebrafish embryonic development were compared with 10 ng/mL single chemical-exposure group as a positive control. The mixture effects of CLO and IMD at realistic environmental concentration and mixing ratio, including worst-case scenarios (i.e., ≤ 100 ng/mL), were assessed with the toxic alteration of two different pathways which can affect the development of zebrafish embryos: the expression levels of target genes that are induced to cell damage by oxidative stress response and involved in thyroid hormone biosynthesis.

Aryl hydrocarbon receptor-mediated oxidative stress can induce toxic signaling pathways linked to cell damage, such as irritation of the inflammatory reactions or the induction of peroxidases by cytochrome P450-dependent oxygenase, during the early stages of embryonic development (Jin et al., 2020; Ren et al., 2020; Shankar et al., 2020). Several studies reported that the activation to oxidative stress is regulated by the redox-sensitive nuclear factor erythroid 2-related factors (Rousseau et al., 2015; Ulin et al., 2019; Williams et al., 2013). Because oxidative stress response also may affect the expression of proto-oncogene (*p53*), a tumor suppressor gene that regulates the cell cycle, we targeted genes which are involved aryl

hydrocarbon receptor-mediated oxidative stress response, including *p53*, to examine the mixture toxicity of CLO and IMD at environmental concentrations (Chen, 2016; Fan et al., 2018; Mugoni et al., 2014). The adverse effects caused by the form of realistic mixtures of CLO and IMD in zebrafish embryos were evaluated with the expression levels of targeted genes after binary mixtures exposure.

Interestingly, the expression levels of target genes linked to the cell damage pathway [aryl hydrocarbon receptor (*ahr2*), cytochrome P450 subunits (*cyp1a1* and *cyp1b1*), nuclear factor erythroid 2-related factors (*nrf1a* and *nrf2a*), and *p53*] were markedly up- or downregulated in the mixture exposure groups compared to the corresponding gene expression levels in the control group ($P < 0.05$, Figure 3; Supplementary Table S2). These results indicate that exposure to binary mixtures of CLO and IMD may cause developmental defects in zebrafish embryos through cell damage mediated by chemical stimulation, even at low concentrations. Previously other studies were reported that the transcriptional expression of *ahr2* mRNA, which reacts to chemicals with aromatic carbocyclic rings (e.g., *neonics*), induces the transcriptional activation of cytochrome P450 monooxygenases (*cyp1a1* and *cyp1b1*) and nuclear factor erythroid 2-related factors (*nrf1a* and *nrf2a*), indicating that their transcriptional alterations involve cellular oxidative stress response to xenobiotics (Jin et al., 2020; Ren et al., 2020; Rousseau et al., 2015; Shankar et al., 2020; Ulin et al., 2019; Williams et al., 2013). Excessive oxidative stress downregulated the transcriptional level of *p53*, leading to cell cycle arrest and/or cytotoxicity (Chen, 2016; Fan et al., 2018; Mugoni et al., 2014). Consequently, although abnormalities were not observed in short-term toxicity tests, in the present study, alterations in the transcriptional levels of target genes for cell damage implied that exposure to binary mixtures of CLO and IMD may induce developmental defects in zebrafish embryos through DNA damage linked to acute oxidative stress responses ($P < 0.05$, Figure 3; Supplementary Table S2).

Thyroid hormones are involved in early development and growth-related biological processes and functions in zebrafish embryos (Liu and Chan, 2002). In particular, to determine the zebrafish embryonic toxicity for potentially harmful substances, thyroid stimulating hormone beta (*tsh- β*) which promotes thyroid hormone secretion and thyroid hormone receptor alpha and beta (*thraa* and *thrb*) have been used as toxicological indicators.

In this study, the transcriptional levels of *tsh- β* , *thraa*, and *thrb* were significantly decreased in the single- and binary mixture groups of CLO and IMD compared to those in the control group ($P < 0.05$, Figure 4; Supplementary Table S2). Our findings indicate that CLO and IMD, either singly or combined in mixtures, can disturb thyroid hormone biosynthesis in the embryo-larva development of zebrafish. Similar to our findings, some studies reported that hazardous chemicals

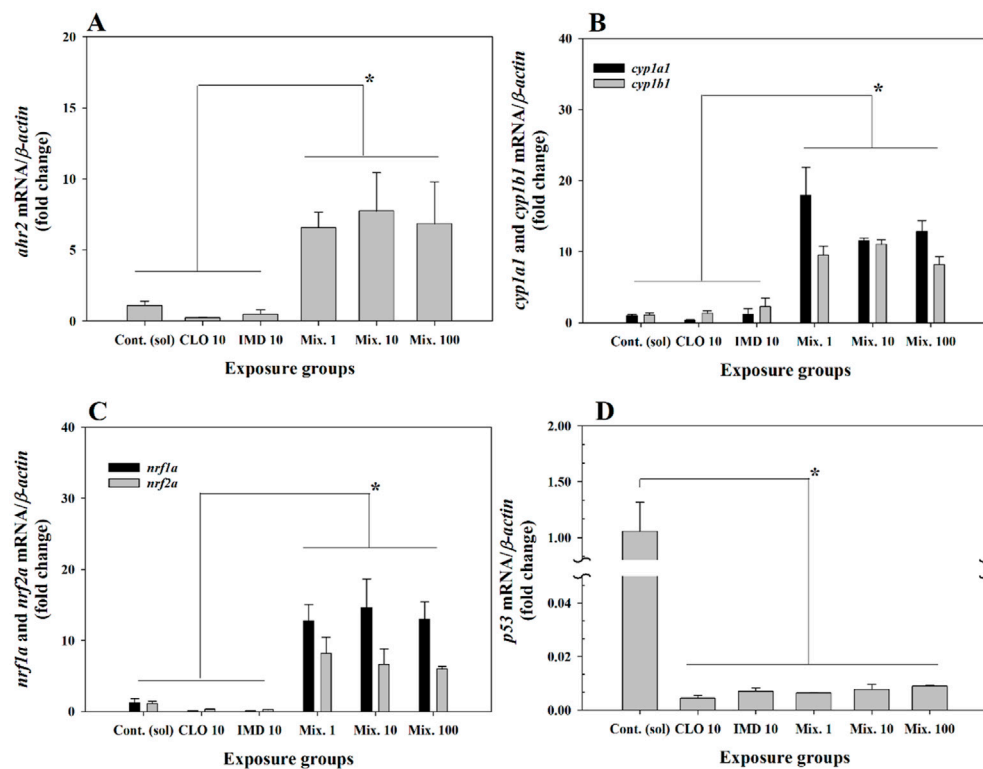


FIGURE 3

Relative fold change of the expression levels for aryl hydrocarbon receptor 2 (*ahr2*), cytochrome P450 monooxygenases (*cypl1a* and *cypl1b*), nuclear factor erythroid 2-related factors (*nrf1a* and *nrf2a*), and tumor suppressor gene (*p53*) in zebrafish embryos exposed to 10 ng/mL of clothianidin (CLO), 10 ng/mL of imidacloprid (IMD), and binary mixtures at three different concentrations (i.e., 1, 10, and 100 ng/mL) with a 1:1 mixing ratio: (A), *ahr2*; (B), *cypl1a* and *cypl1b*; (C), *nrf1a* and *nrf2a*; (D), *p53*. The expression levels of genes were normalized to β -actin and values are presented as the mean value \pm standard error (SEM) ($n = 20$ embryos in each exposure groups with three replicates). *Different letters indicate significant differences between the exposed groups ($P < 0.05$).

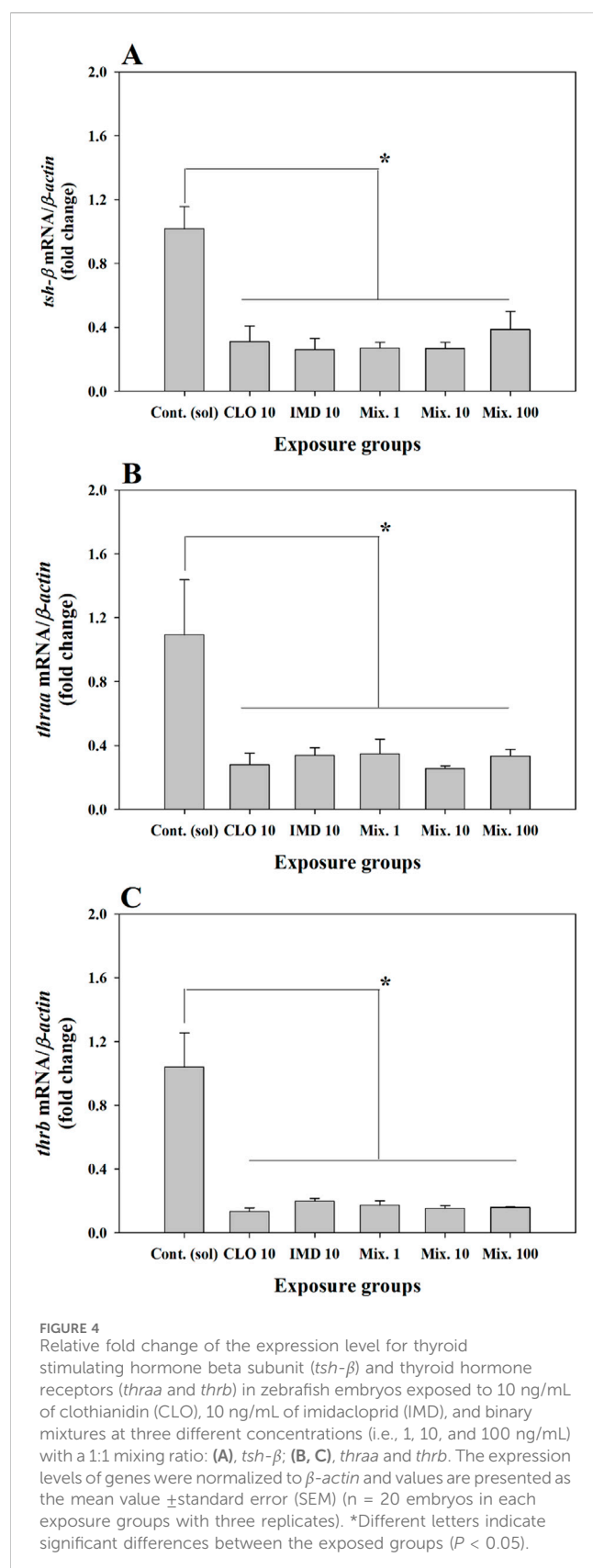
distributed in natural environment, including *neonics*, can interfere with the activation of thyroid hormones through receptor-mediated signal transduction (Boas et al., 2012; Liu et al., 2011; Ma et al., 2019; Walter et al., 2019). Thus, these results imply that the disturbance of thyroid hormone biosynthesis may be due to the intrinsic toxic characteristics of single chemicals and can be promoted by binary mixture exposure ($P < 0.05$, Figure 4; Supplementary Table S2). However, synergistic effects on thyroid hormonal activity were not confirmed in the mixtures. To more clearly elucidate the combined effects on developmental endocrine system in zebrafish, such as thyroid hormone biosynthesis, further studies examining the developmental impairment of zebrafish embryos through chemical interactions in the mixtures are required.

Taken together, a novel finding is that exposure to binary mixtures of CLO and IMD in the aquatic environment (i.e., concentration and ratio) can cause the promotion of cell damage by oxidative stress response and the suppression of thyroid hormone synthesis which is involved embryonic development. This phenomenon indicate that the expression alteration of target genes linked to cell damage and thyroid hormonal synthesis could impair the embryonic development in zebrafish, by the components and concentrations of chemical mixtures (Wang et al., 2020; Wu et al., 2018). Our results will be useful in examining the combined effects of mixtures following short-term exposure, to predict the developmental toxic effects of

chronic exposure to CLO and IMD. However, to clearly confirm the developmental toxicity caused by significant changes of target genes linked to cell damage and thyroid hormonal synthesis, it is necessary to investigate the effects of long-term exposure as well as the expressions of corresponding genes.

4 Conclusion

We confirmed the potential for increased combined concentrations of CLO and IMD in aquatic environments owing to their high stability and continuity. Even at a low concentration reflecting the measured environmental concentration, long-term co-exposure to CLO and IMD was found to induce not only cell damage by oxidative stress response but also developmental disturbance via thyroid hormone biosynthesis disruption, resulting in developmental defects of zebrafish. Therefore, exposure to mixtures of CLO and IMD in the range of environmental concentration may pose a greater threat to zebrafish embryonic development than would exposure to either of the two chemicals. The results from this study can introduce a scientific information for safety application of CLO and IMD to chemical regulation. To provide a comprehensive insight into the combined effects and their action mechanisms of CLO and IMD at the environmental



concentration level, chronic exposure to chemical compounds, including behavioral changes, growth parameters, histological pathology, and reproductive effects, is required.

Data availability statement

The datasets presented in this study can be found in online repositories. The names of the repository/repositories and accession number(s) can be found in the article/[Supplementary Material](#).

Ethics statement

The animal study was approved by the Institutional Animal Care and Use Committee (IACUC) in Korea Institute of Toxicology (IACUC no.2006-0003). The study was conducted in accordance with the local legislation and institutional requirements.

Author contributions

SZ: Formal Analysis, Investigation, Methodology, Writing–original draft. MH: Formal Analysis, Investigation, Methodology, Project administration, Writing–original draft. H-JS: Formal Analysis, Investigation, Writing–original draft. KK: Formal Analysis, Investigation, Writing–original draft. J-CK: Writing–original draft, Writing–review and editing. C-BP: Conceptualization, Funding acquisition, Project administration, Supervision, Writing–original draft, Writing–review and editing.

Funding

The author(s) declare that financial support was received for the research, authorship, and/or publication of this article. This research was supported by the Korea Institute of Toxicology, Republic of Korea (KK-2406_2710008768 and KK-2011-03).

Conflict of interest

The authors declare that the research was conducted in the absence of any commercial or financial relationships that could be construed as a potential conflict of interest.

Publisher's note

All claims expressed in this article are solely those of the authors and do not necessarily represent those of their affiliated organizations, or those of the publisher, the editors and the reviewers. Any product that may be evaluated in this article, or claim that may be made by its manufacturer, is not guaranteed or endorsed by the publisher.

Supplementary material

The Supplementary Material for this article can be found online at: <https://www.frontiersin.org/articles/10.3389/ftox.2024.1464069/full#supplementary-material>

References

- Boas, M., Feldt-Rasmussen, U., and Main, K. M. (2012). Thyroid effects of endocrine disrupting chemicals. *Mol. Cell. Endocrinol.* 355, 240–248. doi:10.1016/j.mce.2011.09.005
- Bonmatin, J.-M., Giorio, C., Girolami, V., Goulson, D., Kreutzweiser, D., Krupke, C., et al. (2015). Environmental fate and exposure; neonicotinoids and fipronil. *Environ. Sci. Pollut. Res.* 22, 35–67. doi:10.1007/s11356-014-3332-7
- Botias, C., David, A., Horwood, J., Abdul-Sada, A., Nicholls, E., Hill, E., et al. (2015). Neonicotinoid residues in wildflowers, a potential route of chronic exposure for bees. *Environ. Sci. & Technol.* 49, 12731–12740. doi:10.1021/acs.est.5b03459
- Casida, J. E., and Durkin, K. A. (2013). Neuroactive insecticides: targets, selectivity, resistance and secondary effects. *Annu. Rev. Entomol.* 58, 99–117. doi:10.1146/annurev-ento-120811-153645
- Chen, J. (2016). The cell-cycle arrest and apoptotic functions of p53 in tumor initiation and progression. *Cold Spring Harb. Perspect. Med.* 6, a026104. doi:10.1101/cshperspect.a026104
- Chen, Y., Zang, L., Liu, M., Zhang, C., Shen, G., Du, W., et al. (2019). Ecological risk assessment of the increasing use of the neonicotinoid insecticides along the east coast of China. *Environ. Int.* 127, 550–557. doi:10.1016/j.envint.2019.04.010
- Chou, T.-C. (2011). The mass-action law based algorithms for quantitative econo-gen bio-research. *Integr. Biol.* 3, 548–559. doi:10.1039/c0ib00130a
- Christen, V., Schirrmann, M., Frey, J. E., and Fent, K. (2018). Global transcriptomic effects of environmentally relevant concentrations of the neonicotinoids clothianidin, imidacloprid, and thiamethoxam in the brain of honey bees (*Apis mellifera*). *Environ. Sci. & Technol.* 52, 7534–7544. doi:10.1021/acs.est.8b01801
- Douglas, M. R., and Tooker, J. F. (2015). Large-scale deployment of seed treatments has driven rapid increase in use of neonicotinoid insecticides and preemptive pest management in U.S. field crops. *Environ. Sci. & Technol.* 49, 5088–5097. doi:10.1021/es506141g
- Embry, M. R., Belanger, S. E., Braunbeck, T. A., Galay-Burgos, M., Halder, M., Hinton, D. E., et al. (2010). The fish embryo toxicity test as an animal alternative method in hazard and risk assessment and scientific research. *Aquat. Toxicol.* 97, 79–87. doi:10.1016/j.aquatox.2009.12.008
- European Food Safety Authority (EFSA) (2013). Scientific Opinion on the public health hazards to be covered by inspection of meat from sheep and goats. *EFSA J.* 11, 3265. doi:10.2903/j.efsa.2013.3265
- Fan, Y., Miao, W., Lai, K., Huang, W., Song, R., and Li, Q. X. (2018). Developmental toxicity and inhibition of the fungicide hymexazol to melanin biosynthesis in zebrafish embryos. *Pestic. Biochem. Physiol.* 147, 139–144. doi:10.1016/j.pestbp.2017.10.007
- Gibbons, D., Morrissey, C. A., and Mineau, P. (2015). A review of the direct and indirect effects of neonicotinoids and fipronil on vertebrate wildlife. *Environ. Sci. Pollut. Res.* 22 (1), 103–118. doi:10.1007/s11356-014-3180-5
- Hladik, M. L., and Kolpin, D. W. (2016). First national-scale reconnaissance of neonicotinoid insecticides in streams across the USA. *Environ. Chem.* 13, 12–20. doi:10.1071/EN15061
- Jin, H., Ji, C., Ren, F., Aniagu, S., Tong, J., Jiang, Y., et al. (2020). AHR-mediated oxidative stress contributes to the cardiac developmental toxicity of trichloroethylene in zebrafish embryos. *J. Hazard. Mater.* 385, 121521. doi:10.1016/j.jhazmat.2019.121521
- Jones, A., Harrington, P., and Turnbull, G. (2014). Neonicotinoid concentrations in arable soils after seed treatment applications in preceding years. *Pest. Manag. Sci.* 70, 1780–1784. doi:10.1002/ps.3836
- Limay-Rios, V., Forero, L. G., Xue, Y., Smith, J., Baute, T., and Schaafsma, A. (2016). Neonicotinoid insecticide residues in soil dust and associated parent soil in fields with a history of seed treatment use on crops in southwestern Ontario. *Environ. Toxicol. Chem.* 35, 303–310. doi:10.1002/etc.3257
- Liu, S., Chang, J., Zhao, Y., and Zhu, G. (2011). Changes of thyroid hormone levels and related gene expression in zebrafish on early life stage exposure to triadimefon. *Environ. Toxicol. Pharmacol.* 32, 472–477. doi:10.1016/j.etap.2011.09.002
- Liu, Y. W., and Chan, W. K. (2002). Thyroid hormones are important for embryonic to larval transitory phase in zebrafish. *Differentiation* 70, 36–45. doi:10.1046/j.1432-0436.2002.700104.x
- Ma, X., Li, H., Xiong, J., Mehler, W. T., and You, J. (2019). Developmental toxicity of a neonicotinoid insecticide, acetamiprid to zebrafish embryos. *J. Agric. Food Chem.* 67, 2429–2436. doi:10.1021/acs.jafc.8b05373
- Main, A. R., Michel, N. L., Cavallaro, M. C., Headley, J. V., Peru, K. M., and Morrissey, C. A. (2016). Snowmelt transport of neonicotinoid insecticides to Canadian Prairie wetlands. *Agric. Ecosyst. Environ.* 215, 76–84. doi:10.1016/j.agee.2015.09.011
- Maloney, E. M., Morrissey, C. A., Headley, J. V., Peru, K. M., and Liber, K. (2017). Cumulative toxicity of neonicotinoid insecticide mixtures to *Chironomus dilutus* under acute exposure scenarios. *Environ. Toxicol. Chem.* 36, 3091–3101. doi:10.1002/etc.3878
- Maloney, E. M., Morrissey, C. A., Headley, J. V., Peru, K. M., and Liber, K. (2018). Can chronic exposure to imidacloprid, clothianidin, and thiamethoxam mixtures exert greater than additive toxicity in *Chironomus dilutus*? *Ecotoxicol. Environ. Safe.* 156, 354–365. doi:10.1016/j.ecoenv.2018.03.003
- Mason, R., Tennekes, H., Sánchez-Bayo, F., and Jepsen, P. (2013). Immune suppression by neonicotinoid insecticides at the root of global wildlife declines. *Environ. Anal. Health. Toxicol.* 1, 3–12. doi:10.7178/jeit.1
- Miles, J. C., Hua, J., Sepulveda, M. S., Krupke, C. H., and Hoverman, J. T. (2017). Effects of clothianidin on aquatic communities: evaluating the impacts of lethal and sublethal exposure to neonicotinoids. *PLoS One* 12, 0174171–e174224. doi:10.1371/journal.pone.0174171
- Morrissey, C. A., Mineau, P., Devries, J. H., Sánchez-Bayo, F., Liess, M., Cavallaro, M. C., et al. (2015). Neonicotinoid contamination of global surface waters and associated risk to aquatic invertebrates: a review. *Environ. Int.* 74, 291–303. doi:10.1016/j.envint.2014.10.024
- Mugoni, V., Camporeale, A., and Santoro, M. M. (2014). Analysis of oxidative stress in zebrafish embryos. *J. Vis. Exp.* 89, e51328. doi:10.3791/51328
- Organization for Economic Co-operation and Development (OECD) (2013) “OECD guidelines for the testing of chemicals 236: fish embryo acute toxicity (FET) test.” Paris, France: OECD. doi:10.1787/9789264203709-en
- Park, C.-B., Kim, G.-E., On, J., Pyo, H., Park, J.-W., and Cho, S.-H. (2022). Sex-specific effects of bisphenol S with tissue-specific responsiveness in adult zebrafish: the antiandrogenic and antiestrogenic effects. *Ecotoxicol. Environ. Safe.* 229, 113102. doi:10.1016/j.ecoenv.2021.113102
- Ren, F., Ji, C., Huang, Y., Aniagu, S., Jiang, Y., and Chen, T. (2020). AHR-mediated ROS production contributes to the cardiac developmental toxicity of PM2.5 in zebrafish embryos. *Sci. Total Environ.* 719, 135097. doi:10.1016/j.scitotenv.2019.135097
- Rousseau, M. E., Sant, K. E., Borden, L. R., Franks, D. G., Hahn, M. E., and Timme-Laragy, A. R. (2015). Regulation of Ahr signaling by Nrf2 during development: effects of Nrf2a deficiency on PCB126 embryotoxicity in zebrafish (*Danio rerio*). *Aquat. Toxicol.* 167, 157–171. doi:10.1016/j.aquatox.2015.08.002
- Sadaria, A. M., Supowit, S. D., and Halden, R. U. (2016). Mass balance assessment for six neonicotinoid insecticides during conventional wastewater and wetland treatment: nationwide reconnaissance in United States wastewater. *Environ. Sci. & Technol.* 50, 6199–6206. doi:10.1021/acs.est.6b01032
- Sánchez-Bayo, F., Goka, K., and Hayasaka, D. (2016). Contamination of the aquatic environment with neonicotinoids and its implication for ecosystems. *Front. Environ. Sci.* 4, 71. doi:10.3389/fenvs.2016.00071
- Shankar, P., Dasgupta, S., Hahn, M. E., and Tanguay, R. L. (2020). A review of the functional roles of the zebrafish aryl hydrocarbon receptors. *Toxicol. Sci.* 178, 215–238. doi:10.1093/toxsci/kfaa143
- Shukla, S., Jhamtani, R. C., Dahiya, M. S., and Agarwal, R. (2017). Oxidative injury caused by individual and combined exposure of neonicotinoid, organophosphate and herbicide in zebrafish. *Toxicol. Rep.* 4, 240–244. doi:10.1016/j.toxrep.2017.05.002
- Simon-Delso, N., Amaral-Rogers, V., Belzunces, L. P., Bonmatin, J. M., Chagnon, M., Downs, C., et al. (2015). Systemic insecticides (neonicotinoids and fipronil): trends, uses, mode of action and metabolites. *Environ. Sci. Pollut. Res.* 22, 5–34. doi:10.1007/s11356-014-3470-y
- Sparks, T. C. (2013). Insecticide discovery: an evaluation and analysis. *Pestic. Biochem. Physiol.* 107, 8–17. doi:10.1016/j.pestbp.2013.05.012
- Struger, J., Grabuski, J., Gagampan, S., Sverko, E., McGoldrick, D., and Marvin, C. H. (2017). Factors influencing the occurrence and distribution of neonicotinoid insecticides in surface waters of southern Ontario, Canada. *Chemosphere* 169, 516–523. doi:10.1016/j.chemosphere.2016.11.036
- Ulin, A., Henderson, J., Pham, M.-T., Meyo, J., Chen, Y., Karchner, S. I., et al. (2019). Developmental regulation of nuclear factor erythroid-2 related factors (nrf) by AHR1b in zebrafish (*Danio rerio*). *Toxicol. Sci.* 167, 536–545. doi:10.1093/toxsci/kfy257
- United States Environmental Protection Agency (USEPA) (2020). EPA releases proposed interim decisions for neonicotinoids. Available at: <https://www.epa.gov/pesticides/epa-releases-proposed-interim-decisions-neonicotinoids>.
- Van der Sluijs, J. P., Amaral-Rogers, V., Belzunces, L. P., Bijleveld van Lexmond, M. F. I. J., Bonmatin, J.-M., Chagnon, M., et al. (2015). Conclusions of the worldwide integrated assessment on the risks of neonicotinoids and fipronil to biodiversity and ecosystem functioning. *Environ. Sci. Pollut. Res.* 22, 148–154. doi:10.1007/s11356-014-3229-5
- Van Dijk, T. C., Van Staalduinen, M. A., and Van Der Sluijs, J. P. (2013). Macro-invertebrate decline in surface water polluted with imidacloprid. *PLoS One* 8, e62374. doi:10.1371/journal.pone.0062374 Available at: <https://journals.plos.org/plosone/article?id=10.1371/journal.pone.0062374>.
- Walter, K. M., Miller, G. W., Chen, X., Yaghoobi, B., Puschner, B., and Lein, P. J. (2019). Effects of thyroid hormone disruption on the ontogenetic expression of thyroid hormone signaling genes in developing zebrafish (*Danio rerio*). *Gen. Comp. Endocrinol.* 272, 20–32. doi:10.1016/j.ygcen.2018.11.007
- Wang, Y., Xu, P., Chang, J., Li, W., Yang, L., and Tian, H. (2020). Unraveling the toxic effects of neonicotinoid insecticides on the thyroid endocrine system of lizards. *Environ. Pollut.* 258, 113731. doi:10.1016/j.envpol.2019.113731

- Wang, Y., Yang, G., Dai, D., Xu, Z., Cai, L., Wang, Q., et al. (2017). Individual and mixture effects of five agricultural pesticides on zebrafish (*Danio rerio*) larvae. *Environ. Sci. Pollut. Res.* 24 (5), 4528–4536. doi:10.1007/s11356-016-8205-9
- Williams, L. M., Timme-Laragy, A. R., Goldstone, J. V., McArthur, A. G., Stegeman, J. J., Smolowitz, R. M., et al. (2013). Developmental expression of the Nfe2-related factor (Nrf) transcription factor family in the zebrafish, *Danio rerio*. *PLoS ONE* 8, e79574. doi:10.1371/journal.pone.0079574
- Wood, T. J., and Goulson, D. (2017). The environmental risks of neonicotinoid pesticides: a review of the evidence post 2013. *Environ. Sci. Pollut. Res.* 24, 17285–17325. doi:10.1007/s11356-017-9240-x
- Woodward, E. E., Hladik, M. L., Main, A. R., Cahn, M., Orlando, J. L., and Teerlink, J. (2022). Comparing imidacloprid, clothianidin, and azoxystrobin runoff from lettuce fields using a soil drench or treated seeds in the Salinas Valley, California. *Environ. Pollut.* 315, 120325. doi:10.1016/j.envpol.2022.120325
- Wu, S., Li, X., Liu, X., Yang, G., An, X., Wang, Q., et al. (2018). Joint toxic effects of triazophos and imidacloprid on zebrafish (*Danio rerio*). *Environ. Pollut.* 234, 470–481. doi:10.1016/j.envpol.2017.12.120
- Xiong, X., Luo, S., Wu, B., and Wang, J. (2017). Comparative developmental toxicity and stress protein responses of dimethyl sulfoxide to rare minnow and zebrafish embryos/larvae. *Zebrafish* 14, 60–68. doi:10.1089/zeb.2016.1287



OPEN ACCESS

EDITED BY

Sanjeeb Mohapatra,
Delft University of Technology, Netherlands

REVIEWED BY

Manjari Mishra,
Stanford University, United States
Jublee Jasmine,
Berhampur University, India

*CORRESPONDENCE

Ruwaya AlKendi,
✉ ruwayaa@uaeu.ac.ae

RECEIVED 12 August 2024

ACCEPTED 30 October 2024

PUBLISHED 27 November 2024

CITATION

De Jesus R, Iqbal S, Mundra S and AlKendi R (2024) Heterogenous bioluminescence patterns, cell viability, and biofilm formation of *Photobacterium leiognathi* strains exposed to ground microplastics. *Front. Toxicol.* 6:1479549. doi: 10.3389/ftox.2024.1479549

COPYRIGHT

© 2024 De Jesus, Iqbal, Mundra and AlKendi. This is an open-access article distributed under the terms of the [Creative Commons Attribution License \(CC BY\)](#). The use, distribution or reproduction in other forums is permitted, provided the original author(s) and the copyright owner(s) are credited and that the original publication in this journal is cited, in accordance with accepted academic practice. No use, distribution or reproduction is permitted which does not comply with these terms.

Heterogenous bioluminescence patterns, cell viability, and biofilm formation of *Photobacterium leiognathi* strains exposed to ground microplastics

Rener De Jesus¹, Sameera Iqbal², Sunil Mundra^{1,2} and Ruwaya AlKendi^{1*}

¹Department of Biology, College of Science, United Arab Emirates University, Al Ain, United Arab Emirates, ²Khalifa Center for Genetic Engineering and Biotechnology, United Arab Emirates University, Al Ain, United Arab Emirates

Microplastics (MPs) have been detected in various aquatic environments and negatively affect organisms, including marine luminous bacteria. This study investigated the differences in bioluminescence patterns, cell viability, and biofilm formation of *Photobacterium leiognathi* strains (LB01 and LB09) when exposed to various concentrations of ground microplastics (GMPs; 0.25%, 0.50%, 1%, or 2% [w/v] per mL) at 22°C or 30°C for 3.1 days (75 h) and 7 days. The strains exhibited heterogenous responses, including variable bioluminescence patterns, cell viability, and biofilm formation, due to the GMPs having effects such as hormesis and bioluminescence quenching. Moreover, the bioluminescence and cell viability differed between the two strains, possibly involving distinct cellular mechanisms, suggesting that GMPs affect factors that influence quorum sensing. Furthermore, the biofilm formation of LB01 and LB09 was observed following exposure to GMPs. Both strains showed increased biofilm formation at higher GMP concentrations (1% and 2%) after 3.1 days at 30°C and 22°C. However, in the 7-day experiment, LB01 significantly ($p < 0.05$) increased biofilms at 22°C, while LB09 significantly ($p < 0.05$) produced biofilms at 30°C. These findings highlight the strain-specific responses of *Phb. leiognathi* to MP pollutants. Therefore, this study underscores the importance of evaluating MPs as environmental stressors on marine microorganisms and their role in the ecophysiological repercussions of plastic pollution in aquatic environments.

KEYWORDS

plastic pollution, quorum sensing, luminous bacteria, hormesis, ecophysiology

1 Introduction

The inexorable influx of plastics into the marine environment represents a profound ecological challenge, with microplastics (MPs) and nanoplastics emerging as pervasive contaminants (Alimi et al., 2018; Zhang and Xu, 2020). MPs, typically measuring <5 mm (<0.2 inches), are characterized by their small size, elasticity, and ability to permeate diverse environments, including aquatic ecosystems (Andrady, 2017; Mattson et al., 2018; Boyle and Örmeci, 2020). The extensive distribution of these plastic particles poses significant risks to aquatic life. Aquatic organisms, from microscopic zooplankton to large aquatic

mammals, can ingest MPs that can cause adverse effects (Lusher et al., 2015; Rummel et al., 2016). In particular, the leaching of adsorbed or inherent toxic substances from ingested plastic particles (such as phthalates, bisphenol A, and persistent organic pollutants) can disrupt their endocrine and reproductive systems. These toxins can be transferred up the food chain, thereby posing risks to predator species and human health (Gallo et al., 2018). These risks extend not only to the organisms that form the backbone of aquatic food webs but also to marine microorganisms, including luminous bacteria (LB).

LB are fundamental to the maintenance of a marine ecosystem's integrity, from nutrient recycling (Thompson and Polz, 2006) to the health of higher trophic organisms, which involves symbiosis (Stabb et al., 2008). LB are involved in nutrient turnover, breaking down organic materials and converting them into molecules for use by other marine organisms. Moreover, LB often engage in symbiotic interactions with fish and invertebrates, providing them with benefits such as camouflage, attraction of prey, or deterrence of predators due to their light-emitting capabilities. Examples of LB are species belonging to the genera of *Aliivibrio* (such as *Aliivibrio fischeri*, and *Aliivibrio salmonicida*), *Vibrio* (such as *Vibrio harveyi*), and *Photobacterium* (such as *Phb. phosphoreum*, and *Phb. leiognathi*). Many LB are equipped with a sophisticated cell-to-cell communication system known as quorum sensing (QS) system, which regulates numerous physiological responses including bioluminescence (Chong et al., 2013; Wang et al., 2022) and biofilm formation (Hammer and Bassler, 2003).

QS is mediated by the production and detection of signaling molecules, which enable the bacterial population to collectively coordinate gene expression and effectively “decide” when to activate certain genes based on the density of their population (Anetzberger et al., 2009; Lupp et al., 2003). This mechanism also influences cell viability in several ways, including by affecting virulence factor production, resource allocation, stress responses, and biofilm formation. The latter is particularly significant, with QS triggering a cascade of genetic and biochemical events that lead to the establishment, development, and maturation of biofilms, which are critical for bacterial survival and adaptation in various environments (Subramani and Jayaprakashvel, 2019). Therefore, this regulatory system enables bacteria within biofilms to optimize resource use, enhance defense mechanisms, and synchronize activities, such as dispersal or virulence, significantly impacting their interactions with hosts and the environment (Subramani and Jayaprakashvel, 2019; Warriar et al., 2021).

Environmental pollutants, including MPs and heavy metals, have been shown to affect QS in marine bacteria, with potential implications for their survival and ecological functions. For example, a range of compounds, including MP beads, Cu^{2+} , Gd^{3+} , and nanoAg, have been shown to affect QS in *A. fischeri* at non-toxic concentrations (Gagné, 2017). Although the changes were more modest, the study found that exposure to these compounds disrupted bioluminescence and altered the QS between *A. fischeri* cells. This is particularly noteworthy as it provides the first evidence that MPs and other toxic chemicals can disrupt bacterial QS. In addition, previous studies have reported that MPs acted as substrates for microbial communities that allowed biofilm communities to form and thrive (Tu et al., 2020; Valentin et al., 2016). In the present study, the impact of ground MPs (GMPs) on *Phb. leiognathi* was

investigated, with a focus on three critical aspects: bioluminescence, cell viability, and biofilm formation. *Phb. leiognathi* is a marine LB that thrives in symbiosis with certain marine organisms (e.g., fish and squids), and is also free-living in the ocean (Thirukumar et al., 2022; Naguit et al., 2014; Yaser et al., 2014). The presence of MPs in aquatic ecosystems has raised concerns about potential ecophysiological effects. By observing changes in bioluminescence, the present study assessed the effects of GMPs on *Phb. leiognathi* QS. Additionally, using MTT assays provided insights into the effects of GMPs on bacterial viability. A post-exposure recovery experiment was conducted to evaluate whether *Phb. leiognathi* could achieve the same state as the unexposed group, using bioluminescence response as an indicator, after GMP exposure. Finally, examining the biofilm formation by *Phb. leiognathi* helps us to understand the implications of plastic pollution for bacterial colonization. Hence, this study contributes to the understanding of how plastic particles as environmental stressors affect LB and their potential ecophysiological roles in aquatic environments.

2 Materials and methods

2.1 LB isolation and purification

Freshly caught squids were bought from a local wet market in Al Ain, United Arab Emirates. The squids were placed in an ice box and transported immediately to the laboratory. The squids were dissected, and the ink sac was identified. The ink sac was gently opened using a sterile scalpel and the ink was collected by absorption using a sterile cotton swab and aseptically transferred into a test tube containing 0.85% saline solution. The solution was then serially diluted up to 10^{-4} and 0.1 mL was spread plated onto sea water agar (SWA; HiMedia®) plates and incubated at 28°C for 48 h. The spread plating was conducted in duplicates. After incubation, each plate was visually observed in the dark for LB colonies. The plates without LB colonies were further incubated for another 24 h. To obtain pure isolates, an LB colony from each plate was picked using an inoculating needle, streaked onto a new SWA plate, and observed after incubation at 28°C for 48 h. The pure LB isolates were then subjected to bioluminescence screening.

2.2 Bioluminescence screening

To determine the bioluminescence intensity and select the most suitable isolates for further study, 14 LB isolates were subjected to bioluminescence screening (Bao et al., 2023). The positive control was *Escherichia coli* DH108 transformed with plasmid pJE202 expressing the Lux operon genes from *Vibrio fischeri*. Overnight cultures of the LB isolates were incubated on SWA plates at 28°C for 48 h. *E. coli* DH108 was incubated on a plate containing Luria–Bertani agar with ampicillin at 35°C for 48 h. After incubation, colonies were picked from the plates and transferred to a test tube containing 0.85% saline solution. The cell density of each suspension was determined with reference to the 0.5 McFarland standard ($\sim 1.5 \times 10^8$ CFU/mL). A loopful (HiMedia® Hi-FlexiLoop 2; 2.0 mm in diameter, calibrated to 0.005 mL) of each suspension

was inoculated in tubes containing 10 mL artificial sea water broth (HiMedia®) with 0.25% [w/v] yeast extract (HiMedia®) and 0.5% [w/v] tryptone type-1 (HiMedia®) (ASW-YE-T) and incubated at 28°C while shaking (120 rpm) in a shaking incubator (Bioevopeak Co., Ltd., shaking incubator) for 48 h. For *E. coli* DH108, Luria–Bertani broth with ampicillin was used. After incubation, 200 µL of inoculum from each culture was transferred to a well of a microtiter plate (black, flat bottom, 96 wells, Costar®), with nine replicates. The microtiter plate was covered with foil and left to stand for 10 min before reading. The bioluminescence intensity was measured using a GloMax® Discover Microplate Reader (Promega Corporation, Madison, WI, USA) with a 10-s integration period prior to reading. Bioluminescence is reported as specific bioluminescence (SB), which is the log-transformed values relative light unit (RLU). As a result, two LB strains were selected: LB01 and LB09. Stock cultures of these bacteria were maintained in cryovials containing 20% [w/v] NaCl–trypticase soy broth with 20% [v/v] glycerol and stored at –20°C for further study.

2.3 Identification of LB isolates

2.3.1 DNA extraction

DNA materials were extracted from the two LB strains using a G-spin™ genomic DNA extraction kit (iNtRON Biotechnology Inc., South Korea) following the manufacturer's protocol. Briefly, 24-h old cultures were prepared and 1 mL aliquot was transferred into a microcentrifuge tube to collect cells by centrifugation ($15,500 \times g$ for 1 min). The supernatant was discarded and 300 µL of buffer solution was added. The tubes were vortexed and incubated in a heat block at 65°C for 15 min with gentle invert mixing every 5 min. Next, 250 µL of binding buffer was added and gently vortexed. Thereafter, the cell lysates (~550 µL) were loaded into spin columns, centrifuged ($15,500 \times g$ for 1 min), and washed twice with 500 µL of washing buffer. The columns were then placed in a new microcentrifuge tube and 50 µL of elution buffer was added directly onto the membrane of each column. The tubes were incubated at 25°C for 1 min and then centrifuged ($15,500 \times g$ for 1 min). Finally, the DNA concentrations were measured using a NanoDrop™ 2000/2000c spectrophotometer (Thermo Fisher Scientific Inc., MA, USA).

2.3.2 PCR amplification, purification, and gel electrophoresis

The extracted DNA was amplified using a PCR amplification kit (TaKaRa Bio Inc., Japan). The primers 27f (5'-AGAGTTTGA TCCTGGCTCAG-3') and 1492r (5'-CTACGGCTACCTTGTTAC GA-3') were purchased from Gene Link™, Inc. The PCR mixtures were prepared by combining 38.75 µL of sterile nuclease-free water, 2.5 µL of 10× PCR buffer, 2.5 µL of MgCl₂, 4 µL of dNTP mixture, 0.5 µL of each primer, 1 µL of DNA sample, and 0.25 µL of Taq DNA Polymerase (TaKaRa). Touchdown PCR was performed using a T-100™ thermal cycler (Bio-Rad Laboratories Inc., Hercules, CA, USA) under the following conditions: initial denaturation at 95°C for 3 min; 29 cycles of denaturation at 95°C for 30 s, annealing at 68°C for 30 s, and extension at 72°C for 30 s; then another 29 cycles of denaturation at

95°C for 30 s, annealing at 60°C for 30 s, and extension at 72°C for 30 s; termination at 72°C for 5 min; and storage at 4°C until use. The PCR amplicons were purified using a MEGAquick-spin™ plus Total Fragment DNA Purification Kit (iNtRON Biotechnology Inc., South Korea). Next, 10 µL of the PCR amplicons was transferred to a microcentrifuge tube and 250 µL of lysis buffer was added. The mixture was then loaded into a column in a collection tube and centrifugation (at $11,000 \times g$ for 30 s). Next, 750 µL of washing buffer was added to the column and centrifuged (at $11,000 \times g$ for 30 s). To dry the column membrane, centrifugation at full speed ($18,000 \times g$) for 3 min was conducted. Thereafter, the column was placed into a new microcentrifuge tube and 40 µL of elution buffer was added to the membrane center and left to stand for 1 min. Finally, centrifugation at full speed for 1 min was conducted to elute the DNA. The purified PCR amplicons were subjected to gel electrophoresis to check the quality and quantity. Next, 8 µL of each purified PCR product with 2 µL of loading dye was loaded onto 1% agarose gel well and run in 1X Tris–acetate–EDTA (TAE) buffer at 100 V for 45 min. A 1-kb molecular DNA ladder (New England Biolabs®, Beverly, MA, USA) was used. The gel was viewed under UV light using a Gel Doc™ EZ Imager with Image Lab™ software version 5.0 (Bio-Rad Laboratories Inc., Hercules, CA, USA).

2.3.3 DNA sequencing

The purified PCR amplicons were subjected to Sanger sequencing and fragment analysis by capillary electrophoresis using a 3,500 Genetic Analyzer (Applied Biosystems, Thermo Fisher Scientific). The obtained sequences were checked and cleaned using 4peaks version 1.8 (www.nucleobytes.com). The cleaned sequences were run against the 16S ribosomal RNA sequence database for Bacteria and Archaea available from GenBank® (<https://www.ncbi.nlm.nih.gov>) using Basic Local Alignment Search Tool (BLAST; National Center for Biotechnology Information, Bethesda, MD, USA). LB01 was identified as *Phb. leiognathi* subsp. *mandapamensis*, while LB09 was identified as *Phb. leiognathi*.

2.4 Preparation of ground microplastics (GMPs)

Microbeads, which made of polyethylene with inorganic metal pigments, extracted from cosmetic products by Habib et al. (2020) were used in this study. First, 10 g of microbeads were rinsed using type 1 ultrapure water to remove unwanted particulates, submerged in 70% ethanol for 30 min, washed with deionized water, and dried at 45°C in a hot air oven (Daihan Scientific Co., South Korea). The beads were ground using a sterile pestle and mortar and then exposed to UV light overnight. A small amount (0.01 g) of the GMPs were observed under a stereomicroscope (Leica Zoom 2000). The size of GMPs was measured using the ImageJ software (<https://imagej.net/ij/>) and the size distribution was determined (Supplementary Figure S1). To ensure asepsis, 0.1 g of GMPs was transferred into several tubes containing trypticase soy broth and incubated at 35°C for 48 h. After incubation, no tube showed turbidity.

2.5 Growth kinetics and bioluminescence profiles of *Phb. leiognathi* strains

The *Phb. leiognathi* strains in stock cultures were revived in tubes containing ASW-YE-T broth and incubated at 28°C for 48 h. Revived bacterial cells were collected by repeated centrifugation ($6,000 \times g$ for 10 min) and resuspended in phosphate-buffered solution (PBS, pH 7.4). The optical density at 600 nm (OD_{600}) was determined and adjusted to 0.5–0.8 (Swift et al., 1993; Ahmad et al., 2012; Muneeswaran et al., 2021). To initially determine the optimal temperature for peak bioluminescence, an experiment was conducted across a temperature range of 15°C–35°C. After 48 h of incubation, bioluminescence intensity was measured at each temperature, revealing that the highest levels were observed at 22°C and 30°C. The said temperatures were selected for this study to characterize growth kinetics and bioluminescence of *Phb. leiognathi* strains.

Freshly revived bacterial cells were collected, and new suspensions were prepared. Subsequently, 3 μ L of the suspension was inoculated into tubes containing 15 mL ASW-YE-T broth and incubated at 22°C or 30°C while shaking (120 rpm). The bacterial growth was monitored over time (until it reached the death phase) by transferring 200 μ L to a microtiter plate well and measuring the OD_{600} using a GloMax® Discover Microplate Reader (Promega Corporation, Madison, WI, USA).

2.6 GMP exposure experiment

To investigate the effects of GMPs on *Phb. leiognathi* strains, fresh cultures of the strains in the exponential growth phase were prepared. An aliquot was transferred into a microcentrifuge tube and the cells were harvested by centrifugation ($6,000 \times g$ for 10 min). The supernatant was carefully discarded, and the pellet was washed twice with PBS (pH 7.4) and then centrifuged again ($6,000 \times g$ for 10 min). After washing twice with PBS (pH 7.4), the supernatant was carefully discarded, ensuring the pellet remained undisturbed. The OD_{600} was adjusted to 0.5–0.8 and the bacterial suspension was immediately used for the GMP exposure experiment. Various GMP concentrations (0.25%, 0.50%, 1.00%, and 2.00% [w/v] per mL) were added to tubes containing 15 mL of ASW-YE-T broth. Control tubes contained ASW-YE-T broth without GMPs. Next, 10 μ L of the bacterial suspension was transferred into each tube. The tubes were then incubated at 22°C or 30°C while shaking (120 rpm) in a shaking incubator (Bioevopeak Co., Ltd.). The bioluminescence responses of the bacteria to different GMP concentrations and temperatures were monitored over two timeframes: (1) every 5 h for 3.1 days (75 h) to assess immediate effects, and (2) every 24 h for 7 days to assess long-term effects. To prevent nutrient depletion, double-strength ASW-YE-T broth was added in the 7-day experiment. To assess the bioluminescence, 200 μ L ($n = 3$) from each tube was transferred to each well of a black microtiter plate. The plate was covered with foil and left undisturbed for 10 min. SB was then measured as described in the Bioluminescence Screening section. This experiment was conducted three times on separate occasions, with triplicate wells ($n = 9$).

2.7 Post-exposure recovery experiment

This experiment was conducted to determine whether *Phb. leiognathi* strains previously exposed to GMPs for 3.1 days and 7 days can recuperate based on their bioluminescence intensities. A 1-mL aliquot of the bacterial culture was carefully pipetted from the tubes in 3.1-day and 7-day GMP exposure experiment, transferred into a microcentrifuge tube, and centrifuged ($6,000 \times g$ for 10 min). Next, the supernatant was carefully discarded, the pellet was washed three times with PBS (pH 7.4), and then resuspended in PBS (pH 7.4). The OD_{600} was measured, adjusted to 0.5–0.8, and 10 μ L of each prepared bacterial suspension was transferred into tubes containing 15 mL ASW-YE-T broth. The tubes were then incubated for 35 h at 22°C or 30°C while shaking (120 rpm). The bioluminescence responses of the strains were monitored every 5 h for 35 h. Then, 200 μ L ($n = 3$) from each tube was transferred to the wells of a black microtiter plate. The plate was covered with foil and left undisturbed for 10 min. Next, the SB was measured as described in the Bioluminescence Screening section. This experiment was conducted three times on separate occasions, with triplicate wells ($n = 9$).

2.8 MTT assay

The cell viability of *Phb. leiognathi* strains after exposure to varying GMP concentrations were assessed using MTT (3-(4,5-dimethylthiazol-2-yl)-2,5-diphenyltetrazolium bromide) assays with modifications (Wang et al., 2010). To prepare the MTT solution, 50 mg of MTT powder (bioWORLD, GeneLinx International, Inc. USA) was dissolved in 10 mL deionized water while stirring at 37°C. The solution was stored in microcentrifuge tubes at -20°C until use. 3 μ L of each bacterial suspension was inoculated in a well of a microtiter plate (clear, flat bottom, 96 wells, Costar®) containing 100 μ L of ASW broth. The plate was incubated at 22°C or 30°C for 8 h. Next, 10 μ L of MTT solution was added using a multi-channel pipette (Eppendorf Research®) and left to stand for 20 min. Thereafter, the broth was removed by gentle pipetting and 100 μ L of dimethyl sulfoxide (purity >99%; Merck, Darmstadt, Germany) was added. The OD_{560} was measured using a microtiter plate reader after shaking the plate for 10 s. Each OD value was corrected based on the blank (medium without cells), and the mean corrected OD values were then calculated. This experiment was conducted with replicates ($n = 12$).

2.9 Crystal violet biofilm formation assay

The biofilm formation of *Phb. leiognathi* strains after GMP was assessed using the method (De Jesus and Dedeles, 2020) with modifications. To initiate biofilm formation, 1% (w/v) squid's ink solution was used to coat the wells of a microtiter plate (clear, flat bottom, 96 wells, Costar®). The ink was collected from a squid's ink sac using a sterile syringe and added to sterile deionized water. The ink solution was heated at 55°C for 10 min and then 100 μ L was transferred to the wells and the microtiter plate was placed in an

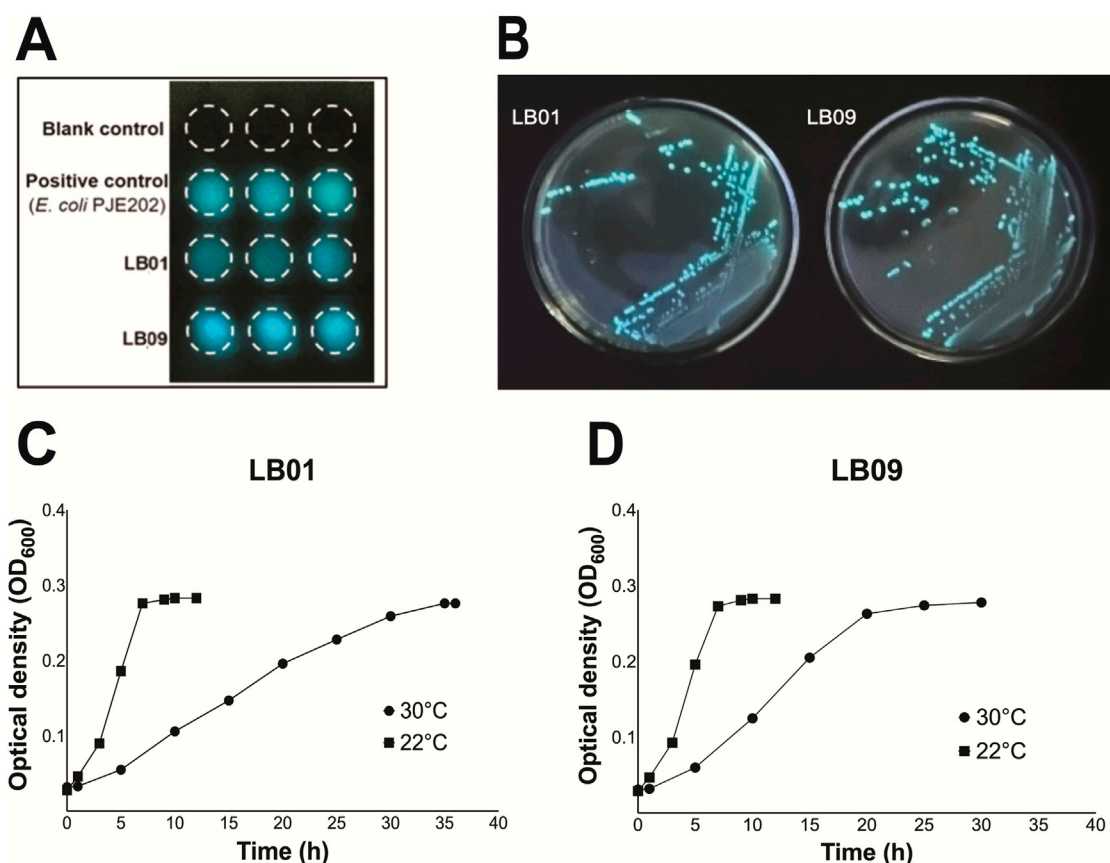


FIGURE 1

Bioluminescence assay and growth phases of *Phb. leiognathi* strains LB01 and LB09. (A) Bioluminescence assays. The mean specific bioluminescence (SB) was 6.04×10^6 for LB01, 1.04×10^7 for LB09, and 6.60×10^6 for the positive control (*E. coli* DH108 transformed with plasmid pJE202 expressing the Lux operon genes from *V. fischeri*). (B) LB01 and LB09 grown on seawater agar (SWA) plates after a 48-h incubation period at 28°C. (C, D) Growth phases of LB01 and LB09 at two distinct temperatures: 22°C and 30°C.

incubator overnight. Next, the contents were removed from the wells and 100 μ L of double-strength ASW-YE-T broth was added to the wells. The wells were then inoculated with 3 μ L of bacterial suspension and incubated at 22°C or 30°C while shaking (150 rpm) for 48 h. After incubation, the broth was removed by gentle pipetting, replenished with freshly prepared ASW-YE-T to support the biofilm formation, and incubated again at the previously mentioned temperatures for 48 h. The growth in microtiter plate wells was assessed based on the OD₆₀₀ using the GloMax® Discover Microplate Reader. Using a multi-channel pipette (Eppendorf Research®), the broth of each well was removed, and the wells were gently washed once with 200 μ L of sterile PBS (pH 7.2), and then air-dried for 20 min. The attached biofilms in the wells were stained with 130 μ L of 1% (v/v) crystal violet solution (HiMedia®) for 5 min and washed three times with 200 μ L of sterile distilled water. The stained biofilms in the wells were solubilized with 130 μ L of absolute ethanol (Carlo Erba, Milan, Italy) and the OD₅₆₀ was assessed. The results were expressed as specific biofilm formation (SBF), calculated as $(A - B)/C$, where *A* is the OD₅₆₀ of the stained biofilms, *B* is the OD₅₆₀ of the stained blank control wells (to eliminate non-specific or abiotic OD values), and *C* is the OD₆₀₀ of bacterial growth in ASW-YE-T broth. The assay was performed in replicates (*n* = 9).

2.10 Data analysis

The bioluminescence intensities were normalized (min-max scaling; 0–1) to reduce potential errors. The differences in mean OD values in MTT assays and the mean SBF in biofilm formation assays (control groups vs. exposed groups) were examined using two-way ANOVA, followed by Dunnett's *post hoc* analysis in Graphpad Prism 10 (version 10.2.3). *p* < 0.05 was accepted as statistically significant, indicating reliable differences between control groups and exposed groups.

3 Results

3.1 Bioluminescence and growth dynamics of *Phb. leiognathi* strains

Two LB isolates, LB01 and LB09, identified as *Phb. leiognathi* subsp. *mandapemensis* and *Phb. leiognathi*, respectively, were selected based on their increased bioluminescence intensity after incubation at 28°C for 48 h (Figures 1A, B). The mean SB of LB01 was 6.04×10^6 , whereas LB09 exhibited a 1.7 times higher mean SB of 1.04×10^7 . This indicates that LB09 has a significantly

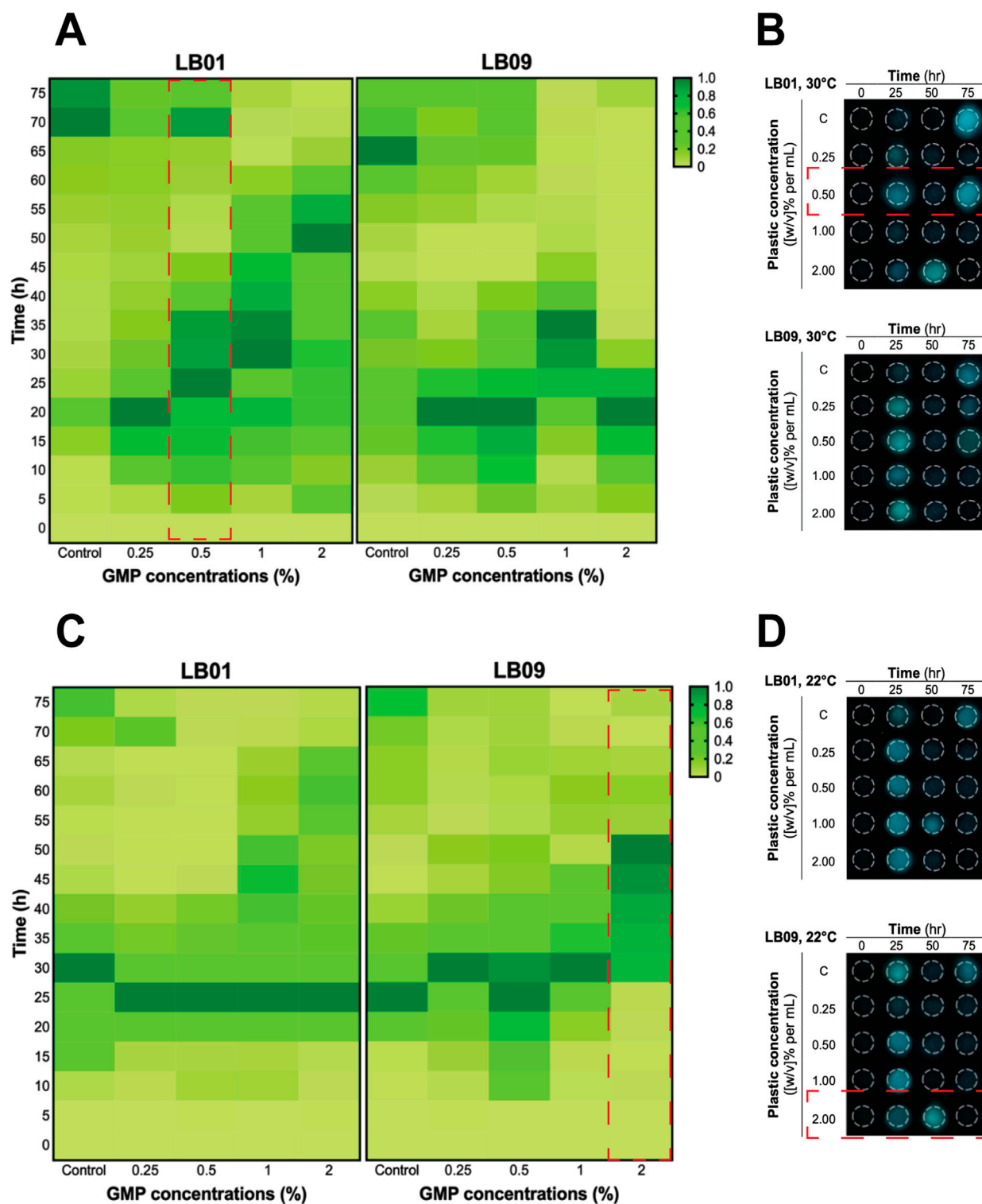


FIGURE 2

Heatmaps of the heterogeneous bioluminescence responses of *Phb. leiognathi* strains LB01 and LB09 over 3.1 days at different ground microplastic (GMP) concentrations and two different temperatures, 30°C and 22°C. (A) At 30°C, prolonged bioluminescence activity of LB01 were observed with higher concentrations vs. lower GMP concentrations, indicating an enhanced response to GMPs, while the bioluminescence of LB09 exhibited shorter bioluminescence responses at this temperature, suggesting a possible inhibitory threshold. (B) Microtiter plate displaying bioluminescence of LB strains exposed to different GMP concentrations at 30°C and specified time points. Biphasic bioluminescence was observed in LB01 exposed to 0.5% GMP concentrations (in red broken lines). (C) At 22°C, both strains demonstrated uniform patterns of bioluminescence when compared to the control group. (D) Microtiter plate displaying bioluminescence of LB strains exposed to different GMP concentrations at 22°C and specified time points. LB09 exposed at a 2% GMP concentration exhibited prolonged and gradual bioluminescence response, as indicated by the red broken lines.

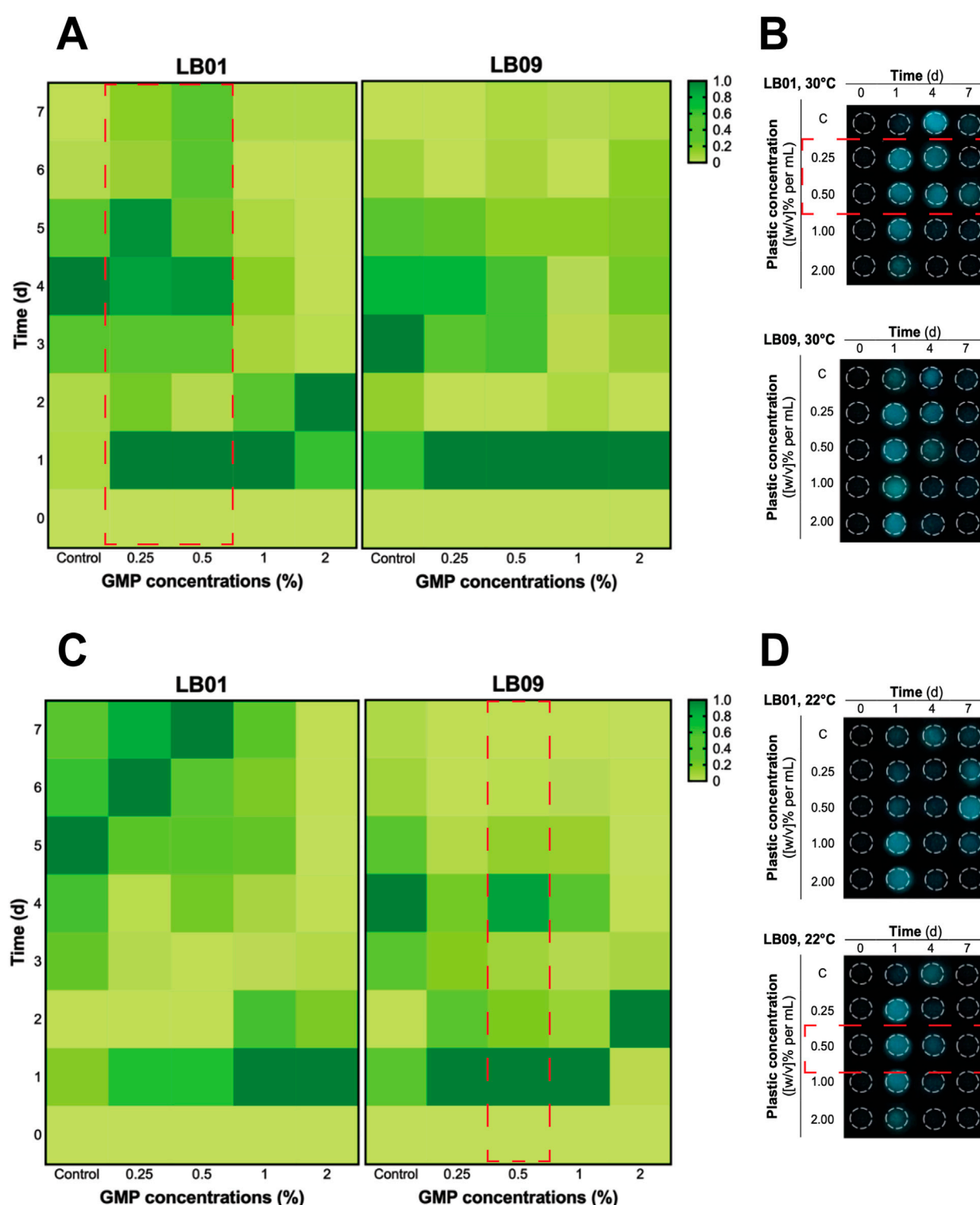


FIGURE 3

Heatmaps of the heterogeneous bioluminescence responses of *Phb. leiognathi* strains LB01 and LB09 over 7 days at different ground microplastic (GMP) concentrations and two different temperatures, 30°C and 22°C. (A) At 30°C, both strains exhibited early pronounced bioluminescence compared to control groups. Biphasic bioluminescence patterns were observed in LB01 exposed to lower GMP concentrations (0.25% and 0.5%) (red broken lines). (B) Microtiter plate displaying bioluminescence of LB strains exposed to different GMP concentrations at 30°C and specified time points. (C) At 22°C, delayed bioluminescence was observed in LB01 exposed to lower GMP concentrations but earlier peaks at higher concentrations (1% and 2%). Potential biphasic bioluminescence pattern was observed in LB09 at 0.5% GMP concentration, as indicated in red broken lines. (D) Microtiter plate displaying bioluminescence of LB strains exposed to different GMP concentrations at 22°C and specified time points.

higher bioluminescence capability than LB01. Nevertheless, both strains were studied further.

The growth dynamics of both strains were monitored at two distinct temperatures, 22°C and 30°C, to assess temperature-dependent growth variations (Figures 1C, D). At 22°C, both strains exhibited similar growth phases. The lag phase started <1 h and was immediately followed by the exponential phase. However, at 30°C, LB01 had a <2 h lag phase then followed by a prolonged exponential phase, which continued until approximately 32 h (Figure 1C). On the other hand, LB09 had a 1.5-h lag phase and a shorter exponential phase, which lasted until between approximately 22.5 h (Figure 1D). Both strains exhibited faster growth at the lower temperature.

3.2 *Phb. leiognathi* bioluminescence varied with GMPs concentration

The effects of GMPs on the bioluminescence intensities of the two *Phb. leiognathi* strains at 22°C or 30°C were investigated. The SB values were presented in Supplementary Tables S1, S2). The bioluminescence intensities of the two strains exposed to varying GMP concentrations were found heterogeneous (Figures 2, 3).

In the 3.1-day experiment, which was used to assess the immediate effects, both strains displayed early peaked of bioluminescence intensity compared to the control group at 30°C (Figures 2A, B), suggesting an upregulation of QS in response to GMP exposure. Interestingly, a biphasic bioluminescence was observed in LB01 exposed at 0.5% GMP concentration that could reflect adjusted QS in response to the presence of GMPs (Figure 2A). These early bioluminescent responses of the two strains are indication of hormetic effect, where low-dose exposure triggers a stimulatory response. At 22°C, both strains exhibited uniform patterns of bioluminescence when compared to the control group, except for LB09 exposed to 2% GMP concentration (Figures 2C, D).

The 7-day experiment involved monitoring the bioluminescence of both strains at both temperatures, with varying GMP concentrations, which was used to assess the long-term effects of plastic particles (Figure 3). At 30°C, an obvious biphasic bioluminescence phenomenon was observed in LB01 at lower concentrations (0.25% and 0.5%) (Figure 3A). Furthermore, the strain also demonstrated biphasic-dose response, where biphasic bioluminescence observed at lower concentrations and a potential bioluminescence quenching (an inhibitory effect) at higher concentrations (1% and 2%) (Figure 3A). At 22°C, both strains showed complex bioluminescence responses (Figures 3C, D). LB01 exposed to lower concentrations showed delayed bioluminescence peaks (Figure 3C). In contrast, LB09 displayed initial bioluminescence peaks across all GMP concentrations, with a potential biphasic bioluminescence pattern observed specifically at the 0.5% GMP (Figure 3C).

Overall, these results highlight the heterogeneous bioluminescence patterns of *Phb. leiognathi* strains to GMP exposure, with strain-specific responses emerging based in GMP concentration and temperature that lead to differences in their physiological adaptation. Furthermore, the observed biphasic

bioluminescence and hormesis underscore the complex interactions between bacterial metabolic processes and MP stressors.

3.3 *Phb. leiognathi* demonstrated heterogeneous recovery responses

A post-exposure recovery experiment was conducted to determine whether the two strains previously exposed to GMPs for 3.1 days and 7 days could recuperate from the effects of this exposure. The SB values for the first 35 h were presented in Supplementary Tables S3, S4). Following the 3.1-day GMP exposure, the bioluminescence responses of LB01 exposed to all GMP concentrations were comparable to those of the control group, except at 2% GMP, indicating that the strain was able to recuperate from the effects of GMPs at low concentrations (Figure 4A). However, early bioluminescence peaks were observed in LB09 following exposure to 0.5%, 1%, and 2% GMPs, but the bacteria exposed to 0.25% displayed slower peaking of bioluminescence (Figure 4B). At 22°C, early bioluminescence peaks were still observed in LB01 following 3.1-day exposure to GMPs (Figure 4C), while LB09 showed contrasting responses, where the bacteria exposed at higher GMP concentrations have bioluminescence patterns comparable to the control group (Figure 4D).

Following the 7 days GMP exposure, LB01 at 30°C displayed slower peaking of bioluminescence, while exposure to higher GMP concentrations (1% and 2%) remained incomparable with the control group (Figure 5A). Similarly, LB09 exposed to 0.25% GMP concentration at the same temperature also showed slower peaking of bioluminescence, but exposure to 0.5%, 1% and 2% GMP concentrations created initial peaks of bioluminescence (Figure 5B). At 22°C, the bioluminescence responses of LB01 exposed to lower GMP concentrations were comparable to those of the control group (especially at 0.5% GMP concentration), except at 2%, indicating that the strain was able to recuperate from the effects of GMPs at low concentrations (Figure 5C). However, early bioluminescence peaks were observed in LB09 following exposure to 0.5%, 1%, and 2% GMPs, but the bacteria exposed to lowest GMP concentration also displayed slower peaking of bioluminescence (Figure 5D).

3.4 *Phb. leiognathi* viability varied with GMP concentrations

MTT assays were performed to evaluate the effects of GMPs on the cell viability of both strains under different experimental conditions (Figure 6). Then, the mean OD₅₆₀ readings were determined and presented in Supplementary Tables S5, S6). In the 3.1-day experiment at 30°C, LB09 showed no significant decrease in viability compared to the control group (Figure 6A). LB01, where a hormetic effect of low GMP concentrations was previously observed, exhibited with no significant differences in viability at 0.25% and 0.50% GMP concentrations compared to the control groups (Figure 6A). At 22°C, LB01 revealed a significant ($p <$

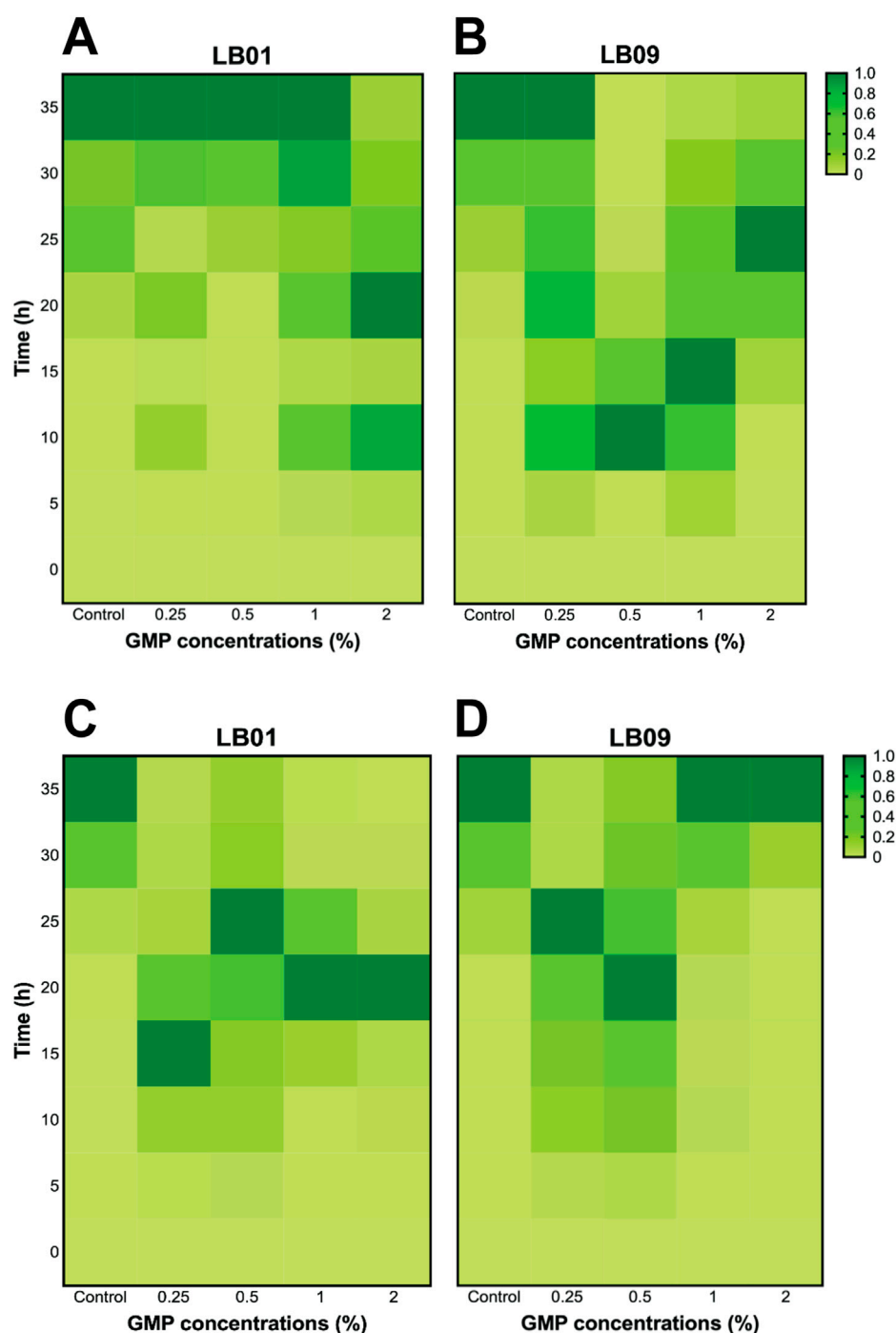


FIGURE 4
Heatmaps of the bioluminescence recovery patterns in *Photobacterium leiognathi* strains LB01 and LB09 following 3.1-day GMP exposure at 30°C (A, B) and 22°C (C, D).

0.05) decrease in viability after exposure at all GMP concentrations compared to the control group (Figure 6B). Conversely, LB09 had distinct MTT assays results at the same temperature. The viability decreased significantly ($p < 0.05$) at low concentrations (0.25% and 0.5%) compared to the control group, but not at high concentrations (1% and 2%), indicating possible adaptive mechanisms (Figure 6B).

Extending the exposure period to 7 days yielded substantial differences (Figures 6C, D). At 30°C, LB01 exhibited a significant ($p < 0.05$) increase in viability at low concentrations (0.25% and 0.5%) vs. to the control group, but not at high concentrations (1% and 2%) (Figure 6C). In contrast, LB09 demonstrated a significant ($p < 0.05$) decrease in viability compared to the control group at all concentrations (Figure 6C). At 22°C, LB01 showed a significant ($p <$

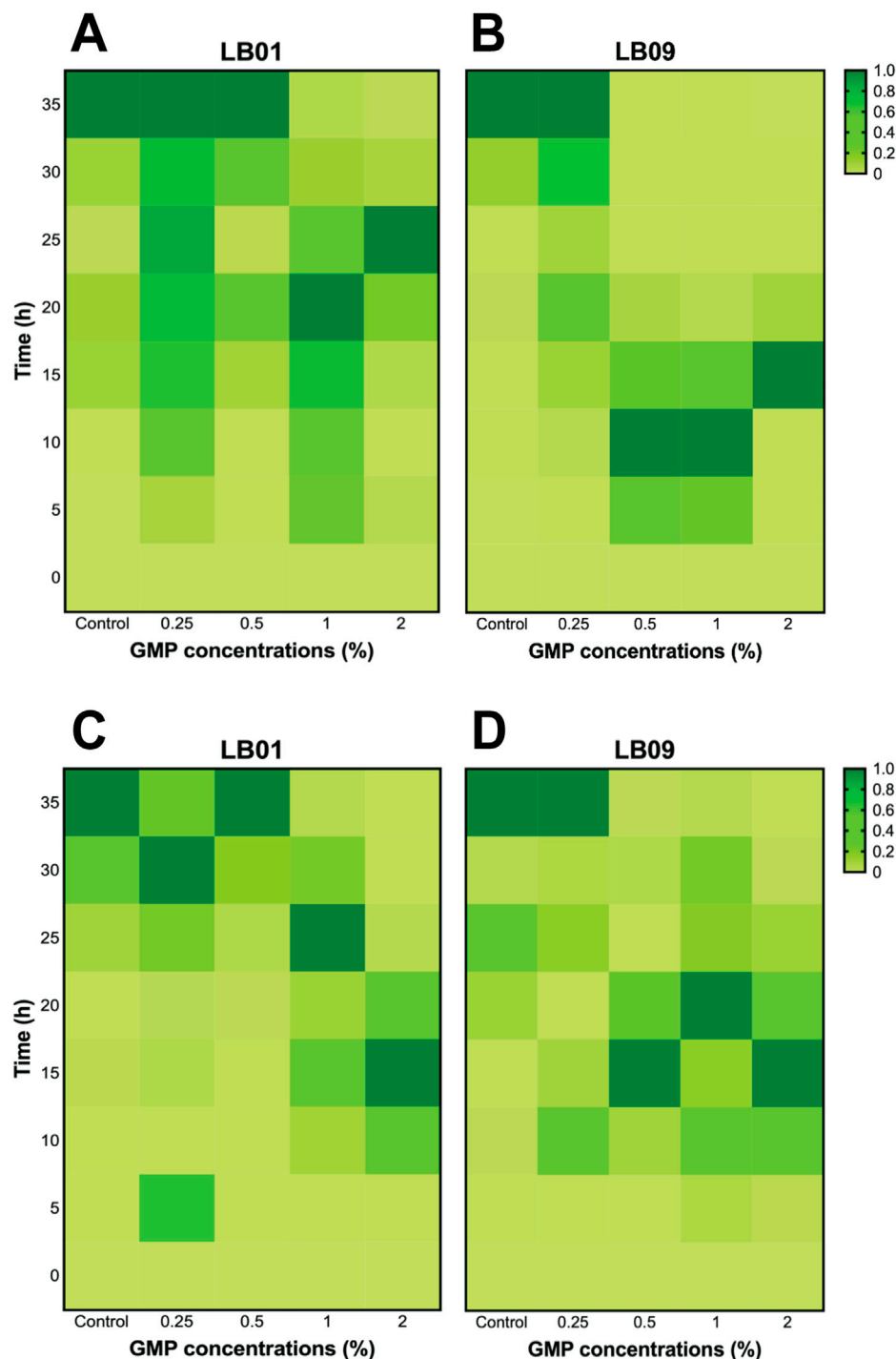
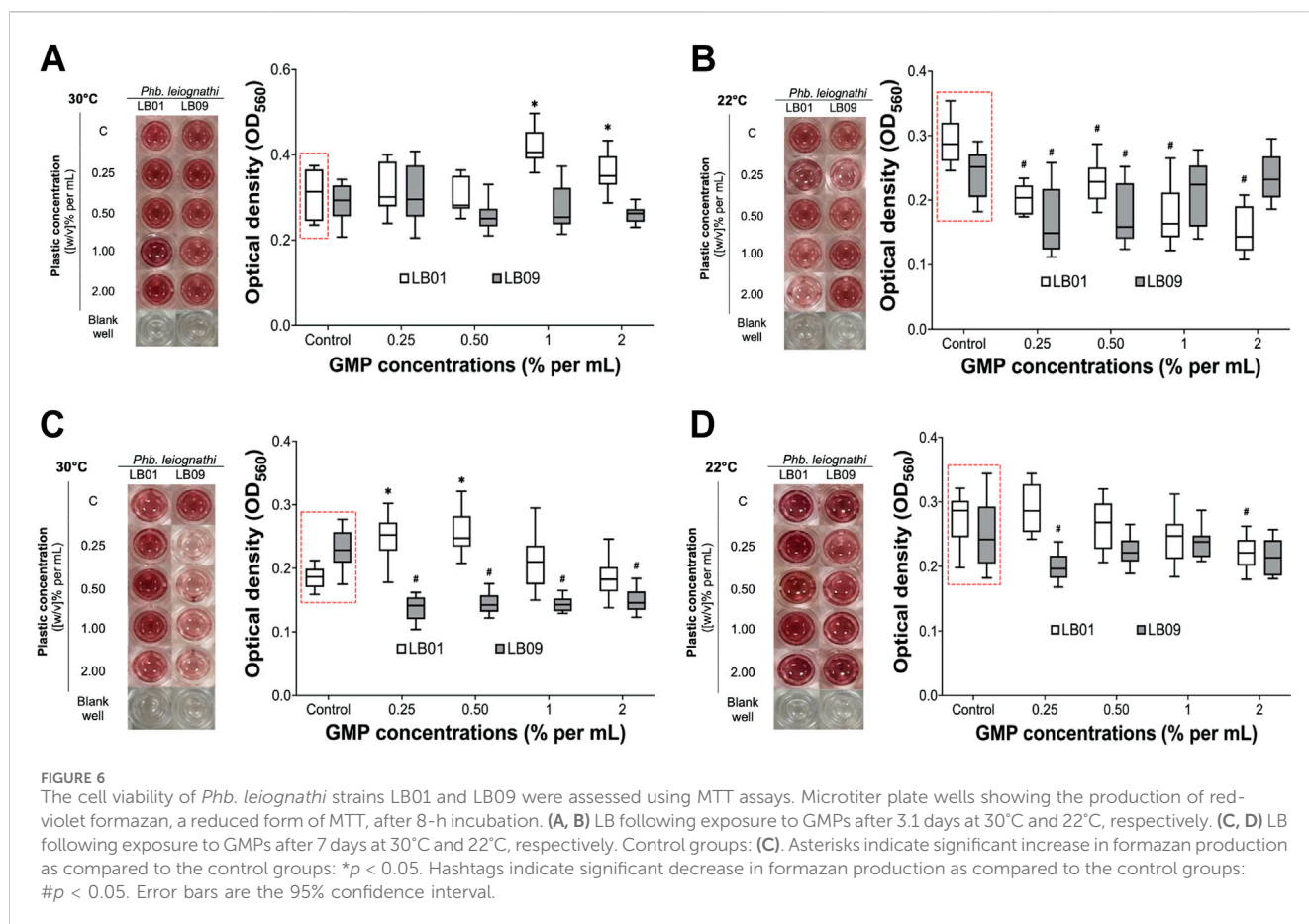


FIGURE 5
Heatmaps of the bioluminescence recovery patterns in *Photobacterium leiognathi* strains LB01 and LB09 following 7-day GMP exposure at 30°C (A, B) and 22°C (C, D).

0.05) decrease in viability compared to the control groups at the 2% GMP concentration, whereas LB09 generally exhibited a decrease in viability at the 0.25% GMP concentration compared to control group (Figure 6D). These observations suggest strain-specific differences in bacterial viability to MPs through QS regulation, which influenced by GMP concentration, temperature, and time exposure.

3.5 Effects of GMPs in biofilm formation of *Phb. leiognathi* strains

The biofilm formation of the two strains was assessed by crystal violet biofilm formation assays following GMP exposure (Figure 7). The biofilms were quantified and



expressed as SBF, which were presented in [Supplementary Tables S7, S8](#)).

In the 3.1-day experiment at 30°C, the SBF of LB09 increased significantly ($p < 0.05$) as the GMP concentration increases compared to the control group (Figure 7A). Similarly, LB01 produced significantly ($p < 0.05$) high SBF at all GMP concentrations, except at 0.50%, compared to the control group (Figure 7A). On the other hand, at 22°C, the SBF in both strains increased vs. control group following exposure to GMP concentrations, except at 0.50% (Figure 7B). In the 7-day experiment, both strains showed contrasting SBF results at different temperatures (Figures 7C, D). It was observed that the LB01 and LB09 produced significantly ($p < 0.05$) low SBF as compared to the control group at 30°C and 22°C, respectively (Figures 7C, D). These observations suggest that there were strain-specific responses based on their biofilm formation after exposure to GMPs at lower temperature.

4 Discussion

The presence of plastics in the aquatic environment is widespread and varied. Studies have shown that 94% of the plastics entering the ocean settle on the sea floor, with an estimated 70 kg of plastics per square kilometer of seabed. About 1% of marine plastics are found floating at or near the

ocean surface, with a global average concentration of less than 1 kg/km². However, this concentration increases in certain mid-ocean locations, with the highest recorded concentration in the North Pacific Gyre at 18 kg/km² (Author Anonymous, 2016). Plastic pollutants exist in ecosystems in various forms and sizes, which can be classified as megaplastics, macroplastics, mesoplastics, and MPs (Thushari and Senevirathna, 2020). Both primary MPs (produced directly as MPs) and secondary MPs (produced by the breakdown of larger plastic items) are widely distributed across marine and coastal environments, in both water, and sediments (Scherer et al., 2020; Lu et al., 2021). The concentrations of MPs in global marine and coastal ecosystems varies, ranging from 0.001 to 140 particles/m³ in water and from 0.2 to 8,766 particles/m³ in sediments globally (Thushari and Senevirathna, 2020; Quaglia et al., 2023; Veettil et al., 2024). These plastic particles can be ingested by fish and bivalves, causing physical harm, and potentially blocking digestive tracts, which can lead to starvation (Ryan, 2016; Egbeocha et al., 2018). Chemical pollutants from plastics can leach into the tissues of these animals, and the plastics can carry pathogens that increase the risk of disease (Gallo et al., 2018). In addition, marine LB, such as *Phb. leiognathi*, may exhibit impaired bioluminescence and cell viability due to plastic exposure, as observed in this study. Furthermore, biofilm formation on plastics can alter microbial communities within marine ecosystems (Pinto et al., 2019; Rummel et al., 2017; Zettler et al., 2013).

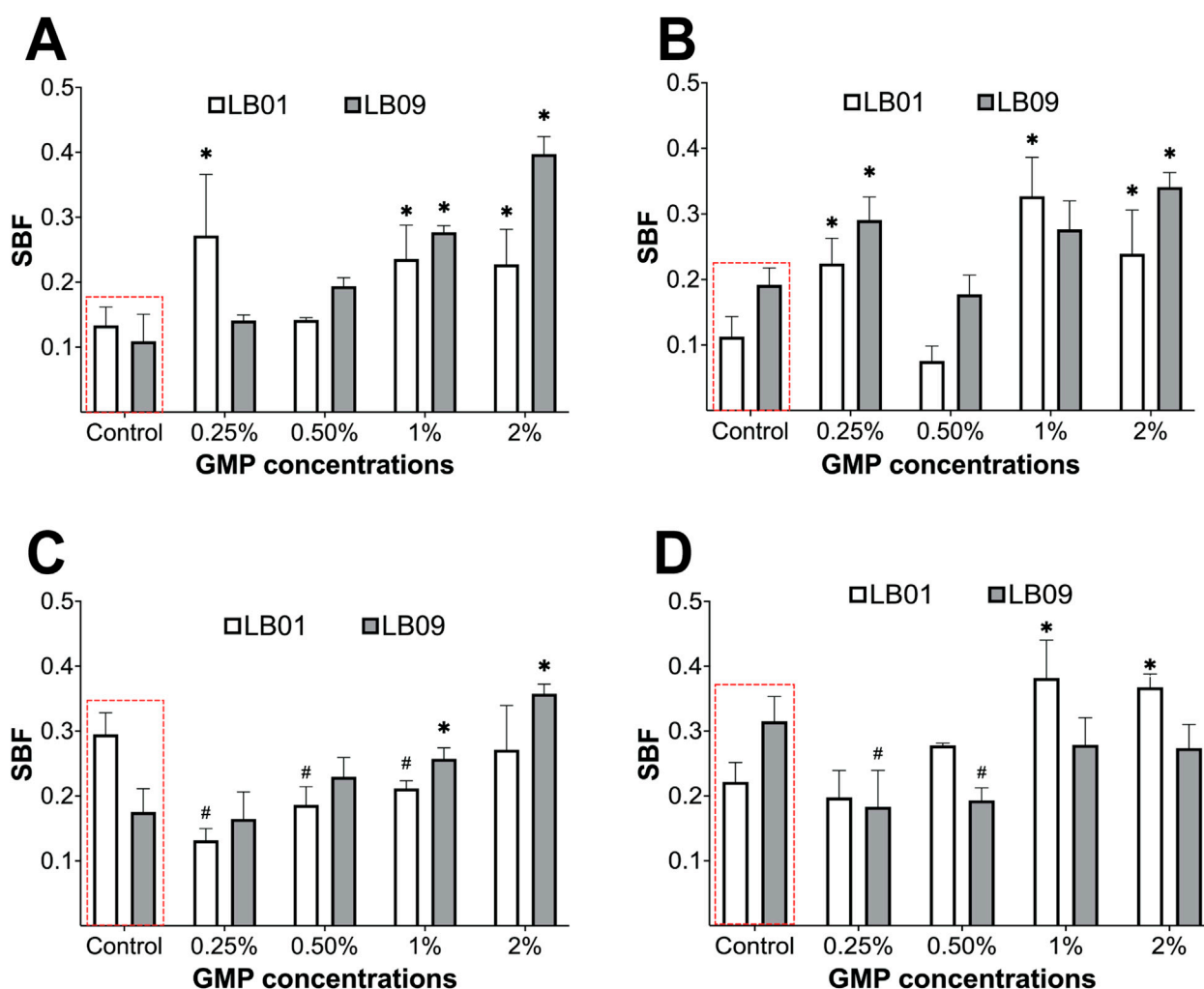


FIGURE 7 Biofilm formation of *Phb. leiognathi* strains LB01 and LB09 was assessed using crystal violet biofilm formation assays. (A, B) Biofilm formation of both strains exposed to GMPs vs. the control groups (red broken lines) for 3.1 days at 30°C and 22°C, respectively. (C, D) Biofilm formation of both strains exposed to GMPs vs. the control groups (red broken lines) for 7 days at 30°C and 22°C, respectively. Asterisks indicate significant increase in biofilm formation as compared to the control groups: * $p < 0.05$. Hash tags indicate significant decrease in biofilm formation as compared to the control groups: # $p < 0.05$. Error bars are the 95% confidence interval.

Bacterial bioluminescence is a complex mechanism regulated by QS that plays a vital role in both ecological and physiological processes (Anetzberger et al., 2009; Lupp et al., 2003). It has been reported that microbeads disrupted QS in bacterial populations by binding to autoinducer molecules (Gagné, 2017). The present study revealed intricate disparities in the bioluminescence patterns of *Phb. leiognathi* strains when exposed to different GMP concentrations at different temperatures. One of the critical observations in this study is the hormetic effect of low GMP concentrations in LB01 at 30°C in 3.1-day experiment. Hormesis is a dose-response phenomenon characterized by low-dose stimulation and high-dose inhibition (Calabrese and Baldwin, 2003), which is regulated by the QS system (Lin et al., 2023; Sun et al., 2018). Numerous studies have reported on the hormesis in various biota caused by environmental pollutants. Fan et al. (2021) reported on induced hormesis in soil microbial populations induced by cadmium and lead. Similar results were found for *Microcystis aeruginosa* exposed to halogenated

organic pollutants (Zhang et al., 2022), *Phb. phosphoreum* exposed to sulfonamides (Deng et al., 2012), and plant species exposed to urban metal pollutants (Salinitro et al., 2021). Moreover, a recent meta-analysis on the effects of MPs at environmentally relevant concentrations (≤ 1 mg/L⁻¹) on aquatic biota also revealed hormesis regarding various endpoints, such as behavior, genotoxicity, immunotoxicity, neurotoxicity, and reproduction (Sun et al., 2021).

Another critical observation in this study is the bioluminescence of high GMP concentrations in LB01 exposed for 7 days at 30°C. Several environmental contaminants exhibit inhibitory effects, resulting in various types of metabolic dysfunction. Aged tire wear particles, which are among the microplastic pollutants in the environment, were found to inhibit bacteria community leading to negatively affecting nitrogen metabolism in marine sediments (Liu et al., 2022). Aromatic compounds (such as benzene, toluene, and furfural) detected in wastewater were

identified as growth inhibitors as they inhibited the metabolic assimilation processes of purple phototrophic bacteria (San Martín et al., 2021). It has been reported that membrane barrier impairment and direct inhibition of enzyme systems by toxic pollutants are likely to underlie bioluminescence quenching (Ismailov et al., 2000). In the present study, bioluminescence was not directly correlated with cell viability; while some conditions resulted in bioluminescence quenching, the *Phb. leiognathi* strains' cells remained largely unaffected in terms of their ability to survive and grow (based on MTT assays). This discrepancy suggests that the factors influencing bioluminescence and cell viability are distinct and may involve different cellular mechanisms. Sully et al. (2014) found that the QS inhibitors disrupt bacterial behaviors, including biofilm formation, without directly killing or inhibiting *Staphylococcus aureus* cells. In addition, MPs are capable of adhering contaminants, which raises the possibility the MPs could also bind signaling molecules involved in QS resulting to disrupted QS mechanism (Gagné, 2017). Thus, bioluminescence alone may not be a reliable indicator of bacterial viability in this context.

Previous studies have reported the effects of plastic particles at different concentrations. For example, Liu et al. (2021) exposed *Streptomyces coelicolor* to nanoplastics and found that the fatality rate peaked (at 64.8%), when the particle size was 20 nm (tested range: 20 nm–1 mm) and the concentration was 10 mg/L (tested range: 0.1–10 mg/L). Tang et al. (2022) found that the polyethylene MPs at 100 and 500 MP/L shifted the community structure of sulfate-reducing bacteria. However, both *Phb. leiognathi* strains showed notably strain-specific response patterns, which highlights microbial variances in the presence of MPs. Yi et al. (2021) reported that 160 mg/L polystyrene microspheres, with sizes ranging from 0.323 to 0.656 μm , inhibited *E. coli* growth but promoted *Bacillus cereus* growth. They concluded that this difference is attributed to the cell wall compositions and surface interactions between each species and the polystyrene microspheres. The size of GMPs, ranging from 25.5 μm to 2.81 mm (Supplementary Figure S1). Larger particles (closer to 2.81 mm) may cause physical disruption by blocking signaling molecules or altering the microenvironment around the cells, which potentially hindering QS. In contrast, smaller particles (closer to 25.5 μm) have a larger surface area-to-volume ration, making them more likely to adsorb chemicals or release additives, which could affect bacterial metabolism more directly, resulting to bioluminescence alteration either through stress responses or metabolic interference. Both *Phb. leiognathi* strains used in the present study belong to the same genus and share similar cell wall compositions, so their differing “behaviors” under specific conditions suggest that other cellular functions may influence their responses to GMPs.

The post-exposure recovery experiments conducted in this study demonstrated that both strains exhibited heterogenous recovery responses possibly that the response dynamics change within 3-day and 7-day GMPs exposure due to the alteration in gene expression, which eventually affecting QS mechanism responsible for bioluminescence. For instance, genes regulating light production can be upregulated or downregulated in response to environmental stress, shifting in the timing of peak bioluminescence (Tu et al., 2008; de Nadal et al., 2011; Zavilgelsky et al., 2015). Additionally, this study suggests that the bioluminescence response to GMP exposure in *Phb. leiognathi* strains is concentration-, time-, and temperature-dependent, which

emphasize the importance of temporal and physical factors on evaluating the environmental impacts of pollutants on marine organisms. The bacterial response from GMPs might influences QS mechanisms, which are essential for coordinating bioluminescence in bacterial populations. Plastic particles may influence signaling molecules that bacteria use to communicate, resulting in a collective bioluminescence response (Gagné, 2017). The premature bioluminescence activities observed in this study emphasize the need for further studies to understand the full ecophysiological consequences of plastic exposure. Future research should focus on elucidating the genetic and molecular mechanisms underlying these responses.

The present study indicates that biofilm formation in *Phb. leiognathi* strains LB01 and LB09 is influenced by exposure to different GMP concentrations, temperature, and exposure duration. The crystal violet biofilm formation assays revealed distinct biofilm development under varying conditions, suggesting complex interactions between the set laboratory conditions and bacterial behavior. The increased biofilm formation observed with higher concentrations vs. lower GMP concentrations was due to bacteria utilizing the GMPs as a substrate, which promoted adherence and aggregation of bacterial cells. Plastics have been reported to be utilized by bacteria as substrates and they induce bacterial aggregation (Ganesan et al., 2022; Hossain et al., 2018; Ayush et al., 2022). For instance, plastics with reduced hydrophobicity increased *E. coli* biofilm formation and exopolysaccharide content (Ganesan et al., 2022). Conversely, both strains have opposite biofilm formation responses in 7-day experiment at 22°C. These observations may be attributable to the differential metabolic responses of the bacteria at low temperature (Price and Sowers, 2004). Additionally, the zeta potential of plastic particles plays a significant role in biofilm formation (Ganesan et al., 2022; Okshevsky et al., 2020; Saygin and Baysal, 2020). A more negative zeta potential generally enhances bacterial adhesion by reducing electrostatic repulsion between bacterial cells and the plastic surface (Abram et al., 2021). This effect was particularly evident at higher GMP concentrations in the present study. Furthermore, the increased biofilm production observed in this study corroborated previous findings that plastics provide additional surface area that facilitates biofilm growth (Ganesan et al., 2022; Webb et al., 2009; Semcesen and Wells, 2021). However, at 22°C in 7-day experiment, the results for LB01 and LB09 differed, pointing again to strain-specific responses to GMPs. The increase in biofilm formation with higher GMPs, especially at 30°C and over longer exposure periods, suggests that temperature and exposure duration are critical factors in biofilm dynamics. Higher temperatures generally enhance microbial activity and biofilm stability, while longer exposure times allow bacteria to adapt and optimize their biofilm-forming capabilities (Stepanović et al., 2003; Bhagwat et al., 2021; Tu et al., 2021). These findings align with studies that have shown that biofilm formation is a complex adaptive response to environmental conditions, which includes factors such as nutrient availability, temperature, and the presence of surfaces for attachment.

The environmental implications of our findings are significant, given the escalating concerns surrounding plastic pollution in marine ecosystems. The present study suggests that plastic particles, prevalent in marine environments, may alter the natural bioluminescence behavior of *Phb. leiognathi* potentially impacting ecological interactions and energy transfer in these ecosystems, which can be applied to explore the combined effects of multiple pollutants, on microbial physiology in real marine environments. For instance,

xenobiotics may alter bacterial biofilm formation, quorum sensing, and bioluminescence (Gagné, 2017; Kumari et al., 2016), as well as microbial interactions with MPs. On the other hand, this research will benefit environmental scientists, marine biologists, and policymakers by offering insights into the ecophysiological repercussions of MP pollution. Understanding these interactions opens potential avenues for biotechnological applications, such as developing sensitive bioindicators for monitoring environmental pollution levels, including the MPs. For future research, exploring longer exposure durations, investigating gene regulation changes underlying the cellular mechanisms, using different types of plastics, and simulating more natural conditions to reflect the full complexity of marine environments and MP interactions are warranted to better understand the ecophysiological consequences of MP pollution.

Data availability statement

The datasets presented in this study can be found in online repositories. The names of the repository/repository and accession number(s) can be found in the article/[Supplementary Material](#).

Ethics statement

The manuscript presents research on animals that do not require ethical approval for their study.

Author contributions

RD: Conceptualization, Data curation, Formal Analysis, Methodology, Validation, Visualization, Writing—original draft, Writing—review and editing. SI: Methodology, Visualization, Writing—review and editing. SM: Resources, Writing—review and editing. RA: Conceptualization, Funding acquisition, Resources, Supervision, Validation, Writing—review and editing.

References

- Abram, A., Zore, A., Lipovž, U., Košak, A., Gavras, M., Boltežar, Ž., et al. (2021). Bacterial adhesion on prosthetic and orthotic material surfaces. *Coatings* 11 (12), 1469. doi:10.3390/coatings11121469
- Ahmad, R., Hansen, G., Hansen, H., Hjerde, E., Pedersen, H., Paulsen, S., et al. (2012). Prediction, microarray and northern blot analyses identify new intergenic small RNAs in *Aliivibrio salmonicida*. *J. Mol. Microbiol. Biotechnol.* 22, 352–360. doi:10.1159/000345769
- Alimi, O., Budarz, J., Hernandez, L., and Tukenji, N. (2018). Microplastics and nanoplastics in aquatic environments: aggregation, deposition, and enhanced contaminant transport. *Environ. Sci. and Technol.* 52, 1704–1724. doi:10.1021/acs.est.7b05559
- Andrady, A. (2017). The plastic in microplastics: a review. *Mar. Pollut. Bull.* 119 (1), 12–22. doi:10.1016/j.marpolbul.2017.01.082
- Anetzberger, C., Pirch, T., and Jung, K. (2009). Heterogeneity in quorum-sensing-regulated bioluminescence of *Vibrio harveyi*. *Mol. Microbiol.* 73 (2), 267–277. doi:10.1111/j.1365-2958.2009.06768.x
- Author Anonymous (2016). Plastics in the marine environment. Available at: <https://eunomia.eco/reports/plastics-in-the-marine-environment/#:~:text=Barely%201%25%20of%20marine%20plastics>.
- Ayush, P., Ko, J.-H., and Oh, H.-S. (2022). Characteristics of initial attachment and biofilm formation of *Pseudomonas aeruginosa* on microplastic surfaces. *Appl. Sci.* 12 (10), 5245. doi:10.3390/app12105245
- Bao, X.-C., Tang, H.-T., Li, X.-G., Li, A.-Q., Qi, X.-Q., Li, D.-H., et al. (2023). Bioluminescence contributes to the adaptation of deep-sea bacterium *Photobacterium phosphoreum* ANT-2200 to high hydrostatic pressure. *Microorganisms* 11 (6), 1362. doi:10.3390/microorganisms11061362
- Bhagwat, G., O'Connor, W., Grainge, I., and Palanisami, T. (2021). Understanding the fundamental basis for biofilm formation on plastic surfaces: role of conditioning films. *Front. Microbiol.* 12, 687118. doi:10.3389/fmicb.2021.687118
- Boyle, K., and Örmeci, B. (2020). Microplastics and nanoplastics in the freshwater and terrestrial environment: a review. *Water* 12 (9), 2633. doi:10.3390/w12092633
- Calabrese, E., and Baldwin, L. (2003). Toxicology rethinks its central belief. *Nature* 421, 691–692. doi:10.1038/421691a
- Chong, G., Kimyon, O., and Manfield, M. (2013). Quorum sensing signal synthesis may represent a selective advantage independent of its role in regulation of bioluminescence in *Vibrio fischeri*. *PLoS One* 8 (6), e67443. doi:10.1371/journal.pone.0067443
- De Jesus, R., and Dedes, G. (2020). Data on quantitation of *Bacillus cereus sensu lato* biofilms by microtiter plate biofilm formation assay. *Data Brief* 28, 104951. doi:10.1016/j.dib.2019.104951
- de Nadal, E., Ammerer, G., and Posas, F. (2011). Controlling gene expression in response to stress. *Nat. Rev. Genet.* 12, 833–845. doi:10.1038/nrg3055

Funding

The author(s) declare that financial support was received for the research, authorship, and/or publication of this article. This research was partially funded by the UAEU Program for Advanced Research (UPAR 2020/2022).

Acknowledgments

The authors would like to thank Dr. Biduth Kundu and Ayesha Alotaibi for their assistance with some of the experiments.

Conflict of interest

The authors declare that the research was conducted in the absence of any commercial or financial relationships that could be construed as a potential conflict of interest.

Publisher's note

All claims expressed in this article are solely those of the authors and do not necessarily represent those of their affiliated organizations, or those of the publisher, the editors and the reviewers. Any product that may be evaluated in this article, or claim that may be made by its manufacturer, is not guaranteed or endorsed by the publisher.

Supplementary material

The Supplementary Material for this article can be found online at: <https://www.frontiersin.org/articles/10.3389/ftox.2024.1479549/full#supplementary-material>

- Deng, Z., Lin, Z., Zou, X., Yao, Z., Tian, D., Wang, D., et al. (2012). Model of hormesis and its toxicity mechanism based on *quorum* sensing: a case study on the toxicity of sulfonamides to *Photobacterium phosphoreum*. *Environ. Sci. and Technol.* 46 (14), 7746–7754. doi:10.1021/es203490f
- Egbeocha, C., Malek, S., Emenike, C., and Milow, P. (2018). Feasting on microplastics: ingestion by and effects on marine organisms. *Aquat. Biol.* 27, 93–106. doi:10.3354/ab00701
- Fan, D., Sun, J., Liu, C., Wang, S., Han, J., Agathokleous, E., et al. (2021). Measurement and modeling of hormesis in soil bacteria and fungi under single and combined treatments of Cd and Pb. *Sci. Total Environ.* 783, 147494. doi:10.1016/j.scitotenv.2021.147494
- Gagné, F. (2017). Toxicity and disruption of *quorum* sensing in *Aliivibrio fischeri* by environmental chemicals: impacts of selected contaminants and microplastics. *J. Xenobiotics* 7 (1), 7101. doi:10.4081/xeno.2017.7101
- Gallo, F., Fossi, C., Weber, R., Santillo, D., Sousa, J., Ingram, I., et al. (2018). Marine litter plastics and microplastics. *Environ. Sci. Eur.* 30 (13), 1–14. doi:10.1186/s12302-018-0139-z
- Ganesan, S., Ruendee, T., Kimura, S., Chawengkijwanich, C., and Janjaroen, D. (2022). Effect of biofilm formation on different types of plastic shopping bags: structural and physicochemical properties. *Environ. Res.* 206, 112542. doi:10.1016/j.envres.2021.112542
- Habib, R., Abdoon, M., Al Meqbaali, R., Ghebremedhin, F., Elkashlan, M., Kittaneh, W., et al. (2020). Analysis of microbeads in cosmetic products in the United Arab Emirates. *Environ. Pollut.* 258, 113831. doi:10.1016/j.envpol.2019.113831
- Hammer, B., and Bassler, B. (2003). *Quorum* sensing controls biofilm formation in *Vibrio cholerae*. *Mol. Microbiol.* 50 (1), 101–104. doi:10.1046/j.1365-2958.2003.03688.x
- Hossain, M., Jiang, M., Wei, Q., and Leff, L. (2018). Microplastic surface properties affect bacterial colonization in freshwater. *J. Basic Microbiol.* 59 (1), 54–61. doi:10.1002/jobm.201800174
- Ismailov, A., Pogossyan, S., Mitrofanova, T., Egorov, N., and Netrusov, A. (2000). Bacterial bioluminescence inhibition by chlorophenols. *Appl. Biochem. Microbiol.* 36 (4), 404–408. doi:10.1007/BF02738051
- Kumari, S., Mangwani, N., and Das, S. (2016). Synergistic effect of *quorum* sensing genes in biofilm development and PAHs degradation by a marine bacterium. *Bioengineered* 7 (3), 205–211. doi:10.1080/21655979.2016.1174797
- Lin, H., Ning, X., Wang, D., Wang, Q., Bai, Y., and Qu, J. (2023). *Quorum*-sensing gene regulates hormetic effects induced by sulfonamides in Comamonadaceae. *Appl. Environ. Microbiol.* 89, e0166223–23. doi:10.1128/aem.01662-23
- Liu, X., Ma, J., Yang, C., Wang, L., and Tang, J. (2021). The toxicity effects of nano/microplastics on an antibiotic producing *Streptomyces coelicolor* M145. *Sci. Total Environ.* 764, 142804. doi:10.1016/j.scitotenv.2020.142804
- Liu, Y., Zhou, H., Yan, M., Liu, Y., Ni, X., Song, J., et al. (2022). Toxicity of tire wear particles and the leachates to microorganisms in marine sediments. *Environ. Pollut.* 309, 119744. doi:10.1016/j.envpol.2022.119744
- Lu, H.-C., Ziajahromi, S., Neale, P., and Leusch, F. (2021). A systematic review of freshwater microplastics in water and sediments: recommendations for harmonisation to enhance future study comparisons. *Sci. Total Environ.* 781, 146693. doi:10.1016/j.scitotenv.2021.146693
- Lupp, C., Urbanowski, M., Greenberg, E., and Ruby, E. (2003). The *Vibrio fischeri* *quorum*-sensing systems *ain* and *lux* sequentially induce luminescence gene expression and are important for persistence in the squid host. *Mol. Microbiol.* 50 (1), 319–331. doi:10.1046/j.1365-2958.2003.t01-1-03585.x
- Lusher, A., Hernandez-Milian, G., O'Brien, J., Berrow, S., O'Connor, I., and Officer, R. (2015). Microplastic and macroplastic ingestion by a deep diving, oceanic cetacean: the True's beaked whale *Mesoplodon mirus*. *Environ. Pollut.* 199, 185–191. doi:10.1016/j.envpol.2015.01.023
- Mattson, K., Jovic, S., Doverbratt, I., and Hansson, L.-A. (2018). "Nanoplastics in the aquatic environment," in *Microplastic contamination in aquatic environments*. Editor E. Zeng (Elsevier Inc), 379–399. doi:10.1016/B978-0-12-813747-5.00013-8
- Muneswaran, T., Kalyanaraman, N., Vennila, T., Kannan, M., and Ramakritinan, C. (2021). Rapid assessment of heavy metal toxicity using bioluminescent bacteria *Photobacterium leiognathi* strain GoMGM1. *Environ. Monit. Assess.* 193, 109. doi:10.1007/s10661-021-08860-2
- Naguit, M., Plata, K., Abisado, R., and Calugay, R. (2014). Evidence of bacterial bioluminescence in a Philippine squid and octopus hosts. *Int. J. Bioflux Soc.* 7 (6), 497–507.
- Okshevsky, M., Gautier, E., Farner, J., Schreiber, L., and Tufenkji, N. (2020). Biofilm formation by marine bacteria is impacted by concentration and surface functionalization of polystyrene nanoparticles in a species-specific manner. *Environ. Microbiol.* 12 (2), 203–213. doi:10.1111/1758-2229.12824
- Pinto, M., Langer, T., Hüffer, T., Hofmann, T., and Herndl, G. (2019). The composition of bacterial communities associated with plastic biofilms differs between different polymers and stages of biofilm succession. *PLoS One* 14 (6), e0217165. doi:10.1371/journal.pone.0217165
- Price, P., and Sowers, T. (2004). Temperature dependence of metabolic rates for microbial growth, maintenance, and survival. *Proc. Natl. Acad. Sci.* 101 (13), 4631–4636. doi:10.1073/pnas.0400522101
- Quaglia, N., Capuzzo, F., Ceci, E., Cometa, S., Di Pinto, A., Mottola, A., et al. (2023). Preliminary survey on the occurrence of microplastics in bivalve mollusks marketed in Apulian fish markets. *Italian J. Food Saf.* 12 (2), 10906. doi:10.4081/ijfs.2023.10906
- Rummel, C., Jahnke, A., Gorokhova, E., Kühnel, D., and Schmitt-Jansen, M. (2017). Impacts of biofilm formation on the fate and potential effects of microplastic in the aquatic environment. *Environ. Sci. and Technol. Lett.* 4 (7), 258–267. doi:10.1021/acs.estlett.7b00164
- Rummel, C., Löder, M., Fricke, N., Lang, T., Griebeler, E.-M., Janke, M., et al. (2016). Plastic ingestion by pelagic and demersal fish from the North sea and Baltic sea. *Mar. Pollut. Bull.* 102 (1), 134–141. doi:10.1016/j.marpolbul.2015.11.043
- Ryan, P. (2016). "Ingestion of plastics by marine organisms," in *Hazardous chemicals associated with plastics in the marine environment*. Editors H. Takada and H. Karapanagioti (Cham: Springer), 235–266. doi:10.1007/978_2016_21
- Salinitro, M., Mattarello, G., Guardigli, G., Odajiu, M., and Tassoni, A. (2021). Induction of hormesis in plants by urban trace metal pollution. *Sci. Rep.* 11, 20329. doi:10.1038/s41598-021-99657-3
- San Martín, J., Puyol, D., Melero, J., Segura, Y., and Martínez, F. (2021). Inhibition of the metabolism of mixed cultures of purple phototrophic bacteria by typical refinery and petrochemistry wastewater pollutants. *J. Chem. Technol. and Biotechnol.* 96 (7), 1893–1901. doi:10.1002/jctb.6708
- Saygin, H., and Baysal, A. (2020). Biofilm formation of clinically important bacteria on bio-based and conventional micro/submicron-sized plastics. *Bull. Environ. Contamination Toxicol.* 105, 18–25. doi:10.1007/s00128-020-02876-z
- Scherer, C., Weber, A., Stock, F., Vurusic, S., Egerci, H., Kochleus, C., et al. (2020). Comparative assessment of microplastics in water and sediment of a large European river. *Sci. Total Environ.* 738, 139866. doi:10.1016/j.scitotenv.2020.139866
- Semcesen, P., and Wells, M. (2021). Biofilm growth on buoyant microplastics leads to changes in settling rates: implications for microplastic retention in the Great Lakes. *Mar. Pollut. Bull.* 170, 112573. doi:10.1016/j.marpolbul.2021.112573
- Stabb, E., Schaefer, A., Bose, J., and Ruby, E. (2008). "Quorum signaling and symbiosis in the marine luminous bacterium *Vibrio fischeri*," in *Chemical communication among bacteria*. Editors S. Winans and B. Bassler (Washington, DC: ASM Press), 233–250.
- Stepanović, S., Ćirković, I., Mijač, V., and Švabić-Vlahović, M. (2003). Influence of the incubation temperature, atmosphere and dynamic conditions on biofilm formation by *Salmonella* spp. *Food Microbiol.* 20 (3), 339–343. doi:10.1016/S0740-0020(02)00123-5
- Subramani, R., and Jayaprakashvel, M. (2019). "Bacterial *quorum* sensing: biofilm formation, survival behaviour and antibiotic resistance," in *Implication of quorum sensing and biofilm formation in medicine, agriculture and food industry*. Editor P. Bramhachari (Singapore: Springer), 21–37. doi:10.1007/978-981-32-9409-7_3
- Sully, E., Malachowa, N., Elmore, B., Alexander, S., Femling, J., Gray, B., et al. (2014). Selective chemical inhibition of *agr* *quorum* sensing in *Staphylococcus aureus* promotes host defense with minimal impact on resistance. *PLoS Pathog.* 10 (6), e1004174. doi:10.1371/journal.ppat.1004174
- Sun, H., Pan, Y., Gu, Y., and Lin, Z. (2018). Mechanistic explanation of time-dependent cross-phenomenon based on *quorum* sensing: a case study of the mixture of sulfonamide and *quorum* sensing inhibitor to bioluminescence of *Aliivibrio fischeri*. *Sci. Total Environ.* 630, 11–19. doi:10.1016/j.scitotenv.2018.02.153
- Sun, T., Zhan, J., Li, F., Ji, C., and Wu, H. (2021). Effect of microplastics on aquatic biota: a hormetic perspective. *Environ. Pollut.* 285, 117206. doi:10.1016/j.envpol.2021.117206
- Swift, S., Winson, M., Chan, P., Bainton, N., Birdsall, M., Reeves, P., et al. (1993). A novel strategy for the isolation of luxI homologues: evidence for the widespread distribution of a LuxR:luxI superfamily in enteric bacteria. *Mol. Microbiol.* 10 (3), 511–520. doi:10.1111/j.1365-2958.1993.tb00923.x
- Tang, M., Zhou, S., Huang, J., Sun, L., and Lu, H. (2022). Stress responses of sulfate-reducing bacteria sludge upon exposure to polyethylene microplastics. *Water Res.* 220, 118646. doi:10.1016/j.watres.2022.118646
- Thirukumar, S., Selvaraj, U., Rath, S., Shankar, K., and Muthuvel, A. (2022). Evaluation of bioactive secondary metabolites from ponyfish associated bacteria (*Photobacterium leiognathi*). *J. Trop. Biodivers. Biotechnol.* 07 (3), jtb71758. doi:10.22146/jtb.71758
- Thompson, J., and Polz, M. (2006). "Dynamics of *Vibrio* populations and their role in environmental nutrient cycling," in *The biology of vibrios*. Editors F. Thompson, B. Austin, and J. Swings (Wiley), 190–203.
- Thushari, G., and Seneviratna, J. (2020). Plastic pollution in the marine environment. *Heliyon* 6, e04709. doi:10.1016/j.heliyon.2020.e04709
- Tu, C., Chen, T., Zhou, Q., Liu, Y., Wei, J., Wanek, J., et al. (2020). Biofilm formation and its influences on the properties of microplastics as affected by exposure time and depth in the seawater. *Sci. Total Environ.* 734, 139237. doi:10.1016/j.scitotenv.2020.139237
- Tu, C., Liu, Y., Li, L., Li, Y., Vogts, A., Luo, Y., et al. (2021). Structural and functional characteristics of microplastic associated biofilms in response to temporal dynamics and polymer types. *Bull. Environ. Contamination Toxicol.* 107, 633–639. doi:10.1007/s00128-021-03333-1

- Tu, K., Waters, C., Svenningsen, S., and Bassler, B. (2008). A small-RNA-mediated negative feedback loop controls *quorum*-sensing dynamics in *Vibrio harveyi*. *Mol. Microbiol.* 70 (4), 896–907. doi:10.1111/j.1365-2958.2008.06452.x
- Valentin, F., Frederique, L., Christophe, L., Arnaud, H., Philippe, S., and Ika, P.-P. (2016). Colonization of polystyrene microparticles by *Vibrio*. *ACS Environ. Sci. and Technol.* 50 (20), 10988–10996. doi:10.1021/acs.est.6b02720
- Veettil, B., Puri, V., Acharki, S., Ward, R., and Khoa, N. (2024). Microplastic pollution in Vietnam's estuarine, coastal and riverine environments: research advances and future prospects. *Estuar. Coast. Shelf Sci.* 301, 108749. doi:10.1016/j.ecss.2024.108749
- Wang, D., Bai, L., Li, S., and Yan, W. (2022). Similarities and differences in *quorum* sensing-controlled bioluminescence between *Photobacterium phosphoreum* T3 and *Vibrio ginghaiensis* sp.-Q67. *Appl. Sci.* 12 (4), 2066. doi:10.3390/app12042066
- Wang, H., Cheng, H., Wang, F., Wei, D., and Wang, X. (2010). An improved 3-(4,5-dimethylthiazol-2-yl)-2,5-diphenyl tetrazolium bromide (MTT) reduction assay for evaluating the viability of *Escherichia coli* cells. *J. Microbiol. Methods* 82, 330–333. doi:10.1016/j.mimet.2010.06.014
- Warrier, A., Satyamoorthy, K., and Murali, T. (2021). *Quorum*-sensing regulation of virulence factors in bacterial biofilm. *Future Microbiol.* 16 (13), 1003–1021. doi:10.2217/fmb-2020-0301
- Webb, H., Crawford, R., Sawabe, T., and Ivanova, E. (2009). Poly(ethylene terephthalate) polymer surfaces as a substrate for bacterial attachment and Biofilm Formation. *Microbes Environ.* 24 (1), 39–42. doi:10.1264/jsme2.ME08538
- Yaser, N., Abdullah, M., Aris, A., and Zainudin, I. (2014). Isolation and identification of bioluminescent bacteria in squid and water of Malaysia. *Int. J. Adv. and Environ. Eng.* 1 (2), 225–228. doi:10.15242/IJAAEE.C0215136
- Yi, X. L. W., Liu, Y., Yang, K., Wu, M., and Zhou, H. (2021). Effect of polystyrene microplastics of different sizes to *Escherichia coli* and *Bacillus cereus*. *Bull. Environ. Contam. Toxicol.* 107, 626–632. doi:10.1007/s00128-021-03215-6
- Zavilgelsky, G., Melkina, O., Kotova, V., Konopleva, M., Manukhov, I., and Pustovoyt, K. (2015). Photoreactivating activity of bioluminescence: repair of UV-damaged *Escherichia coli* DNA proceeds with assistance of the *lux* genes of marine bacteria. *Biophysics* 60, 739–744. doi:10.1134/S0006350915050243
- Zettler, E., Mincer, T., and Amaral-Zettler, L. (2013). Life in the “plastisphere”: microbial communities on plastic marine debris. *Environ. Sci. and Technol. Lett.* 47 (13), 7137–7146. doi:10.1021/es401288x
- Zhang, M., and Xu, L. (2020). Transport of micro- and nanoplastics in the environment: trojan-horse effect for organic contaminants. *Crit. Rev. Environ. Sci. and Technol.* 52 (5), 810–846. doi:10.1080/10643389.2020.1845531
- Zhang, Y., Gao, Q., Liu, S., Tang, L., Li, X.-G., and Sun, H. (2022). Hormetic dose-response of halogenated organic pollutants on *Microcystis aeruginosa*: joint toxic action and mechanism. *Sci. Total Environ.* 829, 154581. doi:10.1016/j.scitotenv.2022.154581

Frontiers in Environmental Science

Explores the anthropogenic impact on our natural world

An innovative journal that advances knowledge of the natural world and its intersections with human society. It supports the formulation of policies that lead to a more inhabitable and sustainable world.

Discover the latest Research Topics

[See more →](#)

Frontiers

Avenue du Tribunal-Fédéral 34
1005 Lausanne, Switzerland
frontiersin.org

Contact us

+41 (0)21 510 17 00
frontiersin.org/about/contact

